PLASTICITY AND RECONSTRUCTION OF NEURAL NETWORK IN BRAIN INJURY

EDITED BY: Zhang Pengyue, Yuchuan Ding, Yulong Bai, Xiangjian Zhang and Yunping Deng

PUBLISHED IN: Frontiers in Cellular Neuroscience

frontiers Research Topics

ISSN 1664-8714
ISBN 978-2-88971-220-5
DOI 10.3389/978-2-88971-220-5

About Frontiers

Frontiers is more than just an open-access publisher of scholarly articles: it is a pioneering approach to the world of academia, radically improving the way scholarly research is managed. The grand vision of Frontiers is a world where all people have an equal opportunity to seek, share and generate knowledge. Frontiers provides immediate and permanent online open access to all its publications, but this alone is not enough to realize our grand goals.

Frontiers Journal Series

The Frontiers Journal Series is a multi-tier and interdisciplinary set of open-access, online journals, promising a paradigm shift from the current review, selection and dissemination processes in academic publishing. All Frontiers journals are driven by researchers for researchers; therefore, they constitute a service to the scholarly community. At the same time, the Frontiers Journal Series operates on a revolutionary invention, the tiered publishing system, initially addressing specific communities of scholars, and gradually climbing up to broader public understanding, thus serving the interests of the lay society, too.

Dedication to Quality

Each Frontiers article is a landmark of the highest quality, thanks to genuinely collaborative interactions between authors and review editors, who include some of the world's best academicians. Research must be certified by peers before entering a stream of knowledge that may eventually reach the public - and shape society; therefore, Frontiers only applies the most rigorous and unbiased reviews.
Frontiers revolutionizes research publishing by freely delivering the most outstanding research, evaluated with no bias from both the academic and social point of view. By applying the most advanced information technologies, Frontiers is catapulting scholarly publishing into a new generation.

What are Frontiers Research Topics?

Frontiers Research Topics are very popular trademarks of the Frontiers Journals Series: they are collections of at least ten articles, all centered on a particular subject. With their unique mix of varied contributions from Original Research to Review Articles, Frontiers Research Topics unify the most influential researchers, the latest key findings and historical advances in a hot research area! Find out more on how to host your own Frontiers Research Topic or contribute to one as an author by contacting the Frontiers Editorial Office: frontiersin.org/about/contact

PLASTICITY AND RECONSTRUCTION OF NEURAL NETWORK IN BRAIN INJURY

Topic Editors:
Zhang Pengyue, Yunnan University of Traditional Chinese Medicine, China
Yuchuan Ding, Wayne State University, United States
Yulong Bai, Huashan Hospital Affiliated to Fudan University, China
Xiangjian Zhang, Second Hospital of Hebei Medical University, China
Yunping Deng, University of Tennessee Health Science Center, United States

Citation: Pengyue, Z., Ding, Y., Bai, Y., Zhang, X., Deng, Y., eds. (2021). Plasticity and Reconstruction of Neural Network in Brain Injury. Lausanne: Frontiers Media SA. doi: 10.3389/978-2-88971-220-5

Table of Contents

frontiers in Cellular Neuroscience

EDITORIAL
published: 22 June 2021
doi: 10.3389/fncel.2021.710499

Editorial: Plasticity and Reconstruction of Neural Network in Brain Injury

Pengyue Zhang[1]*, *Roxanne Ilagan*[2], *Yulong Bai*[3], *Xiangjian Zhang*[4], *Yunping Deng*[5] and *Yuchuan Ding*[2]

[1] College of Acupuncture, Tuina and Rehabilitation, Yunnan University of Traditional Chinese Medicine, Kunming, China, [2] Department of Neurosurgery, Wayne State University School of Medicine, Detroit, MI, United States, [3] Department of Rehabilitation Medicine, Huashan Hospital Affiliated to Fudan University, Shanghai, China, [4] Department of Neurology, Second Hospital of Hebei Medical University, Shijiazhuang, China, [5] University of Tennessee Health Science Center (UTHSC), Memphis, TN, United States

Keywords: plasticity, neural network, brain injury, reconstruction, synaptogenesis

Editorial on the Research Topic

Plasticity and Reconstruction of Neural Network in Brain Injury

OPEN ACCESS

Edited and reviewed by:
Enrico Cherubini, European Brain Research Institute, Italy

***Correspondence:**
Pengyue Zhang
zpy19802000@163.com

Specialty section:
This article was submitted to Cellular Neurophysiology, a section of the journal Frontiers in Cellular Neuroscience

Received: *16 May 2021*
Accepted: *27 May 2021*
Published: *22 June 2021*

Citation:
Zhang P, Ilagan R, Bai Y, Zhang X, Deng Y and Ding Y (2021) Editorial: Plasticity and Reconstruction of Neural Network in Brain Injury. Front. Cell. Neurosci. 15:710499. doi: 10.3389/fncel.2021.710499

The brain is a complex organ which controls all our functions such as movements, balance, thoughts, memory, emotions, circadian clock, and hormone secretion. One of its characteristics is to be very plastic where by plasticity we mean its ability to modify its connections in order to adapt to new internal or external stimuli including traumatic injury, and ischemic or hemorrhagic stroke. Brain injuries lead to the loss of brain parenchyma through necrosis, apoptosis and autophagic cell death of neural cell (Liao et al., 2020). Regardless of the etiology, the breakdown of the entire neural network is the direct result of brain injury and the immediate cause of dysfunction. The exact symptoms of brain disorders depend on the damaged area of the brain. Damages in the language centers or hippocampus result in speech dysfunction or spatial learning and memory disorders. Damages in the motorsensory cortex result in motor and sensory dysfunction of limbs despite normal structure of the spine, peripheral nervous system, bones, and muscles. Thus, the repair and reconstruction of the injured neural network is the ultimate goal for the treatment of brain injury. A thorough clarification of the cellular and molecular mechanisms of plasticity in brain injury and of the mechanisms of neural network reconstruction is a necessary endeavor in the search for new therapeutic targets.

The plasticity found in brain injury differs from the regeneration seen in spinal cord injury: it occurs in a complex environment that includes neural stem cells, injured neurons (surviving bodies and dead axons or synapses), denervated intact neurons, and numerous glial cells. Thus, reconstruction of the neural network after brain injury is affected by multiple cellular and molecular mechanisms, and the synergy among these factors contributes to the reconstruction and recovery of function.

The microenvironment is the functional foundation of the neural network both in the normal and injured brain. The components of the microenvironment include a variety of cell types

(i.e., normal and dysfunctional neurons, activated endogenous neural stem cells, astrocytes and microglia in different activated states), blood capillaries, glial scars, secreted factors (such as free radicals, neuroinflammatory factors, and neurotrophic factor), and the extracellular matrix (see the findings from Roll et al. in this topic). Some components are beneficial to the plasticity of the injured brain, but others are damaging. In this topic, Lei et al. found that NF-κB activated miR-146a-5p and induced oxidative stress and pyroptosis via TIGAR in a hippocampal neuronal cell model of AD; knockdown of NF-κB markedly attenuated oxidative stress and pyroptosis which protected neurons. Results from Hou et al. suggested that pharmacological inhibition of CSF1R caused acute activation of the microglia, promoted inflammatory response, and aggravated neuronal degeneration; this in turn caused loss of dendritic spines and behavioral deficits after transient global cerebral ischemia.

In addition, the newly formatted microvessels in the injured region are an important component of the microenvironment for neural plasticity and repair—damage activates the proliferation of endothelial cells and vascular remodeling through up-regulating the expression of a group of angiogenic factors including vascular endothelial growth factor (VEGF), Ang1/2, and their receptor Tie2. In addition, arteriogenesis (i.e. collateral artery growth, a process in which pre-existing collateral arterioles transform into functional collateral arteries) plays an important role in maintaining cerebral blood flow and improving the microenvironment in ischemic regions after brain injury (Sugiyama et al., 2011). Thus, in order to create a suitable microenvironment for neural plasticity and repair, we must promote the favorable factors and inhibit the adverse factors simultaneously.

Another key component to the reconstruction and repair of the neural network is endogenous neural stem cells (NSCs) (Jinno, 2021). Under external stimuli, such as brain injury, these NSCs from the subventricular zone (SVZ) and dentate gyrus (DG) can proliferate, migrate, and differentiate into neurons, oligodendrocytes, and astrocytes. The new neurons can incorporate into network circuitry, the oligodendrocytes can repair myelin sheaths, and the astrocytes can support, protect, and nourish neural networks in reconstruction. Because of the low immunogenicity and good histocompatibility as well as self-renewal and multi-directional differentiation potential, exogenous NSC transplantation has been used as a treatment for various neurological diseases. Numerous preclinical studies demonstrated that transplantation of exogenous NSCs could complement or replace damaged tissues and improve function (Chen et al., 2016; Zhang et al., 2019). Findings from Bai et al. demonstrated that bone marrow mesenchymal stem cells (BM-MSCs) could differentiate into mature and functional nerve cells, promote nerve regeneration, and improve functional recovery.

Creating the neural connection is a critical step for the reconstruction of the neural network and it requires axon formation, synaptogenesis, and myelination. Axons can sprout from new neurons derived from neural stem cells, injured neurons with surviving bodies and dead axons or synapses, and existing normal neurons located outside of the damaged zone. Axon formation goes through multiple steps including neuritogenesis, axon growth, axon maturation, axon branching, and pruning. The whole process is regulated by multiple mechanisms involved in astrocyte regulation (Fossati et al., 2020). Axon formation creates neuronal polarity and is a prerequisite to synaptogenesis and neural connection. Afterwards, the synapse begins to form between neuron terminals and the dendrites or body of another neuron, and the neural network is reconstituted (Zheng, 2020). The reconstituted neural network then needs to further mature and stabilize under the stimulation of rehabilitative training as well as activities of daily living. At this point, the injured neural network has been reconstructed and the dysfunction has been recovered wholly or partly.

Although the injury can initiate the spontaneous reconstruction of neural networks, the regenerative process is not sufficient for the complete reconstruction of the neural network and full recovery of function. Thus, therapies that stimulate the endogenous neural plasticity and reconstruction of the neural network are critical. Clinical and preclinical trials have determined that neuromodulation techniques such as repetitive transcranial magnetic stimulation (rTMS), transcranial direct current stimulation (tDCS), intermittent theta-burst stimulation (iTBS), and deep brain stimulation (DBS) can promote neural plasticity and improve recovery of function. However, the parameters of treatment such as the dose, frequency, location, and timing after stroke need further study. Ding et al. demonstrated that iTBS in the motor cortex (M1) did not enhance the accuracy or facilitate neuroplasticity after brain-computer interface (BCI) training.

Several other treatments and their effects on neural plasticity have also been studied. Physical exercise and enriched environment have been proven to improve neural plasticity after brain injury–the involved mechanism includes modulation of several mechanisms such as inhibition of the acute inflammatory response as well as enhancement of angiogenesis and synaptogenesis (Zhang et al., 2013, 2020; Hannan, 2014). In addition, Chinese herbs extracts have been shown to promote the reconstruction of the neural network and improve neurobehavioral deficits. Results from Hu et al. showed that notoginsenoside R1 derived from Panax notoginseng promoted neural repair through regulation of Nav proteins in an Alzheimer Disease model. Kang et al. demonstrated that Cannabidiol extracted from cannabis rescued mitochondrial dysfunction induced by MPP+ by activating autophagy. These results suggested that Cannabidiol could be used for the treatment of Parkinson's disease. In addition, electro-acupuncture was identified to improve the functional recovery in ischemic stroke through suppression of neuronal autophagy and apoptosis and by promoting the differentiation of endogenous neural stem cell (eNSC) (see results from Wang et al., Xing et al., and Zhang et al. in this topic).

Although numerous therapeutic methods have been proven effective in animal and preclinical experiments, the clinical application of these treatments

needs to be further investigated. A comprehensive therapeutic regimen including a variety of therapeutic methods could contribute to the plasticity and reconstruction of the neural network and requires further research.

AUTHOR CONTRIBUTIONS

PZ, YDi, YB, XZ, and YDe discussed the contents of this topic. PZ written the editor article. YDi, YB, XZ, YDe, and RI revised the article. All authors contributed to the article and approved the submitted version.

FUNDING

This study was supported by the National Natural Science Foundation of China (81960731, 81660384, and 81460351) and Joint Special Project of Traditional Chinese Medicine in Science and Technology Department of Yunnan Province (2019FF002(-008)).

REFERENCES

Chen, L., Zhang, G., Gu, Y., and Guo, X. (2016). Meta-analysis and systematic review of neural stem cells therapy for experimental ischemia stroke in preclinical studies. *Sci. Rep.* 6:32291. doi: 10.1038/srep32291

Fossati, G., Matteoli, M., and Menna, E. (2020). Astrocytic factors controlling synaptogenesis: a team play. *Cells* 9:2173. doi: 10.3390/cells9102173

Hannan, A. J. (2014). Environmental enrichment and brain repair: harnessing the therapeutic effects of cognitive stimulation and physical activity to enhance experience-dependent plasticity. *Neuropathol. Appl. Neurobiol.* 40, 13–25. doi: 10.1111/nan.12102

Jinno, H. (2021). Regeneration using endogenous neural stem cells following neonatal brain injury. *Pediatr. Int.* 263, 13–21. doi: 10.1111/ped.14368

Liao, S., Apaijai, N., Chattipakorn, N., and Chattipakorn, S. C. (2020). The possible roles of necroptosis during cerebral ischemia and ischemia/reperfusion injury. *Arch. Biochem. Biophys.* 695:108629. doi: 10.1016/j.abb.2020.108629

Sugiyama, Y., Yagita, Y., Oyama, N., Terasaki, Y., Omura-Matsuoka, E., Sasaki, T., et al. (2011). granulocyte colony-stimulating factor enhances arteriogenesis and ameliorates cerebral damage in a mouse model of ischemic stroke. *Stroke* 42, 770–775. doi: 10.1161/STROKEAHA.110.597799

Zhang, G. L., Zhu, Z. H., and Wang, Y. Z. (2019). Neural stem cell transplantation therapy for brain ischemic stroke: review and perspectives. *World J. Stem Cells* 11, 817–830. doi: 10.4252/wjsc.v11.i10.817

Zhang, P. Y., Yang, L. Q., Li, G. X., Jin, Y. J., Wu, D. J., Wang, Q. M., et al. (2020). Agrin involvement in synaptogenesis induced by exercise in a rat model of experimental stroke. *Neurorehabil. Neural Repair.* 34, 1124–1137. doi: 10.1177/1545968320969939

Zhang, P. Y., Yu, H. X., Zhou, N. Y., Zhang, J., Wu, Y., Zhang, Y. L., et al. (2013). Early exercise improves cerebral blood flow through increased angiogenesis in experimental stroke rat model. *J. Neuroeng. Rehabil.* 10:43. doi: 10.1186/1743-0003-10-43

Zheng, S. (2020). Alternative splicing programming of axon formation. *Wiley Interdiscip. Rev. RNA* 11:e1585. doi: 10.1002/wrna.1585

Conflict of Interest: The authors declare that the research was conducted in the absence of any commercial or financial relationships that could be construed as a potential conflict of interest.

frontiers in Cellular Neuroscience

MINI REVIEW
published: 24 May 2019
doi: 10.3389/fncel.2019.00228

The Relationship Between Autophagy and Brain Plasticity in Neurological Diseases

*Man-Man Wang[1], Ya-Shuo Feng[1], Si-Dong Yang[2], Ying Xing[1], Jing Zhang[1], Fang Dong[3] and Feng Zhang[1,4]**

[1] Department of Rehabilitation Medicine, The Third Hospital of Hebei Medical University, Shijiazhuang, China, [2] Department of Spine Surgery, The Third Hospital of Hebei Medical University, Shijiazhuang, China, [3] Department of Clinical Laboratory Medicine, The Third Hospital of Hebei Medical University, Shijiazhuang, China, [4] Hebei Provincial Orthopedic Biomechanics Key Laboratory, The Third Hospital of Hebei Medical University, Shijiazhuang, China

OPEN ACCESS

Edited by:
Zhang Pengyue,
Yunnan University of Traditional Chinese Medicine, China

Reviewed by:
Yuchuan Ding,
Wayne State University, United States
Yulong Bai,
Huashan Hospital Affiliated to Fudan University, China
Qiang Wang,
The Affiliated Hospital of Qingdao University, China
Long Yu Wei,
Beijing University of Chinese Medicine, China

***Correspondence:**
Feng Zhang
zjk20019@126.com

Specialty section:
This article was submitted to Cellular Neurophysiology, a section of the journal Frontiers in Cellular Neuroscience

Received: 23 March 2019
Accepted: 07 May 2019
Published: 24 May 2019

Citation:
Wang M-M, Feng Y-S, Yang S-D, Xing Y, Zhang J, Dong F and Zhang F (2019) The Relationship Between Autophagy and Brain Plasticity in Neurological Diseases. Front. Cell. Neurosci. 13:228. doi: 10.3389/fncel.2019.00228

Autophagy, a catabolic degradation system, is utilized for destroying and recycling the damaged or unnecessary cellular components. Brain plasticity refers to the remarkable characteristics of brain neurons that change their structure and function according to previous experience. This review was performed by searching the relevant articles in databases of SCIENCEDIRECT, PUBMED, and Web of Science, from respective inception to January 2019. Here, we review the neuroprotective effect of autophagy in neurological diseases and the mechanism of autophagy in brain plasticity. Moreover, the mechanism of autophagy in the process of brain plasticity can provide the possibility for the development of new treatment methods in the future, thus benefiting patients with neurological diseases. In summary, autophagy and brain plasticity play important roles in neurological diseases.

Keywords: autophagy, brain plasticity, neuroprotective effect, signal pathway, neurological disease

INTRODUCTION

Autophagy is a lysosome-reliant degradation mechanism that regulate many biological courses, such as neuroprotection and cellular stress reactions (Shen and Ganetzky, 2009). There are different kinds of autophagy in most mammalian cells, and each type of autophagy performs very specific tasks in the course of intracellular degradation (Tasset and Cuervo, 2016). The autophagy-lysosomal pathway is a main proteolytic pathway, which mainly embraces chaperone-mediated autophagy and macroautophagy in mammalian systems (Xilouri and Stefanis, 2010). Macroautophagy, as a lysosomal pathway in charge of the circulation of long-lived proteins and organelles, is mainly considered as the inducible course in neurons, which is activated in conditions of injury and stress (Boland and Nixon, 2006). Coupled with macro-autophagy, chaperone-mediated autophagy (CMA) is crucial for maintaining intracellular survival and homeostasis via selectively reducing oxidized, misfolded, or degraded cytoplasmic proteins (Cai et al., 2015).

The plasticity of the central nervous system(CNS) can be regarded as changes of functional interaction between different types of cells, astrocytes, neurons, and oligodendrocytes (Aberg et al., 2006). The mature brain, as a highly dynamic organ, constantly alters its structure via eliminating and forming new connections. In general, these changes are known as brain plasticity and are related to functional changes (Viscomi and D'Amelio, 2012). Brain plasticity can be divided into

structure plasticity and function plasticity. The structural plasticity of the brain refers to the fact that the connections between synapses and neurons in the brain can be established due to the influence of learning and experience. It includes the plasticity of synapses and neurons. Synaptic plasticity refers to the changes of pre-existing relationship between two neurons including structure and function alteration (De Pitta et al., 2016). Synaptic plasticity is considered as the representative of cellular mechanisms of memory and learning. Mitochondria are related to the modulation of complicated course of synaptic plasticity (Todorova and Blokland, 2017). For a long period, synaptic plasticity has been considered as a neuronal mechanism under the regulation of neural network action (Ronzano, 2017). Recent data indicate that autophagy is a homeostatic mechanism which is compatible with the microenvironment of the synapse, with the purpose of serving local functions linked with synaptic transmission (Todorova and Blokland, 2017). Neuronal plasticity is maintained by the fine modulation of organelle biogenesis and degradation and protein synthesis and degradation to assure high-efficiency turnover (Viscomi and D'Amelio, 2012). Protein degradation plays an important role in the course of synaptic plasticity, but the involved molecular mechanisms are unclear (Haynes et al., 2015). Therefore, Autophagy is a quality control mechanism of organelles and proteins in neurons, which plays a crucial role in their physiology and pathology (Viscomi and D'Amelio, 2012). In a word, there is a close relationship between autophagy and brain plasticity, and the related mechanisms are summarized in this review paper (as **Table 1** and **Figure 1** demonstrate).

THE NEUROPROTECTIVE EFFECT OF AUTOPHAGY IN NEUROLOGICAL DISEASES

Autophagy is involved in the occurrence and treatment for a series of neurological diseases. However, there are only sporadic reports for the relationship between autophagy and some types of the neurological diseases, which have not been accumulated enough to be reviewed. Therefore, in this review, we summarize the relationship between autophagy and brain plasticity in stroke, traumatic brain injury, cerebral tumor, and neurodegenerative diseases.

Autophagy and Stroke

Autophagy plays different roles in various conditions, and both autophagy activation and autophagy inhibition could exert neuroprotective effects in the process of stroke.

The Neuroprotective Effect of Autophagy Activation in Stroke

The co-modulation of autophagy and apoptosis is involved in ischemic stroke (IS)-induced injuries, and apoptosis and mitochondrial autophagy play an important role in this process (Guo Y. et al., 2017). RIPer (Remote ischemic perconditioning) has obvious neuroprotective effect on cerebral ischemia reperfusion injury in rats, and the autophagic lysosomal pathway is activated by RIPer. Autophagy activation promotes the neuroprotective effect of RIPer on focal cerebral ischemia in rats (Su et al., 2014). Liu et al. (2018b) report that activation of autophagy flux in astrocytes might conduce to neural recovery mechanisms and endogenous neuroprotective following stroke. Nampt promotes neuronal survival via inducing autophagy by modulating the TSC2-mTOR-S6K1 signaling pathway in a SIRT1-reliant manner during cerebral ischemia (Wang et al., 2012).

The Neuroprotective Effect of Autophagy Inhibition in Stroke

There is increasing evidence that autophagy dysfunction leads to the accumulation of damaged organelles and/or abnormal proteins. This accumulation is associated with synaptic functional disorder, neuronal death, and cellular stress (Xilouri and Stefanis, 2010). RIPreC (Remote ischemic preconditioning) + IPOC(ischemic post-conditioning) reduced the plasma HMGB1 level to exert its neuroprotective effect on cerebral ischemia reperfusion injury by suppressing the autophagy process (Wang et al., 2016a). SMXZF, which is a kind of compound extracted from Chinese traditional medicine, plays a neuroprotective part in focal ischemia-reperfusion injury, which might be related to the autophagy inactivation via AMPK/mTOR and JNK pathways (Guo et al., 2014).

TABLE 1 | The summary for involved signal pathways for the neuroprotective effect via regulating autophagy.

References	Pathway	Neuroprotective effect via activating / inhibiting autophagy	Diseases
Wang et al., 2012	TSC2-mTOR-S6K1	Activating	Cerebral ischemia.
Guo et al., 2014	AMPK/mTOR and JNK pathways	Inhibiting	Ischemia-reperfusion injury
Chen et al., 2018	mTOR/p70S6K	Inhibiting	Ischemia/ reperfusion injury
Jiang J. et al., 2018	mTOR/Ulk1	Inhibiting	Ischemic stroke
He et al., 2018	PI3K/AKT	Activating	Traumatic Brain Injury
Feng et al., 2017	PERK and IRE1	Inhibiting	Ischemic stroke
Shen et al., 2017	AMPK	Activating	Stroke
Wang et al., 2014	MiRNA-30a	Activating	Ischemic stroke
Zhou et al., 2011	Gsk-3	Activating	Ischemic brain injury
Zhang Y. et al., 2016	MiR-214-3p	Inhibiting	Sporadic Alzheimer's disease
Hu et al., 2017	ATG5	Activating	Parkinson's Disease

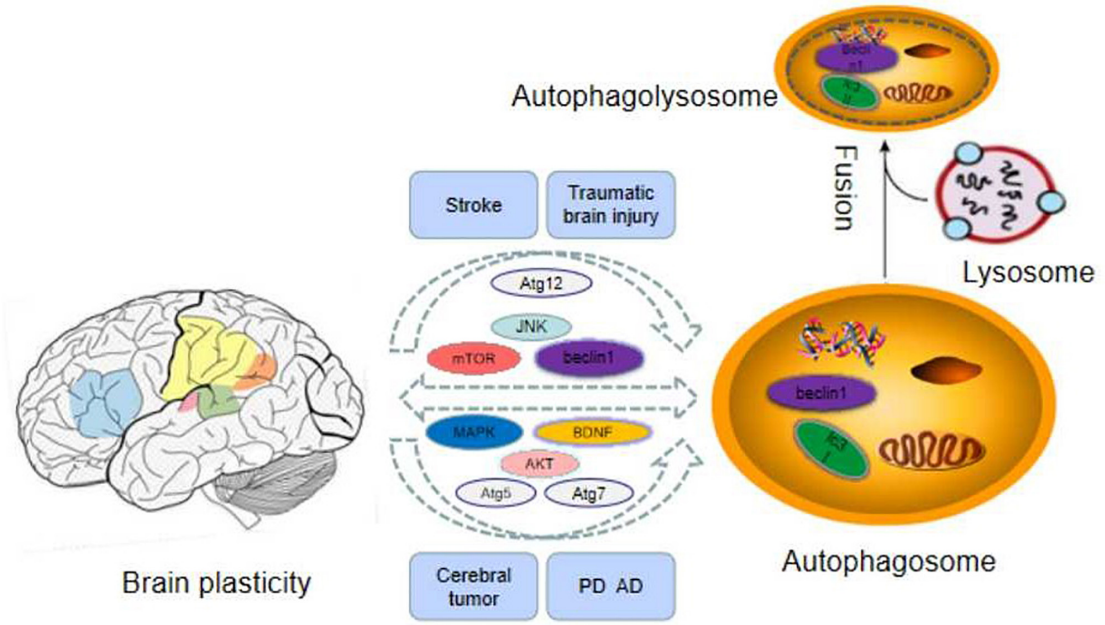

FIGURE 1 | The related important factors of autophagy and brain plasticity.

Guo D. et al. (2017) demonstrate for the first time that suppression of MALAT1 reduces beclin1-reliant autophagy via regulating the expression of mir-30a in cerebral IS, thereby reducing neuron cell death. Moreover, autophagy is regulated by mammalian target proteins in the PI3K/AKT/mTOR/p70S6K signaling pathway (Fan et al., 2015). RIPostC could suppress autophagy via activating the mTOR/p70S6K signaling pathway, thus reducing the brain I/R damage (Chen et al., 2018). Vitexin regulated autophagy dysfunction to alleviate MCAO-induced cerebral IS through mTOR/Ulk1 pathway (Jiang J. et al., 2018). The increasing evidence indicates that the AMPK-mTOR signaling pathway mediates the autophagy activity by the coordinated phosphorylation of ULK1 (Wang et al., 2018). Zheng et al. (2012) have demonstrated that NAD(+) administration reduced ischemic brain injury at least partly via inhibiting autophagy. LncRNA H19 inhibits autophagy through dusp5-erk1/2 axis. Blood samples from patients with IS showed that H19 gene mutation increased the risk of IS. LncRNA H19 could be a novel therapeutic target for IS (Wang et al., 2017a).

In summary, different studies obtained various results for the role of autophagy in the process of stroke, and further studies are required to explore the relationship between autophagy and stroke.

Autophagy and Traumatic Brain Injury

Similar to the relationship between autophagy and stroke, the relationship between autophagy and traumatic brain injury is also not simple. Both inhibition and activation of autophagy could exert neuroprotective effects following the occurrence of traumatic brain injury.

The Neuroprotective Effect of Autophagy Activation in Traumatic Brain Injury (TBI)

The promotion of autophagy and neuronal apoptosis are related to the secondary neural injury after Traumatic Brain Injury (TBI). Sevoflurane post-conditioning regulates autophagy through PI3K/AKT signaling, which alleviates the TBI-triggered neuronal apoptosis (He et al., 2018). Zhang L. et al. (2016) for the first time reveal that FTY720 plays a neuroprotective role following TBI, at least partially through the activation of the PI3K/AKT pathway and autophagy. In addition, Melatonin promotes autophagy, and suppresses mitochondrial apoptosis pathway, thus alleviating secondary brain injury of mice following traumatic brain injury (Ding et al., 2015). RIPoC alleviates brain IR injury via activating AMPK-reliant autophagy (Guo et al., 2018). Calcitriol treatment promotes the expression of VDR protein and alleviated the neural defect in the TBI model of rats. Its protective effect might be related to the decrease of apoptosis and the recovery of autophagy flux in the cortex area of rat brain (Cui et al., 2017). HS (heat stroke) can lead to brain injury via impaired autophagy flux and lysosomal dysfunction, and HA (heat acclimation) has a protective exerts neuroprotection on HS-induced brain injury through the mechanism of autophagy - lysosomal pathway (Yi et al., 2017).

The Neuroprotective Effect of Autophagy Inhibition in Traumatic Brain Injury

The autophagy pathway is associated with the pathophysiological reactions following TBI, and suppression of this pathway might contribute to the alleviation of traumatic injury and functional outcome defects (Luo et al., 2011). Melatonin administration before ischemia could notably alleviate brain IR damage by

suppressing ER stress-reliant autophagy (Feng et al., 2017). The over-expression of mir-27a may mitigate brain injury by inhibiting Foxo3a-regulated neuronal autophagy after TBI (Sun et al., 2017). Jiang H. et al. (2018) report that the down-regulation of TLR4 improves the neuroinflammatory response and brain injury following TBI by inhibiting astrocyte activation and autophagy induction. Therefore, the effect of activation and inhibition of autophagy on traumatic brain injury should be further clarified before future clinical applications.

Autophagy and Neurodegenerative Disease

Autophagy is the core regulator of central nervous system senescence and neurodegeneration. The delivery of organelles and toxic molecules to lysosomes by autophagy is critical for the health and survival of neurons (Plaza-Zabala et al., 2017). Most of the neurodegenerative diseases that perplex humans are related to the intracytoplasmic deposition of proteins that tend to accumulate in neurons, and autophagy is a powerful process for removing these proteins (Frake et al., 2015). Autophagy up-regulation is a promising treatment due to its potential to protect cells from the toxicity of accumulated proteins in neurodegenerative diseases (Karabiyik et al., 2017). Autophagy-regulated degradation of synaptic elements sustains synaptic homeostasis but also involves in a mechanism of neurodegeneration (Luningschror et al., 2017). Autophagy is vital for neuronal integrity, and the reduction of important autophagic components results in the structural defects and progressive neurodegenerative changes in pre- and post-synaptic morphologies (Nikoletopoulou et al., 2017). It is demonstrated that autophagy defects arise in the early stage of Alzheimer's disease (AD) (Li et al., 2017). A considerable amount of evidence indicates that the p38-mitogen-activated protein kinase (MAPK) signaling pathway plays an important part in neurodegenerative diseases and synaptic plasticity (Correa and Eales, 2012). MiR-181a regulates apoptosis and autophagy in PD(Parkinson's Disease) by inhibiting the p38 MAPK/JNK pathway (Liu Y. et al., 2017). In addition, RhEPO may alleviate hippocampal injury in epileptic seizure rats via regulating autophagy in a time-reliant manner through the S6 protein (Li et al., 2018).

In summary, autophagy has a close relationship with neurodegenerative disease, and activation of autophagy could improve the neurodegenerative changes, which might be a novel target in clinical treatment for such diseases.

Autophagy and Cerebral Tumor

The role of autophagy in tumor cell survival and death has attracted much attention in recent years (Noonan et al., 2016). As for glioblastoma (GBM), the most lethal tumor of the CNS, there is increasing evidence that the autophagy process is closely related to the tumorigenesis of GBM (Jawhari et al., 2017). Glioblastoma multiform is the most common and invasive primary brain tumor. Due to its adaptive ability of autophagy, it is highly resistant to various treatments (Jawhari et al., 2017). (Gammoh et al. (2016) elucidate that autophagy is the key to the occurrence and growth of GBM, which is an important therapeutic target for the treatment of GBM. The inhibition of autophagy is a promising strategy against GBM, and ATG9 is identified as a new target for hypoxic-induced autophagy (Abdul Rahim et al., 2017). Autophagy played a critical role in the formation of vasculogenic mimicry(VM) via Glioma stem cells (GSCs), which could be used as a therapeutic target for drug-resistant gliomas (Wu et al., 2017). The inhibition of autophagy promotes the anti-tumor activity of ibrutinib in GBM. Wang et al. (2017b) provides important insights into the role of anticancer drugs combined with autophagy inhibitors in the treatment of GBM.

In summary, autophagy provides new therapeutic expectations for cerebral tumor which is a big challenging for human. Therefore, the application of novel therapy for cerebral tumor on the basis of autophagy mechanisms elucidation should be explored in depth.

THE MECHANISM OF AUTOPHAGY IN BRAIN PLASTICITY

The Role of Mammalian Target of Rapamycin (mTOR) in the Relationship Between Autophagy and Brain Plasticity

Brain Plasticity and mTOR

The mTOR-controlled signaling pathways regulate many integrated physiological functions of the nervous system including neuronal development, synaptic plasticity, memory storage, and cognition (Bockaert and Marin, 2015). Mammalian target of rapamycin, as a protein kinase, is implicated in long-lasting synaptic plasticity and translation control of synapse (Hoeffer and Klann, 2010). It is reported that mTOR modulates many functions in the process of brain development, including proliferation, differentiation, migration, and dendrite formation. Moreover, mTOR plays an important role in the formation and plasticity of synapses (LiCausi and Hartman, 2018). Moreover, the mammalian target of rapamycin complex 1 (mTORC1) is a key modulator for cap-dependent protein synthesis, which is necessary for many forms of long-lasting memory and long-term synaptic plasticity (Santini et al., 2014). Therefore, it is demonstrated that mTOR plays a key role in the process of brain plasticity.

Autophagy and mTOR

As a key regulator of autophagy, the mTOR plays an important role in autophagy, translation, cell growth and survival (Hwang et al., 2017). Mammalian target of rapamycin and autophagy are tightly bound within cells, and defects of mTOR and autophagy process might lead to a variety of human diseases (Hoeffer and Klann, 2010). Studies have shown that mTOR is widely involved in autophagy activation and synaptic plasticity (Ryskalin et al., 2018). The mTOR modulates long-lasting synaptic plasticity, memory and learning via regulating the synthesis of dendritic proteins (Liu et al., 2018a). Macroautophagy can degrade organelles and long-lived proteins in case of mTOR inactivation. Synaptic plasticity is further modulated by mTOR and neurodegeneration occurs when macroautophagy

is absent (Hernandez et al., 2012). Therefore, macroautophagy following mTOR inactivation at the presynaptic terminal rapidly changes the neural transmission and presynaptic structure (Hernandez et al., 2012). The mechanisms for the target of rapamycin have been involved in modulating neurodegeneration and synaptic plasticity, but the role of mTOR in regulating presynaptic function via autophagy has not been clarified clearly (Torres and Sulzer, 2012).

In summary, there is a close relationship among mTOR, brain plasticity and autophagy. The mTOR related pathways play important role in regulating the process of autophagy and brain plasticity.

The Related Signaling Pathways of Autophagy and Brain Plasticity

The PI3K/Akt Pathway

Autophagy acts as a central mediator of cellular disease and health, and this self-balancing process seems to affect synaptic growth and plasticity in the CNS (Alirezaei et al., 2011). The inhibition of autophagy was necessary for memory improvement and for brain-derived neurotrophic factor (BDNF)-caused synaptic plasticity under the circumstances of nutritional stress, indicating that autophagy was a key component of BDNF signaling pathway, which was critical to BDNF-induced synaptic plasticity (Nikoletopoulou et al., 2017). The BDNF-activated ILK-Akt and PI3K-Akt signaling pathway play an important role in structural synaptic plasticity (Li et al., 2012). The activation of PI3K/Akt pathway might conduce to the memory consolidation and mechanisms of synaptic plasticity via increasing protein synthesis via mTOR pathway and promoting cell survival through FKHR pathway (Horwood et al., 2006). (Xu et al. (2017) reported that the neuroprotection of L-3-n-Butylphthalide (L-NBP) in attenuating learning and memory deficits in mice after repeated cerebral ischemia-reperfusion (RCIR) might be associated with the modulation of the expressions of proteins involved in apoptosis and autophagy and the promotion of Akt/mTOR signaling pathway. Moreover, the activation of PI3 kinase-Akt signaling pathway played an important role in promoting the survival of newly generated granule cells originated during exercise and the related increase of synaptic plasticity of dentate gyrus through an anti-apoptosis function (Bruel-Jungerman et al., 2009). Tetrahydrocurcumin alleviated the damage on neurons against TBI-induced apoptotic neuronal death, possibly through regulating autophagy and the PI3K/AKT pathway (Gao et al., 2016).

Moreover, neuronal stimulation led to NMDA receptor (NMDAR)-dependent autophagy via PI3K-Akt-mTOR pathway suppression, which might work in AMPA receptor (AMPAR) degradation, thus showing autophagy as a promoting factor to brain functions and NMDAR-reliant synaptic plasticity (Shehata et al., 2012). Curcumin exerts neuroprotective role through regulating the PI3K/Akt/mTOR pathway and down-regulating the autophagy activities (Huang et al., 2018). However, the interaction between the PI3K/AKT/mTOR pathway and the autophagy process is complicated, more detailed studies on the mechanism of disease as well as animal and cell models is needed.

The MAPK/Erk Pathway

There is increasing evidence that MAPKs can regulate autophagy/macroautophagy (Wang et al., 2016b). MAPK/ErK and p38 play key roles in the strict control of the autophagy process during maturation (Corcelle et al., 2007). In addition, some studies have shown that mitophagy requires MAPKs MAPK1/ERK2 and MAPK14/p38 (Hirota et al., 2015). As a protein kinase, MAPK/Erk is mobilized by neurotrophic factors involved in synaptic plasticity and formation, acting at both the cytoplasmic and nuclear levels (Giachello et al., 2010). The activity-reliant short-term plasticity and formation of these synapses are relied on the MAPK/Erk pathway (Giachello et al., 2010). Recently, there is increasing evidence that Ras and MAPK signaling plays a key role in neuronal function related to synaptic plasticity (Mazzucchelli and Brambilla, 2000).

In summary, the related signaling pathways of autophagy and brain plasticity has not be well clarified, which is worthy of further exploration.

THE ROLE OF AUTOPHAGY MECHANISM IN THE TREATMENT OF NERVOUS SYSTEM DISEASES

The dysfunction of autophagy pathway is related to a variety of neuropathologic conditions, and numerous studies have demonstrated that autophagy is a potential target for pharmacological regulation of neuroprotection (Russo et al., 2015). Autophagy and AMPK play a key role in CSD-induced ischemic tolerance. AMPK-regulated autophagy might be a novel target for stroke (Shen et al., 2017). Wang et al. (2014) report that the suppression of mirna-30a ameliorates ischemic injury by enhancing beclin1-regulated autophagy, which represents a possible therapeutic target for IS. Gsk-3 depressor hinders neuroinflammation following ischemic brain injury via activating autophagy, thereby providing a novel target for the prevention of ischemic brain damage (Zhou et al., 2011). (Peng et al. (2018) definitely indicates that mitofusin 2 mitigates I/R injury primarily by promoting autophagy, providing a potential new strategy for the neuroprotection of brain I/R injury. In addition, miR-214-3p inhibits autophagy and reduces the apoptosis of hippocampal neurons, suggesting that miR-214-3p is a new potential target for sporadic Alzheimer's disease (SAD) (Zhang Y. et al., 2016). The effect of autophagy related gene 5 (ATG5) in protecting dopaminergic neurons in zebrafish PD model is induced by 1-methyl-4-phenyl-1,2,3, 6-tetrahydropyridine (MPTP) (Hu et al., 2017). Autophagy is closely related to the occurrence and development of various neurological diseases in humans. Therefore, the study of autophagy mechanism has important clinical significance for the diagnosis of diseases and the search for new drug targets.

CONCLUSION

Brain plasticity is one of the most fundamental mechanism for neural function recovery following neurological diseases.

Autophagy is a crucial lysosome-reliant degradation process that controls various physiological and pathological courses in the brain. The summary for the interaction of autophagy and brain plasticity might provide novel therapy targets for neurological diseases, thus benefiting the patients in clinic.

AUTHOR CONTRIBUTIONS

M-MW and FZ conceived the main ideas and wrote the manuscript. Y-SF, JZ, FD, S-DY, and YX searched the references and designed the framework.

REFERENCES

Abdul Rahim, S. A., Dirkse, A., Oudin, A., Schuster, A., Bohler, J., Barthelemy, V., et al. (2017). Regulation of hypoxia-induced autophagy in glioblastoma involves ATG9A. *Br. J. Cancer* 117, 813–825. doi: 10.1038/bjc.2017.263

Aberg, N. D., Brywe, K. G., and Isgaard, J. (2006). Aspects of growth hormone and insulin-like growth factor-I related to neuroprotection, regeneration, and functional plasticity in the adult brain. *ScientificWorldJournal* 6, 53–80. doi: 10.1100/tsw.2006.22

Alirezaei, M., Kemball, C. C., and Whitton, J. L. (2011). Autophagy, inflammation and neurodegenerative disease. *Eur. J. Neurosci.* 33, 197–204. doi: 10.1111/j.1460-9568.2010.07500.x

Bockaert, J., and Marin, P. (2015). mTOR in brain physiology and pathologies. *Physiol. Rev.* 95, 1157–1187. doi: 10.1152/physrev.00038.2014

Boland, B., and Nixon, R. A. (2006). Neuronal macroautophagy: from development to degeneration. *Mol. Aspects Med.* 27, 503–519. doi: 10.1016/j.mam.2006.08.009

Bruel-Jungerman, E., Veyrac, A., Dufour, F., Horwood, J., Laroche, S., Davis, S., et al. (2009). Inhibition of PI3K-Akt signaling blocks exercise-mediated enhancement of adult neurogenesis and synaptic plasticity in the dentate gyrus. *PLoS One* 4:e7901. doi: 10.1371/journal.pone.0007901

Cai, Z., Zeng, W., Tao, K., Wang, Z. E. B., and Yang, Q. (2015). Chaperone-mediated autophagy: roles in neuroprotection. *Neurosci. Bull.* 31, 452–458. doi: 10.1007/s12264-015-1540-x

Chen, G. Z., Shan, X. Y., Li, X. S., and Tao, H. M. (2018). Remote ischemic postconditioning protects the brain from focal ischemia/reperfusion injury by inhibiting autophagy through the mTOR/p70S6K pathway. *Neurol. Res.* 40, 182–188. doi: 10.1080/01616412.2018.1424696

Corcelle, E., Djerbi, N., Mari, M., Nebout, M., Fiorini, C., Fenichel, P., et al. (2007). Control of the autophagy maturation step by the MAPK ERK and p38: lessons from environmental carcinogens. *Autophagy* 3, 57–59. doi: 10.4161/auto.3424

Correa, S. A., and Eales, K. L. (2012). The role of p38 Mapk and its substrates in neuronal plasticity and neurodegenerative disease. *J. Signal. Transduct.* 2012:649079. doi: 10.1155/2012/649079

Cui, C., Cui, J., Jin, F., Cui, Y., Li, R., Jiang, X., et al. (2017). Induction of the vitamin D receptor attenuates autophagy dysfunction-mediated cell death following traumatic brain injury. *Cell Physiol. Biochem* 42, 1888–1896. doi: 10.1159/000479571

De Pitta, M., Brunel, N., and Volterra, A. (2016). Astrocytes: orchestrating synaptic plasticity? *Neuroscience* 323, 43–61. doi: 10.1016/j.neuroscience.2015.04.001

Ding, K., Xu, J., Wang, H., Zhang, L., Wu, Y., and Li, T. (2015). Melatonin protects the brain from apoptosis by enhancement of autophagy after traumatic brain injury in mice. *Neurochem. Int.* 91, 46–54. doi: 10.1016/j.neuint.2015.10.008

Fan, S., Zhang, B., Luan, P., Gu, B., Wan, Q., Huang, X., et al. (2015). PI3K/AKT/mTOR/p70S6K pathway is involved in Abeta25-35-induced autophagy. *Biomed. Res. Int.* 2015:161020. doi: 10.1155/2015/161020

Feng, D., Wang, B., Wang, L., Abraham, N., Tao, K., Huang, L., et al. (2017). Pre-ischemia melatonin treatment alleviated acute neuronal injury after ischemic stroke by inhibiting endoplasmic reticulum stress-dependent autophagy via PERK and IRE1 signalings. *J. Pineal Res.* 62:e12395. doi: 10.1111/jpi.12395

Frake, R. A., Ricketts, T., Menzies, F. M., and Rubinsztein, D. C. (2015). Autophagy and neurodegeneration. *J. Clin. Invest.* 125, 65–74.

Gammoh, N., Fraser, J., Puente, C., Syred, H. M., Kang, H., Ozawa, T., et al. (2016). Suppression of autophagy impedes glioblastoma development and induces senescence. *Autophagy* 12, 1431–1439. doi: 10.1080/15548627.2016.1190053

Gao, Y., Li, J., Wu, L., Zhou, C., Wang, Q., Li, X., et al. (2016). Tetrahydrocurcumin provides neuroprotection in rats after traumatic brain injury: autophagy and the PI3K/AKT pathways as a potential mechanism. *J. Surg. Res.* 206, 67–76. doi: 10.1016/j.jss.2016.07.014

Giachello, C. N., Fiumara, F., Giacomini, C., Corradi, A., Milanese, C., Ghirardi, M., et al. (2010). MAPK/Erk-dependent phosphorylation of synapsin mediates formation of functional synapses and short-term homosynaptic plasticity. *J. Cell Sci.* 123, 881–893. doi: 10.1242/jcs.056846

Guo, D., Ma, J., Yan, L., Li, T., Li, Z., Han, X., et al. (2017). Down-regulation of lncrna MALAT1 attenuates neuronal cell death through suppressing beclin1-dependent autophagy by regulating mir-30a in cerebral ischemic stroke. *Cell Physiol. Biochem.* 43, 182–194. doi: 10.1159/000480337

Guo, H., Zhao, L., Wang, B., Li, X., Bai, H., Liu, H., et al. (2018). Remote limb ischemic postconditioning protects against cerebral ischemia-reperfusion injury by activating AMPK-dependent autophagy. *Brain Res. Bull.* 139, 105–113. doi: 10.1016/j.brainresbull.2018.02.013

Guo, Y., Ma, Y., Zhang, Y., Zhou, L., Huang, S., Wen, Y., et al. (2017). Autophagy-related gene microarray and bioinformatics analysis for ischemic stroke detection. *Biochem. Biophys. Res. Commun.* 489, 48–55. doi: 10.1016/j.bbrc.2017.05.099

Guo, Z., Cao, G., Yang, H., Zhou, H., Li, L., Cao, Z., et al. (2014). A combination of four active compounds alleviates cerebral ischemia-reperfusion injury in correlation with inhibition of autophagy and modulation of AMPK/mTOR and JNK pathways. *J. Neurosci. Res.* 92, 1295–1306. doi: 10.1002/jnr.23400

Haynes, K. A., Smith, T. K., Preston, C. J., and Hegde, A. N. (2015). Proteasome inhibition augments new protein accumulation early in long-term synaptic plasticity and rescues adverse Abeta effects on protein synthesis. *ACS Chem. Neurosci.* 6, 695–700. doi: 10.1021/acschemneuro.5b00068

He, H., Liu, W., Zhou, Y., Liu, Y., Weng, P., Li, Y., et al. (2018). Sevoflurane post-conditioning attenuates traumatic brain injury-induced neuronal apoptosis by promoting autophagy via the PI3K/AKT signaling pathway. *Drug Des. Devel. Ther.* 12, 629–638. doi: 10.2147/DDDT.S158313

Hernandez, D., Torres, C. A., Setlik, W., Cebrian, C., Mosharov, E. V., Tang, G., et al. (2012). Regulation of presynaptic neurotransmission by macroautophagy. *Neuron* 74, 277–284. doi: 10.1016/j.neuron.2012.02.020

Hirota, Y., Yamashita, S., Kurihara, Y., Jin, X., Aihara, M., Saigusa, T., et al. (2015). Mitophagy is primarily due to alternative autophagy and requires the MAPK1 and MAPK14 signaling pathways. *Autophagy* 11, 332–343. doi: 10.1080/15548627.2015.1023047

Hoeffer, C. A., and Klann, E. (2010). mTOR signaling: at the crossroads of plasticity, memory and disease. *Trends Neurosci.* 33, 67–75. doi: 10.1016/j.tins.2009.11.003

Horwood, J. M., Dufour, F., Laroche, S., and Davis, S. (2006). Signalling mechanisms mediated by the phosphoinositide 3-kinase/Akt cascade in synaptic plasticity and memory in the rat. *Eur. J. Neurosci.* 23, 3375–3384. doi: 10.1111/j.1460-9568.2006.04859.x

Hu, Z. Y., Chen, B., Zhang, J. P., and Ma, Y. Y. (2017). Up-regulation of autophagy-related gene 5 (ATG5) protects dopaminergic neurons in a zebrafish model of Parkinson's disease. *J. Biol. Chem.* 292, 18062–18074. doi: 10.1074/jbc.M116.764795

Huang, L., Chen, C., Zhang, X., Li, X., Chen, Z., Yang, C., et al. (2018). Neuroprotective effect of curcumin against cerebral ischemia-reperfusion via mediating autophagy and inflammation. *J. Mol. Neurosci.* 64, 129–139. doi: 10.1007/s12031-017-1006-x

Hwang, J. Y., Gertner, M., Pontarelli, F., Court-Vazquez, B., Bennett, M. V., Ofengeim, D., et al. (2017). Global ischemia induces lysosomal-mediated degradation of mTOR and activation of autophagy in hippocampal neurons destined to die. *Cell Death. Differ.* 24, 317–329. doi: 10.1038/cdd.2016.140

Jawhari, S., Bessette, B., Hombourger, S., Durand, K., Lacroix, A., Labrousse, F., et al. (2017). Autophagy and TrkC/NT-3 signaling joined forces boost the hypoxic glioblastoma cell survival. *Carcinogenesis* 38, 592–603. doi: 10.1093/carcin/bgx029

Jiang, H., Wang, Y., Liang, X., Xing, X., Xu, X., and Zhou, C. (2018). Toll-Like Receptor 4 knockdown attenuates brain damage and

neuroinflammation after traumatic brain injury via inhibiting neuronal autophagy and astrocyte activation. *Cell Mol. Neurobiol.* 38, 1009–1019. doi: 10.1007/s10571-017-0570-5

Jiang, J., Dai, J., and Cui, H. (2018). Vitexin reverses the autophagy dysfunction to attenuate MCAO-induced cerebral ischemic stroke via mTOR/Ulk1 pathway. *Biomed. Pharmacother.* 99, 583–590. doi: 10.1016/j.biopha.2018.01.067

Karabiyik, C., Lee, M. J., and Rubinsztein, D. C. (2017). Autophagy impairment in Parkinson's disease. *Essays Biochem.* 61, 711–720. doi: 10.1042/EBC20170023

Li, M., Dai, F. R., Du, X. P., Yang, Q. D., Zhang, X., Chen, Y., et al. (2012). Infusion of BDNF into the nucleus accumbens of aged rats improves cognition and structural synaptic plasticity through PI3K-ILK-Akt signaling. *Behav. Brain Res.* 231, 146–153. doi: 10.1016/j.bbr.2012.03.010

Li, Q., Han, Y., Du, J., Jin, H., Zhang, J., Niu, M., et al. (2018). Recombinant human erythropoietin protects against hippocampal damage in developing rats with seizures by modulating autophagy via the s6 protein in a time-dependent manner. *Neurochem. Res.* 43, 465–476. doi: 10.1007/s11064-017-2443-1

Li, Q., Liu, Y., and Sun, M. (2017). Autophagy and alzheimer's disease. *Cell Mol. Neurobiol* 37, 377–388.

LiCausi, F., and Hartman, N. W. (2018). Role of mTOR Complexes in Neurogenesis. *Int. J. Mol. Sci.* 19:1544. doi: 10.3390/ijms19051544

Liu, X., Li, Y., Yu, L., Vickstrom, C. R., and Liu, Q. S. (2018a). VTA mTOR signaling regulates dopamine dynamics, cocaine-induced synaptic alterations, and reward. *Neuropsychopharmacology* 43, 1066–1077. doi: 10.1038/npp.2017.247

Liu, X., Tian, F., Wang, S., Wang, F., and Xiong, L. (2018b). Astrocyte autophagy flux protects neurons against oxygen-glucose deprivation and ischemic/reperfusion injury. *Rejuven. Res.* 21, 405–415. doi: 10.1089/rej.2017.1999

Liu, Y., Song, Y., and Zhu, X. (2017). MicroRNA-181a regulates apoptosis and autophagy process in parkinson's disease by inhibiting p38 mitogen-activated protein kinase (MAPK)/c-Jun N-terminal kinases (JNK) signaling pathways. *Med. Sci. Monit.* 23, 1597–1606. doi: 10.12659/msm.900218

Luningschror, P., Binotti, B., Dombert, B., Heimann, P., Perez-Lara, A., Slotta, C., et al. (2017). Plekhg5-regulated autophagy of synaptic vesicles reveals a pathogenic mechanism in motoneuron disease. *Nat. Commun.* 8:678. doi: 10.1038/s41467-017-00689-z

Luo, C. L., Li, B. X., Li, Q. Q., Chen, X. P., Sun, Y. X., Bao, H. J., et al. (2011). Autophagy is involved in traumatic brain injury-induced cell death and contributes to functional outcome deficits in mice. *Neuroscience* 184, 54–63. doi: 10.1016/j.neuroscience.2011.03.021

Mazzucchelli, C., and Brambilla, R. (2000). Ras-related and MAPK signalling in neuronal plasticity and memory formation. *Cell Mol. Life Sci.* 57, 604–611. doi: 10.1007/pl00000722

Nikoletopoulou, V., Sidiropoulou, K., Kallergi, E., Dalezios, Y., and Tavernarakis, N. (2017). Modulation of autophagy by BDNF underlies synaptic plasticity. *Cell Metab.* 26, 230.e5–242.e5. doi: 10.1016/j.cmet.2017.06.005

Noonan, J., Zarrer, J., and Murphy, B. M. (2016). Targeting autophagy in glioblastoma. *Crit. Rev. Oncog.* 21, 241–252. doi: 10.1615/critrevoncog.2016017008

Peng, C., Rao, W., Zhang, L., Gao, F., Hui, H., Wang, K., et al. (2018). Mitofusin 2 exerts a protective role in ischemia reperfusion injury through increasing autophagy. *Cell Physiol. Biochem.* 46, 2311–2324. doi: 10.1159/000489621

Plaza-Zabala, A., Sierra-Torre, V., and Sierra, A. (2017). Autophagy and microglia: novel partners in neurodegeneration and aging. *Int. J. Mol. Sci.* 18:E598. doi: 10.3390/ijms18030598

Ronzano, R. (2017). Astrocytes and microglia: active players in synaptic plasticity. *Med. Sci.* 33, 1071–1078. doi: 10.1051/medsci/20173312014

Russo, R., Nucci, C., Corasaniti, M. T., Bagetta, G., and Morrone, L. A. (2015). Autophagy. dysregulation and the fate of retinal ganglion cells in glaucomatous optic neuropathy. *Prog. Brain Res.* 220, 87–105. doi: 10.1016/bs.pbr.2015.04.009

Ryskalin, L., Limanaqi, F., Frati, A., Busceti, C. L., and Fornai, F. (2018). mTOR-related brain dysfunctions in neuropsychiatric disorders. *Int. J. Mol. Sci.* 19:E2226. doi: 10.3390/ijms19082226

Santini, E., Huynh, T. N., and Klann, E. (2014). Mechanisms of translation control underlying long-lasting synaptic plasticity and the consolidation of long-term memory. *Prog. Mol. Biol. Transl. Sci.* 122, 131–167. doi: 10.1016/B978-0-12-420170-5.00005-2

Shehata, M., Matsumura, H., Okubo-Suzuki, R., Ohkawa, N., and Inokuchi, K. (2012). Neuronal stimulation induces autophagy in hippocampal neurons that is involved in AMPA receptor degradation after chemical long-term depression. *J. Neurosci.* 32, 10413–10422. doi: 10.1523/JNEUROSCI.4533-11.2012

Shen, P., Hou, S., Zhu, M., Zhao, M., Ouyang, Y., and Feng, J. (2017). Cortical spreading depression preconditioning mediates neuroprotection against ischemic stroke by inducing AMP-activated protein kinase-dependent autophagy in a rat cerebral ischemic/reperfusion injury model. *J. Neurochem.* 140, 799–813. doi: 10.1111/jnc.13922

Shen, W., and Ganetzky, B. (2009). Autophagy promotes synapse development in *Drosophila*. *J. Cell Biol.* 187, 71–79. doi: 10.1083/jcb.200907109

Su, J., Zhang, T., Wang, K., Zhu, T., and Li, X. (2014). Autophagy activation contributes to the neuroprotection of remote ischemic perconditioning against focal cerebral ischemia in rats. *Neurochem. Res.* 39, 2068–2077. doi: 10.1007/s11064-014-1396-x

Sun, L., Zhao, M., Wang, Y., Liu, A., Lv, M., Li, Y., et al. (2017). Neuroprotective effects of miR-27a against traumatic brain injury via suppressing FoxO3a-mediated neuronal autophagy. *Biochem. Biophys. Res. Commun.* 482, 1141–1147. doi: 10.1016/j.bbrc.2016.12.001

Tasset, I., and Cuervo, A. M. (2016). Role of chaperone-mediated autophagy in metabolism. *FEBS J.* 283, 2403–2413. doi: 10.1111/febs.13677

Todorova, V., and Blokland, A. (2017). Mitochondria and synaptic plasticity in the mature and aging nervous system. *Curr. Neuropharmacol.* 15, 166–173. doi: 10.2174/1570159x14666160414111821

Torres, C. A., and Sulzer, D. (2012). Macroautophagy can press a brake on presynaptic neurotransmission. *Autophagy* 8, 1540–1541. doi: 10.4161/auto.21330

Viscomi, M. T., and D'Amelio, M. (2012). The "Janus-faced role" of autophagy in neuronal sickness: focus on neurodegeneration. *Mol. Neurobiol.* 46, 513–521. doi: 10.1007/s12035-012-8296-3

Wang, J., Cao, B., Han, D., Sun, M., and Feng, J. (2017a). Long non-coding RNA H19 induces cerebral ischemia reperfusion injury via activation of autophagy. *Aging Dis.* 8, 71–84. doi: 10.14336/AD.2016.0530

Wang, J., Han, D., Sun, M., and Feng, J. (2016a). A combination of remote ischemic perconditioning and cerebral ischemic postconditioning inhibits autophagy to attenuate plasma HMGB1 and induce neuroprotection against stroke in rat. *J. Mol. Neurosci.* 58, 424–431. doi: 10.1007/s12031-016-0724-9

Wang, J., Liu, X., Hong, Y., Wang, S., Chen, P., Gu, A., et al. (2017b). Ibrutinib, a Bruton's tyrosine kinase inhibitor, exhibits antitumoral activity and induces autophagy in glioblastoma. *J. Exp. Clin. Cancer Res.* 36:96. doi: 10.1186/s13046-017-0549-6

Wang, J., Zhou, J. Y., Kho, D., Reiners, J. J. Jr., and Wu, G. S. (2016b). Role for DUSP1 (dual-specificity protein phosphatase 1) in the regulation of autophagy. *Autophagy* 12, 1791–1803. doi: 10.1080/15548627.2016.1203483

Wang, J. F., Mei, Z. G., Fu, Y., Yang, S. B., Zhang, S. Z., Huang, W. F., et al. (2018). Puerarin protects rat brain against ischemia/reperfusion injury by suppressing autophagy via the AMPK-mTOR-ULK1 signaling pathway. *Neural Regen. Res.* 13, 989–998. doi: 10.4103/1673-5374.233441

Wang, P., Guan, Y. F., Du, H., Zhai, Q. W., Su, D. F., Miao, C. Y., et al. (2012). Induction of autophagy contributes to the neuroprotection of nicotinamide phosphoribosyltransferase in cerebral ischemia. *Autophagy* 8, 77–87. doi: 10.4161/auto.8.1.18274

Wang, P., Liang, J., Li, Y., Li, J., Yang, X., Zhang, X., et al. (2014). Down-regulation of miRNA-30a alleviates cerebral ischemic injury through enhancing beclin 1-mediated autophagy. *Neurochem. Res.* 39, 1279–1291. doi: 10.1007/s11064-014-1310-6

Wu, H. B., Yang, S., Weng, H. Y., Chen, Q., Zhao, X. L., Fu, W. J., et al. (2017). Autophagy-induced KDR/VEGFR-2 activation promotes the formation of vasculogenic mimicry by glioma stem cells. *Autophagy* 13, 1528–1542. doi: 10.1080/15548627.2017.1336277

Xilouri, M., and Stefanis, L. (2010). Autophagy in the central nervous system: implications for neurodegenerative disorders. *CNS Neurol Disord. Drug Targets* 9, 701–719. doi: 10.2174/187152710793237421

Xu, J., Huai, Y., Meng, N., Dong, Y., Liu, Z., Qi, Q., et al. (2017). L-3-n-butylphthalide activates Akt/mTOR signaling, inhibits neuronal apoptosis and autophagy and improves cognitive impairment in mice with repeated cerebral ischemia-reperfusion injury. *Neurochem. Res.* 42, 2968–2981. doi: 10.1007/s11064-017-2328-3

Yi, J., He, G., Yang, J., Luo, Z., Yang, X., and Luo, X. (2017). Heat acclimation regulates the autophagy-lysosome function to protect against heat stroke-induced brain injury in mice. *Cell Physiol. Biochem.* 41, 101–114. doi: 10.1159/000455979

Zhang, L., Ding, K., Wang, H., Wu, Y., and Xu, J. (2016). Traumatic brain injury-induced neuronal apoptosis is reduced through modulation of PI3K and autophagy pathways in mouse by FTY720. *Cell Mol. Neurobiol.* 36, 131–142. doi: 10.1007/s10571-015-0227-1

Zhang, Y., Li, Q., Liu, C., Gao, S., Ping, H., Wang, J., et al. (2016). MiR-214-3p attenuates cognition defects via the inhibition of autophagy in SAMP8 mouse model of sporadic Alzheimer's disease. *Neurotoxicology* 56, 139–149. doi: 10.1016/j.neuro.2016.07.004

Zheng, C., Han, J., Xia, W., Shi, S., Liu, J., Ying, W., et al. (2012). NAD(+) administration decreases ischemic brain damage partially by blocking autophagy in a mouse model of brain ischemia. *Neurosci. Lett.* 512, 67–71. doi: 10.1016/j.neulet.2012.01.007

Zhou, X., Zhou, J., Li, X., Guo, C., Fang, T., Chen, Z., et al. (2011). GSK-3beta inhibitors suppressed neuroinflammation in rat cortex by activating autophagy in ischemic brain injury. *Biochem. Biophys. Res. Commun.* 411, 271–275. doi: 10.1016/j.bbrc.2011.06.117

Conflict of Interest Statement: The authors declare that the research was conducted in the absence of any commercial or financial relationships that could be construed as a potential conflict of interest.

frontiers in Cellular Neuroscience

REVIEW
published: 09 July 2019
doi: 10.3389/fncel.2019.00302

Consciousness: New Concepts and Neural Networks

Tong Zhao[1†], Yiqian Zhu[1†], Hailiang Tang[1†], Rong Xie[1†], Jianhong Zhu[1] and John H. Zhang[2*]*

[1] Department of Neurosurgery, Huashan Hospital, State Key Laboratory of Medical Neurobiology, Institutes of Brain Science, Collaborative Innovation Center for Brain Science, Shanghai Medical College, Fudan University, Shanghai, China, [2] Center for Neuroscience Research, Loma Linda University School of Medicine, Loma Linda, CA, United States

The definition of consciousness remains a difficult issue that requires urgent understanding and resolution. Currently, consciousness research is an intensely focused area of neuroscience. However, to establish a greater understanding of the concept of consciousness, more detailed, intrinsic neurobiological research is needed. Additionally, an accurate assessment of the level of consciousness may strengthen our awareness of this concept and provide new ideas for patients undergoing clinical treatment of consciousness disorders. In addition, research efforts that help elucidate the concept of consciousness have important scientific and clinical significance. This review presents the latest progress in consciousness research and proposes our assumptions with regard to the network of consciousness.

Keywords: consciousness, neural network, vegetative state, plasticity, brain injury

OPEN ACCESS

Edited by:
Yuchuan Ding,
Wayne State University, United States

Reviewed by:
Anatol Manaenko,
University Hospital Erlangen, Germany
Allen Ho,
Stanford University, United States

****Correspondence:***
Jianhong Zhu
jzhu@fudan.edu.cn
John H. Zhang
johnzhang3910@yahoo.com

† These authors have contributed equally to this work

Specialty section:
This article was submitted to Cellular Neurophysiology, a section of the journal Frontiers in Cellular Neuroscience

Received: *02 May 2019*
Accepted: *20 June 2019*
Published: *09 July 2019*

Citation:
Zhao T, Zhu Y, Tang H, Xie R, Zhu J and Zhang JH (2019) Consciousness: New Concepts and Neural Networks. Front. Cell. Neurosci. 13:302. doi: 10.3389/fncel.2019.00302

INTRODUCTION

Neuroscientists have conducted extensive research on consciousness for many years. In the past, the traditional viewpoint was that consciousness required the proper functioning of midline brain structures and that the content of an experience was supported by the activity of neurons in specific areas of the cerebral cortex (Jang and Lee, 2015). The reticular neurons, and especially the neurons of the ascending reticular activation system, play a vital role in maintaining behavioral arousal and consciousness (Jones, 2003; Englo et al., 2017). However, in recent times, many different opinions have been proposed. For example, some researchers believe that consciousness is aroused in the frontal region of the brain, including the prefrontal and central anterior cortex. Others believe that consciousness is created in areas of the hindbrain, including the occipital/parietal and central posterior regions of the brain (Koch et al., 2016; Seth, 2018). Questions that should be asked include: where is the material basis of consciousness? The physical basis of consciousness is the most important internal factor of consciousness.

IMPORTANT COMPONENT OF CONSCIOUSNESS: WAKEFULNESS

According to the latest neurosurgical research there are two key features of consciousness: (1) the state of consciousness (i.e., wakefulness) and (2) the content of consciousness (i.e., awareness) (Zeman, 2006; Bayne et al., 2016; Fazekas and Overgaard, 2016). Furthermore, there are additional features of the content of consciousness across the context of our brain (**Figure 1**). From the

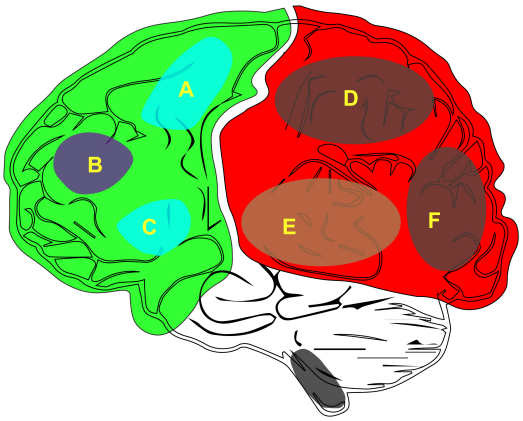

FIGURE 1 | The distribution of the neurobiological basis of consciousness in the brain. **(A)** M1, primary motor cortex. **(B)** Attention or working memory. **(C)** Verbal report (Broca). **(D)** Other content of consciousness. **(E)** Auditory consciousness. **(F)** Visual consciousness.

perspective of neurosurgeons, more attention is paid on wakefulness than on awareness because a disorder of this state can lead to coma. In the clinic, comas, and the associated vegetative state, are difficult to resolve (van Erp et al., 2015; Baricich et al., 2017).

Consciousness includes both the level of consciousness and its content. The level of consciousness is key to maintaining sobriety (Bayne et al., 2016). The generation of consciousness content (**Figure 1**) depends on the integration of the various sensations in the posterior cortex of the brain. Being able to stay awake and aware of the outside world is a characteristic that we associate with a conscious person (Fazekas and Overgaard, 2016). In addition, to perceive the outside world, one must first keep a clear head; that is, waking is the first step in the generation of consciousness. Therefore, if one wishes to study the generation of consciousness, one can start with wakefulness. Furthermore, the opposite of awakening is coma, which is helpful for the study of the mechanisms associated with clinical coma. Wakefulness research is relatively easy when compared to the study of the content of conscious because, unlike awareness, wakefulness can be quantified and is easier to observe and record.

As a state of consciousness, wakefulness is different in the context of both sleeping and coma. These states are mild or severe. For instance, one can wake up or semi-wake up, just as one could have mild or deep anesthesia. We are usually confident in judging a person's state of consciousness (Zeman, 2006). In the first sense, with the help of objective criteria, including the Glasgow Coma Scale (GCS), opening of the eyes usually indicates the state of being awake, and being able to talk almost always indicates further wakefulness. It is often thought that an awake individual is also aware; however, this is not always true. Actually, most of the content of consciousness is based on the state of awakening, and brain activity during sleep is a special case.

Research on consciousness has always been difficult. For example, the definition of consciousness is very vague and includes many aspects, such as the disciplines of psychology and philosophy. Thus, there is no definitive conclusion. In addition, the assessment of the level of consciousness is not an easy task. Awakening is an important component of consciousness and is also a well measured state by the availability of existing means. Therefore, the scientific exploration of consciousness should begin with research that is focused on the state of awakening. This information may further reveal the mysteries of consciousness.

KEY NUCLEAR EVENTS RELATED TO CONSCIOUSNESS: THE PARAVENTRICULAR NUCLEUS AND CLAUSTRUM

Paraventricular

The paraventricular nucleus is an important neurosecretory nucleus of the hypothalamus. Located in the medial area of the hypothalamus, above the upper nucleus, the paraventricular nucleus transmits from the pituitary gland to the posterior pituitary (Maejima et al., 2017; Qin et al., 2018). Previous studies have suggested that the paraventricular nucleus is an endocrine nucleus that produces a variety of hormones, including antidiuretic hormone and oxytocin. Further, scientists have revealed that there is an association between the paraventricular nucleus and hunger, appetite, drug addiction, and behavioral control (Krashes et al., 2014; Kirouac, 2015; Millan et al., 2017). However, the paraventricular nucleus also promotes sleep awakening and increases arousal (Kirouac, 2015). Orexin acts upon orexin receptors and are involved in the regulation of sleep-wakefulness (Ohno and Sakurai, 2008). Orexin neurons around the lateral fornix of the hypothalamus are mainly projected to the paraventricular nucleus of the thalamus, which is deeply involved in the control of motivated behaviors. Orexin-activated paraventricular thalamus (PVT) neurons play roles in the integration of sleep-wakefulness (Ishibashi et al., 2005). Therefore, the paraventricular nucleus of the thalamus may be the key site involved in the control of arousal. This is consistent with the view that the PVT and thalamic midline nuclei are associated with important physiological mechanisms, such as attention, arousal, and consciousness (Groenewegen and Berendse, 1994; Nascimento et al., 2008). Moreover, the PVT is a member of the midline and intralaminar group of thalamic nuclei that were originally hypothesized to function as the thalamocortical arousal system (Jones, 2003) and transmit information related to the state of awakening (Van der Werf et al., 2002).

Clinical observations have indicated that the central region of the thalamus is a key node for controlling the state of awakening; however, the key nuclei or neural circuits of this functional region remain unknown. By using *in vivo* fiber photometry and multi-channel electrophysiological recordings in mice, Dr. Hu (Ren et al., 2018) found that glutamatergic neurons of the PVT showed high activity during waking, and inhibition of PVT neuronal activity led to decreased arousal. Additionally, activation of PVT neurons induced a transition from sleep to arousal and from a waking-up process after

accelerated general anesthesia. This study also demonstrated that the projection of the PVT nucleus accumbens and the projection of orexin-secreting neurons from the lateral hypothalamus to the PVT glutamatergic neurons represent the pathways that control arousal. These results indicated that the PVT is the key thalamic nucleus that controls arousal.

Claustrum

The claustrum is a thin, irregular sheet of neurons that is attached to the underside of the neocortex in the center of brain. It is suspected to be present in the brains of all mammals. Although it is known that the claustrum and the cerebral cortex are reciprocally connected, little is known about the actual function of the claustrum. The claustrum and the frontal lobe are interconnected, and it includes the motor cortex, prefrontal cortex, and cingulate cortex; it also includes the occipital lobe of the visual cortex, the temporal and temporal cortex, the occipital and posterior parietal cortex, the frontal cap, the somatosensory area, and the anterior axillary olfactory and entorhinal cortex (Gattass et al., 2014; Goll et al., 2015; Torgerson et al., 2015; Dehaene et al., 2017; Kitanishi and Matsuo, 2017; White et al., 2018), which also projects into the hippocampus, amygdala and the caudate nucleus (Milardi et al., 2015). The claustrum may be closely related to the generation of consciousness since it provides functional anatomical links between the frontal cortices and the posterior sensory/association cortices (White and Mathur, 2018). The extensive reciprocal connections of the claustrum with almost the entire neocortex prompted us to propose its role as a gateway for perceptual information to the arousal system.

Koubeissi et al. (2014) reported that they were able to control a woman's consciousness by stimulating the claustrum. The woman in this study was epileptic; thus, the researchers used electrodes implanted deep in her brain to record signals from different brain regions during seizures in an attempt to cure her. One of the electrodes was next to the claustrum, and when they stimulated this area with a high-frequency current, the woman lost consciousness. Additionally, she stopped reading, showed "fragments" blankly, breathed slowly, and was unresponsive to the audience and visual instructions. When the stimulus stopped, she immediately regained consciousness and was completely unaware of what had happened. The same situation occurred several times during the test (Koubeissi et al., 2014). Another experiment in 2015 also supported the fact that claustrum may be associated with consciousness. The scientists in this study examined 171 veterans with traumatic brain injuries and observed the effects of claustrum damage on consciousness. They found that claustrum damage was associated with the duration of the loss of consciousness, but not with the frequency. Moreover, they believed that the claustrum played an important role in the restoration of consciousness but that it had little to do with the maintenance of consciousness (Chau et al., 2015).

Based on previous research, we assumed that consciousness was generated by the claustrum, which acted as a command center and formed a network covering the entire brain through the interconnection of three types of neurons, including neurons in the prefrontal lobe, the posterior frontal sulcus and the occipital lobe region. We also assumed that the prefrontal lobe and the state of high-level consciousness (cognition) were functionally related. In addition, we believed that the most basic form of consciousness may be generated by the posterior and occipital regions of the central sulcus. Although the claustrum is closely related to the cerebral cortex and various important nuclei, its connection is different. Most of the projection fibers of the cerebral cortex and nucleus that connect with the claustrum are derived from the bilateral brain, and the nerve fibers emitted from the claustrum are mostly directed to one side. In other words, the projection of the claustrum to the outside is asymmetrical (Smith et al., 2017). Damage to the claustrum of each cerebral hemisphere may also show some differences, although these differences still need to be confirmed (Zingg et al., 2014).

VITAL CORTICAL CONSCIOUSNESS REGIONS: THE HINDBRAIN AND POSTERIOR CORTICAL REGION

By using functional magnetic resonance imaging (MRI), we are able to observe when the brain is unable to stimulate, when corresponding regions are activated, and when neurons become abnormally active. These differences were used in word stimulation and visual decision task experiments, and it was concluded that activation of the cerebral hemisphere depends on the nature of the task rather than the stimulus itself. Whether activated on the left or the right side, activation of the brain is not in the prefrontal cortex. Rather, activation is observed in the vicinity of the central sulcus and the back of the brain (Stephan et al., 2003). In patients who underwent post-traumatic surgery to remove some of brain regions, the vast majority of patients (98%) remained in a persistent vegetative state after one year if the resected section involved the posterior cortex (Boly et al., 2017). Bianchi's research also reached a similar conclusion, and believed that lesions in the posterior cortex of the brain may lead to permanent coma (Bianchi and Sims, 2008). Neurological awareness is primarily anatomically located in the posterior cortical thermal region, including the sensory region, rather than the prefrontal network that is involved in task monitoring and reporting (Merker, 2007). Reports of patients that remain conscious after bilateral frontal lobe resection indicate that the prefrontal cortex is not essential for consciousness (Rowland and Mettler, 1949). Other parts of the cerebral hemisphere may be potential candidates for the maintenance of consciousness, including the back part of the brain.

CRUCIAL THEORIES OF CONSCIOUSNESS: GLOBAL WORKSPACE THEORY, INTEGRATED INFORMATION THEORY, AND QUANTUM THEORY

The most effective way to solve problems associated with consciousness is to use descriptions that have been introduced

by psychologists and cognitive scientists who strive to connect different aspects of their models to the neuroanatomy and neurophysiology of the brain (Harris and Shepherd, 2015). In the history of consciousness research, several theories have attempted to conceptually explain consciousness by presenting neural correlations of the stream of consciousness. In the following sections, we will discuss three of the most popular theories.

Global Workspace Theory

The global workspace (GW) theory of consciousness was first proposed by Baars in 1988 (Baars, 2005) and developed by Dehaene et al. (1998). The GW theory is based on competition, and its core idea is that conscious cognitive content can be used globally for a variety of cognitive processes, including attention, assessment, memory, and verbal reporting. According to the GW theory, a single brain region cannot independently accomplish the task of generating consciousness. Instead, consciousness requires the joint participation and coordination of different parts of the cerebrum. This encourages us to not limit the concept of consciousness to a single brain functional area or a star nucleus and to explore the brain as a whole.

The GW theory posits that computers of the future will be conscious (Thagard and Stewart, 2014; Dehaene et al., 2017). There are some disadvantages of the GW theory. First, it provides, at best, an account of the cognitive function of consciousness but fails to address the deeper problem of the nature of consciousness (i.e., what consciousness is) and how any mental process can be conscious (i.e., the "hard problem of consciousness" hypothesis) (Thagard and Stewart, 2014; LeDoux and Brown, 2017). Second, "while this hypothesis does not address the 'hard problem,' namely, the very nature of consciousness, it constrains a theory that attempts to do so, and provides important insights into the relationship between consciousness and cognition" (Northoff and Huang, 2017).

Integrated Information Theory

The essence of the integrated information theory (IIT) is that consciousness is the capacity of a system to integrate information. It is the most audacious current proposal of Giulio Tononi's hypothesis (Tononi, 2004). Instead of focusing on the function of the cerebrum the IIT starts from the results in an attempt to determine the reason. Moreover, the IIT presents a mathematical framework for evaluating the quality and quantity of consciousness (Tononi, 2012; Oizumi et al., 2014; Tononi et al., 2016; Tsuchiya et al., 2016). This theory posits that the physical basis of consciousness must be the maximization of internal causal power and provide a means to determine the quality and quantity of an experience (Tononi, 2004). The theory leads to some counterintuitive predictions and can be used to develop new tools for assessing consciousness in non-communicative patients. However, the IIT proposes conditions that are necessary for consciousness but that are not entirely sufficient (Nathan and Barbosa, 2011). The IIT claims that all of its axioms are self-evident (Kung et al., 2019). Since the IIT is not a functionalist theory of consciousness, criticisms of non-functionalism have been levied against it (Kung et al., 2019), and the limits of the IIT's definition of consciousness have led to criticism (Nathan and Barbosa, 2011; Kung et al., 2019).

Quantum Theory

It is well known that consciousness is inextricably linked to anesthesia. Hameroff et al. (2002) have conducted many complementary and engaging studies to refine their quantum theory of consciousness. Moreover, a series of mechanics of anesthetic agent function were proposed and included the following: (1) selective binding in hydrophobic pockets comprising non-polar amino acid groups in brain proteins [e.g., microtubule-associated proteins (MAPs); tubulin; and van der Waals (London dispersion) forces, which can inhibit the quantum process by impairing electron mobility]; (2) a specialized combination with "qubits," fundamental information units that abide by quantum events that induce disruption of the quantum computation; (3) a concept of "quantum channels" that consist of tryptophan tings in tubulin that are olive-like, non-polar, and hydrophobic; (4) probability for π-electron resonant energy transfer through quantum channels and weakening of anesthetic agents that could therefore weaken this π-resonance energy transfer (a theorem that accounts for loss of consciousness); and (5) alterations of collective terahertz dipole oscillations in tubulins (Hameroff, 1998, 2006; Hameroff et al., 2002; Craddock et al., 2015, 2017; Mayner et al., 2018). The systematic theory of "Orch OR" proposed that consciousness is constituted by discrete events that correspond with varying oscillation frequencies of distinct brain regions (Crick and Koch, 2003; Hameroff and Penrose, 2014; Li et al., 2018), which is similar with respect to the "snapshots," which is one of the ten frameworks for consciousness proposed by Koch (Li et al., 2018). In addition, an "integrate-and-fire" brain neuronal model and three time-steps of a microtubule automaton have emerged from the above studies that embody specific processing in neuronal microtubules when consciousness has occurred. It seems increasingly feasible to explain consciousness on the basis of quantum mechanics because Li et al. (2018) demonstrated that an isotope of the anesthetic xenon (129Xe) displayed half the quantum property of nuclear spin and was conspicuously less potent than xenon isotopes lacking spin, despite no observed differences in terms of chemical reactions (Craddock et al., 2015, 2017).

Since the enigmatic riddle of consciousness is so intractable, we need additional theorems and hypotheses to be generated with the intent of increasing the level of attention. Perhaps this quantum theory will fade with elapsing time and gradually lose its "charm;" however, it is also possible to disperse the fog of our ignorance and shed light on a new level of comprehending consciousness and adopt a system of "wait and see."

HYPOTHESES: FUNDAMENTAL HUGE NEURAL NETWORK OF CONSCIOUSNESS

From the above literature, we have identified three key areas associated with the generation of consciousness, including the

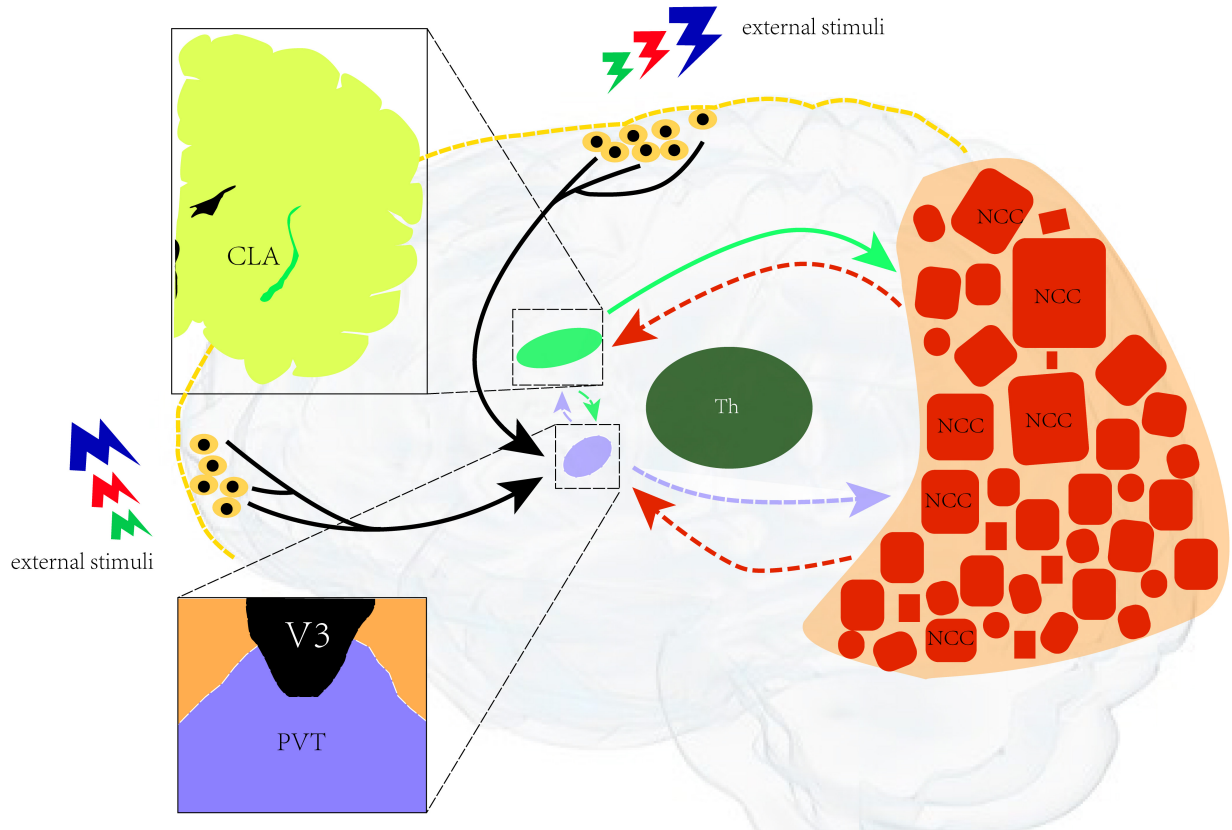

FIGURE 2 | Illustration of the neural network for consciousness. A neural network of consciousness. The paraventricular nucleus is in control of arousal (closely related to the maintenance of consciousness) and the neurons in the posterior cerebral cortex. It is related to the integration of feelings and the generation of consciousness content. The claustrum is the key channel of the consciousness loop and the transmission of control information. CLA, claustrum; PVT, paraventricular; Th, thalamus; NCC, neural correlates of consciousness; V3, third ventricular.

PVT (Groenewegen and Berendse, 1994; Van der Werf et al., 2002; Ishibashi et al., 2005; Nascimento et al., 2008; Ohno and Sakurai, 2008; Kirouac, 2015), the claustrum (Gattass et al., 2014; Koubeissi et al., 2014; Chau et al., 2015; Goll et al., 2015; Milardi et al., 2015; Torgerson et al., 2015; Dehaene et al., 2017; Kitanishi and Matsuo, 2017; White and Mathur, 2018; White et al., 2018), and the posterior cortex (the occipital and temporal lobe) (Rowland and Mettler, 1949; Stephan et al., 2003; Merker, 2007; Bianchi and Sims, 2008; Koch et al., 2016; Boly et al., 2017). Recent experimental studies have confirmed that the PVT plays a key role in animal arousal and that the animal's arousal state can be regulated by the PVT (Hameroff, 2012; Kirouac, 2015). In patients with epilepsy, the state of consciousness can be reversed by stimulating the claustrum. Stimulation of the claustrum can cause loss of consciousness and stop epilepsy (Koubeissi et al., 2014). In addition, modern neuroscience research has suggested that consciousness includes both awakening and consciousness content. The generation of consciousness is from the awakening to the transformation of the content of consciousness (Tononi and Koch, 2015). Any problem that is associated with any one of the links could lead to the decline of the level of consciousness or even coma. The generation of consciousness depends on a neurobiological basis. The neural mechanism that produces the least consciousness is called the related neuron of consciousness (NCC) (Crick and Koch, 2005; Cerullo, 2015; Tononi and Koch, 2015; Reddy and Pereira, 2017; Xie et al., 2017), which was first proposed by Crick and Koch (1990). The study of the NCC is a key step toward research of consciousness. The NCC are distributed in all parts of the brain (Koch et al., 2016; Boly et al., 2017) and rely on neural networks or loops to function with each other.

Based on recent research, we hypothesize that there is a neural network of consciousness in which the paraventricular nucleus formally serves as the control nucleus of arousal, which is closely related to the maintenance of consciousness, and the neurons in the posterior cerebral cortex. It is related to the integration of feelings and the generation of consciousness content. Besides, the claustrum also represents the key channel of the consciousness loop and the transmission of control information (**Figure 2**).

CONCLUSION

At present, consciousness is a very vague concept that lacks a specific and accurate definition. It is now widely accepted that

there are two categories of consciousness: (1) content-related consciousness (i.e., the local state) and (2) the awakening state (i.e., the global state) (Crick and Koch, 2003, 2005; Tononi, 2012; Tononi and Koch, 2015). Although we need to establish a definition of consciousness, we should not be confined by the lack of definition. The cortex of each part of the brain plays an important role in the production of consciousness, especially the prefrontal and posterior occipital cortices and the claustrum. From this review, we are more inclined to believe that consciousness does not originate from a single brain section; instead, we believe that it originates globally.

The exploration of the intrinsic neurobiological mechanism of consciousness is of great significance. According to the latest research on consciousness, the paraventricular nucleus plays an important role in awakening, and the claustrum may represent the nucleus that controls information transmission and regulates the generation of consciousness. The aspects involved in consciousness include the level of consciousness and also the content of consciousness. In the past, consciousness was thought to emanate from the frontal hemispheres of the brain, but current research has found that the content of consciousness mainly originates from the hindbrain. According to the GW theory and the IIT, awareness research requires a large neural network. In order to understand the neurobiological mechanisms of consciousness, the generation of consciousness needs to link all of the critical nucleus functions and the cerebral cortex of the essential brain parts. Consciousness is not split, but instead the overall effects of consciousness are critical.

AUTHOR CONTRIBUTIONS

TZ wrote the manuscript. YZ revised the manuscript. HT proposed the idea for the manuscript. RX created the figures. JZ was responsible for checking the manuscript. JHZ was responsible for checking the whole manuscript as well.

FUNDING

This study was funded by grants (2018YFA0107900, 31771491, and 2019CXJQ01) from the Ministry of Science and Technology of China, the National Natural Science Foundation of China, and Shanghai Municipal Government.

REFERENCES

Baars, B. J. (2005). Global workspace theory of consciousness: toward a cognitive neuroscience of human experience. *Prog. Brain Res.* 150, 45–53. doi: 10.1016/s0079-6123(05)50004-9

Baricich, A., de Sire, A., Antoniono, E., Gozzerino, F., Lamberti, G., and Cisari, C. (2017). Recovery from vegetative state of patients with a severe brain injury: a 4-year real-practice prospective cohort study. *Funct. Neurol.* 32, 131–136.

Bayne, T., Hohwy, J., and Owen, A. M. (2016). Are there levels of consciousness? *Trends Cogn. Sci.* 20, 405–413. doi: 10.1016/j.tics/2016.03.009

Bianchi, M. T., and Sims, J. R. (2008). Restricted diffusion in the splenium of the corpus callosum after cardiac arrest. *Open Neuroimage J.* 2, 1–4. doi: 10.2174/1874440000802010001

Boly, M., Massimini, M., Tsuchiya, N., Postle, B. R., Koch, C., and Tononi, G. (2017). Are the neural correlates of consciousness in the front or in the back of the cerebral cortex? clinical and neuroimaging evidence. *J. Neurosci.* 37, 9603–9613. doi: 10.1523/JNEUROSCIE.3218-16.2017

Cerullo, M. A. (2015). The problem with phi: a critique of integrated information theory. *PLoS Comput. Biol.* 11:e1004286. doi: 10.1371/journal/pcbi.1004286

Chau, A., Salazar, A. M., Krueger, F., Cristofori, I., and Grafman, J. (2015). The effect of claustrum lesions on human consciousness and recovery of function. *Cons. Cogn.* 36, 256–264. doi: 10.1016/j.concog.2015.06.017

Craddock, T. J., Hameroff, S. R., Ayoub, A. T., Klobukowski, M., and Tuszynski, J. A. (2015). Anesthetics act in quantum channels in brain microtubules to prevent consciousness. *Curr. Top. Med. Chem.* 15, 523–533. doi: 10.2174/1568026615666150225104543

Craddock, T. J. A., Kurian, P., Preto, J., Sahu, K., Hameroff, S. R., Klobukowski, M., et al. (2017). Anesthetic alterations of collective terahertz oscillations in tubulin correlate with clinical potency: implications for anesthetic action and post-operative cognitive dysfunction. *Sci. Rep.* 7:9877. doi: 10.1038/s41598-017-09992-7

Crick, F., and Koch, C. (1990). Towards a neurobiological theory of consciousness. *Semin. Neurosci.* 2, 263–275.

Crick, F., and Koch, C. (2003). A framework for consciousness. *Nat. Neurosci.* 6, 119–126.

Crick, F. C., and Koch, C. (2005). What is the function of the claustrum? *Philos. Trans. R. Soc. Lond. B Biol. Sci.* 360, 1271–1279. doi: 10.1098/rstb.2005.1661

Dehaene, S., Kerszberg, M., and Changeux, J. P. (1998). A neuronal model of a global workspace in effortful cognitive tasks. *Proc. Natl. Acad. Sci. U.S.A.* 95, 14529–14534. doi: 10.1073/pnas.95.24.14529

Dehaene, S., Lau, H., and Kouider, S. (2017). What is consciousness, and could machines have it? *Science* 358, 486–492. doi: 10.1126/science.aan8871

Englo, D. J., D'Haese, P. F., Konrad, P. E., Jacobs, M. L., Gore, J. C., Abou-Khalil, B. W., et al. (2017). Functional connectivity disturbances of the ascending reticular activating system in temporal lobe epilepsy. *J. Neurol. Neurosurg. Psychiatry* 88, 925–932. doi: 10.1136/jnnp-2017-315732

Fazekas, P., and Overgaard, M. (2016). Multidimensional models of degrees and levels of consciousness. *Trends Cogn. Sci* .20, 715–716. doi: 10.1016/j.tics.2016.06.011

Gattass, R., Soares, J. G., Desimone, R., and Ungerleider, L. G. (2014). Connectional subdivision of the claustrum: two visuotopic subdivisions in the macaque. *Front. Syst. Neurosci.* 8:63. doi: 10.3389/fnsys.2014.00063

Goll, Y., Atlan, G., and Citri, A. (2015). Attention: the claustrum. *Trends Neurosci.* 38, 486–495. doi: 10.1016/j.tins.2015.006

Groenewegen, H. J., and Berendse, H. W. (1994). The specificity of the 'nonspecific' midline and intralaminar thalamic nuclei. *Trends Neurosci.* 17, 52–57. . doi: 10.1016/0166-2236(94)90074-4

Hameroff, S. (1998). Anesthesia, consciousness and hydrophobic pockets – a unitary quantum hypothesis of anesthetic action. *Toxicol. Lett.* 100-101, 31–39. doi: 10.1016/s0378-4274(98)00162-3

Hameroff, S. (2012). How quantum brain biology can rescue conscious free will. *Front. Integr. Neurosci.* 6:93. doi: 10.3389/fnint.2012.00093

Hameroff, S., Nip, A., Porter, M., and Tuszynski, J. (2002). Conduction pathways in microtubules, biological quantum computation, and consciousness. *Biosystems* 64, 149–168. doi: 10.1016/s0303-2647(01)00183-6

Hameroff, S., and Penrose, R. (2014). Consciousness in the universe: a review of the 'Orch OR' theory. *Phys. Life Rev.* 11, 39–78. doi: 10.1016/j.plrev.2013.08.002

Hameroff, S. R. (2006). The entwined mysteries of anesthesia and consciousness: is there a common underlying mechanism? *Anesthesiology* 105, 400–412. . doi: 10.1097/00000542-200608000-00024

Harris, K. D., and Shepherd, G. M. (2015). The neocortical circuit: themes and variations. *Nat. Neurosci.* 18, 170–181. doi: 10.1038/nn.3917

Ishibashi, M., Takano, S., Yanagida, H., Takatsuna, M., Nakajima, K., and Oomura, Y. (2005). Effects of orexins/hypocretins on neuronal activity in the paraventricular nucleus of the thalamus in rats in vitro. *Peptides* 26, 471–481. doi: 10.1016/j.peptides.2004.10.014

Jang, S. H., and Lee, H. D. (2015). Ascending reticular activating system recovery in a patient with brain injury. *Neurology* 84, 997–999.

Jones, B. E. (2003). Arousal systems. *Front. Biosci.* 8, s438–s451.
Kirouac, G. J. (2015). Placing the paraventricular nucleus of the thalamus within the brain circuits that control behavior. *Neurosci. Biobehav. Rev.* 56, 315–329. doi: 10.1016/j.neubiorev.2015.08.005
Kitanishi, T., and Matsuo, N. (2017). Organization of the claustrum-to-entorhinal cortical connection in mice. *J. Neurosci.* 37, 269–280. doi: 10.1523/JNEUROSCI.1360-16.2016
Koch, C., Massimini, M., Boly, M., and Tononi, G. (2016). Neural correlates of consciousness: progress and problems. *Nat. Rev. Neurosci.* 17, 307–321. doi: 10.1038/nrn.2016.22
Koubeissi, M. Z., Bartolomei, F., Beltagy, A., and Picard, F. (2014). Electrical stimulation of a small brain area reversibly disrupts consciousness. *Epilepsy Behav.* 37, 32–35. doi: 10.1016/j.yebah.2014.05.027
Krashes, M. J., Shah, B. P., Madara, J. C., Olson, D. P., Strochlic, D. E., Garfield, A. S., et al. (2014). An excitatory paraventricular nucleus to AgRP neuron circuit that drives hunger. *Nature* 507, 238–242. doi: 10.1038/nature12956
Kung, Y. C., Li, C. W., Chen, S., Chen, S. C., Lo, C. Z., Lane, T. J., et al. (2019). Instability of brain connectivity during nonrapid eye movement sleep reflects altered properties of information integration. *Hum. Brain Mapp.* doi: 10.1002/hbm.24590 [Epub ahead of print].
LeDoux, J. E., and Brown, R. (2017). A higher-order theory of emotional consciousness. *Proc. Natl. Acad. Sci. U.S.A.* 114, E2016–E2025. doi: 10.1073/pnas.1619316114
Li, N., Lu, D., Yang, L., Tao, H., Xu, Y., Wang, C., et al. (2018). Nuclear spin attenuates the anesthetic potency of xenon isotopes in mice: implications for the mechanisms of anesthesia and consciousness. *Anesthesiology* 129, 271–277. doi: 10.1097/ALN.0000000000002226
Maejima, Y., Takahashi, S., Takasu, K., Takenoshita, S., Ueta, Y., and Shimomura, K. (2017). Orexin action on oxytocin neurons in the paraventricular nucleus of the hypothalamus. *Neuroreport* 28, 360–366. doi: 10.1097/WNR.0000000000000773
Mayner, W. G. P., Marshall, W., Albantakis, L., Findlay, G., Marchman, R., and Tononi, G. (2018). PyPhi: A toolbox for integrated information theory. *PLoS Comput. Bio.* 14:e1006343. doi: 10.1371/journal.pcbi.1006343
Merker, B. (2007). Consciousness without a cerebral cortex: a challenge for neuroscience and medicine. *Behav. Brain Sci.* 30, 63–81. doi: 10.1017/s0140525x07000891
Milardi, D., Bramanti, P., Milazzo, C., Finocchio, G., Arrigo, A., Santoro, G., et al. (2015). Cortical and subcortical connections of the human claustrum revealed in vivo by constrained spherical deconvolution tractography. *Cereb. Cortex* 25, 406–414. doi: 10.1093/cercor/bht231
Millan, E. Z., Ong, Z., and McNally, G. P. (2017). Paraventricular thalamus: gateway to feeding, appetitive motivation, and drug addiction. *Prog. Brain Res.* 235, 113–137. doi: 10.1016/bs.pbr.2017.07.006
Nascimento, E. S. Jr., Duarte, R. B., Silva, S. F., Engelberth, R. C., Toledo, C. A., and Cavalcante, J. S. (2008). Retinal projections to the thalamic paraventricular nucleus in the rock cavy (Kerodon rupestris). *Brain Res.* 1241, 56–61. doi: 10.1016/j.brainres.2008.09.017
Nathan, A., and Barbosa, V. C. (2011). Network algorithmics and the emergence of information integration in cortical models. *Phys. Rev. E* 84:011904. doi: 10.1103/PhusRevE.84.011904
Northoff, G., and Huang, Z. (2017). How do the brain's time and space mediate consciousness and its different dimensions? temporo-spatial theory of consciousness (TTC). *Neurosci. Biobehav. Rev.* 80, 630–645. doi: 10.1016/j.neubiorev.2017.07.013
Ohno, K., and Sakurai, T. (2008). Orexin neuronal circuitry: role in the regulation of sleep and wakefulness. *Front. Neuroendocrinol.* 29, 70–87. doi: 10.1016/j.yfrne.2007.08.001
Oizumi, M., Albantakis, L., and Tononi, G. (2014). From the phenomenology to the mechanisms of consciousness: integrated information theory 3.0. *PLoS Comput. Biol.* 10:e1003588. doi: 10.1371/journa.pcvi.1003588
Qin, C., Li, J., and Tang, K. (2018). The paraventricular nucleus of the hypothalamus: development, function, and human diseases. *Endocrinology* 159, 3458–3472. doi: 10.1210/en.2018-00453
Reddy, J. S. K., and Pereira, C. (2017). Understanding the emergence of microbial consciousness: from a perspective of the subject-object model (SOM). *J. Integr. Neurosci.* 16, S27–S36. doi: 10.3233/JIN-170064
Ren, S., Wang, Y., Yue, F., Cheng, X., Dang, R., Qiao, Q., et al. (2018). The paraventricular thalamus is a critical thalamic area for wakefulness. *Science* 362, 429–434. doi: 10.1126/science.aat2512
Rowland, L. P., and Mettler, F. A. (1949). Cell concentration and laminar thickness in the frontal cortex of psychotic patients; studies on cortes removed at operation. *J. Comp. Neurol.* 90, 255–280. doi: 10.1002/cne.900900302
Seth, A. K. (2018). Consciousness: The last 50 years (and the next). *Brain Neurosci. Adv.* 2, 1–6.
Smith, J. B., Liang, Z., Watson, G. D. R., Alloway, D. K., and Zhang, N. (2017). Interhemispheric resting-state functional connectivity of the claustrum in the awake and anesthetized states. *Brain Struct. Funct.* 222, 2041–2058. doi: 10.1007/s00429-016-1323-9
Stephan, K. E., Marshall, J. C., Friston, K. J., Rowe, J. B., Ritzl, A., Zilles, K., et al. (2003). Lateralized cognitive processes and lateralized task control in the human brain. *Science* 301, 384–386. doi: 10.1126/science.1086025
Thagard, P., and Stewart, T. C. (2014). Two theories of consciousness: semantic pointer competition vs. information integration. *Cons. Cogn.* 30, 73–90. doi: 10.1016/j.concog.2014.07.001
Tononi, G. (2004). An information integration theory of consciousness. *BMC Neurosci.* 5:42.
Tononi, G. (2012). The integrated information theory of consciousness: an updated account. *Arch. Ital. Biol.* 150, 293–329.
Tononi, G., Boly, M., Massimini, M., and Koch, C. (2016). Integrated information theory: from consciousness to its physical substrate. *Nat. Rev. Neurosci.* 17, 450–461. doi: 10.1038/nrn.2016.44
Tononi, G., and Koch, C. (2015). Consciousness: here, there and everywhere? *Philos. Trans. R. Soc. Lond. B Biol. Sci.* 370:20140167. doi: 10.1098/rstb.2014.0167
Torgerson, C. M., Irimia, A., Goh, S. Y., and Van Horn, J. D. (2015). The DTI connectivity of the human claustrum. *Hum. Brain Mapp.* 36, 827–838. doi: 10.1002/hbm.22667
Tsuchiya, N., Taguchi, S., and Saigo, H. (2016). Using category theory to assess the relationship between consciousness and integrated information theory. *Neurosci. Res.* 107, 1–7. doi: 10.1016/j.neures.2015.12.007
Van der Werf, Y. D., Witter, M. P., and Groenewegen, H. J. (2002). The intralaminar and midline nuclei of the thalamus. Anatomical and functional evidence for participation in processes of arousal and awareness. *Brain Res. Brain Res. Rev.* 39, 107–140. doi: 10.1016/s0165-0173(02)00181-9
van Erp, W. S., Lavrijsen, J. C., Vos, P. E., Bor, H., Laureys, S., and Koopmans, R. T. (2015). The vegetative state: prevalence, misdiagnosis, and treatment limitations. *J. Am. Med. Dir. Assoc.* 16, 85.e9–85.e14. doi: 10.1016/j.jamda.2014.10.014
White, M. G., and Mathur, B. N. (2018). Frontal cortical control of posterior sensory and association cortices through the claustrum. *Brain Struct. Funct.* 223, 2999–3006. doi: 10.1007/s00429-081-1661
White, M. G., Panicker, M., Mu, C., Carter, A. M., Roberts, B. M., Dharmasri, P. A., et al. (2018). Anterior cingulate cortex input to the claustrum is required for top-down action control. *Cell Rep.* 22, 84–95. doi: 10.1016/j.celrep.2017.12.023
Xie, F., Xing, W., Wang, X., Liao, W., and Shi, W. (2017). Altered states of consciousness in epilepsy: a DTI study of the brain. *Int. J. Neurosci.* 127, 667–672. doi: 10.1080/00207454.2016.1229668
Zeman, A. (2006). What do we mean by "conscious" and "aware"? *Neuropsychol. Rehabil.* 16, 356–376. doi: 10.1080/09602010500484581
Zingg, B., Hintiryan, H., Gou, L., Song, M. Y., Bay, M., Bienkowski, M. S., et al. (2014). Neural networks of the mouse neocortex. *Cell* 156, 1096–1111. doi: 10.1016/j.cell.2014.02.023

Conflict of Interest Statement: The authors declare that the research was conducted in the absence of any commercial or financial relationships that could be construed as a potential conflict of interest.

frontiers in Cellular Neuroscience

SYSTEMATIC REVIEW
published: 24 October 2019
doi: 10.3389/fncel.2019.00469

Age-Related Changes in the Plasticity of Neural Networks Assessed by Transcranial Magnetic Stimulation With Electromyography: A Systematic Review and Meta-Analysis

Xiaorong Tang[1†], Peidong Huang[2†], Yitong Li[1], Juanchao Lan[1], Zhonghua Yang[1], Mindong Xu[1], Wei Yi[1], Liming Lu[3], Lin Wang[3*] and Nenggui Xu[1*]*

[1] Medical College of Acu-Moxi and Rehabilitation, Guangzhou University of Chinese Medicine, Guangzhou, China, [2] Acupuncture and Massage Rehabilitation Institute, Yunnan University of Chinese Medicine, Kunming, China, [3] Clinical Research Center, South China Research Center for Acupuncture and Moxibustion, Medical College of Acu-Moxi and Rehabilitation, Guangzhou University of Chinese Medicine, Guangzhou, China

Objective: The excitability of cerebral cortical cells, neural pathway, and neural networks, as well as their plasticity, are key to our exploration of age-related changes in brain structure and function. The combination of transcranial magnetic stimulation (TMS) with electromyography (EMG) can be applied to the primary motor cortex; it activates the underlying neural group and passes through the corticospinal pathway, which can be quantified using EMG. This meta-analysis aimed to analyze changes in cortical excitability and plasticity in healthy elderly individuals vs. young individuals through TMS-EMG.

Methods: The Cochrane Library, Medline, and EMBASE databases were searched to identify eligible trials published from database inception to June 3, 2019. The Cochrane Risk of Bias Tool and improved Jadad scale were used to assess the methodological quality. A meta-analysis of the comparative effects was conducted using the Review Manager 5.3 software and Stata 14.0 software.

Results: The pooled results revealed that the resting motor threshold values in the elderly group were markedly higher than those reported in the young group (mean difference [MD]: −2.35; 95% confidence interval [CI]: −3.69 to −1.02]; $p <$ (0.00001). The motor evoked potential amplitude significantly reduced in the elderly group vs. the young group (MD: 0.18; 95% CI: 0.09–0.27; $p < 0.0001$). Moreover, there was significantly longer motor evoked potential latency in the elderly group (MD: −1.07; 95% CI: −1.77 to −0.37]; $p =$(0.003). There was no significant difference observed in the active motor threshold between the elderly and young groups (MD: −1.52; 95% CI: −3.47 to −0.42]; $p =$(0.13). Meanwhile, only two studies reported the absence of adverse events.

OPEN ACCESS

Edited by:
Zhang Pengyue,
Yunnan University of Chinese Medicine, China

Reviewed by:
Sulukkana Noiprasert,
Mae Fah Luang University, Thailand
Hong Xu,
University of Pennsylvania, United States

***Correspondence:**
Nenggui Xu
Ngxu8018@gzucm.edu.cn
Lin Wang
Wanglin16@gzucm.edu.cn
Liming Lu
Lulimingleon@126.com

[†] These authors have contributed equally to this work as co-first authors

Specialty section:
This article was submitted to Cellular Neurophysiology, a section of the journal Frontiers in Cellular Neuroscience

Received: *19 July 2019*
Accepted: *01 October 2019*
Published: *24 October 2019*

Citation:
Tang X, Huang P, Li Y, Lan J, Yang Z, Xu M, Yi W, Lu L, Wang L and Xu N (2019) Age-Related Changes in the Plasticity of Neural Networks Assessed by Transcranial Magnetic Stimulation With Electromyography: A Systematic Review and Meta-Analysis. Front. Cell. Neurosci. 13:469. doi: 10.3389/fncel.2019.00469

Conclusion: We found that the excitability of the cerebral cortex declined in elderly individuals vs. young individuals. The findings of the present analysis should be considered with caution owing to the methodological limitations in the included trials. Additional high-quality studies are warranted to validate our findings.

Keywords: plasticity of neural networks, age-related, transcranial magnetic stimulation, resting motor threshold, meta-analysis

INTRODUCTION

As the birth rate decreases and life expectancy increases, the aging problem of the global population becomes more prominent (Tatti et al., 2016). One of the most striking features of human motor behavior is the ability to respond rapidly and appropriately to environmental changes. However, this ability gradually declines with age. In particular, the decline in cognitive and motor abilities is associated with advancing age (Hunter et al., 2001). This age-related decline is a precursor of various diseases. An enhanced understanding of the impact of aging on cortical functioning may provide us more insight into understanding of age-related diseases (Seidler et al., 2010).

The human motor cortex is capable of undergoing persistent morphological or functional changes depending on stimuli from the environment; this is termed neuroplasticity (Boroojerdi et al., 2001). Cortical plasticity decreases with extensive changes in neurochemistry and neurophysiology during physiological aging (Brunso-Bechtold et al., 2000; Rossini et al., 2007). Although the regulatory mechanisms of related brain neurons are unclear, an increasing body of evidence suggests that aging is associated with alterations in the neural projections. Normal aging is associated with impairments in dendritic morphology, loss of synaptic contact cellular connectivity, and gene expression, which subsequently cause a relative decrease in the excitability of the cortex (Godde et al., 2002; Sawaki et al., 2003; Burke and Barnes, 2006; Hortobágyi et al., 2006; Oliviero et al., 2006). This eventually leads to a decrease in sensation, motor performance, and cognitive function (Mora et al., 2007; Ward et al., 2008).

Several studies showed that the decline in cognitive, memory, and behavioral abilities in healthy elderly individuals are closely related to vascular damage and amyloid deposition (DeCarli et al., 2012). Further research indicated that ischemia and amyloid deposition are connected through the utilitarian bunch of cerebrovascular cells, supporting glial tissue and neurons. Moreover, as a potential mediator of reactive aging, amyloid deposition may lead to changes in neural networks and circuits (Iadecola, 2010). In this way, the interaction of blood vessels and neurodegenerative injuries may influence the cortical and subcortical neural systems. Importantly, this damage may alter the local field potentials. In other words, we can assess age-related cognitive decline by measuring changes in the local field potentials. Recently, neuroscience research has explored the opportunity to apply Non-Invasive Brain Stimulation technology, which measures changes in the local field potentials of the cerebral cortex, to healthy elderly populations. This approach aims to explore aging-related mechanisms and the changes of cerebral cortex under physiological conditions.

The combination of transcranial magnetic stimulation with electromyography may provide information regarding the local and global potentials of the cerebral cortex, and may be used to measure changes in cortical properties following age-related changes in the plasticity of neural networks. A few studies have investigated age-related changes in the plasticity of neural networks among young and elderly individuals (Godde et al., 2002; Sawaki et al., 2003; Oliviero et al., 2006). Owing to the small sample sizes, device characteristics, parameter settings, and experimental procedures of these studies, the current excitability of the cerebral cortex at different ages remains inconclusive. We conducted a systematic review and meta-analysis of the available data to further examine this trend. Therefore, this meta-analysis aimed to analyze changes in cortical excitability and plasticity in healthy elderly individuals vs. young individuals through TMS-EMG.

METHODS

This study was performed according to the guidelines of the Preferred Reporting Items for Systematic Reviews and Meta-analysis checklist. The checklist and flowchart are shown in **Figure 1**, Appendix 1 in **Supplementary Material**.

Search Strategy

We searched the Cochrane Library, Medline, and EMBASE databases for eligible trials published from database inception to June 3, 2019 without language restriction. The search terms are shown in Appendix 2 **(Supplementary Material)**. In addition, we searched the websites of the international clinical trial registry provided by the U.S. National Institutes of Health to avoid missing unpublished studies. Furthermore, the references cited in the searched articles were also carefully reviewed. The search terms were listed in the Appendix 2 **(Supplementary Material)**.

Inclusion Criteria

(1) Patients: healthy individuals aged >18 years. (2) Interventions: all studies that used the TMS to detect

Abbreviations: AMT, active motor threshold; EMG, electromyography; APB, the abductor pollicis brevis muscle; ECR, the extensor carpi radialis muscle; FDI, the first dorsal interosseous muscle; FCR, the flexor carpi radialis muscle; FPB, the flexor pollicis brevis muscle; LTP, long-term potentiation; LTD, long-term depression; NIBS, Non-Invasive Brain Stimulation; PRISMA, Preferred Reporting Items for Systematic Reviews and Meta-analysis checklist; RMT, resting motor threshold; TMS, transcranial magnetic stimulation; TP, thenar and plantar muscle; TES, transcranial electrical stimulation; MEP, motor evoked potential.

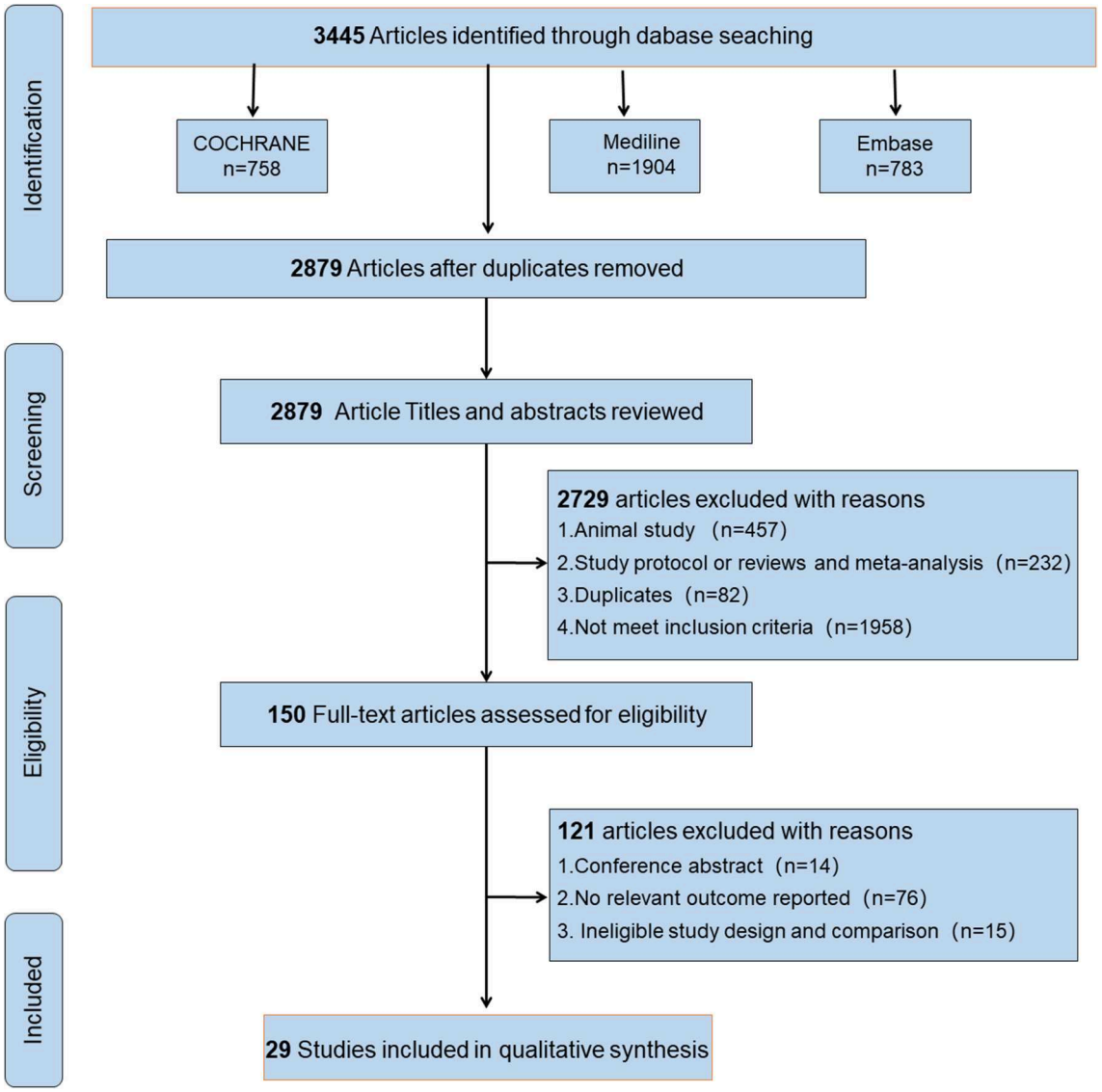

FIGURE 1 | Flow diagram of studies identified, included, and excluded.

brain cortical excitability and plasticity were included. (3) Comparison: healthy elderly (≥50 years) vs. healthy young (<50 years) individuals. (4) Outcomes: primary outcome measures included resting motor threshold (RMT); secondary outcome measures included any of the following: (a) motor evoked potentials (MEPs) amplitude or latency, (b) active motor threshold (AMT), and (c) adverse events. (5) Trial design: cohort or case-control studies.

Exclusion Criteria

(1) Patients with a history of neurological or psychiatric disease, or currently receiving treatment with psychoactive drugs (i.e., sedatives, antipsychotics, antidepressants, etc.). (2) Studies with insufficient data or irrelevant outcomes.

Study Selection and Data Extraction

All potentially eligible studies were independently selected by two reviewers (JL and YL) based on the titles and abstracts. The full text of the selected articles was subsequently obtained and independently reviewed by the reviewers based on the inclusion and exclusion criteria. The following information was independently extracted from the included trials by these two reviewers: title and authors, year of publication, sample size, age and sex of participants, target muscle and hemisphere for TMS, and outcomes (i.e., outcome measures and adverse events). Any disagreements were resolved through discussion with the third reviewer (WY) or further evaluation. The original investigators of studies with missing or incomplete data were contacted to request the data.

Assessment of Risk of Bias (ROB)

The ROB tool of Cochrane (Savović et al., 2014) was used to assess the methodological quality. In addition, the quality of the study was evaluated using the improved Jadad scale. The full score is 7 points, and the threshold for high-quality research is ≥4 points. Two reviewers (JL and YL) independently judged the quality; any disagreements were resolved through discussion with the third reviewer (WY) acting as an arbiter. Moreover, we completed the Standards for Reporting Interventions in Controlled Trials checklist to assess the risk of bias.

Statistical Analysis

The RevMan software (version 5.3; Cochrane Collaboration, Oxford, UK) and Stata software (version 12.0; Stata Corp LP, College Station, TX, USA) were used for statistical analysis. Dichotomous outcomes were expressed with the odds ratio and 95% confidence intervals (CI), while continuous outcomes were expressed with the mean difference (MD, indicators changed from baseline) with 95% CI. Cochran's Q test and I^2 statistic were used to assess the homogeneity; the I^2 test was performed for further analysis. A random-effects model was used to calculate the pooled effect size for the presence of significant heterogeneity ($p \leq 0.1$, $I^2 \geq 50\%$), and a fixed-effects model was applied for the absence of significant heterogeneity (Higgins et al., 2003). We explored the possible sources of heterogeneity through a subgroup analysis, and repeated the sensitivity analysis to study its effect on the overall effect size. A $p \leq 0.05$ denoted statistically significant difference.

RESULTS

Study Selection

We initially retrieved 3,445 publications, and 566 duplicate citations were removed. After screening the abstracts and titles, a total of 2,729 publications were excluded. A total of 121 publications from the 150 publications further identified as potentially eligible trials according to the review of the full text were excluded for the following reasons: 14 were conference abstracts, 76 did not report a relevant outcome, and 15 had ineligible study design and comparison. We did not identify any other studies for evaluation after reviewing the bibliographies of the full-text articles collected during the initial search. Finally, 29 studies (Rossini et al., 1992; Kossev et al., 2002; Sale and Semmler, 2005; Hortobágyi et al., 2006; Fujiyama et al., 2009, 2011, 2012, 2014; Pellicciari et al., 2009; Rogasch et al., 2009; Smith et al., 2009, 2011; Cirillo et al., 2010, 2011; Fathi et al., 2010; Todd et al., 2010; Degardin et al., 2011; Levin et al., 2011; Bernard and Seidler, 2012; Young-Bernier et al., 2012, 2014; Cuypers et al., 2013; Bashir et al., 2014; Opie and Semmler, 2014; Dickins et al., 2015, 2017; Opie et al., 2017, 2018; Emonson et al., 2019) fulfilled our inclusion criteria and were selected. **Figure 1** depicts the search process and trial selection.

Description of Included Studies

The studies included in the analysis involved a total of 914 participants. The age ranged 18–84 years. The brain cortical excitability and plasticity were examined by TMS-EMG in these studies. The muscles which evoked motor potentials in these studies included the first dorsal interosseous muscle, the abductor pollicis brevis muscle, the extensor carpi radialis muscle, the flexor carpi radialis muscle, the flexor pollicis brevis muscle, and the thenar and plantar muscles. The outcomes used to assess cortical excitability and plasticity included RMT, AMT, MEP amplitude, and MEP latency. The detailed characteristics are shown in **Table 1**.

Methodological Quality of Included Studies

Randomization was not used in the 29 selected studies, and none of the studies described concealment of allocation. Nine studies (Fathi et al., 2010; Todd et al., 2010; Fujiyama et al., 2011, 2014; Young-Bernier et al., 2012, 2014; Opie and Semmler, 2014; Dickins et al., 2015, 2017) used appropriate blinding methods for the participants, and nine studies (Fathi et al., 2010; Cirillo et al., 2011; Fujiyama et al., 2012, 2014; Opie and Semmler, 2014; Dickins et al., 2017; Opie et al., 2017, 2018; Emonson et al., 2019) blinded the outcome assessments. All studies reported complete outcome data. Overall, the methodological quality all the included studies was low. The details are listed in the Appendix 3 **(Supplementary Material)**. The summary of bias in each domain across the included studies is shown in **Figures 2**, **3**.

Primary Outcomes

A total of 28 studies (Rossini et al., 1992; Kossev et al., 2002; Sale and Semmler, 2005; Hortobágyi et al., 2006; Pellicciari et al., 2009; Rogasch et al., 2009; Smith et al., 2009, 2011; Cirillo et al., 2010, 2011; Fathi et al., 2010; Todd et al., 2010; Degardin et al., 2011; Fujiyama et al., 2011, 2012, 2014; Levin et al., 2011; Bernard and Seidler, 2012; Young-Bernier et al., 2012, 2014; Cuypers et al., 2013; Bashir et al., 2014; Opie and Semmler, 2014; Dickins et al., 2015, 2017; Opie et al., 2017, 2018; Emonson et al., 2019) assessed the changes in RMT between the elderly and young groups (**Figure 4**). Owing to the significant heterogeneity among the studies (I^2: 85%; $p < 0.00001$), we selected the random-effects model. The pooled results revealed that the RMT values in the elderly group were markedly higher than those observed in the young group (MD: −2.65; 95% CI: −3.97 to −1.33; $p = 0.008$).

Subgroup Analysis of Primary Outcomes

Owing to the high heterogeneity among the pooled results of RMT evaluation ($I^2 = 85\%$; $p < 0.00001$), we divided the studies according to the year of publication and region, and the varied stimulated muscles were examined through a subgroup analysis (**Table 2**, **Figure 4**, Appendices 4, 5 in **Supplementary Material**). The subgroup analysis showed that the muscle, region, or year of publication may be the sources of high heterogeneity.

Subgroup Analysis Based on Different Stimulated Muscles

The pooled results showed that the excitability of the cerebral cortex in the elderly group was significantly reduced compared with that reported in the young group. However, subgroup differences were detected, and when the stimulated muscle was the abductor pollicis brevis muscle (MD: −1.10; 95% CI:

TABLE 1 | Characteristics of trials included in this review.

References	Region	Participants (Y/O)	Age Y (years)	Age O (years)	Gender T (F/M)	Gender C (F/M)	Muscle	Hemisphere	Outcome indicator	Risk of bias
Rossini et al., 1992	Italy	25/40	25.3 ± 5.3	66.0 ± 10.4	15/10	26/14	TP	All	RMT\MEP Amplitude\MEP Latency	UUUULLU
Kossev et al., 2002	Germany	10/10	28.5 ± 5.2	56.1 ± 4.9	6/4	7/3	ECR	Left	RMT\MEP Amplitude\MEP Latency	UUUULHU
Sale and Semmler, 2005	Australia	10/10	26.6 ± 1.3	67.6 ± 2.3	5/5	5/5	FDI	Left	RMT\MEP Amplitude	UUUULLU
Hortobágyi et al., 2006	USA	6/6	27.2 ± 3.7	72.7 ± 6.3	4/2	5/1	FCR	Left	RMT\MEP Amplitude	UUUULLU
Rogasch et al., 2009	Australia	14/14	20.7 ± 1.9	68.3 ± 5.6	6/8	6/8	APB	Left	RMT\AMT\MEP Amplitude	UUUULLU
Pellicciari et al., 2009	Italy	16/16	26.2 ± 0.8	62.1 ± 1.5	8/8	8/8	APB	Left	RMT\MEP Latency	UUUULLU
Fujiyama et al., 2009	Australia	15/15	18–33	61–75	9/6	9/6	ECR	Left	MEP Amplitude	UUUULLU
Smith et al., 2009	Australia	13/17	20.0 ± 2.0	63.1 ± 4.2	0/13	0/17	FDI	Left	RMT\MEP Amplitude\AMT	UUUULLU
Fathi et al., 2010	Japan	16/16	21–39	60–79	2/14	5/11	APB	Left	RMT\MEP	UULLLLU
Cirillo et al., 2010	Australia	12/14	22 ± 2	67 ± 4	7/5	7/7	APB	Left	RMT\AMT\MEP Amplitude	UUUULLU
Todd et al., 2010	Australia	15/15	25 ± 4	67 ± 5	6/9	6/9	FDI	Left	RMT\MEP\AMT	UULULLU
Cirillo et al., 2011	Australia	16/16	23 ± 3	67 ± 5	9/7	9/7	FDI	Left	RMT\AMT\MEP Amplitude	UUULLLU
Degardin et al., 2011	France	14/14	26.4 ± 2.7	62.4 ± 7.1	6/8	8/6	APB	N/A	RMT\AMT	UUUULLU
Fujiyama et al., 2011	Australia	13/13	18–34	62–74	9/4	9/4	FPB	Left	RMT	UULULLU
Levin et al., 2011	Belgium	6/5	23.7 ± 2.3	63.8 ± 1.8	N/A	N/A	APB	Left	RMT\MEP Amplitude	UUUULLU
Smith et al., 2011	Australia	15/15	20.1 ± 2.1	65.5 ± 3.9	0/15	0/15	FDI	Left	RMT\AMT	UUUULLU
Bernard and Seidler, 2012	USA	16/17	21 ± 1.83	69.53 ± 4.07	12/4	10/7	FDI	Left	RMT\MEP Amplitude\MEP Latency	UUUULLU
Fujiyama et al., 2012	Australia	15/15	18–29	58–84	8/7	9/6	ECR	Left	RMT\MEP Amplitude	UUULLLU
Young-Bernier et al., 2012	Canada	25/31	22.5 ± 3.5	70.3 ± 3.8	14/11	18/13	FDI	Left	RMT\MEP Amplitude\MEP Latency	UULULLU
Cuypers et al., 2013	Belgium	14/10	22.8 ± 1.7	69.3 ± 2.8	8/6	8/2	FDI	Left	RMT\MEP Amplitude	UUUULLU
Bashir et al., 2014	USA	10/8	23.40 ± 3.50	57.38 ± 9.61	4/6	5/3	FDI	Left	RMT\MEP Amplitude	UUUULLU
Fujiyama et al., 2014	Australia	20/20	22.7 ± 3.3	68.3 ± 7.9	13/7	10/10	FCR	Left	RMT	UULLLLU
Opie and Semmler, 2014	Australia	22/18	22.3 ± 3.1	70.8 ± 5.0	N/A	N/A	FDI	N/A	RMT\AMT\MEP Amplitude	UULLLLU
Young-Bernier et al., 2014	Canada	20/18	22.3 ± 3.2	70.1 ± 5.6	13/7	9/9	FDI	N/A	RMT\MEP Amplitude\MEP Latency	UULULLU
Dickins et al., 2015	Australia	20/20	22.95 ± 2.52	70.15 ± 3.07	10/10	10/10	APB	N/A	RMT\MEP	UULULLU
Dickins et al., 2017	Australia	20/20	24.4 ± 3.86	69.55 ± 3.99	10/10	10/10	APB	N/A	RMT\MEP	UULLLLU
Opie et al., 2017	Australia	15/15	22.9 ± 0.5	70.8 ± 1.6	8/7	7/8	FDI	Left	RMT\MEP	UUULLLU
Opie et al., 2018	Australia	15/18	22.5 ± 2.9	70.1 ± 6.0	8/7	12/6	FDI	Left	RMT\MEP\AMT	UUULLLU
Emonson et al., 2019	Australia	20/20	24.5 ± 4.48	65.47 ± 5.62	N/A	N/A	N/A	N/A	RMT	UUULLLU

Y, young group; O, old group; F, female; M, male; N/A, not applicable; TP, thenar and plantar muscles; ECR, the extensor carpi radialis muscle; APB, the abductor pollicis brevis muscle; FDI, the first dorsal interosseous muscle; FCR, the flexor carpi radialis muscles; FPB, the flexor pollicis brevis muscle.

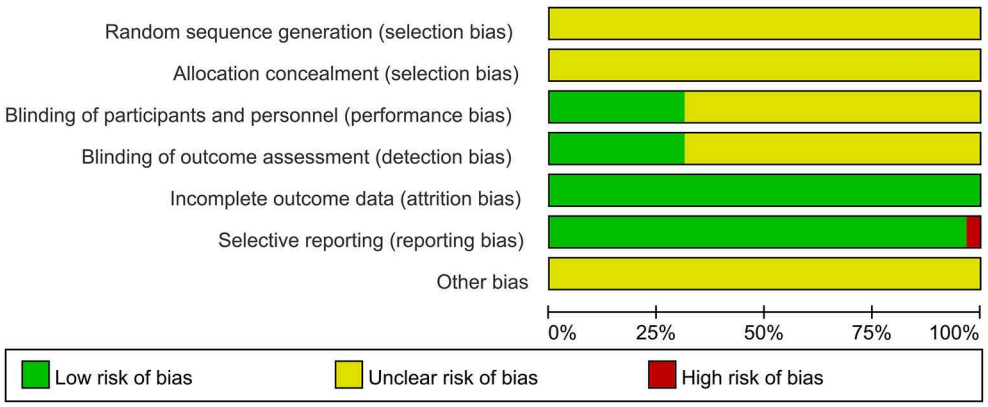

FIGURE 2 | Graph of the risk of bias in the included trials by Cochrane risk of bias toll based upon reviewers' judgment of each domain.

−4.54–2.33; $p = 0.53$), extensor carpi radialis (MD: −0.49; 95% CI: −2.79–1.80; $p = 0.67$), and flexor carpi radialis (MD: −0.72; 95% CI: −2.24–0.80; $p = 0.35$), there was no significant difference between two groups (**Figure 4**). This indicates that the measurement effects of different muscles vary. Therefore, different muscles may be representative of high heterogeneity.

Subgroup Analysis Based on Different Regions

We divided the regions of study into Oceania, Europe, Asia, and America. The results showed that the excitability of the cerebral cortex in the elderly group was significantly reduced compared with that recorded in the young group. However, one study in Asia showed a decrease in RMT in the control group (Appendix 4 in **Supplementary Material**). It is possible that the statistical power was inadequate due to the small number of studies performed in Asia.

Subgroup Analysis Based on the Year of Publication

We divided the studies according to the year of publication (i.e., in and prior to 2011, and after 2011). The results showed that the excitability of the cerebral cortex in the elderly group was markedly lower than that reported in the young group. However, we did not find significant differences in the two groups among the studies performed in and prior to 2011 (MD: −1.65; 95% CI: −3.97–0.68; $p = 0.17$) (Appendix 5 in **Supplementary Material**). This may be related to device characteristics (e.g., type of coil and accuracy of the EMG) or the level of operational proficiency.

Sensitivity Analysis

We excluded one study at a time to determine the effect of each study on the estimated pooled effect size. The results did not show instability (**Figure 5**).

Secondary Outcomes

MEP Amplitude

A total of 20 studies (Rossini et al., 1992; Sale and Semmler, 2005; Fujiyama et al., 2009, 2012; Rogasch et al., 2009; Smith et al., 2009; Cirillo et al., 2010, 2011; Fathi et al., 2010; Todd et al., 2010; Levin et al., 2011; Bernard and Seidler, 2012; Young-Bernier et al., 2012, 2014; Cuypers et al., 2013; Bashir et al., 2014; Dickins et al., 2015, 2017; Opie et al., 2017, 2018) providing numerical data for the MEP amplitude were included. Owing to the heterogeneity, a random-effects model was applied (I^2: 89%; $p < 0.00001$). The pooled data analysis showed that the MEP amplitude was markedly reduced in the elderly group vs. the young group (MD: 0.18; 95% CI: 0.09–0.27; $p < 0.00001$) (**Figure 6A**).

MEP Latency

Seven studies (Rossini et al., 1992; Kossev et al., 2002; Pellicciari et al., 2009; Todd et al., 2010; Bernard and Seidler, 2012; Young-Bernier et al., 2012, 2014) providing numerical data for the MEP latency were included. Owing to the heterogeneity, a random-effects model was used (I^2: 79%; $p < 0.00001$). The pooled results showed that there was a significantly longer MEP latency in the elderly group (MD: −1.07; 95% CI:−1.77 to −0.37; $p = 0.003$) (**Figure 6B**).

AMT

Nine studies (Rogasch et al., 2009; Smith et al., 2009, 2011; Cirillo et al., 2010, 2011; Todd et al., 2010; Degardin et al., 2011; Opie and Semmler, 2014; Opie et al., 2018) providing numerical data for the AMT were included. Owing to the heterogeneity, a random-effects model was used (I^2: 82%; $p < 0.00001$). There was no significant difference observed in the AMT between the two groups (MD: −1.52; 95% CI: −3.47 to −0.42; $p = 0.13$) (**Figure 6C**).

Adverse Outcomes

Only two (Hortobágyi et al., 2006; Opie et al., 2017) studies did not report adverse events related to TMS. The remaining studies did not report adverse outcomes.

Publication Bias

According to Egger's test, there was no evidence of publication bias among the primary outcome (RMT outcome, Egger's test $p = 0.257$).

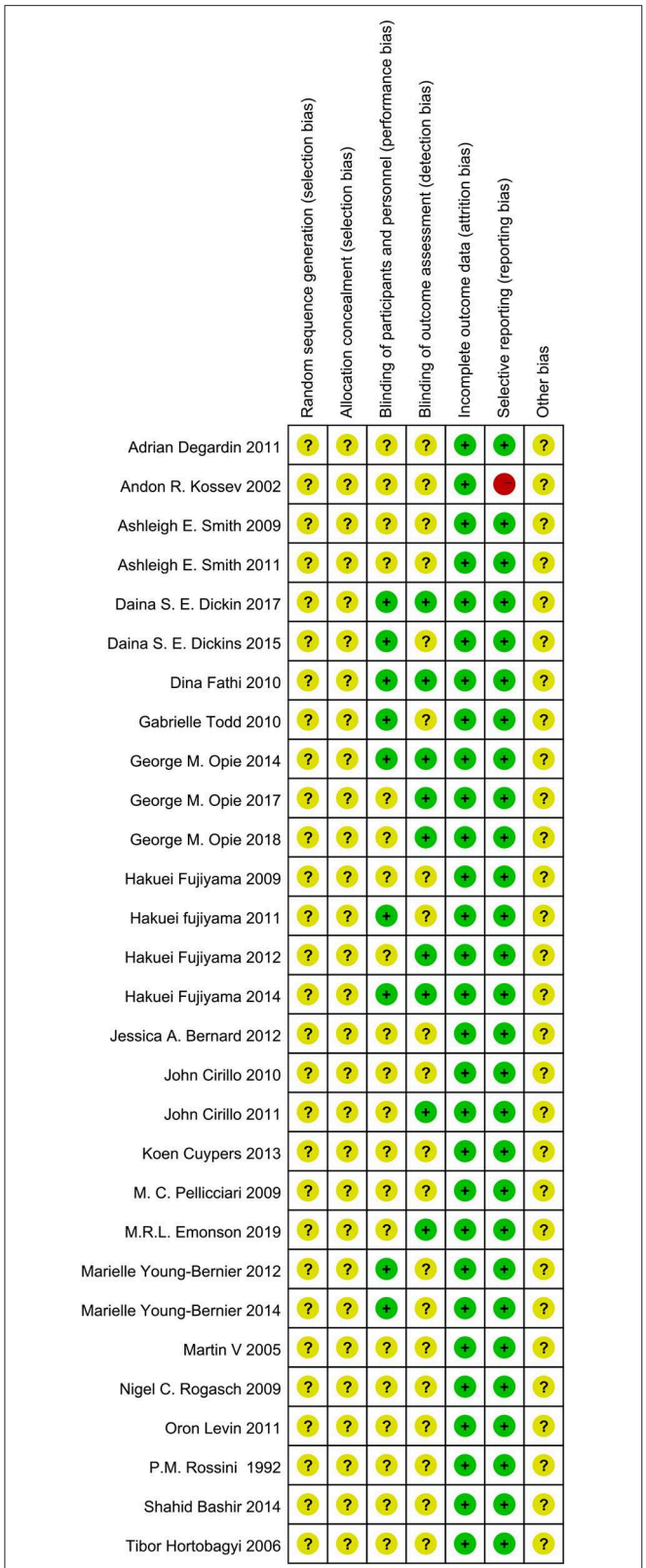

FIGURE 3 | Summary Graph of the risk of bias in the included trials by Cochrane risk of bias toll based upon reviewers' judgment of each domain.

DISCUSSION

Summary of the Main Findings

We conducted a meta-analysis including 29 studies with 914 patients. We used TMS-EMG, including RMT, AMT, MEP amplitude, and MEP latency to evaluate the age-related changes in the plasticity of neural networks among young and elderly individuals. The results indicated that the excitability of the cerebral cortex declined in elderly individuals vs. young individuals. Three important points were noted. Firstly, the RMT and MEP latency in the elderly group was higher than that in the young group. In contrast, the MEP amplitude in the elderly group was lower than that in the young group. Secondly, there was no significant difference in the AMT between the two groups. Third, there were no common adverse reactions reported in the included studies, suggesting that TMS-EMG technology is relatively safe.

Age-Related Changes in the Plasticity of Neural Networks

Driven by a decline in birth rates and an increase in life expectancy, the global demographic structure is rapidly aging. Demographic projections show that the proportion of individuals aged ≥65 years is expected to increase by >150% in 35 years (Tatti et al., 2016). According to this projection, the number of individuals aged >65 years will exceed 1.6 billion by 2050. Age-related diseases profoundly impact the daily activities and quality of life of the elderly (Logsdon et al., 2002; Craik and Bialystok, 2006), posing a great and urgent challenge to society (Ballard, 2010). Therefore, it is essential to fully understand the mechanisms involved in aging.

Aging is associated with functional decline in numerous cognitive areas, such as attention, memory, language, and executive functions (Morrison and Baxter, 2012). The structure and function of many brain regions undergo extensive changes with aging, including reduction in cerebral cortex thickness (Tatti et al., 2016), decreases in neurotransmitter binding potential, and synaptic receptor density and efficacy (Celsis, 2000), change in cortical and cerebellar metabolism (Dukart et al., 2013), gray matter atrophy, white matter loss ventricular enlargement, etc. (Scahill et al., 2003; Bolandzadeh et al., 2012; Bennett and Madden, 2014).

Research on the mechanism of aging and the related physiological and pathological changes is insufficient. However, in recent years, numerous studies investigating age-related changes in the plasticity of neural networks have achieved breakthroughs in this field. A number of studies have shown that elderly individuals with normal cognition mainly showed functional changes in the neural network during memory coding, especially in the posterior medial cortex (Wellman and Sengelaub, 1995; Ahmed et al., 2018). Converging evidence from positron emission tomography studies indicates that nearly one-third of clinically normal elderly individuals harbor fibrillar β-amyloid deposition (Dickerson et al., 2009; Sperling et al., 2009). Animal experiments confirmed that with increasing age, fibrous β-amyloid is gradually deposited, and functional changes in the default network were observed in the posterior medial

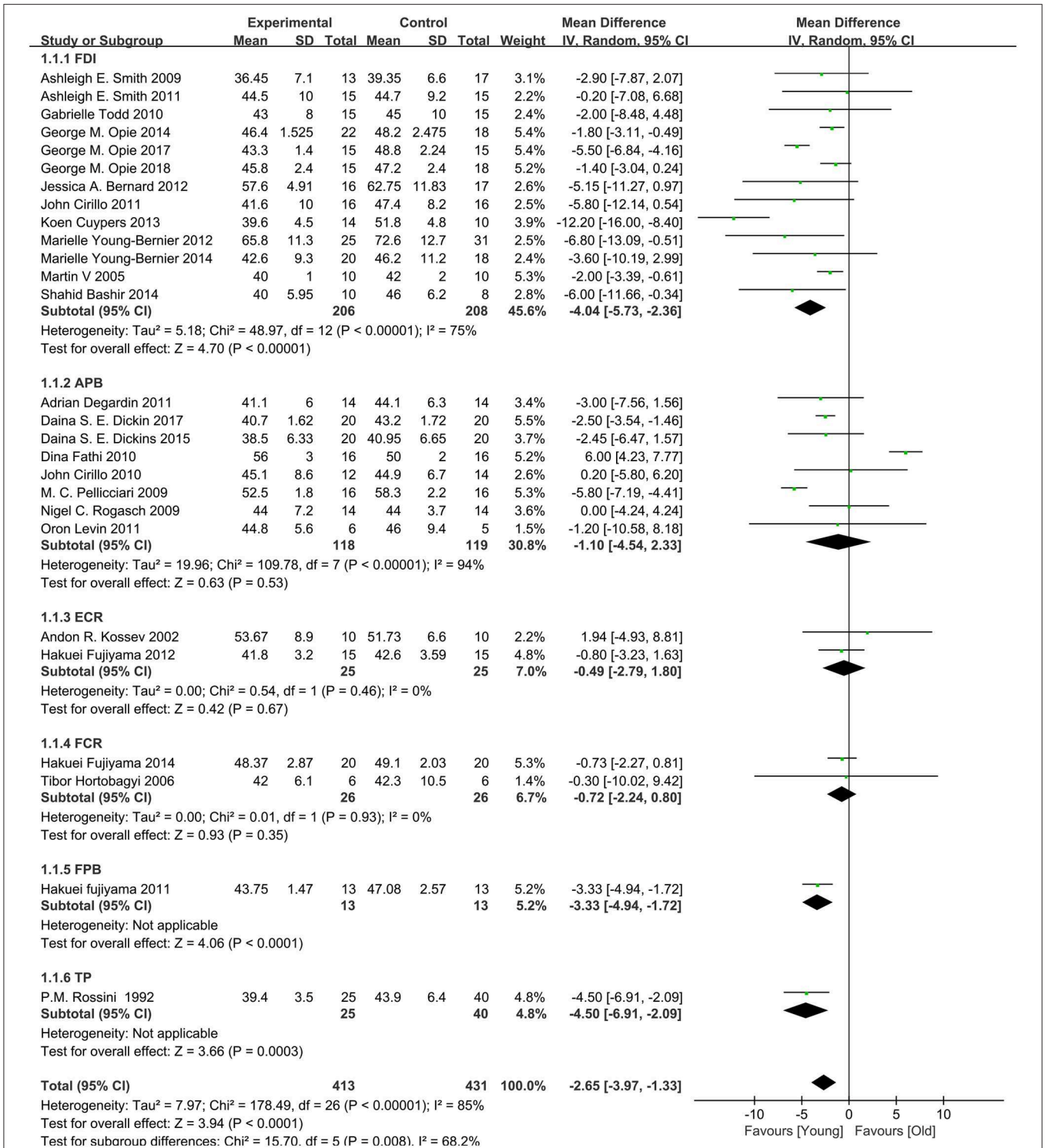

FIGURE 4 | Young group vs. old group, RMT.

cortex of rats (Becker et al., 2011; Sousa et al., 2017). These studies suggested that many of the age-related changes in neural network function may be attributed to amyloid deposition (Iadecola, 2010).

Multi-dimensional observations of changes in the neural networks of the brain may deepen our understanding of aging, and its physiological and pathological mechanisms. Non-invasive brain stimulation techniques (e.g., TMS) are used in

TABLE 2 | Subgroup analysis based on the RMT.

Group	No. of studies	No. of participants	*MD*	95% *CI*	*Z*	*p* (Effect)	I^2 (%)	χ^2
Muscle								
FDI	13	414	−4.04	[−5.73, −2.36]	4.70	<0.00001	75	48.97
APB	8	237	−1.10	[−4.54, 2.33]	0.63	0.53	94	109.78
ECR	2	50	−0.49	[−2.79, 1.80]	0.42	0.67	0	0.54
FCR	2	52	−0.72	[−2.24, 0.80]	0.93	0.35	0	0.01
FPB	1	26	−3.33	[−4.94, −1.72]	4.06	<0.00001		
TP	1	65	−4.50	[−6.91, −2.09]	3.66	0.0003		
Publication region								
Oceania	16	515	−1.90	[−2.95, −0.85]	3.56	0.0004	69	48.82
Europe	6	180	−5.10	[−7.95, −2.25]	3.51	0.0005	74	19.21
Asia	1	32	6	[4.23, 7.77]	6.66	<0.00001		
America	5	157	−4.99	[−7.91, −2.06]	3.34	0.0008	0	1.51
Publication year								
≤2011	15	422	−1.65	[−3.97, 0.68]	1.38	0.17	88	118.78
>2011	13	462	−2.94	[−4.55, −1.33]	9.35	0.0004	84	73.13

ECR, the extensor carpi radialis muscle; APB, the abductor pollicis brevis muscle; FDI, the first dorsal interosseous muscle; FCR, the flexor carpi radialis muscles; FPB, the flexor pollicis brevis muscle; TP, thenar and plantar muscles.

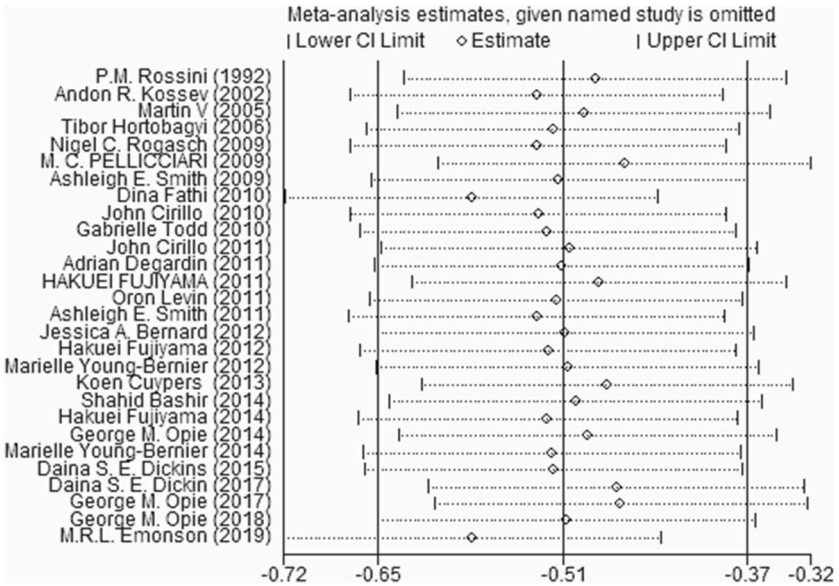

FIGURE 5 | Sensitivity analysis by excluding each article.

numerous studies to detect changes in the neural networks. Recently, neuroscience research has explored the possibility of applying this technology to examine the elderly population. Early detection of changes may enable the development of new treatments, thereby increasing the likelihood of effectively preventing or delaying the occurrence of disease.

Diagnostic Applications of TMS for the Plasticity of Neural Networks

Since its introduction by Professor Anthony Barker of the University of Sheffield in 1985 (Barker et al., 1985), TMS has been used to activate the human motor cortex, non-invasively assess the net level of cortical excitability, and determine the integrity of the central motor pathways (Tatti et al., 2016). TMS removes short and powerful magnetic pulses from the skull and generates a secondary electrical current according to the principle of electromagnetic induction of Faraday. The current generated in the cerebral cortex changes the excitability of the underlying neurons and induces neuronal firing. This ultimately results in movement of the corresponding muscles through the corticospinal, corticonuclear, callosal fiber, nerve roots, and peripheral motor pathways (Sanes and Donoghue,

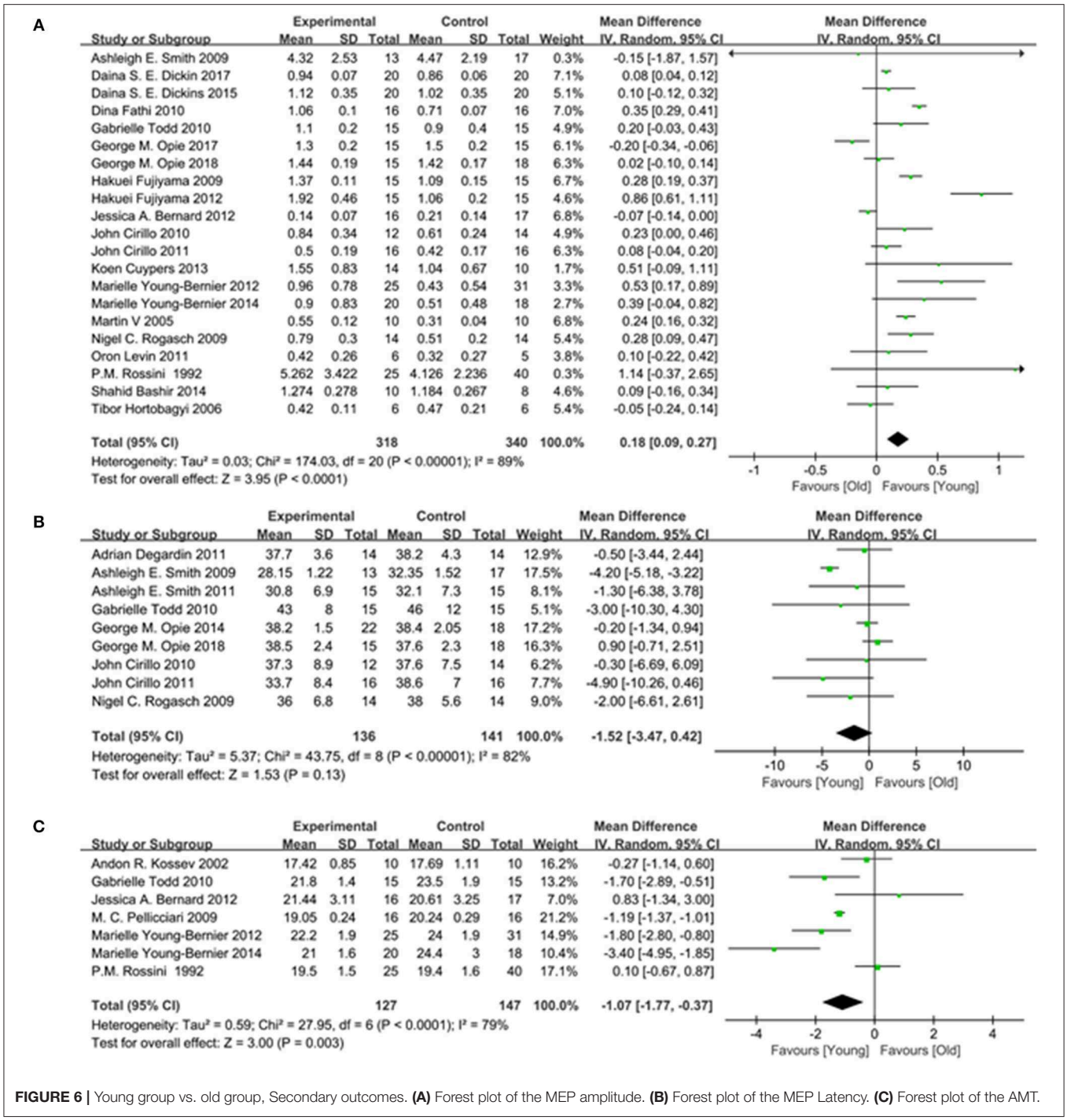

FIGURE 6 | Young group vs. old group, Secondary outcomes. **(A)** Forest plot of the MEP amplitude. **(B)** Forest plot of the MEP Latency. **(C)** Forest plot of the AMT.

2000; Müller-Dahlhaus et al., 2010). In this manner, TMS may directly reflect the excitability information of different motor cortices and functional integrity of the intracortical neuronal structures. EMG refers to the muscle bioelectrical pattern recorded using an electromyograph. It is often used to determine the functional status of peripheral nerves, neurons, neuromuscular junctions, and muscles. When TMS-EMG is applied to the monitoring of primary motor cortex excitability, it activates the underlying neural group and passes through the corticospinal pathway. This ultimately leads to a motor response to the contralateral muscle MEP, which can be quantified using EMG. The motor thresholds, the MEP amplitude, the MEP latency, and short intracortical inhibition are the most commonly applied techniques for TMS (Edwards et al., 2008). Notably, the results of these techniques are largely influenced by device characteristics, parameter settings, and experimental

procedures. In addition, subject-related variables (e.g., eventual pharmacological treatments) affect the outcome indicators of TMS stimulation.

In recent years, investigations regarding the plasticity of neural networks have attracted considerable attention, and researchers use the TMS-EMG technology to evaluate the sensitivity of the motor system to plastic changes. Some studies showed that following the induction of the M1 cortical region of the brain by TMS in the elderly, their ability to stimulate excitability and stimulation-induced adaptations was limited compared with that reported in the young individuals (Dayan et al., 2013; Li et al., 2015). Consistent with the findings of the present meta-analysis, these results indicate that the function and ability of the M1 cortical region in older individuals decrease with age.

Limitations

This meta-analysis had several limitations. Firstly, heterogeneity was detected, which reduced the reliability of the comparisons. Although all the included studies were examined using only TMS-EMG, there was also heterogeneity detected in different characteristics, parameter settings, experimental procedures, and subject-related variables (including state dependency and eventual pharmacological treatments), which may reduce the generalizability of the conclusions. Secondly, only 29 randomized controlled trials were included in this review. Moreover, limitations in the quality of research design and sample sizes affect the extrapolation and strength of this evidence. In addition, due to the limitations of the inclusion of the literature, we can only be included in the cohort and case-control studies. Therefore, it is possible that the statistical power may have been inadequate due to the small number of studies, and it is difficult to precisely evaluate the excitability of neural networks in the different groups. Thirdly, there was no report of adverse events. In the included studies, we only found limited information related to safety owing to poor reporting of adverse events. Hence, the pooled results should be treated with caution. Another limitation is that, in this review, behavioral meta-analysis results are only provided by the included TMS-EMG studies, which may lead to publication bias. This suggests that some studies without significant cortical activation results may not be published.

CONCLUSIONS

We found that the excitability of the cerebral cortex declined in elderly individuals vs. young individuals. The findings of this review should be considered with caution owing to the methodological limitation of the included trials. Further high-quality studies are warranted to validate the present findings. It is well established that the normal process of aging is the result of degeneration and compensation of the neural network and its related conduction functions. However, the existing models of age-related changes in the brain do not cover the full spectrum of alterations (Li et al., 2015). Thus, the use of various detection methods is necessary to dynamically observe the age-related changes in neural networks. This approach may assist researchers in developing a new aging model, which reflects the age-related changes in the plasticity of neural networks.

DATA AVAILABILITY STATEMENT

The data supporting the results reported in this article may be obtained from the corresponding author upon reasonable request.

AUTHOR CONTRIBUTIONS

NX and PH: study concept and design. WY and ZY: data curation. YL and LW: formal analysis. YL and JL: investigation. XT: methodology. YL: resources. LW, MX, and PH: software. XT and PH: supervision and writing-original draft. NX: validation. XT: writing-review and editing. All authors read and approved to publish the final version of the manuscript.

FUNDING

This study was supported by Project Grant National Natural Science Foundation of China (Grants nos. 81774406, 81774394, 81804167, and 81904297), the Qi-Huang Scholar of National Traditional Chinese Medicine Leading Talents Support Program (2018) and 2012A061400017, 2014GKXM031, 2017KYTD03, 2017B030314143, 2017KCXTD006 from the Department of Education of Guangdong Province, China.

ACKNOWLEDGMENTS

We would like to thank the staff of South China Research Center for Acupuncture of Guangdong Province for their support of this study.

SUPPLEMENTARY MATERIAL

The Supplementary Material for this article can be found online at: https://www.frontiersin.org/articles/10.3389/fncel.2019.00469/full#supplementary-material

REFERENCES

Ahmed, R. M., Ke, Y. D., Vucic, S., Ittner, L. M., Seeley, W., Hodges, J. R., et al. (2018). Physiological changes in neurodegeneration - mechanistic insights and clinical utility. *Nat. Rev. Neurol.* 14, 259–271. doi: 10.1038/nrneurol.2018.23

Ballard, J. (2010). Forgetfulness and older adults: concept analysis. *J. Adv. Nurs.* 66, 1409–1419. doi: 10.1111/j.1365-2648.2010.05279.x

Barker, A. T., Jalinous, R., and Freeston, I. L. (1985). Non-invasive magnetic stimulation of human motor cortex. *Lancet* 1, 1106–1107. doi: 10.1016/S0140-6736(85)92413-4

Bashir, S., Perez, J. M., Horvath, J. C., Pena-Gomez, C., Vernet, M., Capia, A., et al. (2014). Differential effects of motor cortical excitability and plasticity in young and old individuals: a Transcranial Magnetic Stimulation (TMS) study. *Front. Aging Neurosci.* 6:111. doi: 10.3389/fnagi.2014.00111

Becker, J. A., Hedden, T., Carmasin, J., Maye, J., Rentz, D. M., Putcha, D., et al. (2011). Amyloid-beta associated cortical thinning in clinically normal elderly. *Ann. Neurol.* 69, 1032–1042. doi: 10.1002/ana.22333

Bennett, I. J., and Madden, D. J. (2014). Disconnected aging: cerebral white matter integrity and age-related differences in cognition. *Neuroscience* 276, 187–205. doi: 10.1016/j.neuroscience.2013.11.026

Bernard, J. A., and Seidler, R. D. (2012). Evidence for motor cortex dedifferentiation in older adults. *Neurobiol. Aging* 33, 1890–1899. doi: 10.1016/j.neurobiolaging.2011.06.021

Bolandzadeh, N., Davis, J. C., Tam, R., Handy, T. C., and Liu-Ambrose, T. (2012). The association between cognitive function and white matter lesion location in older adults: a systematic review. *BMC Neurol.* 12:126. doi: 10.1186/1471-2377-12-126

Boroojerdi, B., Ziemann, U., Chen, R., Bütefisch, C. M., and Cohen, L. G. (2001). Mechanisms underlying human motor system plasticity. *Muscle Nerve* 24, 602–613. doi: 10.1002/mus.1045

Brunso-Bechtold, J. K., Linville, M. C., and Sonntag, W. E. (2000). Age-related synaptic changes in sensorimotor cortex of the Brown Norway X fischer 344 rat. *Brain Res.* 872, 125–133. doi: 10.1016/S0006-8993(00)02515-4

Burke, S. N., and Barnes, C. A. (2006). Neural plasticity in the ageing brain. *Nat. Rev. Neurosci.* 7, 30–40. doi: 10.1038/nrn1809

Celsis, P. (2000). Age-related cognitive decline, mild cognitive impairment or preclinical Alzheimer's disease? *Ann. Med.* 32, 6–14. doi: 10.3109/07853890008995904

Cirillo, J., Rogasch, N. C., and Semmler, J. G. (2010). Hemispheric differences in use-dependent corticomotor plasticity in young and old adults. *Exp. Brain Res.* 205, 57–68. doi: 10.1007/s00221-010-2332-1

Cirillo, J., Todd, G., and Semmler, J. (2011). Corticomotor excitability and plasticity following complex visuomotor training in young and old adults. *Eur. J. Neurosci.* 34, 1847–1856. doi: 10.1111/j.1460-9568.2011.07870.x

Craik, F. I., and Bialystok, E. (2006). Planning and task management in older adults: cooking breakfast. *Mem. Cognit.* 34, 1236–1249. doi: 10.3758/BF03193268

Cuypers, K., Thijs, H., Duque, J., Swinnen, S. P., Levin, O., and Meesen, R. L. (2013). Age-related differences in corticospinal excitability during a choice reaction time task. *Age* 35, 1705–1719. doi: 10.1007/s11357-012-9471-1

Dayan, E., Censor, N., Buch, E. R., Sandrini, M., and Cohen, L. G. (2013). Noninvasive brain stimulation: from physiology to network dynamics and back. *Nat. Neurosci.* 16, 838–844. doi: 10.1038/nn.3422

DeCarli, C., Kawas, C., Morrison, J. H., Reuter-Lorenz, P. A., Sperling, R. A., and Wright, C. B. (2012). Session II: mechanisms of age-related cognitive change and targets for intervention: neural circuits, networks, and plasticity. *J. Gerontol. A Biol. Sci. Med. Sci.* 67, 747–753. doi: 10.1093/gerona/gls111

Degardin, A., Devos, D., Cassim, F., Bourriez, J. L., Defebvre, L., Derambure, P., et al. (2011). Deficit of sensorimotor integration in normal aging. *Neurosci. Lett.* 498, 208–212. doi: 10.1016/j.neulet.2011.05.010

Dickerson, B. C., Bakkour, A., Salat, D. H., Feczko, E., Pacheco, J., Greve, D. N., et al. (2009). The cortical signature of Alzheimer's disease: regionally specific cortical thinning relates to symptom severity in very mild to mild AD dementia and is detectable in asymptomatic amyloid-positive individuals. *Cereb. Cortex.* 19, 497–510. doi: 10.1093/cercor/bhn113

Dickins, D. S. E., Kamke, M. R., and Sale, M. V. (2017). Corticospinal plasticity in bilateral primary motor cortices induced by paired associative stimulation to the dominant hemisphere does not differ between young and older adults. *Neural Plast.* 2017, 1–14. doi: 10.1155/2017/8319049

Dickins, D. S. E., Sale, M. V., and Kamke, M. R. (2015). Plasticity induced by intermittent theta burst stimulation in bilateral motor cortices is not altered in older adults. *Neural Plast.* 2015, 1–9. doi: 10.1155/2015/323409

Dukart, J., Mueller, K., Villringer, A., Kherif, F., Draganski, B., Frackowiak, R., et al. (2013). Relationship between imaging biomarkers, age, progression and symptom severity in Alzheimer's disease. *Neuroimage Clin.* 3, 84–94. doi: 10.1016/j.nicl.2013.07.005

Edwards, M. J., Talelli, P., and Rothwell, J. C. (2008). Clinical applications of transcranial magnetic stimulation in patients with movement disorders. *Lancet Neurol.* 7, 827–840. doi: 10.1016/S1474-4422(08)70190-X

Emonson, M. R. L., Fitzgerald, P. B., Rogasch, N. C., and Hoy, K. E. (2019). Neurobiological effects of transcranial direct current stimulation in younger adults, older adults and mild cognitive impairment. *Neuropsychologia* 125, 51–61. doi: 10.1016/j.neuropsychologia.2019.01.003

Fathi, D., Ueki, Y., Mima, T., Koganemaru, S., Nagamine, T., Tawfik, A., et al. (2010). Effects of aging on the human motor cortical plasticity studied by paired associative stimulation. *Clin. Neurophysiol.* 121, 90–93. doi: 10.1016/j.clinph.2009.07.048

Fujiyama, H., Garry, M. I., Levin, O., Swinnen, S. P., and Summers, J. J. (2009). Age-related differences in inhibitory processes during interlimb coordination. *Brain Res.* 1262, 38–47. doi: 10.1016/j.brainres.2009.01.023

Fujiyama, H., Hinder, M. R., Schmidt, M. W., Garry, M. I., and Summers, J. J. (2012). Age-related differences in corticospinal excitability and inhibition during coordination of upper and lower limbs. *Neurobiol. Aging* 33, 1484.e1–1484.e14. doi: 10.1016/j.neurobiolaging.2011.12.019

Fujiyama, H., Hyde, J., Hinder, M. R., Kim, S. J., McCormack, G. H., Vickers, J. C., et al. (2014). Delayed plastic responses to anodal tDCS in older adults. *Front. Aging Neurosci.* 6:115. doi: 10.3389/fnagi.2014.00115

Fujiyama, H., Tandonnet, C., and Summers, J. J. (2011). Age-related differences in corticospinal excitability during a Go/NoGo task. *Psychophysiology.* 48, 1448–1455. doi: 10.1111/j.1469-8986.2011.01201.x

Godde, B., Berkefeld, T., David-Jürgens, M., and Dinse, H. R. (2002). Age-related changes in primary somatosensory cortex of rats: evidence for parallel degenerative and plastic-adaptive processes. *Neurosci. Biobehav. Rev.* 26, 743–752. doi: 10.1016/S0149-7634(02)00061-1

Higgins, J. P., Thompson, S. G., Deeks, J. J., and Altman, D. G. (2003). Measuring inconsistency in meta-analyses. *BMJ* 327, 557–560. doi: 10.1136/bmj.327.7414.557

Hortobágyi, T., del Olmo, M. F., and Rothwell, J. C. (2006). Age reduces cortical reciprocal inhibition in humans. *Exp. Brain Res.* 171, 322–329. doi: 10.1007/s00221-005-0274-9

Hunter, S. K., Thompson, W., and Roger, D. A. (2001). Reaction time, strength, and physical activity in women aged 20–89 years. *J. Aging Phys. Act.* 9, 32–42. doi: 10.1123/japa.9.1.32

Iadecola, C. (2010). The overlap between neurodegenerative and vascular factors in the pathogenesis of dementia. *Acta Neuropathol.* 120, 287–296. doi: 10.1007/s00401-010-0718-6

Kossev, A. R., Schrader, C., Däuper, J., Dengler, R., and Rollnik, J. D. (2002). Increased intracortical inhibition in middle-aged humans; a study using paired-pulse transcranial magnetic stimulation. *Neurosci. Lett.* 333, 83–86. doi: 10.1016/S0304-3940(02)00986-2

Levin, O., Cuypers, K., Netz, Y., Thijs, H., Nuttin, B., Helsen, W. F., et al. (2011). Age-related differences in human corticospinal excitability during simple reaction time. *Neurosci. Lett.* 487, 53–57. doi: 10.1016/j.neulet.2010.09.072

Li, H. J., Hou, X. H., Liu, H. H., Yue, C. L., Lu, G. M., and Zuo, X. N. (2015). Putting age-related task activation into large-scale brain networks: a meta-analysis of 114 fMRI studies on healthy aging. *Neurosci. Biobehav. Rev.* 57, 156–174. doi: 10.1016/j.neubiorev.2015.08.013

Logsdon, R. G., Gibbons, L. E., McCurry, S. M., and Teri, L. (2002). Assessing quality of life in older adults with cognitive impairment. *Psychosom. Med.* 64, 510–519. doi: 10.1097/00006842-200205000-00016

Mora, F., Segovia, G., and del Arco, A. (2007). Aging, plasticity and environmental enrichment: structural changes and neurotransmitter dynamics in several areas of the brain. *Brain Res. Rev.* 55, 78–88. doi: 10.1016/j.brainresrev.2007.03.011

Morrison, J. H., and Baxter, M. G. (2012). The ageing cortical synapse: hallmarks and implications for cognitive decline. *Nat. Rev. Neurosci.* 13, 240–250. doi: 10.1038/nrn3200

Müller-Dahlhaus, F., Ziemann, U., and Classen, J. (2010). Plasticity resembling spike-timing dependent synaptic plasticity: the evidence in human cortex. *Front. Synaptic Neurosci.* 2:34. doi: 10.3389/fnsyn.2010.00034

Oliviero, A., Profice, P., Tonali, P. A., Pilato, F., Saturno, E., Dileone, M., et al. (2006). Effects of aging on motor cortex excitability. *Neurosci Res.* 55, 74–77. doi: 10.1016/j.neures.2006.02.002

Opie, G. M., Cirillo, J., and Semmler, J. G. (2018). Age-related changes in late I-waves influence motor cortex plasticity induction in older adults. *J. Physiol. (Lond).* 596, 2597–2609. doi: 10.1113/JP274641

Opie, G. M., Post, A. K., Ridding, M. C., Ziemann, U., and Semmler, J. G. (2017). Modulating motor cortical neuroplasticity with priming paired associative stimulation in young and old adults. *Clin. Neurophysiol.* 128, 763–769. doi: 10.1016/j.clinph.2017.02.011

Opie, G. M., and Semmler, J. G. (2014). Age-related differences in short- and long-interval intracortical inhibition in a human hand muscle. *Brain Stimul.* 7, 665–672. doi: 10.1016/j.brs.2014.06.014

Pellicciari, M. C., Miniussi, C., Rossini, P. M., and De Gennaro, L. (2009). Increased cortical plasticity in the elderly: changes in the somatosensory cortex after paired associative stimulation. *Neuroscience* 163, 266–276. doi: 10.1016/j.neuroscience.2009.06.013

Rogasch, N. C., Dartnall, T. J., Cirillo, J., Nordstrom, M. A., and Semmler, J. G. (2009). Corticomotor plasticity and learning of a ballistic thumb training task are diminished in older adults. *J. Appl. Physiol.* 107, 1874–1883. doi: 10.1152/japplphysiol.00443.2009

Rossini, P. M., Desiato, M. T., and Caramia, M. D. (1992). Age-related changes of motor evoked potentials in healthy humans: non-invasive evaluation of central and peripheral motor tracts excitability and conductivity. *Brain Res.* 593, 14–19. doi: 10.1016/0006-8993(92)91256-E

Rossini, P. M., Rossi, S., Babiloni, C., and Polich, J. (2007). Clinical neurophysiology of aging brain: from normal aging to neurodegeneration. *Prog Neurobiol.* 83, 375–400. doi: 10.1016/j.pneurobio.2007.07.010

Sale, M. V., and Semmler, J. G. (2005). Age-related differences in corticospinal control during functional isometric contractions in left and right hands. *J. Appl. Physiol.* 99, 1483–1493. doi: 10.1152/japplphysiol.00371.2005

Sanes, J. N., and Donoghue, J. P. (2000). Plasticity and primary motor cortex. *Annu. Rev. Neurosci.* 23, 393–415. doi: 10.1146/annurev.neuro.23.1.393

Savović, J., Weeks, L., Sterne, J. A., Turner, L., Altman, D. G., Moher, D., et al. (2014). Evaluation of the Cochrane Collaboration's tool for assessing the risk of bias in randomized trials: focus groups, online survey, proposed recommendations and their implementation. *Syst. Rev.* 3:37. doi: 10.1186/2046-4053-3-37

Sawaki, L., Yaseen, Z., Kopylev, L., and Cohen, L. G. (2003). Age-dependent changes in the ability to encode a novel elementary motor memory. *Ann. Neurol.* 53, 521–524. doi: 10.1002/ana.10529

Scahill, R. I., Frost, C., Jenkins, R., Whitwell, J. L., Rossor, M. N., and Fox, N. C. (2003). A longitudinal study of brain volume changes in normal aging using serial registered magnetic resonance imaging. *Arch. Neurol.* 60, 989–994. doi: 10.1001/archneur.60.7.989

Seidler, R. D., Bernard, J. A., Burutolu, T. B., Fling, B. W., Gordon, M. T., Gwin, J. T., et al. (2010). Motor control and aging: links to age-related brain structural, functional, and biochemical effects. *Neurosci. Biobehav. Rev.* 34, 721–733. doi: 10.1016/j.neubiorev.2009.10.005

Smith, A. E., Ridding, M. C., Higgins, R. D., Wittert, G. A., and Pitcher, J. B. (2009). Age-related changes in short-latency motor cortex inhibition. *Experimental Brain Research.* 198, 489–500. doi: 10.1007/s00221-009-1945-8

Smith, A. E., Ridding, M. C., Higgins, R. D., Wittert, G. A., and Pitcher, J. B. (2011). Cutaneous afferent input does not modulate motor intracortical inhibition in ageing men. *Euro. J. Neurosci.* 34, 1461–1469. doi: 10.1111/j.1460-9568.2011.07869.x

Sousa, A. M. M., Meyer, K. A., Santpere, G., Gulden, F. O., and Sestan, N. (2017). Evolution of the human nervous system function, structure, and development. *Cell* 170, 226–247. doi: 10.1016/j.cell.2017.06.036

Sperling, R. A., Laviolette, P. S., O'Keefe, K., O'Brien, J., Rentz, D. M., Pihlajamaki, M., et al. (2009). Amyloid deposition is associated with impaired default network function in older persons without dementia. *Neuron* 63, 178–188. doi: 10.1016/j.neuron.2009.07.003

Tatti, E., Rossi, S., Innocenti, I., Rossi, A., and Santarnecchi, E. (2016). Non-invasive brain stimulation of the aging brain: state of the art and future perspectives. *Ageing Res. Rev.* 29, 66–89. doi: 10.1016/j.arr.2016.05.006

Todd, G., Kimber, T. E., Ridding, M. C., and Semmler, J. G. (2010). Reduced motor cortex plasticity following inhibitory rTMS in older adults. *Clin. Neurophysiol.* 121, 441–447. doi: 10.1016/j.clinph.2009.11.089

Ward, N. S., Swayne, O. B., and Newton, J. M. (2008). Age-dependent changes in the neural correlates of force modulation: an fMRI study. *Neurobiol. Aging* 29, 1434–1446. doi: 10.1016/j.neurobiolaging.2007.04.017

Wellman, C. L., and Sengelaub, D. R. (1995). Alterations in dendritic morphology of frontal cortical neurons after basal forebrain lesions in adult and aged rats. *Brain Res.* 669, 48–58. doi: 10.1016/0006-8993(94)01231-6

Young-Bernier, M., Davidson, P. S., and Tremblay, F. (2012). Paired-pulse afferent modulation of TMS responses reveals a selective decrease in short latency afferent inhibition with age. *Neurobiol Aging* 33, 835.e1–835.e11. doi: 10.1016/j.neurobiolaging.2011.08.012

Young-Bernier, M., Tanguay, A. N., Davidson, P. S., and Tremblay, F. (2014). Short-latency afferent inhibition is a poor predictor of individual susceptibility to rTMS-induced plasticity in the motor cortex of young and older adults. *Front. Aging Neurosci.* 6:182. doi: 10.3389/fnagi.2014.00182

Conflict of Interest: The authors declare that the research was conducted in the absence of any commercial or financial relationships that could be construed as a potential conflict of interest.

The handling editor declared a shared affiliation, though no other collaboration, with the author PH at the time of the review.

frontiers in Cellular Neuroscience

ORIGINAL RESEARCH
published: 05 February 2020
doi: 10.3389/fncel.2019.00590

Blebbistatin Inhibits Neomycin-Induced Apoptosis in Hair Cell-Like HEI-OC-1 Cells and in Cochlear Hair Cells

Song Gao[1†], Cheng Cheng[2,3†], Maohua Wang[4†], Pei Jiang[5], Liyan Zhang[5], Ya Wang[1], Huihui Wu[1], Xuanfu Zeng[1], Hui Wang[6], Xia Gao[2,3]*, Yongming Ma[1]* and Renjie Chai[5,7,8,9,10]**

[1]Department of Otolaryngology, Affiliated People's Hospital of Jiangsu University, Zhenjiang, China, [2]Department of Otolaryngology Head and Neck Surgery, Nanjing Drum Tower Hospital Clinical College of Nanjing Medical University, Jiangsu Provincial Key Medical Discipline (Laboratory), Nanjing, China, [3]Research Institute of Otolaryngology, Nanjing, China, [4]Department of Otolaryngology, Head and Neck Surgery, XiangYa School of Medicine, Central South University, Changsha, China, [5]MOE Key Laboratory for Developmental Genes and Human Disease, Institute of Life Sciences, Southeast University, Nanjing, China, [6]Department of Otolaryngology Head and Neck Surgery, Shanghai Jiao Tong University Affiliated Sixth People's Hospital, Shanghai, China, [7]Co-Innovation Center of Neuroregeneration, Nantong University, Nantong, China, [8]Institute for Stem Cell and Regeneration, Chinese Academy of Science, Beijing, China, [9]Beijing Key Laboratory of Neural Regeneration and Repair, Capital Medical University, Beijing, China, [10]Jiangsu Province High-Tech Key Laboratory for Bio-Medical Research, Southeast University, Nanjing, China

OPEN ACCESS

Edited by:
Zhang Pengyue,
Yunnan University of Traditional Chinese Medicine, China

Reviewed by:
Wenwen Liu,
Shandong University, China
Bingjin Li,
Jilin University, China

***Correspondence:**
Renjie Chai
renjiec@seu.edu.cn
Yongming Ma
maym121@163.com
Xia Gao
xiagaogao@hotmail.com
Hui Wang
wangh2005@alumni.sjtu.edu.cn

†These authors have contributed equally to this work

Received: 29 October 2019
Accepted: 27 December 2019
Published: 05 February 2020

Citation:
Gao S, Cheng C, Wang M, Jiang P, Zhang L, Wang Y, Wu H, Zeng X, Wang H, Gao X, Ma Y and Chai R (2020) Blebbistatin Inhibits Neomycin-Induced Apoptosis in Hair Cell-Like HEI-OC-1 Cells and in Cochlear Hair Cells. Front. Cell. Neurosci. 13:590. doi: 10.3389/fncel.2019.00590

Aging, noise, and ototoxic drug-induced hair cell (HC) loss are the major causes of sensorineural hearing loss. Aminoglycoside antibiotics are commonly used in the clinic, but these often have ototoxic side effects due to the accumulation of oxygen-free radicals and the subsequent induction of HC apoptosis. Blebbistatin is a myosin II inhibitor that regulates microtubule assembly and myosin–actin interactions, and most research has focused on its ability to modulate cardiac or urinary bladder contractility. By regulating the cytoskeletal structure and reducing the accumulation of reactive oxygen species (ROS), blebbistatin can prevent apoptosis in many different types of cells. However, there are no reports on the effect of blebbistatin in HC apoptosis. In this study, we found that the presence of blebbistatin significantly inhibited neomycin-induced apoptosis in HC-like HEI-OC-1 cells. We also found that blebbistatin treatment significantly increased the mitochondrial membrane potential (MMP), decreased ROS accumulation, and inhibited pro-apoptotic gene expression in both HC-like HEI-OC-1 cells and explant-cultured cochlear HCs after neomycin exposure. Meanwhile, blebbistatin can protect the synaptic connections between HCs and cochlear spiral ganglion neurons. This study showed that blebbistatin could maintain mitochondrial function and reduce the ROS level and thus could maintain the viability of HCs after neomycin exposure and the neural function in the inner ear, suggesting that blebbistatin has potential clinic application in protecting against ototoxic drug-induced HC loss.

Keywords: aminoglycoside, hair cell, blebbistatin, apoptosis, ROS, hearing, synaptic plasticity

INTRODUCTION

Aging, noise, and ototoxic drugs are major causes of hair cell (HC) damage leading to sensorineural hearing loss. Aminoglycoside antibiotics are widely used against gram-negative bacterial infections because of their low cost and effectiveness (Becker and Cooper, 2013), but these drugs can cause HC loss by activating the apoptosis pathway (Jiang et al., 2017). Thus, it is important to find an effective way to reduce the ototoxicity of aminoglycosides. Aminoglycoside antibiotics mainly accumulate in the lysosomes and mitochondria in HCs, inducing the accumulation of intracellular reactive oxygen species (ROS), which in turn induce apoptosis and are the major factor leading to HC damage (Coffin et al., 2013; Liu et al., 2016, 2019; Wang et al., 2016; He et al., 2017; Waqas et al., 2017; Yu et al., 2017; Li A. et al., 2018; Li H. et al., 2018). Several studies have shown that ischemia–reperfusion-induced deafness, noise-induced deafness, presbycusis, and ototoxic drug-induced deafness are all closely related to the accumulation of ROS in HCs (Seidman et al., 2000; Sena and Chandel, 2012).

Many studies, including our previous studies, have shown that caspase-associated apoptosis plays an important role in aminoglycoside-induced ototoxicity (Guan et al., 2016; He et al., 2017). The accumulation of ROS in the lysosomes and mitochondria of HCs leads to the upregulation of caspase genes, which further induces apoptosis of HCs (Esterberg et al., 2016; Jiang et al., 2016; Guo et al., 2019). In the central nervous system, myosin contraction plays an important role in oxidative stress-related neuronal apoptosis, myosin contraction, and the formation of relevant complexes needed to activate the expression of caspase-3 through the ROCK1-related pathway, indicating positive feedback regulation between myosin contraction and the oxidative stress-induced apoptosis pathway (Wang et al., 2017). However, the role of myosin contraction in cochlear HC apoptosis remains uninvestigated.

Blebbistatin is a myosin II inhibitor, and it interferes with myosin–actin interactions and microtubule assembly (Kovács et al., 2004). It has been reported that blebbistatin reduces apoptosis in neurons, cardiomyocytes, and erythrocytes, and by inhibiting myosin IIA–actin interactions, blebbistatin increases mitochondrial length and reduces calcium overload, reduces damage from oxygen free radicals and mitochondrial dysfunction, and decreases caspase activity (Lang et al., 2011; Wang et al., 2017; Li F. et al., 2018). Many research has focused on blebbistatin's effects on cellular morphology or modulating cardiac contractility (Chen et al., 2018), and the role of blebbistatin in protecting against aminoglycoside-induced HC apoptosis has not been investigated yet.

In this study, we found that blebbistatin significantly reduced ROS accumulation and maintained mitochondrial function and thus prevented neomycin-induced apoptosis in HEI-OC-1 cells and explant-cultured cochlear HCs *in vitro*. Our results suggest that blebbistatin might serve as a new therapeutic drug for the prevention of aminoglycoside-induced HC loss.

MATERIALS AND METHODS

Animals

All animal procedures were performed according to protocols approved by the Animal Care and Use Committee of Southeast University. All efforts were made to use minimal animals and to prevent their suffering.

Whole Organ Explant Culture

Cochlear sensory epithelium was dissected from postnatal day (P)3 wild-type FVB mice and cultured in DMEM/F12 (Gibco, Gaithersburg, MD, USA, 11330-032) supplemented with 2% B27 (Invitrogen, Waltham, MA, USA, 17504044), 1% N-2 (Invitrogen, Waltham, MA, USA, 17502-048), and 50 μg/ml ampicillin (Sigma–Aldrich, St. Louis, MO, USA, P0781). In the experimental group, the cochleae were treated with 0.5 mM neomycin (Sigma–Aldrich, St. Louis, MO, USA, N6386-5G) and 1 μM blebbistatin (dissolved in DMSO, Boehringer Ingelheim Pharma GmbH, Biberach an der Riß, Germany) for 12 h and allowed to recover for another 12 h. Equivalent amounts of DMSO (Sigma–Aldrich, St. Louis, MO, USA, D8371) were added to the control and neomycin-only groups. The tissues were cultured at 37°C with 5% CO_2.

Cell Culture

HEI-OC-1 cells were divided into three groups and cultured in DMEM (Corning, Corning city, NY, USA, 10-013-CVC) supplemented with 10% FBS (Pansera, P30-2602) and 50 μg/ml ampicillin for 12 h. After this initial incubation, the experimental group was treated with 2 mM neomycin and 0.01 μM to 5 μM blebbistatin in 6-well plates, while the neomycin-only group was treated with 2 mM neomycin and an equivalent volume of DMSO in place of the blebbistatin. After another 24 h of culture, the cells were thoroughly washed with PBS and cultured in DMEM with ampicillin for an additional 12 h recovery. Control cells without neomycin or blebbistatin were treated with an equivalent volume of DMSO and incubated under identical conditions. Finally, the cells were imaged with an inverted phase-contrast microscope.

CCK-8 Assay

Cell death was measured using the Cell Counting CCK-8 Kit (Protein Biotechnology, CC201-01). Briefly, HEI-OC-1 cells were exposed to 2 mM neomycin in 96-well plates for 12 h. After removing the neomycin, the tissues were allowed to recover for another 12 h. Blebbistatin was added throughout the entire process in the experimental group, and an equivalent volume of DMSO was added in the neomycin-only group. All cells were then incubated with 10 μl of CCK-8 in each well for 30 min at 37°C, and a microtiter plate reader (Bio-Rad) was used to measure the optical densities at 450 nm.

Immunofluorescence

The antibodies and staining kits used in this article included the Live-Dead Cell Staining Kit (Biovision, Milpitas, CA, USA, K501-100), stained with fluorescein diacetate (FDA, green) and propidium iodide (PI, red), TUNEL BrightRed

Apoptosis Detection Kit (Vazyme, A113-01), anti-cleaved-caspase-3 antibody (Cell Signaling Technology, Danvers, MA, USA, 9664S), Mito-SOX Red (Life Technologies, Carlsbad, CA, USA, M36008), anti-Ctbp2 (BD Biosciences, San Jose, CA, USA, 612044), anti-myosin7a antibody (Proteus Bioscience, #25-6790, 1:1,000 dilution), Alexa Fluor 647 donkey anti-goat IgG (H + L; Invitrogen, Waltham, MA, USA, A-21447, 1:500 dilution), Alexa Fluor 555 donkey anti-rabbit IgG (H + L; Invitrogen, Waltham, MA, USA, A-31572, 1:500 dilution), and DAPI (Solarbio, C0060, 1:1,000 dilution).

Except for the staining kits, the cells or tissues were incubated with 4% paraformaldehyde (Sigma–Aldrich, St. Louis, MO, USA, 158127) for 1 h and then washed three times with PBST [1× PBS with 0.1% Triton X-100 (Solarbio, 1109F0521)] and incubated for 1 h in blocking medium (PBS with 10% heat-inactivated donkey serum, 1% Triton X-100, 1% BSA, and 0.02% sodium azide at pH 7.2) at room temperature. The samples were marked with primary antibody diluted in PBT-1 (PBS with 10% Triton X-100, 5% heat-inactivated donkey serum, 1% BSA, and 0.02% sodium azide at pH 7.2) for 8 h at 4°C. After washing three times with PBST, the samples were marked with the secondary antibody diluted in PBT-2 (PBS with 1% BSA and 0.1% Triton X-100 at pH 7.2) for 1 h. The samples were washed again three times with PBST and mounted on slides. The samples were imaged with an LSM700 confocal microscope.

Flow Cytometry

An Annexin V-FITC Kit (Beyotime, C1062) was used to detect the apoptotic cells. For determining mitochondrial membrane potential (MMP) and analyzing ROS production, cells were stained using the TMRE Mitochondrial Membrane Potential Assay Kit (Abcam, Cambridge, UK, ab113852) and MitoTracker® Red CMXRos (Yeasen, 40741ES50) and analyzed by flow cytometry (FACSCanto, BD) within 1 h.

PCR

RNA was extracted using TRIzol reagent (Protein Biotechnology), and cDNA was reversed transcribed with the RevertAid First Strand cDNA synthesis kit (Thermo Fisher Scientific, Waltham, MA, USA). For quantitative polymerase chain reaction (qPCR), SYBR Green (Roche, Basel, Switzerland, 17747200) was used on a real-time PCR apparatus (CFX96, Bio-Rad). *Gapdh* was used as the reference endogenous gene.

Gene	Forward sequence (5′–3′)	Reverse sequence (5′–3′)
Gapdh	AGGTCGGTGTGAACGGATTTG	TGTAGACCATGTAGTTGPAGGTCA
Bax	TGAAGACAGGGGCCTTTTTG	AATTCGCCGGAGACACTCG
Casp3	ATGGAGAACAACAAAACCTCAGT	TTGCTCCCATGTATGGTCTTTAC
NF-κB	ATGGCAGATGATCCCTAC	TGTTGACAGTGGTATTTCTGGTG
Bcl-2	ATGCTTTGTGGAACTATATGGC	GGTATGCACCCAGAGTGATGC
Gsr	TGCACTTCCCGGTAGGAAAC	GATCGCAACTGGGGTGAGAA
Sodl	AACCAGTTGTGTTGTCAGGAC	CCACCATGTTTCTTAGAGTGAGG
Nqo1	AGGATGGGAGGTACTCGAATC	AGGCGTCCTTCCTTATATGCTA
Alox15	GGCTCCAACAACGAGGTCTAC	AGGTATTCTGACACATCCACCTT

Statistical Analysis

All experiments were repeated at least three times, and the data are shown as the mean ± SD. All statistical analyses were conducted using Microsoft Excel and GraphPad Prism 7. Two-tailed, unpaired student's *t*-tests were used to determine statistical significance when comparing two groups, and one-way ANOVA followed by a Dunnett multiple comparisons test was used when comparing more than two groups. $P < 0.05$ was considered statistically significant.

RESULTS

Blebbistatin Treatment Significantly Increased the Viability of HC-Like HEI-OC-1 Cells After Neomycin Exposure

To determine the protective effect of blebbistatin in HC-like HEI-OC-1 cells, the cells were pre-treated with different doses of blebbistatin for 12 h before neomycin exposure. We then treated the HEI-OC-1 cells with 2 mM neomycin together with blebbistatin for 24 h and measured the survival of HEI-OC-1 cells using the CCK-8 kit (**Figure 1A**). Survival decreased significantly after 2 mM neomycin exposure, and blebbistatin protected against neomycin-induced cell death (**Figures 1B,C**). The CCK-8 results showed that the viability gradually increased with low concentrations of blebbistatin, but once the concentration of blebbistatin was higher than 2 μM, the viability of HEI-OC-1 cells began to decrease (**Figure 1D**). Cell morphology was significantly altered with 2 μM blebbistatin (**Figure 1B**), so we chose 1 μM blebbistatin pre-treatment for 12 h as the treatment condition in the rest of this study. To confirm this finding, we measured the percentage of live and dead cells in the control group, neomycin-only group, and blebbistatin group using the live-dead cell staining kit. Blebbistatin treatment significantly reduced cell death caused by neomycin exposure (**Figures 1C,E**). At the same time, we used myosin7a to label the HEI-OC-1 cells and found that compared with the neomycin-only group, living cells morphology in blebbistatin group is more similar to the control group (**Supplementary Figure S1**).

Blebbistatin Treatment Reduced Neomycin-Induced Cochlear HC Loss in Whole-Organ Explant Cultures *in vitro*

To determine the effect of blebbistatin in protecting cochlear HCs after neomycin damage, we used whole-organ explant cultures. Consistent with our previous studies (Guan et al., 2016; He et al., 2017), we dissected the cochleae from P3 wild-type mice, and the cultured cochleae were pre-treated with 1 μM blebbistatin for 12 h before neomycin damage. We then treated the cultured cochleae with 0.5 mM neomycin together with blebbistatin for 12 h (**Figure 2A**). Consistent with the

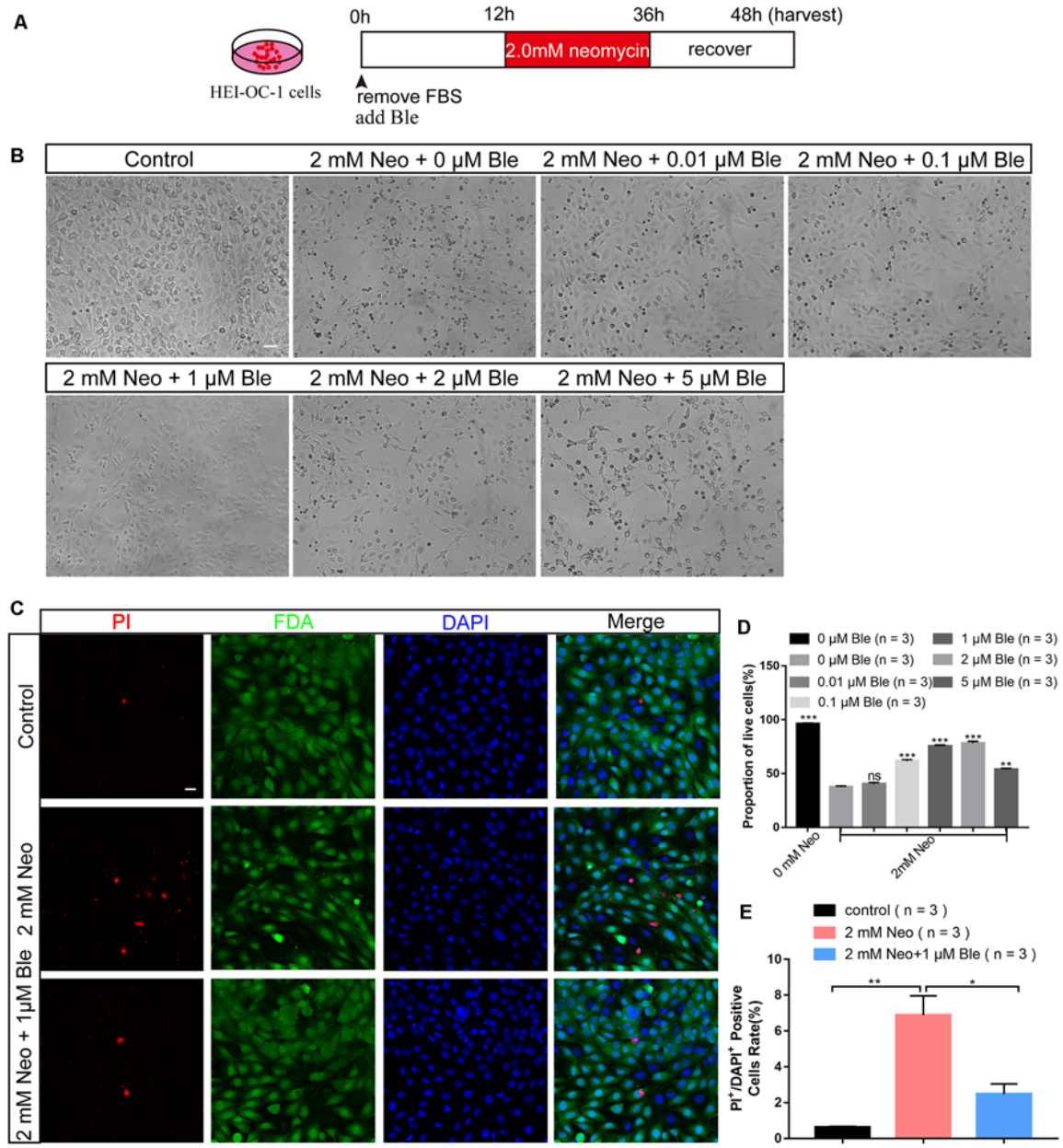

FIGURE 1 | Blebbistatin significantly enhanced the viability of HEI-OC-1 cells after neomycin exposure. **(A)** Schematic diagram of blebbistatin (Ble) and neomycin addition in cell culture. **(B)** The survival of hair cell (HC)-like HEI-OC-1 cells cultured under the same conditions with different concentrations of blebbistatin. Scale bars = 100 μm. **(C)** Images of HEI-OC-1 cells stained with FDA (green) and PI (red). Scale bars = 20 μm. **(D)** The result of the CCK-8 assay. **(E)** The proportions of live and dead cells in **(D)**. $^{*}p < 0.05$, $^{**}p < 0.01$, $^{***}p < 0.001$, ns, no significant.

results in HEI-OC-1 cells, immunofluorescence staining with a myosin7a antibody and DAPI showed that the myosin7a-positive HC numbers of the middle and basal turns of the cochlea were significantly decreased after neomycin exposure, while blebbistatin treatment significantly increased the HC number compared to the neomycin-only group (**Figures 2B–D**). Consistent with previous reports (Li A. et al., 2018), the neomycin-induced HC loss was mainly in the middle and basal turns of the cochlea, and no significant differences were seen in the apical turn in the blebbistatin group, neomycin-only group, and control group (**Figure 2E**).

Blebbistatin Treatment Significantly Decreased Apoptosis in HEI-OC-1 Cells After Neomycin Exposure

To determine the effect of blebbistatin on HEI-OC-1 cell apoptosis after neomycin exposure, we measured the percentage

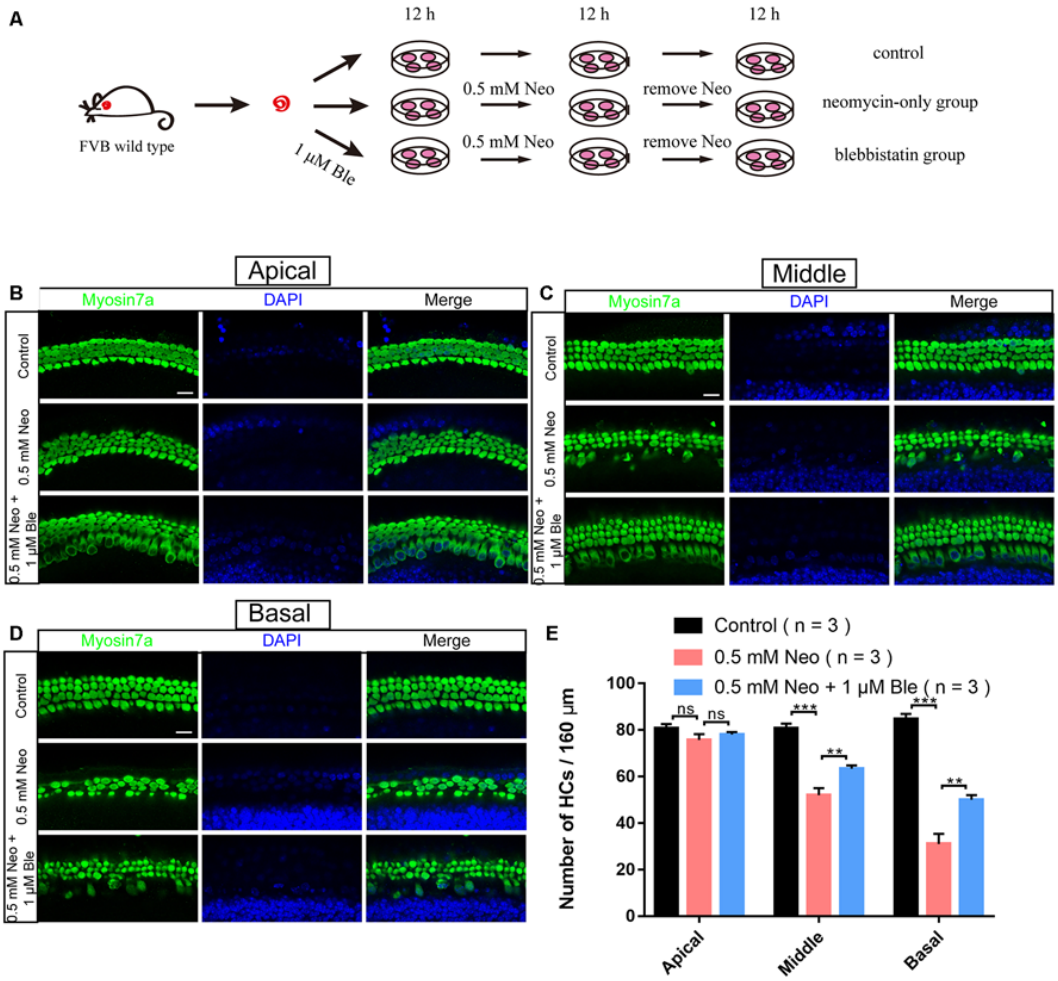

FIGURE 2 | Blebbistatin promoted HC survival in the cochlea after neomycin exposure. **(A)** Schematic diagram of drug addition in tissue culture. **(B–D)** HCs in the apical **(B)**, middle **(C)**, and basal turns **(D)** of the cochlea were stained with anti-myosin7a antibody in the control, 0.5 mM neomycin, and 0.5 mM neomycin + 1 μM blebbistatin groups. **(E)** Quantification of the number of myosin7a-positive cells in the apical, middle, and basal turns of the cochlea. $^{**}p < 0.01$, $^{***}p < 0.001$, ns, no significant. Scale bars = 16 μm.

of cell death and cell apoptosis using flow cytometry. We used propidium iodide to label the dead cells and Annexin V to label the cells undergoing apoptosis and showed that the cells pre-treated with 1 μM blebbistatin had a significantly lower rate of apoptosis compared to the neomycin-only group (**Figures 3A,B**).

To confirm the effect of blebbistatin on inhibiting HEI-OC-1 cell apoptosis, we used TUNEL staining and a cleaved-caspase-3 antibody. The numbers of both TUNEL-positive and cleaved-caspase-3-positive cells in the neomycin-only group were significantly greater than the control group (**Figures 3C,D**), while pre-treatment with 1 μM blebbistatin significantly reduced the proportions of TUNEL-positive and cleaved-caspase-3-positive cells after neomycin exposure (**Figures 3E,F**).

Our qPCR results also showed that the expression of pro-apoptotic genes like *Casp3* and *Bax* were significantly decreased in HEI-OC-1 cells pre-treated with 1 μM blebbistatin, while the expression of the anti-apoptotic genes *Bcl-2* and *NF-kB* were significantly increased in the blebbistatin pre-treated group compared to the neomycin-only group (**Figure 3G**). Together, our results suggest that blebbistatin protects HEI-OC-1 cells against neomycin exposure by inhibiting neomycin-induced apoptosis.

Blebbistatin Treatment Reduced Neomycin-Induced Apoptosis of Cochlear HCs in Whole-Organ Explant Cultures *in vitro*

To verify the effects of blebbistatin on neomycin-induced HC loss in whole-organ explant cultures, we also stained the explant-cultured cochleae for TUNEL and cleaved-caspase-3 after blebbistatin treatment and neomycin exposure. Consistent with the results in HEI-OC-1 cells, the numbers of both TUNEL-positive and cleaved-caspase-3–positive HCs were significantly increased in the neomycin-only group

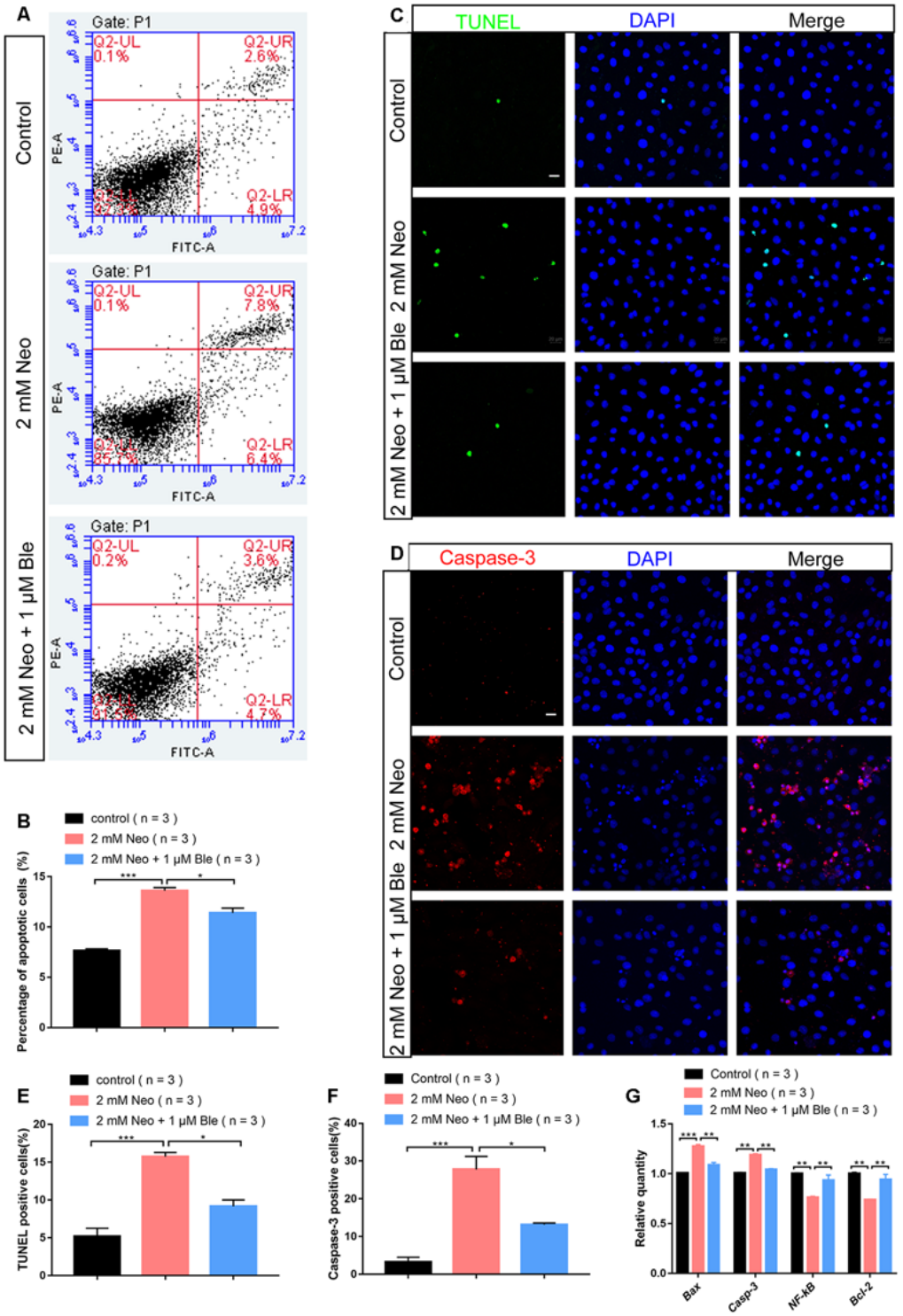

FIGURE 3 | Blebbistatin reduced neomycin-induced apoptosis in HEI-OC-1 cells. **(A)** TUNEL staining showing the apoptotic HEI-OC-1 cells after different treatments. The TUNEL-positive apoptotic cells increased in the neomycin-only group compared with the controls and decreased in the 2 mM neomycin + 1 μM blebbistatin group compared with the neomycin-only group. **(B)** Cleaved-caspase-3 and DAPI double staining showing the apoptotic HEI-OC-1 cells after the different treatments. **(C)** Apoptosis analysis by flow cytometry after different treatments. **(D)** Quantification of the flow cytometry results. **(E)** Quantification of the numbers of TUNEL/DAPI double-positive cells in panel (**A**). **(F)** Quantification of the numbers of Caspase-3/DAPI double-positive cells in panel (**B**). **(G)** Quantitative polymerase chain reaction (qPCR) results showing the expression of pro-apoptotic factors like *caspase-3* and *Bax* and anti-apoptotic factors like *Bcl-2* and *NF-kB* after neomycin and blebbistatin treatment. $^{*}p < 0.05$, $^{**}p < 0.01$, $^{***}p < 0.001$. Scale bars = 20 μm.

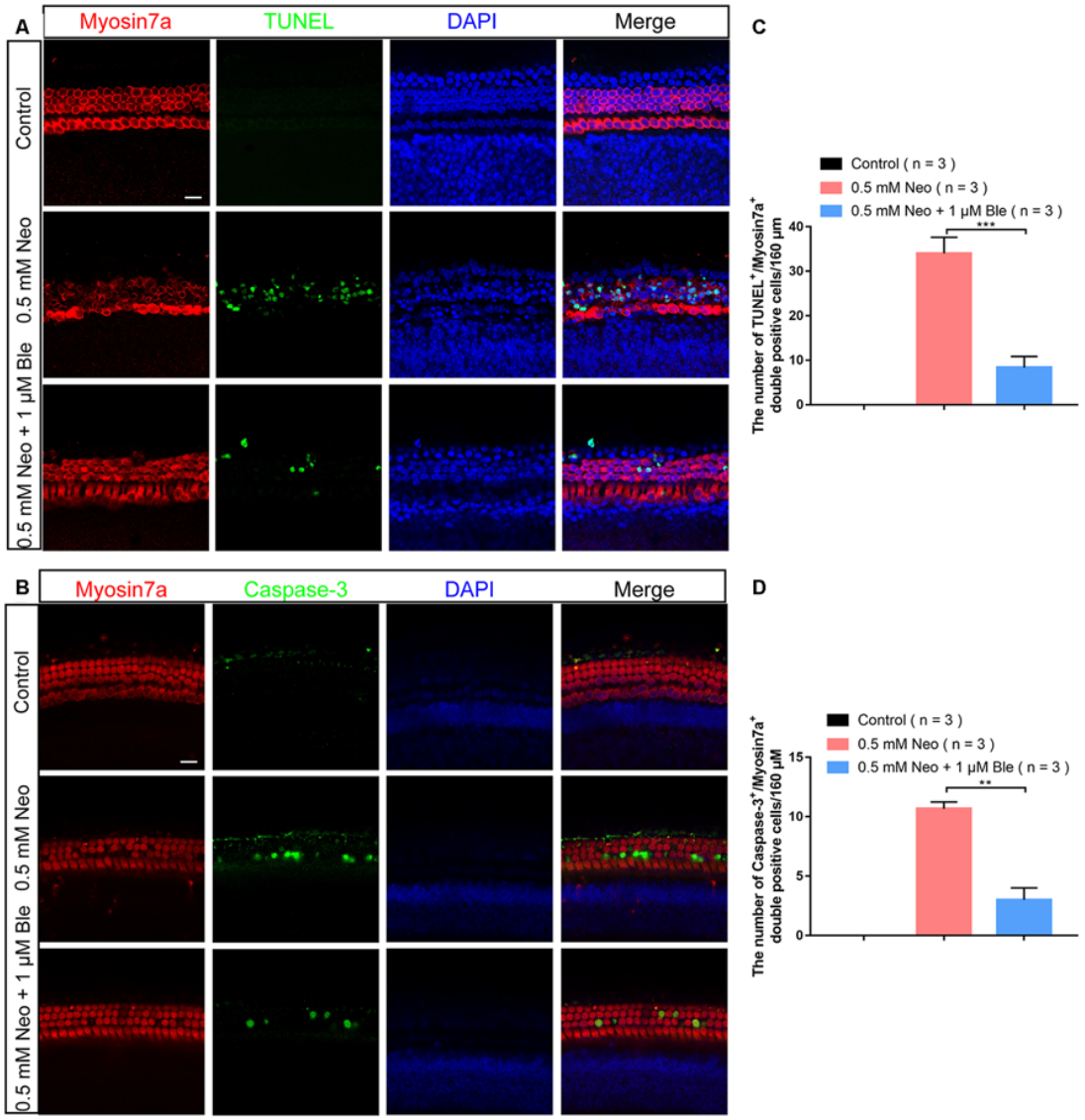

FIGURE 4 | Neomycin-induced HC apoptosis decreased after treatment with blebbistatin. **(A)** The number of TUNEL-positive cells decreased in the 0.5 mM neomycin + 1 μM blebbistatin group compared with the neomycin-only group (middle turns). **(B)** The number of cleaved caspase-3-positive cells decreased in the 0.5 mM neomycin + 1 μM blebbistatin group compared with the neomycin-only group (middle turns). **(C)** Quantification of the numbers of TUNEL/myosin7a double-positive cells in panel (**A**). **(D)** Quantification of the numbers of cleaved caspase-3/myosin7a double-positive cells in panel (**B**). $^{**}p < 0.01$, $^{***}p < 0.001$. Scale bars = 16 μm.

compared to the control group (**Figures 4A–D**). Blebbistatin treatment reduced neomycin-induced HC apoptosis, and the proportions of TUNEL-positive and cleaved-caspase-3-positive HCs were significantly lower after pre-treatment with 1 μM blebbistatin (**Figures 4A–D**).

Blebbistatin Treatment Significantly Increased the MMP of HEI-OC-1 Cells After Neomycin Exposure

Mitochondria are the main site of cellular ROS production, and the production of ROS occurs mainly in the mitochondrial oxidative respiratory chain. Thus, mitochondrial structural and functional disorders can lead to mitochondrial ROS accumulation, which is the main inducer of apoptosis (Liu and Yan, 2007). To investigate the mechanism through which blebbistatin prevents neomycin-induced apoptosis, the TMRE kit was used to evaluate changes in the MMP of HEI-OC-1 cells using flow cytometry analysis and immunofluorescence staining (Samudio et al., 2005). The MMP of HEI-OC-1 cells was significantly lower after 2 mM neomycin exposure, while HEI-OC-1 cells pre-treated with 1 μM blebbistatin had significantly greater TMRE intensity compared to the neomycin-only group (**Figures 5A–C**). These results suggest

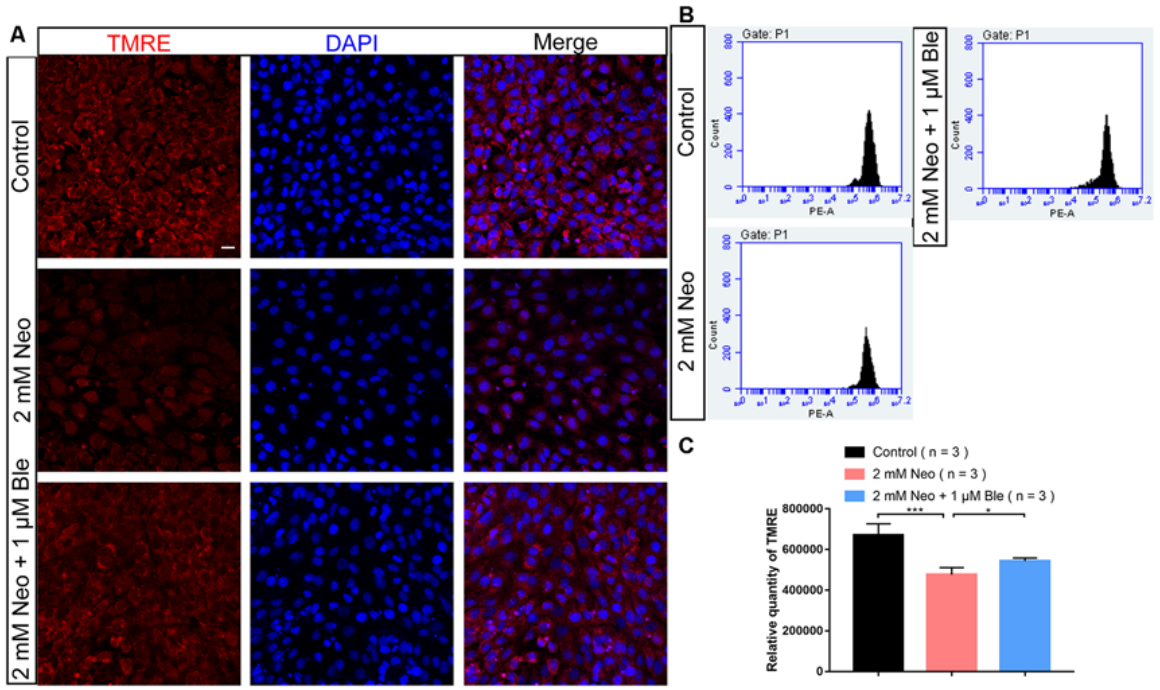

FIGURE 5 | Blebbistatin maintains the mitochondrial membrane potential (MMP) after neomycin exposure. **(A)** HEI-OC-1 cells were labeled using the TMRE staining kit. **(B)** The analysis of MMP by flow cytometry showing that the TMRE intensity was reduced after 2 mM neomycin treatment for 24 h compared with the undamaged controls and that the TMRE intensity in the 2 mM neomycin + 1 μM blebbistatin group was increased significantly compared with the neomycin-only group. **(C)** Quantification of the data in panel **(B)**. $^{*}p < 0.05$, $^{***}p < 0.001$. Scale bars = 20 μm.

that blebbistatin prevents neomycin-induced mitochondrial dysfunction in HEI-OC-1 cells.

Blebbistatin Treatment Significantly Attenuated Neomycin-Induced Oxidative Stress in HEI-OC-1 Cells

Recent studies have demonstrated that the production of ROS by the mitochondria is the major cause of aminoglycoside-induced HC apoptosis (Huang et al., 2000; Balaban et al., 2005). Mito-SOX Red has been reported to selectively detect mitochondrial superoxide (Kalyanaraman et al., 2017), and here we also used Mito-SOX Red to detect mitochondrial ROS levels in HEI-OC-1 cells by immunofluorescence staining and flow cytometry analysis. Neomycin exposure significantly increased the ROS levels, while the HEI-OC-1 cells pre-treated with 1 μM blebbistatin had significantly lower ROS levels compared with the neomycin-only cells (**Figures 6A–C**).

To confirm this result, the expression levels of oxidant genes were also measured using qPCR. We found that after neomycin exposure, the HEI-OC-1 cells pre-treated with 1 μM blebbistatin had significantly higher expression levels of the antioxidant genes *Gsr*, *Alox15*, and *Sod1* compared to the neomycin-only cells (**Figure 6D**). Together, our data demonstrated that blebbistatin treatment significantly increased antioxidant gene expression and prevented the accumulation of mitochondrial ROS in HEI-OC-1 cells and thus protected HEI-OC-1 cells against neomycin-induced apoptosis.

Blebbistatin Treatment Significantly Reduced Neomycin-Induced Oxidative Stress in Cultured Cochlear HCs

To determine the protective mechanism of blebbistatin in cochlear HCs in whole-organ explant cultures, we also stained the cultured cochleae with Mito-SOX Red to detect mitochondrial ROS levels in HCs after blebbistatin treatment and neomycin damage. Consistent with the results in HEI-OC-1 cells, we found that neomycin exposure significantly increased HC loss and ROS levels, while blebbistatin treatment significantly reduced the HC loss and ROS levels compared to the neomycin-only group (**Figures 7A,B**).

Blebbistatin Protects the Synapses Between Hair Cells and Spiral Ganglion Neurons

To confirm whether blebbistatin can protect the synapses between HCs and cochlear spiral ganglion neurons, we used Ctbp2 to label the synapses of the HCs and found that the number of HCs' synapse decreased significantly in the neomycin group compared with the blebbistatin group and the control group (**Figures 8A,B**). These results suggest that blebbistatin prevents neomycin-induced synaptic damage in HCs.

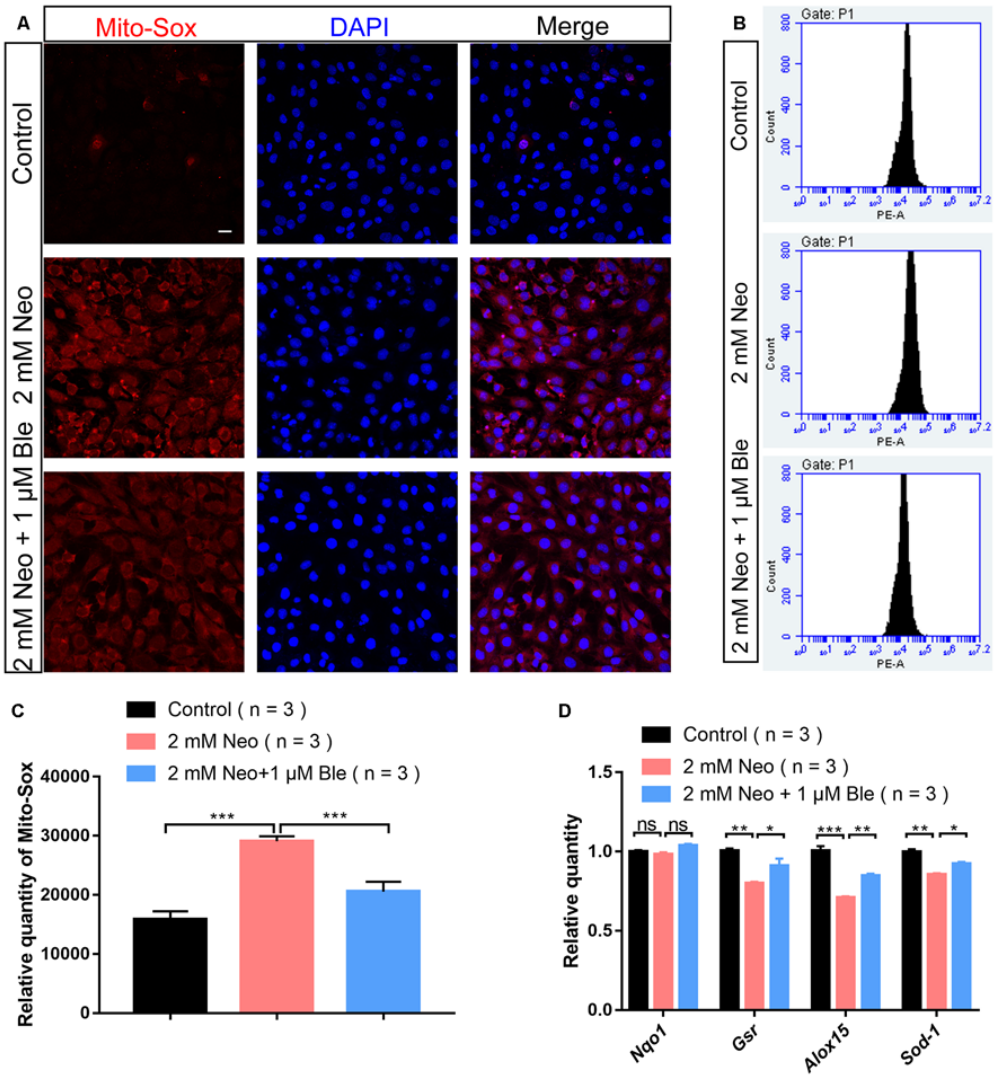

FIGURE 6 | Blebbistatin decreased reactive oxygen species (ROS) levels in HEI-OC-1 cells after neomycin injury. **(A)** The immunofluorescence intensity of Mito-SOX was increased after 2 mM neomycin treatment for 24 h compared with the undamaged controls, and Mito-SOX intensity was significantly reduced in the 2 mM neomycin + 1 μM blebbistatin group compared with the neomycin-only group. Scale bars = 20 μm. **(B)** Flow cytometry data showing the intensity of Mito-SOX in the control, neomycin-only, and 2 mM neomycin + 1 μM blebbistatin groups. **(C)** Quantification of the data in panel (**B**). **(D)** qPCR results showing the expression of the antioxidant genes *Gsr, Sod1, Alox15*, and *Nqo1* after neomycin and blebbistatin treatment. $^{*}p < 0.05$, $^{**}p < 0.01$, $^{***}p < 0.001$, ns, no significant. Scale bars = 16 μm.

DISCUSSION

Ototoxic side effects limit the clinical application of aminoglycoside antibiotics (Durante-Mangoni et al., 2009; Zimmerman and Lahav, 2013). Aminoglycosides can produce a large number of highly toxic ROS, and this occurs mainly in the organ of Corti, which is the main sensory organ for hearing (Nadol, 1993). Under physiological conditions, the ROS produced by mitochondrial metabolism are removed by the antioxidant mechanisms of the HC. However, aminoglycoside exposure increases ROS production in the cochlear HCs, and the excess ROS overwhelm the cellular defense mechanisms and eventually trigger apoptosis in HCs (Chen et al., 2015; Quan et al., 2015; Esterberg et al., 2016). Therefore, finding effective ways to reduce cellular ROS production in HCs is the key to preventing aminoglycoside-induced ototoxicity and is a main focus in the hearing research field.

Blebbistatin is a myosin II inhibitor, and it regulates microtubule assembly and myosin–actin interactions. The activity of blebbistatin on the cytoskeleton has been shown to be involved in the regulation of cell structure, morphology (Yoon et al., 2019), and migration (Hu et al., 2019; Wang et al., 2019) and to maintain the survival and growth of stem cells (Zhao et al., 2015) and to reduce oxidative stress-induced apoptosis. Blebbistatin protects Lgr5+ stem cells against colitis-induced epithelium injury in gastrointestinal tissues

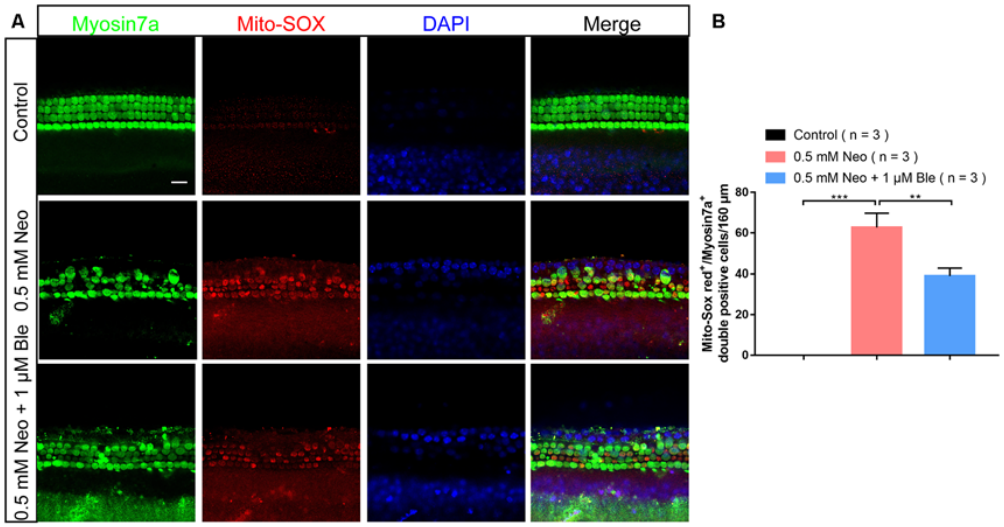

FIGURE 7 | Blebbistatin decreased ROS levels in cochlear HCs after neomycin injury. **(A)** The immunofluorescence intensity of Mito-SOX was increased after 0.5 mM neomycin treatment for 12 h compared with the undamaged controls, and Mito-SOX intensity was significantly reduced in the 0.5 mM neomycin + 1 μM blebbistatin group compared with the neomycin-only group. **(B)** Quantification of the numbers of Mito-SOX/myosin7a double-positive cells in A. $^{**}p < 0.01$, $^{***}p < 0.001$. Scale bars = 16 μm.

through the Myh9-Rac1-PAK1-Akt pathway (Zhao et al., 2015) and induces cell migration through myosin-II-related matrix stretch and recoil (Vicente-Manzanares et al., 2009). Blebbistatin has also been reported to inhibit apoptosis by reducing the accumulation of ROS in neuronal tissues (Wang et al., 2017). The interconnections and differences in these effects in various cells and tissues are also of interest and need to be explored further.

To explore the effects of blebbistatin in protecting against neomycin-induced damage, we used HC-like HEI-OC-1 cells and cochlear whole-organ explant cultures *in vitro*. Results in both systems showed that blebbistatin significantly reduced mitochondrial ROS accumulation and inhibited cell apoptosis, thus preventing the neomycin-induced apoptotic cell death of HEI-OC-1 cells and cultured cochlear HCs. Cochlear whole-organ explant cultures showed that blebbistatin protected against neomycin-induced HC loss in the middle and basal turns of the cochlea, while the damage in the apical turn was only mild and thus no protection by blebbistatin was observed. This was because aminoglycosides are preferentially localized at the base of cochlea, and both the aminoglycoside concentration and the extent of HC damage form a decreasing gradient from the base to the apex (Karasawa et al., 2008; Marcotti et al., 2010). Moreover, aminoglycoside-induced hearing loss also shows a decreasing gradient from high frequency to low frequency, which is consistent with the HC damage occurring primarily in the base and decreasing towards the apex (Chen et al., 2015; Guo et al., 2019). Because basal HCs are more sensitive to neomycin, we have paid the most attention to the protection of HCs in the basal turn.

We also found that the protective effect of blebbistatin is dose dependent, and 1 μM blebbistatin had significantly greater protective effects than 0.1 μM blebbistatin (**Figures 1A–D**). A similar level of protection was seen for 2 μM blebbistatin,

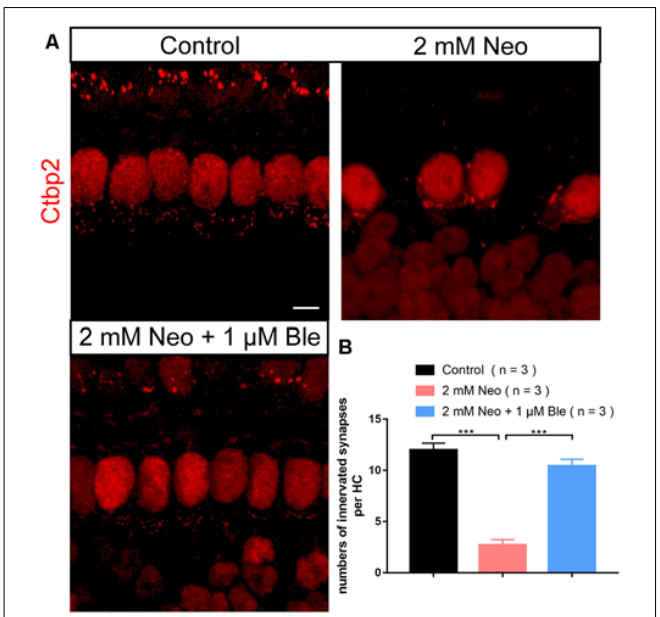

FIGURE 8 | Pre-synapse staining of the HCs. **(A)** The presynaptic marker Ctbp2 was used to label the ribbon synapses on HCs. **(B)** Quantification of the presynaptic number in HCs. $^{***}p < 0.001$. Scale bar = 5 μm.

but at 5 μM, the protective effect began to decline, suggesting that high concentrations of blebbistatin might damage HCs. Previous studies also showed that at concentrations higher than 1 μM, blebbistatin shows toxic effects in cardiomyocytes (Li F. et al., 2018). Also, in the concentration range of 0.5–5 μM, blebbistatin preferentially blocks the connection between myosin and actin (Kovács et al., 2004), and in neurons, 1 μM blebbistatin treatment maintains the cellular structure after H_2O_2 exposure

(Wang et al., 2017). Thus, in this study we used 1 μM blebbistatin in both the HC-like HEI-OC-1 cells and the cochlear whole-organ explant cultures.

ROS accumulation and mitochondrial dysfunction have been reported to be involved in HC apoptosis (Hu et al., 2008; He et al., 2016). ROS accumulation leads to mitochondrial depolarization, which results in a decrease in the MMP and the subsequent release of apoptotic factors. Under physiological conditions, spontaneous generation and elimination keep the ROS level stable, and this is regulated by numerous antioxidant and oxidant genes. This study found that blebbistatin significantly increased the expression of the antioxidant genes *Gsr*, *Sod1*, and *Alox15* after neomycin exposure, which significantly decreased the ROS levels and increased the MMP in HEI-OC-1 cells. Our results suggest that blebbistatin is an effective drug in reducing the ROS level and maintaining mitochondrial function after neomycin exposure. This is consistent with observations in myocardial and other nucleated cells that blebbistatin protects mitochondrial function by stabilizing the morphology of the cytoskeleton and that it reduces ROS accumulation in order to prevent apoptosis (Lang et al., 2011; Wang et al., 2017; Li F. et al., 2018; Miura et al., 2018).

Regarding plasticity and reconstruction of neural network after hearing injury, Ctpb2 was usually used to label the synapse, and the number of innervated synapses was compared to assess the structure and function of neural connections (Zhang et al., 2019). Our results suggest that blebbistatin has a good protective effect on synaptic damage caused by neomycin in HCs.

Compared to other drugs known to reduce HC damage caused by aminoglycosides, we think that blebbistatin can reduce the accumulation of ROS more stably and efficiently. But it has to be pointed out that high concentrations of blebbistatin correspond to the low efficiency of treatment and change the normal shape of cells to some extent. Drug dosage is essential to be fully considered for future animal or human experiments.

In conclusion, our results suggest that blebbistatin can maintain the balance of oxidant and anti-oxidant gene expression and reduce the accumulation of ROS and thus maintain mitochondrial function and prevent apoptosis in HEI-OC-1 cells and cultured cochlear HCs after neomycin exposure. These results suggest that blebbistatin might have potential clinical application in preventing aminoglycoside-induced HC loss and subsequent hearing loss, and we will further investigate its protective mechanism and clinical application in future studies.

DATA AVAILABILITY STATEMENT

The raw data supporting the conclusions of this article will be made available by the authors, without undue reservation, to any qualified researcher.

ETHICS STATEMENT

The animal study was reviewed and approved by Animal Care and Use Committee of Southeast University.

AUTHOR CONTRIBUTIONS

All authors listed have made a substantial, direct and intellectual contribution to the work, and approved it for publication.

FUNDING

This work was supported by grants from the National Key R&D Program of China (2017YFA0103903), the Strategic Priority Research Program of the Chinese Academy of Science (XDA16010303), Innovative Research Group Project of the National Natural Science Foundation of China (81970884, 81900941, 81900944, 81622013, 81970882, 81570919, 81870721, 81771019, 81700913, 81670928, and 81570921), Jiangsu Province Natural Science Foundation (BK20190121), Boehringer Ingelheim Pharma GmbH, and the Project of Invigorating Health Care Through Science, Technology and Education, and K. C. Wong Education Foundation.

The authors declare that this study received funding from Boehringer Ingelheim Pharma. The funder was not involved in the study design, collection, analysis, interpretation of data, the writing of this article, or the decision to submit it for publication.

SUPPLEMENTARY MATERIAL

The Supplementary Material for this article can be found online at: https://www.frontiersin.org/articles/10.3389/fncel.2019.00590/full#supplementary-material.

REFERENCES

Balaban, R. S., Nemoto, S., and Finkel, T. (2005). Mitochondria, oxidants, and aging. *Cell* 120, 483–495. doi: 10.1016/j.cell.2005.02.001

Becker, B., and Cooper, M. A. (2013). Aminoglycoside antibiotics in the 21st century. *ACS Chem. Biol.* 8, 105–115. doi: 10.1021/cb3005116

Chen, Y., Li, L., Ni, W., Zhang, Y., Sun, S., Miao, D., et al. (2015). Bmi1 regulates auditory hair cell survival by maintaining redox balance. *Cell Death Dis.* 6:e1605. doi: 10.1038/cddis.2014.549

Chen, P., Xu, D. Q., Xu, S. L., Xiao, H., Wan, S. H., Wang, X. H., et al. (2018). Blebbistatin modulates prostatic cell growth and contrapctility through myosin II signaling. *Clin. Sci.* 132, 2189–2205. doi: 10.1042/cs20180294

Coffin, A. B., Rubel, E. W., and Raible, D. W. (2013). Bax, Bcl2, and p53 differentially regulate neomycin- and gentamicin-induced hair cell death in the zebrafish lateral line. *J. Assoc. Res. Otolaryngol.* 14, 645–659. doi: 10.1007/s10162-013-0404-1

Durante-Mangoni, E., Grammatikos, A., Utili, R., and Falagas, M. E. (2009). Do we still need the aminoglycosides? *Int. J. Antimicrob. Agents* 33, 201–205. doi: 10.1016/j.ijantimicag.2008.09.001

Esterberg, R., Linbo, T., Pickett, S. B., Wu, P., Ou, H. C., Rubel, E. W., et al. (2016). Mitochondrial calcium uptake underlies ROS generation during aminoglycoside-induced hair cell death. *J. Clin. Invest.* 126, 3556–3566. doi: 10.1172/jci84939

Guan, M., Fang, Q., He, Z., Li, Y., Qian, F., Qian, X., et al. (2016). Inhibition of ARC decreases the survival of HEI-OC-1 cells after neomycin

damage *in vitro*. *Oncotarget* 7, 66647–66659. doi: 10.18632/oncotarget.11336

Guo, J., Chai, R., Li, H., and Sun, S. (2019). Protection of hair cells from ototoxic drug-induced hearing loss. *Adv. Exp. Med. Biol.* 1130, 17–36. doi: 10.1007/978-981-13-6123-4_2

He, Z., Guo, L., Shu, Y., Fang, Q., Zhou, H., Liu, Y., et al. (2017). Autophagy protects auditory hair cells against neomycin-induced damage. *Autophagy* 13, 1884–1904. doi: 10.1080/15548627.2017.1359449

He, Z., Sun, S., Waqas, M., Zhang, X., Qian, F., Cheng, C., et al. (2016). Reduced TRMU expression increases the sensitivity of hair-cell-like HEI-OC-1 cells to neomycin damage *in vitro*. *Sci. Rep.* 6:29621. doi: 10.1038/srep29621

Hu, B. H., Henderson, D., and Yang, W. P. (2008). The impact of mitochondrial energetic dysfunction on apoptosis in outer hair cells of the cochlea following exposure to intense noise. *Hear. Res.* 236, 11–21. doi: 10.1016/j.heares.2007.break11.002

Hu, X., Weston, T. A., He, C., Jung, R. S., Heizer, P. J., Young, B. D., et al. (2019). Release of cholesterol-rich particles from the macrophage plasma membrane during movement of filopodia and lamellipodia. *Elife* 8:e50231. doi: 10.7554/eLife.50231

Huang, T., Cheng, A. G., Stupak, H., Liu, W., Kim, A., Staecker, H., et al. (2000). Oxidative stress-induced apoptosis of cochlear sensory cells: otoprotective strategies. *Int. J. Dev. Neurosci.* 18, 259–270. doi: 10.1016/s0736-5748(99)00094-5

Jiang, M., Karasawa, T., and Steyger, P. S. (2017). Aminoglycoside-induced cochleotoxicity: a review. *Front. Cell. Neurosci.* 11:308. doi: 10.3389/fncel.2017.00308

Jiang, P., Ray, A., Rybak, L. P., and Brenner, M. J. (2016). Role of STAT1 and oxidative stress in gentamicin-induced hair cell death in organ of corti. *Otol. Neurotol.* 37, 1449–1456. doi: 10.1097/mao.0000000000001192

Kalyanaraman, B., Hardy, M., Podsiadly, R., Cheng, G., and Zielonka, J. (2017). Recent developments in detection of superoxide radical anion and hydrogen peroxide: opportunities, challenges, and implications in redox signaling. *Arch. Biochem. Biophys.* 617, 38–47. doi: 10.1016/j.abb.2016.08.021

Karasawa, T., Wang, Q., Fu, Y., Cohen, D. M., and Steyger, P. S. (2008). TRPV4 enhances the cellular uptake of aminoglycoside antibiotics. *J. Cell Sci.* 121, 2871–2879. doi: 10.1242/jcs.023705

Kovács, M., Tóth, J., Hetényi, C., Málnási-Csizmadia, A., and Sellers, J. R. (2004). Mechanism of blebbistatin inhibition of myosin II. *J. Biol. Chem.* 279, 35557–35563. doi: 10.1074/jbc.M405319200

Lang, E., Qadri, S. M., Zelenak, C., Gu, S., Rotte, A., Draeger, A., et al. (2011). Inhibition of suicidal erythrocyte death by blebbistatin. *Am. J. Physiol. Cell Physiol.* 301, C490–C498. doi: 10.1152/ajpcell.00043.2011

Li, F., Fan, X., Zhang, Y., Zhang, Y., Ma, X., Kou, J., et al. (2018). Inhibition of myosin IIA-actin interaction prevents ischemia/reperfusion induced cardiomyocytes apoptosis through modulating PINK1/Parkin pathway and mitochondrial fission. *Int. J. Cardiol.* 271, 211–218. doi: 10.1016/j.ijcard.2018.04.079

Li, H., Song, Y., He, Z., Chen, X., Wu, X., Li, X., et al. (2018). Meclofenamic acid reduces reactive oxygen species accumulation and apoptosis, inhibits excessive autophagy, and protects hair cell-like HEI-OC1 cells from cisplatin-induced damage. *Front. Cell. Neurosci.* 12:139. doi: 10.3389/fncel.2018.00139

Li, A., You, D., Li, W., Cui, Y., He, Y., Li, W., et al. (2018). Novel compounds protect auditory hair cells against gentamycin-induced apoptosis by maintaining the expression level of H3K4me2. *Drug Deliv.* 25, 1033–1043. doi: 10.1080/10717544.2018.1461277

Liu, L., Chen, Y., Qi, J., Zhang, Y., He, Y., Ni, W., et al. (2016). Wnt activation protects against neomycin-induced hair cell damage in the mouse cochlea. *Cell Death Dis.* 7:e2136. doi: 10.1038/cddis.2016.35

Liu, W., Xu, X., Fan, Z., Sun, G., Han, Y., Zhang, D., et al. (2019). Wnt signaling activates TIGAR and protects against cisplatin-induced spiral ganglion neuron damage in the mouse cochlea. *Antioxid. Redox Signal.* 30, 1389–1410. doi: 10.1089/ars.2017.7288

Liu, X. Z., and Yan, D. (2007). Ageing and hearing loss. *J. Pathol.* 211, 188–197. doi: 10.1002/path.2102

Marcotti, W., van Netten, S. M., and Kros, C. J. (2010). The aminoglycoside antibiotic dihydrostreptomycin rapidly enters mouse outer hair cells through the mechano-electrical transducer channels. *J. Physiol.* 567, 505–521. doi: 10.1113/jphysiol.2005.085951

Miura, M., Taguchi, Y., Handoh, T., Hasegawa, T., Takahashi, Y., Morita, N., et al. (2018). Regional increase in ROS within stretched region exacerbates arrhythmias in rat trabeculae with nonuniform contraction. *Pflugers Arch.* 470, 1349–1357. doi: 10.1007/s00424-018-2152-x

Nadol, J. B. Jr. (1993). Hearing loss. *N. Eng. J. Med.* 329, 1092–1102. doi: 10.1056/NEJM199310073291507

Quan, Y., Xia, L., Shao, J., Yin, S., Cheng, C. Y., Xia, W., et al. (2015). Adjudin protects rodent cochlear hair cells against gentamicin ototoxicity *via* the SIRT3-ROS pathway. *Sci. Rep.* 5:8181. doi: 10.1038/srep08181

Samudio, I., Konopleva, M., Hail, N. Jr., Shi, Y. X., McQueen, T., Hsu, T., et al. (2005). 2-cyano-3,12-dioxooleana-1,9-dien-28-imidazolide (CDDO-Im) directly targets mitochondrial glutathione to induce apoptosis in pancreatic cancer. *J. Biol. Chem.* 280, 36273–36282. doi: 10.1074/jbc.m507518200

Seidman, M. D., Khan, M. J., Bai, U., Shirwany, N., and Quirk, W. S. (2000). Biologic activity of mitochondrial metabolites on aging and age-related hearing loss. *Am. J. Otol.* 21, 161–167. doi: 10.1016/s0196-0709(00)80003-4

Sena, L. A., and Chandel, N. S. (2012). Physiological roles of mitochondrial reactive oxygen species. *Mol. Cell* 48, 158–167. doi: 10.1016/j.molcel.2012.09.025

Vicente-Manzanares, M., Ma, X., Adelstein, R. S., and Horwitz, A. R. (2009). Non-muscle myosin II takes centre stage in cell adhesion and migration. *Nat. Rev. Mol. Cell Biol.* 10, 778–790. doi: 10.1038/nrm2786

Wang, W. Y., Davidson, C. D., Lin, D., and Baker, B. M. (2019). Actomyosin contractility-dependent matrix stretch and recoil induces rapid cell migration. *Nat. Commun.* 10:1186. doi: 10.1038/s41467-019-09121-0

Wang, X., Ling, C. C., Li, L., Qin, Y., Qi, J., Liu, X., et al. (2016). MicroRNA-10a/10b represses a novel target gene mib1 to regulate angiogenesis. *Cardiovasc. Res.* 110, 140–150. doi: 10.1093/cvr/cvw023

Wang, Y., Xu, Y., Liu, Q., Zhang, Y., Gao, Z., Yin, M., et al. (2017). Myosin IIA-related actomyosin contractility mediates oxidative stress-induced neuronal apoptosis. *Front. Mol. Neurosci.* 10:75. doi: 10.3389/fnmol.2017.00075

Waqas, M., Sun, S., Xuan, C., Fang, Q., Zhang, X., Islam, I., et al. (2017). Bone morphogenetic protein 4 promotes the survival and preserves the structure of flow-sorted Bhlhb5+ cochlear spiral ganglion neurons *in vitro*. *Sci. Rep.* 7:3506. doi: 10.1038/s41598-017-03810-w

Yoon, C., Choi, C., Stapleton, S., Mirabella, T., Howes, C., Dong, L., et al. (2019). Myosin IIA-mediated forces regulate multicellular integrity during vascular sprouting. *Mol. Biol. Cell* 30, 1974–1984. doi: 10.1091/mbc.e19-02-0076

Yu, X., Liu, W., Fan, Z., Qian, F., Zhang, D., Han, Y., et al. (2017). c-Myb knockdown increases the neomycin-induced damage to hair-cell-like HEI-OC1 cells *in vitro*. *Sci. Rep.* 7:41094. doi: 10.1038/srep41094

Zhang, S., Zhang, Y., Dong, Y., Guo, L., Zhang, Z., Shao, B., et al. (2019). Knockdown of Foxg1 in supporting cells increases the trans-differentiation of supporting cells into hair cells in the neonatal mouse cochlea. *Cell. Mol. Life Sci.* doi: 10.1007/s00018-019-03291-2 [Epub ahead of print].

Zhao, B., Qi, Z., Li, Y., Wang, C., Fu, W., and Chen, Y. G. (2015). The non-mu scle-myosin-II heavy chain Myh9 mediates colitis-induced epithelium injury by restricting Lgr5+ stem cells. *Nat. Commun.* 6:7166. doi: 10.1038/ncomms8166

Zimmerman, E., and Lahav, A. (2013). Ototoxicity in preterm infants: effects of genetics, aminoglycosides, and loud environmental noise. *J. Perinatol.* 33, 3–8. doi: 10.1038/jp.2012.105

Conflict of Interest: The authors declare that the research was conducted in the absence of any commercial or financial relationships that could be construed as a potential conflict of interest.

frontiers in Cellular Neuroscience

ORIGINAL RESEARCH
published: 12 March 2020
doi: 10.3389/fncel.2020.00049

Isolation and Characterization of Neural Progenitor Cells From Bone Marrow in Cell Replacement Therapy of Brain Injury

Wen-fang Bai[1†], Yuling Zhang[2,3†], Weicheng Xu[1], Weikun Li[4], Meihui Li[5], Fengying Yuan[6], Xun Luo[7,8] and Mingsheng Zhang[1]*

[1]Department of Rehabilitation Medicine, Guangdong Provincial People's Hospital, Guangdong Academy of Medical Sciences, Guangdong Provincial Institute of Geriatrics, Guangzhou, China, [2]School of Medical Instrument and Food Engineering, The University of Shanghai for Science and Technology, Shanghai, China, [3]Stroke Biological Recovery Laboratory, Spaulding Rehabilitation Hospital, a Teaching Affiliate of Harvard Medical School, Charlestown, MA, United States, [4]Department of Rehabilitation Medicine, Zengcheng District People's Hospital of Guangzhou, Guangzhou, China, [5]Department of Rehabilitation Medicine, The First Affiliated Hospital of Guangdong Pharmaceutical University, Guangzhou, China, [6]Department of Rehabilitation Medicine, Guangdong Provincial Hospital of Integrated Traditional Chinese and Western Medicine, Foshan, China, [7]Kerry Rehabilitation Medicine Research Institute, Shenzhen, China, [8]Shenzhen Sanming Project Group, Spaulding Rehabilitation Hospital, a Teaching Affiliate of Harvard Medical School, Charlestown, MA, United States

OPEN ACCESS

Edited by:
Zhang Pengyue,
Yunnan University of Traditional Chinese Medicine, China

Reviewed by:
Xingping Qin,
Renmin Hospital of Wuhan University, China
Yunyuan Li,
University of British Columbia, Canada

****Correspondence:***
Mingsheng Zhang
mszrch@163.com

[†]These authors have contributed equally to this work

Received: *18 December 2019*
Accepted: *21 February 2020*
Published: *12 March 2020*

Citation:
Bai W, Zhang Y, Xu W, Li W, Li M, Yuan F, Luo X and Zhang M (2020) Isolation and Characterization of Neural Progenitor Cells From Bone Marrow in Cell Replacement Therapy of Brain Injury. Front. Cell. Neurosci. 14:49. doi: 10.3389/fncel.2020.00049

Many studies supported that bone marrow mesenchymal stem cells (BM-MSCs) can differentiate into neural cells, but few researchers detected mature and function of nerve cells, especially *in vivo* study. Some researchers even suggested that BM-MSCs transplantation would not be able to differentiate into functional neural cells. To figure out the dispute, this study examined bone marrow-derived sphere-like cells, harvested *via* neural stem cell suspension culture, then identified as bone marrow-derived neural progenitor cells (BM-NPCs) by finding the expression of neural progenitor cells genes and proteins, neural progenitor cells characteristic and nerve cell differentiation induced through both methods. Moreover, BM-NPCs transplantation showed long-term survival and improved the ethological and histological indexes of brain injury rats, demonstrating functional nervous cells differentiated from BM-NPCs. These *in vitro* and *in vivo* results confirmed BM-NPCs differentiating into mature and functional nerve cells. This study provided valuable experimental data for BM-NPCs, suggesting a potential alternative treatment of central nervous injury disease.

Keywords: mesenchymal stem cells, bone marrow-derived neural progenitor cells, nerve cells, differentiation, cell transplantation

INTRODUCTION

Research on stem cells and regenerative medicine is the most popular in current life science frontiers (Chen et al., 2019; Dupont et al., 2019; Stoddard-Bennett and Reijo Pera, 2019; Yamada et al., 2019). Differentiating into functional neural cells plays an important role in the neural network plasticity after brain injury. The stem cell transplant to treat central nervous injury has made great progress (Xu et al., 2017; Hosseini et al., 2018; Ludwig et al., 2018; Zamproni et al., 2019).

Mesenchymal stem cells (MSCs) are the most studied potential stem cells (Bhartiya, 2019). Global clinical trials on MSCs have been over 750 projects[1]. The United States approved more than 40 items in brain injury in Clinical trials. MSCs will be promising treatment strategies for the recovery of brain damage (Sherman et al., 2019). One of the reasons is that MSCs with strong proliferation and multi-directional differentiation potential can transdifferentiate into neurons and glial cells of ectoderm cells *in vivo* or *in vitro* in an appropriate environment, and plays a vital role of nerve repair (Kabos et al., 2002; Zhang et al., 2004; Munoz et al., 2005; Robinson et al., 2011; Tang et al., 2012; Huat et al., 2015). However, there are some problems in the transplantation of MSCs, such as lack of long-term survival in intracranial and limited direct evidence of nerve regeneration (Matsuse et al., 2011).

Although in recent years, lots of studies supported that bone-marrow MSCs (BM-MSCs) could transdifferentiate into neural cells, *in vitro* most of them (Long et al., 2005; Lei et al., 2007; Sun et al., 2007; Mu et al., 2018; Luo et al., 2019; Ruan et al., 2019), but few researchers could detect mature and function nerve cells, especially *in vivo* study (Tomita et al., 2006; Raedt et al., 2007; Nojiri et al., 2008). Even some researchers suggested that transplanted BM-MSCs were not able to differentiate into functional neural cells, at least expressed a limited set of neural markers and no cells replaced effect (Raedt et al., 2007). But in most cases of BM-MSCs transplantation, functional recovery was recognized even if just a few transplanted cells survived in the host tissue (Parr et al., 2008). The main role of promoting neural functional recovery probably was raised by inhibiting apoptosis, regulating the body's immune response to reduce inflammation, and so on (Shi et al., 2018).

It is much more than that. The possibility of committed tissue-specific stem cells pre-existing in the bone marrow has not been dealt with adequately. Any trans-differentiation studies employing populations of bone marrow cells should rule out the possibility that the apparently pure hematopoietic stem cell population could, in fact, contain pre-existing tissue-specific stem/progenitors (Kucia et al., 2004). It is reported that mRNA of several early markers for neural is detectable in peripheral blood mononuclear cells (Kucia et al., 2004). Our previous study examined the nerve cells culture environment, including which bone marrow-derived nerve cells may exist a phase of bone marrow-derived neural progenitor cells (BM-NPCs). BM-NPCs might be more suitable than BM-MSCs, served as seed cells for cell transplantation, playing the role of cell replacement therapy in the central nervous injury disease (Bai et al., 2013). Therefore, how to isolate neural progenitor cells from BM-MSCs and directly differentiate these progenitor cells into functional neural cells, looking the convincing proof for BM-NPCs, and observing the bone marrow derived neurons in long-term intracranial survival, and participating in nerve regeneration, are the urgent problems to be solved in clinical cell transplantation for treating brain injury. here, our study provide evidence that a neural progenitor cell population (BM-NPCs) could be separated from BM-MSCs and these BM-NPCs are able to further differentiate into neural cells *in vitro* based on the cell morphology and cell marker expression, and improve damaged brain function after cell transplantation. These results provide valuable experimental data for BM-NPCs in the central nerve regeneration application.

[1]https://clinicaltrials.gov/

MATERIALS AND METHODS

Isolation and Culture of BM-MSCs

Adult (3 weeks) specific-pathogen-free (SPF)-class SD rats were purchased from the Laboratory Animal Centre of Sun Yat-sen University. Rats BM-MSCs were generated using the whole bone marrow adherent culture method. Briefly, bone marrow was obtained as in our previous study (Bai et al., 2013) and then centrifuged at 1,500 rpm for 5 min. The supernatant was discarded, and the cell pellet was re-suspended in α-MEM medium plus with 10% FBS, transferred into a petri dish, and cultured in an incubator at 37°C and 5% CO_2. The medium was replaced every 2 days, as the cells were subcultured when the cell confluency reaches 90%.

Isolation and Culture of BM-NPCs

After two generations of BM-MSCs, cells were detached by trypsin-EDTA and cultured in a serum-free medium of neural stem cells culture medium Neurobal-A with 1% N2-supplement, 2 mmol/L L-glutamine and 20 ng/ml b-FGF and EGF in suspension culture bottles induction. After 48 h, there were cells in suspended growth, using Accutase™ enzyme digestion batches, some of these cells have the ability of proliferation as a sphere suspension growth.

Flow Cytometry Analysis of BM-MSCs and BM-NPCs

BM-MSCs or BM-NPCs were harvested with trypsin and washed twice with PBS. After filtering through a 200-mesh screen, the cell density was adjusted to $2–6 \times 10^6$/ml. The surface markers molecules on the BM-MSCs were then examined by flow cytometry with the following antibodies: CD3-PE, CD4-FITC, CD11b-PE, CD29-FITC, CD34-APC, CD14-APC, CD45-FITC, CD105-APC, and CD133-PE.

Immunofluorescent Staining

Cells were plated on the coverslips on the six-well plates. After attaching to the plates, the cells were fixed with 4% Paraformaldehyde (PFA) for 30 min, and then washed with PBS, permeabilized with 0.1% Triton X-100 for 5 min, and blocked with 1% BSA for 30 min. The cells were added to the primary antibody against Nestin/SOX2/CD133/Tuj1 or Texas Red conjugated phalloidin (Invitrogen, Waltham, MA, USA) for 2 h and FITC-conjugated second antibody. The samples were washed three additional times then mounted using Mowiol. The stained cells were viewed by a confocal microscope (TCS SP5, Leica, German). Antibodies and dilutions were as follows: rabbit polyclonal antibody Nestin (1:200) and SOX2 (1:100) both from Capital Bio Corporation in Beijing; mouse

monoclonal CD133 (1:40, Miltenyi Biotec, Auburn, CA, USA); polyclonal antibody Tuj-1 (1:500, Life Technologies, Carlsbad, CA, USA).

RT-PCR and qPCR

Total RNA was isolated from cells samples by Trizol Reagent. The quality and purity of RNA were assessed by the ratio of OD_{260} and OD_{280}, which of the value of all samples ranged from 1.8 to 2.2. RNA integrity assessed the Agilent 2100 bioanalyzer (Agilent Technologies, Santa Clara, CA, USA). The RNA integrity number (RIN) value of all samples ranged from 8.1 to 8.9 (scale1–10), indicating high-quality RNA.

First-strand cDNA was prepared from total RNA (1 μg) by Prime Script^{TM} RT reagent Kit With gDNA Eraser form RNA (Takara, Dalian China) according to the manufacturer's specifications. One microliter of 5-fold dilution of cDNA and 0.4 μM of primer pair (**Supplementary Table S1**) were used in 20 μl reaction volume with SYBRs Premix Ex Taq II (Perfect Real Time; Takara, Dalian, China) in master cycler real plex (Eppendorf, Germany), 5 ng of template cDNA, 45 cycles: 95°C/15 s, 60°C/15 s. These qRT-PCR procedures were run in duplicate to correct for variances in loading. All PCR results were determined using the relative quantification method ($2^{-\Delta\Delta}$Ct) with GADPH as the normalization control.

Adipogenesis Differentiation

BM-MSCs (6×10^4 cells/well) were seeded in 24-well plates and cultured at 37°C in a humidified atmosphere with 5% CO_2 in DMEM supplemented with 10% volume fraction of FBS, 10 mmol/L dexamethasone, 10 mg/L insulin, 100 mg/L 1-methyl-3-isobutyl xanthine, 100 mg/L indomethacin, 100 U/ml penicillin, and 100 mg/L streptomycin. This adipogenesis differentiation medium was replaced every 3–4 days. After 14 days of culture, the cells can be processed for Oil Red O staining, to detect adipogenesis.

Animal Model

Brain injury rat models were divided randomly into cell group (n = 20) and control group (n = 20; device as **Supplementary Figure S2**). Cell group rat tracer injected with CD-Dil tagged BM-NPCs 10 μl (1 million) through the microsyringe transplantation to cerebral injury rats, under the condition of the same set as control group with injecting medium. Movement function Wayne Clark test and grooming test were carried out respectively after transplantation of 1 day, 3 days, 7 days, and 30 days and 60 days. At the same time, 7 days, 30 days and 90 days after transplantation, brain tissue pathological conditions were detected, using immunofluorescence test to analyze Dil tagged BM-NPCs migration in brain injury and nerve cell markers NeuN. Antibodies and dilutions were as follows: neuron-specific enolase (NeuN) monoclonal, 1:200 (BD Bioscience).

Histological Observations

After treatment, the brains were carefully excised, rinsed in PBS, and then fixed in 4% PFA. The samples were dehydrated in a graded ethanol series (70–100%) and embedded in paraffin. Five-micrometer sections were prepared. According to the standard procedures, samples were stained with hematoxylin and eosin (HE).

Animal Behavior Test

Wayne Clark and grooming scores were carried out according to the score table (Bertelli and Mira, 1994; Finnie, 2001).

Statistical Analysis

Data were expressed as mean ± SEM. Comparisons of mean values among the groups were compared using Student's t-test. A five percent probability ($P < 0.05$) was used as the level of significance. Differences were considered statistically significant with $P < 0.01$.

RESULTS

Characterization of BM-MSCs

BM-MSCs were generated using the whole bone marrow adherent culture method, identified by analysis extending cell morphology and the surface markers using flow cytometry (**Figure 1A**). The results showed that characteristic of BM-MSCs in accordance with the international appraisal standard of MSCs, identified by microscope morphological observation and the flow cytometry of CD34/45/3/4/11b/14/133 (−) and CD29/105 (+) (**Figure 1B**).

Characterization of BM-NPCs

Through the method of neural stem cell suspension culture, bone marrow-derived sphere-like cells were harvested, which was measured by the flow cytometry cycle, and the results showed that 79.2% of the third generation of sphere-like cells was in G0/G1 phase (**Figure 2A**).

To analyze cell differentiation potential of sphere-like cells, cell immunofluorescence and RT-PCR method were carried out to detect the pluripotent surface markers expression. The results showed sphere-like cells express protein CD133, Sox2, and Nestin (**Figure 2B**).

To detect the mRNA level, semi-quantitative RT-PCR was executed. Pluripotent stem cell gene namely c-myc, klf4, sox2, Sca-1, oct4 and neural progenitor cells gene including Muashil1, CD184, CD133, CD56, Nestin, Muashil2, Notch1 were both stronger expressed in sphere-like cells (**Figures 2C,D**). To further confirm the pluripotency, sphere-like cells were induced to adipose differentiation. The result showed positive lipid drops with oil O staining (**Figure 2E**).

BM-NPCs Differentiation Into Neuron-Like Cells

To analyze the differentiation ability of BM-NPCs to nerve cells, genetic level changes in the process of cell differentiation was detected using both direct adherent differentiation and neuron co-culture induction method.

The third generation of BM-NPCs was cultured in neurons medium for 15 days. BM-NPCs adhered to the wall directly and neuron-like cells can be observed after 10 days, some of which like glial cells, linked with each other to grow. When continue to induce the other 5 days, a typical morphology of nerve cells, similar to normal cortex

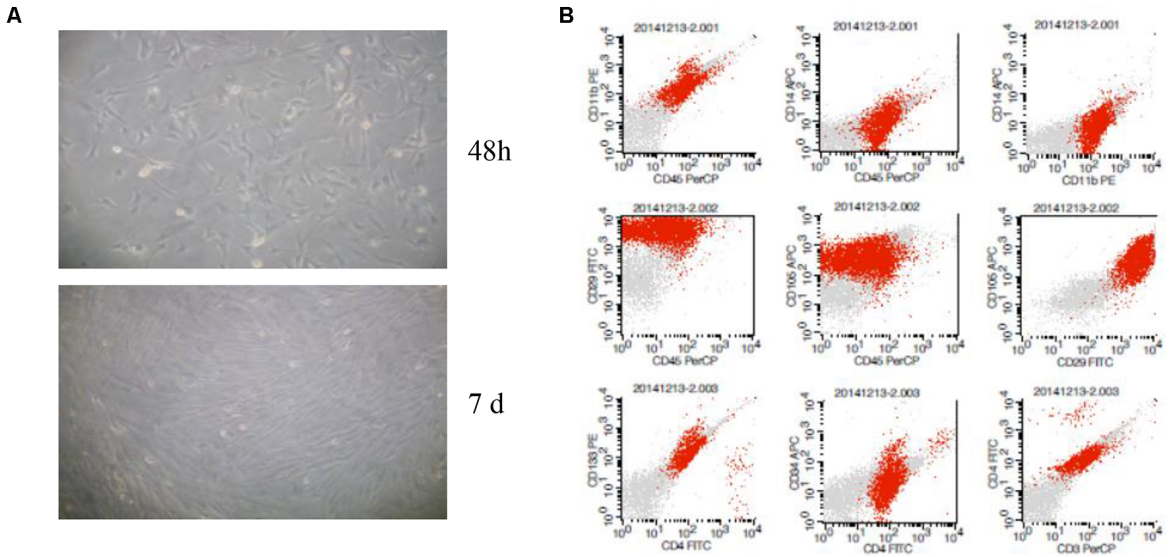

FIGURE 1 | Characterization of bone marrow-derived mesenchymal stem cells (BM-MSCs). **(A)** Microscope morphological observation of BM-MSCs. **(B)** Analysis of BM-MSCs for the expression of surface markers by flow cytometric analysis.

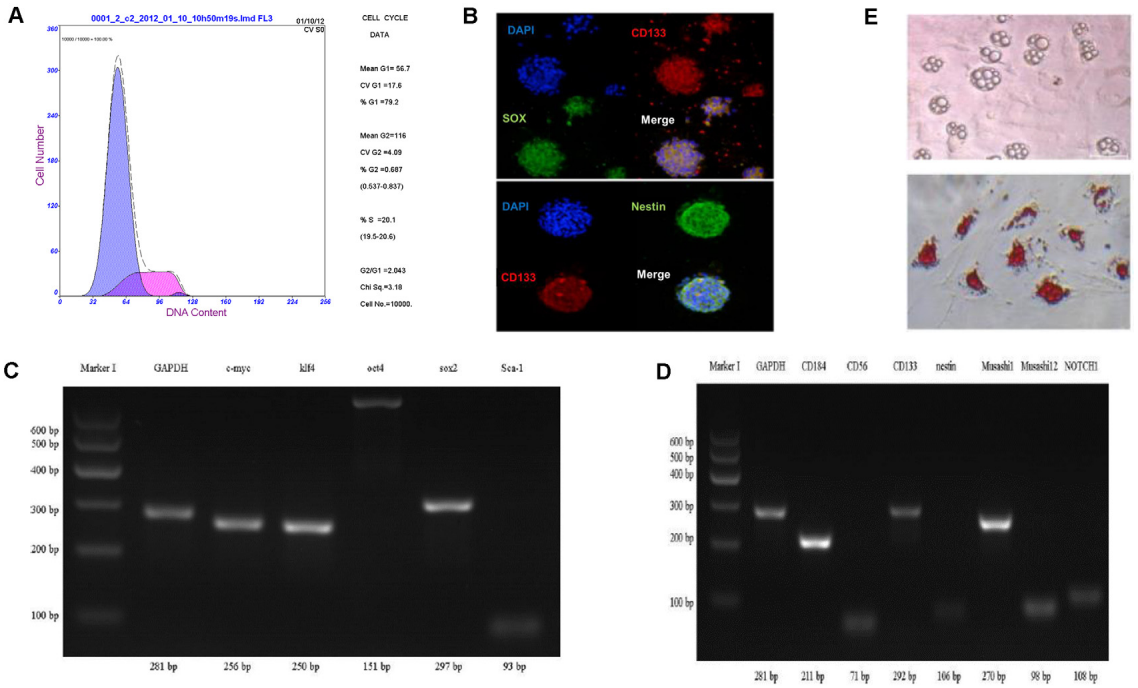

FIGURE 2 | Characterization of bone marrow-derived neural progenitor cells. **(A)** The cell cycle by flow cytometry. **(B–D)** Identification of cell differentiation potential and neural progenitor cells related to gene protein expression using cell immunofluorescence staining and RT-PCR method. **(E)** Oil Red O staining to detect adipogenesis differentiation.

neuron cells and completely different from BM-MSCs, can be observed (**Figure 3**).

Then analysis of neuronal markers was detected. Using semi-quantitative RT-PCR and quantitative qPCR to detect mRNA expression level before and after inducing BM-NPCs about neural stem cell marker genes (Nestin/CD56/CD133), the nerve cells marker genes (the beta-III-tubulin/Neun/5-HT/ACHE/GABA, and CNPase and neurotrophic factor gene

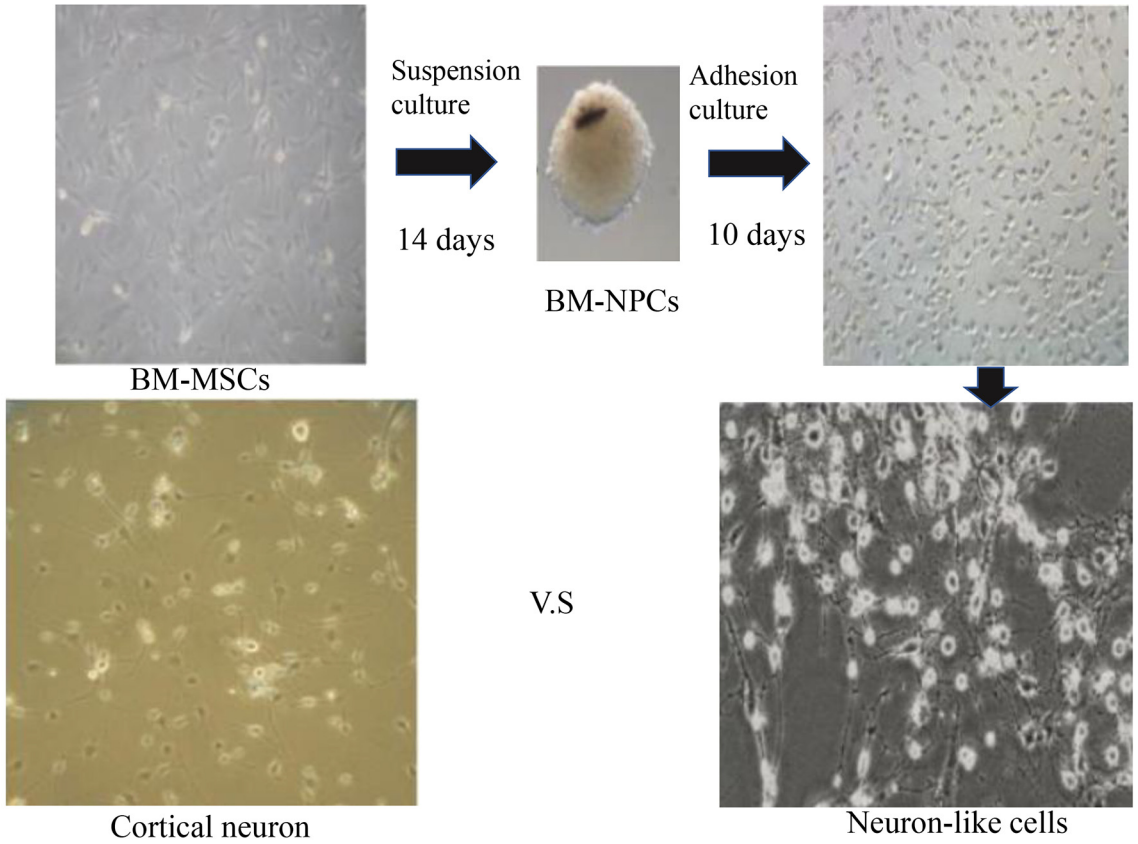

FIGURE 3 | Direct adherent induces differentiation of bone marrow neural progenitor cells into neuron-like cells.

NGF/BDNF/GDNF gene (**Figures 4A–C**). Quantitative gene expression results showed BM-NPCs was higher expression of neural progenitor cell gene CD56 and CD133 compared to BM-MSCs. What's more, results showed higher CNPase expression and NGF nutrition factor gene-level increased significantly (**Figure 4D**). To confirm the expression of neuronal markers. Tuj-1/NF200 and glial cell marker GFAP were detected by immunofluorescence technique. These nerve-like cells expressed Tuj-1 (+)/NF200 (−) and GFAP (+)/S100 (+) (**Figure 5**).

In addition, the CM-Dil cells tracer tagged BM-NPCs was cocultured with the original generation cortex neurons for 10 days, the result showed neurons-like morphology and network growth with neurons (**Figure 6A**), like primary cortex neurons (**Supplementary Figure S1**). For 15 days, using an inverted microscope and immunofluorescence observations to detect neuronal markers Tuj-1 expression. When CM-Dil cells tracer tagged BM-NPCs in the more suitable environment for neuronal growth was co-culture with the original generation of cortex neuron cell, BM-NPCs can be differentiated into more typical neuron morphological characteristics, with Tuj1 fluorescent protein-positive expression, and normal neural network connected into the growth cells (**Figure 6B**). However, unlike BM-NPCs, BM-MSCs cocultured with neurons did not show the appearance (**Figure 6C**).

Long-Term Survival of Bone Marrow-Derived Neurons Involved in Nerve Regeneration

Bone marrow-derived neural progenitor cells (BM-NPCs) transplantation in the brain injury rats was carried out followed by a search for the evidence about long-term survival *in vivo*, and participating in nerve regeneration of brain damage.

First, the immunofluorescence results showed that 7 days of transplantation, the Dil labeled cells transplanted into the area of injury around brain tissue. However, Dil labeled cells still not show NeuN positive. Transplantation for 30 days, brain damage tissue around GFAP positive astrocytes, some Dil+ cells, in the region of the hippocampus and cerebral cortex neurons, with normal nerve cells express integration expressed NeuN. After 4 weeks, cell group was still visible Dil tagged positive cells expressed NeuN, which integrated in normal nerve cells in the brain tissue, and the damage zone of the surrounding tissue growth (**Figure 7A**).

Second, HE staining showed 1 week after cell transplantation, the control group damage surrounding tissue with edema, oven visible cystic cavity, significantly reduced the number of nerve

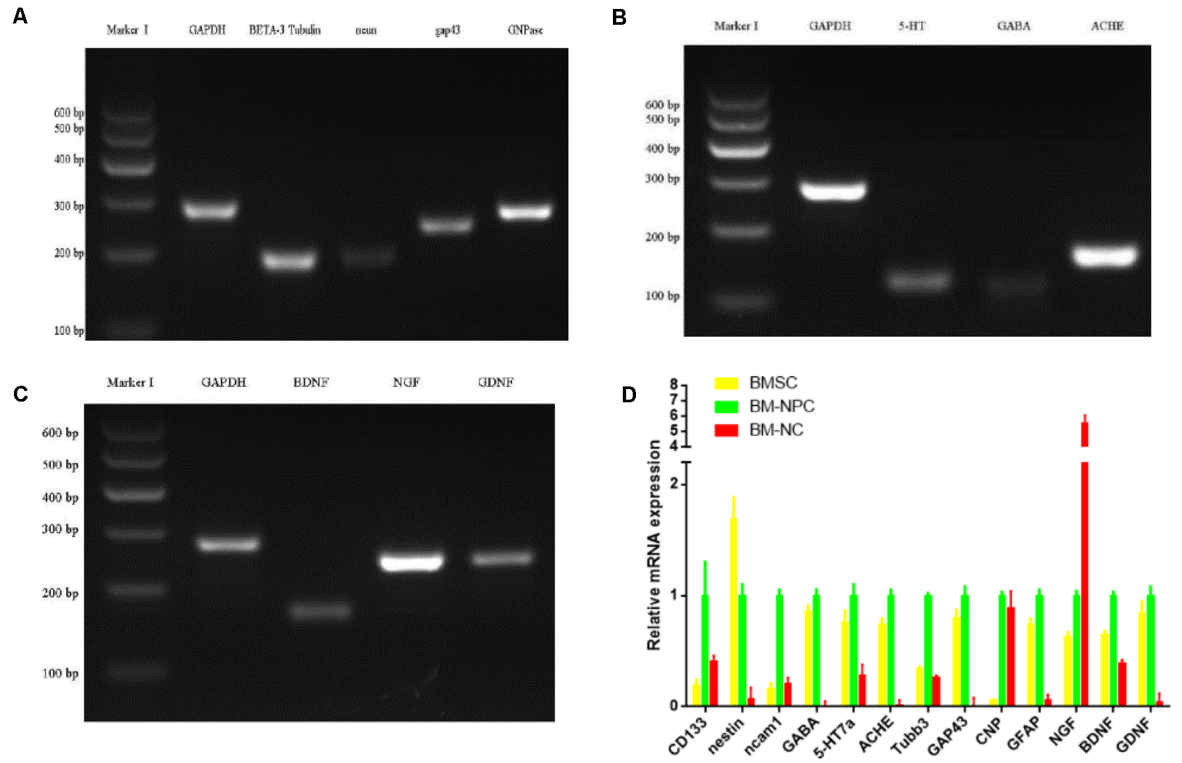

FIGURE 4 | Direct adherent induces differentiation of bone marrow neural progenitor cells into neuron-like cells, whose neuronal markers were detected by semi-quantitative RT-PCR (**A–C** from BM-NC) and quantitative qPCR **(D)**.

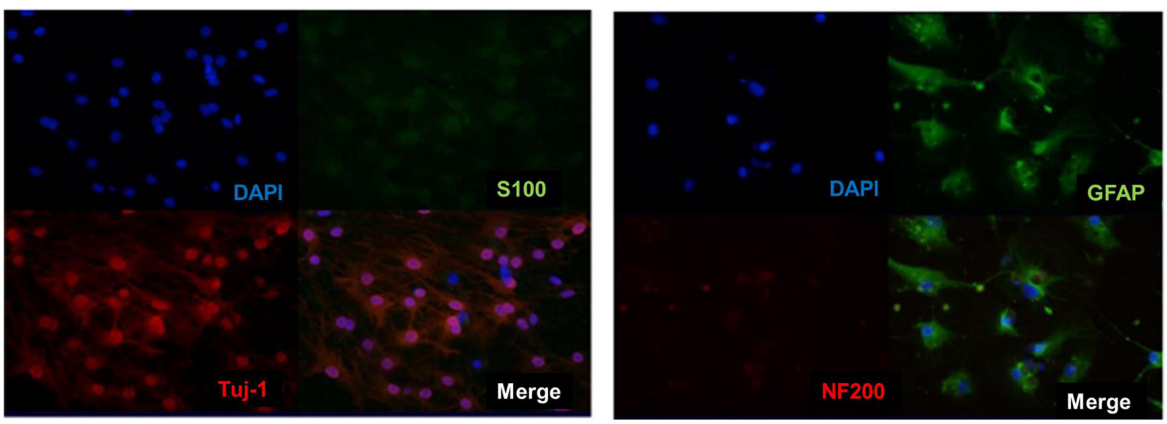

FIGURE 5 | Direct adherent induced differentiation of bone marrow neural progenitor cells into neuron-like cells, whose neuronal markers Tuj-1 (+)/NF200 (–) and S100 (+)/GFAP (+) was detected by immunofluorescence.

cells, inflammatory cells infiltration around, cell group edema, lighter, cystic cavity range limit, glial cells. Transplantation for 4 weeks, focal brain injury recovered from the surrounding tissue, compared with the control group. The cystic cavity was small in a cell group, and the row of the surrounding cell of the class was neat, tissue edema and inflammatory cells disappeared (**Figure 7B**).

Third, the behavioral score showed two groups of Wayne Clark and grooming score results were no significant difference ($P < 0.05$) on 1 day. But transplantation for 3 days, 7 days, 30 days, 60 days, Wayne Clark, grooming score results had significant difference ($P < 0.05$ or $P < 0.01$). The cell group had better functional recovery (**Figures 8A,B**).

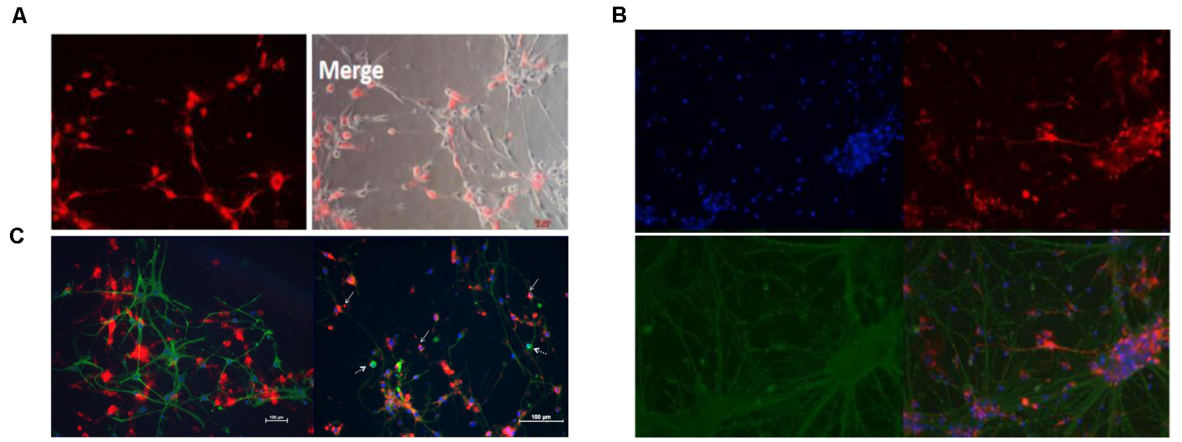

FIGURE 6 | Neuron co-culture induced differentiation of bone marrow neural progenitor cells into neuron-like cells followed by immunofluorescence observations. **(A)** BM-NPCs cocultured with cortical neurons for 10 days. **(B)** BM-NPCs cocultured with cortical neurons for 15 days. **(C)** BM-MSCs (left) and BM-NPCs cocultured with the cortical neuron. CM-Dil (red), Tuj1 (green) and DAPI (blue).

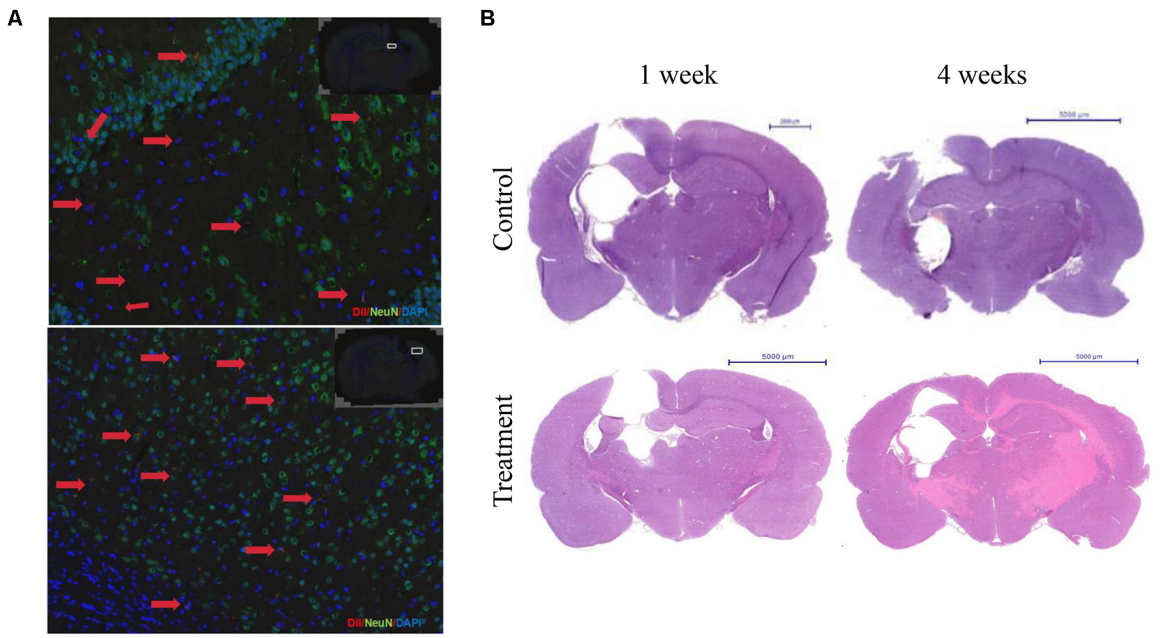

FIGURE 7 | Bone marrow-derived neurons can long-term survival in brain injury rats and promote nerve regeneration. **(A)** The immunofluorescence staining results showed that the Dil labeled cells after 4 weeks of transplantation. Dil (red), NeuN(green), DAPI (blue). **(B)** HE staining after 1 or 4 weeks of transplantation.

DISCUSSION

More and more focus on the capacity of stem cell-derived neural progenitor cells following brain injury (Pati et al., 2016), but less evidence ensure that these cells transdifferentiate into neural cells (Shinoyama et al., 2013). This article explored that bone marrow sphere-like cells were obtained from the BM-MSCs using the method of neural stem cell suspension culture, identified as BM-NPCs by neural progenitor cells gene and protein expression, and neural progenitor cells characteristic and nerve cell differentiation *in vitro*. Moreover, BM-NPCs transplantation improved the behavior and histological indexes of brain injury rats.

First, the pluripotent stem cell gene and neural progenitor cells gene were both stronger expressed in sphere-like cells, that suggested the bone marrow-derived sphere-like cells was pluripotent and able to differentiate into neural cells, in other words, they were bone marrow-derived neural progenitor cells (BM-NPCs; **Figures 2A–E**).

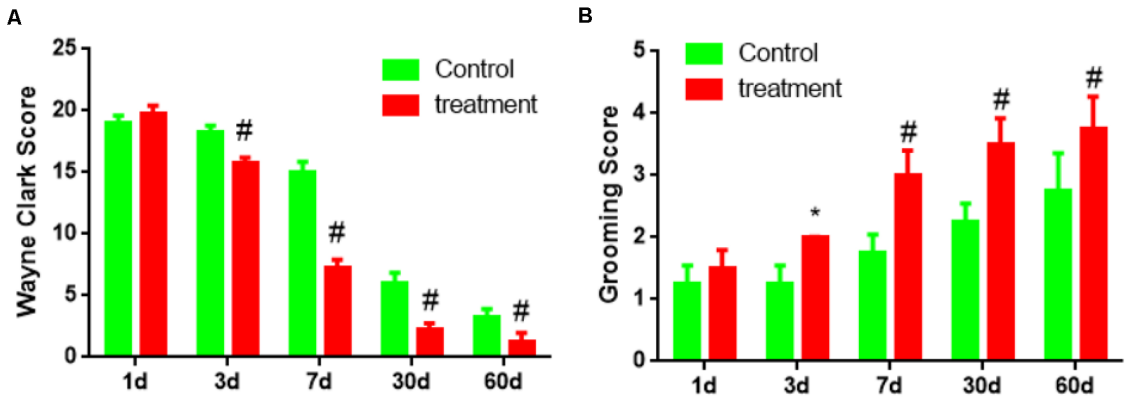

FIGURE 8 | The behavioral score of brain damage rats after BM-NPCs transplantation. **(A)** Wayne Clark and **(B)** grooming score after transplantation for different time points. $^{*}P < 0.05$, $^{\#}P < 0.01$.

These cells adhered to the wall directly, then showed a typical morphology of neuron-like cells and nerve cells, different from BM-MSCs (**Figure 3**). Further, after induced differentiation of BM-NPCs, the Nestin, NCAM1, and CD133 gene expression decreased obviously because maybe the cells differentiate into different nerve cells. beta-III-tubulin/Neun/5-HT/ACHE gene expression also decreased obviously, which suggested that the "stick-to-wall" differentiation environment was not conducive to neuron differentiation, so these cells were unable to form mature neurons with neurotransmitter expression. Cells may easily differentiate into glial cells with cultivation over a long time because glial cells were more easy to survive and proliferate, then with higher CNPase and NGF nutrition factor expression (**Figures 4A–D**). What's more, expression of neuronal markers suggested the more appropriate neuron growth environment, BM-NPCs might have the capacity to differentiate into mature functional neurons.

These results *in vitro* showed that suspension-cultured BM-NPCs have more ability to differentiate into nerve cells compared with BM-MSCs and that BM-NPCs induced neuronal cells were similar to fully mature neurons cell, however, a certain difference in the gene expression still exists. BM-NPCs probably have the ability to differentiate into functional neural cells in the appropriate environment, playing a role in the central nervous system injury disease (**Figures 5**, **6**).

Finally, the results that BM-NPCs transplantation can promote brain injury of limb motor function recovery in rats, that supply the evidence of long-term survival in intracranial, integrating into damage brain and participating in nerve regeneration (**Figures 7**, **8**). The behavioral score of brain damage rats improved 3 days after BM-NPCs transplantation. This time point was in accord with the study that concludes that the critical time period for manipulating endogenous NPCs following a spinal cord injury in rats was between 24 h when Nestin expression in ependymal cells increased and 1 week when astrocytes were activated in large numbers (Mao et al., 2016).

CONCLUSION

This study identified the BM-NPCs and provided valuable experimental basis data for BM-NPCs transplantation, suggesting the alternative treatment of central nervous injury disease.

DATA AVAILABILITY STATEMENT

All datasets generated for this study are included in the article/**Supplementary Material**.

ETHICS STATEMENT

The animal study was reviewed and approved by The ethics committee of Guangdong Provincial People's Hospital.

AUTHOR CONTRIBUTIONS

WB wrote the manuscript. YZ revised the manuscript. MZ proposed the idea for the manuscript. WX created the figures. XL was responsible for checking the manuscript. WL, ML, and FY contributed to the analysis and interpretation of data. WB and YZ were responsible for data collection, study design, and critical review. Finally, we thank all patients who took part in this study.

FUNDING

This study was funded by grants of Natural Science Foundation of China (Grant No. 81871842) and Science and Technology Planning Project of Guangdong Province, China (Grant No. 2016A02014014). All sources of funding received for the research being submitted.

SUPPLEMENTARY MATERIAL

The Supplementary Material for this article can be found online at: https://www.frontiersin.org/articles/10.3389/fncel.2020.00049/full#supplementary-material.

REFERENCES

Bai, W. F., Xu, W. C., Feng, Y., Huang, H., Li, X. P., Deng, C. Y., et al. (2013). Fifty-Hertz electromagnetic fields facilitate the induction of rat bone mesenchymal stromal cells to differentiate into functional neurons. *Cytotherapy* 15, 961–970. doi: 10.1016/j.jcyt.2013.03.001

Bertelli, J. A., and Mira, J. C. (1994). Brachial plexus repair by peripheral nerve grafts directly into the spinal cord in rats. Behavioral and anatomical evidence of functional recovery. *J. Neurosurg.* 81, 107–114. doi: 10.3171/jns.1994.81.1.0107

Bhartiya, D. (2019). Clinical translation of stem cells for regenerative medicine. *Circ. Res.* 124, 840–842. doi: 10.1161/CIRCRESAHA.118.313823

Chen, L., Qu, J., and Xiang, C. (2019). The multi-functional roles of menstrual blood-derived stem cells in regenerative medicine. *Stem Cell Res. Ther.* 10:1. doi: 10.1186/s13287-018-1105-9

Dupont, G., Yilmaz, E., Loukas, M., Macchi, V., De Caro, R., and Tubbs, R. S. (2019). Human embryonic stem cells: distinct molecular personalities and applications in regenerative medicine. *Clin. Anat.* 32, 354–360. doi: 10.1002/ca.23318

Finnie, J. (2001). Animal models of traumatic brain injury: a review. *Aust. Vet. J.* 79, 628–633. doi: 10.1111/j.1751-0813.2001.tb10785.x

Hosseini, S. M., Sani, M., Haider, K. H., Dorvash, M., Ziaee, S. M., Karimi, A., et al. (2018). Concomitant use of mesenchymal stem cells and neural stem cells for treatment of spinal cord injury: a combo cell therapy approach. *Neurosci. Lett.* 668, 138–146. doi: 10.1016/j.neulet.2018.01.008

Huat, T. J., Khan, A. A., Abdullah, J. M., Idris, F. M., and Jaafar, H. (2015). MicroRNA expression profile of neural progenitor-like cells derived from rat bone marrow mesenchymal stem cells under the influence of IGF-1, bFGF and EGF. *Int. J. Mol. Sci.* 16, 9693–9718. doi: 10.3390/ijms16059693

Kabos, P., Ehtesham, M., Kabosova, A., Black, K. L., and Yu, J. S. (2002). Generation of neural progenitor cells from whole adult bone marrow. *Exp. Neurol.* 178, 288–293. doi: 10.1006/exnr.2002.8039

Kucia, M., Ratajczak, J., Reca, R., Janowska-Wieczorek, A., and Ratajczak, M. Z. (2004). Tissue-specific muscle, neural and liver stem/progenitor cells reside in the bone marrow, respond to an SDF-1 gradient and are mobilized into peripheral blood during stress and tissue injury. *Blood Cells Mol. Dis.* 32, 52–57. doi: 10.1016/j.bcmd.2003.09.025

Lei, Z., Yongda, L., Jun, M., Yingyu, S., Shaoju, Z., Xinwen, Z., et al. (2007). Culture and neural differentiation of rat bone marrow mesenchymal stem cells *in vitro*. *Cell Biol. Int.* 31, 916–923. doi: 10.1016/j.cellbi.2007.02.006

Long, X., Olszewski, M., Huang, W., and Kletzel, M. (2005). Neural cell differentiation *in vitro* from adult human bone marrow mesenchymal stem cells. *Stem Cells Dev.* 14, 65–69. doi: 10.1089/scd.2005.14.65

Ludwig, P. E., Thankam, F. G., Patil, A. A., Chamczuk, A. J., and Agrawal, D. K. (2018). Brain injury and neural stem cells. *Neural Regen. Res.* 13, 7–18. doi: 10.4103/1673-5374.224361

Luo, H., Xu, C., Liu, Z., Yang, L., Hong, Y., Liu, G., et al. (2019). Neural differentiation of bone marrow mesenchymal stem cells with human brain-derived neurotrophic factor gene-modified in functionalized self-assembling peptide hydrogel *in vitro*. *J. Cell Biochem.* 120, 2828–2835. doi: 10.1002/jcb.26408

Mao, Y., Mathews, K., and Gorrie, C. A. (2016). Temporal response of endogenous neural progenitor cells following injury to the adult rat spinal cord. *Front. Cell. Neurosci.* 10:58. doi: 10.3389/fncel.2016.00058

Matsuse, D., Kitada, M., Ogura, F., Wakao, S., Kohama, M., Kira, J., et al. (2011). Combined transplantation of bone marrow stromal cell-derived neural progenitor cells with a collagen sponge and basic fibroblast growth factor releasing microspheres enhances recovery after cerebral ischemia in rats. *Tissue Eng. Part A* 17, 1993–2004. doi: 10.1089/ten.tea.2010.0585

Mu, T., Qin, Y., Liu, B., He, X., Liao, Y., Sun, J., et al. (2018). *In vitro* neural differentiation of bone marrow mesenchymal stem cells carrying the FTH1 reporter gene and detection with MRI. *Biomed Res. Int.* 2018:1978602. doi: 10.1155/2018/1978602

Munoz, J. R., Stoutenger, B. R., Robinson, A. P., Spees, J. L., and Prockop, D. J. (2005). Human stem/progenitor cells from bone marrow promote neurogenesis of endogenous neural stem cells in the hippocampus of mice. *Proc. Natl. Acad. Sci. U S A* 102, 18171–18176. doi: 10.1073/pnas.0508945102

Nojiri, Y., Takeda, S., Enomoto, M., Nishitsuji, H., Masuda, T., Sotome, S., et al. (2008). Co-overexpression of GDNF and GFRα1 induces neural differentiation in neural progenitor cells in comparison to bone marrow stromal cells. *J. Med. Dent. Sci.* 55, 121–128.

Parr, A. M., Kulbatski, I., Wang, X. H., Keating, A., and Tator, C. H. (2008). Fate of transplanted adult neural stem/progenitor cells and bone marrow-derived mesenchymal stromal cells in the injured adult rat spinal cord and impact on functional recovery. *Surg. Neurol.* 70, 600–607; discussion 607. doi: 10.1016/j.surneu.2007.09.043

Pati, S., Muthuraju, S., Hadi, R. A., Huat, T. J., Singh, S., Maletic-Savatic, M., et al. (2016). Neurogenic plasticity of mesenchymal stem cell, an alluring cellular replacement for traumatic brain injury. *Curr. Stem Cell Res. Ther.* 11, 149–157. doi: 10.2174/1574888x10666151019120050

Raedt, R., Pinxteren, J., Van Dycke, A., Waeytens, A., Craeye, D., Timmermans, F., et al. (2007). Differentiation assays of bone marrow-derived multipotent adult progenitor cell (MAPC)-like cells towards neural cells cannot depend on morphology and a limited set of neural markers. *Exp. Neurol.* 203, 542–554. doi: 10.1016/j.expneurol.2006.09.016

Robinson, A. P., Foraker, J. E., Ylostalo, J., and Prockop, D. J. (2011). Human stem/progenitor cells from bone marrow enhance glial differentiation of rat neural stem cells: a role for transforming growth factor beta and Notch signaling. *Stem Cells Dev.* 20, 289–300. doi: 10.1089/scd.2009.0444

Ruan, H., Xiao, R., Jiang, X., Zhao, B., Wu, K., Shao, Z., et al. (2019). Biofunctionalized self-assembly of peptide amphiphile induces the differentiation of bone marrow mesenchymal stem cells into neural cells. *Mol. Cell. Biochem.* 450, 199–207. doi: 10.1007/s11010-018-3386-9

Sherman, L. S., Romagano, M. P., Williams, S. F., and Rameshwar, P. (2019). Mesenchymal stem cell therapies in brain disease. *Semin Cell Dev Biol.* 95, 111–119. doi: 10.1016/j.semcdb.2019.03.003

Shi, Y., Wang, Y., Li, Q., Liu, K., Hou, J., Shao, C., et al. (2018). Immunoregulatory mechanisms of mesenchymal stem and stromal cells in inflammatory diseases. *Nat. Rev. Nephrol.* 14, 493–507. doi: 10.1038/s41581-018-0023-5

Shinoyama, M., Ideguchi, M., Kida, H., Kajiwara, K., Kagawa, Y., Maeda, Y., et al. (2013). Cortical region-specific engraftment of embryonic stem cell-derived neural progenitor cells restores axonal sprouting to a subcortical target and achieves motor functional recovery in a mouse model of neonatal hypoxic-ischemic brain injury. *Front. Cell. Neurosci.* 7:128. doi: 10.3389/fncel.2013.00128

Stoddard-Bennett, T., and Reijo Pera, R. (2019). Treatment of Parkinson's disease through personalized medicine and induced pluripotent stem cells. *Cells* 8:E26. doi: 10.3390/cells8010026

Sun, X., Jiang, H., and Yang, H. (2007). *In vitro* culture of bone marrow mesenchymal stem cells in rats and differentiation into retinal neural-like cells. *J. Huazhong Univ. Sci. Technol. Med. Sci.* 27, 598–600. doi: 10.1007/s11596-007-0531-1

Tang, Y., Cui, Y. C., Wang, X. J., Wu, A. L., Hu, G. F., Luo, F. L., et al. (2012). Neural progenitor cells derived from adult bone marrow mesenchymal stem cells promote neuronal regeneration. *Life Sci.* 91, 951–958. doi: 10.1016/j.lfs.2012.09.005

Tomita, M., Mori, T., Maruyama, K., Zahir, T., Ward, M., Umezawa, A., et al. (2006). A comparison of neural differentiation and retinal transplantation with bone marrow-derived cells and retinal progenitor cells. *Stem Cells* 24, 2270–2278. doi: 10.1634/stemcells.2005-0507

Xu, C., Fu, F., Li, X., and Zhang, S. (2017). Mesenchymal stem cells maintain the microenvironment of central nervous system by regulating the polarization of macrophages/microglia after traumatic brain injury. *Int. J. Neurosci.* 127, 1124–1135. doi: 10.1080/00207454.2017.1325884

Yamada, Y., Nakamura-Yamada, S., Kusano, K., and Baba, S. (2019). Clinical potential and current progress of dental pulp stem cells for various systemic

diseases in regenerative medicine: a concise review. *Int. J. Mol. Sci.* 20:E1132. doi: 10.3390/ijms20051132

Zamproni, L. N., Grinet, M., Mundim, M., Reis, M. B. C., Galindo, L. T., Marciano, F. R., et al. (2019). Rotary jet-spun porous microfibers as scaffolds for stem cells delivery to central nervous system injury. *Nanomedicine* 15, 98–107. doi: 10.1016/j.nano.2018.08.014

Zhang, H., Wang, J. Z., Sun, H. Y., Zhang, J. N., and Yang, S. Y. (2004). The effects of GM1 and bFGF synergistically inducing adult rat bone marrow stromal cells to form neural progenitor cells and their differentiation. *Chin. J. Traumatol.* 7, 3–6.

Conflict of Interest: The authors declare that the research was conducted in the absence of any commercial or financial relationships that could be construed as a potential conflict of interest.

frontiers in Cellular Neuroscience

BRIEF RESEARCH REPORT
published: 15 May 2020
doi: 10.3389/fncel.2020.00134

Electroacupuncture Inhibits Neuronal Autophagy and Apoptosis *via* the PI3K/AKT Pathway Following Ischemic Stroke

*Man-Man Wang[1], Min Zhang[2], Ya-Shuo Feng[1], Ying Xing[1], Zi-Xuan Tan[1], Wen-Bin Li[2], Fang Dong[3] and Feng Zhang[1,4]**

[1]*Department of Rehabilitation Medicine, The Third Hospital of Hebei Medical University, Shijiazhuang, China,* [2]*Department of Pathophysiology, Hebei Medical University, Shijiazhuang, China,* [3]*Department of Clinical Laboratory Medicine, The Third Hospital of Hebei Medical University, Shijiazhuang, China,* [4]*Hebei Provincial Orthopedic Biomechanics Key Laboratory, The Third Hospital of Hebei Medical University, Shijiazhuang, China*

OPEN ACCESS

Edited by:
Zhang Pengyue, Yunnan University of Traditional Chinese Medicine, China

Reviewed by:
Bei Zhang, University of Texas Health Science Center at Houston, United States
Wen Shi, University of Nebraska Medical Center, United States

***Correspondence:**
Feng Zhang
zjk20019@126.com

Specialty section:
This article was submitted to Cellular Neuropathology, a section of the journal Frontiers in Cellular Neuroscience

Received: *17 March 2020*
Accepted: *21 April 2020*
Published: *15 May 2020*

Citation:
Wang M-M, Zhang M, Feng Y-S, Xing Y, Tan Z-X, Li W-B, Dong F and Zhang F (2020) Electroacupuncture Inhibits Neuronal Autophagy and Apoptosis via the PI3K/AKT Pathway Following Ischemic Stroke. Front. Cell. Neurosci. 14:134. doi: 10.3389/fncel.2020.00134

Electroacupuncture (EA) is a safe and effective therapy for ischemic stroke in both clinical and laboratory settings. However, the underlying mechanism behind EA treatment for stroke remains unclear. Here, we aimed to evaluate whether EA treatment at the acupoints of Zusanli (ST36) and Quchi (LI11) exerted a neuroprotective effect on ischemic stroke rats by modulating autophagy and apoptosis *via* the PI3K/AKT/mTOR signaling pathway. EA was performed at 24 h following brain ischemia/reperfusion (I/R) for 30 min per day for 3 days. Our results indicated that EA treatment significantly decreased neurological deficits and cerebral infarct volume in ischemic stroke rats. Also, EA intervention markedly reduced neuronal apoptosis by suppressing the activation of cleaved caspase-3 (CCAS3) at 72 h following I/R, as shown by a Western blot analysis. Furthermore, EA treatment after ischemic stroke suppressed the ischemia activated expression level of LC3II/I and Atg7 and increased the ischemia inhibited expression level of PI3K, phosphorylation of mTOR, phosphorylation of AKT, P62 and LAMP1, hence mediating the autophagy level of the neurocyte, which was reversed by the PI3K inhibitor Dactolisib. In summary, our results indicate that the protective effects of EA treatment at points of Quchi (LI11) and Zusanli (ST36) in rats following cerebral I/R injury was associated with the inhibition of neuronal apoptosis and autophagy *via* activating the PI3K/AKT/mTOR signaling pathway.

Keywords: electroacupuncture, ischemic stroke, autophagy, PI3K, apoptosis

INTRODUCTION

Ischemic stroke is a type of cerebrovascular disease with high morbidity, disability, and mortality; it represents a critical threat to human health and life and is a leading reason for permanent disability and death for adults (Liu et al., 2019; Yang et al., 2019). The pathogenesis of ischemic stroke is complicated. During ischemia/reperfusion (I/R) injury, neuronal cells undergo various acute changes that can result in alterations of various signaling pathways (Xie et al., 2013).

As a result of ischemia, the blood supply to neurons is interrupted, which then promotes a series of pathophysiological responses. Various pathological changes are involved individually or jointly in the ischemic process, including autophagy, apoptosis, inflammation, excitatory toxicity, mitochondrial death pathways and free radical release (Khoshnam et al., 2017; Sekerdag et al., 2018), all of which lead to neuronal cell death, hindering important motor (Sun et al., 2012), sensory (Graf et al., 1986) and cognitive functions (Escobar et al., 2019; Liu et al., 2019). Ischemic stroke has been considered one of the main factors that cause aging of the brain and the pathological state of neurodegenerative diseases (Sommer, 2017; Graham and Liu, 2017). However, reliable therapies for ischemic stroke have been very limited until now. Therefore, effective and safe treatments are urgently required.

Comprising the integration of acupuncture and electric stimulation, electroacupuncture (EA) is a safe and effective treatment method in the treatment of various diseases. EA is widely used in experimental research and clinical therapy for ischemic stroke (Liu et al., 2019). According to our previous studies, EA can improve neurological dysfunction, decrease the infarct volumes, and decrease the number of ischemic lesions (Xing et al., 2018a,b). Moreover, EA treatment could generate neuro regenerative effects for ischemic stroke, including promoting brain blood flow, regulating oxidative stress, reducing excitatory amino acids with neurotoxicity, maintaining the integrity of the blood-brain barrier, inhibiting neuronal apoptosis, increasing neurotrophic factors and producing brain ischemic tolerance (Xing et al., 2018c). Therefore, early intervention with EA in the acute stage of ischemic stroke has very important clinical significance.

It is well established that following I/R injury, the brain will undergo more serious damage than with ischemia alone. The mechanisms behind brain I/R damage are complex and associated with neuronal autophagy and apoptosis. Autophagy, which is a key process for cell survival following a stroke, plays a crucial role in the pathogenesis of cerebral ischemia-reperfusion injury (He et al., 2019). Moreover, there is mounting evidence proving that after cerebral I/R, the suppression of apoptosis plays a key role in preventing neuron injury and even death (Zhang et al., 2018).

EA preconditioning can effectively improve cerebral ischemia/reperfusion injury (CIRI) in rats, which may be related to the suppression of autophagy in the ischemic cerebral cortex tissue (Huang et al., 2019). EA preconditioning can reduce the number of autophagosomes and the expression of autophagy markers in the ischemic cortex. Also, both 100 Hz and 2 Hz/10 0HZ-EA are effective in improving the recovery of hindlimb motor function in spinal cord injury (SCI) rats; this may be associated with the function of reducing neuronal apoptosis and promoting the autophagy of damaged nerve cells (Luo et al., 2019). The PI3K/AKT pathway plays an important role in regulating cell proliferation, differentiation, migration, and apoptosis in various types of cells (Samakova et al., 2019). Therefore, the PI3K/AKT pathway is a key target for ischemic stroke treatment. However, whether EA could suppress neuronal autophagy and apoptosis *via* the PI3K/AKT pathway following ischemic stroke is not clear, and the related mechanisms remain unknown.

In the present study, we investigated whether EA treatment at the Quchi (LI11) and Zusanli (ST36) acupoints can provide neuroprotection by regulating autophagy and apoptosis through the PI3K/AKT pathway after ischemic stroke.

MATERIALS AND METHODS

Middle Cerebral Artery Occlusion/Reperfusion (MCAO/R) Model

The MCAO/R animal model was induced by middle cerebral artery (MCA) occlusion. Briefly, each rat fasted in a 12 h light/dark cycle and then anesthetized by intraperitoneal injection of 10% chloral hydrate (300 mg/kg); the left external carotid artery (ECA), left common carotid artery (CCA) and internal carotid artery (ICA) were exposed *via* a midline neck incision. The left MCA was occluded by inserting a surgical nylon suture (diameter, 0.26 mm; Beijing Shandong Biotech Co., Ltd., Beijing, China) through the ICA. After blocking for 2 h, the nylon cord was slowly removed for reperfusion to restore blood supply in the MCA area. This model was measured with the MCAO method, as described previously (Xing et al., 2018a,b). The rectal temperatures of the rats were kept at 37°C throughout the whole surgical process. The rats of the sham-operated group underwent the same surgical procedure without suture insertion. The conditions of occlusions and reperfusion were monitored by laser-doppler flowmetry.

Animals and Groups

Sprague–Dawley (SD) rats, weighing 250–280 g, were purchased from the Hebei Province Laboratory Animal Center. The SD rats were housed in a 12 h light/dark cycle at a temperature of 22 ± 2°C and 60–70% humidity. Food and water were available *ad libitum*. The experimental protocol was permitted by the Animal Use and Care Committee of Hebei Medical University.

As shown in **Figure 1A**, the 75 rats were randomly divided into five groups (n = 15/group) as follows: (i) in the sham group, the rats underwent neck dissection and vascular exposure but no MCA occlusion; (ii) in the MCAO/R group, the left MCA was blocked for 2 h before reperfusion; (iii) in the EA group, the surgical method was the same as that in the MCAO/R group. Reperfusion was performed 2 h after surgery, and EA treatment was administered for 30 min daily for 3 days following MCAO (24, 48, 72 h following ischemia); (iv) in the EA + NC group, NC (the non-specific control of Dactolisib) was provided by intraperitoneal injection daily for 3 days, and the last injection was performed at 30 min before surgery. The rest of the procedures were the same as the EA group; and (v) in the EA+D group, the PI3K inhibitor Dactolisib (Selleck Chemicals, Houston, TX, USA) was dissolved with DMSO, PEG300 and Tween 80 according to the instructions(concentration = 5 mM), which were provided to the rats by intraperitoneal injection daily for 3 days, and the last injection was performed at 30 min before surgery. The other processing methods were the same as those in the EA+NC.

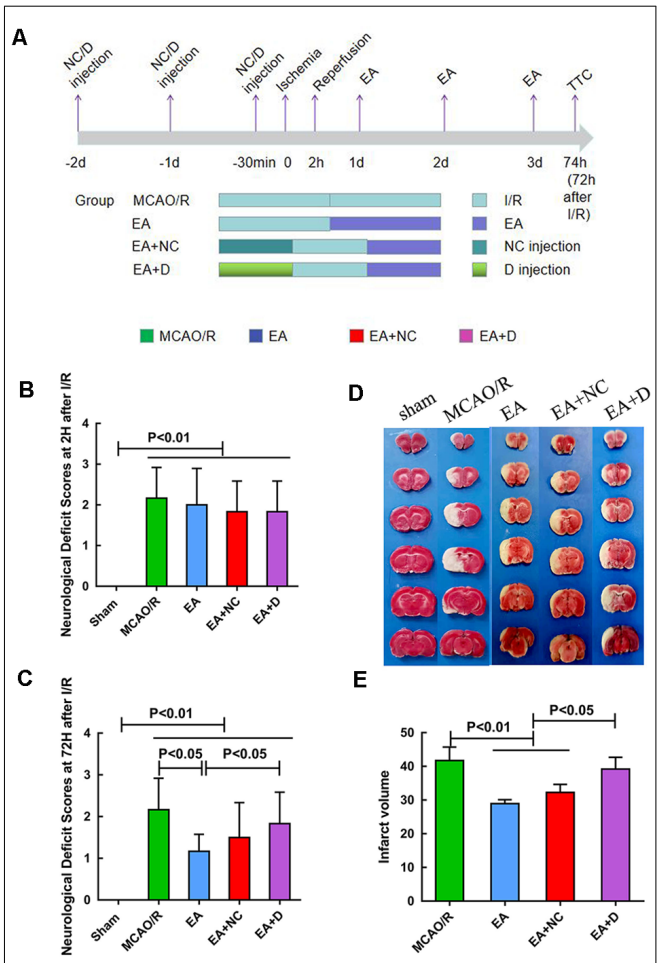

FIGURE 1 | The pathology of an injury following ischemia/reperfusion (I/R) within 3 days. **(A)** Experimental groups and the protocol. **(B)** Neurological deficit assessment at 2 h after I/R injury. **(C)** Neurological deficit assessment at 72 h after I/R injury. **(D)** 2,3,5-triphenyl tetrazolium chloride (TTC) staining for cerebral infarct volume of the sham, MCAO/R, EA, EA+NC, and EA+D groups. **(E)** Bar graph showing the percentage of cerebral infarct volume among the four groups.

Assessment of Neurological Deficit Scores

At 2 h and 72 h after I/R, the neurological deficit score was evaluated in a blinded manner: score 0, indicated no neurological deficits; score 1, failure to fully extend right forepaw; score 2, circling to the opposite side; score 3, falling to contralateral side; score 4, not able to walk independently; and score 5, died. Finally, rats with scores of 1–3 points at 2 h following I/R injury were enrolled in the current study.

EA Intervention

EA intervention was measured with a method previously described. EA intervention was administered at the points Zusanli (ST36) and Quchi (LI11) on the right paralyzed limb *via* an EA apparatus (Model G6805-2A; Shanghai Huayi Co., Shanghai, China). Rats underwent 10% chloral hydrate anesthesia before EA treatment. Two acupuncture needles that were 0.3 mm in diameter were inserted at approximately a 2–3 mm depth at the ST36 and LI11 acupoints. The intervention parameters were set as continuous waves of 2 Hz and an intensity of 1 mA. However, the rats in the sham-operated group and MCAO/R groups were also anesthetized without EA treatment. Finally, the rats were sacrificed at 72 h after MCAO/R for the experiment.

TTC Staining

The volume of cerebral infarction was detected using TTC staining. Five rats in each group were executed to assess the infarct volume by the TTC method. At 72 h after cerebral I/R injury, the rats were sacrificed under anesthesia with 10% chloral hydrate *via* intraperitoneal injection and stored at −20°C for 15 min. The brain was dissected into six sections in the coronal plane into 2 mm thick slices. The slices were placed in a 2% 2,3,5-triphenyl tetrazolium chloride (TTC, Solarbio, China) solution in 0.1 M phosphate-buffered saline (PBS) at 37°C for 20–30 min and fixed in a 4% paraformaldehyde buffer. The normal brain area was dark red, but no staining was observed in the infarcted area. The infarct was measured using imaging software (Adobe Photoshop 7.0). The formula was used to calculate infarct volume as follows:

$$\begin{aligned}\text{Infarct volume} = {} & \text{contralateral hemisphere region} \\ & - \text{a noninfarcted region in the} \\ & \text{ipsilateral hemisphere.} \\ \text{Infarct percentage} = {} & \text{infract volume} - \text{volume of the} \\ & \text{contralateral hemisphere} \times 100\%.\end{aligned}$$

Western Blot Analysis

Western blotting was performed to detect the proteins in the PI3K/AKT/mTOR pathway and autophagy/apoptosis-related proteins. Five rats in each group were executed to detect target proteins. The total proteins were collected from the hippocampal tissue on the left hemisphere of the brain. The hippocampal tissues were homogenized in lysis buffer and centrifuged at 12,000× *g* for 15 min. The supernatants were collected and frozen at −80°C. The protein concentration of each group was detected by the Enhanced BCA Protein Assay Kit (#PC0020, Solarbio, China). Equal amounts of protein (30 μg) were loaded into 12% sodium dodecyl sulfate-polyacrylamide gel electrophoresis (SDS-PAGE) gels for electrophoresis and then transferred onto a PVDF membrane (Roche, Mannheim, Germany). After blocking in a 5% bovine serum albumin solution for 1 h at 37°C, the membranes were incubated at 4°C overnight with primary antibodies against LC3 (1:500, #18725-1-AP, proteintech), P62 (1:1,000, #18420-1-AP, proteintech), LAMP-1 (1:1,000, #62562, Abcam), cleaved-caspase3 (1:500, #66470-2-lg, proteintech), Atg7 (1:1,000, #32345, Cell Signalling Technology, Danvers, MA, USA), PI3K (1:1,000, #4249, Cell Signalling Technology, Danvers, MA, USA), mTOR (1:1,000, #2972 Cell Signalling Technology, Danvers, MA, USA), Phospho-mTOR (1:1,000, #5536, Cell Signalling Technology, Danvers, MA, USA), AKT (1:1,000, #4691, Cell Signalling Technology, Danvers, MA, USA), Phospho-AKT (Thr308, #13038, Cell Signalling Technology,

Danvers, MA, USA) and GAPDH (1:5,000, #10494-1-AP, proteintech). After washing with TBST, the membrane was incubated with a goat antimouse IgM (1:5,000) or antirabbit IgG (1:5,000) for 1 h at room temperature. The protein bands were detected using enhanced chemiluminescence (ECL), and the images were analyzed using an Amersham Imager 600. Finally, the optical density of each band was quantified by ImageJ software.

Immunofluorescence

Rats (n = 5/group) were sacrificed without pain. Brain tissue was fixed in formaldehyde, embedded in paraffin, and sectioned with a thickness of 5 mm. Nonspecific antigen binding was blocked with normal sheep serum for 60 min. The sections were separately incubated with primary rabbit antibodies against LC3 (1:200; Cell Signalling Technology, Danvers, MA, USA) and CCAS3 (1:200; Cell Signalling Technology, Danvers, MA, USA) at 4°C overnight. After washing with PBS, the sections were incubated with Rhodamine (TRITC)-conjugated goat antirabbit IgG (H+L) secondary antibody (1:500; proteintech) at room temperature for 1 h in the darks and then washed three times with PBS. Nuclei were counterstained with 4′,6-diamidino-2-phenylindole (DAPI). Cells were observed at 200× magnification under a fluorescence microscope (OLYMPUS 905). Outcomes are shown as optical density (OD). In our present study, immunofluorescence analysis demonstrated the expression difference of LC3 in the ipsilateral hippocampus of the rats in different groups.

Statistical Analysis

All data were processed using SPSS 21.0. Quantitative data were expressed as the mean ± standard deviation. Differences among the various groups were performed by one-way analysis of variance (ANOVA), followed by a Bonferroni test. The neurological deficits scores among the five groups were analyzed by a nonparametric test. $P < 0.05$ was considered a statistically significant difference.

RESULTS

EA Alleviates the Neurological Deficit Scores and Infarct Volumes in Cerebral I/R Injury Rats

The neurological deficit scores were evaluated at 2 h and 72 h after I/R surgery. As shown in **Figure 1B**, when compared with the sham group, the rats in the other groups exhibited significant neurological deficits ($P < 0.01$), even though there was no significant difference in the neurological deficits score between the MCAO/R group and the EA group at 2 h following I/R. However, EA treatment at the LI11 and ST36 acupoints significantly decreased the neurological deficits score at 72 h following I/R compared with the MCAO/R group ($P < 0.05$), and the neurological deficits of the EA+D group were increased compared with the EA group ($P < 0.05$), as shown in **Figure 1C**.

EA Treatment Alleviates Infarct Volumes in Rats following I/R Injury

An infarct volume evaluation was performed at 72 h after I/R injury. As shown in **Figure 1D**, the rats in the sham group showed no infarct volumes, and there was a significant infarct area in the rest groups. As shown in **Figure 1E**, the infarct volume of the rats in the MCAO group was significantly higher than the EA group ($P < 0.01$) and EA+NC group ($P < 0.01$). Compared with the EA and EA+NC groups, the infarct volume of the rats in the EA+D group was significantly increased ($P < 0.05$).

EA Treatment Regulates Autophagy-Related Proteins

The autophagy-related and apoptosis-related proteins were examined by Western blot, including LC3I, LC3II, P62, LAMP-1, and CCAS3, as shown in **Figure 2A**. As shown in **Figure 2B**, the ratio of LC3I/II markedly increased in the MCAO/R group compared with the sham group ($P < 0.01$), but EA treatment reversed this change in the EA ($P < 0.01$) and EA+NC groups ($P < 0.01$). Furthermore, the ratio of LC3-I/II in the EA+D group was significantly increased compared with the EA ($P < 0.01$) and EA+NC groups ($P < 0.01$). As shown in **Figure 2C**, the level of P62 was significantly decreased in the MCAO/R group ($P < 0.01$) compared with the sham group, but EA treatment reversed this change in the EA ($P < 0.01$) and EA+NC groups ($P < 0.05$) compared with the MCAO group, and the expression of P62 in the EA+D group was significantly decreased compared with the EA ($P < 0.01$) and EA+NC groups ($P < 0.01$). Also, as shown in **Figure 2D**, compared with the sham group, the expression of LAMP-1 in the MCAO/R group was decreased ($P < 0.01$). Moreover, the expression of LAMP-1 was increased in both the EA and EA+NC groups compared with the MCAO group ($P < 0.01$). And the expression of LAMP-1 in the EA+D group was significantly decreased compared with the EA ($P < 0.01$) and EA+NC groups ($P < 0.01$). As shown in **Figure 2E**, the expression of CCAS3 in the MCAO/R group was significantly increased compared with the sham group ($P < 0.01$). EA intervention at the ST36 and LI11 acupoints significantly decreased neuronal apoptosis *via* reversing the upregulation of CCAS3 in EA ($P < 0.01$) and EA+NC groups ($P < 0.01$). Furthermore, the expression of CCAS3 in the EA+D groups was significantly increased compared with the EA ($P < 0.01$) and EA+NC groups ($P < 0.01$).

To confirm the effect of EA on LC3 expression level, the protein expression of LC3 was evaluated by immunofluorescence, as shown in **Figure 3A**. As shown in **Figure 3B**, the LC3 expression level was also significantly decreased in the EA ($P < 0.05$) and EA+NC ($P < 0.05$) groups compared with the MCAO/R group. Comparatively, with the PI3K inhibitor Dactolisib, the level of LC3 in the EA+D group was markedly increased compared with the EA ($P < 0.05$) and EA+NC groups ($P < 0.05$). These results demonstrate that EA treatment after MCAO surgery may inhibit autophagy, which

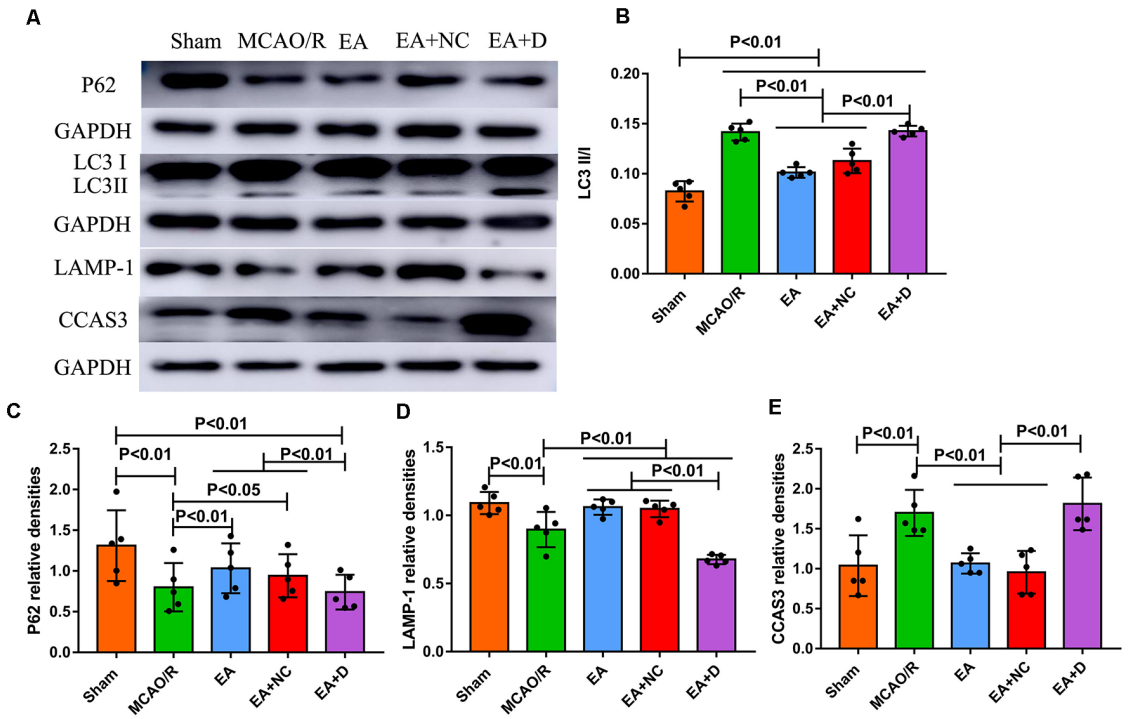

FIGURE 2 | Effect of electroacupuncture (EA) treatment on CCAS3 and autophagy-related proteins. **(A)** Western blot analysis of the expression levels of P62, LC3I, LC3II, LAMP-1, and CCAS3. **(B)** Bar diagram shows the difference of LC3II/I in the ipsilateral hippocampus of the rats (n = 5/group). **(C)** Statistical analysis showing the expression of P62 in the ipsilateral hippocampus of the rats. **(D)** Statistical analysis showing the difference of LAMP-1 in the ipsilateral hippocampus of the rats. **(E)** Statistical analysis showing the expression of CCAS3 in the ipsilateral hippocampus of the rats.

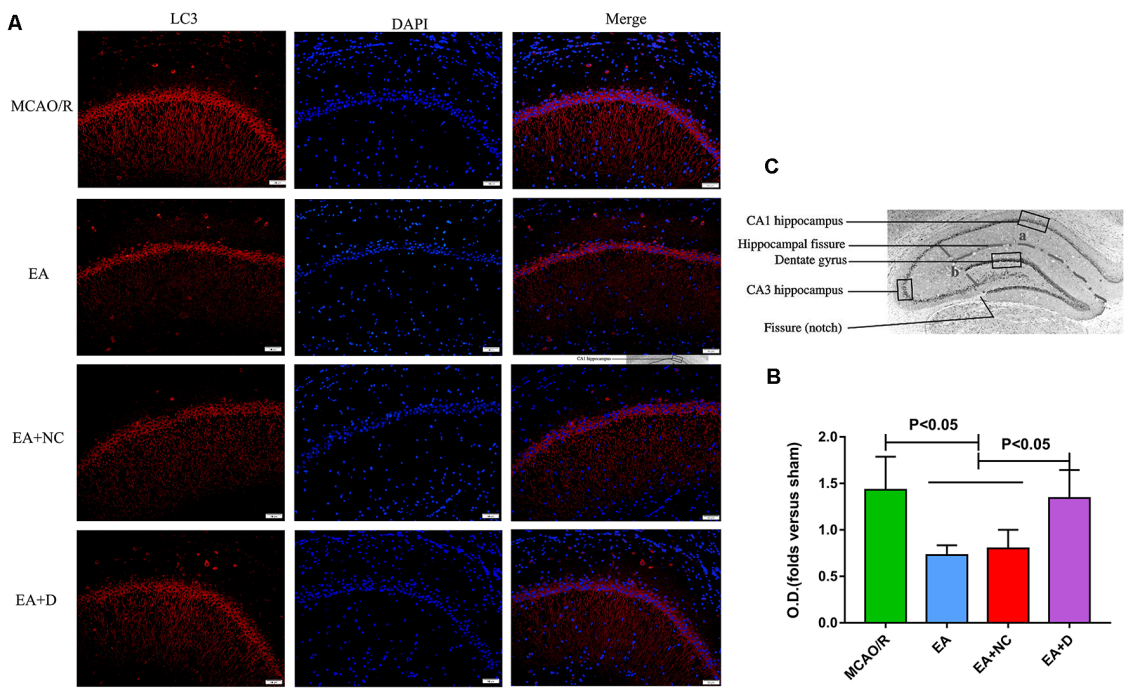

FIGURE 3 | IF analysis of the effect of EA treatment on autophagy-related proteins. **(A)** IF analysis showing the expression difference of LC3 in the ipsilateral hippocampus of the rats. **(B)** Statistical analysis of the LC3 expression assessed by IF. **(C)** The anatomical illustration of the hippocampus in the rat.

can exert a neuroprotective effect on EA treatment in ischemic stroke. As shown in **Figure 3C**, the anatomical illustration of the hippocampus in the rat.

EA Intervention Activates the PI3K/AKT/mTOR Pathway in Cerebral I/R-Injured Rats

As shown in **Figure 4A**, to investigate the effect of EA intervention on the PI3K/AKT/mTOR pathway following an ischemic stroke, Western blotting was performed to examine the expression levels of PI3K, Atg7, total-mTOR (t-mTOR), phosphorylated-mTOR (P-mTOR), total-AKT (t-AKT) and phosphorylated-AKT (P-AKT) in the ischemic cerebral hippocampus. As shown in **Figure 4B**, the level of PI3K was significantly decreased in the MCAO/R group ($P < 0.01$) compared with the sham group, but EA treatment reversed this change in the EA ($P < 0.01$) and EA+NC groups ($P < 0.01$). However, the expression of PI3K in the EA+D group was significantly decreased compared with the EA ($P < 0.01$) and EA+NC groups ($P < 0.01$). As shown in **Figure 4C**, the expression level of Atg7 was increased in the MCAO/R group compared with the sham group ($p < 0.01$). Compared with the MCAO/R group, the expression level of Atg7 was significantly decreased in the EA ($p < 0.05$) and EA+NC groups ($p < 0.05$). Moreover, the expression level of Atg7 was significantly increased in the EA+D group compared with the EA ($p < 0.05$) and EA+NC groups ($p < 0.05$).

As shown in **Figure 4D**, the levels of phosphorylation of mTOR (P-mTOR/t-mTOR) in the MCAO/R ($P < 0.01$) group were significantly decreased compared with the sham group, whereas EA treatment reversed this change in the EA ($P < 0.01$) and EA+NC groups ($P < 0.01$) compared with the MCAO/R group, and the level of phosphorylation of mTOR in the EA+D group was significantly decreased compared with the EA ($P < 0.01$) and EA+NC groups ($P < 0.01$). The level of phosphorylation of AKT (P-mAkt/t-mAkt) in the MCAO/R group was significantly decreased compared with the sham group ($P < 0.01$). Compared with the MCAO/R group, the level of phosphorylation of AKT was significantly increased in the EA group ($p < 0.01$), but there was no significant difference between the MCAO/R group and EA+NC group. Moreover, the level of phosphorylation of AKT was significantly decreased in the EA+D group compared with the EA group ($p < 0.01$), as shown in **Figure 4E**. These results demonstrate that EA treatment exerted neuroprotection *via* regulating the PI3K/AKT/mTOR pathway in cerebral I/R rats.

DISCUSSION

The Effect of EA Treatment on Autophagy and Apoptosis of Neuronal Cells after Stroke

The protective effect of electroacupuncture on ischemic stroke and other neurological diseases was confirmed by the current study. Our previous studies indicated that EA improved the symptoms of neurological impairment and decreased the volume of cerebral infarction in rats (Xing et al., 2018a,b). However, the exact mechanisms are still not clear. Autophagy plays an important role in the process of cerebral I/R injury and is crucial for neuronal cell survival and death (Harvey, 1979). It was reported that EA preconditioning protected the brain from I/R damage by inhibiting the autophagy process (Wu et al., 2015). Furthermore, EA has been shown to exert a protective effect on ischemic stroke by inhibiting autophagy and autophagosome formation, which is mediated by the mTORC1-ULK complex-Beclin1 pathway (Liu et al., 2016). In the current study, we demonstrated that the expression of P62 and LAMP1 were significantly decreased in the hippocampus after MCAO surgery and were increased in the hippocampus after EA treatment and reversed by the PI3K inhibitor Dactolisib; also, the LC3-II/I ratio was significantly increased after MCAO surgery and was decreased in the hippocampus after EA treatment and was reversed by Dactolisib administration. These results indicate that EA exerted a neuroprotective effect *via* inhibiting neuronal autophagy, which is following the above-mentioned results. Moreover, our results demonstrate that PI3K plays a key role in the process of EA exerting neuroprotection. However, Wu et al. (2016) reported that the protective effect of EA preconditioning for cerebral ischemic injury was mainly because of upregulated autophagy expression. This result was different from our results regarding whether the activation or inhibition of autophagy could play a protective role. The contradictory results might be because of the different time points of EA intervention or the different stages in the pathological process of stroke.

Apoptosis is one important pathophysiological change following an ischemic stroke. Here, a neuroprotective effect is defined as the suppression of neuronal apoptosis to rescue or inhibit the progress of neuronal death (Hou et al., 2018). EA pretreatment can inhibit the expression of proapoptotic genes and proteins, reduce cell apoptosis, and modulate the activation of microglia (Yao et al., 2019). Moreover, EA can alleviate neuronal apoptosis in the ischemic in the penumbral region surrounding the ischemic cores. In the meanwhile, EA activated the expression level of p-AKT, p-Bad, and BCL-2 and inhibited the expression level of Bax and CCAS3 (Xue et al., 2014). In the current study, we found that the expression of CCAS3 was significantly increased after MCAO surgery and was decreased after EA treatment. Moreover, the inhibition of PI3K by Dactolisib abolished the neuroprotective effect of EA. According to these results, EA intervention markedly suppressed neuronal autophagy and apoptosis, thus alleviating brain damage following I/R.

Also, as for acupoint selection, the related animal experiments have shown that electroacupuncture stimulation at LI11 and ST36 acupoints can reduce motor dysfunction, improve the degree of neurological impairment and reduce the volume of cerebral infarction (Xing et al., 2018b,c; Liu et al., 2019). In consideration of the therapeutic dose of EA, based on the results of related articles, we select the 72 h time point and decide on a 3 times*30 min treatment plan in the present study (Liu et al., 2016; Huang et al., 2019).

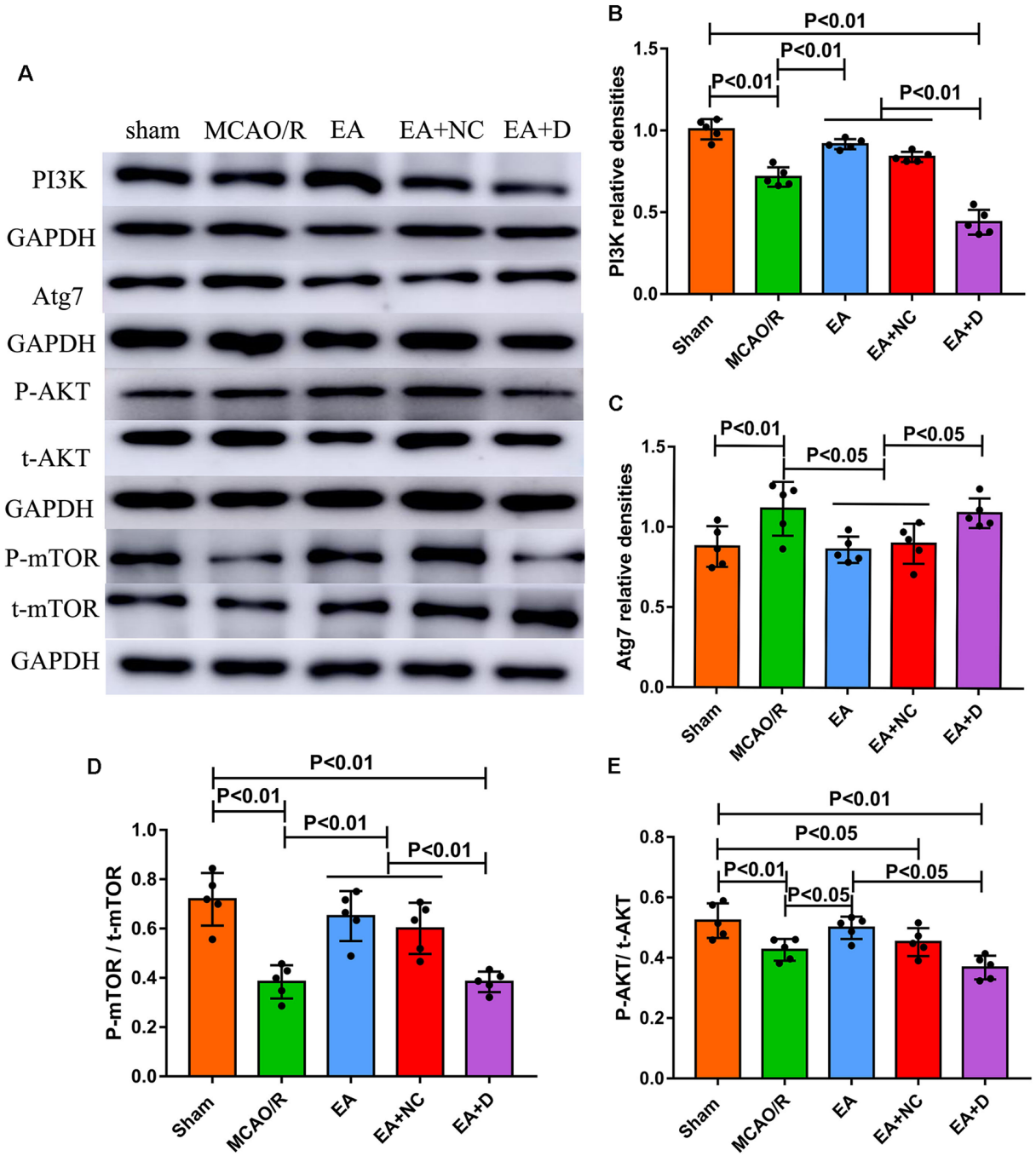

FIGURE 4 | Effect of EA intervention on the protein of the PI3K/AKT pathway in cerebral I/R-injured rats. **(A)** Western blot analysis showing the levels of PI3K, Atg7, P-AKT, t-AKT, P-mTOR, and t-mTOR among the sham, MCAO/R, EA, EA+NC, and EA+D groups. **(B)** Statistical analysis showing the difference of PI3K in the ipsilateral hippocampus of the rats (n = 5/group). **(C)** Statistical analysis showing the expression of Atg7 in the ipsilateral hippocampus of the rats. **(D)** Statistical analysis showing the level of P-mTOR/t-mTOR in the ipsilateral hippocampus of the rats. **(E)** Statistical analysis showing the level of P-AKT/t-AKT in the ipsilateral hippocampus of the rats.

In summary, EA treatment could exert a neuroprotective effect possibly *via* inhibiting neuronal autophagy and apoptosis following an ischemic stroke, and here, PI3K played a key role in this mechanism.

The Effect of EA Intervention on PI3K/AKT/mTOR Pathway

Because of the key role of PI3K in the process of inducing neuroprotection *via* EA following an ischemic

stroke, the downstream protein targets of PI3K were investigated.

In the present study, the levels of PI3K, phosphorylation of AKT, and phosphorylation of mTOR were significantly decreased following I/R injury, were activated by EA treatment, and were reversed by Dactolisib administration. Moreover, the expression of Atg7 was significantly increased after MCAO surgery, decreased in the hippocampus after EA treatment and reversed by Dactolisib administration. Furthermore, there is substantial evidence that the mammalian targets of rapamycin complex 1 (mTORC1) have an important effect on autophagy after ischemic stroke (Liu et al., 2016). Gabapentin (GBP) pretreatment has been shown to reduce brain IR injury by activating the PI3K/Akt/mTOR pathway, which exerted the neuroprotective effect *via* inhibiting the neurons autophagy associated with oxidative stress (Yan et al., 2019). Moreover, EA treatment could suppress hippocampal neuron apoptosis and improve neurological impairments in rats with cerebral palsy *via* regulating the PI3K/AKT signaling pathway (Zhang et al., 2018). The neuroprotective effect of EA seems to be regulated *via* activating the PI3K pathway rather than the ERK pathway (Sun et al., 2005). Therefore, we could conclude that AKT, mTOR, and Atg7 are the downstream proteins of PI3K.

The PI3K-Akt-mTOR signaling pathway plays an important role in cell autophagy, and it is also a main signal transduction cascade involved in cell proliferation, metabolism, and survival (Wang et al., 2018). LC3, P62, and Beclin-1 are autophagy-related proteins. Beclin-1 interacts with PI3K to trigger autophagy and then participates in the subsequent steps of the fusion of autophagosomes and lysosomes (Zhao et al., 2020). LC3 combines with the autophagosome membrane to form a complete autophagosome, and then fuses and degrades with lysosomes (Currarino et al., 1976). P62 interacts with LC3 II to aggregate for achieving autophagy -specific degradation (Parzych and Klionsky, 2014). The present study demonstrated that EA treatment can activate the PI3K/AKT signaling pathway after ischemic stroke. EA activated the expression level of PI3K, p-AKT, and P-mTOR and inhibited the expression level of Atg7. Moreover, Wang et al. (2019) reported that EA intervention also suppressed the activation of the mTOR signaling pathway and attenuated hermal pain responses in SCI rats. Catalpa may be involved in axonal regeneration *via* regulating the PI3K/AKT/mTOR pathway (Wang et al., 2019). And Rhy (Rhynchophylline) can activate the PI3K/Akt/mTOR signaling pathway possibly by regulating the AKT/mTOR pathway to alleviate ischemic injury (Huang et al., 2014). According to these results, we can conclude that EA treatment exerted neuroprotective effects by regulating the PI3K/AKT/mTOR pathway after ischemic stroke.

CONCLUSION

In conclusion, our results indicate that EA at the LI11 and ST36 acupoints inhibited neuronal autophagy and apoptosis in rats following ischemic stroke. Also, the mechanism of EA treatment exerted neuroprotection after ischemic stroke by regulating the PI3K/AKT/mTOR pathway. Furthermore, our research also may provide a possible interventional target point for novel therapeutic methods.

DATA AVAILABILITY STATEMENT

All datasets generated for this study are included in the article.

ETHICS STATEMENT

The animal study was reviewed and approved by Animal Use and Care Committee of Hebei Medical University.

AUTHOR CONTRIBUTIONS

M-MW and FZ designed the study. YX, MZ, and Y-SF performed the experiments. W-BL, Z-XT, FD, M-MW, and FZ analyzed the results together. M-MW and FZ wrote the article. All authors read and approved the final version.

REFERENCES

Currarino, G., Willis, K. W., Johnson, A. F. Jr., and Miller, W. W. (1976). Pulmonary telangiectasia. *Am. J. Roentgenol.* 127, 775–779. doi: 10.2214/ajr.127.5.775

Escobar, I., Xu, J., Jackson, C. W., and Perez-Pinzon, M. A. (2019). Altered neural networks in the Papez circuit: implications for cognitive dysfunction after cerebral ischemia. *J. Alzheimers Dis.* 67, 425–446. doi: 10.3233/jad-180875

Graf, R., Kataoka, K., Rosner, G., and Heiss, W. D. (1986). Cortical deafferentation in cat focal ischemia: disturbance and recovery of sensory functions in cortical areas with different degrees of cerebral blood flow reduction. *J. Cereb. Blood Flow. Metab.* 6, 566–573. doi: 10.1038/jcbfm.1986.103

Graham, S. H., and Liu, H. (2017). Life and death in the trash heap: the ubiquitin proteasome pathway and UCHL1 in brain aging, neurodegenerative disease and cerebral Ischemia. *Ageing Res. Rev.* 34, 30–38. doi: 10.1016/j.arr.2016.09.011

Harvey, R. J. (1979). Interaction between rifampicin and trimethoprim. *J. Antimicrob. Chemother.* 5, 113–115. doi: 10.1093/jac/5.1.113

He, H., Zeng, Q., Huang, G., Lin, Y., Lin, H., Liu, W., et al. (2019). Bone marrow mesenchymal stem cell transplantation exerts neuroprotective effects following cerebral ischemia/reperfusion injury by inhibiting autophagy *via* the PI3K/Akt pathway. *Brain Res.* 1707, 124–132. doi: 10.1016/j.brainres.2018.11.018

Hou, Y., Wang, K., Wan, W., Cheng, Y., Pu, X., and Ye, X. (2018). Resveratrol provides neuroprotection by regulating the JAK2/STAT3/PI3K/AKT/mTOR pathway after stroke in rats. *Genes Dis.* 5, 245–255. doi: 10.1016/j.gendis.2018.06.001

Huang, Y. G., Yang, S. B., Du, L. P., Cai, S. J., Feng, Z. T., and Mei, Z. G. (2019). [Electroacupuncture pretreatment alleviated cerebral ischemia-reperfusion injury *via* suppressing autophagy in cerebral cortex tissue in rats]. *Zhen Ci Yan Jiu* 44, 867–872. doi: 10.13702/j.1000-0607.190307

Huang, H., Zhong, R., Xia, Z., Song, J., and Feng, L. (2014). Neuroprotective effects of rhynchophylline against ischemic brain injury *via* regulation of the Akt/mTOR and TLRs signaling pathways. *Molecules* 19, 11196–11210. doi: 10.3390/molecules190811196

Khoshnam, S. E., Winlow, W., Farzaneh, M., Farbood, Y., and Moghaddam, H. F. (2017). Pathogenic mechanisms following ischemic stroke. *Neurol. Sci.* 38, 1167–1186. doi: 10.1007/s10072-017-2938-1

Liu, X., Feng, Z., Du, L., Huang, Y., Ge, J., Deng, Y., et al. (2019). The potential role of MicroRNA-124 in cerebral ischemia injury. *Int. J. Mol. Sci.* 21:E120. doi: 10.3390/ijms21010120

Liu, W., Shang, G., Yang, S., Huang, J., Xue, X., Lin, Y., et al. (2016). Electroacupuncture protects against ischemic stroke by reducing autophagosome formation and inhibiting autophagy through the mTORC1-ULK1 complex-Beclin1 pathway. *Int. J. Mol. Med.* 37, 309–318. doi: 10.3892/ijmm.2015.2425

Liu, L., Wang, N. H., Zhang, Q., Li, S. Y., Gu, W. J., and Wu, Y. (2019). [Micro-ribonucleic acids participate in electroacupuncture intervention-induced improvement of ischemic stroke]. *Zhen Ci Yan Jiu* 44, 686–692. doi: 10.13702/j.1000-0607.180643

Luo, H. Y., Zeng, Z. W., Yu, X. B., He, J., Cao, J., and Xu, B. (2019). [Effect of electroacupuncture with different frequencies on hindlimb locomotor function and expression of LC3, Beclin 1 and cleaved Caspase-3 proteins in spinal cord injury rats]. *Zhen Ci Yan Jiu* 44, 625–631. doi: 10.13702/j.1000-0607.190068

Parzych, K. R., and Klionsky, D. J. (2014). An overview of autophagy: morphology, mechanism, and regulation. *Antioxid. Redox Signal.* 20, 460–473. doi: 10.1089/ars.2013.5371

Samakova, A., Gazova, A., Sabova, N., Valaskova, S., Jurikova, M., and Kyselovic, J. (2019). The PI3k/Akt pathway is associated with angiogenesis, oxidative stress and survival of mesenchymal stem cells in pathophysiologic condition in ischemia. *Physiol. Res.* 68, S131–S138. doi: 10.33549/physiolres.934345

Sekerdag, E., Solaroglu, I., and Gursoy-Ozdemir, Y. (2018). Cell death mechanisms in stroke and novel molecular and cellular treatment options. *Curr. Neuropharmacol.* 16, 1396–1415. doi: 10.2174/1570159x16666180302115544

Sommer, C. J. (2017). Ischemic stroke: experimental models and reality. *Acta Neuropathol.* 133, 245–261. doi: 10.1007/s00401-017-1667-0

Sun, F., Wang, X., Mao, X., Xie, L., and Jin, K. (2012). Ablation of neurogenesis attenuates recovery of motor function after focal cerebral ischemia in middle-aged mice. *PLoS One* 7:e46326. doi: 10.1371/journal.pone.0046326

Sun, N., Zou, X., Shi, J., Liu, X., Li, L., and Zhao, L. (2005). Electroacupuncture regulates NMDA receptor NR1 subunit expression *via* PI3-K pathway in a rat model of cerebral ischemia-reperfusion. *Brain Res.* 1064, 98–107. doi: 10.1016/j.brainres.2005.09.060

Wang, J., Wan, D., Wan, G., Wang, J., Zhang, J., and Zhu, H. (2019). Catalpol induces cell activity to promote axonal regeneration *via* the PI3K/AKT/mTOR pathway *in vivo* and *in vitro* stroke model. *Ann. Transl. Med.* 7:756. doi: 10.21037/atm.2019.11.101

Wang, Y., Zhao, Y., Ma, X., Li, J., Hou, J., and Lv, X. (2019). Beneficial effects of electroacupuncture on neuropathic pain evoked by spinal cord injury and involvement of PI3K-mTOR mechanisms. *Biol. Res. Nurs.* 21, 5–13. doi: 10.1177/1099800418804896

Wang, B. J., Zheng, W. L., Feng, N. N., Wang, T., Zou, H., Gu, J. H., et al. (2018). The effects of autophagy and PI3K/AKT/m-TOR signaling pathway on the cell-cycle arrest of rats primary sertoli cells induced by zearalenone. *Toxins* 10:E398. doi: 10.3390/toxins10100398

Wu, Z. Q., Cui, S. Y., Zhu, L., and Zou, Z. Q. (2016). Study on the mechanism of mTOR-mediated autophagy during electroacupuncture pretreatment against cerebral ischemic injury. *Evid. Based Complement. Alternat. Med.* 2016:9121597. doi: 10.1155/2016/9121597

Wu, Z., Zou, Z., Zou, R., Zhou, X., and Cui, S. (2015). Electroacupuncture pretreatment induces tolerance against cerebral ischemia/reperfusion injury through inhibition of the autophagy pathway. *Mol. Med. Rep.* 11, 4438–4446. doi: 10.3892/mmr.2015.3253

Xie, G., Yang, S., Chen, A., Lan, L., Lin, Z., Gao, Y., et al. (2013). Electroacupuncture at Quchi and Zusanli treats cerebral ischemia-reperfusion injury through activation of ERK signaling. *Exp. Ther. Med.* 5, 1593–1597. doi: 10.3892/etm.2013.1030

Xing, Y., Wang, M. M., Feng, Y. S., Dong, F., and Zhang, F. (2018a). Possible involvement of PTEN signaling pathway in the anti-apoptotic effect of electroacupuncture following ischemic stroke in rats. *Cell. Mol. Neurobiol.* 38, 1453–1463. doi: 10.1007/s10571-018-0615-4

Xing, Y., Yang, S. D., Wang, M. M., Dong, F., Feng, Y. S., and Zhang, F. (2018b). Electroacupuncture alleviated neuronal apoptosis following ischemic stroke in rats *via* midkine and ERK/JNK/p38 signaling pathway. *J. Mol. Neurosci.* 66, 26–36. doi: 10.1007/s12031-018-1142-y

Xing, Y., Zhang, M., Li, W. B., Dong, F., and Zhang, F. (2018c). Mechanisms involved in the neuroprotection of electroacupuncture therapy for ischemic stroke. *Front. Neurosci.* 12:929. doi: 10.3389/fnins.2018.00929

Xue, X., You, Y., Tao, J., Ye, X., Huang, J., Yang, S., et al. (2014). Electro-acupuncture at points of Zusanli and Quchi exerts anti-apoptotic effect through the modulation of PI3K/Akt signaling pathway. *Neurosci. Lett.* 558, 14–19. doi: 10.1016/j.neulet.2013.10.029

Yan, B. C., Wang, J., Rui, Y., Cao, J., Xu, P., Jiang, D., et al. (2019). Neuroprotective effects of gabapentin against cerebral ischemia reperfusion-induced neuronal autophagic injury *via* regulation of the PI3K/Akt/mTOR signaling pathways. *J. Neuropathol. Exp. Neurol.* 78, 157–171. doi: 10.1093/jnen/nly119

Yang, S., Wang, H., Yang, Y., Wang, R., Wang, Y., Wu, C., et al. (2019). Baicalein administered in the subacute phase ameliorates ischemia-reperfusion-induced brain injury by reducing neuroinflammation and neuronal damage. *Biomed. Pharmacother.* 117:109102. doi: 10.1016/j.biopha.2019.109102

Yao, S. Q., Yi, W., Liu, R., and Xu, N. G. (2019). [Development of research on mechanisms of electroacupuncture intervention underlying improvement of cerebral ischemia rats in recent five years]. *Zhen Ci Yan Jiu* 44, 383–387. doi: 10.13702/j.1000-0607.180260

Zhang, X., Du, Q., Yang, Y., Wang, J., Liu, Y., Zhao, Z., et al. (2018). Salidroside alleviates ischemic brain injury in mice with ischemic stroke through regulating BDNK mediated PI3K/Akt pathway. *Biochem. Pharmacol.* 156, 99–108. doi: 10.1016/j.bcp.2018.08.015

Zhang, H., Gao, J., Wang, M., Yu, X., Lv, X., Deng, H., et al. (2018). Effects of scalp electroacupuncture on the PI3K/Akt signalling pathway and apoptosis of hippocampal neurons in a rat model of cerebral palsy. *Acupunct. Med.* 36, 96–102. doi: 10.1136/acupmed-2016-011335

Zhao, Y., Feng, X., Li, B., Sha, J., Wang, C., Yang, T., et al. (2020). Dexmedetomidine protects against lipopolysaccharide-induced acute kidney injury by enhancing autophagy through inhibition of the PI3K/AKT/mTOR pathway. *Front. Pharmacol.* 11:128. doi: 10.3389/fphar.2020.00128

Conflict of Interest: The authors declare that the research was conducted in the absence of any commercial or financial relationships that could be construed as a potential conflict of interest.

frontiers in Cellular Neuroscience

ORIGINAL RESEARCH
published: 21 May 2020
doi: 10.3389/fncel.2020.00102

Laser Lesion in the Mouse Visual Cortex Induces a Stem Cell Niche-Like Extracellular Matrix, Produced by Immature Astrocytes

Lars Roll[1,2], *Ulf T. Eysel*[2,3] *and Andreas Faissner*[1,2]*

[1] Department of Cell Morphology and Molecular Neurobiology, Faculty of Biology and Biotechnology, Ruhr University Bochum, Bochum, Germany, [2] International Graduate School of Neuroscience, Ruhr University Bochum, Bochum, Germany, [3] Department of Neurophysiology, Faculty of Medicine, Ruhr University Bochum, Bochum, Germany

OPEN ACCESS

Edited by:
Yuchuan Ding,
Wayne State School of Medicine, United States

Reviewed by:
Jorge Matias-Guiu, Complutense University of Madrid, Spain
Yu-Feng Wang, Harbin Medical University, China

***Correspondence:**
Andreas Faissner
andreas.faissner@rub.de

Specialty section:
This article was submitted to Non-Neuronal Cells, a section of the journal Frontiers in Cellular Neuroscience

Received: *07 January 2020*
Accepted: *03 April 2020*
Published: *21 May 2020*

Citation:
Roll L, Eysel UT and Faissner A (2020) Laser Lesion in the Mouse Visual Cortex Induces a Stem Cell Niche-Like Extracellular Matrix, Produced by Immature Astrocytes. Front. Cell. Neurosci. 14:102. doi: 10.3389/fncel.2020.00102

The mammalian central nervous system (CNS) is characterized by a severely limited regeneration capacity. Comparison with lower species like amphibians, which are able to restore even complex tissues after damage, indicates the presence of an inhibitory environment that restricts the cellular response in mammals. In this context, signals provided by the extracellular matrix (ECM) are important regulators of events like cell survival, proliferation, migration, differentiation or neurite outgrowth. Therefore, knowledge of the post-lesional ECM and of cells that produce these factors might support development of new treatment strategies for patients suffering from traumatic brain injury and other types of CNS damage. In the present study, we analyzed the surround of focal infrared laser lesions of the adult mouse visual cortex. This lesion paradigm avoids direct contact with the brain, as the laser beam passes the intact bone. Cell type-specific markers revealed a distinct spatial distribution of different astroglial subtypes in the penumbra after injury. Glial fibrillary acidic protein (GFAP) as marker for reactive astrocytes was found broadly up-regulated, whereas the more immature markers vimentin and nestin were only expressed by a subset of cells. Dividing astrocytes could be identified via the proliferation marker Ki-67. Different ECM molecules, among others the neural stem cell-associated glycoprotein tenascin-C and the DSD-1 chondroitin sulfate epitope, were found on astrocytes in the penumbra. *Wisteria floribunda* agglutinin (WFA) and aggrecan as markers for perineuronal nets, a specialized ECM limiting synaptic plasticity, appeared normal in the vicinity of the necrotic lesion core. In sum, expression of progenitor markers by astrocyte subpopulations and the identification of proliferating astrocytes in combination with an ECM that contains components typically associated with neural stem/progenitor cells suggest that an immature cell fate is facilitated as response to the injury.

Keywords: astrocyte, chondroitin sulfate, cortical plasticity, extracellular matrix, neural stem cell, niche, regeneration, tenascin

INTRODUCTION

Lesions of the mammalian central nervous system (CNS) are characterized by a limited regeneration capacity. In the light of patients' recovery it is of interest to understand the molecular and cellular mechanisms underlying this limitation on the one hand and to identify the potential of cells in this region on the other hand. In this study, laser-induced lesions of the mouse visual cortex were employed as a model for brain injury and the lesion response was assessed with a focus on the fate of astrocytes and on different factors of the extracellular matrix (ECM). The visual cortex is easily accessible for manipulation and has been used for several plasticity studies (Eysel and Schweigart, 1999; Eysel et al., 1999). Originally established in cats and rats, the visual cortex lesions were also adapted to mice, where the lesion is inflicted by an infrared laser (Roll et al., 2012). In this lesion paradigm, direct contact of the brain with surgical instruments and exposure to the environment are avoided, as the laser beam passes the intact bone. This provides well-defined conditions and a direct infection of the brain with contaminating pathogens can be excluded. In the close surround of laser-induced lesions, reduced blood flow comparable to the penumbra of ischemic infarctions has been described (Kiessling et al., 1990; Lindsberg et al., 1991). The well-defined border of the lesion core enables the post-lesional study of the vulnerable surround with high spatial precision.

Astrocytes respond to injuries and participate in a process called reactive gliosis. They produce cytokines and ECM molecules, are involved in glial scar formation and can show stem cell properties under specific circumstances (Robel et al., 2011; Pekny and Pekna, 2014). Therefore astrocytes are interesting as a potential source for new cells that might contribute to new networks.

Cell behavior and the cell fate are tightly regulated by external signals. Accordingly the ECM, a complex network that serves as reservoir for a multitude of factors, and its composition are of interest. The importance of the ECM for CNS function is undisputed, for example as one part of the neural stem cell niche (Reinhard et al., 2016). A factor that is associated with immature neural cells is the glycoprotein tenascin-C (Tnc). During development it is expressed by astrocytes, before it is downregulated and restricted to the adult neural stem cell niche (Faissner et al., 2017). Tnc regulates processes such as adhesion, migration, neurite outgrowth, but also modulates the immune system (Loers and Schachner, 2007; Piccinini and Midwood, 2012). Interestingly, Tnc is re-expressed in the diseased CNS (Roll et al., 2012; Roll and Faissner, 2019). Typically ECM molecules are glycosylated and these carbohydrate modifications can modulate the properties of the carrier molecules, for example resulting in an altered interaction of different factors (reviewed by Hayes and Melrose, 2018). Specific glycoepitopes, which can be detected by monoclonal antibodies (mAbs), have been identified that show distinct expression patterns and therefore are expected to fulfill specific functions. The DSD-1 (dermatan sulfate-dependent 1) chondroitin sulfate epitope, recognized by mAb 473HD, is associated with neural stem cells and its blockage has been shown to affect proliferation of neural stem cells *in vitro* (von Holst et al., 2006). Glycoepitopes of the LewisX (LeX; also SSEA-1) type are trisaccharides. Specific antibodies are available that recognize LeX in distinct contexts: mAb 487^{LeX} detects terminal LeX motifs, whereas mAb 5750^{LeX} binds internal motifs (Hennen et al., 2011). Here, both antibodies have been shown to label different subpopulations of neural stem/progenitor cells. A related epitope, detected by the mAb 4860, has been found on cells of the oligodendrocyte lineage in the developing CNS (Czopka et al., 2009). Perineuronal nets (PNNs) are a specialized form of matrix that enwraps subtypes of neurons and is associated with plasticity restriction in the adult CNS. In the context of potentially increased plasticity after brain injury, analysis of PNN integrity can shed light on the underlying mechanisms. Indeed, PNN degradation in the diseased CNS has been described, but seems to depend on the type of damage (reviewed by Bozzelli et al., 2018).

MATERIALS AND METHODS

Animals

129S2/SvPasCrl (RRID:IMSR_CRL:287) mice were originally obtained from Charles River and held in the animal facility of the Ruhr University Bochum (Germany).

Infrared Laser Lesion of the Visual Cortex

All procedures were performed in accordance with the German law (§15 TierSchG) and approved by the animal protection commission of the Landesamt für Natur, Umwelt und Verbraucherschutz Nordrhein-Westfalen (file number 84-02.04.2012.A363). Laser lesions were performed according to a standardized protocol (Roll et al., 2012). In short, young adult mice (12 weeks old) were anesthetized with 65 mg ketamine, 13 mg xylazine and 2 mg acepromazine (all CP-Pharma, Burgdorf, Germany) per kg body weight (i.p.). Body temperature was stabilized by a heating pad. The scalp covering the cortex was cut with a scalpel, and the bone was drilled thin. A row of overlapping, round lesions (each 0.5 mm in diameter, 2 W, 810 nm) was inflicted to the right visual cortex through the wet (PBS), intact bone by an infrared laser (OcuLight SLx; Iris Medical/Iridex, Mountain View, CA, United States). Eventually, an area 2 mm long (A-P) and 0.5 mm wide (M-L), located 1 mm anterior from lambda suture and 1 mm lateral from sagittal suture, was affected by necrosis (lesion core). The skin wound was closed with tissue glue and the mice were allowed to recover in their cage under close monitoring.

Tissue Preparation and Immunohistochemistry

3, 7, 14, or 28 days post-lesion (dpl), animals were anesthetized with 65 mg ketamine, 13 mg xylazine and 2 mg acepromazine per kg body weight (i.p.). The heart was exposed and the mouse

was transcardially perfused for 5 min with heparin-supplemented (Liquemin N 25000, Roche, Mannheim, Germany; diluted 1:500) physiological salt solution (0.9% NaCl) to remove blood from the vascular system. Afterward animals were perfused for 15 min with 4% PFA to fix the tissue. The brain was dissected and fixed in 4% PFA for 24 h at 4°C, before it was transferred into 30% sucrose solution for cryoprotection. Finally, the tissue was mounted in Tissue-Tek (Sakura Finetek, Torrance, CA, United States) on dry ice and stored at −70°C.

Cryosections were prepared using a cryostat. 20-µm-thick frontal sections were collected either on Superfrost Plus microscope slides (Thermo Scientific, Braunschweig, Germany) or free-floating with a brush in cold PBS, supplemented with 1 mM EDTA. Tissue on glass was stored at −70°C, free-floating tissue was transferred into cryo vials filled with 1 mL mixture of glycerol and 30% (w/v) sucrose in PBS (1:1), supplemented with 1 mM EDTA.

Two immunohistochemistry protocols, for free-floating slices or slices on glass, were applied, depending on the antibody. Usually, stainings of ECM molecules were performed with free-floating slices in 96-well-plates. The slices were moved from one well to the next with a curved glass pipette. Slices were incubated in blocking solution (PBS supplemented with 1% bovine serum albumin, 5% goat serum and 0.5% Triton X-100) for 1 h at RT, in primary antibodies over night at 4°C, washed with PBS (3 min × 15 min), treated with secondary antibodies (diluted in blocking solution w/o Triton X-100) for 3 h, followed by washing in PBS (3 min × 15 min) before mounting in Immu-Mount (Thermo Fisher Scientific, Waltham, MA, United States) at RT. Alternatively, slices on glass slides were thawed and dried for 15 min at RT and washed in PBS. For PNN stainings, slices were heated in citrate buffer and kept at 100°C for 5 min. After 10 min the buffer was cooled on ice and the slices were washed in PBS for 5 min. The tissue was surrounded with Roti-Liquid barrier marker (Carl Roth, Karlsruhe, Germany). The following steps were performed in a dark, humidified chamber: after blocking for 1 h at RT, the primary antibody was applied over night at 4°C. Unbound antibodies were removed by washing in PBS (3 min × 5 min), before secondary antibodies were applied for 1 h, followed by washing in PBS (3 min × 5 min) and mounting in Immu-Mount (all at RT). Antibodies are listed in **Tables 1**, **2**. Cell nuclei were counterstained with Hoechst 33258 or To-Pro-3.

In situ Hybridization

In situ hybridization was performed according to a protocol described by N. P. Pringle and W. D. Richardson (Wolfson Institute for Biomedical Research, London, United Kingdom). The composition of buffers and solutions is listed in **Supplementary Table 1**. In short, 20-µm-thick slices on glass slides were thawed and dried for 10 min at RT. Digoxigenin-labeled RNA riboprobes (sequence: see **Supplementary Table 2**) were diluted 1:500 in hybridization mix and 250 µL of this solution were given onto each slice. The solution was covered with cover slips to avoid evaporation when the tissue was incubated for hybridization at 65°C over night in a humidified (2x SSC, 50% formamide) chamber. The cover slips were carefully removed by rinsing with wash buffer in a cuvette. Subsequently, two washing steps with pre-heated wash buffer at 65°C and three steps with MABT buffer at RT followed. The slices were transferred to a humidified (aqua dest) chamber and encircled with barrier marker. 150 µL blocking solution were added for 1 h at RT and subsequently replaced by 150 µL anti-DIG-AP (Roche Diagnostics, Mannheim, Germany) antibody solution, which was incubated at 4°C over night. After three washing steps with MABT buffer (each 10 min) at RT the samples were incubated in pre-developing buffer (2 min × 5 min at RT). Afterward, 200 µL developing solution were applied for at least 2 h at 37°C in the dark. Staining induced by the alkaline phosphatase was controlled under the microscope and stopped by incubation in aqua dest for 5 min. The slices were mounted with Immu-Mount and stored at 4°C.

Microscopy

After *in situ* hybridization, tissue was documented with a Leica MZ6 stereomicroscope (Leica Microsystems, Wetzlar, Germany), for higher magnifications with an Axioplan 2 microscope (Carl Zeiss, Oberkochen, Germany). Immunohistochemical stainings were documented with an Axio Zoom.V16, for higher magnifications with an Axioplan 2 or an LSM 510 META (all Carl Zeiss, Oberkochen, Germany). Images were exported and processed with Adobe Photoshop, Adobe Illustrator (both CS6; Adobe, Dublin, Ireland) and ImageJ (Fiji; Schindelin et al., 2012).

Quantitative Analysis

Cells in immunohistochemical stainings were counted manually using the cell counter tool in ImageJ (Fiji; Schindelin et al., 2012). Data were analyzed with Excel software (Office 2010; Microsoft Corporation, Redmond, WA, United States) and visualized with Adobe Illustrator (CS6; Adobe, Dublin, Ireland). To quantify the relative proliferation rate of reactive astrocytes (GFAP/Ki-67 double-positive cells in relation to all GFAP-positive cells), the cells in the penumbra of three brains (n = 3; three slices per brain) were counted. The total number of cells positive for GFAP, vimentin and nestin was determined by counting the cells in a defined area of 500 µm x 500 µm, directly adjacent to the border of the necrotic lesion core (n = 3; one slice per brain; 20-µm-thick slices).

SDS-Polyacrylamide Gel Electrophoresis (SDS-PAGE), Western Blot

1-mm-thick frontal sections of fresh brain tissue were sectioned with razor blades in cooled PBS (4°C). Each section was divided into four parts of equal size by a horizontal and a vertical cut. These parts were individually shock-frozen in reaction tubes on dry ice and stored at −70°C. The composition of buffers and solutions used for SDS-PAGE and Western blot is listed in **Supplementary Table 3**. In short, proteins were isolated by addition of 1 mL lysis buffer under trituration, first with a 1,000 µL pipette and subsequently with a fine insulin syringe. Samples were incubated on ice for 1 h, centrifuged (15 min at 4°C) and the supernatant was isolated and stored at −20°C before use. For SDS-PAGE, 15 µL of the supernatant were

TABLE 1 | Primary antibodies used for immunohistochemical analysis (IHC) and Western Blot (WB).

	Target	Species	Dilution	Reference/RRID
Antibody				
473HD	DSD-1 epitope	Rat IgM	IHC: 1:250	Faissner et al., 1994
4860	Glycolipid	Rat IgM	IHC: 1:200	Czopka et al., 2009
487^{LeX} (L5)	LeX epitope	Rat IgM	IHC: 1:350	Streit et al., 1990
5750^{LeX}	LeX epitope	Rat IgM	IHC: 1:50	Hennen et al., 2011
Aggrecan	Aggrecan	Rabbit poly.	IHC: 1:300	Merck Millipore RRID:AB_90460
βIII Tubulin	βIII Tubulin	Mouse IgG	IHC: 1:250	Sigma-Aldrich RRID:AB_477590
DM1A	α Tubulin	Mouse IgG	WB: 1:10,000	Sigma-Aldrich RRID:AB_477593
GFAP	Glial fibrillary acidic protein	Mouse IgG	IHC: 1:300	Sigma-Aldrich RRID:AB_477010
GFAP	Glial fibrillary acidic protein	Rabbit poly.	IHC: 1:200	DAKO RRID:AB_10013382
GFAP	Glial fibrillary acidic protein	Rat IgG	IHC: 1:400	Merck Millipore RRID:AB_211868
Iba1	Ionized calcium-binding adapter molecule 1	Goat IgG	IHC: 1:125	Abcam RRID:AB_2224402
Ki-67	Nuclei of dividing cells	Mouse IgG	IHC: 1:20	Novocastra/Leica RRID:AB_563841
Ki-67	Nuclei of dividing cells	Rabbit IgG	IHC: 1:50	Thermo Scientific RRID:AB_2341197
Nestin	Nestin	Mouse IgG	IHC: 1:250	Merck Millipore RRID:AB_94911
Tnc (Kaf 14.1)	Tenascin-C	Rabbit poly.	IHC: 1:250 WB: 1:300	Faissner and Kruse, 1990
Tnc (Kaf 12F)	Tenascin-C	Rabbit poly.	IHC: 1:250	Faissner and Kruse, 1990
Vimentin	Vimentin	Mouse IgM	IHC: 1:200	Sigma-Aldrich RRID:AB_261856
Lectin				
WFA (biotinylated)	Perineuronal nets	*Wisteria floribunda*	1:100	Sigma-Aldrich L1516-2MG

mixed with 5 μL loading buffer, heated (95°C for 5 min) and cooled on ice. Proteins were separated according to their molecular weight in polyacrylamide gels by an electric field (20 mA) for ca. 1 h in an electrophoresis unit (Hoefer, Heidelberg, Germany). Subsequently, proteins were transferred onto a PVDF membrane (Carl Roth, Karlsruhe, Germany) in an electric field of 75 mA for 1.5 h. The membrane was blocked with 5% milk powder in TBST for 1 h at RT. Primary antibodies were diluted in 5% milk powder in TBST and incubated at 4°C over night. After three washing steps with TBST (each 5 min) the secondary antibody was incubated for 1 h. Three washing steps with TBST and one step with TBS followed, before 5 mL of the ECL solution (Carl Roth, Karlsruhe, Germany) were applied for 5 min. The membrane was documented with a MicroChemi imaging system (DNR, Neve Yamin, Israel).

Reverse Transcription Polymerase Chain Reaction (RT-PCR)

1-mm-thick frontal sections of fresh brain tissue were sectioned with razor blades in cooled PBS (4°C). Each section was divided into four parts of equal size by a horizontal and a vertical cut. These parts were individually shock-frozen in reaction tubes on dry ice and stored at −70°C. RNA was isolated using the GenElute Total RNA purification kit (Sigma-Aldrich, St. Louis, MO, United States). 1 μg RNA was used for cDNA synthesis with the First strand cDNA synthesis kit (Thermo Scientific,

TABLE 2 | Secondary antibodies used for immunohistochemical analysis (IHC) and Western blot (WB).

Antibody	Species	Dilution	RRID
Anti goat, AF488	Donkey	1:300; IHC	Dianova RRID:AB_2336933
Anti mouse IgM, AF488	Goat	1:300; IHC	Dianova RRID:AB_2338849
Anti mouse IgG, Cy3	Goat	1:300; IHC	Dianova RRID:AB_2338687
Anti mouse IgG + IgM, AF488	Goat	1:300; IHC	Dianova RRID:AB_2338844
Anti mouse IgG + IgM, Cy3	Goat	1:300; IHC	Dianova RRID:AB_2338686
Anti mouse IgG + IgM, AF647	Goat	1:300; IHC	Dianova RRID:AB_2338908
Anti mouse IgG + IgM, Cy3	Rabbit	1:300; IHC	Dianova RRID:AB_2340139
Anti rabbit IgG, AF488	Goat	1:300; IHC	Dianova RRID:AB_2338049
Anti rabbit IgG, AF488	Donkey	1:300; IHC	Dianova RRID:AB_2313584
Anti rabbit IgG, Cy3	Goat	1:300; IHC	Dianova RRID:AB_2338003
Anti rabbit IgG, AF647	Goat	1:300; IHC	Dianova RRID:AB_2338078
Anti rat IgG + IgM, AF488	Goat	1:300; IHC	Dianova RRID:AB_2338357
Anti rat IgM, FITC	Goat	1:300; IHC	Dianova RRID:AB_2338198
Anti rat IgM, Cy3	Goat	1:300; IHC	Dianova RRID:AB_2338249
Anti mouse IgG + IgM, HRP	Goat	1:10,000; WB	Dianova RRID:AB_2338505
Anti rabbit IgG, HRP	Goat	1:10,000; WB	Dianova RRID:AB_2307391

Waltham, MA, United States). Details of the PCR buffers, primer sequences and the PCR program are provided in **Supplementary Table 4**. In short, PCR was performed with 1 μl of cDNA in a Mastercycler gradient (Eppendorf, Hamburg, Germany). The number of cycles was reduced from a standard of 25 to 20 for β *Actin* samples to avoid saturation effects. DNA amplicons were separated by agarose gel electrophoresis according to their size. Gels were documented with a digital camera under UV light (LTF, Wasserburg am Inn, Germany). Band intensity was measured densitometrically with ImageJ: after background subtraction, a box of equal size was drawn around each band and the "mean" value was determined using the "Measure" tool. Each value was normalized to the housekeeping gene β *Actin*. Data were analyzed with Excel software and visualized with Adobe Illustrator.

RESULTS

The cell fate as well as the expression of ECM molecules associated with immature neural cell populations and PNNs were assessed in the laser lesion model.

Reactive Gliosis After Cortical Laser Lesion

Reactive gliosis, which includes reactive astrocytes, is a hallmark in the lesion response of the CNS. Accordingly, the fate of astrocytes was examined in a first step with immunohistochemical stainings. Reactive gliosis could be observed by comparing the GFAP signal of the lesioned hemisphere with the contralateral side 3 days after laser lesion (3 dpl; **Figures 1A,B**). In the healthy, contralateral cortex only a faint GFAP signal in few cells was observed. The majority of these cells was found in close vicinity to the corpus callosum and in the outer cortical layers. In contrast, the penumbra was characterized by high levels of GFAP expressed by hypertrophic, reactive astrocytes that occurred in all cortical layers. This region (**Figure 1C**) was then analyzed in detail.

Reactive gliosis does not only involve astrocytes, but also activated microglia cells. Iba1, a marker for resting and activated microglia, was used to detect this cell type in the penumbra. Double staining for the astrocyte marker GFAP and the microglia marker Iba1 showed distinct signals that did not overlap (**Figure 2**). Microglia were detected throughout the whole cortex, in the healthy as well as in the lesioned hemisphere (**Figures 2A–B″**). No obvious difference in the density of Iba1 signals was observed in the lesioned hemisphere. Microglia were also present directly adjacent to the necrotic lesion core (**Figures 2C–C″**). In contrast, this region was completely free of GFAP-labeled astrocytes. They appeared in high numbers in the penumbra as described above, but they were completely absent in a radius of more than 300 μm around the lesion core, with an abrupt border.

Progenitor Marker Expression by Reactive Astrocytes

Astrocytes represent a heterogeneous cell type with numerous subpopulations. To assess these astroglial subtypes, distribution of the markers GFAP, nestin, and vimentin was analyzed in the penumbra. Triple staining for the markers (**Figure 3**) shows a prominent expression of the astrocyte marker GFAP and only a subset of the cells coexpressed vimentin. Even fewer cells were also positive for the progenitor marker nestin. We quantified the cells in a defined area of 500 μm x 500 μm adjacent to the border of the necrotic lesion core and found that 71.2 ± 5.5 cells expressed GFAP, 30.7 ± 11.0 cells expressed vimentin and only 16 ± 13 cells expressed nestin in 20 μm-thick slices (**Supplementary Figure 1**). The distribution of marker-expressing cells appeared not arbitrarily. Instead, vimentin and even more obviously the nestin-positive cells were restricted to the region close to the lesion core. Outside

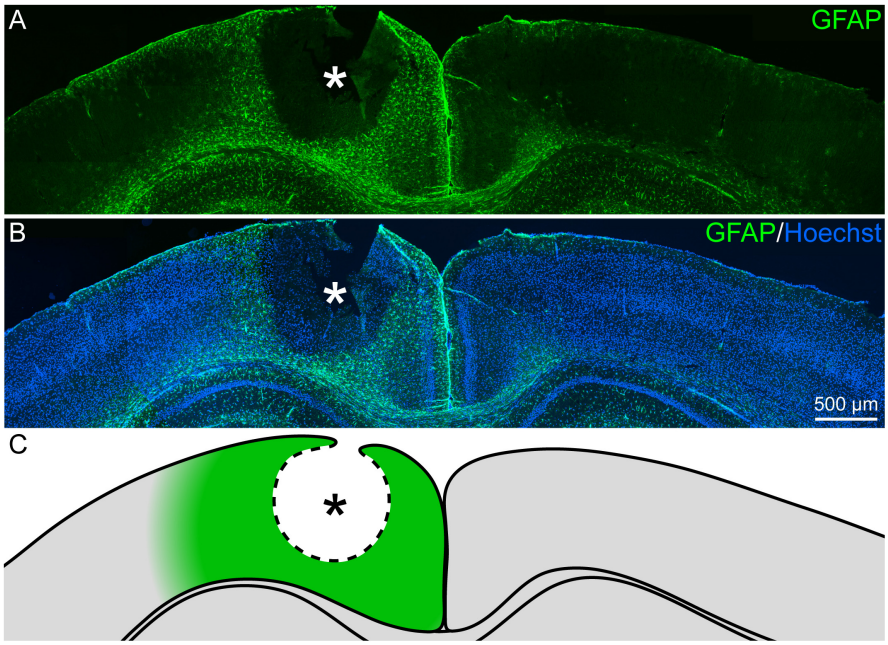

FIGURE 1 | Reactive gliosis after cortical laser lesion, 3 dpl. **(A,B)** GFAP-positive astrocytes appeared in the penumbra of the necrotic lesion core in the adult visual cortex (frontal brain section). Under healthy conditions, GFAP was only sparsely expressed. **(C)** Scheme of the lesion that indicates the penumbra around the lesion core in green. Asterisk: lesion core; Hoechst: nuclear counterstaining; scale bar: 500 µm.

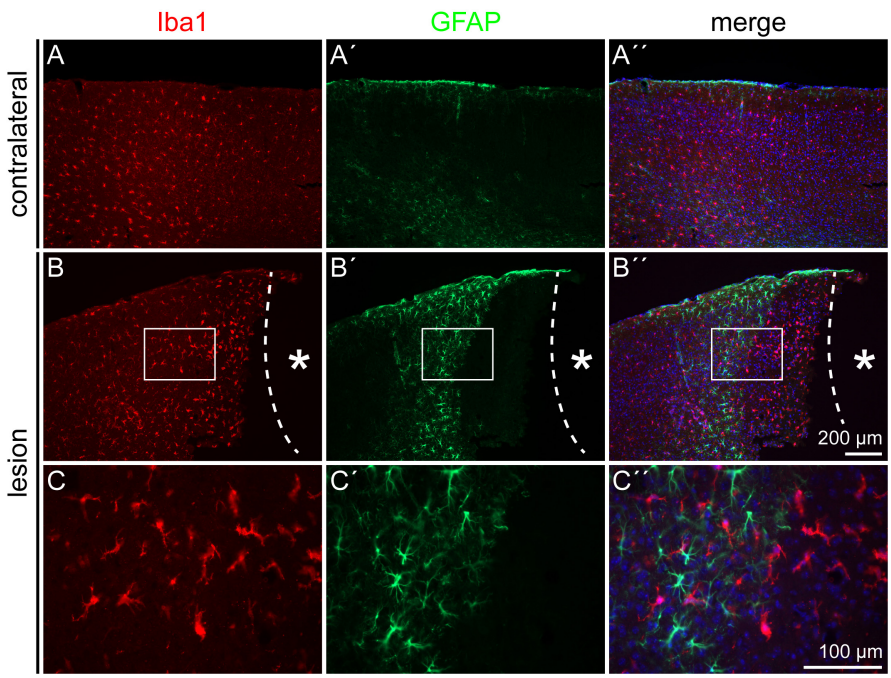

FIGURE 2 | Microglia and astrocyte distribution after lesion, 3 dpl. Iba1 staining showed no colocalization with the GFAP signal. As on the contralateral side **(A–A′′)**, Iba1-positive microglia were distributed also throughout the cortex in the penumbra **(B–B′′)**. GFAP-positive astrocytes kept a distance of more than 300 µm from the lesion core, whereas Iba1-positive microglia could be found directly adjacent to it. **(C–C′′)** Show higher magnifications of the boxes in **(B–B′′)**. Asterisk: lesion core; scale bars: 200 µm **(A–B′′)**, 100 µm **(C–C′′)**.

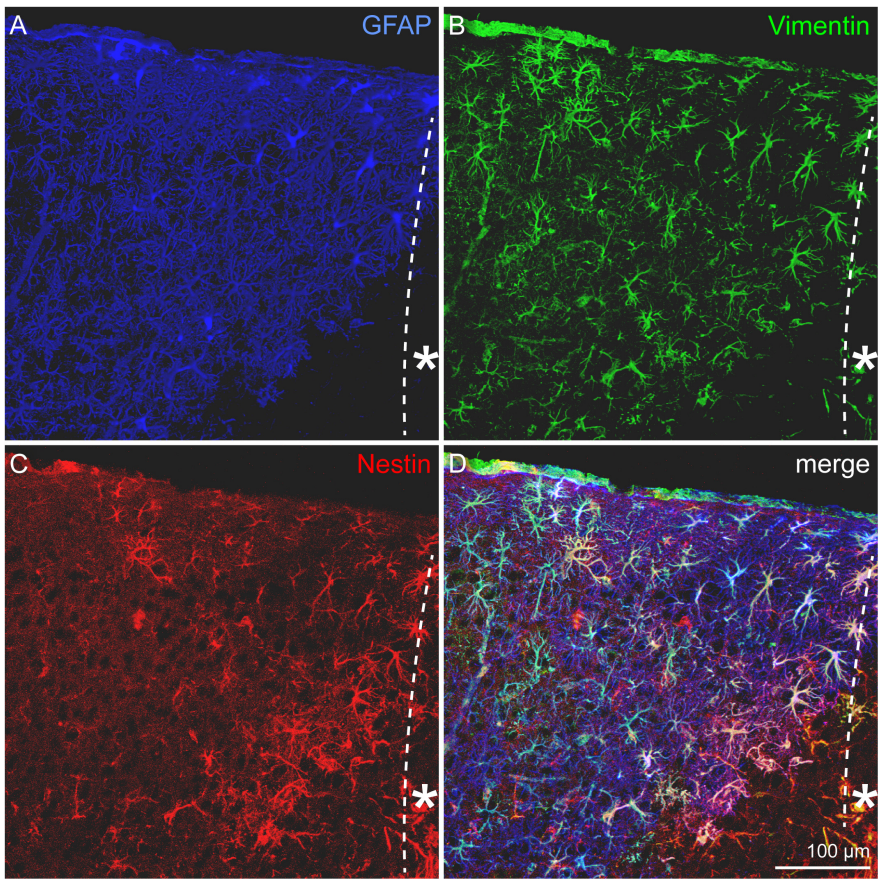

FIGURE 3 | Astrocytic subpopulations in the lesioned cortex, 3 dpl. **(A)** GFAP-positive, reactive astrocytes appeared in high numbers in the penumbra. GFAP was broadly upregulated, whereas vimentin **(B)** and most strikingly nestin **(C)** were restricted to cells near the lesion core. Nearly all of the vimentin- and nestin-expressing cells were also positive for GFAP **(D)**. Asterisk: direction toward the lesion core; scale bar: 100 µm.

the penumbra, cells positive for these markers are absent in the healthy cortex.

Proliferation of Reactive Astrocytes

Depending on the lesion paradigm, reactive astrocytes can re-enter the cell cycle. To examine if laser lesion of the mouse visual cortex induced astrocyte proliferation in the penumbra, double stainings of nestin and GFAP with the proliferation marker Ki-67 were performed. Ki-67 labels proliferating cells in all phases of the cell cycle. A huge number of cells in the lesioned cortex were positive for Ki-67 (**Figures 4A–A‴**). For an unambiguous allocation of a nucleus with a certain cell to avoid false-positive results from nuclei of other cells, and therefore of a potentially different cell type, three-dimensional reconstructions of confocal images were analyzed. The fact that nestin and GFAP both are constituents of intermediate filaments and therefore part of the cytoskeleton allowed a clear allocation. Double staining of nestin and Ki-67 3 days after lesion indeed revealed proliferating cells that expressed the progenitor marker nestin. Detailed analysis of one cell shows the labeled cytoskeleton encasing the nucleus (**Figures 4B–B″**). The cell shown in this example had three long, fine processes that contacted a blood vessel (arrows). Also proliferating GFAP-expressing cells were identified in the penumbra, as shown by the clear coexpression of GFAP in the cytoskeleton around a Ki-67-positive nucleus (**Figures 5A–B″**). Quantification revealed that 1.5 ± 0.4% of the GFAP-positive, reactive astrocytes in the cortical penumbra expressed Ki-67 (**Supplementary Figure 2**).

Extracellular Matrix After Lesion

After characterization of the cell fate in the penumbra, with a focus on the astrocytic lineage, the extracellular environment was analyzed. Tnc was re-expressed in the penumbra by nestin-positive, reactive astrocytes (**Figures 6A–B″**). Immunohistochemical analyses in the lesioned brain are always critical with regard to unspecific staining and strong background due to the damaged tissue containing cell debris, immune cells and other factors. *In situ* hybridization independently confirmed a prominent re-expression of *Tnc* mRNA in the penumbra after 3 days, whereas no expression was detected on the contralateral side (**Figure 6C**). The negative control with the sense riboprobe showed no staining in the whole brain slice (**Figure 6C′**). We performed RT-PCR and Western blot as pilot experiments with a time series to assess Tnc

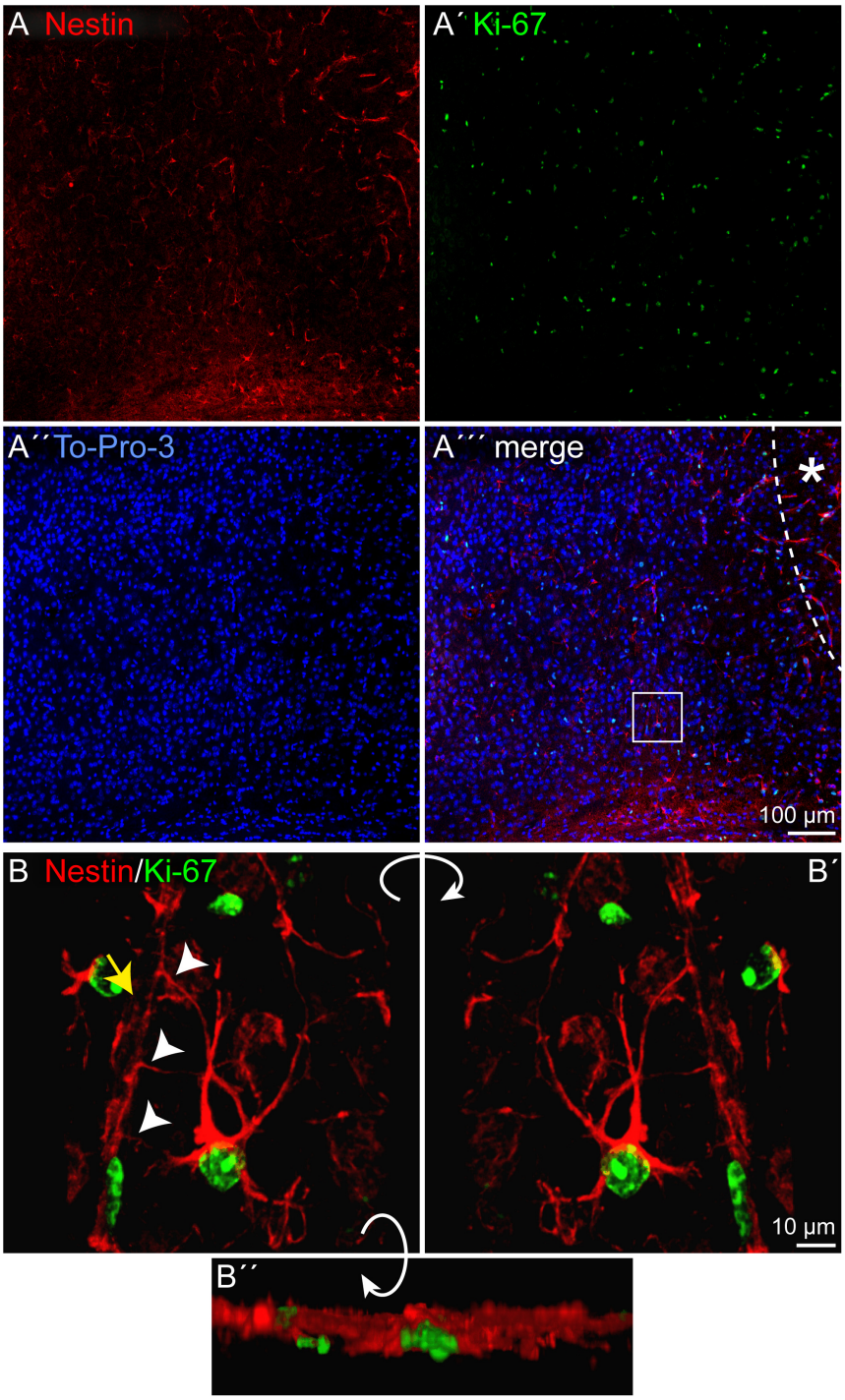

FIGURE 4 | Proliferation of nestin-positive cells, 3 dpl. **(A–A′′′)** Staining of the proliferation marker Ki-67 revealed numerous proliferating cells in the penumbra after lesion. Some of these cells were also nestin-positive. **(B–B′′)** An example of such a cell boxed in **(A′′′)** is shown after three-dimensional reconstruction of confocal images. The cell formed at least three contacts (arrowheads) to vasculature (yellow arrow). Asterisk: direction toward the lesion core; scale bars: 100 µm **(A–A′′′)**, 10 µm **(B–B′′)**.

expression independently (n = 1; **Supplementary Figure 3**). RT-PCR revealed an increase in relative *Tnc* expression in the lesioned hemisphere 3 dpl (fivefold increase compared to the healthy control and to the contralateral side). Expression levels on mRNA level returned to normal values already 7 dpl. In contrast, the Western blot showed stronger signals at 3 dpl

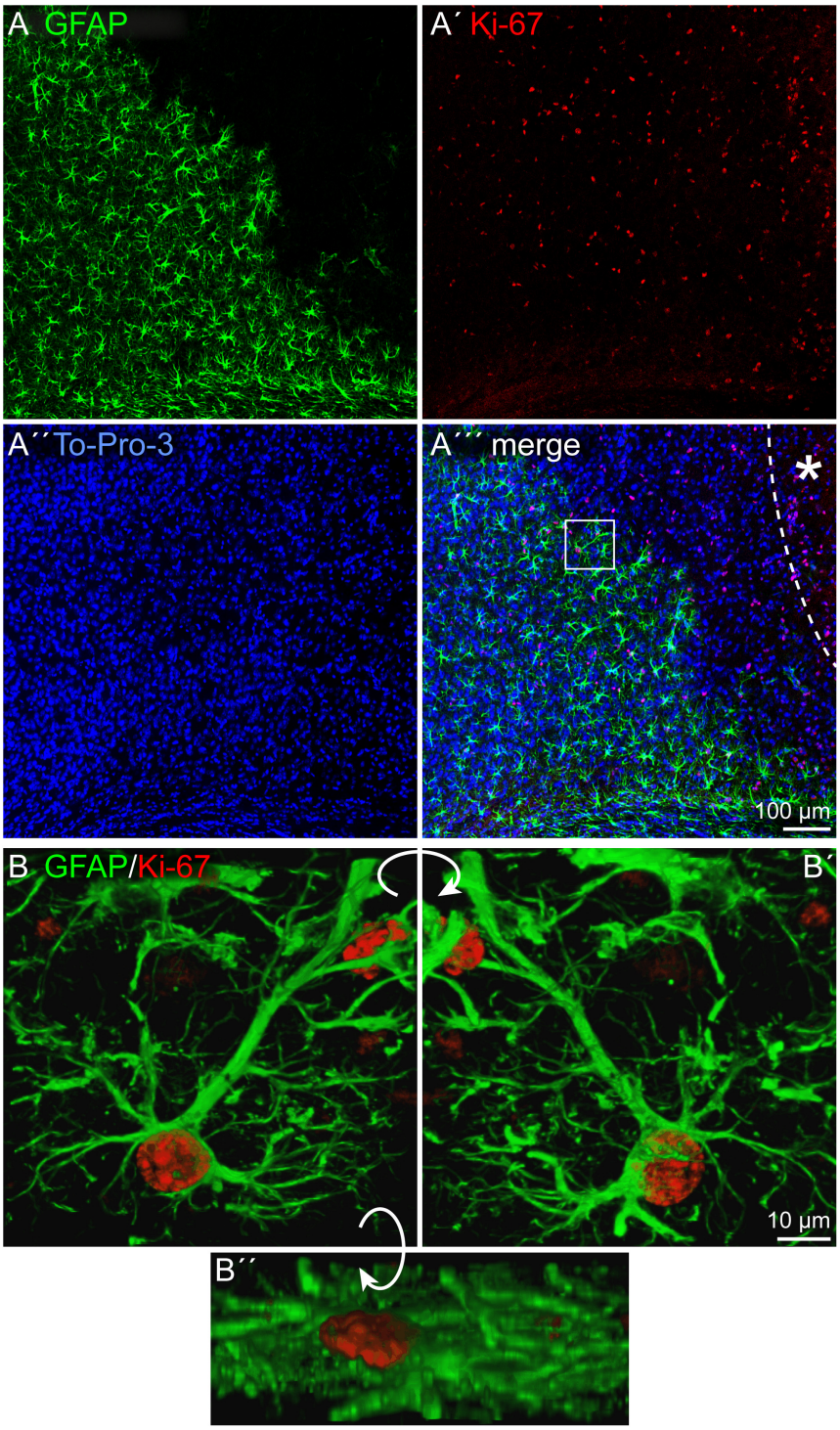

FIGURE 5 | Proliferation of reactive astrocytes, 3 dpl. **(A–A´´´)** Immunohistochemical stainings for Ki-67 labeled numerous proliferating cells in the penumbra after lesion. Some of these cells were also GFAP-positive. **(B–B´´)** An example of a proliferating astrocyte (boxed in **A´´´**) is shown after three-dimensional reconstruction of confocal images. Asterisk: direction toward the lesion core; scale bars: 100 µm **(A–A´´´)**, 10 µm **(B–B´´)**.

and also at 7 dpl, indicating that the increase in Tnc protein levels exceeded the short upregulation seen on mRNA level (**Supplementary Figure 3**).

The expression of the stem cell-related DSD-1 glycoepitope, detected by the mAb 473HD, and other glycoepitopes in the penumbra was examined by immunohistochemical analyses.

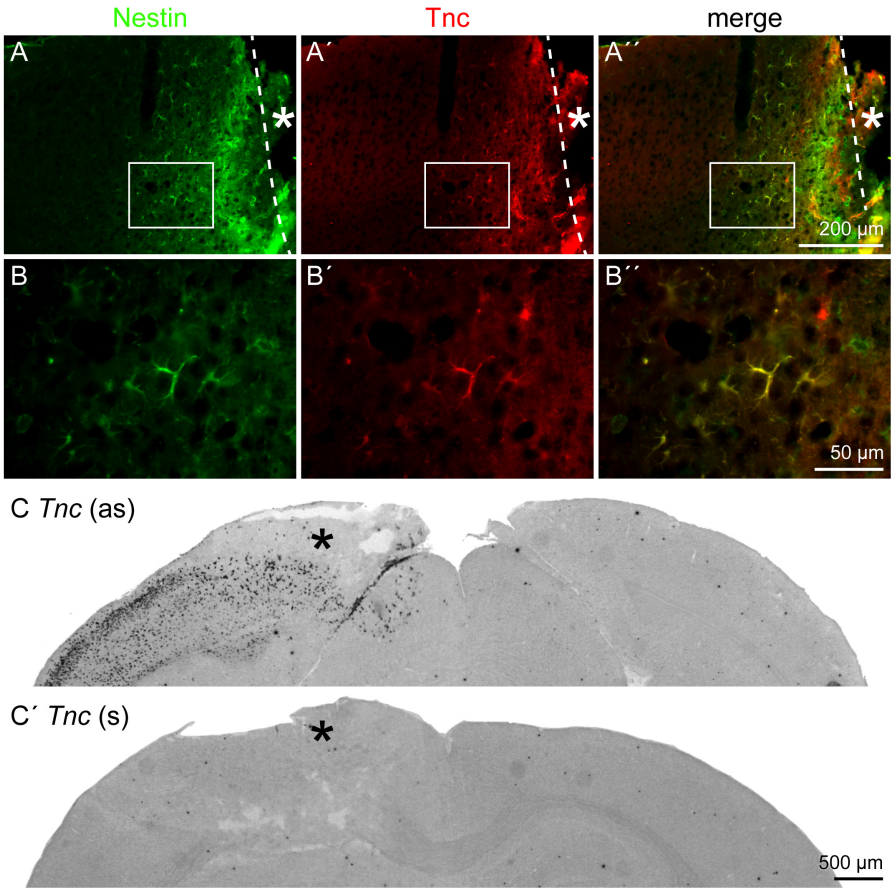

FIGURE 6 | Tnc expression by reactive astrocytes, 3 dpl. **(A–B′′)** Tnc was expressed by nestin-positive reactive astrocytes in the penumbra. **(B–B′′)** Higher magnifications of the boxed region in **A–A′′**. **(C,C′)** *In situ* hybridization revealed a prominent re-expression of *Tnc* mRNA in the lesioned cortex, whereas no expression was found on the contralateral side. The sense riboprobe (s), used as a negative control, showed no unspecific staining. Asterisk: lesion core; scale bars: 200 µm **(A–A′′)**, 50 µm **(B–B′′)**, 500 µm **(C,C′)**.

The DSD-1 was detected in the penumbra, on cells near the lesion core (**Figures 7A,A′**). The expression pattern of LeX-type glycoepitopes and a related epitope recognized by mAb 4860 was analyzed in a next step. mAb 487^{LeX} led to a diffuse signal and did not reveal a lesion-specific expression of its epitope (**Figures 7B,B′**). 5750^{LeX} staining showed a characteristic, patchy expression pattern. This was also not altered in the penumbra, except at the direct border to the lesion core (**Figures 7C,C′**). In addition to a diffuse staining in both hemispheres, the 4860 epitope was found on distinct cells in the penumbra that showed an astrocytic morphology (**Figures 7D,D′**), similar to the cells stained with GFAP earlier.

The DSD-1 epitope is associated with GFAP- and nestin-positive cells after laser lesion (Roll et al., 2012). To confirm also the astroglial identity of 4860 epitope-expressing cells, double stainings of GFAP and the 4860 epitope were performed (**Figure 8**). In the healthy cortex on the contralateral side, mAb 4860 only stained very few cells. These were double-positive for GFAP (**Figures 8A–A′′**). In contrast, the penumbra contained a large number of 4860-positive cells, distributed throughout all cortical layers. These cells represented a subpopulation of GFAP-positive astrocytes (**Figures 8B–B′′**). As shown in a higher magnification, not all GFAP-positive cells coexpressed the 4860 epitope, instead the epitope expression was restricted to astrocytic subpopulations (**Figures 8C–C′′**).

Perineuronal Nets After Lesion

Beside ECM related to immature neural cell types, PNNs as a specialized form of ECM were immunohistochemically analyzed. Detected by double stainings of the two PNN markers *Wisteria floribunda* agglutinin (WFA) and aggrecan (Acan), PNNs appeared with a punctate staining pattern around individual neurons in the cortex (**Figure 9**). As the relative intensity of individual PNN markers can differ, also depending on the brain region, both markers were used. In contrast to WFA staining, which produced a clear staining pattern with intensely stained PNNs, the Acan staining appeared less prominent, at least in the cortex. In the penumbra of the laser lesion, PNN markers were not affected 3 dpl (**Figures 9A–A′′′**). The same was true 28 dpl, when morphologically intact PNNs were labeled (**Figures 9B–B′′′**). The location of GFAP-positive astrocytes shows the high degree of reactive gliosis. The presence of PNN markers in

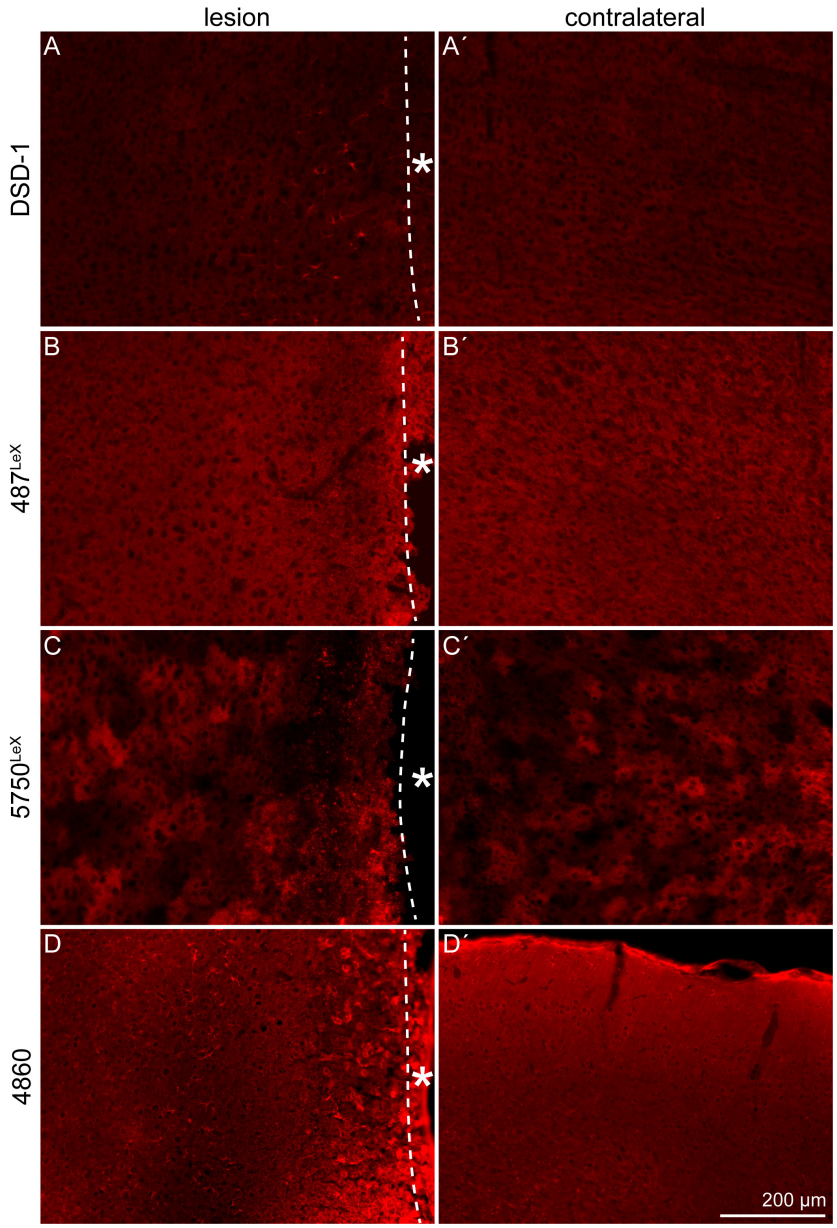

FIGURE 7 | Expression of the DSD-1, 487^{LeX}, 5750^{LeX}, and 4860 glycoepitopes, 3 dpl. **(A,A′)** The DSD-1 glycoepitope was detected on cells, restricted to the penumbra. **(B,B′)** Staining with mAb 487^{LeX} did not show a lesion-specific expression of the epitope. **(C,C′)** The 5750^{LeX} staining revealed a characteristic, patchy expression pattern that was not altered in the penumbra. **(D,D′)** The 4860 epitope was found on distinct cells in the penumbra, in contrast to a diffuse staining in the healthy hemisphere. Asterisk: direction toward the lesion core; scale bar: 200 µm.

this environment suggests that PNNs were relatively stable in the penumbra.

DISCUSSION

Heterogeneous Subpopulations of Astrocytes After Lesion

Reactive astrocytes play a crucial role in the lesion response of the CNS. They are involved in the formation of the glial scar and secrete a variety of ECM and other signaling molecules like cytokines (Dowell et al., 2009). In addition, reactive astrocytes can show characteristics of neural stem/progenitor cells. To assess the cell fate of reactive astrocytes after laser lesion, the expression of GFAP, vimentin, and nestin was immunohistochemically analyzed by triple stainings (**Figure 3**). In the healthy CNS, GFAP is expressed by astrocyte subpopulations (Sofroniew and Vinters, 2010), vimentin is present in the radial glia type of neural stem cells during development (Bignami et al., 1982) and nestin is the prototypical neural stem/progenitor cell marker

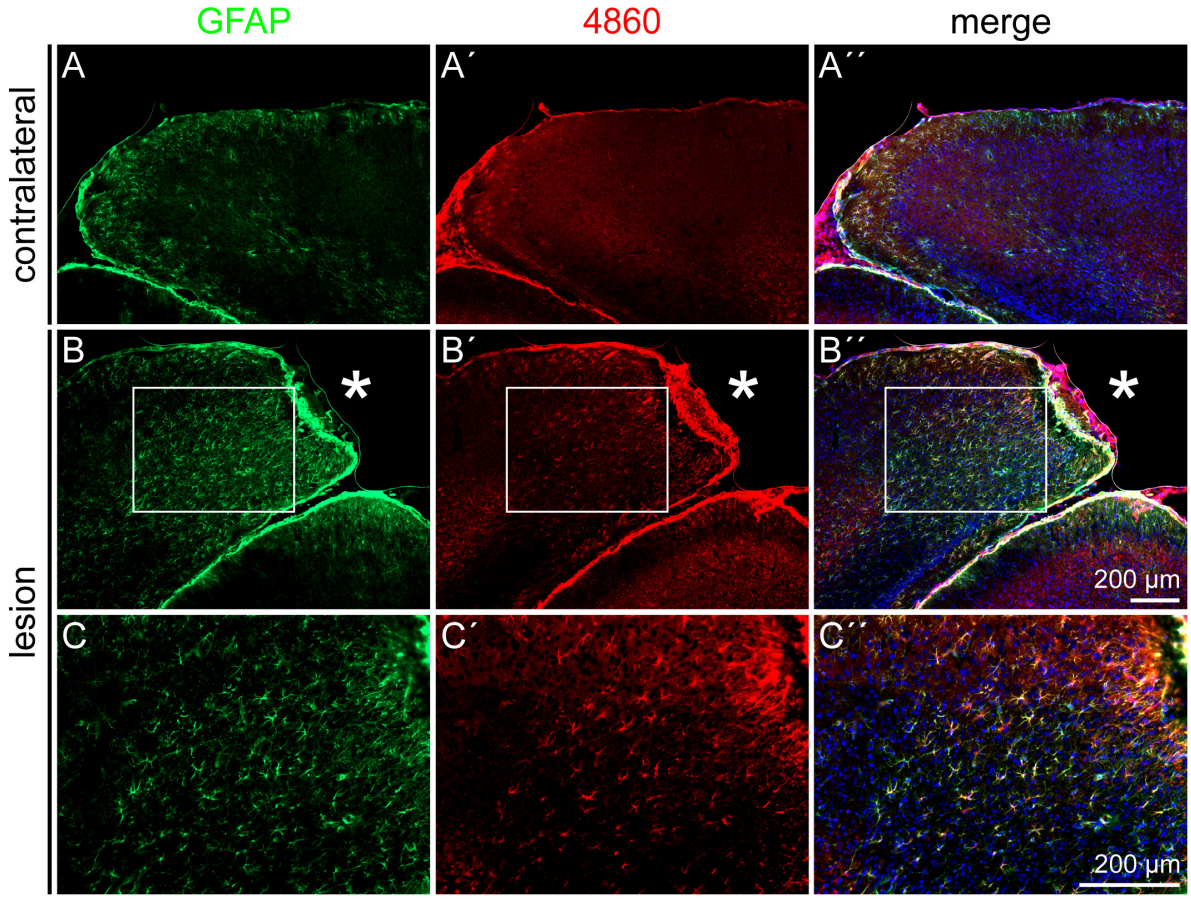

FIGURE 8 | 4860 glycoepitope expression on astrocytes after lesion, 3 dpl. **(A–A′′)** In the contralateral hemisphere, mAb 4860 labeled only few GFAP-positive cells. **(B–C′′)** In contrast, the penumbra was rich in 4860-positive cells, representing a subpopulation of GFAP-positive astrocytes. **(C–C′′)** Higher magnifications of the boxed region in **B–B′′**. Asterisk: lesion core; scale bars: 200 µm.

(Dahlstrand et al., 1995). Under pathological conditions, all three markers can be expressed by reactive astrocytes (Robel et al., 2011). The observed expression pattern in our laser lesion model with broad GFAP expression, fewer cells coexpressing vimentin and only very few cells adjacent to the lesion core that were also positive for nestin suggests the emergence of distinct astrocytic subpopulations. Similar results have been obtained in the rat model after laser lesion of the visual cortex (Sirko et al., 2009). Regional progenitor marker expression that is limited to the close vicinity of the lesion site has also been detected in other lesion models, for example after spinal cord injury (SCI) and cryogenic traumatic brain injury (White et al., 2010; Kim et al., 2012; Wanner et al., 2013). Astroglial expression of progenitor markers can reflect an immature state of the cells. If they indeed re-enter the cell cycle depends on the type of damage. For example, in many models of long-term neurodegenerative diseases such as Alzheimer's, proliferation is not or only rarely observed (Ben Haim et al., 2015). In contrast, proliferating astrocytes have been described in many cases after acute damage with blood–brain barrier disruption (Dimou and Götz, 2014).

In our laser lesion model, proliferating nestin- as well as GFAP-positive cells were detected by double stainings with the proliferation marker Ki-67 (**Figures 4**, **5**). The fact that astrocytes proliferate does not mean that they form new neurons and replace lost cells after injury. Under many conditions, neurogenesis from reactive astrocytes has not been observed *in vivo* (Götz et al., 2015). Progenitor marker expression seems to indicate the intrinsic potential of the cells rather than the cell fates they actually adopt in the lesioned environment. The hypothesis that the cell fate is not only a question of cell-intrinsic properties but also depends on appropriate external signals is supported by severe differences reported in the astrocytes' potential *in vivo* and *in vitro*. Astrocytes isolated after stab wound formed neurospheres and gave rise to neurons, astrocytes, and oligodendrocytes *in vitro* but not *in vivo*, indicating an anti-neurogenic environment in the adult brain, also after damage (Buffo et al., 2008).

An important question concerns the origin of the reactive astrocytes present in the penumbra. Two mechanisms are conceivable. Activation of local astrocytes on the one hand, and attraction of astrocytes with stem/progenitor characteristics from

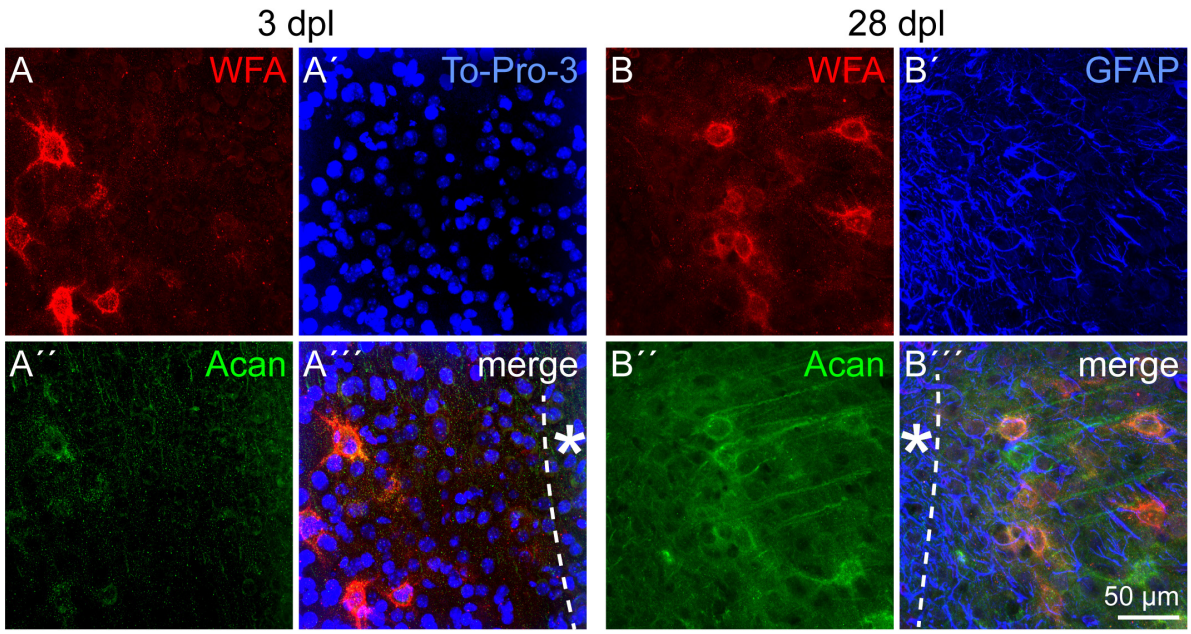

FIGURE 9 | PNNs in the lesioned visual cortex. **(A–A′′′)** WFA intensely stained PNNs in the penumbra 3 dpl. Aggrecan (Acan) signals appeared more diffuse. **(B–B′′′)** The same was observed 28 dpl, when morphologically intact PNNs could still be detected. GFAP-positive astrocytes **(B′–B′′′)** indicate the high degree of reactive gliosis in the region where the PNN markers were still detectable. Asterisk: direction toward the lesion core; scale bar: 50 µm.

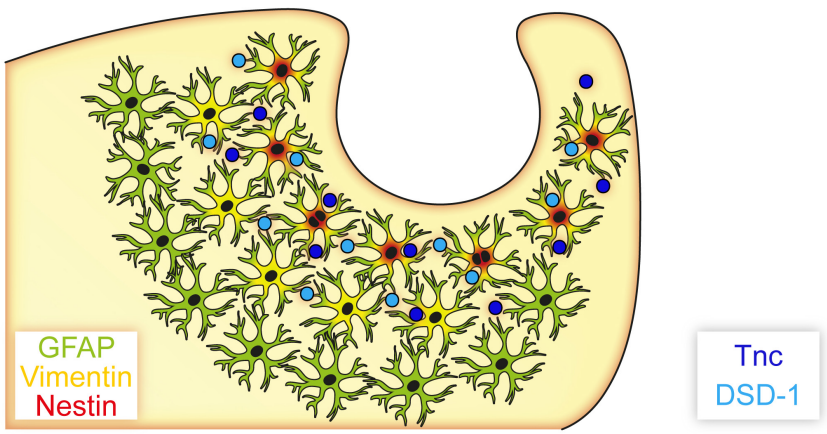

FIGURE 10 | Astrocyte subpopulations and extracellular matrix after cortical laser lesion. Reactive astrocytes with distinct marker profiles were observed in a region-specific manner. GFAP-positive cells were found in a broad region of the penumbra, whereas only subpopulations of these cells also coexpressed vimentin or nestin. These markers combined with an extracellular matrix containing neural stem/progenitor cell-associated factors like Tnc and the DSD-1 epitope indicate an immature cell fate of these astrocyte subpopulations, potentially facilitated by an environment resembling parts of the neural stem cell niche.

the adult stem cell niches, namely the subventricular zone (SVZ) or subgranular zone (SGZ), on the other hand. Both mechanisms have been described for different types of CNS damage. Local activation has been detected following stab wound injury (Buffo et al., 2008). After stroke, an increased proliferation in the SVZ and an attraction of SVZ cells to the damaged area were shown (Arvidsson et al., 2002). In the present study, the organized spatial distribution of astroglial subtypes, depending on their position in the penumbra, as soon as 3 days after injury suggests that local astrocytes are activated. Otherwise, nestin-positive cells could also be expected in regions outside the penumbra, on their way from the niche to their target region. This does not exclude the possibility of additional stem/progenitor cells that might be attracted from the adult stem cell niches, but favors a model where local activation is the predominant mechanism after laser lesion.

ECM Remodeling After Lesion

As the ECM provides important signals for the cells in the penumbra (reviewed by Roll and Faissner, 2014), its composition

after laser lesion was assessed with regard to Tnc (**Figure 6**) and the DSD-1 glycoepitope, recognized by the mAb 473HD (**Figure 7**). These molecules have in common that they are expressed during CNS development and are downregulated under healthy conditions in the adult.

Tnc and the DSD-1 epitope were detected exclusively in the penumbra, and they are associated with reactive astrocytes in close vicinity of the lesion (Roll et al., 2012). *Tnc* mRNA detected by *in situ* hybridization was very prominent in the lesioned hemisphere. The area was broader than Tnc detection by immunohistochemical analysis, indicating a regulation on the translational or post-translational level. An isoform-specific Tnc expression after brain injury in the rat has been reported, with isoforms containing the FNIII domains B and D specifically upregulated after cortical injury (Dobbertin et al., 2010). The findings are also in line with other reports. Tnc is expressed in the injured human cortex and is strongly restricted to those GFAP-positive cells that were very close to the lesion site in cortical lesions of the rat (McKeon et al., 1991; Brodkey et al., 1995). Tnc and Phosphacan/RPTPβ/ζ, which can carry the DSD-1 epitope, colocalize with GFAP after SCI and entorhinal cortex lesion (Deller et al., 1997; Tang et al., 2003). Expression of the DSD-1 epitope by reactive astrocytes has been described for laser lesions of the rat visual cortex, in this case the carrier molecule RPTPβ/ζ was also found upregulated (Sirko et al., 2009). Similar results have been obtained in the injured cortex, where the short isoform of RPTPβ/ζ was upregulated most prominently (Dobbertin et al., 2003).

In addition to the DSD-1 epitope, expression of the glycoepitopes recognized by the mAbs 4860, 487^{LeX}, and 5750^{LeX} was analyzed immunohistochemically (**Figure 7**). The 4860 epitope was found on astroglial cells, shown by double staining with GFAP (**Figure 8**). In the healthy CNS, the epitope is part of glycolipids on cells of the oligodendrocyte lineage that have nearly completed differentiation and have already downregulated NG2 and other earlier markers (Czopka et al., 2009). During postnatal development, the epitope is strongly expressed and shows a diffuse staining pattern in the adult cortex. Under normal conditions a colocalization of the 4860 epitope with nestin and GFAP has not been described. This leads to the question how the ectopic expression of this epitope on reactive astrocytes can be interpreted. It is obvious that under pathological conditions markers can be coexpressed that do not overlap in the healthy brain. For example, nestin and GFAP are normally not coexpressed in mature astrocytes (Götz et al., 2015). This might indicate that de- or *trans*-differentiation of reactive astrocytes proceeds slowly or is not completed compared to immature cells in the developing organism. In this context, new markers are of interest to refine the characterization by the combination of markers.

Two mAbs directed against the LeX motif in specific molecular contexts, 487^{LeX} and 5750^{LeX}, were employed to investigate a potential role of the LeX structures in response to laser lesion (**Figure 7**). These LeX antibodies had already been used to investigate glycoepitope expression in human induced pluripotent stem cell (hiPSC)-derived human neural stem/progenitor cells, where they revealed an increased epitope expression in the later neuroepithelium and radial glia state (Kandasamy et al., 2017). In the adult brain, the LeX motif is found on SVZ stem cells (Capela and Temple, 2002). The staining patterns were not modified in the penumbra. Accordingly, neither mAb 487^{LeX} nor mAb 5750^{LeX} are promising candidates for the characterization of reactive astrocytes or other cell types in the laser lesion model. The observation that LeX epitopes are not upregulated following damage has also been described for SCI (Wanner et al., 2013). It is not trivial to assign secreted molecules of the interstitial ECM to distinct cells. Once released, the molecules can diffuse or can be enriched on the surface of the producing cell but also on other cells by expression of appropriate receptors. Expression analysis on mRNA level via *in situ* hybridization is possible, but faces the problem of potential differences between mRNA level and the actual amount of protein as a result of translational regulation or proteolytic degradation.

Perineuronal Nets and Plasticity After Lesion

PNNs as a specialized form of ECM were investigated in the light of synaptic plasticity that might be increased after lesion to allow the formation of new networks. PNN distribution was not changed in the penumbra after cortical laser lesion (**Figure 9**). The PNN markers WFA and aggrecan did not show differences, neither compared to the contralateral side nor to a healthy control without lesion (data not shown). PNNs were still present 28 days after injury in a region with a dense network of GFAP-positive astrocytes, indicating massive gliosis. In contrast to stable PNN marker detection in our lesion model, a very rapid PNN degradation has been described within hours after photothrombosis (Karetko-Sysa et al., 2011), which shows the huge differences between lesion paradigms. TGF-β signaling has been identified as a critical factor for PNN degradation in different lesion models (Kim et al., 2017).

Beside plastic changes based on potential PNN destabilization, plasticity has been studied on different levels in the rat laser lesion model. In the penumbra of the lesion core an increased LTP (Mittmann and Eysel, 2001; Dohle et al., 2009), associated with a special contribution of NR2B subunits, was found in *ex vivo* – *in vitro* experiments (Huemmeke et al., 2004). Increased intracellular Ca^{2+} levels and Ca^{2+} transients – both NMDA receptor- and AMPA receptor-dependent – were detected as a molecular basis of the augmented LTP (Barmashenko et al., 2001, 2003). Furthermore, cells in the surround of the lesions showed increased excitability and reduced GABAergic inhibition (Mittmann et al., 1994). All the latter changes reinstall mechanisms that support plasticity in early postnatal development but are downregulated in adulthood. Interestingly, this corresponds to the immature marker expression profile of astrocyte subpopulations and to the ECM composition found in the penumbra. It has to be considered that PNNs enwrap only some neuronal subtypes. Predominantly, but not exclusively, parvalbumin-positive GABAergic interneurons are surrounded by PNNs (Lensjo et al., 2017). So neuronal subtypes can be specifically affected after damage and show distinct responses, which is seen by a general tendency to an increased

excitation:inhibition ratio, resulting in hyperexcitability after damage (Carron et al., 2016). This observation has been confirmed for the laser lesion model in the rat by the studies mentioned above.

CONCLUSION

Reactive astrocytes with potential progenitor characteristics were found in the laser lesion model (**Figure 10**). Cellular subpopulations coexpressing distinct progenitor markers like vimentin and nestin showed a spatial distribution in the penumbra of the necrotic lesion core, which suggests activation of local astrocytes as response to the injury. Their potential *in vivo* and *in vitro* remains to be elucidated and is a potential target for future therapeutic approaches. Manipulation of the extracellular environment could be one way to alter cell behavior. After laser lesion, the ECM composition resembled, at least in part, the ECM present in the developing organism. Presence of molecules like Tnc in the penumbra is meaningful in two respects. First, these factors might be used as markers to label astrocytic subpopulations with potential progenitor characteristics, as they are associated with the abovementioned markers GFAP, vimentin and nestin. Second, it is tempting to speculate that an ECM enriched in these molecules promotes an immature cell fate by forming a niche-like environment. Astroglial expression of the glycoepitope recognized by mAb 4860, associated with oligodendrocytes in the healthy CNS, might indicate an intrinsic potential of the reactive cells to generate new oligodendrocytes. Manipulation of these cells, via their environment or by other means, could release brain-intrinsic stem cells to improve regeneration. The fact that PNN markers were found even after weeks in the direct vicinity of the lesion suggests that synaptic plasticity might not be increased by degradation of the PNN matrix following cortical laser lesion.

A limitation of the study is the determination of the cells that produce ECM molecules and the quantification of such factors based on immunohistochemistry in the lesion environment. On the one hand, cells can bind soluble factors by expression of receptors on the cell surface, on the other hand tissue damage with cell debris, immune cell infiltration and protease activity can affect the quality of the staining. The long-term fate of reactive astrocytes including possible neurogenesis is an interesting question that remains open for future studies. Analysis of PNNs in the penumbra could be refined with regard to the ultrastructure level, as PNN function might be impaired by alterations more subtle than complete loss of typical markers.

DATA AVAILABILITY STATEMENT

All datasets generated for this study are included in the article/**Supplementary Material**.

ETHICS STATEMENT

The animal study was reviewed and approved by the Animal protection commission of the Landesamt für Natur, Umwelt und Verbraucherschutz Nordrhein-Westfalen (LANUV).

AUTHOR CONTRIBUTIONS

LR and UE performed the experiments. AF, LR, and UE wrote and revised the manuscript.

FUNDING

The study was funded by the German Research Foundation (DFG), SFB 509, FA 159/16-1 and FA 159/23-1 to AF, the International Graduate School of Neuroscience of the Ruhr University Bochum (IGSN) and by the German Academic Exchange Service (DAAD).

ACKNOWLEDGMENTS

We thank Sabine Kindermann, Ute Neubacher, and Marion Voelzkow for excellent technical assistance.

SUPPLEMENTARY MATERIAL

The Supplementary Material for this article can be found online at: https://www.frontiersin.org/articles/10.3389/fncel.2020.00102/full#supplementary-material

REFERENCES

Arvidsson, A., Collin, T., Kirik, D., Kokaia, Z., and Lindvall, O. (2002). Neuronal replacement from endogenous precursors in the adult brain after stroke. *Nat. Med.* 8, 963–970. doi: 10.1038/nm747

Barmashenko, G., Eysel, U. T., and Mittmann, T. (2001). Intracellular calcium signals in the surround of rat visual cortex lesions. *Neuroreport* 12, 3023–3028. doi: 10.1097/00001756-200110080-00009

Barmashenko, G., Eysel, U. T., and Mittmann, T. (2003). Changes in intracellular calcium transients and LTP in the surround of visual cortex lesions in rats. *Brain Res.* 990, 120–128. doi: 10.1016/s0006-8993(03)03447-4

Ben Haim, L., Carrillo-de Sauvage, M. A., Ceyzeriat, K., and Escartin, C. (2015). Elusive roles for reactive astrocytes in neurodegenerative diseases. *Front. Cell. Neurosci.* 9:278. doi: 10.3389/fncel.2015.00278

Bignami, A., Raju, T., and Dahl, D. (1982). Localization of vimentin, the nonspecific intermediate filament protein, in embryonal glia and in early differentiating neurons. In vivo and in vitro immunofluorescence study of the rat embryo with vimentin and neurofilament antisera. *Dev. Biol.* 91, 286–295. doi: 10.1016/0012-1606(82)90035-5

Bozzelli, P. L., Alaiyed, S., Kim, E., Villapol, S., and Conant, K. (2018). Proteolytic remodeling of perineuronal nets: effects on synaptic plasticity and neuronal population dynamics. *Neural Plast.* 2018:5735789. doi: 10.1155/2018/5735789

Brodkey, J. A., Laywell, E. D., O'Brien, T. F., Faissner, A., Stefansson, K., Dorries, H. U., et al. (1995). Focal brain injury and upregulation of a developmentally

regulated extracellular matrix protein. *J. Neurosurg.* 82, 106–112. doi: 10.3171/jns.1995.82.1.0106

Buffo, A., Rite, I., Tripathi, P., Lepier, A., Colak, D., Horn, A. P., et al. (2008). Origin and progeny of reactive gliosis: a source of multipotent cells in the injured brain. *Proc. Natl. Acad. Sci. U.S.A.* 105, 3581–3586. doi: 10.1073/pnas.0709002105

Capela, A., and Temple, S. (2002). LeX/ssea-1 is expressed by adult mouse CNS stem cells, identifying them as nonependymal. *Neuron* 35, 865–875. doi: 10.1016/s0896-6273(02)00835-8

Carron, S. F., Alwis, D. S., and Rajan, R. (2016). Traumatic brain injury and neuronal functionality changes in sensory cortex. *Front. Syst. Neurosci.* 10:47. doi: 10.3389/fnsys.2016.00047

Czopka, T., Hennen, E., von Holst, A., and Faissner, A. (2009). Novel conserved oligodendrocyte surface epitope identified by monoclonal antibody 4860. *Cell Tissue Res.* 338, 161–170. doi: 10.1007/s00441-009-0868-9

Dahlstrand, J., Lardelli, M., and Lendahl, U. (1995). Nestin mRNA expression correlates with the central nervous system progenitor cell state in many, but not all, regions of developing central nervous system. *Brain Res. Dev. Brain Res.* 84, 109–129. doi: 10.1016/0165-3806(94)00162-s

Deller, T., Haas, C. A., Naumann, T., Joester, A., Faissner, A., and Frotscher, M. (1997). Up-regulation of astrocyte-derived tenascin-C correlates with neurite outgrowth in the rat dentate gyrus after unilateral entorhinal cortex lesion. *Neuroscience* 81, 829–846. doi: 10.1016/s0306-4522(97)00194-2

Dimou, L., and Götz, M. (2014). Glial cells as progenitors and stem cells: new roles in the healthy and diseased brain. *Physiol. Rev.* 94, 709–737. doi: 10.1152/physrev.00036.2013

Dobbertin, A., Czvitkovich, S., Theocharidis, U., Garwood, J., Andrews, M. R., Properzi, F., et al. (2010). Analysis of combinatorial variability reveals selective accumulation of the fibronectin type III domains B and D of tenascin-C in injured brain. *Exp. Neurol.* 225, 60–73. doi: 10.1016/j.expneurol.2010.04.019

Dobbertin, A., Rhodes, K. E., Garwood, J., Properzi, F., Heck, N., Rogers, J. H., et al. (2003). Regulation of RPTPbeta/phosphacan expression and glycosaminoglycan epitopes in injured brain and cytokine-treated glia. *Mol. Cell. Neurosci.* 24, 951–971. doi: 10.1016/s1044-7431(03)00257-4

Dohle, C. I., Eysel, U. T., and Mittmann, T. (2009). Spatial distribution of long-term potentiation in the surround of visual cortex lesions *in vitro*. *Exp. Brain Res.* 199, 423–433. doi: 10.1007/s00221-009-1964-5

Dowell, J. A., Johnson, J. A., and Li, L. (2009). Identification of astrocyte secreted proteins with a combination of shotgun proteomics and bioinformatics. *J. Proteome Res.* 8, 4135–4143. doi: 10.1021/pr900248y

Eysel, U. T., and Schweigart, G. (1999). Increased receptive field size in the surround of chronic lesions in the adult cat visual cortex. *Cereb. Cortex* 9, 101–109. doi: 10.1093/cercor/9.2.101

Eysel, U. T., Schweigart, G., Mittmann, T., Eyding, D., Qu, Y., Vandesande, F., et al. (1999). Reorganization in the visual cortex after retinal and cortical damage. *Restor Neurol. Neurosci.* 15, 153–164.

Faissner, A., Clement, A., Lochter, A., Streit, A., Mandl, C., and Schachner, M. (1994). Isolation of a neural chondroitin sulfate proteoglycan with neurite outgrowth promoting properties. *J. Cell Biol.* 126, 783–799. doi: 10.1083/jcb.126.3.783

Faissner, A., and Kruse, J. (1990). J1/tenascin is a repulsive substrate for central nervous system neurons. *Neuron* 5, 627–637. doi: 10.1016/0896-6273(90)90217-4

Faissner, A., Roll, L., and Theocharidis, U. (2017). Tenascin-C in the matrisome of neural stem and progenitor cells. *Mol. Cell Neurosci.* 81, 22–31. doi: 10.1016/j.mcn.2016.11.003

Götz, M., Sirko, S., Beckers, J., and Irmler, M. (2015). Reactive astrocytes as neural stem or progenitor cells: *in vivo* lineage, *in vitro* potential, and Genome-wide expression analysis. *Glia* 63, 1452–1468. doi: 10.1002/glia.22850

Hayes, A. J., and Melrose, J. (2018). Glycans and glycosaminoglycans in neurobiology: key regulators of neuronal cell function and fate. *Biochem. J.* 475, 2511–2545. doi: 10.1042/BCJ20180283

Hennen, E., Czopka, T., and Faissner, A. (2011). Structurally distinct LewisX glycans distinguish subpopulations of neural stem/progenitor cells. *J. Biol. Chem.* 286, 16321–16331. doi: 10.1074/jbc.M110.201095

Huemmeke, M., Eysel, U. T., and Mittmann, T. (2004). Lesion-induced enhancement of LTP in rat visual cortex is mediated by NMDA receptors containing the NR2B subunit. *J. Physiol.* 559(Pt 3), 875–882. doi: 10.1113/jphysiol.2004.069534

Kandasamy, M., Roll, L., Langenstroth, D., Brüstle, O., and Faissner, A. (2017). Glycoconjugates reveal diversity of human neural stem cells (hNSCs) derived from human induced pluripotent stem cells (hiPSCs). *Cell Tissue Res.* 368, 531–549. doi: 10.1007/s00441-017-2594-z

Karetko-Sysa, M., Skangiel-Kramska, J., and Nowicka, D. (2011). Disturbance of perineuronal nets in the perilesional area after photothrombosis is not associated with neuronal death. *Exp. Neurol.* 231, 113–126. doi: 10.1016/j.expneurol.2011.05.022

Kiessling, M., Herchenhan, E., and Eggert, H. R. (1990). Cerebrovascular and metabolic effects on the rat brain of focal Nd:YAG laser irradiation. *J. Neurosurg.* 73, 909–917. doi: 10.3171/jns.1990.73.6.0909

Kim, S. Y., Senatorov, V. V. Jr., Morrissey, C. S., Lippmann, K., Vazquez, O., Milikovsky, D. Z., et al. (2017). TGFbeta signaling is associated with changes in inflammatory gene expression and perineuronal net degradation around inhibitory neurons following various neurological insults. *.Sci Rep.* 7:7711. doi: 10.1038/s41598-017-07394-3

Kim, W. R., Kim, J. Y., Moon, Y., Kim, H. J., Kim, H., and Sun, W. (2012). Regional difference of reactive astrogliosis following traumatic brain injury revealed by hGFAP-GFP transgenic mice. *Neurosci. Lett.* 513, 155–159. doi: 10.1016/j.neulet.2012.02.023

Lensjo, K. K., Christensen, A. C., Tennoe, S., Fyhn, M., and Hafting, T. (2017). Differential expression and Cell-type specificity of perineuronal nets in hippocampus, medial entorhinal cortex, and visual cortex examined in the rat and mouse. *eNeuro* 4:ENEURO.379-16.2017. doi: 10.1523/ENEURO.0379-16.2017

Lindsberg, P. J., Frerichs, K. U., Burris, J. A., Hallenbeck, J. M., and Feuerstein, G. (1991). Cortical microcirculation in a new model of focal laser-induced secondary brain damage. *J. Cereb. Blood Flow Metab.* 11, 88–98. doi: 10.1038/jcbfm.1991.10

Loers, G., and Schachner, M. (2007). Recognition molecules and neural repair. *J. Neurochem.* 101, 865–882. doi: 10.1111/j.1471-4159.2006.04409.x

McKeon, R. J., Schreiber, R. C., Rudge, J. S., and Silver, J. (1991). Reduction of neurite outgrowth in a model of glial scarring following CNS injury is correlated with the expression of inhibitory molecules on reactive astrocytes. *J. Neurosci.* 11, 3398–3411.

Mittmann, T., and Eysel, U. T. (2001). Increased synaptic plasticity in the surround of visual cortex lesions in rats. *Neuroreport* 12, 3341–3347. doi: 10.1097/00001756-200110290-00039

Mittmann, T., Luhmann, H. J., Schmidt-Kastner, R., Eysel, U. T., Weigel, H., and Heinemann, U. (1994). Lesion-induced transient suppression of inhibitory function in rat neocortex *in vitro*. *Neuroscience* 60, 891–906. doi: 10.1016/0306-4522(94)90270-4

Pekny, M., and Pekna, M. (2014). Astrocyte reactivity and reactive astrogliosis: costs and benefits. *Physiol. Rev.* 94, 1077–1098. doi: 10.1152/physrev.00041.2013

Piccinini, A. M., and Midwood, K. S. (2012). Endogenous control of immunity against infection: tenascin-C regulates TLR4-mediated inflammation via microRNA-155. *Cell Rep.* 2, 914–926. doi: 10.1016/j.celrep.2012.09.005

Reinhard, J., Brosicke, N., Theocharidis, U., and Faissner, A. (2016). The extracellular matrix niche microenvironment of neural and cancer stem cells in the brain. *Int. J. Biochem. Cell Biol.* 81(Pt A), 174–183. doi: 10.1016/j.biocel.2016.05.002

Robel, S., Berninger, B., and Götz, M. (2011). The stem cell potential of glia: lessons from reactive gliosis. *Nat. Rev. Neurosci.* 12, 88–104. doi: 10.1038/nrn2978

Roll, L., and Faissner, A. (2014). Influence of the extracellular matrix on endogenous and transplanted stem cells after brain damage. *Front. Cell. Neurosci.* 8:219. doi: 10.3389/fncel.2014.00219

Roll, L., and Faissner, A. (2019). Tenascins in CNS lesions. *Semin. Cell Dev. Biol.* 89, 118–124. doi: 10.1016/j.semcdb.2018.09.012

Roll, L., Mittmann, T., Eysel, U. T., and Faissner, A. (2012). The laser lesion of the mouse visual cortex as a model to study neural extracellular matrix remodeling during degeneration, regeneration and plasticity of the CNS. *Cell. Tissue Res.* 349, 133–145. doi: 10.1007/s00441-011-1313-4

Schindelin, J., Arganda-Carreras, I., Frise, E., Kaynig, V., Longair, M., Pietzsch, T., et al. (2012). Fiji: an open-source platform for biological-image analysis. *Nat. Methods* 9, 676–682. doi: 10.1038/nmeth.2019

Sirko, S., Neitz, A., Mittmann, T., Horvat-Brocker, A., von Holst, A., Eysel, U. T., et al. (2009). Focal laser-lesions activate an endogenous population of neural stem/progenitor cells in the adult visual cortex. *Brain* 132(Pt 8), 2252–2264. doi: 10.1093/brain/awp043

Sofroniew, M. V., and Vinters, H. V. (2010). Astrocytes: biology and pathology. *Acta Neuropathol.* 119, 7–35. doi: 10.1007/s00401-009-0619-8

Streit, A., Faissner, A., Gehrig, B., and Schachner, M. (1990). Isolation and biochemical characterization of a neural proteoglycan expressing the L5 carbohydrate epitope. *J. Neurochem.* 55, 1494–1506. doi: 10.1111/j.1471-4159.1990.tb04931.x

Tang, X., Davies, J. E., and Davies, S. J. (2003). Changes in distribution, cell associations, and protein expression levels of NG2, neurocan, phosphacan, brevican, versican V2, and tenascin-C during acute to chronic maturation of spinal cord scar tissue. *J. Neurosci. Res.* 71, 427–444. doi: 10.1002/jnr.10523

von Holst, A., Sirko, S., and Faissner, A. (2006). The unique 473HD-Chondroitinsulfate epitope is expressed by radial glia and involved in neural precursor cell proliferation. *J. Neurosci.* 26, 4082–4094. doi: 10.1523/JNEUROSCI.0422-06.2006

Wanner, I. B., Anderson, M. A., Song, B., Levine, J., Fernandez, A., Gray-Thompson, Z., et al. (2013). Glial scar borders are formed by newly proliferated, elongated astrocytes that interact to corral inflammatory and fibrotic cells via STAT3-dependent mechanisms after spinal cord injury. *J. Neurosci.* 33, 12870–12886. doi: 10.1523/JNEUROSCI.2121-13.2013

White, R. E., McTigue, D. M., and Jakeman, L. B. (2010). Regional heterogeneity in astrocyte responses following contusive spinal cord injury in mice. *J. Comp. Neurol.* 518, 1370–1390. doi: 10.1002/cne.22282

Conflict of Interest: The authors declare that the research was conducted in the absence of any commercial or financial relationships that could be construed as a potential conflict of interest.

frontiers in Cellular Neuroscience

ORIGINAL RESEARCH
published: 25 June 2020
doi: 10.3389/fncel.2020.00186

In Search of a Dose: The Functional and Molecular Effects of Exercise on Post-stroke Rehabilitation in Rats

Fengwu Li[1], *Xiaokun Geng*[1,2,3]*, *Christian Huber*[3], *Christopher Stone*[3] *and Yuchuan Ding*[3,4]*

[1]China-America Institute of Neuroscience, Luhe Hospital, Capital Medical University, Beijing, China, [2]Department of Neurology, Beijing Luhe Hospital, Capital Medical University, Beijing, China, [3]Department of Neurosurgery, Wayne State University School of Medicine, Detroit, MI, United States, [4]Department of Research and Development Center, John D. Dingell VA Medical Center, Detroit, MI, United States

OPEN ACCESS

Edited by:
Claudio Rivera,
Aix-Marseille Université, France

Reviewed by:
Jérôme Laurin,
Aix-Marseille Université, France
Anne Sophie Tessier,
INSERM U1093 Cognition, Action et Plasticité Sensomotrice, France

***Correspondence:**
Xiaokun Geng
xgeng@ccmu.edu.cn
Yuchuan Ding
yding@med.wayne.edu

Specialty section:
This article was submitted to Cellular Neuropathology, a section of the journal Frontiers in Cellular Neuroscience

Received: 01 November 2019
Accepted: 28 May 2020
Published: 25 June 2020

Citation:
Li F, Geng X, Huber C, Stone C and Ding Y (2020) In Search of a Dose: The Functional and Molecular Effects of Exercise on Post-stroke Rehabilitation in Rats. Front. Cell. Neurosci. 14:186. doi: 10.3389/fncel.2020.00186

Although physical exercise has been demonstrated to augment recovery of the post-stroke brain, the question of what level of exercise intensity optimizes neurological outcomes of post-stroke rehabilitation remains unsettled. In this study, we aim to clarify the mechanisms underlying the intensity-dependent effect of exercise on neurologic function, and thereby to help direct the clinical application of exercise-based neurorehabilitation. To do this, we used a well-established rat model of ischemic stroke consisting of cerebral ischemia induction through middle cerebral artery occlusion (MCAO). Ischemic rats were subsequently assigned either to a control group entailing post-stroke rest or to one of two exercise groups distinguished by the intensity of their accompanying treadmill regimens. After 24 h of reperfusion, exercise was initiated. Infarct volume, apoptotic cell death, and neurological defects were quantified in all groups at 3 days, and motor and cognitive functions were tracked up to day-28. Additionally, Western blotting was used to assess the influence of our interventions on several proteins related to synaptogenesis and neuroplasticity (growth-associated protein 43, a microtubule-associated protein, postsynaptic density-95, synapsin I, hypoxia-inducible factor-1α, brain-derived neurotrophic factor, nerve growth factor, tyrosine kinase B, and cAMP response element-binding protein). Our results were in equal parts encouraging and surprising. Both mild and intense exercise significantly decreased infarct volume, cell death, and neurological deficits. Motor and cognitive function, as determined using an array of tests such as beam balance, forelimb placing, and the Morris water maze, were also significantly improved by both exercise protocols. Interestingly, while an obvious enhancement of neuroplasticity proteins was shown in both exercise groups, mild exercise rats demonstrated a stronger effect on the expressions of Tau ($p < 0.01$), brain-derived neurotrophic factor ($p < 0.01$), and tyrosine kinase B ($p < 0.05$). These findings contribute to the growing body of literature regarding the positive effects of both mild and intense long-term treadmill exercise on brain injury, functional outcome, and

neuroplasticity. Additionally, the results may provide a base for our future study regarding the regulation of HIF-1α on the BDNF/TrkB/CREB pathway in the biochemical processes underlying post-stroke synaptic plasticity.

Keywords: ischemia/reperfusion, functional outcome, synaptogenesis, BDNF, TrkB, CREB, HIF-1α

INTRODUCTION

Exercise therapy has long been considered a promising strategy to ameliorate physical disability after stroke (Saposnik et al., 2016). However, neurological outcomes of post-stroke rehabilitation appear to differ according to the intensity of the exercise regimen that is used (Bell et al., 2015; Xing et al., 2018). Some previous studies have demonstrated that higher intensity exercise may yield better functional recovery and neuroplasticity (Linder et al., 2019; Luo et al., 2019; Andrews et al., 2020), while other studies have suggested that mild exercise results in superior neuroprotection and synaptic plasticity after stroke (Lee et al., 2009; Shih et al., 2013). These conflicting results underscore the principle that exercise intensity is an important determinant of post-stroke neurological outcomes. Therefore, clarifying the mechanisms that underlie an intensity-dependent effect of exercise on neurologic function may help direct the clinical application of exercise-based neurorehabilitation. Currently, these mechanisms have not been fully explored, and are consequently incompletely understood.

Recently, brain-derived neurotrophic factor (BDNF) has become the subject of increasing attention as a possible mediator of the neurological benefits of exercise. BDNF is an abundant growth factor that is involved in activity-induced neuroplasticity and is upregulated in the animal brain by exercise. The regulation of neuroplasticity depends on a complex set of interactions between a variety of neural proteins, including postsynaptic density 95 (PSD-95; Wang et al., 2019), synapsin I (SYN; Pan et al., 2017), growth-associated protein 43 (GAP-43), and microtubule-associated protein (also known as Tau; Biundo et al., 2018; Mercerón-Martínez et al., 2018; Pu et al., 2019). Changes in these neuroplastic factors are related to exercise-induced activation of BDNF (Kim and Leem, 2016; Belviranli and Okudan, 2019). Previous research has suggested a pivotal regulatory role for BDNF and its receptor, BDNF-tyrosine kinase B (TrkB), regarding neuroplasticity after physical exercise (Lee et al., 2018), mediated through the expression of the transcription factor cyclic AMP response element-binding protein (CREB; Hu et al., 2004). Moreover, activation of the BDNF/TrkB/CREB signaling pathway has also been shown to promote functional recovery after stroke (Liu H. et al., 2018). Taken together, these lines of evidence suggest that post-stroke exercise regimens such as the one used in this study may induce neuroplasticity and influence rehabilitative outcomes through the changes they provoke in the BDNF pathway.

Another factor that may be involved in determining the outcomes of post-stroke exercise regimens is hypoxia-inducible factor-1α (HIF-1α). Upregulation of HIF-1α by exercise has been reported to play a role in reducing infarct volumes following ischemia/reperfusion injury (Li C. et al., 2017), and in post-stroke neuroplasticity (Wu et al., 2018). Previous studies demonstrated that HIF-1α also induced the expression of BDNF (Shi et al., 2009; Nakamura et al., 2011; Helan et al., 2014), and thereby promoted neuroplasticity, reduced neuronal death, and improved neurological function in a rat model of ischemic stroke (Chen et al., 2017). HIF-1α has further been shown to stimulate the expression of the TrkB receptor (Martens et al., 2007), and the CREB receptor in various cancer cells (Yu et al., 2020). However, despite this considerable circumstantial evidence, previous studies have not yet explored the effect of HIF-1α on BDNF/TrkB/CREB pathway in improving synaptic plasticity following ischemia/reperfusion injury. Although the present study did not determine this relation, as the first step, we intended to assess the expression of HIF-1α and BDNF/TrkB/CREB proteins following ischemia/reperfusion injury. These results might suggest a potential association of these molecules and provide a base for our future study regarding the regulation of HIF-1α on the BDNF/TrkB/CREB pathway.

MATERIALS AND METHODS

Animals

A total of 150 adult male Sprague–Dawley rats (280–300 g, Vital River Laboratory Animal Technology Company Limited, Beijing, China) were used in this study. The protocol by which they were studied was approved by the Animal Care and Use Committee of Capital Medical University, and the study was conducted following the NIH Guide for the Care and Use of Laboratory Animals. Animals were randomly divided into three groups: middle cerebral artery occlusion (MCAO) without exercise (50), MCAO plus intense treadmill exercise (50), and MCAO plus mild treadmill exercise (50). Both exercise protocols were initiated after 24 h reperfusion, and animals in each group were sacrificed at days 3, 14, and 28 after reperfusion for further biochemical analysis.

Focal Cerebral Ischemia

The animals were subjected to transient right MCAO according to the method we described previously (Li F. et al., 2019). Briefly, rats were anesthetized in a chamber using 3% isoflurane and a mixture of 70% nitrous oxide and 30% oxygen. Then rats were then transferred to a surgical table, where anesthesia was maintained with a facemask that delivered 1% isoflurane from a calibrated precision vaporizer, and poly-L-lysine-coated nylon (4.0) sutures were used to generate infarcts with minimal inter-animal variability. During the unilateral, 2-h MCAO procedure, cerebral blood flow (CBF), blood pCO_2 and pO_2, mean arterial pressure (MAP), and rectal temperature were monitored continuously. Rectal temperatures were maintained between 36.5°C and 37.5°C using a heating pad and a heating

lamp. Ipsilesional ischemic cerebral hemispheres were used for molecular analysis.

Treadmill Exercise

Animals were randomly assigned either to the exercise groups or the non-exercise control group. Exercise animals were run on a four-lane treadmill (ZS-PT-II, ZS Dichuang Instruments, Inc., Beijing, China), either at a constant speed of 30 m/min for 30 min each day (intense); or at 5 m/min for the first 10 min, 9 m/min for the second 10 min, and 12 m/min for the last 10 min on days 1 and 2, followed by 12 m/min on the third and subsequent days (mild). The mild exercise was begun at a shorter intensity (days 1–2) and ultimately ended with the final mild speed at 3 days and thereafter, such that low intensity was maintained throughout. This gradual start could not be achieved for the intense exercise group, however, as we would, in this case, have been unable to accurately assess the effects of high intensity in the short-term (3 days) when rats were sacrificed. Both exercise and non-exercise animals were housed in groups of three in standard cages for equal time.

Neurological Deficit

The modified scoring systems proposed by Zea Longa (5-point) and Belayev et al. (1996) (12-point) were used to examine the severity of neurological deficits in rats before and after 24 h reperfusion (Li F. et al., 2019). After MCAO, rats with scores of 2 or below were considered to represent the unsuccessful establishment of the MCAO model and were consequently excluded (about 10%); exclusion was then confirmed on autopsy by lack of a core, indicating a faulty surgery.

Cerebral Infarct Volume

At 3 days of ischemia and reperfusion in rats that underwent MCAO, brains were resected and cut into 2-mm-thick slices, which were then treated with 2,3,5-triphenyltetrazolium chloride (TTC; Sigma–Aldrich, St. Louis, MO, USA) for staining (Li et al., 2017b), facilitating the use of an indirect method for calculating infarct volume to minimize error caused by edema.

Apoptotic Cell Death

For quantification of apoptosis-related DNA fragmentation, a commercial enzyme immunoassay was used to determine cytoplasmic histone-associated DNA fragments (Cell Death Detection ELISA; mlbio, Shanghai, China). The degree of apoptosis was quantified according to the amount of cytoplasmic histone-associated DNA fragments in the control and experimental groups at 3 days after physical exercise.

Neurobehavioral Tests

These tests included adhesive removal, beam balance, forelimb placing, grid walking, and Rota-rod performance (R03–1; Xin-Ruan Instruments, Inc., Shanghai, China), as assessed at days 1, 3, 7, 14, 21, and 28. The Morris water maze (ZS-II; ZS Dichuang Instruments, Inc., Beijing, China) was also employed, in our case at 24–28 days; this is following a previous report that showed no obvious suppressive effect on swimming at 24 days after the ischemic event (Ran et al., 2018). In the adhesive removal test, the tape was attached to the palmar surface of the forepaw, and the time taken for the first attempt to touch and to remove the tape was recorded. In the beam balance test, rats were placed on a narrow wooden beam (122 × 2.5 × 42 cm), and performance was scored from 0 to 6 (0 = no attempt to stay on the beam; 1 = attempted to stay on the beam but no movement; 2 = attempted to cross the beam but failed; 3 = crossed the beam with contralateral hindlimb slips >50% of the time; 5 = crossed the beam with contralateral hindlimb slips <50% of the time; 6 = crossed the beam without slips; see Ran et al. (2018). In the forelimb placing test, rats were held gently with forelimbs close to the tabletop while the surface was lightly brushed using each side of their vibrissa. The ability of rats to place the preferred forelimb on the edge of the table in this context was recorded 10 times, and placing rates were calculated. In the grid walk test, rats were placed on a wire grid (100 × 25 × 50 cm) and allowed to walk from one end to the other; the total number of foot slips during this crossing was recorded. In the Rota-rod test, rats were placed on a rotating drum that accelerated from 4 to 40 rpm within 300 s; the time that the animals stayed on the rotating rod was then recorded. Finally, in the Morris water maze, rats were placed into a pool (diameter = 150 cm) at one of the four locations, and allowed to swim for 90 s to find a hidden platform (diameter = 10 cm); swim speed and the time taken to find the hidden platform were recorded using a camera positioned above the pool that transmitted data to an analysis system for calculation. Tests were conducted on non-consecutive days to mitigate possible confounding due to motor learning that might have occurred if these tests were performed in close succession.

Neuron Isolation and Flow Cytometry Assay

As described previously by our group (Chen et al., 2018), an adult brain dissociation kit (Miltenyi Biotec, Bergisch Gladbach, Germany) was used for neuron isolation. Briefly, rats were sacrificed at 3, 14, and 28 days after exercise and ipsilesional brains were finely cut, ground, and filtered through a 70-μm cell strainer (Miltenyi Biotec, Bergisch Gladbach, Germany) to obtain a single-cell suspension. Cell pellets (5×10^6 cells) were stained with primary antibodies against Tau or GAP-43 (1 μg/1 × 10^6 cells, rabbit anti-Tau, and rabbit anti-GAP43, Abcam, MA, USA) in darkness for 30 min at room temperature. Cells were washed three times with PBS and incubated with Alexa Fluor® 488 fluorescein-conjugated secondary antibodies (Sigma, St. Louis, MO, USA) for 30 min at room temperature, and then washed again and analyzed on a FACS Calibur flow cytometer (Accuri C6, BD, San Jose, CA, USA) with Cell Quest software (BD, San Jose, CA, USA).

Protein Expression

At 3, 14, and 28 days after initiation of the exercise regimens, rats were sacrificed for Western blot analysis. Tissue samples from the ipsilesional ischemic cerebral hemispheres of all experimental groups were harvested, and total protein extraction was performed using cell lysis solutions (Thermo Fisher Scientific, Inc., Waltham, MA, USA). Protein concentration was then determined by the BCA method. Electrophoresis (10% SDS-PAGE gel) was performed

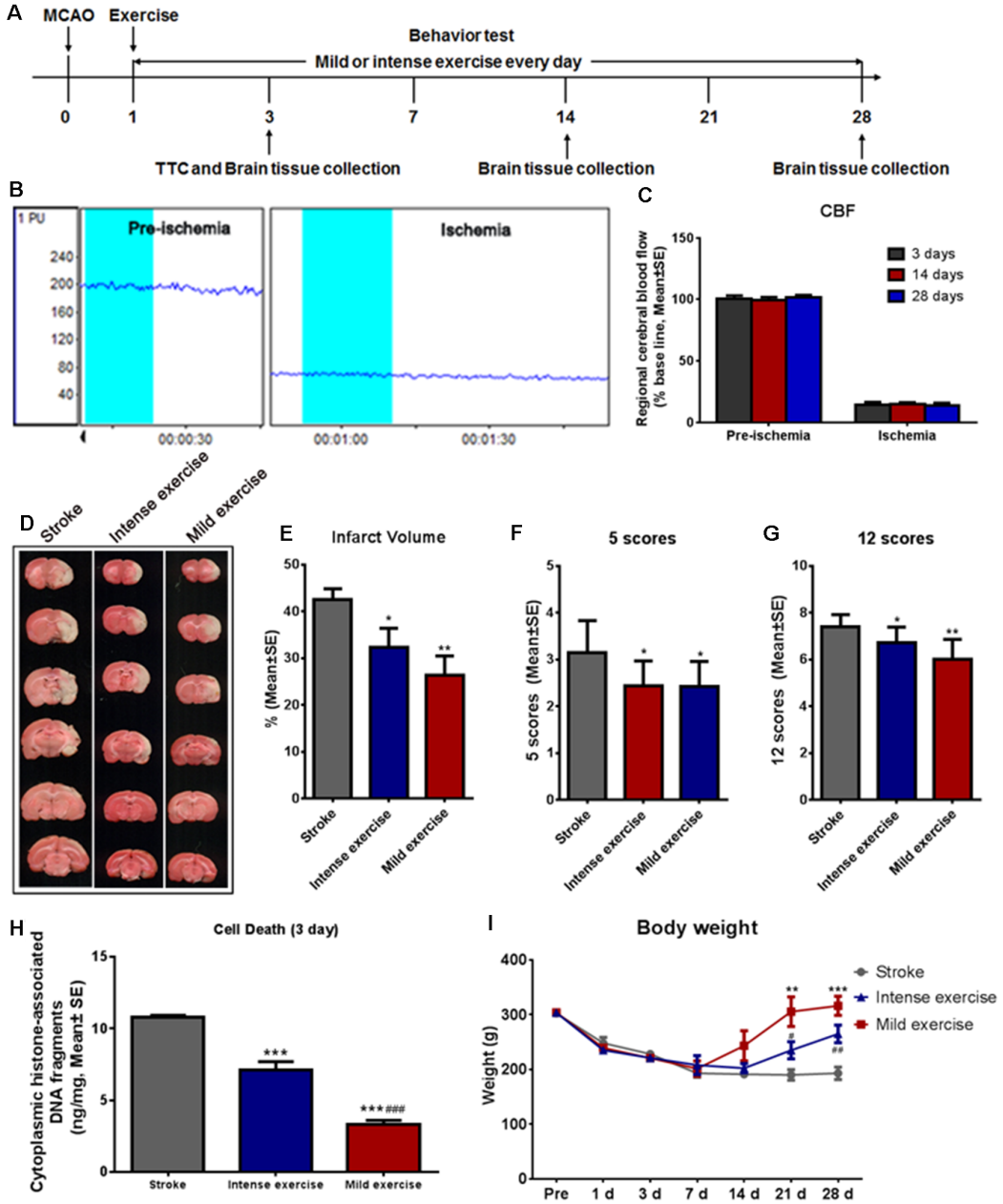

FIGURE 1 | Mild or intense exercise reduced brain infarct. **(A)** Illustration of the experimental timelines. Rats were subjected to 2 h middle cerebral artery occlusion (MCAO), followed by daily treadmill exercise 1 day after reperfusion for up to 28 days. **(B,C)** Representative images and quantification of cerebral blood flow (CBF) monitoring of the three study groups for 2 min before and after the onset of ischemia. There were no significant differences in CBF between groups. **(D)** 2,3,5-triphenyltetrazolium chloride (TTC) histology demonstrating exercise-induced infarct volume reduction in the penumbra region of the ischemic territory supplied by the middle cerebral artery. **(E)** Quantification of the infarct volume reduction exercise. Both mild (**$p < 0.01$) and intense (*$p < 0.05$) exercise significantly decreased infarct volumes, but the reduction was more pronounced with mild exercise. Neurological deficits were tracked after both types of exercise using both the 5- **(F)** and 12- **(G)** point systems. ANOVA analyses indicated that both mild (**$p < 0.01$) and intense exercise (*$p < 0.05$) reduced neurological deficits. **(H)** Cell death reduction due to exercise quantified at 3 days. Both mild and intense exercise reduced apoptotic cell death significantly (***$p < 0.001$), but a more significant ($^{\#\#\#}p < 0.001$) decrease was shown in the mild exercise group. **(I)** Bodyweight was recorded at days 1, 3, 7, 14, 21 and 28. ** or *** Represent mild exercise vs. control; $^{\#}$ or $^{\#\#}$ represent intense exercise vs. control.

with 30 μg of protein per lane. Gel transfer to a PVDF membrane was performed under 200 V for 1 h. Membranes were blocked with 5% skimmed milk, followed by incubation with primary antibodies (1:1,000 rabbit anti-BDNF, rabbit anti-NGF, rabbit anti-PSD-95, rabbit anti-SYN, rabbit anti-Tau, and rabbit anti-GAP43, Abcam, MA, USA; 1:500 rabbit anti-HIF-1α, Santa Cruz Biotechnology, Inc., Santa Cruz, CA, USA) overnight at 4°C. The next day, membranes were

washed three times and further incubated with a goat anti-rabbit IgG-HRP secondary antibody (1:1,000, Santa Cruz) at room temperature for 1 h. After washing, the ECL method was used to detect signals. Western blot images for each antibody were analyzed using an image analysis program (ImageJ 1.42, National Institutes of Health, Bethesda, MD, USA) to quantify protein expression according to relative image density.

Statistical Analysis

Statistical analyses were performed with SPSS Statistics for Windows, Version 17.0 (SPSS Inc., Chicago, IL, USA). Differences among groups were assessed using one-way ANOVA with a significance level of $p < 0.05$. *Post hoc* comparison among groups was performed using the least significant difference method.

RESULTS

Experimental Design and Physiological Parameters

Illustration of the experimental timelines (**Figure 1A**). There were no significant differences in CBF (**Figures 1B,C**), blood MAP, pO_2, or pCO_2 (**Table 1**) between these groups.

TABLE 1 | Physiological parameters during surgery.

	Stroke	Intense exercise	Mild exercise
MAP (mm Hg)			
Prior to MCAO	86.8 ± 3.3	87.0 ± 3.5	87.5 ± 3.4
Onset of reperfusion	86.7 ± 2.4	86.8 ± 2.5	86.4 ± 3.5
After reperfusion	82.3 ± 2.9	85.3 ± 3.1	85.8 ± 4.0
pCO_2 (mm Hg)			
Prior to MCAO	44.8 ± 1.7	45.0 ± 2.2	47.2 ± 3.5
Onset of reperfusion	42.4 ± 2.7	45.4 ± 2.0	43.2 ± 2.1
After reperfusion	45.2 ± 4.0	44.3 ± 2.7	43.4 ± 4.4
pO_2 (mm Hg)			
Before MCAO	132.9 ± 5.9	139.5 ± 5.6	132.4 ± 5.7
Onset of reperfusion	135.2 ± 5.1	132.7 ± 5.6	134.7 ± 4.9
After reperfusion	134.1 ± 9.1	138.2 ± 6.4	132.4 ± 4.1

MAP, mean arterial pressure; MCAO, middle cerebral artery occlusion.

Brain Infarction and Correlates

A large infarct volume (42.5%) was seen following 2 h MCAO and 3 days reperfusion. Both mild ($^{**}p < 0.01$) and intense ($^{*}p < 0.05$) exercise significantly decreased infarct volumes (32.3% vs. 26.3%, respectively; **Figures 1D,E**). Neurological deficits were detected by the 5- (**Figure 1F**) or 12- (**Figure 1G**) point score systems; compared to the control group, deficits were decreased significantly ($^{*}p < 0.05$) after either mild or intense exercise. Apoptotic cell death was detected at 3 days as described above; both mild and intense exercise significantly ($^{***}p < 0.001$) decreased cell death (0.07 and 0.14 ng/ml, respectively, vs. 0.22 ng/ml), but a further significant decrease was noted ($^{***}p < 0.001$) in the mild exercise group (**Figure 1H**). Also, a significant ($^{***}p < 0.001$) increase in weight was seen in both exercise groups, with mild exercise rats demonstrating additional gain (**Figure 1I**).

Functional Outcomes

As shown in **Figure 2A**, the time taken to fall off the grid was significantly reduced after both mild ($p < 0.01$) or intense ($p < 0.05$) exercise as compared to rest at 3, 7, 14, 21, and 28 days (**Figure 2A**); this reduction was significantly more pronounced in mild exercise rats on 7, 21, and 28 days. Similar results were observed in beam balance (**Figure 2B**), Rota-rod (**Figure 2C**), adhesive removal (**Figures 2D–E**), and forelimb placing tests (**Figure 2F**). On assessment using the Morris water maze (**Figures 2G–J**) at 24–28 days, exercised rats demonstrated significantly shorter latency to locate the hidden platform as compared to rested controls, with mildly exercised rats attaining significantly better outcomes (**Figures 2G–H**). Exercised rats spent more time ($^{*}p < 0.05$) in the target quadrant to find the hidden submerged platform than rested rats (**Figure 2I**). In contrast, there was no significant difference between groups concerning swim speed, suggesting similar gross motor skills (**Figure 2J**). These results demonstrate the significant role of exercise generally, and mild exercise in particular, in the long-term recovery of sensorimotor functions and spatial learning capability after ischemia/reperfusion injury.

Neuroplasticity

Flow cytometry assay demonstrated that both mild ($^{**}p < 0.01$) and intense ($^{**}p < 0.01$) exercise increased expression of Tau (**Figures 3A,C**) and GAP-43 (**Figures 3B,D**) at 3, 14, and 28 days; significantly more Tau expression was seen in mildly exercised rats ($^{**}p < 0.01$). Also, compared to the control group, mild and intense exercise both significantly increased protein expression of Tau, GAP-43, and PSD-95 at 3, 14, and 28 days. Compared to the control group, levels of Tau ($^{**}p < 0.01$, **Figure 3E**), GAP-43 ($^{***}p < 0.001$, **Figure 3F**), PSD-95 ($^{*}p < 0.05$, **Figure 3G**), and SYN (**Figure 3H**) were found by Western Blot to be increased in mildly exercised rats at 3, 14, and 28 days; the same results were also seen in the intense exercise group. Taken together, these results demonstrate the capacity of exercise to augment neuroplasticity after ischemia/reperfusion injury.

Expression of HIF-1α, BDNF, TrkB, and CREB

Both exercise protocols yielded a significant increase in levels of these proteins at 3, 14, and 28 days. Compared to the control group, levels of HIF-1α (3 days, $^{*}p < 0.05$; 28 days, $^{**}p < 0.01$, **Figure 4A**), BDNF (**Figure 4B**), NGF (14 days and 28 days, $^{***}p < 0.001$, **Figure 4C**), TrkB ($^{*}p < 0.05$, **Figure 4D**), and CREB ($^{**}p < 0.01$, **Figure 4E**) were significantly increased in both the mild and intense exercise groups. Levels of HIF-1α (3 days, $^{*}p < 0.05$, **Figure 4A**), BDNF (14 days, $^{**}p < 0.01$, **Figure 4B**), NGF (3 days, $^{**}p < 0.01$, **Figure 4C**), TrkB (14 days, $^{*}p < 0.05$, **Figure 4D**), and CREB (**Figure 4E**) were further increased in mildly exercised rats. These results demonstrate the alterations in HIF-1α, BDNF, TrkB, and CREB in association with synaptic plasticity following ischemia/reperfusion injury.

DISCUSSION

The results obtained in this study, confirmed the augmentation in neuroplasticity in the ipsilesional hemisphere and functional

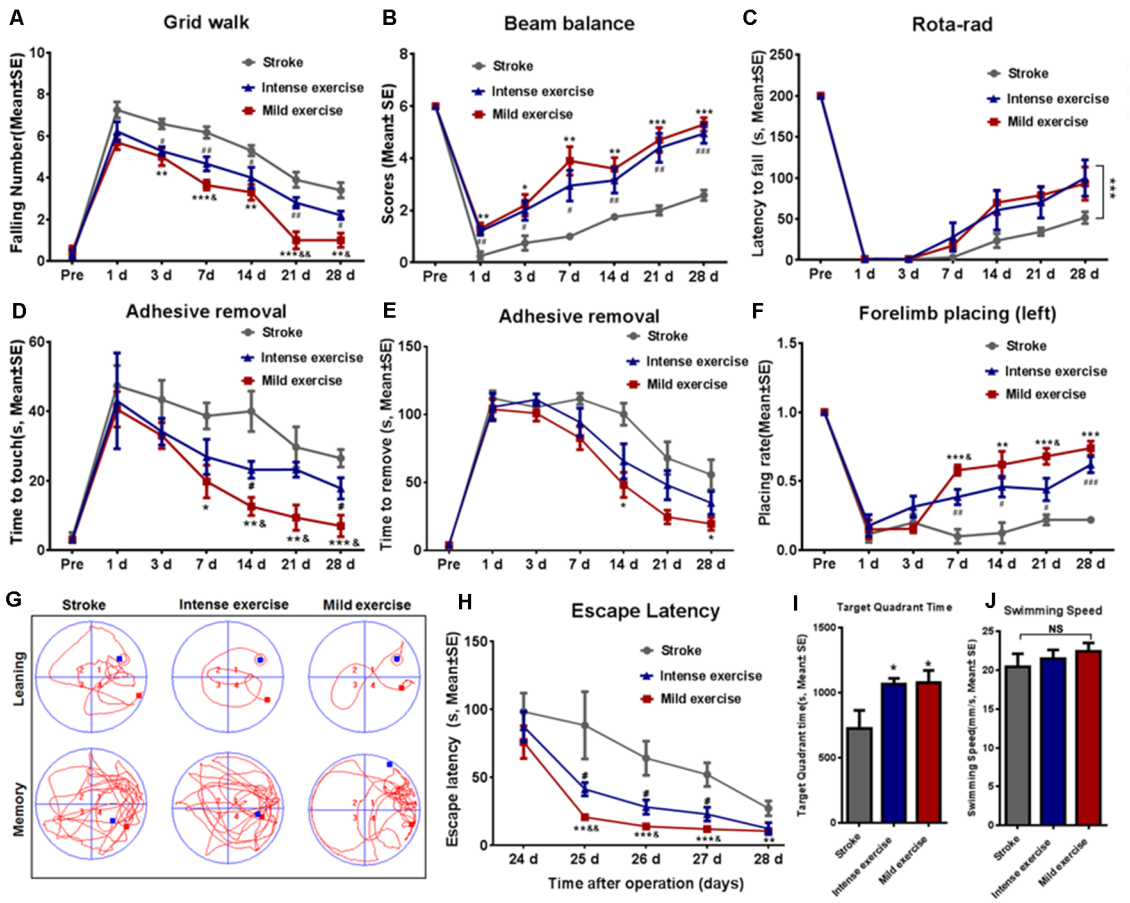

FIGURE 2 | Exercise-mediated enhancement of functional recovery. **(A)** Grid walk test. Foot slips from the grid were significantly reduced after both mild (5.0 vs. 6.6 at 3 days, $^{**}p < 0.01$; 3.6 vs. 6.2 at 7 days, $^{***}p < 0.001$; 3.3 vs. 5.3 at 14 days, $^{**}p < 0.01$; 1.0 vs. 3.9 at 21 days, $^{***}p < 0.001$; 1.0 vs. 3.4 at 28 days, $^{**}p < 0.01$) and intense (5.2 vs. 6.6 at 3 days, $^{\#}p < 0.05$; 4.7 vs. 6.2 at 7 days, $^{\#\#}p < 0.01$; 4.0 vs. 5.3 at 14 days, $^{\#}p < 0.05$; 2.8 vs. 3.9 at 21 days, $^{\#}p < 0.05$; 2.2 vs. 3.4 at 28 days, $^{\#\#}p < 0.01$) exercise rats as compared to control rats at 3, 7, 14, 21, and 28 days. Mild exercise conferred further benefit over intense exercise in this respect (5.7 vs. 6.2 at 1 day; 5.0 vs 5.2 at 3 days; 3.6 vs. 4.7 at 7 days, $^{\&}p < 0.05$; 3.3 vs. 4.0 at 14 days; 1.0 vs. 2.8 at 21 days, $^{\&\&}p < 0.01$; 1.0 vs. 2.2 at 28 days, $^{\&}p < 0.05$). Similar results were observed in beam balance **(B)**, Rota-rod **(C)**, adhesive removal **(D,E)**, and forelimb placing tests **(F)**. Learning ability was examined by the Morris water maze test at 24–28 days of exercise **(G–J).** Representative images of the swim paths at 28 days **(G)**. Latency to locate the submerged platform at 24–28 days **(H)**. Target quadrant time **(I)** and swim speed **(J)** at 28 days. $^{*}p \leq 0.05$, $^{**}p \leq 0.01$, $^{***}p \leq 0.001$ represent mild exercise vs. control; $^{\#}p \leq 0.05$, $^{\#\#}p \leq 0.01$, $^{\#\#\#}p \leq 0.001$ represent intense exercise vs. control; $^{\&}p \leq 0.05$ represent intense exercise vs. mild exercise. NS, not significant.

outcomes provided by physical exercise after ischemic brain injury. Specifically, we showed that both mild and intense exercise regimens reduced brain infarct volume and apoptotic cell death, and improved motor and cognitive function at 3, 14, and 28 days after ischemia/reperfusion injury. The early improvement in infarct volume seen in these results aligned with a previous meta-analysis, in which infarct volume was reduced most effectively by exercise administered with the shortest delays after ischemia (Egan et al., 2014); data from our group derived from pre-conditioning experimentation suggest that this may be related to the capacity of exercise to mitigate inflammatory damage during reperfusion (Ding et al., 2005), with the caveat that the exercise initiation too early after ischemia may be detrimental (Li et al., 2017a). More recent work by our group further substantiated these findings by demonstrating that exercise improved glycometabolism in the ischemic area and decreased neuroinflammation and apoptosis as early as 1 day post-stroke, and also at 3 days (Shen et al., 2016; Li et al., 2017a,b,c). These findings suggest that it is beneficial to initiate exercise early after ischemia/reperfusion, as was done in the present study.

Furthermore, our biochemical analyses showed that the expression of synaptic plasticity proteins (Tau, GAP-43, and PSD-95) and their potential upstream regulators (HIF-1α, BDNF, NGF, TrkB, and CREB) were significantly increased after exercise. These findings suggest that long-term physical exercise may induce synaptic plasticity through the HIF-1α and BDNF/TrkB/CREB pathway. Brain synaptic regeneration may be related to elevated levels of GAP-43 or Tau proteins, and exercise has been shown to increase expression of GAP-43 in the ischemic area in rats with cerebral ischemia/reperfusion injury (Mizutani et al., 2014). Exercise-induced GAP-43 has

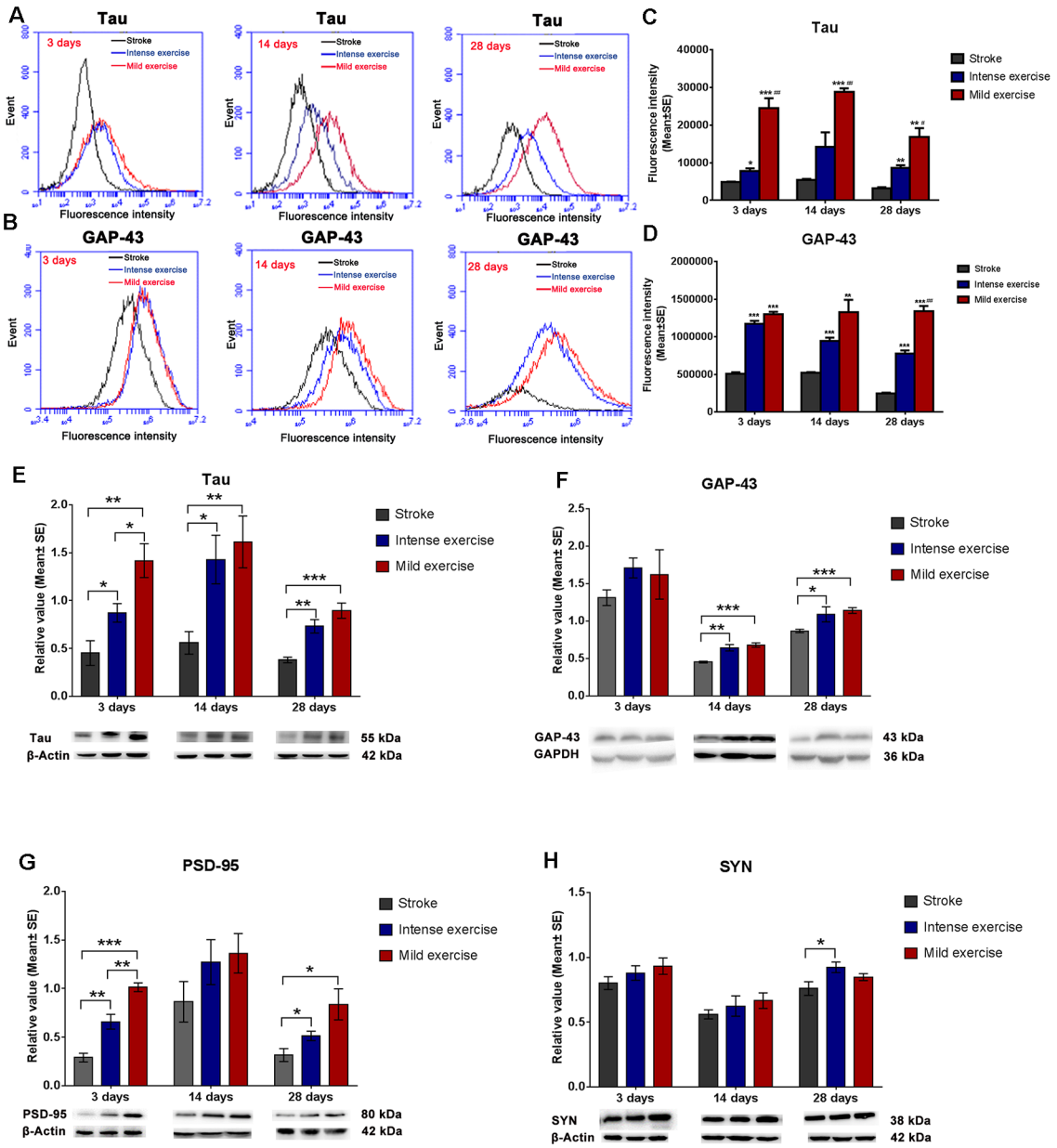

FIGURE 3 | Exercise-induced increased expression of synaptic proteins. **(A–D)** Representative images of Tau and GAP-43 detected by FCM. Both mild (**A,C**; 24,600.2 vs. 4,885.12 at 3 days, $^{***}p < 0.001$; 28,897 vs. 5,408.9 at 14 days, $^{***}p < 0.001$; 16,879.2 vs. 3,186.86 at 28 days, $^{**}p < 0.01$) and intense (7,752.19 vs. 4,885.12 at 3 days, $^{*}p < 0.05$; 14,230.5 vs. 5,408.9 at 14 days; 8,698.12 vs. 3,186.86 at 28 days, $^{**}p < 0.01$) exercise significantly induced Tau expression at 3, 14, and 28 days. Further increases in expression were seen in mildly exercised rats at 3, 14, and 28 days ($^{\#}0.05$, $^{\#\#}0.01$, $^{\#\#\#}0.001$ represent mild exercise vs. intense exercise). The same results were also seen for GAP-43 expression **(B,D)**. **(E–H)** Representative images of Tau, GAP-43, PSD-95, and SYN as detected by Western Blot. Compared to the control group, levels of Tau (**E**; 1.4 vs. 0.5 at 3 days, $^{**}p < 0.01$; 1.6 vs. 0.6 at 14 days, $^{**}p < 0.01$; 0.9 vs. 0.4 at 28 days, $^{***}p < 0.001$), GAP-43 (**F**; 1.6 vs. 1.3 at 3 days; 0.7 vs. 0.5 at 14 days, $^{***}p < 0.001$; 1.1 vs. 0.8 at 28 days, $^{***}p < 0.001$), PSD-95 (**G**; 1.0 vs. 0.3 at 3 days, $^{***}p < 0.001$; 1.4 vs. 0.9 at 14 days; 0.8 vs. 0.3 at 28 days, $^{*}p < 0.05$), and SYN (**H**; 0.9 vs. 0.8 at 3 days; 0.7 vs. 0.6 at 14 days; 0.8 vs. 0.8 at 28 days) in mildly exercised rats were increased. The same results were also seen with intense exercise. Levels of Tau (**E**; 1.4 vs. 0.9 at 3 days, $^{*}p < 0.05$; 1.6 vs. 1.4 at 14 days; 0.9 vs. 0.7 at 28 days), GAP-43 (**F**; 1.6 vs. 1.7 at 3 days; 0.7 vs. 0.6 at 14 days; 1.1 vs. 1.0 at 28 days), PSD-95 (**G**; 1.0 vs. 0.7 at 3 days, $^{**}p < 0.01$; 1.4 vs. 1.3 at 14 days; 0.8 vs. 0.5 at 28 days), and SYN (**H**; 0.9 vs. 0.9 at 3 days; 0.7 vs. 0.6 at 14 days; 0.8 vs. 0.9 at 28 days) were similar between mildly and intensely exercised rats.

been associated with augmented hippocampal neuroplasticity (Liu W. et al., 2018; Rahmati and Kazemi, 2019) in a process that appears to be dependent on BDNF maturation and the TrkB signaling promoted by mature BDNF (Ding et al., 2011). Similarly, exercise has been shown to promote axonal recovery as assessed by the upregulation of Tau and GAP-43 and is associated with functional improvement after cerebral infarction (Li et al., 2015). Short-term moderate exercise also appears to be

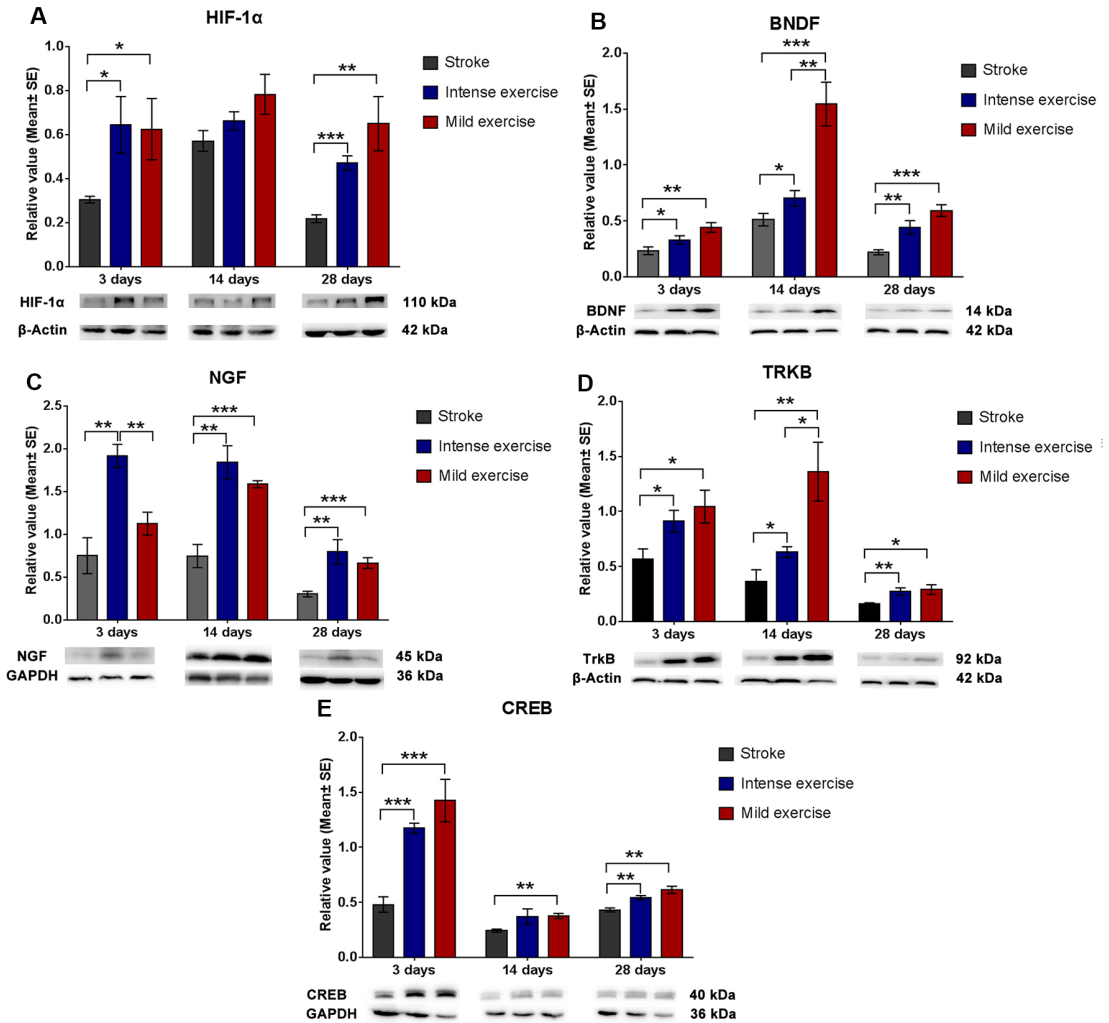

FIGURE 4 | Augmented HIF-1α/BDNF/ TrkB/CREB pathway protein expression after exercise. Compared to rested rats, levels of HIF-1α **(A**; 0.6 vs. 0.3 at 3 days, $^{*}p < 0.05$; 0.8 vs. 0.6 at 14 days; 0.7 vs. 0.2 at 28 days, $^{**}p < 0.01$), BDNF **(B**; 0.4 vs. 0.2 at 3 days; 1.5 vs. 0.5 at 14 days; 0.6 vs. 0.2 at 28 days), NGF **(C**; 1.1 vs. 0.7 at 3 days; 1.6 vs. 0.7 at 14 days, $^{***}p < 0.001$; 0.6 vs. 0.3 at 28 days, $^{***}p < 0.001$), TrkB **(D**; 1.0 vs. 0.6 at 3 days, $^{*}p < 0.05$; 1.4 vs. 0.4 at 14 days, $^{**}p < 0.01$; 0.3 vs. 0.2 at 28 days, $^{*}p < 0.05$), and CREB **(E**; 1.4 vs. 5.5 at 3 days, $^{***}p < 0.001$; 0.4 vs. 0.2 at 14 days, $^{**}p < 0.01$; 0.6 vs. 0.4 at 28 days, $^{**}p < 0.01$) in mildly exercised rats were significantly increased. The same results were seen in intensely exercised rats. Levels of HIF-1α **(A**; 0.6 vs. 0.6 at 3 days, $^{*}p < 0.05$; 0.8 vs. 0.7 at 14 days; 0.7 vs. 0.5 at 28 days), BDNF **(B**; 0.4 vs. 0.3 at 3 days; 1.5 vs. 0.7 at 14 days, $^{**}p < 0.01$; 0.6 vs. 0.4 at 28 days), NGF **(C**; 1.1 vs. 1.9 at 3 days, $^{**}p < 0.01$; 1.6 vs. 1.8 at 14 days; 0.6 vs. 0.8 at 28 days), TrkB **(D**; 1.0 vs. 0.9 at 3 days; 1.4 vs. 0.6 at 14 days, $^{*}p < 0.05$; 0.3 vs. 0.3 at 28 days), and CREB **(E**; 1.4 vs. 1.2 at 3 days; 04 vs. 0.4 at 14 days; 0.6 vs. 0.5 at 28 days) were similar between exercise intensities.

capable of inducing the BDNF-regulated marker of hippocampal and structural plasticity known as SYN (Ferreira et al., 2011). One critical component of synaptic plasticity, the dynamic reorganization of the PSD protein scaffold (Coley and Gao, 2019), is augmented by yet another synaptic protein, PSD-95. PSD-95 is constituent of the postsynaptic membrane that plays a key role in the plasticity and structure of the excitatory chemical synapse (Wu et al., 2017), and multiple studies have associated physical exercise with its induction (Jung and Kim, 2017; Pan et al., 2017). A series of studies have shed light on the relationship between these factors by demonstrating that BDNF/NGF participate in promoting neuroplasticity for motor rehabilitation after focal cerebral infarction (Matsuda et al., 2011; Mizutani et al., 2011; Mang et al., 2013); BDNF was reported to be induced by exercise, and may regulate the expression of synaptic proteins including GAP-43 (Liu W. et al., 2018), SYN (Ferreira et al., 2011), PSD-95 (Li X. et al., 2019) and Tau (Kerling et al., 2017). This research indicates that synaptic plasticity after stroke is determined, at least in part, by the induction and upregulation of axonal or synaptic proteins that, in our study, were found to be increased in both exercise cohorts.

Also, our work helps to elucidate the role occupied by another factor: HIF-1α. The present results are consistent with previous studies showed that the upregulation of HIF-1α promoted synapse plasticity by mediating synaptic markers

(Li G. et al., 2019), and played a beneficial role in post-stroke exercise inducing angiogenesis and neurogenesis (Li C. et al., 2017). Recent work demonstrates that exercise could activate the cerebral motor and cognitive circuits by increasing the expression of HIF-1α, suggesting a regulatory role of HIF-1α in exercise-enhanced neuroplasticity (Halliday et al., 2019). Additionally, previous studies also indicated that HIF-1α regulated BDNF (Chen et al., 2017), TrkB (Martens et al., 2007), and CREB (Yu et al., 2020). Furthermore, the activation of the BDNF/TrkB/CREB pathway has been reported to contribute to the reduction in cerebral ischemic injury and improvement in functional recovery after stroke (Liu H. et al., 2018). Therefore, the enhanced expression of HIF-1α and BDNF/TrkB/CREB proteins after ischemia/reperfusion injury in the present study suggest that HIF-1α might be involved in the BDNF pathway, known to promote synaptic plasticity. Although, we did not explicitly study the regulation of HIF-1α on the BDNF/TrkB/CREB pathway, our results suggest a potential link between the molecules. Our findings could be a basis to further clarify the participation of HIF-1α in BDNF-mediated synaptogenesis.

The results obtained in this experiment are in agreement with previous studies showing that exercise improves motor and cognitive function (Chen et al., 2019; Palasz et al., 2019; Tíglás et al., 2019). Our results also, by suggesting the adequacy of milder post-stroke exercise, address the controversy in the literature regarding the dependence of these beneficial effects on the intensity of the prescribed exercise regimens (Han et al., 2017). A previous investigation supports the findings in the present study, by reporting that higher intensity exercise can exacerbate brain injury after ischemia, whereas the effects of mild intensity training were found to be encouraging (Scopel et al., 2006). Additional work has shown that cell proliferation in the dentate gyrus (Kim et al., 2003), spatial memory function (Lee et al., 2009), and synaptic plasticity (Shih et al., 2013) were more remarkable with mild rather than with heavy exercise after ischemia. In contrast, high-intensity intermittent exercise (HIT) was reported to be superior to moderate-intensity continuous training (MCT) in improving neural plasticity after cerebral ischemia in rats (Pin-Barre et al., 2017; Luo et al., 2019). HIT had a similar effect on cardiac troponin-I as workload-matched continuous exercise in endurance runners, which could be considered as high intensity exercise (Li et al., 2020) and was reported to be acceptable in stroke patients (Boyne et al., 2016). In agreement with these studies, our present results support the beneficial effect of intense exercise, but also indicate that mild exercise is not necessarily worse; and may be adequate to augment neuroprotection and neuroplasticity after stroke. Further investigation is needed in order to optimize exercise intensity post-stroke and determine which intensity may be most beneficial for neurorehabilitation. Furthermore, a standardized definition of exercise intensities may be necessary in order to homogenize methodologies and better compare results between studies in the future.

The protocol utilized in the present study to define exercise intensities was based on prior works (Curry et al., 2010; Zhang et al., 2012). We employed as a standard of achieved exercise training intensity the speed at which rats could not run any longer due to fatigue within three minutes after the onset of exercise. The therapeutic doses of physical exercise training used in our study were calculated as 40% of this maximum velocity in the case of mild exercise training, which amounted to approximately 15 m/min, and 80% in the case of intense exercise training, which was about 32 m/min (Zhang et al., 2012). To further increase the difference between our categories, we reduced speed in the mild group to a maximum of 12 m/min as previous studies (Tian et al., 2013; Zhang P. et al., 2013; Zhang et al., 2017; Tang et al., 2018). For the high-intensity group, we selected 30 m/min because we have employed this speed in previous work, in which we found that it reduced brain damage (Ding et al., 2006), blood-brain barrier dysfunction (Guo et al., 2008), and brain inflammation in stroke (Curry et al., 2010). Recently, studies used physiological parameters, transferable to patients, to determine high and low intensity in rats (Pin-Barre et al., 2017; Luo et al., 2019). To agree with the principle that a physical exercise regimen is reproducible (Gronwald et al., 2019), our further exercise procedure would focus on a physiological indicator such as the lactate threshold. Another key finding from our previous work was the influence of initiation time on post-stroke rehabilitation outcomes: initiation 6 h post-stroke exacerbated brain damage, but this was avoided when exercise was deferred for 1–3 days (Li et al., 2017a,b). Therefore, the initiation time of 24 h after stroke was selected in this study.

In this study, we intended to observe the protective effects of post-stroke exercise on brain infarct at 3 days as previous studies did. Recent work by our group substantiates these findings by demonstrating exercise-improved glycometabolism, decreased neuroinflammation, and apoptosis (Li et al., 2017a,b,c). The present results were largely supported by the findings of other groups, which demonstrated that exercise accelerated CBF (Pianta et al., 2019), decreased infarct volume (Tian et al., 2013; Zhang Y. et al., 2013; Pan et al., 2020) and improved functional outcomes (Pianta et al., 2019). In contrast, a few studies have reported no neuroprotective effects of exercise on the neurological deficit and infarct volume after stroke within 3 days (Matsuda et al., 2011; Cui et al., 2020). Future studies are necessary to fully elucidate the effect of post-stroke exercise on brain injury.

Some limitations are important to consider when interpreting the results of our study. The different constant-intensity regimens were used to demonstrate the concept of mild or intense exercise. Although the exercise protocol in rats cannot be directly transferred to patients, in the present study, as the first step, we intended to use these two exercise procedures to investigate the mechanism underlying the dose-dependent benefit of exercise on recovery after stroke. More careful design is on the way to develop a translational strategy that better applies to human stroke patients (Gronwald et al., 2019). For this purpose, our future work will focus on a connection between animal and clinical exercise procedures by controlling the workload of each training regimen as well as using lactate threshold or oxygen uptake as an indicator. Regarding the interpretation of the neurobehavioral test, possibly the multiple

Rotarod tests served as a training procedure that may have influenced our results. Given our study's focus on the effect and mechanism of different exercise doses on rehabilitation, in each group, the rats received the same test. It is unlikely that this small amount of possible training would change the direction of our results.

In conclusion, this study demonstrates the positive effect on brain injury, functional outcome, and neuroplasticity conferred by both mild and intense long-term treadmill exercise. Additionally, our results suggest that intense exercise did not confer further benefit when compared with its milder counterpart, thus mild exercise may be adequate and sufficient to elicit rehabilitative benefits post-stroke. Moreover, the results may provide a base for our future study regarding the regulation of HIF-1α on the BDNF/TrkB/CREB pathway in the biochemical processes underlying post-stroke synaptic plasticity.

DATA AVAILABILITY STATEMENT

All datasets generated for this study are included in the article/**Supplementary Material**.

ETHICS STATEMENT

The animal study was reviewed and approved by the Animal Care and Use Committee of the Capital Medical University.

AUTHOR CONTRIBUTIONS

FL conducted the animal and biochemical experiments employed in this research. FL, XG, CH, CS, and YD were instrumental in preparing or revising the manuscript. YD was responsible for the experimental design, in addition to assisting with manuscript preparation and revision.

FUNDING

This work was partially supported by the National Natural Science Foundation of China (FL, 81802231 and XG, 81871838), the Organization Department of Beijing talents project (FL, 2018000082595G485), the Beijing Tongzhou District Financial Fund, the Science and Technology Plan of Beijing Tongzhou District (FL, KJ2020CX002 and KJ2019CX004-07).

ACKNOWLEDGMENTS

We thank Sainan Wang, Menglei Liu, Yanlong Zhao, and Chencheng Zhang for technical assistance.

SUPPLEMENTARY MATERIAL

The Supplementary Material for this article can be found online at: https://www.frontiersin.org/articles/10.3389/fncel.2020.00186/full#supplementary-material.

REFERENCES

Andrews, S. C., Curtin, D., Hawi, Z., Wongtrakun, J., Stout, J. C., and Coxon, J. P. (2020). Intensity matters: high-intensity interval exercise enhances motor cortex plasticity more than moderate exercise. *Cereb. Cortex* 30, 101–112. doi: 10.1093/cercor/bhz075

Belayev, L., Alonso, O. F., Busto, R., Zhao, W., and Ginsberg, M. D. (1996). Middle cerebral artery occlusion in the rat by intraluminal suture. *Neurol. patholog. eval. improved model Stroke* 27, 1616–1623; discussion 1623. doi: 10.1161/01.str.27.9.1616.

Bell, J. A., Wolke, M. L., Ortez, R. C., Jones, T. A., and Kerr, A. L. (2015). Training intensity affects motor rehabilitation efficacy following unilateral ischemic insult of the sensorimotor cortex in C57BL/6 mice. *Neurorehabil. Neural Repair* 29, 590–598. doi: 10.1177/1545968314553031

Belviranli, M., and Okudan, N. (2019). Voluntary, involuntary and forced exercises almost equally reverse behavioral impairment by regulating hippocampal neurotrophic factors and oxidative stress in experimental Alzheimer's disease model. *Behav. Brain Res.* 364, 245–255. doi: 10.1016/j.bbr.2019.02.030

Biundo, F., Del Prete, D., Zhang, H., Arancio, O., and D'Adamio, L. (2018). A role for tau in learning, memory and synaptic plasticity. *Sci. Rep.* 8:3184. doi: 10.1038/s41598-018-21596-3

Boyne, P., Dunning, K., Carl, D., Gerson, M., Khoury, J., Rockwell, B., et al. (2016). High-intensity interval training and moderate-intensity continuous training in ambulatory chronic stroke: feasibility study. *Phys. Ther.* 96, 1533–1544. doi: 10.2522/ptj.20150277

Chen, F. T., Chen, Y. P., Schneider, S., Kao, S. C., Huang, C. M., and Chang, Y. K. (2019). Effects of exercise modes on neural processing of working memory in late middle-aged adults: an fMRI study. *Front. Aging Neurosci.* 11:224. doi: 10.3389/fnagi.2019.00224

Chen, C., Jiang, W., Liu, Z., Li, F., Yang, J., Zhao, Y., et al. (2018). Splenic responses play an important role in remote ischemic preconditioning-mediated neuroprotection against stroke. *J. Neuroinflammation* 15:167. doi: 10.1186/s12974-018-1190-9

Chen, J., Yang, Y., Shen, L., Ding, W., Chen, X., Wu, E., et al. (2017). Hypoxic preconditioning augments the therapeutic efficacy of bone marrow stromal cells in a rat ischemic stroke model. *Cell. Mol. Neurobiol.* 37, 1115–1129. doi: 10.1007/s10571-016-0445-1

Coley, A. A., and Gao, W. J. (2019). PSD-95 deficiency disrupts PFC-associated function and behavior during neurodevelopment. *Sci. Rep.* 9:9486. doi: 10.1038/s41598-019-45971-w

Cui, J., Kim, C. S., Kim, Y., Sohn, M. K., and Jee, S. (2020). Effects of repetitive transcranial magnetic stimulation (rTMS) combined with aerobic exercise on the recovery of motor function in ischemic stroke rat model. *Brain Sci.* 10:186. doi: 10.3390/brainsci10030186

Curry, A., Guo, M., Patel, R., Liebelt, B., Sprague, S., Lai, Q., et al. (2010). Exercise pre-conditioning reduces brain inflammation in stroke *via* tumor necrosis factor-α, extracellular signal-regulated kinase 1/2 and matrix metalloproteinase-9 activity. *Neurol. Res.* 32, 756–762. doi: 10.1179/174313209x459101

Ding, Y. H., Mrizek, M., Lai, Q., Wu, Y., Reyes, R. Jr., Li, J., et al. (2006). Exercise preconditioning reduces brain damage and inhibits TNF-α receptor expression after hypoxia/reoxygenation: an *in vivo* and *in vitro* study. *Curr. Neurovasc. Res.* 3, 263–271. doi: 10.2174/156720206778792911

Ding, Y. H., Young, C. N., Luan, X., Li, J., Rafols, J. A., Clark, J. C., et al. (2005). Exercise preconditioning ameliorates inflammatory injury in ischemic rats during reperfusion. *Acta Neuropathol.* 109, 237–246. doi: 10.1007/s00401-004-0943-y

Ding, Q., Ying, Z., and Gómez-Pinilla, F. (2011). Exercise influences hippocampal plasticity by modulating brain-derived neurotrophic factor processing. *Neuroscience* 192, 773–780. doi: 10.1016/j.neuroscience.2011.06.032

Egan, K. J., Janssen, H., Sena, E. S., Longley, L., Speare, S., Howells, D. W., et al. (2014). Exercise reduces infarct volume and facilitates neurobehavioral recovery: results from a systematic review and meta-analysis of exercise

in experimental models of focal ischemia. *Neurorehabil. Neural Repair* 28, 800–812. doi: 10.1177/1545968314521694

Ferreira, A. F., Real, C. C., Rodrigues, A. C., Alves, A. S., and Britto, L. R. (2011). Short-term, moderate exercise is capable of inducing structural, BDNF-independent hippocampal plasticity. *Brain Res.* 1425, 111–122. doi: 10.1016/j.brainres.2011.10.004

Gronwald, T., de Bem Alves, A. C., Murillo-Rodriguez, E., Latini, A., Schuette, J., and Budde, H. (2019). Standardization of exercise intensity and consideration of a dose-response is essential. Commentary on "Exercise-linked FNDC5/irisin rescues synaptic plasticity and memory defects in Alzheimer's models", by Lourenco et al., published 2019 in Nature Medicine. *J. Sport Health Sci.* 8, 353–354. doi: 10.1016/j.jshs.2019.03.006

Guo, M., Lin, V., Davis, W., Huang, T., Carranza, A., Sprague, S., et al. (2008). Preischemic induction of TNF-α by physical exercise reduces blood-brain barrier dysfunction in stroke. *J. Cereb. Blood Flow Metab.* 28, 1422–1430. doi: 10.1038/jcbfm.2008.29

Halliday, M. R., Abeydeera, D., Lundquist, A. J., Petzinger, G. M., and Jakowec, M. W. (2019). Intensive treadmill exercise increases expression of hypoxia-inducible factor 1α and its downstream transcript targets: a potential role in neuroplasticity. *Neuroreport* 30, 619–627. doi: 10.1097/wnr.0000000000001239

Han, P., Zhang, W., Kang, L., Ma, Y., Fu, L., Jia, L., et al. (2017). Clinical evidence of exercise benefits for stroke. *Adv. Exp. Med. Biol.* 1000, 131–151. doi: 10.1007/978-981-10-4304-8_9

Helan, M., Aravamudan, B., Hartman, W. R., Thompson, M. A., Johnson, B. D., Pabelick, C. M., et al. (2014). BDNF secretion by human pulmonary artery endothelial cells in response to hypoxia. *J. Mol. Cell. Cardiol.* 68, 89–97. doi: 10.1016/j.yjmcc.2014.01.006

Hu, B., Liu, C., Bramlett, H., Sick, T. J., Alonso, O. F., Chen, S., et al. (2004). Changes in trkB-ERK1/2-CREB/Elk-1 pathways in hippocampal mossy fiber organization after traumatic brain injury. *J. Cereb. Blood Flow Metab.* 24, 934–943. doi: 10.1097/01.wcb.0000125888.56462.a1

Jung, S. Y., and Kim, D. Y. (2017). Treadmill exercise improves motor and memory functions in cerebral palsy rats through activation of PI3K-Akt pathway. *J. Exerc. Rehabil.* 13, 136–142. doi: 10.12965/jer.1734964.482

Kerling, A., Kück, M., Tegtbur, U., Grams, L., Weber-Spickschen, S., Hanke, A., et al. (2017). Exercise increases serum brain-derived neurotrophic factor in patients with major depressive disorder. *J. Affect. Disord.* 215, 152–155. doi: 10.1016/j.jad.2017.03.034

Kim, Y. P., Kim, H. B., Jang, M. H., Lim, B. V., Kim, Y. J., Kim, H., et al. (2003). Magnitude- and time-dependence of the effect of treadmill exercise on cell proliferation in the dentate gyrus of rats. *Int. J. Sports Med.* 24, 114–117. doi: 10.1055/s-2003-38202

Kim, D. M., and Leem, Y. H. (2016). Chronic stress-induced memory deficits are reversed by regular exercise *via* AMPK-mediated BDNF induction. *Neuroscience* 324, 271–285. doi: 10.1016/j.neuroscience.2016.03.019

Lee, H. W., Ahmad, M., Weldrick, J. J., Wang, H. W., Burgon, P. G., and Leenen, F. H. H. (2018). Effects of exercise training and TrkB blockade on cardiac function and BDNF-TrkB signaling postmyocardial infarction in rats. *Am. J. Physiol. Heart Circ. Physiol.* 315, H1821–H1834. doi: 10.1152/ajpheart.00245.2018

Lee, S. U., Kim, D. Y., Park, S. H., Choi, D. H., Park, H. W., and Han, T. R. (2009). Mild to moderate early exercise promotes recovery from cerebral ischemia in rats. *Can. J. Neurol. Sci.* 36, 443–449. doi: 10.1017/s0317167100007769

Li, F., Geng, X., Khan, H., Pendy, J. T. Jr., Peng, C., Li, X., et al. (2017a). Exacerbation of brain injury by post-stroke exercise is contingent upon exercise initiation timing. *Front. Cell. Neurosci.* 11:311. doi: 10.3389/fncel.2017.00311

Li, F., Pendy, J. T. Jr., Ding, J. N., Peng, C., Li, X., Shen, J., et al. (2017b). Exercise rehabilitation immediately following ischemic stroke exacerbates inflammatory injury. *Neurol. Res.* 39, 530–537. doi: 10.1080/01616412.2017.1315882

Li, F., Shi, W., Zhao, E. Y., Geng, X., Li, X., Peng, C., et al. (2017c). Enhanced apoptosis from early physical exercise rehabilitation following ischemic stroke. *J. Neurosci. Res.* 95, 1017–1024. doi: 10.1002/jnr.23890

Li, F., Geng, X., Yip, J., and Ding, Y. (2019). Therapeutic target and cell-signal communication of chlorpromazine and promethazine in attenuating blood-brain barrier disruption after ischemic stroke. *Cell Transplant.* 28, 145–156. doi: 10.1177/0963689718819443

Li, F., Nie, J., Zhang, H., Fu, F., Yi, L., Hopkins, W., et al. (2020). Effects of matched intermittent and continuous exercise on changes of cardiac biomarkers in endurance runners. *Front. Physiol.* 11:30. doi: 10.3389/fphys.2020.00030

Li, C., Wen, H., Wang, Q., Zhang, C., Jiang, L., Dou, Z., et al. (2015). Exercise training inhibits the nogo-A/NgR1/Rho-a signals in the cortical peri-infarct area in hypertensive stroke rats. *Am. J. Phys. Med. Rehabil.* 94, 1083–1094. doi: 10.1097/phm.0000000000000339

Li, X., Wu, Q., Xie, C., Wang, C., Wang, Q., Dong, C., et al. (2019). Blocking of BDNF-TrkB signaling inhibits the promotion effect of neurological function recovery after treadmill training in rats with spinal cord injury. *Spinal Cord* 57, 65–74. doi: 10.1038/s41393-018-0173-0

Li, C., Zhang, B., Zhu, Y., Li, Y., Liu, P., Gao, B., et al. (2017). Post-stroke constraint-induced movement therapy increases functional recovery, angiogenesis and neurogenesis with enhanced expression of HIF-1α and VEGF. *Curr. Neurovasc. Res.* 14, 368–377. doi: 10.2174/1567202614666171128120558

Li, G., Zhao, M., Cheng, X., Zhao, T., Feng, Z., Zhao, Y., et al. (2019). FG-4592 improves depressive-like behaviors through HIF-1-mediated neurogenesis and synapse plasticity in rats. *Neurotherapeutics* doi: 10.1007/s13311-019-00807-3 [Epub ahead of print].

Linder, S. M., Rosenfeldt, A. B., Davidson, S., Zimmerman, N., Penko, A., Lee, J., et al. (2019). Forced, not voluntary, aerobic exercise enhances motor recovery in persons with chronic stroke. *Neurorehabil. Neural Repair* 33, 681–690. doi: 10.1177/1545968319862557

Liu, W., Xue, X., Xia, J., Liu, J., and Qi, Z. (2018). Swimming exercise reverses CUMS-induced changes in depression-like behaviors and hippocampal plasticity-related proteins. *J. Affect. Disord.* 227, 126–135. doi: 10.1016/j.jad.2017.10.019

Liu, H., Zhong, L., Zhang, Y., Liu, X., and Li, J. (2018). Rutin attenuates cerebral ischemia-reperfusion injury in ovariectomized rats *via* estrogen-receptor-mediated BDNF-TrkB and NGF-TrkA signaling. *Biochem. Cell Biol.* 96, 672–681. doi: 10.1139/bcb-2017-0209

Luo, L., Li, C., Deng, Y., Wang, Y., Meng, P., and Wang, Q. (2019). High-intensity interval training on neuroplasticity, balance between brain-derived neurotrophic factor and precursor brain-derived neurotrophic factor in poststroke depression rats. *J. Stroke Cerebrovasc. Dis.* 28, 672–682. doi: 10.1016/j.jstrokecerebrovasdis.2018.11.009

Mang, C. S., Campbell, K. L., Ross, C. J., and Boyd, L. A. (2013). Promoting neuroplasticity for motor rehabilitation after stroke: considering the effects of aerobic exercise and genetic variation on brain-derived neurotrophic factor. *Phys. Ther.* 93, 1707–1716. doi: 10.2522/ptj.20130053

Martens, L. K., Kirschner, K. M., Warnecke, C., and Scholz, H. (2007). Hypoxia-inducible factor-1 (HIF-1) is a transcriptional activator of the TrkB neurotrophin receptor gene. *J. Biol. Chem.* 282, 14379–14388. doi: 10.1074/jbc.M609857200

Matsuda, F., Sakakima, H., and Yoshida, Y. (2011). The effects of early exercise on brain damage and recovery after focal cerebral infarction in rats. *Acta Physiol.* 201, 275–287. doi: 10.1111/j.1748-1708.2010.02174.x

Mercerón-Martínez, D., Almaguer-Melian, W., Alberti-Amador, E., and Bergado, J. A. (2018). Amygdala stimulation promotes recovery of behavioral performance in a spatial memory task and increases GAP-43 and MAP-2 in the hippocampus and prefrontal cortex of male rats. *Brain Res. Bull.* 142, 8–17. doi: 10.1016/j.brainresbull.2018.06.008

Mizutani, K., Sonoda, S., Wakita, H., Katoh, Y., and Shimpo, K. (2011). Functional recovery and alterations in the expression and localization of protein Kinase C following voluntary exercise in rat with cerebral infarction. *Neurol. Sci.* 35, 53–59. doi: 10.1007/s10072-013-1477-7

Mizutani, K., Sonoda, S., Yamada, K., Beppu, H., and Shimpo, K. (2011). Alteration of protein expression profile following voluntary exercise in the perilesional cortex of rats with focal cerebral infarction. *Brain Res.* 1416, 61–68. doi: 10.1016/j.brainres.2011.08.012

Nakamura, K., Tan, F., Li, Z., and Thiele, C. J. (2011). NGF activation of TrkA induces vascular endothelial growth factor expression *via* induction of hypoxia-inducible factor-1α. *Mol. Cell. Neurosci.* 46, 498–506. doi: 10.1016/j.mcn.2010.12.002

Palasz, E., Niewiadomski, W., Gasiorowska, A., Wysocka, A., Stepniewska, A., and Niewiadomska, G. (2019). Exercise-induced neuroprotection and recovery of

motor function in animal models of Parkinson's disease. *Front. Neurol.* 10:1143. doi: 10.3389/fneur.2019.01143

Pan, X., Jiang, T., Zhang, L., Zheng, H., Luo, J., and Hu, X. (2017). Physical exercise promotes novel object recognition memory in spontaneously hypertensive rats after ischemic stroke by promoting neural plasticity in the entorhinal cortex. *Front. Behav. Neurosci.* 11:185. doi: 10.3389/fnbeh.2017.00185

Pan, G., Jin, L., Shen, W., Zhang, J., Pan, J., Cheng, J., et al. (2020). Treadmill exercise improves neurological function by inhibiting autophagy and the binding of HMGB1 to Beclin1 in MCAO juvenile rats. *Life Sci.* 243:117279. doi: 10.1016/j.lfs.2020.117279

Pianta, S., Lee, J. Y., Tuazon, J. P., Castelli, V., Mantohac, L. M., Tajiri, N., et al. (2019). A short bout of exercise prior to stroke improves functional outcomes by enhancing angiogenesis. *Neuromolecular Med.* 21, 517–528. doi: 10.1007/s12017-019-08533-x

Pin-Barre, C., Constans, A., Brisswalter, J., Pellegrino, C., and Laurin, J. (2017). Effects of high- versus moderate-intensity training on neuroplasticity and functional recovery after focal ischemia. *Stroke* 48, 2855–2864. doi: 10.1161/strokeaha.117.017962

Pu, H., Shi, Y., Zhang, L., Lu, Z., Ye, Q., Leak, R. K., et al. (2019). Protease-independent action of tissue plasminogen activator in brain plasticity and neurological recovery after ischemic stroke. *Proc. Natl. Acad. Sci. U S A* 116, 9115–9124. doi: 10.1073/pnas.1821979116

Rahmati, M., and Kazemi, A. (2019). Various exercise intensities differentially regulate GAP-43 and CAP-1 expression in the rat hippocampus. *Gene* 692, 185–194. doi: 10.1016/j.gene.2019.01.013

Ran, Y., Liu, Z., Huang, S., Shen, J., Li, F., Zhang, W., et al. (2018). Splenectomy fails to provide long-term protection against ischemic stroke. *Aging Dis.* 9, 467–479. doi: 10.14336/ad.2018.0130

Saposnik, G., Cohen, L. G., Mamdani, M., Pooyania, S., Ploughman, M., Cheung, D., et al. (2016). Efficacy and safety of non-immersive virtual reality exercising in stroke rehabilitation (EVREST): a randomised, multicentre, single-blind, controlled trial. *Lancet Neurol.* 15, 1019–1027. doi: 10.1016/s1474-4422(16)30121-1

Scopel, D., Fochesatto, C., Cimarosti, H., Rabbo, M., Bello-Klein, A., Salbego, C., et al. (2006). Exercise intensity influences cell injury in rat hippocampal slices exposed to oxygen and glucose deprivation. *Brain Res. Bull.* 71, 155–159. doi: 10.1016/j.brainresbull.2006.08.011

Shen, J., Huber, M., Zhao, E. Y., Peng, C., Li, F., Li, X., et al. (2016). Early rehabilitation aggravates brain damage after stroke *via* enhanced activation of nicotinamide adenine dinucleotide phosphate oxidase (NOX). *Brain Res.* 1648, 266–276. doi: 10.1016/j.brainres.2016.08.001

Shi, Q., Zhang, P., Zhang, J., Chen, X., Lu, H., Tian, Y., et al. (2009). Adenovirus-mediated brain-derived neurotrophic factor expression regulated by hypoxia response element protects brain from injury of transient middle cerebral artery occlusion in mice. *Neurosci. Lett.* 465, 220–225. doi: 10.1016/j.neulet.2009.08.049

Shih, P. C., Yang, Y. R., and Wang, R. Y. (2013). Effects of exercise intensity on spatial memory performance and hippocampal synaptic plasticity in transient brain ischemic rats. *PLoS One* 8:e78163. doi: 10.1371/journal.pone.0078163

Tang, Y., Zhang, Y., Zheng, M., Chen, J., Chen, H., and Liu, N. (2018). Effects of treadmill exercise on cerebral angiogenesis and MT1-MMP expression after cerebral ischemia in rats. *Brain Behav.* 8:e01079. doi: 10.1002/brb3.1079

Tíglás, T., Németh, Z., Koller, A., Van der Zee, E. A., Luiten, P. G. M., and Nyakas, C. (2019). Effects of long-term moderate intensity exercise on cognitive behaviors and cholinergic forebrain in the aging rat. *Neuroscience* 411, 65–75. doi: 10.1016/j.neuroscience.2019.05.037

Tian, S., Zhang, Y., Tian, S., Yang, X., Yu, K., Zhang, Y., et al. (2013). Early exercise training improves ischemic outcome in rats by cerebral hemodynamics. *Brain Res.* 1533, 114–121. doi: 10.1016/j.brainres.2013.07.049

Wang, Z., Hou, L., and Wang, D. (2019). Effects of exercise-induced fatigue on the morphology of asymmetric synapse and synaptic protein levels in rat striatum. *Neurochem. Int.* 129:104476. doi: 10.1016/j.neuint.2019.104476

Wu, Q., Sun, M., Bernard, L. P., and Zhang, H. (2017). Postsynaptic density 95 (PSD-95) serine 561 phosphorylation regulates a conformational switch and bidirectional dendritic spine structural plasticity. *J. Biol. Chem.* 292, 16150–16160. doi: 10.1074/jbc.M117.782490

Wu, X., Liu, S., Hu, Z., Zhu, G., Zheng, G., and Wang, G. (2018). Enriched housing promotes post-stroke neurogenesis through calpain 1-STAT3/HIF-1α/VEGF signaling. *Brain Res. Bull.* 139, 133–143. doi: 10.1016/j.brainresbull.2018.02.018

Xing, Y., Yang, S. D., Dong, F., Wang, M. M., Feng, Y. S., and Zhang, F. (2018). The beneficial role of early exercise training following stroke and possible mechanisms. *Life Sci.* 198, 32–37. doi: 10.1016/j.lfs.2018.02.018

Yu, Z., Liu, Y., Zhu, J., Han, J., Tian, X., Han, W., et al. (2020). Insights from molecular dynamics simulations and steered molecular dynamics simulations to exploit new trends of the interaction between HIF-1α and p300. *J. Biomol. Struct. Dyn.* 38, 1–12. doi: 10.1080/07391102.2019.1580616

Zhang, A., Bai, Y., Hu, Y., Zhang, F., Wu, Y., Wang, Y., et al. (2012). The effects of exercise intensity on p-NR2B expression in cerebral ischemic rats. *Can. J. Neurol. Sci.* 39, 613–618. doi: 10.1017/s0317167100015341

Zhang, P., Yu, H., Zhou, N., Zhang, J., Wu, Y., Zhang, Y., et al. (2013). Early exercise improves cerebral blood flow through increased angiogenesis in experimental stroke rat model. *J. Neuroeng. Rehabil.* 10:43. doi: 10.1186/1743-0003-10-43

Zhang, Y., Zhang, P., Shen, X., Tian, S., Wu, Y., Zhu, Y., et al. (2013). Early exercise protects the blood-brain barrier from ischemic brain injury *via* the regulation of MMP-9 and occludin in rats. *Int. J. Mol. Sci.* 14, 11096–11112. doi: 10.3390/ijms140611096

Zhang, Q., Zhang, J., Yan, Y., Zhang, P., Zhang, W., and Xia, R. (2017). Proinflammatory cytokines correlate with early exercise attenuating anxiety-like behavior after cerebral ischemia. *Brain Behav.* 7:e00854. doi: 10.1002/brb3.854

Conflict of Interest: The authors declare that the research was conducted in the absence of any commercial or financial relationships that could be construed as a potential conflict of interest.

frontiers in Cellular Neuroscience

BRIEF RESEARCH REPORT
published: 21 July 2020
doi: 10.3389/fncel.2020.00223

Electro-Acupuncture Promotes the Differentiation of Endogenous Neural Stem Cells via Exosomal microRNA 146b After Ischemic Stroke

Shenghang Zhang[1,2†], Tingting Jin[1†], Lulu Wang[1†], Weilin Liu[3], Yuhao Zhang[1], Yi Zheng[1], Yunjiao Lin[1], Minguang Yang[3], Xiaojun He[1], Huawei Lin[1], Lidian Chen[1] and Jing Tao[1]*

[1] College of Rehabilitation Medicine, Fujian University of Traditional Chinese Medicine, Fuzhou, China, [2] The 900 Hospital of the Joint Logistic Team, Fuzhou, China, [3] Fujian University of Traditional Chinese Medicine, The Academy of Rehabilitation Industry, Fuzhou, China

OPEN ACCESS

Edited by:
Zhang Pengyue, Yunnan University of Traditional Chinese Medicine, China

Reviewed by:
Lai Wang, Oklahoma Medical Research Foundation, United States
Ahmet Burak Caglayan, Istanbul Medipol University, Turkey

***Correspondence:**
Jing Tao
taojing01@fjtcm.edu.cn

[†] *These authors have contributed equally to this work*

Specialty section:
This article was submitted to Cellular Neuropathology, a section of the journal Frontiers in Cellular Neuroscience

Received: *29 March 2020*
Accepted: *24 June 2020*
Published: *21 July 2020*

Citation:
Zhang S, Jin T, Wang L, Liu W, Zhang Y, Zheng Y, Lin Y, Yang M, He X, Lin H, Chen L and Tao J (2020) Electro-Acupuncture Promotes the Differentiation of Endogenous Neural Stem Cells via Exosomal microRNA 146b After Ischemic Stroke. Front. Cell. Neurosci. 14:223. doi: 10.3389/fncel.2020.00223

Background: Evidences indicate that exosomes-mediated delivery of microRNAs (miRNAs or miRs) is involved in the neurogenesis of stroke. This study was to investigate the role of exosomal miRNAs in non-drug therapy of electro-acupuncture (EA) regulating endogenous neural stem cells for stroke recovery.

Methods: The model of focal cerebral ischemia and reperfusion in rats were established by middle cerebral artery occlusion (MCAO) and treated by EA. The exosomes were extracted from peri-ischemic striatum and identified by exosomal biomarkers, and detected differentially expressed miRNAs with microarray chip. Primary stem cells were cultured, and oxygen–glucose deprivation and reperfusion (OGD/R) was used to mimic vitro ischemic injury.

Results: The levels of exosomal biomarkers TSG101 and CD81 were increased in peri-ischemic striatum after EA treatment, and we revealed 25 differentially expressed miRNAs in isolated exosomes, of which miR-146b was selected for further analysis, and demonstrated that EA increased miR-146b expression and its inhibitors could block the effects. Subsequently, we confirmed that EA upregulated miR-146b expression to promote neural stem cells differentiation into neurons in peri-ischemic striatum. *In vitro*, it was verified that OGD/R hindered neural stem cells differentiation, and miR-146b inhibitors furtherly suppressed its differentiation, simultaneously NeuroD1 was involved in neural stem cells differentiation into neurons. Moreover, *in vivo* we found EA promoted NeuroD1-mediated neural stem cells differentiation via miR-146b. In addition, EA also could improve neurological deficits through miR-146b after ischemic stroke.

Conclusion: EA promotes the differentiation of endogenous neural stem cells via exosomal miR-146b to improve neurological injury after ischemic stroke.

Keywords: electro-acupuncture, ischemic stroke, neural stem cells, exosomes, MiR-146b

INTRODUCTION

Stroke remains the second-leading cause of death in the world, with ischemic stroke accounting for ˜70% of all strokes, and approximately half of patients died or became disabled within 1–3 months (Wang et al., 2017; Wu et al., 2019). Although extensive advance on the epidemiology, etiology, mechanism, classification, and prognosis of stroke, safe and effective treatment strategies have not been developed for most patients, which seriously threatens human health and life, and bring huge burden to patients and families. Therefore, it is an important issue to comprehensively understand the severity of stroke, improve treatment methods, reduce the incidence, disability, and mortality of stroke, and find safe and effective treatment for stroke patients.

Studies have shown that cells of the adult mammalian central nervous system have destructive repair capabilities, especially the proliferation and differentiation of endogenous neural stem cells that can promote neurogenesis (Shinozuka et al., 2014; Nakagomi et al., 2019). The endogenous neural stem cells of the adult brain are mainly present in the subventricular zone (SVZ) region of the lateral ventricle and the subgranular zone (SGZ) region of the hippocampus (Péron and Berninger, 2015; Boldrini et al., 2018). These neural stem cells could be activated and proliferated after stroke then migrated into the lesion and differentiated into functional neural cells (Yamashita et al., 2006; Ngalula et al., 2015). However, newly generated neural stem cells and neural cells by self-healing are not sufficient to promote neurological recovery after stroke. Therefore, how to promote the proliferation and differentiation of endogenous neural stem cells may be a potentially beneficial treatment for stroke.

The previous study has proved that low-frequency electro-acupuncture (EA) stimulation can promote the proliferation of endogenous neural stem cells in SVZ and hippocampus of rats with focal cerebral ischemia (Guo et al., 2014). It has been reported that proliferated endogenous neural stem cells were migrated from the SVZ region to the damaged region of the striatum after EA treatment (Yang et al., 2005). While in our previous study, we demonstrated that EA could promote the proliferation and differentiation of endogenous neural stem cells, which improved the neurological deficits, thereby saving the brain from ischemic damage (Tao et al., 2014; Chen et al., 2015). However, its mechanism is not completely clear.

As we know, secretory extracellular vesicles (EVs) play an essential role in intercellular signal transduction. Recent studies suggest that exosomes-mediated delivery of microRNAs (miRNAs or miRs) is involved in the neurogenesis of stroke (Zagrean et al., 2018; Geng et al., 2019). Exosomes, as a type of EVs (about 30–100 nm in diameter), target cellular functions by delivering proteins, lipids, and nucleic acids (Mori et al., 2019). They can almost be released by all known cell types, including neurons, astrocytes, etc. (Takeda et al., 2015). In this study, we found that exosomal miR-146b identified by microarray chips affected the differentiation of endogenous neural stem cells in rats with ischemia-reperfusion injury. The miR-146 family (miR-146a and miR-146b) has been proved that it can promote the differentiation of neural stem cells into neurons by regulating the Notch1 signaling pathway (Xiao et al., 2015). As a downstream mediator of Notch1 signaling, NeuroD1 is specifically expressed in developing neurons and it is a key transcription factor regulating the differentiation and maturation of neurons (Beckervordersandforth et al., 2015). NeuroD1 transcription factor induced new neuronal cells in the ipsilateral cerebral cortex and lateral striatum of mouse brain after stroke (Gonçalves et al., 2016). Studies have shown that a single transcription factor NeuroD1 in the mouse brain directly converts reactive astrocytes into functional neurons (Guo et al., 2014). And in their recent study, ectopic expression of NeuroD1 in the ischemic injury model through the adeno-associated virus system could regenerate 30–40% of neurons damaged in the motor cortex, and behavioral tests showed that NeuroD1 treatment significantly relieves motor and fear memory deficits after rodent ischemic injury (Chen et al., 2020). Besides, our previous studies have shown that EA could regulate the Notch1 signal transduction to promote the proliferation and differentiation of neural stem cells after ischemic stroke (Tao et al., 2014; Zhao et al., 2015). Therefore, we aimed to demonstrate whether EA could promote the differentiation of endogenous neural stem cells via exosomal miR-146b regulating the NeuroD1 after ischemic stroke.

MATERIALS AND METHODS

Animals

Sixty healthy SPF male *SD* rats (260 ± 20 g) obtained from the Shanghai Laboratory Animal (SLAC, Co., Ltd., Shanghai, China), license no. SCXK 2014−007. All animal experiments were carried out in a pathogen-free environment at the Animal Experimental Center of Fujian University of Traditional Chinese Medicine, placing the rats in a controlled environment (22–25°C; 50 ± 10% relative humidity; 12 h automatic light/dark cycle).

Experimental Design

This study was divided into two parts. First, to explore which exosomal miRNAs were regulated by EA treatment in rats with ischemic stroke. Rats were divided into three groups (n = 7/group): (i) sham operation group (Sham), (ii) middle cerebral artery occlusion group (MCAO), (iii) middle cerebral artery occlusion with EA treatment group (MCAO+EA). Second, to clarify the function of EA treatment effect miRNAs expression in rats with ischemic stroke. Rats were divided into four groups (n = 10/group): (i) MCAO group (MCAO), (ii) MCAO and miR-146b inhibitor injection group (MCAO+miR-146b inhibitors), (iii) MCAO and EA treatment group (MCAO+EA), (iV) MCAO and EA treatment combined with miR-146b inhibitors injection group (MCAO+EA+miR-146b inhibitors). The EA treatment continued for 21 days after the operation (1/20 Hz, 1 mA, 30 min/day). The EA needle was inserted into the LI11 and ST36 of hemiplegic limb at a depth of 2–3 mm and stimulation generated

with an EA instrument (G6805; SMIF, Shanghai, China). The MCAO+miR-146b inhibitors group and the MCAO+EA+miR-146b inhibitors group were injected with miR-146b inhibitor in the intraventricular 30 min before modeling. The rats were anesthetized with 3% isoflurane (R510, RWD Life Science Co., Ltd., Shenzhen China) and placed on a stereotaxic instrument (68001; RWD Life Science Co., Ltd., Shenzhen China). Stereotactic coordinates were as follows: Anteroposterior, 0.8 mm; Mediolateral, 1.5 mm; Depth, 3.5 mm.

Focal Cerebral Ischemia Model

We used thread occlusion of the right middle cerebral artery (MCAO) to establish a rat model of focal cerebral ischemia and reperfusion according to the Longa EZ method (Longa et al., 1989). All animals were fasted 12 h before surgery, and anesthetized with 3% isoflurane. The wound was cut about 2 cm in the middle of the neck, and the right common carotid artery, external carotid artery, and internal carotid artery were separated. After the common artery and external carotid artery, the internal carotid artery clipped. The common carotid artery was inserted into the wire plug, and the internal carotid artery was finally ligated, and the wound was sutured. After 90 min of ischemia, the plug was slowly withdrawn, and the blood reperfused into the left middle cerebral artery. The rats in the Sham group only separated the vascular arteries but did not ligature and thread.

Drugs Injection

5-Bromo-2′-Deoxyuridine Injection

The 5-bromo-2′-deoxyuridine (BrdU) (B5002, Sigma Co., Ltd., United States) powder dissolved in sterile physiological saline in the dark. Each group of experimental animals was injected intraperitoneally with the appropriate BrdU solution (50 mg/kg) once a day for 21 days before each EA treatment.

miR-146b Inhibitors Injection

The miR-146b inhibitor (GeneCopoeia Inc., Guangzhou China) diluted with 0.7% DMSO to a concentration of 10 μM at -20°C. Then 7 μl of the drug was administered to the left ventricle using a stereotaxic instrument 30 min before modeling (Zhan et al., 2010; Zhao et al., 2013). Simultaneously, 7 μl of 0.7% DMSO was injected into the MCAO group and the MCAO+EA group.

Scoring of Neurological Deficits

We performed neurobehavioral scoring and observed posture before and after EA treatment (modified Neurological Severity Scores, mNSS). The abnormality of the index was 0, the moderate abnormality was 1 point, and the severe abnormality was 2 points. The scores added together, and the total score is 0–18 points. The higher the score, the more serious the neuromotor injury.

Immunofluorescence

At the end of all experiments, rats anesthetized with sodium pentobarbital (800 mg/kg, i.p.). After perfusion, the brain tissue was fixed in 4% paraformaldehyde for 24 h and finally wrapped in paraffin after dehydration with gradient alcohol. The 5 μm thick brain slices were dewaxed and repaired for 15 min, and washed with PBS for 5 min. Then, 2N HCL was added dropwise for DNA denaturation, and the cells were incubated at 37°C for 1 h, washed three times with a boric acid solution (pH 8.5), then washed three times with PBS. The blocking solution was incubated at 37°C for 1 h, and then primary antibody BrdU (1:300; ab74547; Abcam, Cambridge), NeuN (1:200; ab177487; Abcam, Cambridge), DCX (1:100; ab18723; Abcam, Cambridge), NeuroD1 (1:200; ab60704; Abcam, Cambridge) were added dropwise. The next day, PBS washed three times, and the corresponding fluorescent secondary antibody was added dropwise in the dark. Nuclei of all cells counterstained with DAPI (1:1000; Santa Cruz, United States). The tissue slides was mounted in mounting medium (Vector Laboratories, United States), and images captured with a confocal fluorescence microscope (LSM710, Carl Zeiss, Germany). The average number of double-labeled positive cells from three slices for each rat with six fields of view/slice used for statistical analysis.

Western Blotting

The ischemic striatum were taken after the rats sacrificed, 1 ml of cell division fluid (Invitrogen; Thermo Fisher Scientific, Inc., United States) and 10 μl of PMSF storage solution added per 200 mg of brain tissue. It centrifuged, and the supernatant were taken to determine the concentration of protein. The protein samples were loaded to SDS-PAGE gel (Promega Corp., Madison, WI, United States) (20 V, l0 min, 60 V, 2 h), and then transferred to the PVDF membrane, 100 V, 60–120 min. Blocking for 2 h with 5% skim milk at room temperature, then incubation with HSP70 (1:1000; ab181606; Abcam, Cambridge), TSG101 (1:2000; ab125001; Abcam, Cambridge), CD81 (1:500; MA5-13548; Thermo Fisher Scientific, United States), NeuroD1 (1:1000; ab60704; Abcam, Cambridge), and β-action (1:8000; Proteintech, China) primary antibody at 4°C overnight, On the 2nd day, the corresponding secondary antibody goat anti-rabbit IgG (1:2000; ab6721; Abcam, Cambridge), Goat anti-mouse IgG (1:5000; ab6789; Abcam, Cambridge) were added and incubated for 2 h. Finally, the PVDF membrane were incubated with Enhanced Chemiluminescence (ECL) solution (RPN2232, GE Healthcare) and then placed on an image scanner for 1 min, and the expression levels of the target protein were analyzed by Image-Pro Plus software (version 7.0; UVP, LLC, Upland, CA, United States).

Exosome Isolation and miRNA Chip

Fresh frozen peri-ischemic striatum was dissected and treated with 20 units/ml papain (Worthington) in Hibernate E solution (2 ml/sample, BrainBits, Springfield, IL) for 15 min at 37°C. The tissue gently homogenized in 2 volumes (5 ml /sample) of cold Hibernate E solution. The tissue homogenate sequentially filtered through a 40 m mesh filter (BD Biosciences) and a 0.2 m syringe filter (Thermo Scientific). Exosomes were isolated from the filtrate as previously literature (Perez-Gonzalez et al., 2012). The filtrate was sequentially centrifuged at 300 g for

10 min at 4°C, 2,000 g for 10 min at 4°C, and 10,000 g for 30 min at 4°C to discard cells, membranes, and debris. Then, the exosomes were extracted according to the Exosome Isolation Kit (UR52121, Umibio, Shanghai, China). The total exosome RNA was isolated by the Exosome RNA isolation kit (Invitrogen), and microRNA expression profiling analyzed by the miRCURY LNA^{TM} microRNA array system (Exiqon).

Real-Time qRT-PCR

Total RNA was extracted from the peri-ischemic striatum using TRIZOL reagent (Invitrogen, Thermo Fisher Scientific, Inc., United States). Reverse transcription reaction and PCR amplification reaction carried out using the miRNA All-in-one^{TM} qRT-PCR miRNA Detection kit, and amplification performed on an ABI7500 real-time PCR instrument, and the results were normalized to GAPDH gene expression. All experiments were performed in triplicate and repeated at least three times. The following primer sequences used: miR-146b (forward) 5'-UGAGAACUGAAUUCCAUAGGCUGU-3', (reverse) 5'-ACUCUUGACUUAAGGUAUCC GACA-3'. GAPDH (forward) 5'-AGACAGCCGCATCTTCTTGT-3', (reverse) 5'-CTT GCCGT GGGTAGAGTCAT.

Oxygen-Glucose Deprivation and Reperfusion

Neural stem cells were isolated from E13.5 to E14.5 rat embryonic brains. The dissected cerebral tissues were cut into small chunks and were digested with Accutase solution (A6964, Sigma-Aldrich, Millipore, United States) for 5 min at 37°C and washed with PBS solution, plated in a six-well plastic plate in Neurobasal medium (Gibco, United States) supplemented with 20 ng/ml basic fibroblast growth factor (Gibco, United States), 20 ng/ml epidermal growth factor (Gibco, United States), 2% B27 supplement (Gibco, United States), and 1% penicillin/streptomycin, and incubated at 37°C in 5% CO_2.

To mimic the condition of ischemic injury *in vitro*, the neural stem cells were cultured in oxygen-glucose deprivation (OGD) medium with DMEM, then placed in a modular chamber (MC-101 model, Billups-Rothenberg, Del Mar, CA) filled with a gas mixture (1% O_2, 5% CO_2, and 94% N_2) for 6 h. Then, by changing the culture medium for OGD reperfusion (OGD/R), the neural stem cells were restored to a normoxic state for 72 h. Control group of neural stem cells cultured under standard conditions without any treatment.

Cell Model and Experimental Group

This study was divided into three groups, Control group, OGD/R group, OGD/R+miR-146b inhibitors group. Control group: primary neural stem cells were normally cultured; OGD/R group: primary neural stem cells were cultured with OGD 6 h and reperfusion 72 h; OGD/R+miR-146b inhibitors group: neural stem cell were cultured with adding 7 μl 10μM miR-146b inhibitors on OGD 6 h and reperfusion 72 h.

Statistical Analysis

All quantitative data are expressed as the means ± *SD* and were analyzed using SPSS 21.0 statistical analysis software (IBM, Corp., Armonk, NY, United States). One-way ANOVA analyzed the mNSS scores, western blotting, qRT-PCR, and immunofluorescence staining results. $P < 0.05$ was considered to indicate a statistically significant difference.

RESULTS

EA Enhanced the Expression of Exosomal miR-146b in Peri-Ischemic Striatum

Firstly, we found that the expression of HSP70, TSG101, and CD81 of exosomal biomarkers were increased in the MCAO group compared with the Sham group. However, after EA treatment, the expression of CD81 and TSG101 were increased in the MCAO+EA group compared with the MCAO group ($P < 0.05$, **Figures 1A,B**).

Then, exosomes were isolated from peri-ischemic striatum of the MCAO group and the MCAO+EA group, and furtherly analyzed miRNAs expressed changes in these exosomal by microarray chip, using a 1.5-fold change and $P < 0.05$ as the threshold cutoff for screening differentially expressed miRNAs. We found that 25 miRNAs differentially expressed in exosomes, including miR-409a, miR-532, miR-1188, miR-125b, miR-146b, miR-30a, etc. (**Figure 1C**). Furthermore, the expression of three miRNAs (miR-125b, miR-146b, miR-30a) were upregulated, and miR-1949 was downregulated by real-time PCR, consistent with chip results ($P < 0.05$, **Figure 1D**), and miR-92b was not statistically significant but had an upward trend ($P > 0.05$, **Figure 1D**). Due to miR-146b has been proved to be involved in the differentiation of neural stem cells (Xiao et al., 2015) we explored whether EA regulated the miR-146b expression in peri-ischemic striatum. The results showed that the expression of miR-146b was decreased in the MCAO+miR-146b inhibitors group, while higher expression in the MCAO+EA group, which compared with the MCAO group ($P < 0.01$, **Figure 1E**). Moreover, it had lower expression in the MCAO+EA+miR-146b inhibitors group compared with the MCAO+EA group, but no statistical significance ($P > 0.05$, **Figure 1E**). These results suggest that EA is involved in regulating the expression of exosomal miR-146b in peri-ischemic striatum.

EA Promoted the Differentiation of Endogenous Neural Stem Cells via miR-146b in Peri-Ischemic Striatum and SVZ of the Ischemic Hemisphere

To explore whether EA regulated the differentiation of neural stem cells through miR-146b, we used BrdU to label neonatal cells and NeuN to mark neural cells after ischemic stroke. Thus immunofluorescence co-localization with NeuN and BrdU represented neonatal neurons. In peri-ischemic striatum and SVZ of the ischemic hemisphere, we found that the positive cells of co-localization of $NeuN^+$ /$Brdu^+$ were decreased in the MCAO+miR-146b inhibitors group and increased in the MCAO+EA group, compared with the MCAO group ($P < 0.05$ or $P < 0.01$, **Figures 2A–D**). Besides, compared with the MCAO+EA group, the result also

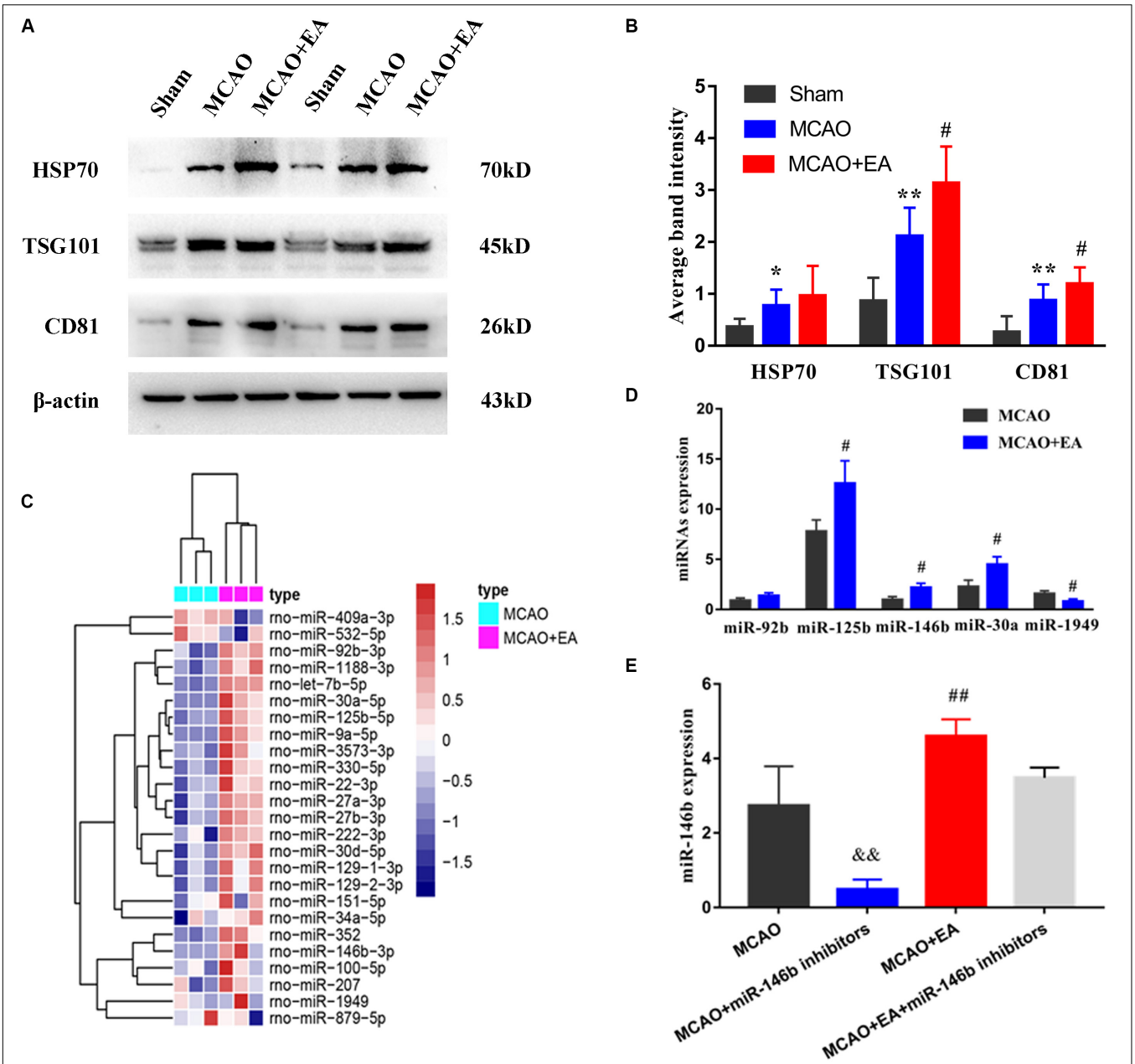

FIGURE 1 | Electro-acupuncture promotes the release of exosomal miR-146b in peri-ischemic striatum. **(A)** The expression of exosome-associated markers HSP70, TSG101, and CD81 were analyzed by Western blotting. **(B)** The expression of markers were quantified on the basis of average band intensity ($n = 4$). **(C)** MiRNA microarray analysis of exosomes from peri-ischemic striatum and clustering of 25 significantly altered miRNAs with ≥1.5-fold difference in expression between MCAO and MCAO+EA groups. **(D)** Four miRNAs were significantly upregulated and 1 miRNA were downregulated in exosomes of the MCAO+EA group compared with the MCAO group were checked by RT-qPCR ($n = 3$). **(E)** The expression of miR-146b in tissues of peri-ischemic striatum were analyzed form MCAO, MCAO+miR-146b inhibitors, MCAO+EA, MCAO+EA+miR-146b inhibitors groups ($n = 3$). Data represent means ± *SD* of the results of representative experiment. $^{*}P < 0.05$, MCAO vs. Sham; $^{**}P < 0.01$, MCAO vs. Sham; $^{\#}P < 0.05$ and $^{\#\#}P < 0.01$, MCAO vs. MCAO+EA; $^{\&\&}P < 0.01$, MCAO vs. MCAO+miR-146b inhibitors; MCAO+EA vs. MCAO+EA+miR-146b inhibitors.

showed that the co-localization of the MCAO+EA+miR-146b inhibitors group was decreased ($P < 0.01$, **Figures 2A–D**). It indicated that EA could promote endogenous neural stem cells differentiation into neurons in peri-ischemic striatum and SVZ of the ischemic hemisphere through miR-146b after ischemic stroke.

MiR-146b Regulated the Differentiation of Neural Stem Cells *in vitro* OGD/R Injury

Furthermore, we performed neural stem cells OGD/R culture to mimic *in vitro* ischemic injury model. The results showed

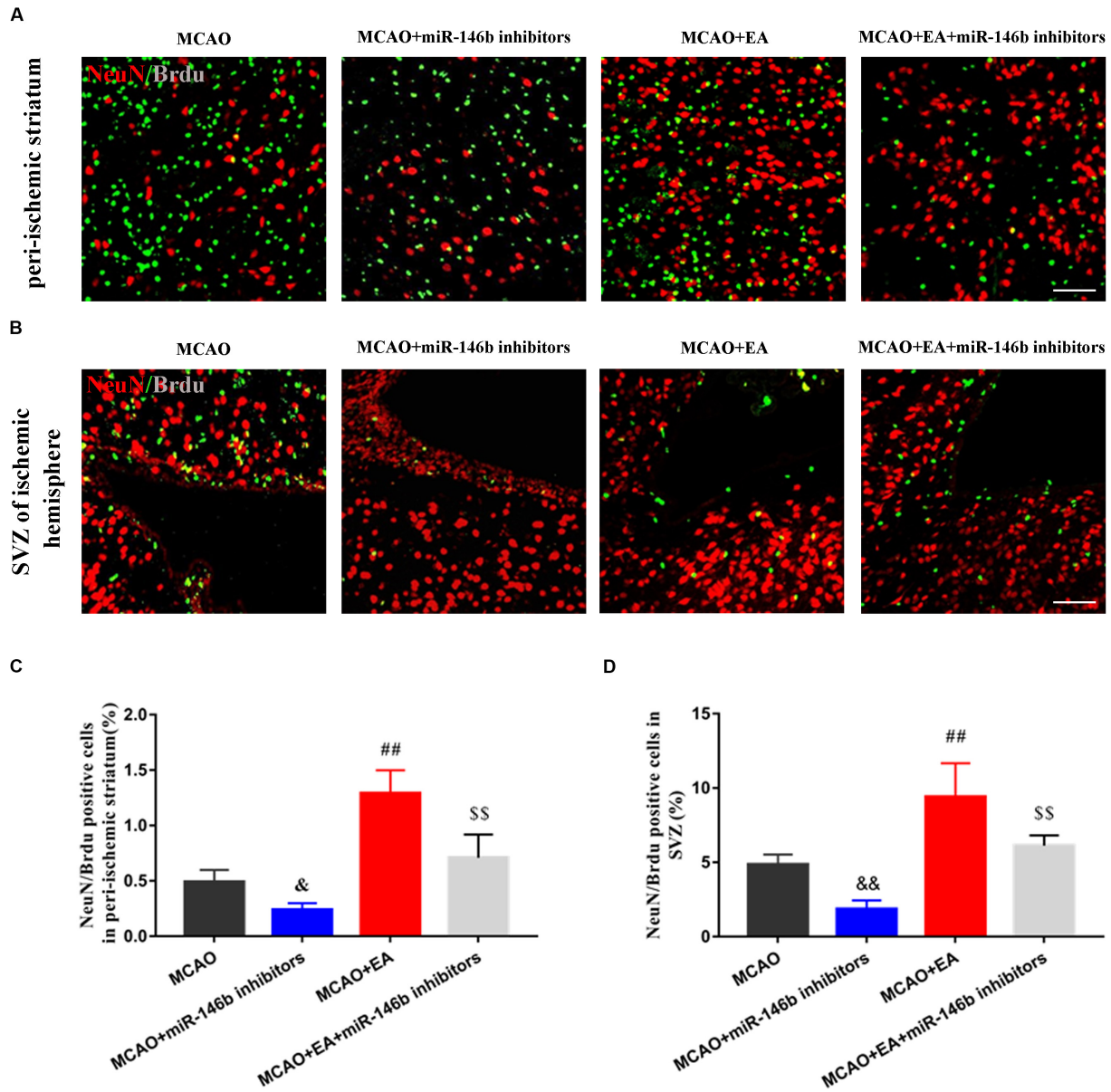

FIGURE 2 | Electro-acupuncture promotes the differentiation of endogenous neural stem cells into neurons in peri-ischemic striatum and SVZ of ischemic hemisphere. **(A)** Immunofluorescence and co-localization of NeuN with BrdU in peri-ischemic striatum **(B)**. Immunofluorescence and co-localization of NeuN with BrdU in the subventricular zone (SVZ) of ischemic hemisphere. **(C,D)** The positive cells of co-localization of NeuN/Brdu in peri-ischemic striatum and SVZ of ischemic hemisphere, respectively ($n = 4$). Data represent means ± *SD* of the results of representative experiment. $^{\&}P < 0.05$ and $^{\&\&}P < 0.01$, MCAO vs. MCAO+miR-146b inhibitors; $^{\#\#}P < 0.01$, MCAO vs. MCAO+EA; $^{\$\$}P < 0.05$, MCAO+miR-146b inhibitors vs. MCAO+EA+miR-146b inhibitors.

that OGD/R induced Nestin-marked neural stem cell injury, and miR-146b inhibitors could suppress the injury, but no statistical significance ($P > 0.05$, **Figures 3A,D**). Simultaneously, OGD/R inhibited the differentiation of neural stem cells, and miR-146b inhibitors further suppressed the differentiation of neural stem cells and NeuroD1 was involved in neural stem cells differentiation into neurons with NeuroD1$^+$/DCX$^+$ and NeuroD1$^+$/NeuN$^+$ ($P < 0.05$, **Figures 3B–E**). These results suggest that miR-146b could regulate NeuroD1-mediated neural stem cells differentiation *in vitro* OGD/R injury.

EA Could Promote NeuroD1-Mediated Neural Stem Cells Differentiation via miR-146b in SVZ of the Ischemic Hemisphere

To furtherly clarify whether EA promoted the differentiation of neural stem cells through miR-146b, firstly, the expression of NeuroD1 of differentiation-associated factors in SVZ of the ischemic hemisphere with miR-146b inhibitors intervention was observed, and the results showed that the expression of NeuroD1

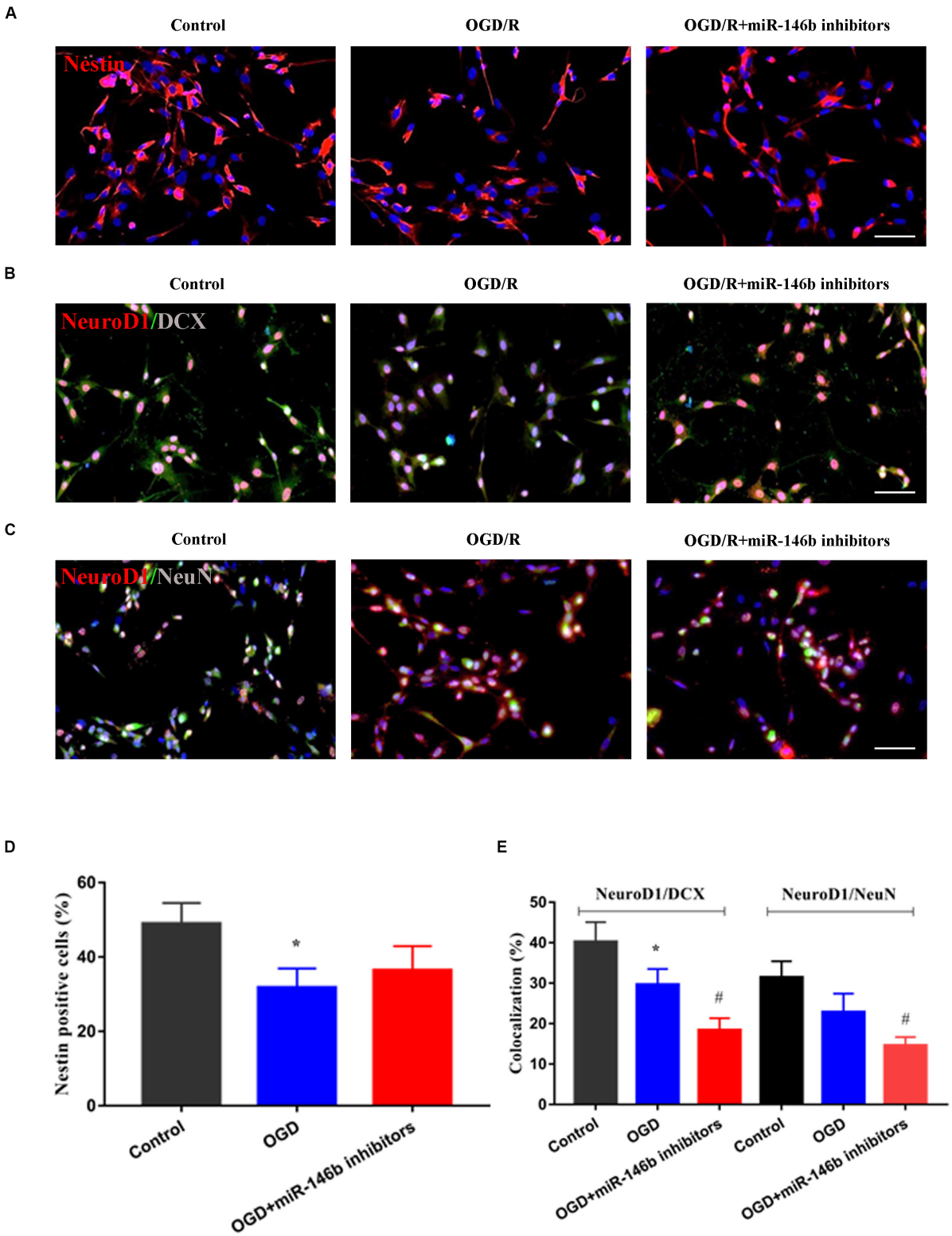

FIGURE 3 | MiR-146b inhibitors suppressed neuronal differentiation of stem cells on OGD 6 h and reperfusion 72 h of *vitro* culture. **(A)** Cells were immunostained for Nestin (red) and DAPI for the nucleus (blue). **(B)** Immunofluorescence and co-localization of NeuroD1 (red) with DCX (green) ($n = 3$). **(C)** Immunofluorescence and co-localization of NeuroD1 (red) with NeuN (green). **(D)** Percentage of Nestin positive cells in control, OGD/R, OGD/R+miR-146b inhibitors groups ($n = 3$). **(E)** Percentage of co-localization with NeuroD1$^+$/DCX$^+$ and NeuroD1$^+$/NeuN$^+$ in control, OGD/R, OGD/R+miR-146b inhibitors groups ($n = 3$). Data represent means ± *SD* of the results of representative experiment. $^*P < 0.05$, Control vs. OGD/R; $^\#P < 0.05$, OGD/R vs. MCAO+miR-146b inhibitors.

in the MCAO+miR-146b inhibitors group was lower trend than that in the MCAO group, and it was significantly increased after EA in SVZ of the ischemic hemisphere ($P < 0.01$, **Figures 4A,B**). Moreover, it had lower expression in the MCAO+EA+miR-146b inhibitors group compared with the MCAO+EA group ($P < 0.05$, **Figures 4A,B**). Subsequently, we used immunofluorescence staining to co-localize NeuroD1 and DCX in SVZ of the ischemic hemisphere. Unsurprisingly, more $NeuroD1^+/DCX^+$ were co-localized in the MCAO+EA group, and injected miR-146b inhibitors could decrease the number of $NeuroD1^+/DCX^+$ co-localization ($P < 0.05$, **Figures 4C,D**).

Furthermore, we assessed the neurological deficits, the results showed that the mNSS score was obviously reduced in the MCAO+EA group compared with the MCAO group, and it was reduced in the MCAO+EA+miR-146b inhibitors group compared with MCAO+miR-146b inhibitor group as well ($P < 0.05$, **Figure 4E**), which proved that EA could improve neurological deficits after stroke.

DISCUSSION

Stroke is considered the leading cause of neurological dysfunction and death worldwide. Currently, recombinant tissue plasminogen activator (rt-PA) is the only thrombolytic drug approved by the FDA for the treatment of ischemic stroke. However, due to the time window limitation of thrombolytic therapy and serious adverse prognosis, its clinical application is greatly limited (Powers et al., 2019). Non-drug treatment of stroke is more and more common in clinic. EA has been shown to effectively improve neurological deficits after stroke (Chang et al., 2017). In this study, we found that the content of exosomes was increased in the peri-ischemic striatum after EA. Then, we revealed 25 differentially expressed miRNAs in exosomes by analysis of miRNA expression profile, of which miR-146b was selected for further analysis, by injecting miR-146b inhibitor into the lateral ventricle of rats, it has been determined that miR-146b was involved in the regulation of EA on neurogenesis. Subsequently, we demonstrated that EA could promote endogenous neural stem cells differentiation into neurons in peri-ischemic striatum and SVZ of the ischemic hemisphere by up-regulating the expression of miR-146b after ischemic stroke. *In vitro* and *in vivo* we verified the role of miR-146b on neurogenesis, which proved that miR-146b was involved in promoting NeuroD1-mediated neural stem cells differentiation. In addition, EA also could improve neurological deficits through miR-146b after ischemic stroke. Therefore, we speculated that exosomal miR-146b might be a potential target for promoting endogenous neural stem cells differentiation after stroke.

Neurogenesis provides a potential therapeutic method for stroke. In an experimental stroke, cerebral ischemic neurogenesis was increased in ipsilateral SVZ, and neuroblasts migrate from SVZ to the ischemic border region of the striatum and cortex, which have the phenotype of mature neurons (Liu et al., 2007). In recent years, studies have shown that exosomes mediated delivery of proteins, lipids, and nucleic acids, which are involved in neurogenesis (Lässer, 2012). These bioactive molecules mediate exosomal cell-to-cell communication which may target specific cell types. Exosomes released by the neural cells not only regulate the occurrence and development of nervous system diseases, but also play a role in regeneration and remodeling of the nervous system after neural injury (Porro et al., 2015). It reported that exosome treatment significantly restore cerebral infarct volume and improve neurological deficits in cerebral ischemia rats (Zheng et al., 2019). In a study, the researchers co-cultured the damaged cortical neurons with adipose stem cells, and found that exosomes secreted by neural stem cells can exert neuroprotective functions by inhibiting neuronal apoptosis, thereby promoting the central nervous system (CNS) regeneration and repair (Hong et al., 2019). Another study showed that mesenchymal stem cell-derived exosomes stimulated neurogenesis in the SVZ region and reduced neurological damage (Reza-Zaldivar et al., 2019). In this study, we found that the content of exosomes was increased in the peri-ischemic striatum after EA treatment, accompanied by the improvement of neurological deficits after stroke.

Stem cells can self-renew or differentiate into multiple cell types, and miRNAs play a central role in determining the fate of stem cells. Thus, does exosomes play an important role by delivering miRNAs? We revealed that exosomal miR-146b identified by microarray chip influenced the differentiation of endogenous neural stem cells. Previous study has shown that miR-146 regulates differentiation of neural stem cells by regulating Notch 1 signaling pathway (Mei et al., 2011). *In vitro* experiment, human neural stem cells (hNSCs) were induced to differentiation with 2D and 3D culture systems, and using miRNA PCR arrays to identify differential expression profiles in differentiated hNSCs, revealing hsa-miR-146b was upregulation, and it further was confirmed that miR-146b regulated the differentiation of hNSCs into neurons by its mimic transfection (Xiao et al., 2015).

Increasing evidence suggests that miRNAs are involved in the process of ischemic stroke (Zhang et al., 2017). A large number of studies have used miRNA treatment to reduce ischemic brain injury and functional recovery after stroke (Volný et al., 2015; Sen, 2019; Van Kralingen et al., 2019; Yuan et al., 2019). Based on this fact, we explored the effect of exosomal miR-146b on neural stem cell differentiation after ischemia-reperfusion injury. We demonstrated that EA could promote endogenous neural stem cells differentiation into neurons in peri-ischemic striatum and SVZ of the ischemic hemisphere via the upregulation of miR-146b after ischemic stroke. Besides, *in vitro* ischemic injury model, we found that OGD/R could inhibit the differentiation of neural stem cells, and miR-146b inhibitors further suppressed the differentiation of neural stem cells. We also confirmed that NeuroD1 was involved in neural stem cells differentiation into neurons. *In vitro* and *in vivo*, we verified the effect of miR-146b on neurogenesis, which proved that miR-146b was involved in promoting NeuroD1-mediated neural stem cells differentiation.

As a neurodifferentiation factor, NeuroD1 is essential for neuronal development, and it can reprogram other cell types into neurons (Pataskar et al., 2016). In our previous study, it has shown that EA could regulate the Notch1 signaling pathway (Tao et al., 2015). While the Notch1 signal transduction may be due to its inhibitory effect on bHLH protein that activates the

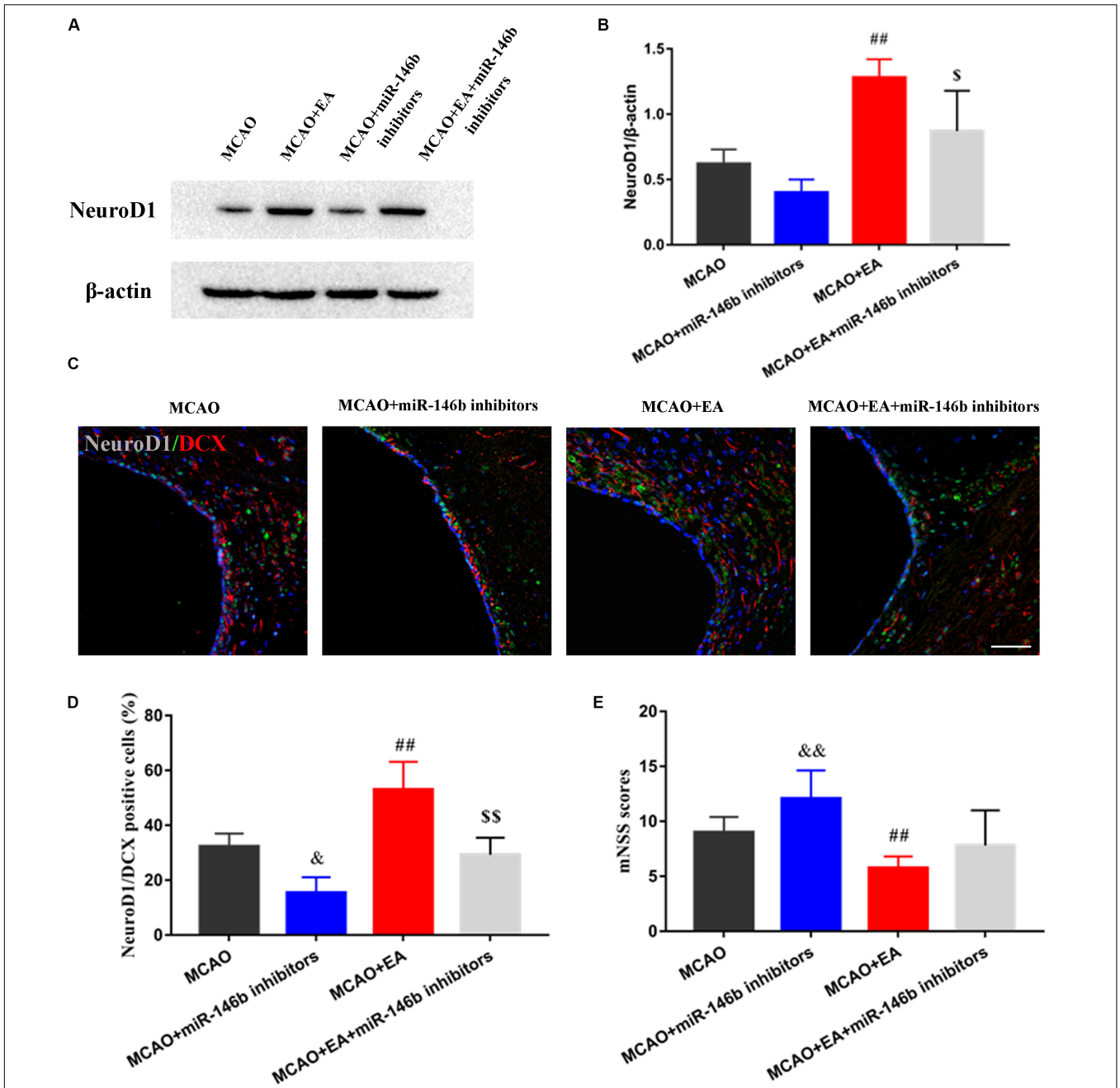

FIGURE 4 | Electro-acupuncture promotes NeuroD1 associated neuron differentiation in SVZ of ischemic hemisphere. **(A)** The expression of NeuroD1 of neuronal differentiation-associated marker was analyzed by Western blotting in SVZ of ischemic hemisphere. **(B)** The expression of markers were quantified on the basis of average band intensity (n = 3). **(C)** Immunofluorescence and co-localization of NeuroD1 with DCX in SVZ of ischemic hemisphere. **(D)** Co-localization of NeuroD1 with DCX positive cells (n = 3). **(E)** The mNSS scores were tested in MCAO, MCAO+miR-146b inhibitors, MCAO+EA, MCAO+EA+miR-146b inhibitors groups (n = 10). Data represent means ± SD of the results of representative experiment. $^{\#\#}P < 0.01$, MCAO vs. MCAO+EA; $^{\&}P < 0.05$ and $^{\&\&}P < 0.05$, MCAO vs. MCAO+miR-146b inhibitors; $^{\$}P < 0.05$ and $^{\$\$}P < 0.05$, MCAO+EA vs. MCAO+EA+miR-146b inhibitors.

cell differentiation program (Kageyama et al., 2005). As a type of bHLH protein, NeuroD1 is a potential downstream target of the Notch signaling pathway. Studies have shown that Notch signaling increased, and the transcription level of NeuroD1 was decreased (Fineberg et al., 2012). Therefore, we speculated that NeuroD1 might be a potential factor for EA to promote the differentiation of endogenous neural stem cells. In our study, EA could promote neurogenesis after stroke and increase the number of $DCX^+/NeuroD1^+$ colocalization in the SVZ. And when we injected miR-146b inhibitor, the number of $DCX^+/NeuroD1^+$ co-localization was decreased. Therefore, our results suggest that NeuroD1 might be a downstream factor of exosomal miR-146b, which could promote the differentiation of endogenous neural stem cells in rats with ischemia-reperfusion injury. However,

in the future, we will further explore how mir-146b regulates NeuroD1-mediated differentiation of neural stem cells.

CONCLUSION

Electro-acupuncture is a prospective therapy that can enhance the differentiation of endogenous neurogenesis and improve neurological deficits after ischemic stroke. We demonstrated that exosomal miR-146b is an important neuromodulator of neurogenesis, which promotes endogenous neural stem cell differentiation into neurons in peri-ischemia after stroke.

DATA AVAILABILITY STATEMENT

The raw data supporting the conclusions of this article will be made available by the authors, without undue reservation, to any qualified researcher.

ETHICS STATEMENT

The animal study was reviewed and approved by the Animal Ethics Committee of Fujian University of Traditional Chinese Medicine (SCXK#2016005).

AUTHOR CONTRIBUTIONS

LC, WL, and JT contributed to the study concept and design. SZ, TJ, LW, YuZ, YiZ, YL, and XH collected and analyzed the data. HL and MY performed the statistical analyses. WL and JT drafted and revised the manuscript. All authors contributed to the critical revision of the manuscript, approved the final manuscript as submitted, and agreed to be accountable for all aspects of the work.

FUNDING

This study was supported by the grants from the science and technology platform construction project of Fujian Science and Technology Department (Grant No. 2018Y2002).

SUPPLEMENTARY MATERIAL

The Supplementary Material for this article can be found online at: https://www.frontiersin.org/articles/10.3389/fncel.2020.00223/full#supplementary-material

REFERENCES

Beckervordersandforth, R., Zhang, C. L., and Lie, D. C. (2015). Transcription-factor-dependent control of adult hippocampal neurogenesis. *Cold Spring Harb. Perspect. Biol.* 7:a018879. doi: 10.1101/cshperspect.a018879

Boldrini, M., Fulmore, C. A., Lu, A. Q., Lee, R., Wang, S., Tartt, A. N., et al. (2018). Human hippocampal neurogenesis persists throughout aging. *Cell Stem Cell* 22, 589–599. doi: 10.1016/j.stem.2018.03.015

Chang, J., Zhang, H., and Tan, Z. (2017). Effect of electroacupuncture in patients with post-stroke motor aphasia: neurolinguistic and neuroimaging characteristics. *Wien. Klin. Wochenschr.* 129, 102–109. doi: 10.1007/s00508-016-1070-1

Chen, B., Tao, J., Lin, Y., Lin, R., Liu, W., and Chen, L. (2015). Electro-acupuncture exerts beneficial effects against cerebral ischemia and promotes the proliferation of neural progenitor cells in the cortical peri-infarct area through the Wnt/β-catenin signaling pathway. *Int. J. Mol. Med.* 36, 1215–1222. doi: 10.3892/ijmm.2015.2334

Chen, Y. C., Ma, N. X., and Pei, Z. F. (2020). A neurod1 AAV-based gene therapy for functional brain repair after ischemic injury through in? vivo astrocyte-to-neuron conversion. *Mol. Ther.* 28, 217–234. doi: 10.1016/j.ymthe.2019.09.003

Fineberg, S. K., Datta, P., Stein, C. S., Lu, A. Q., Lee, R., Wang, S., et al. (2012). MiR-34a represses Numbl in murine neural progenitor cells and antagonizes neuronal differentiation. *PLoS One* 7:38562. doi: 10.1371/journal.pone.0038562

Geng, W., Lu, A. Q., Lee, R., Wang, S., Tang, H., Luo, S., et al. (2019). Exosomes from miRNA-126-modified ADSCs promotes functional recovery after stroke in rats by improving neurogenesis and suppressing microglia activation. *Am. J. Transl. Res.* 11, 780–792.

Gonçalves, J. T., Schafer, S. T., and Gage, F. H. (2016). Adult neurogenesis in the hippocampus: from stem cells to behavior. *Cell* 167, 897–914. doi: 10.1016/j.cell.2016.10.021

Guo, Z., Zhang, L., and Wu, Z. (2014). In vivo direct reprogramming of reactive glial cells into functional neurons after brain injury and in an Alzheimer's disease model. *Cell Stem Cell.* 14, 188–202. doi: 10.1016/j.stem.2013.12.001

Hong, P., Yang, H., and Wu, Y. (2019). The functions and clinical application potential of exosomes derived from adipose mesenchymal stem cells: a comprehensive review. *Stem Cell Res. Ther.* 10:242. doi: 10.1186/s13287-019-1358-y

Kageyama, R., Ohtsuka, T., Hatakeyama, J., and Ohsawa, R. (2005). Roles of bHLH genes in neural stem cell differentiation. *Exp. Cell Res.* 306, 343–348. doi: 10.1016/j.yexcr.2005.03.015

Lässer, C. (2012). Exosomal RNA as biomarkers and the therapeutic potential of exosome vectors. *Expert Opin. Biol. Ther.* 12(Suppl. 1), S189–S197. doi: 10.1517/14712598.2012.680018

Liu, X. S., Zhang, Z. G., Gao, L., Shen, D. H., Guo, X., Zhang, R. L., et al. (2007). Stroke induces gene profile changes associated with neurogenesis and angiogenesis in adult subventricular zone progenitor cells. *J. Cereb. Blood Flow Metab.* 27, 564–574. doi: 10.1038/sj.jcbfm.9600371

Longa, E. Z., Weinstein, P. R., Carlson, S., and Cummins, R. (1989). Reversible middle cerebral artery occlusion without craniectomy in rats. *Stroke* 20, 84–91. doi: 10.1161/01.str.20.1.84

Mei, J., Bachoo, R., and Zhang, C. L. (2011). MicroRNA-146a inhibits glioma development by targeting Notch1. *Mol. Cell. Biol.* 17, 3584–3592. doi: 10.1128/MCB.05821-11

Mori, M. A., Ludwig, R. G., and Garcia-Martin, R. (2019). Extracellular miRNAs: from biomarkers to mediators of physiology and disease. *Cell Metab.* 30, 656–673. doi: 10.1016/j.cmet.2019.07.011

Nakagomi, T., Takagi, T., and Beppu, M. (2019). Neural regeneration by regionally induced stem cells within post-stroke brains: novel therapy perspectives for stroke patients. *World J. Stem Cells* 11, 452–463. doi: 10.4252/wjsc.v11.i8.452

Ngalula, K. P., Cramer, N., and Schell, M. J. (2015). Transplanted neural progenitor cells from distinct sources migrate differentially in an organotypic model of brain injury. *Front. Neurol.* 6:212. doi: 10.3389/fneur.2015.00212

Pataskar, A., Gao, L., Shen, D. H., Guo, X., Jung, J., Smialowski, P., et al. (2016). NeuroD1 reprograms chromatin and transcription factor landscapes to induce the neuronal program. *EMBO J.* 35, 24–45. doi: 10.15252/embj.201591206

Perez-Gonzalez, R., Gauthier, S. A., Kumar, A., and Levy, E. (2012). The exosome secretory pathway transports amyloid precursor protein carboxyl-terminal fragments from the cell into the brain extracellular space. *J. Biol. Chem.* 287, 43108–43115. doi: 10.1074/jbc.m112.40446726

Péron, S., and Berninger, B. (2015). Imported stem cells strike against stroke. *Cell Stem Cell* 17, 501–502. doi: 10.1016/j.stem.2015.10.006

Porro, C., Trotta, T., and Panaro, M. A. (2015). Microvesicles in the brain: biomarker, messenger or mediator? *J. Neuroimmunol.* 288, 70–78. doi: 10.1016/j.jneuroim.2015.09.006

Powers, W. J., Rabinstein, A. A., and Ackerson, T. (2019). Guidelines for the early management of patients with acute ischemic stroke: 2019 update to the 2018 guidelines for the early management of acute ischemic stroke: a guideline for healthcare professionals from the american heart association/american stroke association. *Stroke* 50, 344–418. doi: 10.1161/STR.0000000000000215

Reza-Zaldivar, E. E., Hernández-Sapiéns, M., Gutiérrez-Mercado, K., Sandoval-Ávila, S., Gomez-Pinedo, U., Márquez-Aguirre, L., et al. (2019). Mesenchymal stem cell-derived exosomes promote neurogenesis and cognitive function recovery in a mouse model of alzheimer's disease. *Neural Regen. Res.* 014, 1626–1634. doi: 10.4103/1673-5374.255978

Sen, C. K. (2019). Micrornas as new maestro conducting the expanding symphony orchestra of regenerative and reparative medicine. *Physiol. Genom.* 43, 517–520. doi: 10.1152/physiolgenomics.00037.2011

Shinozuka, K., Dailey, T., and Tajiri, N. (2014). Stem cells for neurovascular repair in stroke. *J. Stem Cell Res. Ther.* 4:12912. doi: 10.1007/978-1-4614-8690-9_11

Takeda, K., Sowa, Y., Nishino, K., Itoh, K., and Fushiki, S. (2015). Adipose-derived stem cells promote proliferation, migration, and tube formation of lymphatic endothelial cells in vitro by secreting lymphangiogenic factors. *Ann. Plast. Surg.* 74, 728–736. doi: 10.1097/SAP.0000000000000084

Tao, J., Chen, B., and Gao, Y. (2014). Electroacupuncture enhances hippocampal NSCs proliferation in cerebral ischemia-reperfusion injured rats via activation of notch signaling pathway. *Int. J. Neurosci.* 124, 204–212. doi: 10.3109/00207454.2013.840781

Tao, J., Xue, X. H., and Chen, L. D. (2015). Electroacupuncture improves neurological deficits and enhances proliferation and differentiation of endogenous nerve stem cells in rats with focal cerebral ischemia. *Neurol. Res.* 32, 198–204. doi: 10.1179/174313209X414506

Van Kralingen, J. C., McFall, A., Ord, E. N. J., Watson, T., and Xang, S. (2019). Altered extracellular vesicle microRNA expression in ischemic stroke and small vessel disease. *Transl. Stroke Res.* 10, 495–508. doi: 10.1007/s12975-018-0682-3

Volný, O., Kašičková, L., and Coufalová, D. (2015). microRNAs in cerebrovascular disease. *Adv. Exp. Med. Biol.* 888, 155–195. doi: 10.1007/978-3-319-22671-2_9

Wang, W., Jiang, B., and Sun, H. (2017). Prevalence, incidence, and mortality of stroke in China: results from a nationwide population-based survey of 480 687 adults. *Circulation* 135, 759–771. doi: 10.1161/CIRCULATIONAHA.116.025250

Wu, S., Wu, B., and Liu, M. (2019). Stroke in China: advances and challenges in epidemiology, prevention, and management. *Lancet Neurol.* 18, 394–405. doi: 10.1016/S1474-4422(18)30500-3

Xiao, W. Z., Lu, A. Q., Lee, R., Wang, S., and Liu, X. W. (2015). Role of miRNA-146 in proliferation and differentiation of mouse neural stem cells. *Biosci. Rep.* 35:88. doi: 10.1042/BSR20150088

Yamashita, T., Ninomiya, M., Hernandez, R., and Acosta, P. (2006). Subventricular zone-derived neuroblasts migrate and differentiate into mature neurons in the post-stroke adult striatum. *J. Neurosci.* 26, 6627–6636. doi: 10.1523/JNEUROSCI.0149-06.2006

Yang, Z. J., Shen, D. H., Guo, X., and Sun, F. Y. (2005). Electroacupuncture enhances striatal neurogenesis in adult rat brains after a transient cerebral middle artery occlusion. *Acupunct. Electrother. Res.* 30, 185–199. doi: 10.3727/036012905815901244

Yuan, Y., Zhang, Z., and Wang, Z. (2019). MiRNA-27b regulates angiogenesis by targeting AMPK in mouse ischemic stroke model. *Neuroscience* 398, 12–22. doi: 10.1016/j.neuroscience.2018.11.041

Zagrean, A. M., Hermann, D. M., Opris, I., Zagrean, L., and Popa-Wagner, A. (2018). Multicellular crosstalk between exosomes and the neurovascular unit after cerebral ischemia, therapeutic implications. *Front. Neurosci.* 12:811. doi: 10.3389/fnins.2018.00811

Zhan, L., Wang, T., and Li, W. (2010). Activation of Akt/FoxO signaling pathway contributes to induction of neuroprotection against transient global cerebral ischemia by hypoxic pre-conditioning in adult rats. *J. Neurochem.* 114, 897–908. doi: 10.1111/j.1471-4159.2010.06816.x

Zhang, Y., Jiang, H., and Yue, Y. (2017). The protein and mRNA expression levels of glial cell line-derived neurotrophic factor in post stroke depression and major depressive disorder. *Sci. Rep.* 7:8674. doi: 10.1038/s41598-017-09000-y

Zhao, H., Wang, J., Gao, L., Shen, D. H., Guo, X., Wang, R., et al. (2013). MiRNA-424 protects against permanent focal cerebral ischemia injury in mice involving suppressing microglia activation. *Stroke* 44, 1706–1713. doi: 10.1161/STROKEAHA.111.000504

Zhao, J., Gui, M., Liu, X., Jin, D., Zhuang, Z., and Yan, T. (2015). Electroacupuncture promotes neural stem cell proliferation and neurogenesis in the dentate gyrus of rats following stroke via upregulation of notch1 expression. *Mol. Med. Rep.* 12, 6911–6917. doi: 10.3892/mmr.2015.4279

Zheng, Y., He, R., and Wang, P. (2019). Exosomes from LPS-stimulated macrophages induce neuroprotection and functional improvement after ischemic stroke by modulating microglial polarization. *Biomater. Sci.* 7, 2037–2049. doi: 10.1039/c8bm01449c

Conflict of Interest: The authors declare that the research was conducted in the absence of any commercial or financial relationships that could be construed as a potential conflict of interest.

frontiers in Cellular Neuroscience

ORIGINAL RESEARCH
published: 04 September 2020
doi: 10.3389/fncel.2020.00280

Notoginsenoside R1–Induced Neuronal Repair in Models of Alzheimer Disease Is Associated With an Alteration in Neuronal Hyperexcitability, Which Is Regulated by Nav

Tao Hu[1†], Shan Li[2†], Wen-Qi Liang[3†], Shan-Shan Li[4†], Min-Nan Lu[5], Bo Chen[5], Li Zhang[6], Rui Mao[7], Wan-Hai Ding[8], Wen-Wei Gao[8], Shi-Wen Chen[8], Yan-Bin XiYang[2], Jie Zhang[9,10]* and Xu-Yang Wang[8]**

[1] Department of Laboratory Medicine, The Third People's Hospital of Yunnan Province, Kunming, China, [2] Institute of Neuroscience, Basic Medical College, Kunming Medical University, Kunming, China, [3] Department of Emergency, Shanghai Changhai Hospital, Naval Medical University, Shanghai, China, [4] Basic Medical College, Experimental Teaching Center, Kunming Medical University, Kunming, China, [5] Science and Technology Achievement Incubation Center, Kunming Medical University, Kunming, China, [6] Editorial Department of Journal of Kunming Medical University, Kunming, China, [7] School of Stomatology, Kunming Medicine University, Kunming, China, [8] Department of Neurosurgery, Shanghai Jiao Tong University Affiliated 6th People's Hospital, Shanghai, China, [9] Yunnan Provincial Key Laboratory for Birth Defects and Genetic Diseases, Department of Medical Genetics, The First People's Hospital of Yunnan Province, Kunming, China, [10] Affiliated Hospital of Kunming University of Science and Technology, Kunming, China*

Alzheimer disease is characterized by a progressive cognitive deficit and may be associated with an aberrant hyperexcitability of the neuronal network. Notoginsenoside R1 (R1), a major activity ingredient from *Panax notoginseng*, has demonstrated favorable changes in neuronal plasticity and induced neuroprotective effects in brain injuries, resulting from various disorders, however, the underlying mechanisms are still not well understood. In the present study, we aimed to explore the possible neuroprotective effects induced by R1 in a mouse model of AD and the mechanisms underlying these effects. Treatment with R1 significantly improved learning and memory functions and redressed neuronal hyperexcitability in amyloid precursor protein/presenilin-1 mice by altering the numbers and/or distribution of the members of voltage-gated sodium channels (Nav). Moreover, we determined whether R1 contributed to the regulation of neuronal excitability in Aβ-42–injured cells. Results of our study demonstrated that treatment with R1 rescued Aβ1-42–induced injured neurons by increasing cell viability. R1-induced alleviation in neuronal hyperexcitability might be associated with reduced Navβ2 cleavage, which partially reversed the abnormal distribution of Nav1.1α. These results suggested that R1 played a vital role in the recovery of Aβ1-42–induced neuronal injury and hyperexcitability, which is regulated by Nav proteins. Therefore, R1 may be a promising candidate in the treatment of AD.

Keywords: notoginsenoside R1, Alzheimer disease, neuronal hyperexcitability, voltage-gated sodium channel, cognitive impairment

OPEN ACCESS

Edited by:
Zhang Pengyue,
Yunnan University of Traditional Chinese Medicine, China

Reviewed by:
Hao Tang,
Manchester University, United States
Xiuyun Liu,
Johns Hopkins University, United States

***Correspondence:**
Yan-Bin XiYang
xiyang_neuro@126.com
Jie Zhang
kmzhjie@aliyun.com
Xu-Yang Wang
wangxuyanglxl@163.com

† These authors have contributed equally to this work

Specialty section:
This article was submitted to Cellular Neuropathology, a section of the journal Frontiers in Cellular Neuroscience

Received: *14 May 2020*
Accepted: *06 August 2020*
Published: *04 September 2020*

Citation:
Hu T, Li S, Liang W-Q, Li S-S, Lu M-N, Chen B, Zhang L, Mao R, Ding W-H, Gao W-W, Chen S-W, XiYang Y-B, Zhang J and Wang X-Y (2020) Notoginsenoside R1–Induced Neuronal Repair in Models of Alzheimer Disease Is Associated With an Alteration in Neuronal Hyperexcitability, Which Is Regulated by Nav. Front. Cell. Neurosci. 14:280. doi: 10.3389/fncel.2020.00280

INTRODUCTION

Alzheimer disease (AD) is the most typical manifestation of dementia, and its incidence is increasing exponentially. It is prevalent among the elderly and has affected 35 million people worldwide (Ghezzi et al., 2013). AD is characterized by a progressive cognitive decline, which may burden the families of patients as well as healthcare systems. Researchers have been trying to identify drugs that may help slow the progression of AD; however, the results obtained so far have not been satisfactory (Ghezzi et al., 2013). Therefore, developing new drugs for the management of AD is a big unmet medical need.

Panax notoginseng is a promising candidate for the management of AD, owing to the multiple types of active components present in this herb. This traditional Chinese herbal medicine is grown in Yunnan and has more than a 100-year history of use in the clinical treatment of a wide range of diseases in China (Ng, 2006; Guo et al., 2010; Kim, 2012). As a major ingredient isolated from *P. notoginseng* saponins (PNSs), notoginsenoside R1 (R1) has been proven to possess anti-inflammatory and antioxidative properties and is useful to reverse damage caused by ischemia–reperfusion (Zhang et al., 1997; Ng, 2006; Zhang and Wang, 2006; Liu et al., 2010; Pang et al., 2017). Recent studies have demonstrated that various ginsenosides contribute to PNS-induced neuroprotective effects in AD (Huang et al., 2014, 2017; Li et al., 2015. By reduction of the amyloid precursor protein (APP) expression, stimulation of α-secretase activity, and inhibition on β-secretase activity, ginsenosides Rb1, Rg1, and Rg3 display protective effects against Aβ production and aggregation (Chen et al., 2006; Wang and Du, 2009; Yang et al., 2009). In addition, a recent study reported that R1 prevented Aβ-induced synaptic dysfunction and improved hippocampal-based memory performance in an AD mouse model through a possible mechanism involved in the modulation of neuronal excitability (Yan et al., 2014). However, the neuroprotection induced by R1 associated with neuronal excitability seen in AD is still not clearly understood.

Voltage-gated sodium channels (Nav) play a crucial role in cell excitability and generate and propagate action potentials (APs) (Hodgkin and Huxley, 1952; Catterall, 2000; Chyung et al., 2005). The main components of Nav include nine α subtypes, namely, Nav1.1 to Nav1.9, and at least one auxiliary β subunit. Nav1.1 is mainly seen in GABAergic interneurons but not in excitatory pyramidal neurons (Yu et al., 2006). The voltage-gated sodium-channel β2 subunit (Navβ2) is indispensable for the generation of normal electric potential and controlling excitability of the neuronal membrane; it also regulates current density and the function of Nav in neurons (Chen et al., 2002; Lopez-Santiago et al., 2006). A previous study conducted by our group demonstrated that the expression of SCN2B (the encoding gene of Navβ2) mRNA was up-regulated in the hippocampus and frontal cortex of senescence-accelerated mice prone 8 (SAMP8). This finding suggested that SCN2B may be closely related to the aging process of the hippocampus and frontal lobe of SAMP8, whereas treatment with Xueshuantong (a trade name of PNS) significantly reversed this trend (XiYang et al., 2016). Administration of PNS also induced an improvement in learning and memory (XiYang et al., 2016). Otherwise, as a novel substrate of BACE1 and γ-secretase, the hydrolyzed Navβ2 expression is significantly increased, and Navβ2 plays an important role in the abnormal intracellular translocation of Nav1.1α and production of Aβ in mice with AD (Hu et al., 2017, 2019). Taken together, these results suggested that the antiaging effect and neuroprotective ability of PNS may be associated with the regulation of Navβ2 expression in the brain in the regions responsible for learning and memory. Our current study presents the first known case of how learning and memory improvement induced by R1, a specific and major ingredient of PNS, is dependent on the alteration of neuronal excitability regulated by Navβ2 in mice with AD.

MATERIALS AND METHODS

Ethics Statement

All experiments and protocols regarding animal care complied with the Guide for the Care and Use of Laboratory Animals published by the US National Institutes of Health (publication no. 85-23; revised 1996). This study was performed in accordance with the Care and Use Guidelines of Experimental Animals established by the Research Ethics Committee of Kunming University of China (permit no. kmu-eac-2018021; Kunming, China). Isoflurane was used to induce anesthesia for surgical procedures. The purchase, storage, and use of isoflurane were approved by Kunming Medical University (license no. kmykdx-D-A00272; Kunming, China).

Drug Preparation

R1 (C47H80O18, molecular weight 933.16, purity > 99.0%) was purchased from MedChemExpress LLC (CAS no. 80418-24-2, Shanghai, China). R1 was dissolved in dimethyl sulfoxide (DMSO) to yield a 1 mM stock solution and stored at −20°C.

Animal Grouping

Two-month-old C57BL/6J mice [wild-type (WT) mice] and APPswe/PS1ΔE9 [APP/presenilin-1 (PS1) transgenic mice with a C57BL/6J genetic background] mice were purchased from the laboratory animal center of Kunming Medical University. A previous study demonstrates that APP/PS1 mice show intact cognition at the age of 2 months, learning deficits at 3.5 months, learning and memory deficits at 5 m, and further learning and memory impairments at 8 m (Li et al., 2016). It appears that APP/PS1 mice at 2 months mimic the preclinical stage of AD (prodromal AD), whereas APP/PS1 mice at 8 months exhibit midclinical signs of AD (symptomatic AD) (Li et al., 2016). In order to explore the impact of R1 on mice at the preclinical stage of AD, we used 2-month-old APP/PS1 mice to explore the possible effects of R1 treatment for a consecutive 6-month period to study the age-specific alterations of memory and neuronal excitability related to AD progression. The APP/PS1 mice were randomly divided into the R1-treated group and control group, with each group comprising 15 mice. Animals in the drug-treated group were administered R1 once a day at a dose of 5 mg/kg per day by gavage for 6 months (APP/PS1 + R1–treated group). The

control group was treated with an equivalent volume of sterile 10% DMSO instead of R1 (APP/PS1 + vehicle group). Age-matched WT mice were administered an equivalent volume of sterile 10% DMSO, and these mice served as the normal control group (WT + vehicle group, $n = 15$). All experimental mice were housed in wood-chip bedded plastic cages in a 12:12 h light–dark cycle with free access to food and water.

Novel Object Recognition Task

After 6 months of continuous administration of the study drug, a novel object recognition (NOR) task was performed to evaluate the spatial memory of mice. The task lasted 3 days. A $40 \times 40 \times 40$ cm^3 transparent plastic box was used to perform this experiment. Previous studies report 24 h as an intertrial interval (ITI) in NOR test when memory function was explored, indicating it to be a promising and reasonable interval for NOR tasks to be performed by APP/PS1 mice (Luo et al., 2020). Therefore, in the present study, we selected 24 h as an ITI for the NOR task. On the first day, a 5-min habituation phase was carried out in the apparatus without introducing any objects. After the 24 h ITI, mice underwent an exploratory phase in the box containing two identical objects for 5 min. On the third day, a novel object (NT) was placed as a substitute for one of the objects in the apparatus. Mice were allowed to move and observe different objects freely; the time spent exploring the NT and familiar object (FT) was recorded. The memory discrimination index (DI), which is considered to be the index of spatial memory ability, was calculated using the following equation: $(NT - FT)/(NT + FT)$.

Marris Water Maze Test

The Marris Water Maze (MWM) consists of a circular pool (100 cm in diameter, 50 cm deep) filled with white water at 24°C ± 1°C to a depth of 20 cm. The MWM test was run as previously described (XiYang et al., 2016). All mice were subjected to a preliminary experiment, which allowed them to adapt to water and enabled them to step on a white platform (hidden below the water surface) so that they could be rescued. This preliminary experiment was carried out the day before the actual test. Briefly, a mouse placed in water was allowed to swim around for 10 s and then placed on a white platform submerged under water for only 1–2 s. For the regular test, the hidden platform was placed in a different location. The time taken by the mouse to find the hidden submerged white platform was recorded as escape latency and recorded for 5 days in a row. On day 6 of the test, the platform was removed for the probe trial, and each mouse was allowed to swim for 60 s to assess their memory regarding the location of the platform. The amount of time spent in the target quadrant, path taken in the target quadrant, and number of target platform crossings were recorded. The time spent and distances traveled in the four quadrants were also noted. The animals were tracked using an overhead video camera, and the data were analyzed using an animal behavior video-analysis system.

Electroencephalogram Recordings

For electroencephalogram (EEG) recordings, a high-resolution mouse EEG using polyimide-based microelectrode array (PBM array) was used. Protocols for electrode implantation, EEG recordings, data acquisition, and analysis were performed according to published studies the literature with some modifications (Lee et al., 2011; Corbett et al., 2013; Hu et al., 2017). Mice were anesthetized using isoflurane (2–3% for induction) mixed with O_2 (0.5–1 L/min) and fixed on the stereotaxic instrument for electrode fixation before subjecting them to EEG recordings. First, a 2 cm incision was made on the middle of the scalp to expose the skull, and the bregma and lambda points were identified. These points are the recognized electrode positions on the surface of the mouse brain on the skull according to the mouse brain atlas (Paxinos and Franklin's the Mouse Brain in Stereotaxic Coordinates). Then, mice were implanted in the hippocampus (anteroposterior −2.1 mm, mediolateral −1.5, dorsoventral −1.5 mm) with bare three-wire electrodes (1.0 mm in diameter), which consisted of three polyimide-coated wires with bare tips. Two microscrews that were used for ground and reference were fixed on the occipital bone above the cerebellum. Mice implanted with microelectrodes recovered within 5–7 days after surgery. The connector was linked to a multichannel EEG amplifier system, and neural electrical signals were recorded. EEG signals were recorded in freely mobile mice between 10 and 11 a.m., and signal acquisition was carried out in the cages of mice. The original recording signal collected by the recording electrode was amplified 1,000× by the amplifier. Analog signals were digitized at a sampling frequency rate of 1 kHz using a CED Micro1401 (CED, Cambridge, United Kingdom) data acquisition system. The A/D sampling rate was not only 128 Hz, and further, the signal was bandpass-filtered between 1 and 64 Hz. Power spectral densities were generated every 30 s for each recording to calculate the amount of time spent at > 6 Hz (time in high frequency). Signal processing ensured that integer values represented the dominant frequency (DF) in Hz for each 30-s epoch. The mean DF was calculated for each mouse from each DF in each 30-s epoch. Time in high frequency was calculated by summing the number of 30-s epochs with a DF > 6 Hz and dividing it by the total number of 30-s epochs (total time of the recording) for each mouse (Corbett et al., 2013; Hu et al., 2017).

Western Blot

Mice were sacrificed by cervical dislocation and decapitation following the EEG recording (a week later). Brains were removed and soaked in cold phosphate-buffered saline. Half of the brain was used for Western blot analysis and the rest for cell-surface biotinylation assay.

For Western blot analysis, the brain tissue was separately homogenized using a homogenizer on ice in lysis buffer, which comprised 10% sodium dodecyl sulfate (SDS), 10 mM Tris-HCl buffer (pH 7.4), 30% Triton-1000, 10 mM ethylenediaminetetraacetic acid, protease inhibitor cocktail (Roche, Switzerland), and NaCl. The homogenates were centrifuged at 5,000 *g* for 10 min at 4°C. Proteins were quantified using the bicinchoninic acid reagent (Sigma–Aldrich; Merck KGaA, Darmstadt, Germany) method. Equal amounts of the proteins were separated using SDS–polyacrylamide gel electrophoresis (PAGE) on 4–12% gels. Proteins were then

transferred to nitrocellulose membranes and incubated with primary antibodies against BACE1 (1:1,000; cat. no. ab2077; Abcam), Nav1.1α (1:800; cat. no. ASC-001; Alomone), or Navβ2 (1:500; cat. no. ASC-007; Alomone). GAPDH (1:800; cat. no. Sc-365062; Santa Cruz, CA, United States) was used as a loading control. The membranes were subsequently incubated with appropriate secondary antibodies at 20–25°C for 2 h. Horseradish peroxidase–conjugated anti–rabbit antibodies were used for the detection of Nav1.1α and Navβ2 (1:2,000; cat. no. PI-1000; Vector Laboratories, Inc.), whereas GAPDH was detected using a peroxidase-conjugated anti–mouse secondary antibody (1:1,000; cat. no. PI-2000; Vector Laboratories, Inc.). Enhanced chemiluminescence luminol reagent (Beyotime Institute of Biotechnology, Shanghai, China) was used for protein quantification. A densitometry analysis of target protein bands was conducted using a Bio-Rad Gel Imaging System (ChemiDoc^{TM} XRS+; Bio-Rad Laboratories, Inc., Hercules, CA, United States) and Quantity One software v4.6.6 (Bio-Rad Laboratories, Inc.) for each group, in order to quantify the expression levels of proteins.

Cell-Surface Biotinylation Assay

The remaining brain tissue was placed into ice-cold Krebs solution containing the components described previously (Corbett et al., 2013) with the following modifications: 120 mM NaCl, 4.5 mM KCl, 1.5 mM KH_2PO_4, 10 mM glucose, 1.5 mM $MgSO_4$, 26 mM $NaHCO_3$, and 1.5 mM $CaCl_2$. Cell-surface biotinylation and detection of cell-surface Nav1.1α were performed as previously described (Corbett et al., 2013; Hu et al., 2017). NeutrAvidin agarose beads (Pierce, United States) were used to pull down the biotinylated proteins, which were eluted by incubation with SDS–PAGE sample buffer at 37°C for 60 min and analyzed using SDS–PAGE followed by Western blotting as described in section "Western Blot." For expression analysis of extracellular proteins, biotinylated cell-surface proteins were bound to the beads. The remaining lysate containing non-biotinylated proteins was used for the detection of intracellular proteins of Nav1.1α.

Cell Culture

Cortical or hippocampal tissues were obtained from postnatal day 0 (P0) C57BL/6J mice as described previously (Kim and Magrane, 2011). The crushed cortical and hippocampal tissues were digested using 1.25% of pancreatin (Gibco) in an incubator at 37°C for 10 min before being resuspended with fetal bovine serum (Gibco). The resulting tissue suspension was filtered using a 70 μm cell strainer to collect the cortical or hippocampal cells. These cells were incubated in six-well culture plates that were precoated with poly-D-lysine (Sigma–Aldrich) and soaked with neuronal medium (Gibco) containing 2% B27 supplement (Gibco), 0.5% penicillin/streptomycin, and 0.25% GlutaMax (Gibco). Half of the culture medium was replaced every 3 days.

Preparation and Treatment With Aβ1-42

Cultured cells were treated with Aβ1-42 peptide to mimic Aβ-induced neuronal injury. The Aβ1-42 peptide (Sigma–Aldrich) was dissolved in 1,1,1,3,3,3- hexafluoro-2-propanol to yield a concentration of 1 mM. After the Aβ1-42 peptide was incubated in the fume hood at room temperature for 24 h, a clear peptide film was formed, which was stored at −20°C. The Aβ1-42 peptide was resuspended in DMSO. The cultured cortical and hippocampal cells were treated using 5 μM Aβ1-42 peptide (preparation described in section "Cell Culture"), which was diluted in neural basal medium for 5 h.

Cell Treatment

We observed that R1 administration induced neuronal restoration in APP/PS1 mice, improved learning and memory, and was useful in redressing in brain hyperexcitatory. In order to identify whether R1 contributed to the regulation of neuronal excitability Aβ1-42–injured cultured cells were treated using 5 μM R1 (named as R1 group). Aβ1-42–injured cells that were treated with DMSO served as one of the control groups (DMSO group), whereas those treated with medium served as the blank (blank group). The cultured cells untreated by Aβ1-42 and PNS monomers were also used as baseline control. Upon establishment of these treatment protocols, the cultured cells were used for further evaluation.

3-(4,5-Dimethylthiazol-2-yl)-2,5-Diphenyltetrazolium Bromide Assay

Cell viability was measured using a 3-(4,5-dimethylthiazol-2-yl)-2,5-diphenyltetrazolium bromide (MTT) assay kit per manufacturer's guidelines (Sigma–Aldrich). Briefly, the primary neuronal cells were seeded in 96-well plates at a density of 2×10^4 cells per well and treated with various exogenous substances according to the followed protocol. Following incubation, MTT reagent was added to the cells at 37°C. After incubation for 4 h, the culture medium was replaced with 100 μL DMSO to dissolve the formazan crystals. The absorbance of each well was measured at 570 nm by using a microplate reader (Microplate Reader, Bio-Rad, 3550).

Electrophysiological Patch Clamp Recording

Previous studies have suggested that increased neuronal hyperexcitability induced by Aβ1-42 is associated with an increased sodium current (Ciccone et al., 2019). Hence, we investigated whether the regulation of sodium current by R1 affected neuronal excitability. Electrophysiological measurements were used to detect APs or sodium currents of the primary cortex or hippocampal neurons at room temperature. Electrophysiological patch clamp recording was performed using a previously described method (Shan et al., 2019). Briefly, cells were patched in voltage clamp mode and kept at −70 mV. The membrane capacitance (Cm), input resistance (Rm), and the time constant (tau) were calculated by applying the depolarization step voltage command (mV) and using the pClamp10 software integration test function of the membrane. Next, recordings were switched to current clamp mode. The resting film potential was adjusted to −80 mV by introducing a positive current (50–100 pA). A series of depolarizing current

pulses was then used, and intrinsic excitation was checked by constructing the input–output (i–o) function.

Statistical Analysis

Statistical analyses were performed using SPSS 19.0 (IBM, Armonk, NY, United States) for Windows covariance software package. The data are expressed at mean ± standard deviation (SD). Student's *t*-test was used to determine significance between two groups. Statistical differences among multiple groups were evaluated using analysis of variance (ANOVA) and Bonferroni *post hoc* test. Two-way repeated-measures (RM) ANOVA followed by Tukey test was used for the analysis of results from the MWM test. NOR data were analyzed using two-way ANOVA. EEG data were analyzed using one-way ANOVA followed by Student's *t*-test for paired groups (two tailed). $p < 0.05$ was considered to be statistically significant.

RESULTS

R1 Improved Cognitive Impairment of APP/PS1 Mice

The effects of R1 on the learning and memory functions of APP/PS1 mice were evaluated by using the NOR task and MWM test. Two-way RM ANOVA revealed that the escape latency progressively decreased over time in all groups (WT + vehicle, APP/PS1 + vehicle, and APP/PS1 + R1 group). There was no significant difference in the escape latency between 2-month-old APP/PS1 mice and 2-month-old WT mice. However, the 8-month-old APP/PS1 mice spent more time to find the hidden platform compared to the age-matched WT mice, while R1 significantly shrank the difference ($p < 0.05$, **Figure 1A**). The platform was removed during the probe test. The 2-month-old mice did not display statistically significant differences in the number of target crossings, the time spent in the target quadrant, and percentages of path in the target quadrant ($p > 0.05$, **Figures 1B,C,E**). The 8-month-old APP/PS1 mice spent shorter time in the target quadrant, showed lesser number of target crossings, and had lower percentages of path in the target quadrant compared to those of the aged-matched WT mice ($p < 0.05$, **Figures 1B,D,E**). As shown in **Figure 1F**, the average swimming speed between the WT and APP/PS1 mice showed no significant difference ($p > 0.05$, **Figure 1F**). Treatment with R1 partially improved the MWM test behavior in APP/PS1 mice (**Figures 1B–E**).

The discrimination index obtained from the NOR task demonstrated that there was no significant difference between the WT and 2-month-old APP/PS1 mice in the task exploring new objects ($p > 0.05$, **Figure 2B**). The 8-month-old APP/PS1 mice spent less time in the NOR task compared to the age-matched

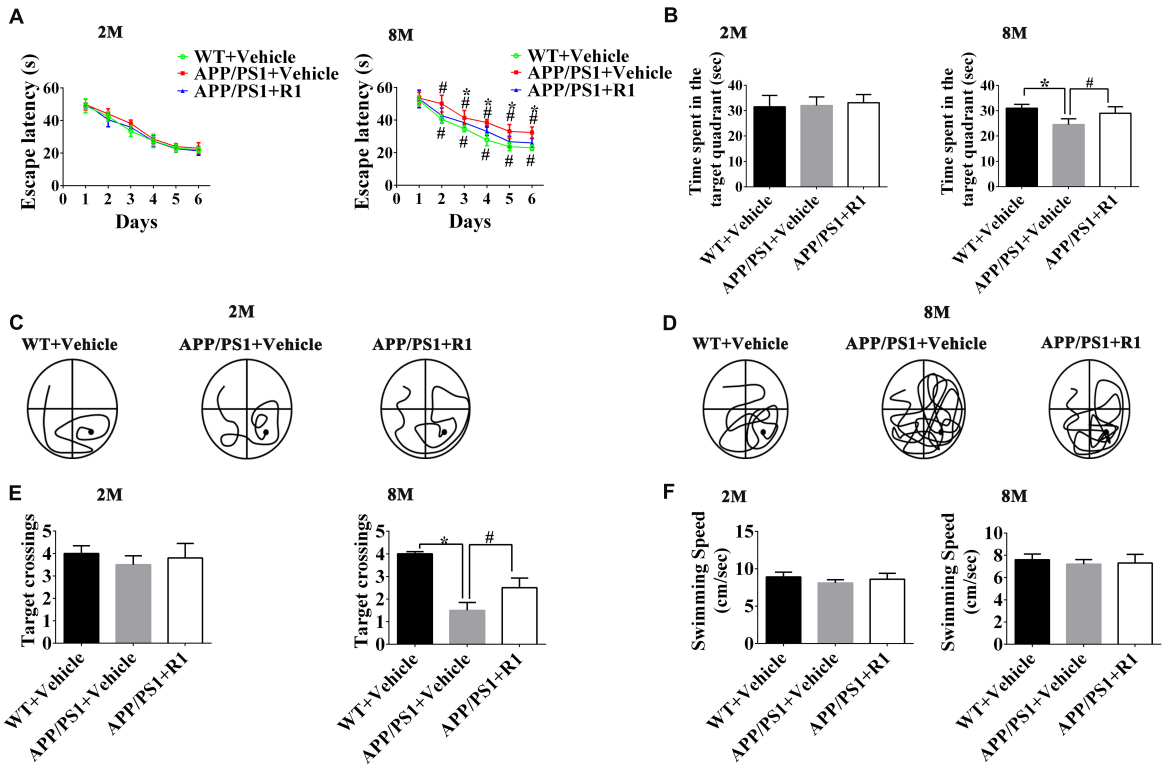

FIGURE 1 | Effects of R1 on spatial learning and memory changes in APP/PS1 mice as indicated by the Morris water maze test. **(A)** Escape latency time of mice in the training period from days 1 to 6. **(B)** Time spent in the target quadrant during the probe test. Swimming paths of 2-month-old **(C)** and 8-month-old **(D)** APP/PS1 mice during the probe test. **(E)** Entries and crossings through the target platform position during the probe test. **(F)** Average swimming speed of mice during probe trial. Data are expressed as mean ± SD, $n = 15$ mice/group. $^{*}p < 0.05$ vs. WT+ vehicle, $^{\#}p < 0.05$ vs. APP/PS1 + R1.

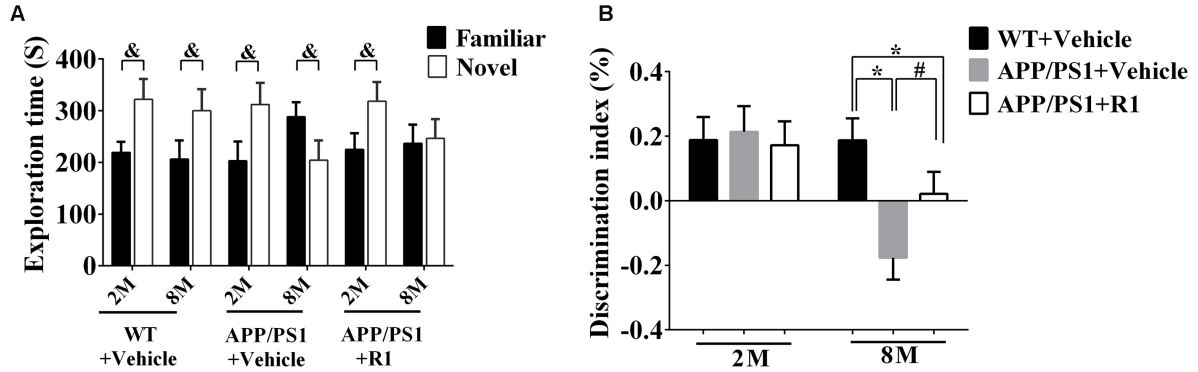

FIGURE 2 | Effects of R1 on NOR tasks in APP/PS1 mice. **(A)** Comparison of the exploration time on familiar objects and novel objects in APP/PS1 mice. **(B)** Discrimination Index obtained from different groups. Data are expressed as mean ± SEM, n = 15 mice/group. $^{*}p < 0.05$ VS. WT + vehicle, $^{\#}p < 0.05$ vs. APP/PS1 + R1, and $^{\&}p < 0.05$ vs. novel.

WT mice ($p < 0.05$) (**Figure 2B**). Treatment with R1 increased the time taken by mice in the NOR task in the APP/PS1 group (APP/PS1 + R1 vs. APP/PS1 + vehicle, $p < 0.05$) (**Figures 2A,B**).

Taken together, the above results indicated that R1 could be a beneficial compound for improving spatial learning and memory loss in transgenic mice with AD (**Figures 1**, **2**).

R1 Reversed Abnormal Neuronal Hyperexcitability of APP/PS1 Mice and Regulated the Expression of BACE1 and Nav

To investigate the possible effects of R1 on the aberrant neuronal hyperexcitability, EEG was recorded in WT and APP/PS1 mice following various treatments. The EEGs of the 8-month-old APP/PS1 mice showed increased spike-wave discharges and time in high frequency significantly compared to those in the age-matched WT mice (**Figure 3**). Although the 8-month-old APP/PS1 mice treated with R1 exhibited ameliorative neuronal excitability, it did not reach the level of the age-matched WT mice (**Figure 3**). These results indicated that R1 treatment improved neuronal hyperexcitability induced by APP/PS1 mutation.

Next, we explored the mechanisms underlying ameliorative neuronal excitability. The crucial roles of the Nav family members and BACE1 in neuronal excitability regulation, the levels of BACE1, enzymolysis status of Navβ2, and the expression and locations of Nav1.1α were determined. R1 treatment significantly decreased the expression of BACE1 in the cortex and hippocampus of APP/PS1 mice (APP/PS1 + R1 vs. APP/PS1 + vehicle, $p < 0.05$) (**Figures 4A,B**). Simultaneously, increased full-length Navβ2 and decreased Navβ2-CTF fragments were detected in APP/PS1 mice treated with R1 (APP/PS1 + R1 vs. APP/PS1 + vehicle, $p < 0.05$) (**Figures 4A,C,D**). These results also demonstrated that the abnormal extracellular and intracellular distributions of Nav1.1α in the cortex or hippocampus were redressed using R1 (APP/PS1 + R1 vs. APP/PS1 + vehicle, $p < 0.05$, **Figures 4E–H**). Taken together, these data suggested that R1-induced alleviation in neuronal excitability might be associated with a reduction in Navβ2 cleavage, which partially reversed the abnormal distribution of Nav1.1α in the cortex and hippocampus.

The Effects of R1 on Cell Viability of Aβ1-42–Induced Injured Neurons

The cell viability of Aβ1-42 (5μM)–injured cultured cortical and hippocampal neurons was measured using an MTT assay at 0, 24, 48, 72, and 96 h posttreatment with R1. Our results demonstrated that there was no significant difference between the DMSO-treated and blank control groups (**Figures 5A–E**). The cellular activity of the blank group significantly decreased when compared to that of baseline control group at 48,72, and 96 h posttreatment ($p < 0.05$) (**Figures 5C–E**). These results demonstrated that treatment with Aβ1-42 led to a significant damage in neurons after 48 h of incubation. Compared to the DMSO group, treatment with R1 induced significant recovery in cell viability in Aβ1-42–injured cells ($p < 0.05$) (**Figures 5C–E**). We observed that R1-treated neurons recovered from injury and showed the highest cellular activity at 96 h (**Figure 5F**). Therefore, the above results confirmed that R1 had therapeutic effects on Aβ1-42–induced neuronal damage.

Effects of R1 on the Neuronal Hyperexcitability and Sodium Current Overload Induced by Aβ1-42

To determine whether R1 contributed to the redressal of neuronal hyperexcitability induced by Aβ1-42, whole-cell patch-clamp recordings were performed on cultured neurons after application, following different treatment protocols. We found that the frequency of neuronal APs after treatment with Aβ1-42 significantly increased compared to the baseline control group ($p < 0.05$) (**Figure 6**). There was also a significant decrease in the threshold ($p < 0.05$) (**Figures 6A,B**). The frequency, threshold, and peak amplitude of the neuronal AP in the DMSO-treated group showed no significant difference when compared to the blank control ($p > 0.05$) (**Figures 6A–C**). These results demonstrated that model of neuronal hyperexcitability induced

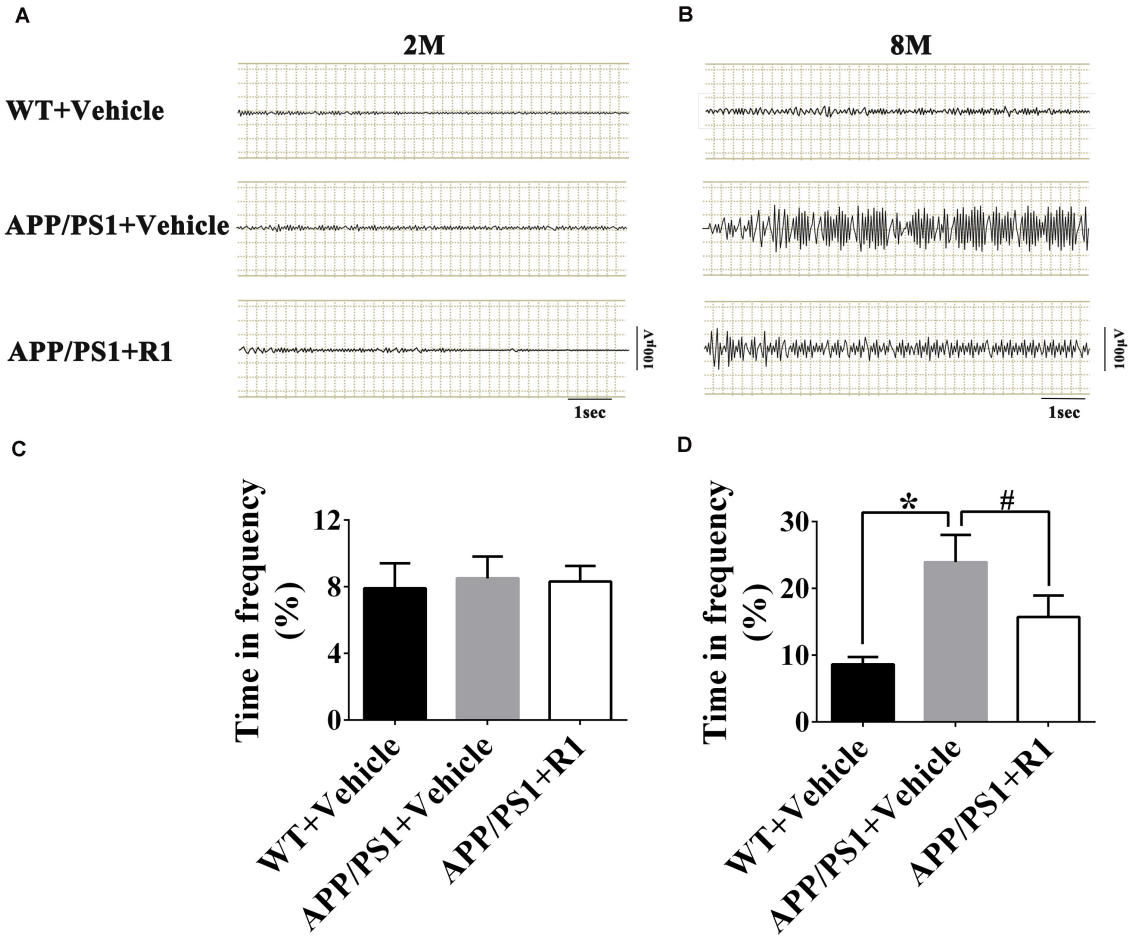

FIGURE 3 | Notoginsenoside R1 administration induced improvement in neuronal hyperexcitability and abnormal neural activity detected using EEG. Spike-wave discharges of APP/PS1 mice, APP/PS1 mice + R1, and APP/PS1 mice + vehicle in 2 m **(A)** and 8 m **(B)**, and the time in high frequency (%) obtained from different groups in 2-month-old **(C)** and 8-month-old mice **(D)** (n = 15), $^{*}p < 0.05$ vs. WT+ Vehicle, $^{\#}p < 0.05$ vs. APP/PS1 + R1.

by Aβ1-42 was reliable and also consistent with a previously published study (Wang et al., 2016).

In Aβ1-42–injured neurons, treatment with R1 induced a decrease in frequency of neuronal AP and increase in threshold potential when compared to that of DMSO-treated neurons ($p < 0.05$, **Figures 6A,B**). It was notable that the threshold potential detected in the R1-treated groups showed no statistically significant difference when compared to that of the baseline group ($p > 0.05$) (**Figure 6B**). Moreover, the peak current density showed no significant difference after R1 treatments ($p > 0.05$) (**Figure 6C**). These results suggested that R1 was responsible for reducing abnormal excitability in Aβ1-42–induced neurons.

Electrophysiological patch clamp recording was used to determine whether neuronal excitability was related to increased sodium current. We found that sodium current density curves and current density of neurons significantly increased after treatment with Aβ1-42 when compared to the untreated baseline control group (**Figure 7A**). The parameters of sodium current in the DMSO group were not significantly different compared to those of the blank group ($p > 0.05$) (**Figures 7A,B**). The current and peak current densities of R1-treated groups were decreased when compared to those of the DMSO-treated group ($p < 0.05$, **Figures 7A,B**). These results indicated that R1 contributed to restore the Aβ1-42–induced neuronal sodium current overload.

Effects of R1 on the Aberrant Status of Sodium-Channel Proteins Induced by Aβ1-42

To understand the underlying mechanism by which R1 redressed neuronal hyperexcitability and sodium-channel overload caused by Aβ1-42, we examined the expression, location, and hydrolysis status of sodium-channel proteins including Nav1.1α, Navβ2, and BACE1 in Aβ1-42–injured neurons.

As shown in **Figure 8**, after Aβ1-42 treatment, the expression of total Nav1.1α, intracellular Nav1.1α, Navβ2-CTF, and BACE1 significantly increased compared to that in the baseline control group ($p < 0.05$) (**Figures 8A,B,D,F,J**). The full-length Navβ2 decreased in the blank and DMSO-treated groups compared to

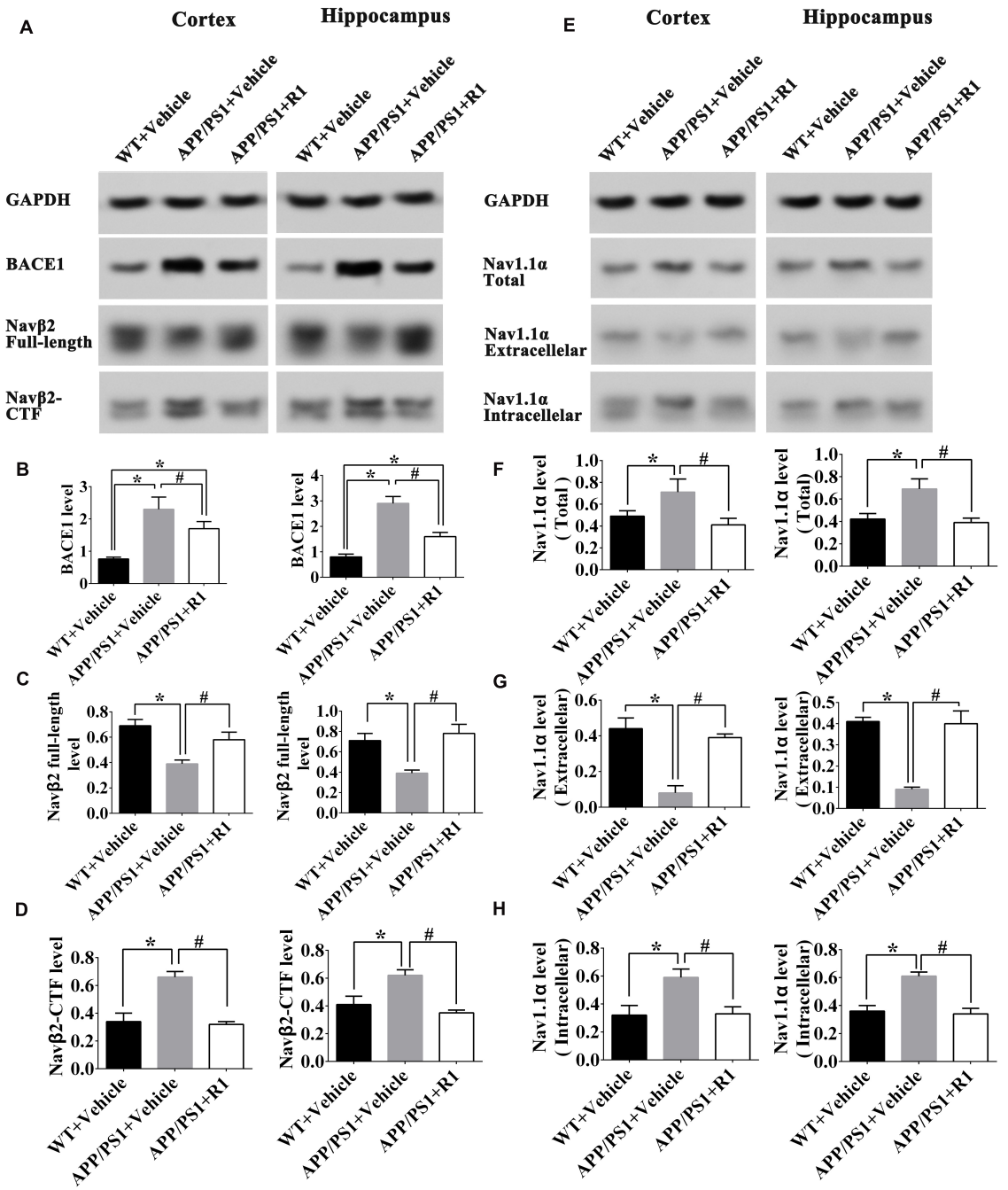

FIGURE 4 | Notoginsenoside R1 altered the distribution of Nav1.1α and cleavage of Navβ2 in the brains of APP/PS1 mice. Representative expression **(A,E)** and densitometric quantification of BACE1 **(B)**, Navβ2 full-length **(C)**, Navβ2-CTF **(D)**, total expression of Nav1.1α **(F)** extracellular Nav1.1α **(G)**, and intracellular Nav1.1α **(H)** protein in the cortex and hippocampus lysates from WT mice, APP/PS1 mice, or APP/PS1 + R1 mice, respectively. Data are shown as mean ± SD (n = 15). $^{*}p < 0.05$ vs. WT + vehicle, $^{\#}p < 0.05$ vs. APP/PS1 + R1.

that in the baseline control group ($p < 0.05$) (**Figures 8A,E**). Moreover, the abnormal release of intracellular Nav1.1α and expression was observed in Aβ1-42–treated groups, which explained the abnormal activation of BACE1 induced by Aβ1-42 (blank group vs. baseline control group, $p < 0.05$) (**Figures 8A,C,D,J**). Additionally, the expression of Nav protein was not significantly different between the blank control and DMSO-treated groups ($p > 0.05$) (**Figures 8A–K**).

Among the PNS monomer–treated groups, the levels of total, intracellular, and extracellular Nav1.1α in the R1-treated group were statistically different in comparison to those of the DMSO group ($p < 0.05$) (**Figures 8B–D**), however, it showed no

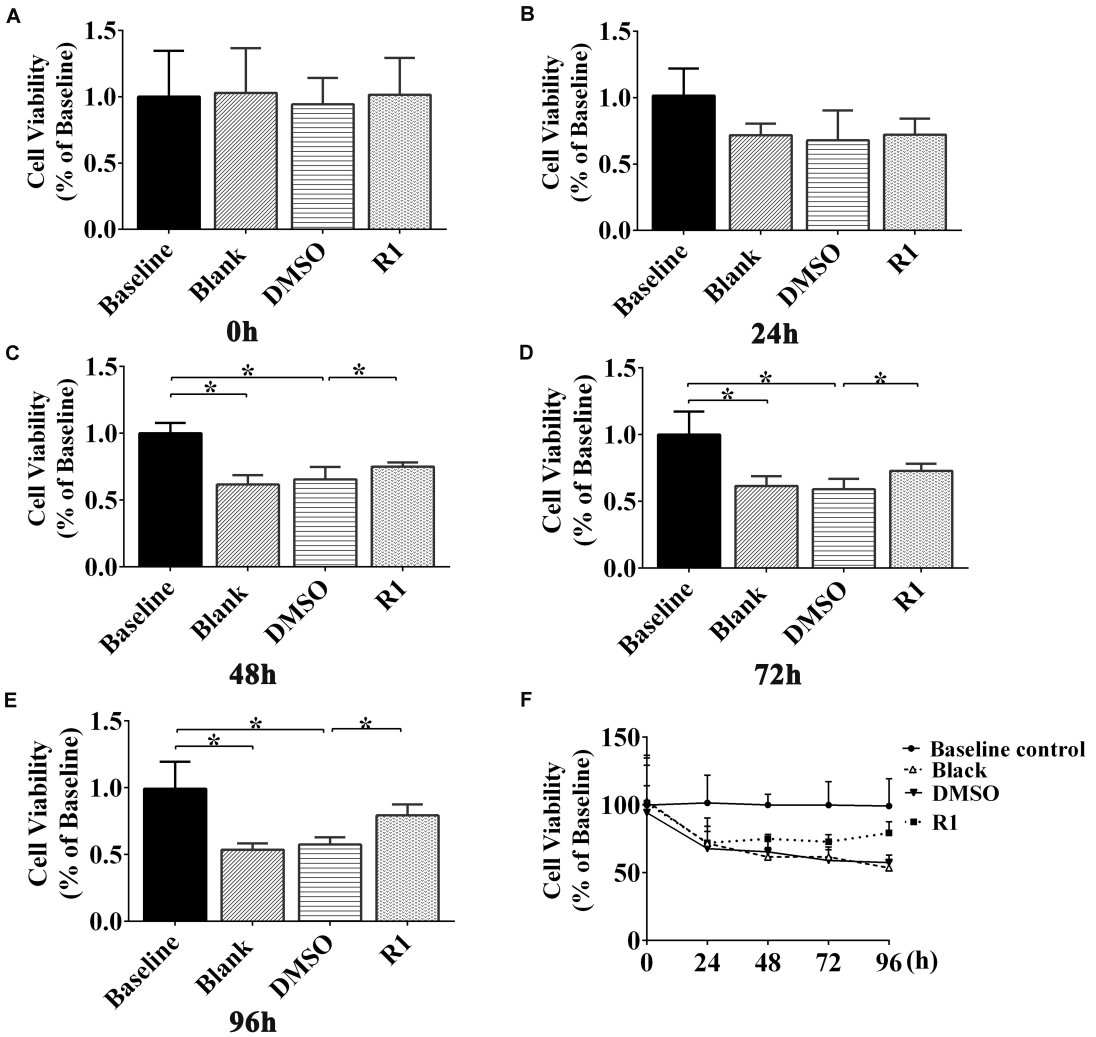

FIGURE 5 | Effect of R1 on Aβ1-42–induced neuron viability determined using MTT assay. Cell viability of cultured neurons treated with different groups at 0 h **(A)**, 24 h **(B)**, 48 h **(C)**, 72 h **(D)**, and 96 h **(E)**. **(F)** Cell viability of cultured neurons in innocent neurons (baseline control), neurons treated with Aβ1-42 (blank group), and Aβ1-42–treated neurons incubated with DMSO (DMSO group) or R1 (R1 group), at different time points. Data are shown as mean ± SD (n = 5). *$p < 0.05$.

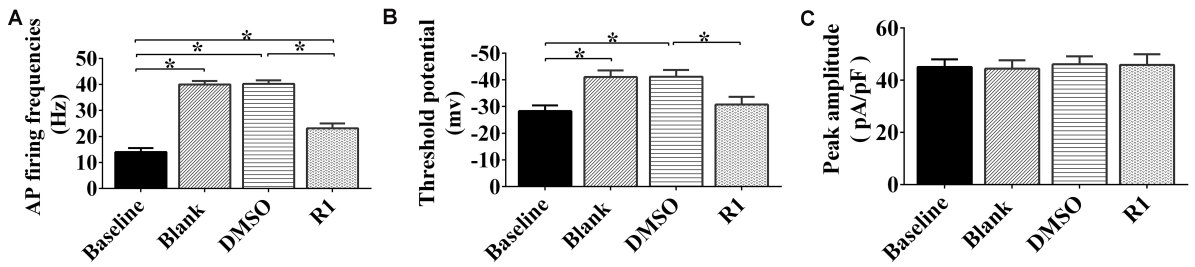

FIGURE 6 | Effects of notoginsenoside R1 on neuronal hyperexcitability induced by Aβ1-42. Changes in the action potential frequency **(A)**, threshold **(B)**, and peak amplitude **(C)** in neurons after R1 treatment. Data are shown as mean ± SD (n = 9). *$p < 0.05$.

statistical difference compared to that of the baseline control group in total and intracellular Nav1.1α levels ($p > 0.05$) (**Figures 8B,D**). Meanwhile, we observed increased Navβ2 full-length levels and reduced Navβ2-CTF in the R1-treated group when compared to the DMSO-treated group ($p < 0.05$) (**Figures 8E,F**). The levels of full-length Navβ2 and Navβ2-CTF in

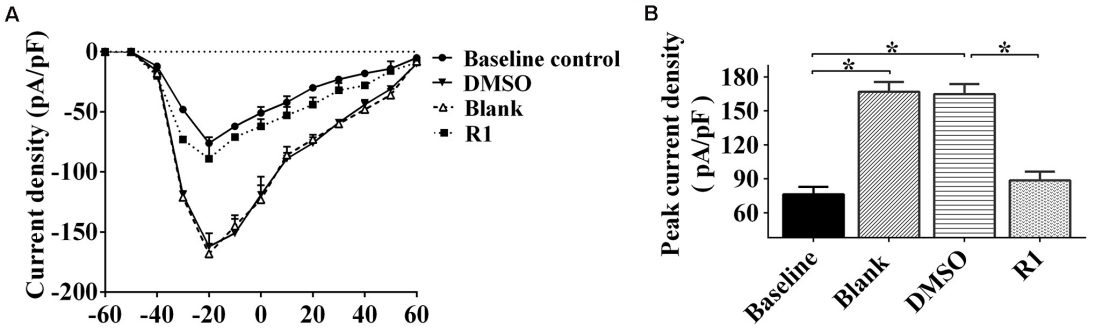

FIGURE 7 | Effects of R1 on the changes of neuronal sodium current. **(A)** Current–voltage relationships of sodium current density in innocent neurons (baseline control) and neurons treated with Aβ1-42 (blank group), Aβ1-42–treated neurons cultured with DMSO (DMSO group), or R1 (R1 group). **(B)** Peak current densities in Aβ1-42–injured neurons after various treatments. Data are shown as mean ± SD ($n = 9$). *$p < 0.05$.

the R1-treated group showed a statistically significant difference in comparison to those of the baseline control group ($p < 0.05$) (**Figures 8J,K**). Additionally, a significant decrease in the level of BACE1 was detected in the R1-treated group ($p < 0.05$, **Figure 8J**). Taken together, these results suggested that the R1-induced alleviation of neuronal excitability might be associated with the reduction in Navβ2 cleavage and partial reversal of the abnormal distribution of Nav1.1α.

The above results collectively demonstrated that neuroprotection induced by R1 was associated with the recovery in the abnormal distribution of Nav1.1α and the abnormal activation of BACE1 induced by Aβ1-42.

DISCUSSION

Previous studies have demonstrated that by binding to the effects of anti-inflammatory properties, reducing blood viscosity, and antiapoptosis, ginsenosides treatment has outstanding advantage in therapy of neurological disorders accompanied with cognitive impairment (Liu et al., 2014, 2018; Sheng et al., 2014; Zhong et al., 2015). For example, individuals with a commonly occurring brain disorder, traumatic brain injury, characterized by intracranial/intracerebral hemorrhage (Regan et al., 2018), generally develop symptoms of cognitive deficit (Ratliff et al., 2020). Researchers report that administration of PNS reduced inflammation, increased hematoma absorption in patients with acute ICH, and improved behavioral function (Gao et al., 2012). Furthermore, treatment with ginsenosides remarkably improved cognitive performance in patients with AD and in rodent models (Lee et al., 2008; Liu et al., 2012). In this study, we identified that R1 had the ability to regulate sodium-channel expression and thus redressed abnormal neuronal excitability, which otherwise contributes to brain damage and cognitive impairment in AD.

Our study results also identified that R1 was involved in regulating Nav proteins and redressing aberrant neuronal hyperexcitability induced by Aβ1-42. R1 treatment significantly improved learning and spatial memory function and ameliorated abnormal brain excitability in APP/PS1 mice. Consistent with these findings, R1 administration also induced the inhibition of BACE1 activity, thus reducing the excessive cleavage of Navβ2 and correcting the abnormal expressions and distribution of Nav1.1α. It also reduced the neuronal hyperexcitability induced by APP/PS1 mutations. These results suggested that neuroprotection exerted by R1 in APP/PS1 model might be associated with the recovery of neuron hyperexcitability regulated by Nav proteins. Our results revealed that R1 was effective in improving neuronal viability and excitability in Aβ1-42–injured neurons. R1 treatment also restored the voltage-gated sodium current and reduced neuronal excitability by regulating the distribution of Nav1.1α and expression of Navβ2.

We observed that the impairment of spatial learning and memory functions and the paradoxical discharge of brain were significantly improved in APP/PS1 mice following R1 treatment. These results suggested that the corrected intrinsic neuronal hyperexcitability might contribute to cognitive recovery after treatment with R1. Previous studies have reported that XST administration significantly improved spatial memory in APP/PS1 mice, which suggests improvements in neuroplasticity and function (Huang et al., 2018). A previous study indicates that APP/PS1 mutation-induced brain injury and cognitive impairment may be caused by changes in neuronal activity (Leonard and McNamara, 2007). Our findings confirmed that administration of R1 in APP/PS1 mice corrected neuronal hyperexcitability. In order to determine signaling mechanisms, Aβ1-42–injured primary cultured neurons of mice were used as an *in vitro* AD model to depict neuronal hyperexcitability injury. Previous studies have demonstrated that soluble Aβ1-42 oligomers play a key role in neuronal hyperactivity, subsequent cognitive deficits, and memory dysfunction in AD (Bakker et al., 2012; Busche et al., 2012). These findings were consistent with results obtained in our study.

As demonstrated in our study, treatment with R1 rescued cell viability after incubation with Aβ1-42. R1 treatment reduced the frequency of AP and increased its threshold in Aβ1-42–injured neurons. The above results suggested the neuroprotective effect of R1 in Aβ1-42–injured neurons. Previous studies have demonstrated multiple mechanisms of R1 in the treatment of AD (Wang et al., 2013). For example, treatment with R1 provided neuroprotection to APP/PS1 mice by increasing the levels of

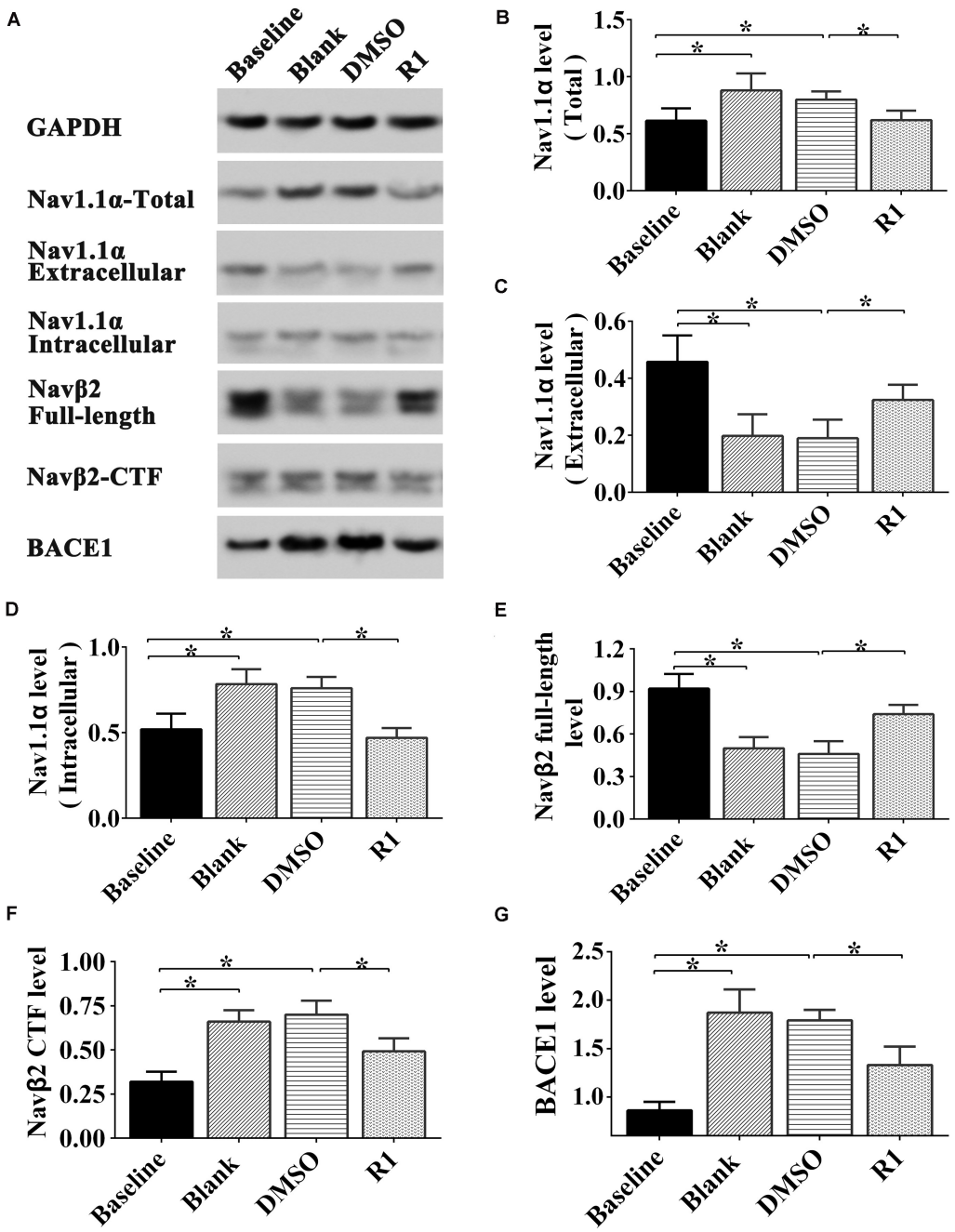

FIGURE 8 | Effect of R1 on the expression, location, and cleavage status of sodium channel proteins after Aβ1-42 treatment. Representative Western blot **(A)** and densitometry quantification of the total Nav1.1α **(B)**, extracellular Nav1.1α **(C)**, intracellular Nav1.1α **(D)**, Navβ2 full-length **(E)**, Navβ2-CTF **(F)**, and BACE1 **(G)** expression. Data are shown as mean ± SD ($n = 5$). *$p < 0.05$.

insulin-degrading enzymes (Li et al., 2015). Moreover, R1 has previously been reported to improve cognitive function in AD mice and may be involved in the regulation of neuroexcitability; these reports are consistent with our conclusions (Yan et al., 2014). The results of our study revealed a molecular mechanism of R1-induced improvement in the learning and memory functions in the mouse model of AD.

To investigate the mechanisms underlying the improved cognitive functions and neuronal excitability, we measured the activity of BACE1 in the cortex and hippocampus of mice. Previous studies demonstrated that increased levels of BACE1, Navβ2 cleavage fragments (Navβ2-CTF), and associated aberrations in Nav1.1α expression and localization were observed in the cortical lysates of APP transgenic mice

(Corbett et al., 2013). Therefore, we proposed that the modulation of neuronal excitability by R1 in the AD model was associated with the regulation of the expression of Nav channels. Previous studies showed that the knockdown of Navβ2 partially reversed the excessive degradation of Navβ2 and aberrant intracellular translocation of Nav1.1α. The knockdown also restored electrical excitability of hippocampal neurons and significantly improved learning and memory functions in transgenic mice (Hu et al., 2017, 2019). Studies have also demonstrated that increased Nav1.1α levels are associated with cognitive deficits in mice (Corbett et al., 2013). BACE1 inhibition is known to effectively reduce the production of Aβ, which proves to be a valuable therapeutic strategy in AD (Cheret et al., 2013; Filser et al., 2015; Zhu et al., 2018). We found that R1 treatment significantly improved cell viability, reduced the cleavage of Navβ2 by BACE1 suppression, and also corrected the abnormal distribution of Nav1.1α. These results also showed that administration of R1 regulated sodium current by regulating the enzymatic hydrolysis of Navβ2. Therefore, R1 administration might prove to be a promising therapeutic strategy for the treatment of AD.

CONCLUSION

Our results demonstrated that administration of R1 significantly promoted neuronal repair and improved cognition in mice with AD by modulating neuronal excitability. R1 improved abnormal neuronal hyperexcitability and memory deficit and was associated with the regulation of Nav proteins. Next, we will test the learning and memory function change between APP/PS1 mice with or without R1 prolonged administration to further understand whether the neuroprotective effect could last or not after the 6-month R1 treatment in APP/PS1 mice.

DATA AVAILABILITY STATEMENT

The raw data supporting the conclusions of this article will be made available by the authors, without undue reservation, to any qualified researcher.

ETHICS STATEMENT

The animal study was reviewed and approved by the Committee of Kunming University of China (permit no. kmu-eac-2018021; Kunming, China).

AUTHOR CONTRIBUTIONS

TH, SL, W-QL, S-SL, X-YW, Y-BX, and JZ designed the study, performed analyses, and prepared the manuscript. TH, SL, W-QL, W-HD, S-SL, M-NL, BC, W-WG, S-WC, X-YW, Y-BX, JZ, and BC conducted animal experiments. TH, SL, W-QL, S-SL, M-NL, BC, W-HD, LZ, RM, X-YW, Y-BX, JZ, and BC performed cell culture, cell transfection, and cell treatment. TH, W-QL, W-WG, Y-BX, SL, X-YW, and JZ conducted the electrophysiology evaluation. TH, S-SL, Y-BX, W-QL, S-WC, SL, LZ, and RM finished the statistical analyses. All authors were substantially involved in the research, acquisition of data, analysis and manuscript preparation and have read and approved the final submitted manuscript.

FUNDING

This work was supported by the National Natural Science Foundation of China (Grant Nos. 81960210 and 81701212), Foundation of Science and Technology Innovative Team Building of Kunming Medical University (Grant No. CXTD201807), Medical Leader Plan of Health Commission of Yunnan Province (D-2017056), and the Medical Reserve Talents Cultivation Project of the Health and Family Planning Commission of Yunnan Province (Grant No. H-2017026).

ACKNOWLEDGMENTS

We thank Dr. Seng Kee Leong for his valuable comments in the writing of this manuscript.

REFERENCES

Bakker, A., Krauss, G. L., Albert, M. S., Speck, C. L., Jones, L. R., Stark, C. E., et al. (2012). Reduction of hippocampal hyperactivity improves cognition in amnestic mild cognitive impairment. *Neuron* 74, 467–474. doi: 10.1016/j.neuron.2012.03.023

Busche, M. A., Chen, X., Henning, H. A., Reichwald, J., Staufenbiel, M., Sakmann, B., et al. (2012). Critical role of soluble amyloid-beta for early hippocampal hyperactivity in a mouse model of Alzheimer's disease. *Proc. Natl. Acad. Sci. U.S.A.* 109, 8740–8745. doi: 10.1073/pnas.1206171109

Catterall, W. A. (2000). From ionic currents to molecular mechanisms: the structure and function of voltage-gated sodium channels. *Neuron* 26, 13–25. doi: 10.1016/s0896-6273(00)81133-81132

Chen, C., Bharucha, V., Chen, Y., Westenbroek, R. E., Brown, A., Malhotra, J. D., et al. (2002). Reduced sodium channel density, altered voltage dependence of inactivation, and increased susceptibility to seizures in mice lacking sodium channel beta 2-subunits. *Proc. Natl. Acad. Sci. U.S.A.* 99, 17072–17077. doi: 10.1073/pnas.212638099

Chen, F., Eckman, E. A., and Eckman, C. B. (2006). Reductions in levels of the Alzheimer's amyloid beta peptide after oral administration of ginsenosides. *FASEB J.* 20, 1269–1271. doi: 10.1096/fj.05-5530fje

Cheret, C., Willem, M., Fricker, F. R., Wende, H., Wulf-Goldenberg, A., Tahirovic, S., et al. (2013). Bace1 and Neuregulin-1 cooperate to control formation and maintenance of muscle spindles. *EMBO J.* 32, 2015–2028. doi: 10.1038/emboj.2013.146

Chyung, J. H., Raper, D. M., and Selkoe, D. J. (2005). Gamma-secretase exists on the plasma membrane as an intact complex that accepts substrates and effects intramembrane cleavage. *J. Biol. Chem.* 280, 4383–4392. doi: 10.1074/jbc.M409272200

Ciccone, R., Franco, C., Piccialli, I., Boscia, F., Casamassa, A., de Rosa, V., et al. (2019). Amyloid beta-Induced Upregulation of Nav1.6 Underlies Neuronal Hyperactivity in Tg2576 Alzheimer's Disease Mouse Model. *Sci. Rep.* 9:13592. doi: 10.1038/s41598-019-50018-50011

Corbett, B. F., Leiser, S. C., Ling, H. P., Nagy, R., Breysse, N., Zhang, X., et al. (2013). Sodium channel cleavage is associated with aberrant neuronal activity

and cognitive deficits in a mouse model of Alzheimer's disease. *J. Neurosci.* 33, 7020–7026. doi: 10.1523/jneurosci.2325-12.2013

Filser, S., Ovsepian, S. V., Masana, M., Blazquez-Llorca, L., Brandt Elvang, A., Volbracht, C., et al. (2015). Pharmacological inhibition of BACE1 impairs synaptic plasticity and cognitive functions. *Biol. Psychiatry* 77, 729–739. doi: 10.1016/j.biopsych.2014.10.013

Gao, L., Zhao, H., Liu, Q., Song, J., Xu, C., Liu, P., et al. (2012). Improvement of hematoma absorption and neurological function in patients with acute intracerebral hemorrhage treated with Xueshuantong. *J. Neurol. Sci.* 323, 236–240. doi: 10.1016/j.jns.2012.09.028

Ghezzi, L., Scarpini, E., and Galimberti, D. (2013). Disease-modifying drugs in Alzheimer's disease. *Drug Des. Devel. Ther.* 7, 1471–1478. doi: 10.2147/dddt.S41431

Guo, H. B., Cui, X. M., An, N., Cai, G. P. (2010). Sanchi ginseng (*Panax notoginseng* (Burkill) F. H. Chen) in China: distribution, cultivation and variations. 57, 453–460. doi: 10.1007/s10722-010-9531-9532

Hodgkin, A. L., and Huxley, A. F. (1952). A quantitative description of membrane current and its application to conduction and excitation in nerve. *J. Physiol.* 117, 500–544. doi: 10.1113/jphysiol.1952.sp004764

Hu, T., Li, S. S., Lu, M. N., Zhang, L., Chen, B., Mao, R., et al. (2019). Neuroprotection induced by Navbeta2knockdown in APP/PS1 transgenic neurons is associated with NEP regulation. *Mol. Med. Rep.* 20, 2002–2011. doi: 10.3892/mmr.2019.10406

Hu, T., Xiao, Z., Mao, R., Chen, B., Lu, M. N., Tong, J., et al. (2017). Navbeta2 knockdown improves cognition in APP/PS1 mice by partially inhibiting seizures and APP amyloid processing. *Oncotarget* 8, 99284–99295. doi: 10.18632/oncotarget.21849

Huang, J., Wu, D., Wang, J., Li, F., Lu, L., Gao, Y., et al. (2014). Effects of Panax notoginseng saponin on alpha, beta, and gamma secretase involved in Abeta deposition in SAMP8 mice. *Neuroreport* 25, 89–93. doi: 10.1097/wnr.0000000000000048

Huang, J. L., Jing, X., Tian, X., Qin, M. C., Xu, Z. H., Wu, D. P., et al. (2017). Neuroprotective Properties of Panax notoginseng Saponins via Preventing Oxidative Stress Injury in SAMP8 Mice. *Evid. Based Complement. Alternat. Med.* 2017:8713561. doi: 10.1155/2017/8713561

Huang, Y., Guo, B., Shi, B., Gao, Q., and Zhou, Q. (2018). Chinese herbal medicine xueshuantong enhances cerebral blood flow and improves neural functions in Alzheimer's disease mice. *J. Alzheimers Dis.* 63, 1089–1107. doi: 10.3233/jad-170763

Kim, H. J., and Magrane, J. (2011). Isolation and culture of neurons and astrocytes from the mouse brain cortex. *Methods Mol. Biol.* 793, 63–75. doi: 10.1007/978-1-61779-328-8_4

Kim, J. H. (2012). Cardiovascular diseases and panax ginseng: a review on molecular mechanisms and medical applications. *J. Ginseng. Res.* 36, 16–26. doi: 10.5142/jgr.2012.36.1.16

Lee, M., Kim, D., Shin, H. S., Sung, H. G., and Choi, J. H. (2011). High-density EEG recordings of the freely moving mice using polyimide-based microelectrode. *J. Vis. Exp.* 47:e2562. doi: 10.3791/2562

Lee, S. T., Chu, K., Sim, J. Y., Heo, J. H., and Kim, M. (2008). Panax ginseng enhances cognitive performance in Alzheimer disease. *Alzheimer Dis. Assoc. Disord.* 22, 222–226. doi: 10.1097/WAD.0b013e31816c92e6

Leonard, A. S., and McNamara, J. O. (2007). Does epileptiform activity contribute to cognitive impairment in Alzheimer's disease? *Neuron* 55, 677–678. doi: 10.1016/j.neuron.2007.08.014

Li, X. Y., Men, W. W., Zhu, H., Lei, J. F., Zuo, F. X., Wang, Z. J., et al. (2016). Age- and Brain Region-Specific Changes of Glucose Metabolic Disorder, Learning, and Memory Dysfunction in Early Alzheimer's Disease Assessed in APP/PS1 Transgenic Mice Using (18)F-FDG-PET. *Int. J. Mol. Sci.* 17:1707. doi: 10.3390/ijms17101707

Li, Z., Li, H., Zhao, C., Lv, C., Zhong, C., Xin, W., et al. (2015). Protective Effect of Notoginsenoside R1 on an APP/PS1 Mouse Model of Alzheimer's Disease by Up-Regulating Insulin Degrading Enzyme and Inhibiting Abeta Accumulation. *CNS Neurol. Disord. Drug Targets* 14, 360–369. doi: 10.2174/1871527314666150225141521

Liu, H., Liang, J. P., Li, P. B., Peng, W., Peng, Y. Y., Zhang, G. M., et al. (2014). Core bioactive components promoting blood circulation in the traditional Chinese medicine compound xueshuantong capsule (CXC) based on the relevance analysis between chemical HPLC fingerprint and in vivo biological effects. *PLoS One* 9:e112675. doi: 10.1371/journal.pone.0112675

Liu, J., Yan, X., Li, L., Zhu, Y., Qin, K., Zhou, L., et al. (2012). Ginsennoside rd attenuates cognitive dysfunction in a rat model of Alzheimer's disease. *Neurochem. Res.* 37, 2738–2747. doi: 10.1007/s11064-012-0866-862

Liu, W. J., Tang, H. T., Jia, Y. T., Ma, B., Fu, J. F., Wang, Y., et al. (2010). Notoginsenoside R1 attenuates renal ischemia-reperfusion injury in rats. *Shock* 34, 314–320. doi: 10.1097/SHK.0b013e3181ceede4

Liu, Y., Liu, T., Ding, K., Liu, Z., Li, Y., He, T., et al. (2018). Phospholipase Cgamma2 signaling cascade contribute to the antiplatelet effect of Notoginsenoside Fc. *Front. Pharmacol.* 9:1293. doi: 10.3389/fphar.2018.01293

Lopez-Santiago, L. F., Pertin, M., Morisod, X., Chen, C., Hong, S., Wiley, J., et al. (2006). Sodium channel beta2 subunits regulate tetrodotoxin-sensitive sodium channels in small dorsal root ganglion neurons and modulate the response to pain. *J. Neurosci.* 26, 7984–7994. doi: 10.1523/jneurosci.2211-06.2006

Luo, Y., Yang, W., Li, N., Yang, X., Zhu, B., Wang, C., et al. (2020). Anodal Transcranial Direct Current Stimulation Can Improve Spatial Learning and Memory and Attenuate Aβ(42) Burden at the Early Stage of Alzheimer's Disease in APP/PS1 Transgenic Mice. *Front. Aging Neurosci.* 12:134. doi: 10.3389/fnagi.2020.00134

Ng, T. B. (2006). Pharmacological activity of sanchi ginseng (*Panax notoginseng*). *J. Pharm. Pharmacol.* 58, 1007–1019. doi: 10.1211/jpp.58.8.0001

Pang, H. H., Li, M. Y., Wang, Y., Tang, M. K., Ma, C. H., and Huang, J. M. (2017). Effect of compatible herbs on the pharmacokinetics of effective components of Panax notoginseng in Fufang Xueshuantong Capsule. *J. Zhejiang Univ. Sci. B* 18, 343–352. doi: 10.1631/jzus.B1600235

Ratliff, W. A., Mervis, R. F., Citron, B. A., Schwartz, B., Rubovitch, V., Schreiber, S., et al. (2020). Effect of mild blast-induced TBI on dendritic architecture of the cortex and hippocampus in the mouse. *Sci. Rep.* 10:2206. doi: 10.1038/s41598-020-59252-59254

Regan, S. L. P., Knight, P. G., Yovich, J. L., Arfuso, F., and Dharmarajan, A. (2018). Growth hormone during in vitro fertilization in older women modulates the density of receptors in granulosa cells, with improved pregnancy outcomes. *Fertil. Steril.* 110, 1298–1310. doi: 10.1016/j.fertnstert.2018.08.018

Shan, L., Galaj, E., and Ma, Y. Y. (2019). Nucleus accumbens shell small conductance potassium channels underlie adolescent ethanol exposure-induced anxiety. *Neuropsychopharmacology* 44, 1886–1895. doi: 10.1038/s41386-019-0415-417

Sheng, S., Wang, Y., Long, C., Su, W., and Rong, X. (2014). Chinese medicinal formula Fufang Xueshuantong capsule could inhibit the activity of angiotensin converting enzyme. *Biotechnol. Biotechnol. Equip.* 28, 322–326. doi: 10.1080/13102818.2014.911611

Wang, X., Zhang, X. G., Zhou, T. T., Li, N., Jang, C. Y., Xiao, Z. C., et al. (2016). Elevated neuronal excitability due to modulation of the voltage-gated sodium channel Nav1.6 by Abeta1-42. *Front. Neurosci.* 10:94. doi: 10.3389/fnins.2016.00094

Wang, Y., Feng, Y., Fu, Q., and Li, L. (2013). Panax notoginsenoside Rb1 ameliorates Alzheimer's disease by upregulating brain-derived neurotrophic factor and downregulating Tau protein expression. *Exp. Ther. Med.* 6, 826–830. doi: 10.3892/etm.2013.1215

Wang, Y. H., and Du, G. H. (2009). Ginsenoside Rg1 inhibits beta-secretase activity in vitro and protects against Abeta-induced cytotoxicity in PC12 cells. *J. Asian Nat. Prod. Res.* 11, 604–612. doi: 10.1080/10286020902843152

XiYang, Y. B., Wang, Y. C., Zhao, Y., Ru, J., Lu, B. T., Zhang, Y. N., et al. (2016). Sodium Channel Voltage-Gated Beta 2 Plays a Vital Role in Brain Aging Associated with Synaptic Plasticity and Expression of COX5A and FGF-2. *Mol. Neurobiol.* 53, 955–967. doi: 10.1007/s12035-014-9048-9043

Yan, S., Li, Z., Li, H., Arancio, O., and Zhang, W. (2014). Notoginsenoside R1 increases neuronal excitability and ameliorates synaptic and memory dysfunction following amyloid elevation. *Sci. Rep.* 4:6352. doi: 10.1038/srep06352

Yang, L., Hao, J., Zhang, J., Xia, W., Dong, X., Hu, X., et al. (2009). Ginsenoside Rg3 promotes beta-amyloid peptide degradation by enhancing gene expression of neprilysin. *J. Pharm. Pharmacol.* 61, 375–380. doi: 10.1211/jpp/61.03.0013

Yu, F. H., Mantegazza, M., Westenbroek, R. E., Robbins, C. A., Kalume, F., Burton, K. A., et al. (2006). Reduced sodium current in GABAergic interneurons in a mouse model of severe myoclonic epilepsy in infancy. *Nat. Neurosci.* 9, 1142–1149. doi: 10.1038/nn1754

Zhang, H. S., and Wang, S. Q. (2006). Notoginsenoside R1 from Panax notoginseng inhibits TNF-alpha-induced PAI-1 production in human aortic smooth muscle cells. *Vascul. Pharmacol.* 44, 224–230. doi: 10.1016/j.vph.2005.12.002

Zhang, W. J., Wojta, J., and Binder, B. R. (1997). Notoginsenoside R1 counteracts endotoxin-induced activation of endothelial cells in vitro and endotoxin-induced lethality in mice in vivo. *Arterioscler. Thromb. Vasc. Biol.* 17, 465–474. doi: 10.1161/01.atv.17.3.465

Zhong, L., Zhou, X. L., Liu, Y. S., Wang, Y. M., Ma, F., Guo, B. L., et al. (2015). Estrogen receptor alpha mediates the effects of notoginsenoside R1 on endotoxin-induced inflammatory and apoptotic responses in H9c2 cardiomyocytes. *Mol. Med. Rep.* 12, 119–126. doi: 10.3892/mmr.2015.3394

Zhu, K., Xiang, X., Filser, S., Marinkovic, P., Dorostkar, M. M., Crux, S., et al. (2018). Beta-Site Amyloid Precursor Protein Cleaving Enzyme 1 Inhibition Impairs Synaptic Plasticity via Seizure Protein 6. *Biol. Psychiatry* 83, 428–437. doi: 10.1016/j.biopsych.2016.12.023

Conflict of Interest: The authors declare that the research was conducted in the absence of any commercial or financial relationships that could be construed as a potential conflict of interest.

frontiers in Cellular Neuroscience

ORIGINAL RESEARCH
published: 16 October 2020
doi: 10.3389/fncel.2020.00267

Pharmacological Targeting of CSF1R Inhibits Microglial Proliferation and Aggravates the Progression of Cerebral Ischemic Pathology

Boru Hou[1]†, Cheng Jiang[1]†, Dong Wang[1], Gang Wang[1], Zening Wang[1], Miaojuan Zhu[2], Yuchen Kang[2], Jiacheng Su[2], Pengfei Wei[3], Haijun Ren[1] and Furong Ju[3,4]*†*

[1]Department of Neurosurgery, Lanzhou University Second Hospital, Lanzhou, China, [2]Second Clinical Medical College, Lanzhou University, Lanzhou, China, [3]Shenzhen Key Lab of Neuropsychiatric Modulation and Collaborative Innovation Center for Brain Science, CAS Center for Excellence in Brain Science, Shenzhen Institutes of Advanced Technology, Chinese Academy of Sciences, Shenzhen, China, [4]School of Life Sciences, Lanzhou University, Lanzhou, China

OPEN ACCESS

Edited by:
Zhang Pengyue,
Yunnan University of Traditional Chinese Medicine, China

Reviewed by:
Maria Dolores Ganfornina,
University of Valladolid, Spain
Bhakta Prasad Gaire,
University of Maryland, Baltimore, United States

***Correspondence:**
Boru Hou
friend7412@126.com
Furong Ju
635201692@qq.com

†These authors have contributed equally to this work

Specialty section:
This article was submitted to Non-Neuronal Cells, a section of the journal Frontiers in Cellular Neuroscience

Received: 25 February 2020
Accepted: 29 July 2020
Published: 16 October 2020

Citation:
Hou B, Jiang C, Wang D, Wang G, Wang Z, Zhu M, Kang Y, Su J, Wei P, Ren H and Ju F (2020) Pharmacological Targeting of CSF1R Inhibits Microglial Proliferation and Aggravates the Progression of Cerebral Ischemic Pathology. Front. Cell. Neurosci. 14:267. doi: 10.3389/fncel.2020.00267

Ischemic stroke can induce rapid activation of the microglia. It has been reported that the microglia's survival is dependent on colony-stimulating factor 1 receptor (CSF1R) signaling and that pharmacological inhibition of CSF1R leads to morphological changes in the microglia in the healthy brain. However, the impact of CSF1R inhibition on neuronal structures and motor ability after ischemia–reperfusion remains unclear. In this study, we investigated microglial de-ramification, proliferation, and activation after inhibition of CSF1R by a tyrosine kinase inhibitor (ki20227) in a mouse model of global cerebral ischemia induced by bilateral common carotid artery ligation (BCAL). In addition to microglial morphology, we evaluated the mRNA expression of cytokines, chemokines, and inflammatory receptors. Our results show that pharmacological inhibition of CSF1R in ischemic mice resulted in the blockade of microglial proliferation and a shift in microglial morphology reflected by excessive de-ramification and a more activated phenotype accompanied by an enhanced innate immune response. Furthermore, we show that pharmacological inhibition of CSF1R in ischemic mice resulted in the aggravation of neuronal degeneration and behavioral impairment. Intravital two-photon imaging revealed that although pharmacological inhibition of CSF1R did not affect the recovery of dendritic structures, it caused a significant increase in spine elimination during reperfusion in ischemic mice. These findings suggest that pharmacological inhibition of CSF1R induces a blockade of microglial proliferation and causes acute activation of the microglia accompanied by a severe inflammatory response. It aggravates neuronal degeneration, loss of dendritic spines, and behavioral deficits after transient global cerebral ischemia.

Keywords: microglia, CSF1R, ischemia, neuron, ki20227

INTRODUCTION

As the primary resident immune cells of the central nervous system (CNS), the microglia play an essential role in physiology and CNS pathologies such as stroke (Kettenmann et al., 2011; Zhan et al., 2014). Importantly, the microglia exhibit changes in morphology and gene expression, particularly in response to stroke (Morrison and Filosa, 2013), and microglial activation is correlated with de-ramification and attenuated process motility after stroke (Orr et al., 2009). Various studies have shown that the microglia continuously survey the cerebral microenvironment with their extensive processes (Davalos et al., 2005; Nimmerjahn et al., 2005), interact with neurons, and regulate the turnover of synaptic structures (Winship and Murphy, 2008; Wake et al., 2009, 2013; Jolivel et al., 2015). Recent studies have shown that microglia positively contribute to normal CNS physiology to allow the completion of multiple learning tasks and motor learning-dependent synapse formation through brain-derived neurotrophic factor (BDNF) signaling (Parkhurst et al., 2013). Besides, two-photon imaging studies have directly demonstrated microglia-induced spine formation in the developing somatosensory cortex *in vivo* (Miyamoto et al., 2016). Activated microglia remove damaged neural cells, cellular debris, and dysfunctional synapses and produce pro- or anti-inflammatory factors after stroke (Turrin and Rivest, 2006; Denes et al., 2010; Iadecola and Anrather, 2011; Vinet et al., 2012; Prinz and Priller, 2014; Masuch et al., 2016). Although there have been many reports on the characteristics of the microglia under both physiological and pathological conditions in the past decades, little is known about whether the recovery of neurons is closely associated with the microglia during the pathological process of stroke. Studying the functional role of the microglia in shaping complex neuronal networks after stroke is difficult since strategies that target the microglia *in vivo* also affect other macrophages. Recently, inhibition of colony-stimulating factor 1 receptor (CSF1R) on the microglia, loss of colony-stimulating factor 1 (CSF-1), and genetic knockout of CSF1R were shown to reduce the population of normal microglia *in vivo* (Li et al., 2006; Erblich et al., 2011; Ginhoux et al., 2014), providing strategies for further research on the microglia. Depletion of the microglia not only causes defects in neuronal structure and function in healthy mice, affecting performance on multiple learning tasks, but also increases the infarct size and causes deregulation of neuronal calcium responses in cerebral ischemia (Parkhurst et al., 2013; Szalay et al., 2016). In addition, some studies suggest that microglia depletion by long-term treatment with a CSF1R inhibitor increases the numbers of neutrophils and the size of the ischemic lesion (Szalay et al., 2016; Otxoa-De-Amezaga et al., 2019), but some other study has indicated that eliminating the microglia does not improve neurogenesis after traumatic brain injury (Willis et al., 2020). Thus, the microglia may act as a double-edged sword in many neural diseases, and its in stroke still remains debatable. PLX3397 and PLX5622 are common and robust inhibitors of CSF1R that can cause a dramatic reduction in the microglial population in the adult brain (Elmore et al., 2014; Willis et al., 2020). GW2580 can specifically block microglial proliferation in APP/PS1 mice, and ki20227 inhibits the turnover/expansion of myeloid cells in an experimental autoimmune encephalomyelitis (EAE) animal model (Ohno et al., 2006, 2008; Uemura et al., 2008; Olmos-Alonso et al., 2016). However, neither of these inhibitors induces significant changes in the microglial survival rate (Hou et al., 2016; Olmos-Alonso et al., 2016).

In the present study, a reversible global cerebral ischemia model and *in vivo* imaging were used to determine the precise roles of the microglia in the brain after stroke. Here, we report that ki20227 treatment blocks microglial proliferation and causes excessive microglial activation after cerebral ischemia. Furthermore, ki20227 aggravates neuronal degeneration, loss of dendritic spines, and behavioral deficits after cerebral ischemia.

MATERIALS AND METHODS

Animals

Transgenic mice (Thy1-YFP line H) expressing yellow fluorescent protein (YFP) in layer 5 pyramidal neurons and CX3CR1$^{GFP/+}$ mice expressing green fluorescent protein (GFP) in the microglia were purchased from Jackson Laboratory. All animals were bred in the Laboratory Centre for Basic Medical Sciences, Lanzhou University. The mice had free access to food and clean water and were housed under a normal 24-h light cycle (12-h light/12-h dark) at 22 ± 2°C. Transgenic mice of both sexes aged 3–5 months and weighing 20–30 g were used in this study. All experiments in this study were carried out strictly following the rules set by the Ethics Committee of Lanzhou University, China.

Global Ischemia Model

The method of bilateral common carotid artery ligation (BCAL), which was used to induce global ischemia, was described in previous studies (Zhang et al., 2005; Winship and Murphy, 2008). Briefly, each animal was deeply anesthetized with a mixture of 2% ketamine and 0.2% xylazine by intraperitoneal injection, and then a thinned-skull cranial window was created above the somatosensory cortex. After that, the animal was placed in the supine position, and the carotid arteries were occluded through a midline incision. To ensure that global ischemia was effectively induced in mice, reduced blood flow and beaded dendrites were confirmed by two-photon imaging through the cranial window. If decreases in blood flow and beading of dendrites were not observed within 10 min after surgery through the cranial window by intravital two-photon imaging, then global ischemia had not been successfully induced. The mice were subjected to 60 min of transient ischemia after occlusion of the common carotid arteries at room temperature by tying surgical sutures. After 60 min of bilateral common carotid artery occlusion, the surgical sutures were untied to allow reperfusion of the blood vessels. To support recovery and enhance the survival rate, we placed the mice on a heating pad after BCAL until they fully awoke.

Antagonism of CSF1R

Inhibition of the tyrosine kinase activity of CSF1R was achieved by the administration of ki20227, and inhibition of protein

kinases was evaluated based on the expression profiles, as previously described (Ohno et al., 2008). The mice were treated intragastrically with ki20227 (each mouse was given 2 mg g^{-1} day^{-1}) once daily for 3 days of reperfusion. Vehicle (0.5% methylcellulose in distilled water) was administered intragastrically during reperfusion after 60 min of ischemia, and reperfusion was continued for 3 days. The mice were divided into four groups: the intragastric ki20227 administration group (ki20227-treated sham mice), vehicle group (vehicle-treated sham mice), ki20227 treatment (once daily) during reperfusion after 60 min of ischemia group (ki20227-treated stroke mice), and vehicle treatment (once daily) during reperfusion after 60 min of ischemia group (vehicle-treated stroke mice).

Two-Photon Imaging and Data Analysis

Intravital two-photon imaging was performed as described in previous studies (Grutzendler et al., 2002; Zhang et al., 2005). Briefly, to ensure the immobility of the animals, a custom-made metal frame and a steel plate were used to fix the skulls. Then, the skulls of anesthetized mice were exposed and the region of interest, i.e., the imaging site (a 2 × 2-mm^2 area of the skull with the center located −1.5 mm from Bregma and 2.0 mm from the midline), was marked and then thinned to a thickness of 25 μm by a high-speed dental drill. After the step distance was set to an appropriate depth for dendritic spines (0.75 μm), real-time images of the dendritic structure were acquired with a two-photon microscope with a ×25 water-immersion objective lens at zoom 4 (×25/1.05, Olympus) at a wavelength of 920 nm. Two-photon image analysis was carried out as described previously (Ju et al., 2018). To quantify the percentage of blebbed dendrites, we used a custom-designed macro to mark dendrites at a fixed length of 20 μm and calculated the total length of the selected dendritic segments. The percentage of blebbed dendrites was calculated as the total length of blebbed dendrites/total length of dendrites. To quantify blood flow, we intravenously administered Evans blue (EB) solution (10 mg/ml; 2.5 ml/kg) before surgery. Blood flow was evaluated with a two-photon microscope with a ×25 water-immersion objective lens at zoom 4 (×25/1.05, Olympus) at a wavelength of 920 nm. A line was drawn along the center axis of an arteriole (10–15 μm in diameter), and repeated line scanning was used to measure the velocity of red blood cells (RBCs). To estimate RBC velocity, we fit a line to the arcs created by moving RBCs in line scans and calculated the change in position ($\Delta x/\Delta t$). Thus, the x-axis presents the distance which the red blood cells have traveled; each interval between the lines aligned along the y-axis reflects the period between each scan. The velocity was presented as pixel distance/line time. Raw data have been extracted from the ImageJ measurement. Dividing the distance along the x-axis (calculated by pixels' edge) by the time period along the y-axis (in seconds) can result in the velocity of blood cells (in micrometers per second). Six to 10 vessels were analyzed per mouse (n = 6). To quantify dendritic spine changes, the same dendritic segments were carefully imaged at different time points. More than 200 spines selected from the image stacks were counted for each mouse. Spine elimination was calculated as the number of lost spines/the number of preexisting spines, and spine formation was calculated as the number of new spines/the number of preexisting spines.

Nissl and Immunofluorescence Staining

Brain tissues fixed with 4% paraformaldehyde (PFA) were washed in phosphate-buffered saline (PBS) and sectioned (30 μm) on a vibrating microtome (Leica). We visualized Nissl bodies in layers 1–3 of the somatosensory cortex at −1.5 to −2.0 mm from Bregma and 2.0 mm from the midline. Nissl bodies were stained with cresyl violet. Serial brain sections were collected at 120-μm intervals. Then, the slices were treated as follows: air-dried for 15 min and immersed in 95% ethanol for 15 min, 70% ethanol for 1 min, 50% ethanol for 1 min, ddH_2O twice for 1 min each, cresyl violet for 10 min, ddH_2O for 1 min, 50% ethanol for 1 min, 70% ethanol for 2 min, 95% ethanol for 2 min, 100% ethanol for 2 min, and xylene for 10 min. After these procedures, the sections were sealed with neutral balsam for microscopy. All images were analyzed using ImageJ software[1] to count the Nissl bodies. Eight to 10 somatosensory cortex slices (−1.0 to −2.5 mm from Bregma) per mouse were analyzed (n = 6).

To immunofluorescently label neurons, the brain sections were washed with PBS and blocked with 10% goat serum in PBS for 0.5 h. The sections were incubated with a primary antibody against NeuN (1:200; Millipore) diluted in buffer containing 0.01% Triton X-100 and 10% goat serum for 12 h at 4°C. The brain sections were incubated with rhodamine-conjugated goat anti-rat secondary antibody (1:100; ZSGB-BIO) for 1 h at room temperature. For each confocal experiment, all brain sections containing layers 1–3 of the somatosensory cortex, located −1.5 to −2.0 mm from Bregma and 2.0 mm from the midline, were imaged. All images were analyzed using ImageJ software to count the number of cells. Eight to 10 brain slices per mouse were analyzed (n = 6).

To identify proliferating microglia after stroke, bromodeoxyuridine (BrdU) immunofluorescence was performed as described in our preliminary studies. Briefly, BrdU (50 mg/kg; Sigma) was administered to the mice *via* intraperitoneal injection two times per day starting from the 12th hour after BCAL. After 3 days of reperfusion, the brain tissues of the mice were fixed with 4% PFA. For BrdU immunofluorescence, the brain sections were washed with PBS for 10 min, treated with 2 M HCl at 37°C for 30 min, neutralized with 0.1 M borate buffer (pH 8.5) for 3 × 15 min, and incubated overnight with a rat monoclonal antibody against BrdU (1:500; AbD Serotec). The brain tissues were incubated with rhodamine-conjugated goat anti-rat secondary antibody (1:100; ZSGB-BIO) for 1 h at room temperature. For each confocal experiment, all brain sections containing layers 1–3 of the somatosensory cortex, located −1.5 to −2.0 mm from Bregma and 2.0 mm from the midline, were imaged. All images were analyzed using ImageJ software to count the number of cells. Eight to 10 brain slices per mouse were analyzed (n = 6).

[1] http://rsb.info.nih.gov/ij/

Microglial Skeleton and Soma Size Analysis

We observed microglial morphology changes in layers 1–3 of the somatosensory cortex, located −1.5 to −2.0 mm from Bregma and 2.0 mm from the midline. This area was also observed *in vivo*. For microglial skeleton analysis, GFP-positive microglia extracted from CX3CR1$^{GFP/+}$ mice were used to acquire images of microglial morphology. Brain tissues fixed with 4% PFA were washed in PBS and sectioned (60 μm) on a vibrating microtome (Leica). For cell skeletonization analysis, repeated *z*-series of about 60 optical sections [1,024 × 1,024 pixel arrays, *z*-stack at 1-μm intervals, zoom 4 (×25/1.05)] were obtained with an Olympus confocal microscope. All images were analyzed using ImageJ software. The *z*-stack of a single microglia was approximately 60 μm, and 10–15 microglia in the somatosensory cortex of each mouse were analyzed (n = 6). The analytic skeleton plugin[2] was applied to collect data focused on the branch point number and the total length of the microglial process. The images were analyzed with a custom-coded macro plugin to perform skeletonized analysis ("Plugin" < "Process" < "Smooth 3D"; radius, 0.3–0.8). The file was properly converted to binary format after the final images had been stacked ("Image" < "Adjust" < "Threshold"). The skeletonization plugin (2D/3D) was used to generate skeletonized images (Lee et al., 1994). For microglial skeleton analysis, approximately 10 relatively intact microglia per mouse were analyzed (n = 6). For microglial soma size analysis, the soma was outlined and analyzed with ImageJ ("Polygon selections" < "Measure" < "Area"). Approximately 30 relatively intact microglial soma per mouse were analyzed (n = 6).

Behavioral Tests

The open-field test was carried out as described previously to evaluate animal behavioral deficits after reperfusion for different durations (Olmos-Alonso et al., 2016). The mice were placed in individual cages (25 cm × 25 cm × 31 cm) for 10 min, and the total distance traveled (in centimeters) was measured. The rotarod test was performed on an apparatus (ZB-200 rotarod system, TME Technology) as described previously (Zhu et al., 2017a). Mice were placed on the rod and allowed to run, and the speed of the rod accelerated from 10 to 40 rpm within 300 s. The mice were subjected to three trials per day for 3 days before surgery. The mice were tested 3 days after reperfusion. The body weight and food intake of each mouse were monitored during the experiment.

Analysis of Gene Expression by qPCR

Mice from both the ischemic and control groups were treated with vehicle or ki20227 (n = 6/group), and tissue samples of the somatosensory cortex (centered around the area −1.5 mm from Bregma and 2.0 mm from midline) were extracted under a dissecting microscope after transcardial perfusion with PBS. RNA was extracted with an RNA Extraction Kit (TaKaRa) and quantified with a Nanodrop spectrophotometer (Thermo Fisher Scientific), and RNA integrity was checked *via* gel (2% agarose) electrophoresis. The RNA was then reverse-transcribed with a reverse-transcription kit with gDNA Eraser (Applied Biosystems, Foster City, CA, USA). The expression of genes was analyzed *via* quantitative polymerase chain reaction (qPCR) using iTaq^{TM} Universal SYBR® Green Supermix (Bio-Rad). Glyceraldehyde-3-phosphate dehydrogenase (GAPDH) was chosen as the reference gene. The relative quantity of messenger RNAs (mRNAs) was determined by the $2^{-\triangle\triangle CT}$ method. The custom-designed gene-specific primers (GENEWIZ) were as follows: CSF1 (FW: GGAACAGCTGGATGATC, RV: GAGGAG CAGAACAAGGC); BCL2 (FW: GTGCAAGTGTAAATTGCC GAG, RV: GAGACTTCTGAAGATCGATGG); CCL3 (FW: CCATATGGAGCTGACACCCC, RV: GAGCAAAGGCTGCT GGTTTC); CXCL10 (FW: CCAAGTGCTGCCGTCATTTT, RV: CTCAACACGTGGGCAGGATA); CSF1R (FW: GCAGTA CCACCATCCACTTGTA, RV: GTGAGACACTGTCCTTCA GTGC); IL34 (FW: CTTTGGGAAACGAGAATTTGGAGA, RV: GCAATCCTGTAGTTGATGGGGAAG); Cd4 (FW: GTT TTCGCTACATGACTGCACA, RV: AGGTTGTCCAACTGAC ATCTTTC); Cd80 (FW: AGTTTCTCTTTTTCAGGTTGTGAA, RV: ACATGATGGGGAAAGCCAGG); CCR2 (FW: AGGA GCCATACCTGTAAATGCC, RV: TGTGGTGAATCCAATGC CCT); CCL19 (FW: CCTGCCTCAGATTATCTGCCA, RV: GT GACCCAGCGCCCCATCCCTGG); Ccl5 (FW: GTGCCCAC GTCAAGGAGTAT, RV: TTCTCTGGGTTGGCACACAC): TNF-α (FW: GACGTGGAACTGGCAGAAGA, RV: ACTGA TGAGAGGGAGGCCAT); Ccl4 (FW: GGCTCTGACCCTCC CACTTCCT, RV: CCAGTGAGCCCTGGGTCAC); Ccl2 (FW: TTAAAAACCTGGATCGGAACCAA, RV: GCATTAGCTT CAGATTTACGGGT); TGF-β (FW: GGCGATACCTCAGCA ACCG, RV: CTAAGGCGAAAGCCCTCAAT); and GAPDH (FW: CGTGCCGCCTGGAGAAACCTG, RV: AGAGTGGG AGTTGCTGTTGAAGTCG). The RNA samples were derived from six pregnant mice, and at least three technical replicates of each RNA sample were analyzed by qRT-PCR.

Statistical Analysis

SPSS software was used for all statistical analyses. Analysis of variance and two-tailed unpaired *t*-test was used to compare two groups, and one-way ANOVA was performed to compare three or more groups. Two-way ANOVA was performed to analyze the behavioral data. The results are presented as the mean ± standard error of the mean, with $^{*}p < 0.05$ and $^{**}p < 0.01$.

RESULTS

BCAL Induces Ischemia and Alters Dendritic Structure and Blood Flow

Whole-brain ischemia was induced to observe changes in neurons, microglial activity, and mobility during stroke (**Figure 1A**). In the whole-brain ischemia model, blood flow was controlled based on the duration of common carotid artery ligation, plasma was labeled with EB by intravenous injection, and the success of the model was judged based on the slowing or stopping of blood flow (marked by red fluorescence) *via*

[2]http://imagejdocu.tudor.lu/

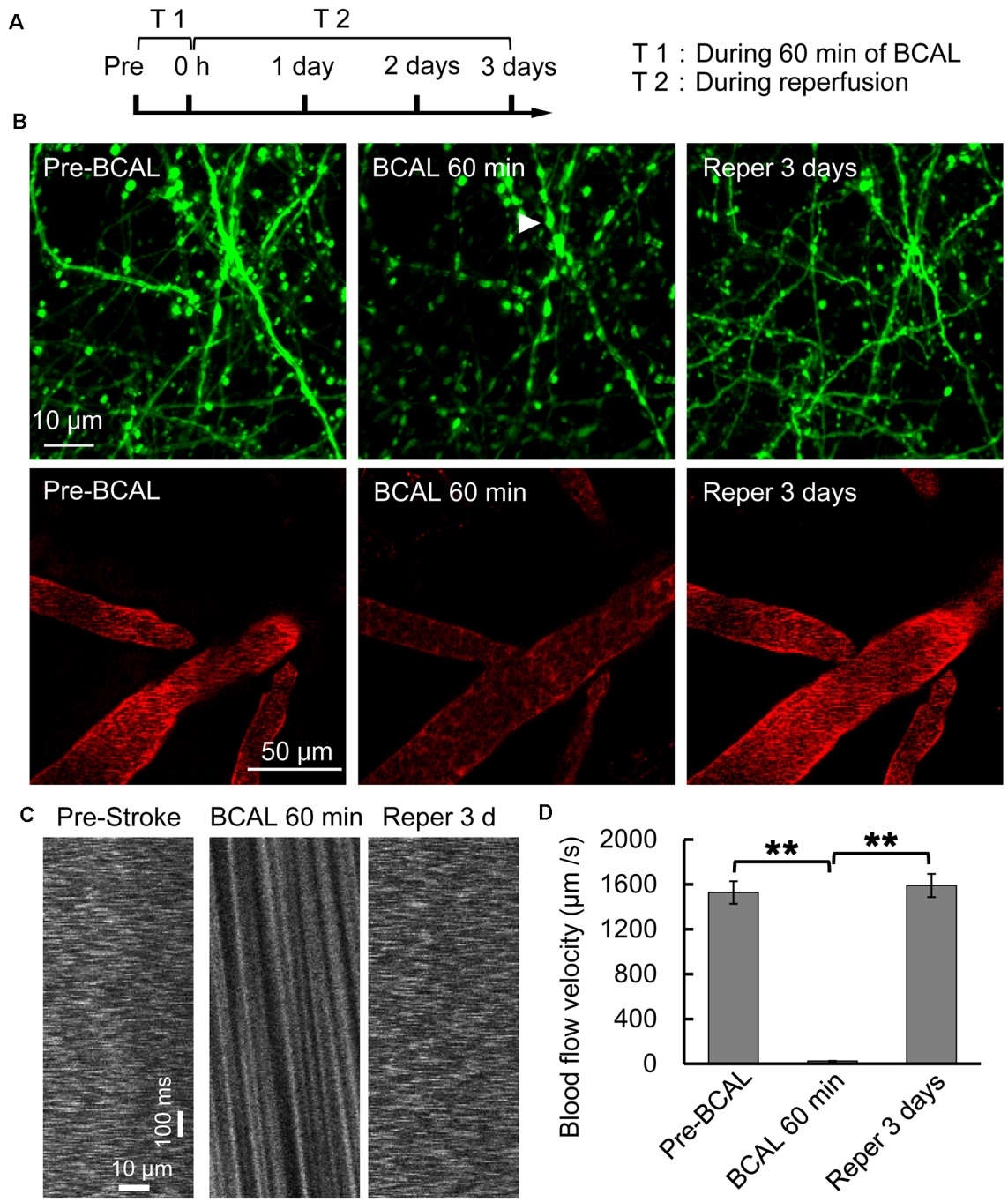

FIGURE 1 | Two-photon imaging of a murine model of global ischemia. **(A)** Timeline showing the time points of tyrosine kinase inhibitor (ki20227) treatment in the transient ischemia–reperfusion model. **(B)** Two-photon images showing Evans blue (EB)-labeled blood vessels (*red*; *scale bar*, 50 μm) and dendritic structures labeled with Thy1-YFP line H (*green*; *scale bar*, 10 μm) before surgery, after 60 min of bilateral common carotid artery ligation (BCAL), and after 3 days of reperfusion. The *arrowheads* indicate blebbed dendrites. **(C)** Two-photo line-scanning imaging of the blood flow velocity before ischemia, 60 min after ischemia, and 3 days after reperfusion. *Scale bar*, 10 μm and100 ms. **(D)** Quantification of blood flow velocity. Six to 10 vessels were analyzed per mouse. $n = 6$, $^{**}p < 0.01$.

intravital two-photon imaging (**Figure 1B**). Transgenic mice (Thy1-YFP line H) expressing YFP in layer 5 pyramidal neurons were used for imaging. In previous studies by our laboratory (Zhang et al., 2005; Zhu et al., 2017a), *in vivo* two-photon imaging revealed blebbed dendrites on layer 5 pyramidal neurons in the somatosensory cortex and blocked blood flow, as visualized with EB, after 60 min of BCAL (**Figure 1B**). Subsequently, after 3 days of reperfusion, blood flow velocity was restored to normal levels and the dendritic structure rapidly recovered [blood flow velocity (in micrometers per second): before BCAL,

1,563.9 ± 185.0; after 560 min of BCAL, 20.5 ± 6.8; after 3 days of reperfusion, 1,578.3 ± 167.1; $^{**}p < 0.01$; **Figures 1C,D**].

Morphological Transition of Microglia in Response to CSF1R Signaling Inhibition

The effects of cerebral ischemia on the microglia were then evaluated. To clarify the response of the microglia after the inhibition of CSF1R, newly proliferated microglia in the somatosensory cortex were imaged, and the density and soma size of the microglia were also measured. We first assessed the effect of ki20227-induced inhibition of CSF1R in sham CX3CR1$^{GFP/+}$ mice. Although the number of newly proliferated microglia was slightly increased in sham mice compared to control mice, the density and soma size of the microglia were not significantly changed after the inhibition of CSF1R by ki20227 (**Figures 2A–E**). We further assessed the effect of ki20227 on microglial activation after stroke. In the present study, confocal imaging indicated that the density of the microglia was significantly decreased in ki20227-treated stroke mice compared with vehicle-treated stroke mice 3 days after reperfusion [density (per square millimeter): vehicle-treated stroke mice, 294.3 ± 10.2, vs. ki20227-treated stroke mice, 204.6 ± 15.4; $^{*}p < 0.05$; **Figures 2A,B**]. In addition, there was a significant change in microglial soma size between the ki20227-treated and vehicle-treated stroke mice on day 3 after reperfusion [soma size (per square micrometer): vehicle-treated stroke mice, 102.3 ± 20.8, vs. ki20227-treated stroke mice, 140.3 ± 15.9; $^{*}p < 0.05$; **Figure 2C**]. Furthermore, there were significantly fewer newly proliferated microglia in the ki20227-treated than in vehicle-treated stroke mice on day 3 after reperfusion (number of proliferated microglia: vehicle-treated stroke mice, 93.5 ± 10.1, vs. ki20227-treated stroke mice, 32.8 ± 21.4; $^{**}p < 0.01$; **Figures 2D,E**).

To precisely investigate how the microglia from CX3CR1$^{GFP/+}$ mice respond to global ischemia following ki20227 treatment at the morphological level, ImageJ software was used to quantitatively analyze the skeletonized microglial morphology. All images of the microglia were collected from the somatosensory cortex. In the sham groups, we summarized the length of the microglial processes and the number of branch points in the vehicle-treated and the ki20227-treated sham groups. There was a significant difference in the number of branch endpoints, but no difference in the total process length of individual microglia between the vehicle-treated and ki20227-treated sham groups. We also found that there was a significant difference in the total process length of individual microglia between the vehicle-treated and ki20227-treated sham groups. We further evaluated the effect of ki20227 on microglial morphology in ischemic mice. In mice not treated with the antagonist, the total number of microglial branch endpoints and the total process length of each microglia were significantly reduced by global ischemia after 3 days of reperfusion. Remarkably, we found significant reductions in the number of microglial total branch endpoints and the process length in the ki20227-treated stroke group compared to the vehicle-treated stroke group on day 3 after reperfusion [total number of microglial branch endpoints/cell: vehicle-treated stroke group, 246.3 ± 13.7, vs. ki20227-treated stroke group, 207.8 ± 13.3; total length of microglial processes/cell (in micrometers): vehicle-treated stroke group, 999.6 ± 86.6, vs. ki20227-treated stroke group, 688.7 ± 110.6; $^{**}p < 0.01$; **Figures 2F–I**].

Inflammation Is Induced by Ischemia Combined With ki20227 Treatment

To determine whether inflammation is involved in the effect of ki20227 treatment, TGF-β, CSF1R, CSF1, CXCL10, BCL-2, iNOS, CCL5, TGF-α, IL34, CD86, CD80, CCR2, CCL2, CCL3, CCL4, and CD4 were detected in ki20227-treated sham mice. The expression levels were barely changed in the ki20227-treated sham mice compared to the vehicle-treated sham mice. However, the expressions of several of the above-mentioned genes were significantly increased in vehicle-treated stroke mice compared to vehicle-treated sham mice 3 days after reperfusion. We found that the expression levels of some chemokines and cytokine receptors, such as CSF1R, CSF1, CCL3, CD4, and CCR2, were significantly different in ki20227-treated stroke mice compared to vehicle-treated stroke mice (**Figures 3A,C**). Furthermore, in the ki20227-treated stroke mice, the mRNA expression levels of pro-inflammatory factors such as iNOS and BCL-2 (**Figure 3B**) and the cytokine-related gene TNF-α were significantly increased compared with those in the vehicle-treated stroke mice on day 3 after reperfusion (**Figure 3A**), but the mRNA expression levels of anti-inflammatory factors such as TGF-β were significantly decreased in the ki20227-treated stroke mice compared with the vehicle-treated stroke mice on day 3 after reperfusion (**Figure 3A**). Additionally, quantitative analysis showed no marked difference in the mRNA expressions of other chemokines and inflammatory genes, such as CD80, IL34, CD86, CXCL10, CCL2, CCL4, and CCL5, between the vehicle-treated and ki20227-treated stroke mice on day 3 (**Figures 3B,C**).

CSF1R Inhibition Promotes the Degeneration of Neurons During the Progression of Global Ischemia

To determine the effect of ki20227 on the degeneration of neurons, the density of Nissl bodies was analyzed after Nissl staining (**Figures 4A,B**). In the ki20227-treated sham group, the density of Nissl bodies was not significantly different from that in the vehicle-treated sham group. However, in the ki20227-treated stroke mice, the density of Nissl bodies was significantly lower than that in the vehicle-treated stroke mice on day 3 after reperfusion [density (per square millimeter): vehicle-treated stroke mice, 4,756.8 ± 292.1, vs. ki20227-treated stroke mice, 4,116.9 ± 355.4; $^{**}p < 0.01$; **Figure 4C**]. We assessed the effect of ki20227-induced inhibition of CSF1R on the density of neurons (**Figures 4D,E**). There was no significant difference in the density of neurons in sham mice before and after inhibition of CSF1R by ki20227. However, the density of neurons was significantly decreased in the ki20227-treated stroke mice compared with the vehicle-treated stroke mice on day 3 after reperfusion [density (per square millimeter): vehicle-treated stroke mice,

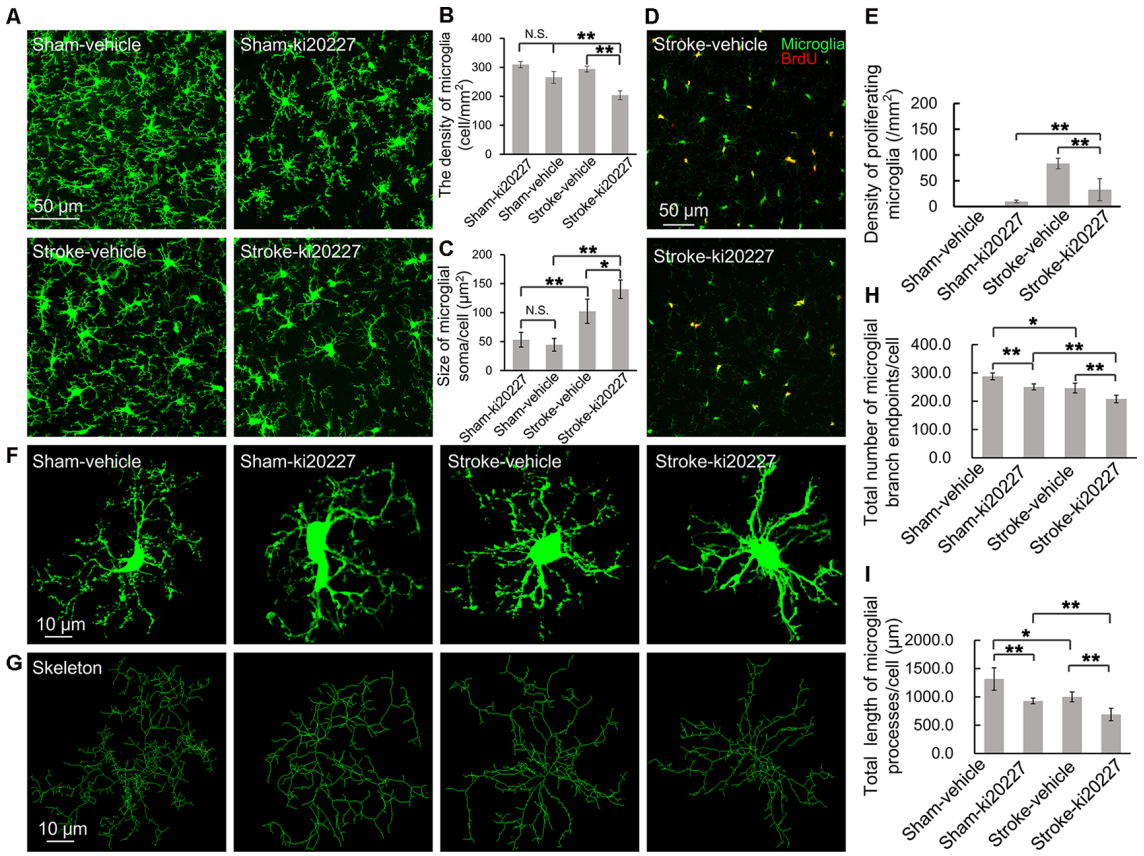

FIGURE 2 | ki20227-induced morphological changes in the microglia following reperfusion after ischemia. **(A)** Representative confocal images of the microglia [*green*, green fluorescent protein (GFP)-positive microglia] in different groups. *Scale bar*, 50 μm. **(B)** Quantification of microglial density showing a significant difference between groups. $n = 6$ mice per group; N.S.: $p < 0.05$, $^{**}p < 0.01$, $n = 6$. **(C)** Quantification of microglial soma size showing a significant difference between groups ($n = 6$ mice per group). N.S.: $p < 0.05$, $^{*}p < 0.05$, $^{**}p < 0.01$, $n = 6$. **(D)** Representative confocal images of microglial proliferation (*green*, GFP-positive microglia; *red*, BrdU-positive cells) in different groups. *Scale bar*, 50 μm. **(E)** Quantification of microglial proliferation showing a significant difference between groups ($n = 6$ mice per group). $^{**}p < 0.01$, $n = 6$. **(F,G)** Representative confocal images of the microglia (*green*, GFP-positive microglia) and skeletonized microglia in the vehicle-treated sham, ki20227-treated sham, vehicle-treated stroke, and ki20227-treated stroke mice. The image sizes (*scale bars*) in panels **(F,G)** are of the same length. *Scale bar*, 10 μm. **(H,I)** Analysis of the total number of microglial branch endpoints and the total length of microglial processes in all groups. Note that there was a significant difference between the vehicle-treated and ki20227-treated groups. The total number of microglial branch endpoints and the total length of microglial processes were significantly decreased after treatment with ki20227 on day 3 after global ischemia. $^{*}p < 0.05$, $^{**}p < 0.01$, $n = 6$.

3,050.4 ± 216.7, vs. ki20227-treated stroke mice, 2,529.1 ± 204.8; $^{*}p < 0.05$; **Figure 4F**].

We further examined whether ki20227 affects the recovery of the dendritic structure by evaluating the percentage of blebbed dendrites after stroke (**Figure 4G**). Time-lapse imaging revealed no significant dendritic structural damage in mice after ki20227 treatment, but a significant difference in damage between the vehicle-treated sham mice and the vehicle-treated stroke mice on day 3. Noteworthy is that there was a significant difference in damage between the ki20227-treated sham mice and ki20227-treated stroke mice on day 3. Furthermore, we examined the recovery of the dendritic structure in the vehicle-treated and ki20227-treated stroke mice and found no significant difference in the recovery of the dendritic structure on day 3 (percentage of blebbed dendrites: vehicle-treated stroke group, 3.8 ± 0.8, vs. ki20227-treated stroke group, 3.8 ± 1.0; $p < 0.05$, $n = 6$; **Figure 4H**). To further investigate the effect of ki20227 on dendritic spine plasticity after global cerebral ischemia, we assessed the formation and elimination of spines (**Figures 4I,J**). *In vivo* imaging showed that there were no significant differences in the spine elimination rate or formation rate between the vehicle-treated and ki20227-treated sham mice on day 3. However, when we further evaluated the formation and elimination rates of dendritic spines in ischemia mice, live imaging revealed that both the elimination rate and the formation rate were significantly higher in the vehicle-treated stroke mice than in the vehicle-treated sham mice on day 3 after reperfusion (**Figures 4I,G**). Importantly, the spine elimination rate in the ki20227-treated stroke mice was even higher than that in the vehicle-treated stroke mice, and the formation rate was significantly lower in the ki20227-treated than in vehicle-treated stroke mice on day 3 after reperfusion (before reperfusion: vehicle-treated stroke group: elimination rate, 8.74 ± 0.82%; formation rate, 6.06 ± 0.83%; ki20227-treated stroke group:

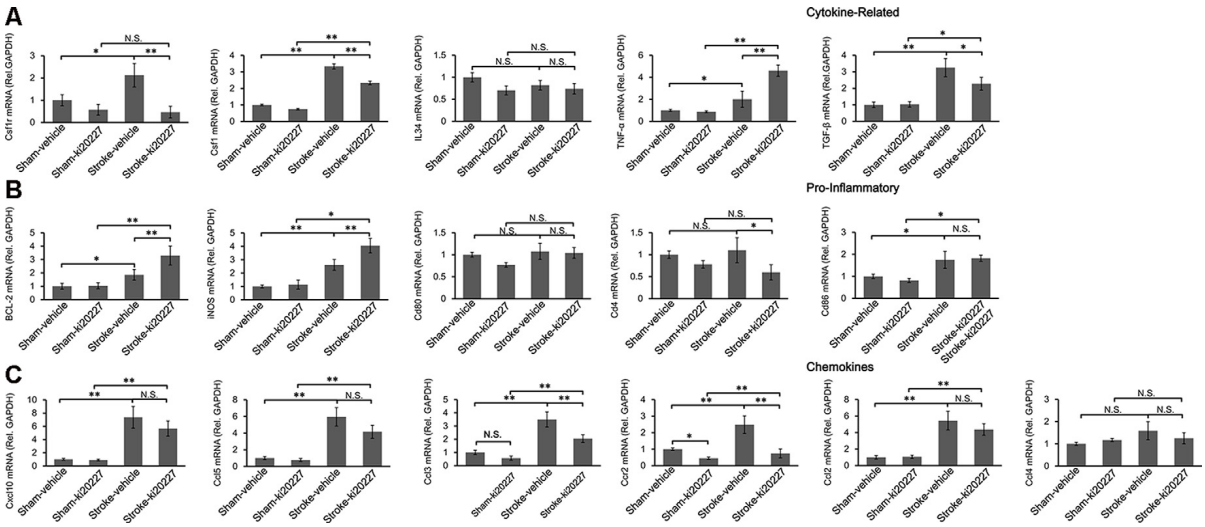

FIGURE 3 | Response of the relative mRNA expressions of various inflammatory gene markers to ki20227 treatment. **(A)** Cytokines-related genes. **(B)** Pro-inflammatory genes. **(C)** Chemokines. There was little difference in the mRNA expression levels of inflammatory cytokines between the vehicle-treated and ki20227-treated sham mice on day 3. However, the mRNA expression levels of the cytokine-related genes, pro-inflammatory genes, and chemokines were significantly different between the ki20227-treated and vehicle-treated stroke mice on day 3 after reperfusion ($n = 6$ mice per group). N.S.: $p > 0.05$, $^{*}p < 0.05$, $^{**}p < 0.01$.

elimination rate, 10.35 ± 1.68%; formation rate, 4.79 ± 0.64%; $^{*}p < 0.05$, $^{**}p < 0.01$, $n = 6$; **Figures 4K,L**).

CSF1R Inhibition Prevents the Progression of Stroke Pathology

The open-field test and rotarod test were performed to evaluate behavioral deficits in stroke mice. There were no significant differences in the total distance traveled, total time spent on the rotarod, or weight between the vehicle-treated and ki20227-treated sham mice (**Figures 5A–C**). However, significant decreases in the total distance traveled, total time spent on the rotarod, and weight were detected in the vehicle-treated stroke mice compared with the vehicle-treated sham mice after reperfusion (**Figures 5A–C**). Importantly, we found that, in the ki20227-treated stroke mice, there were significant decreases in the total distance traveled, total time spent on the rotarod, and weight compared with those in the vehicle-treated stroke mice after reperfusion (**Figures 5A–C**).

DISCUSSION

The microglia are ramified and dynamic brain-resident myeloid cells (Mosher et al., 2012; Michell-Robinson et al., 2015), and the complexity of their morphology and function is determined by the physical conditions under which their dynamic ramified processes surveil the microenvironment and by the pathology driving their phagocytosis of pathogens or cellular debris (Tremblay et al., 2010; Fontainhas et al., 2011). Studies have elucidated the role of stimuli in altering microglial activity in models of CNS injury pathology (Fontainhas et al., 2011; Tremblay et al., 2011; Masuch et al., 2016). Our results show that treatment with the CSF1R kinase inhibitor ki20227 inhibits the proliferation of microglia and alters microglial morphology after ischemic stroke. Furthermore, these changes aggravate neurodegeneration and change the plasticity of neuronal dendrites after global cerebral ischemia.

De-ramification is one of the cellular morphological properties of activated microglia (Kreutzberg, 1996; Stence et al., 2001); the microglia can retract their processes and alter their gene expression profiles in response to ischemia (Khan et al., 2017; Ju et al., 2018). Such morphological alterations are closely related to the velocity of local blood flow. When blood flow is completely stopped, the mobility of microglial protrusions, including extension and retraction, is lost (Masuda et al., 2011). In addition to the altered morphology, modified gene expression is considered the main event in microglial activation. Such alterations, which include pro- and anti-inflammatory effects, are dependent on the specific stage of pathology (Bell et al., 2010; Denieffe et al., 2013). Based on these findings, our study aimed to investigate the effect of a predominant factor, CSF1R, which is a cytokine that participates in morphological changes in and proliferation of microglia, on the functional and phenotypical modification of the microglia during ischemia–reperfusion. CSF1R and its downstream pathway are closely related to the survival and maintenance of the microglia. PLX3397 is an efficient, selective, ATP-competitive inhibitor of CSF1R, and as a robust inhibitor, it can cause a dramatic reduction in the microglial population in the adult brain. However, unlike PLX3397, ki20227 is a highly selective c-Fms tyrosine kinase (CSF1R) inhibitor like GW2580. In adult mice, ki20227 has little effect on the survival rate of microglia, and GW2580 (75 mg/kg) has been used in the past without having a significant effect

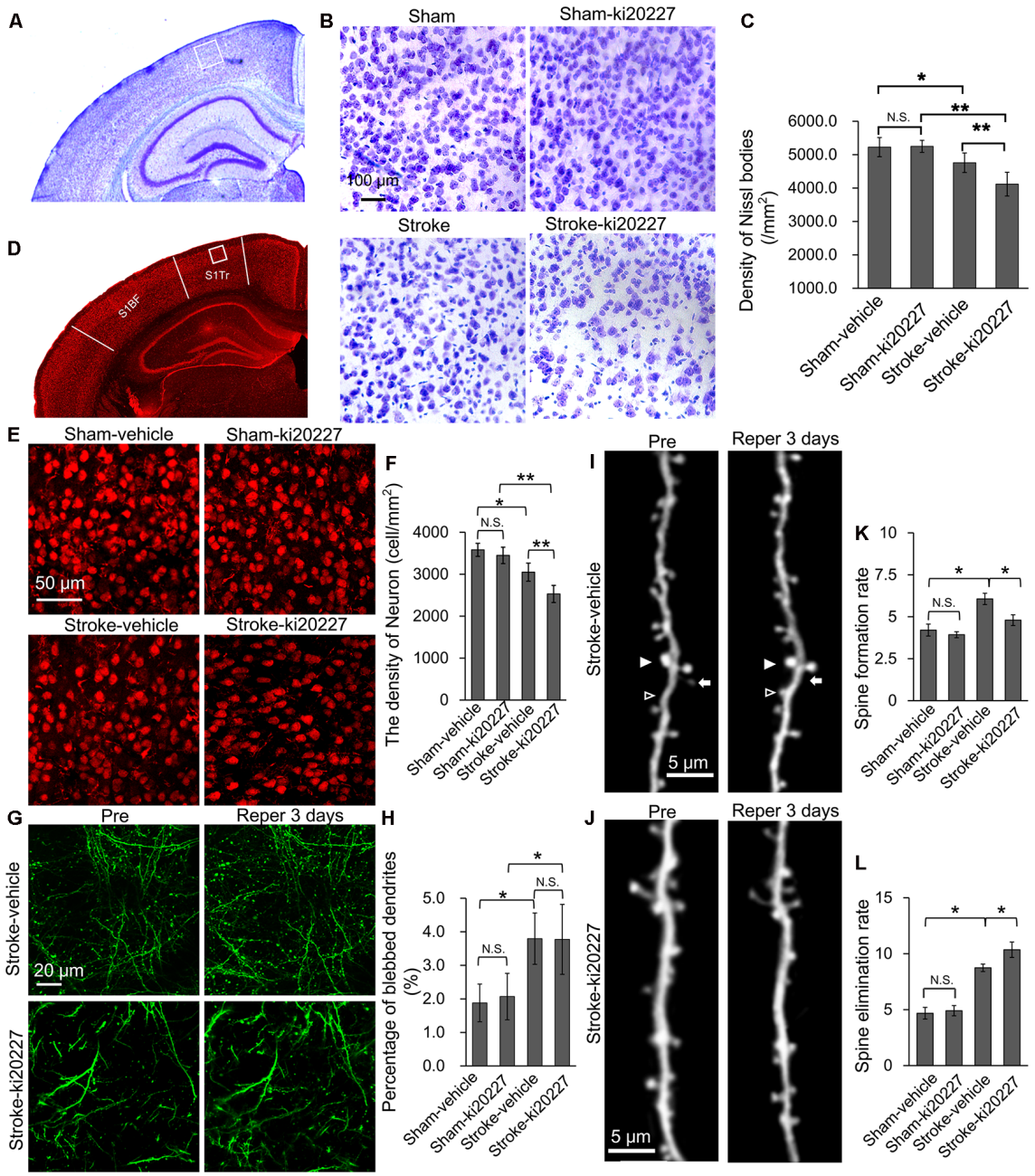

FIGURE 4 | ki20227-induced neuronal degeneration in the cerebral cortex following reperfusion after transient global cerebral ischemia. **(A,B)** Representative image of Nissl bodies in the vehicle-treated sham, ki20227-treated sham, vehicle-treated stroke, and ki20227-treated stroke mice. The region of interest (ROI) is indicated by the *white box*. High-magnification images in panel **(B)** showing Nissl bodies in different groups. *Scale bar*, 100 μm. **(C)** Analysis of Nissl bodies in the vehicle-treated sham, ki20227-treated sham, vehicle-treated stroke, and ki20227-treated stroke mice. There was no difference between the vehicle-treated and ki20227-treated sham mice, but a significant difference was found between the vehicle-treated and ki20227-treated stroke mice ($n = 6$). *$p < 0.05$, **$p < 0.01$. **(D,E)** Confocal images showing neurons (*red*) of the somatosensory cortex in different groups. The ROI is indicated by the *white box*. High-magnification images in panel **(E)** show neurons in the different groups. *S1Tr*, primary somatosensory cortex, trunk region; *S1BF*, primary somatosensory cortex, barrel field. *Scale bar*, 50 μm. **(F)** Analysis of the density of neuron in the vehicle-treated sham, ki20227-treated sham, vehicle-treated stroke, and ki20227-treated stroke mice. Significant differences were found between the vehicle-treated and ki20227-treated stroke mice ($n = 6$). N.S: $p < 0.05$, *$p < 0.05$, **$p < 0.01$. **(G)** ki20227 did not affect the reversible recovery of the dendritic structure (*green*) following global cerebral ischemia–reperfusion. Morphological changes in dendritic structures before ischemia and 3 days after reperfusion. *Scale bar*, 20 μm. **(H)** Quantification of the percentage of blebbed dendritic structures in vehicle-treated sham, ki20227-treated sham, vehicle-treated stroke, and ki20227-treated stroke mice. Note that there was a significant difference in dendritic beading between sham and stroke mice ($n = 6$). N.S.: $p < 0.05$, *$p < 0.05$. **(I,J)** *In vivo* imaging of the dendritic structure in the different groups. The *open arrowheads*, *arrows*, and *filled arrowheads* indicate newly formed spines, eliminated spines, and stable spines, respectively. *Scale bar*, 5 μm. **(K,L)** The spine formation rate and spine elimination rate were significantly different between groups ($n = 6$ mice per group). *$p < 0.05$, **$p < 0.01$.

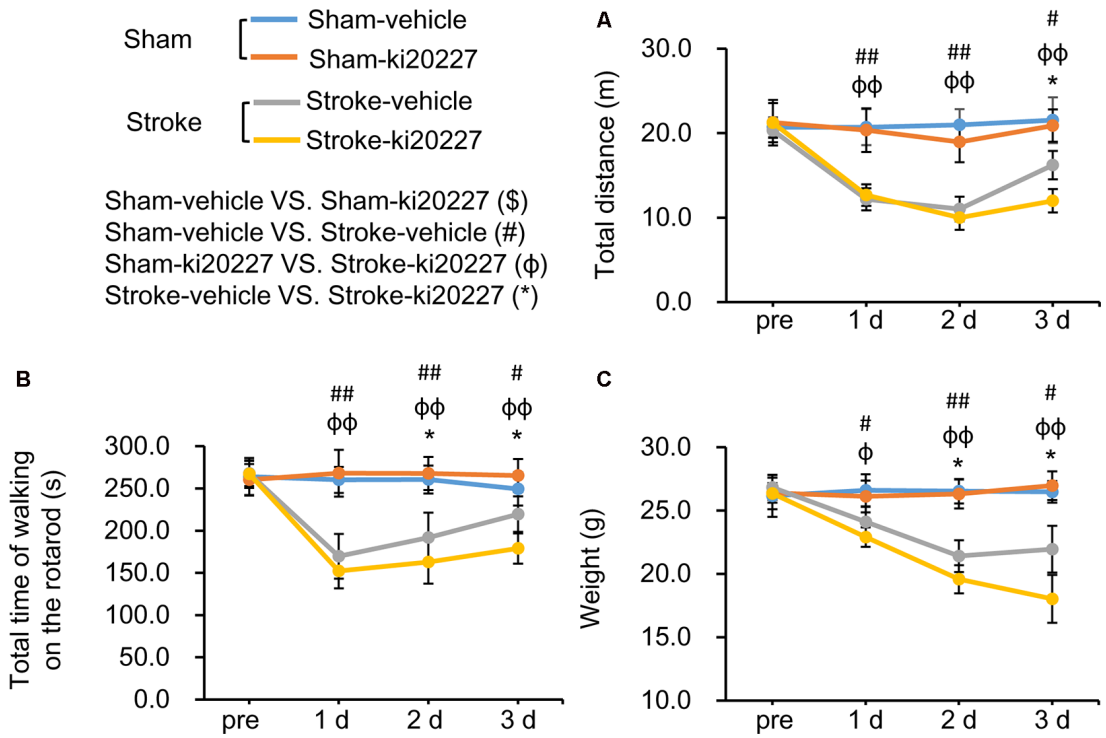

FIGURE 5 | ki20227-induced behavioral deficits after global ischemia–reperfusion. **(A)** The tracks of the vehicle-treated sham, ki20227-treated sham, vehicle-treated stroke, and ki20227-treated stroke mice before and after the experiments. **(B)** There were significant differences in the total time spent on the rotarod between groups. **(C)** There were significant differences in mouse weight between groups. Vehicle-treated vs. ki20227-treated sham mice ($), vehicle-treated sham mice vs. vehicle-treated stroke mice (#), ki20227-treated sham mice vs. ki20227-treated stroke mice (ϕ), and vehicle-treated vs. ki20227-treated stroke mice (*). $^{*}p < 0.05$, $^{\#}p < 0.05$, $^{\#\#}p < 0.01$, $^{\phi}p < 0.05$, $^{\phi\phi}p < 0.01$, $n \geq 6$.

on the microglial survival rate. The role of the microglia after stroke is still controversial. Treatment with PLX3397 may cause a remarkable change in microglial cell density, while ki20227-induced inhibition of CSF1R does not induce a notable change in the number of microglia. In this study, we selected ki20227 to prevent the elimination of a large number of microglia due to CSF1R inhibition.

Used as an antagonist, ki20227 induced a marked microglial de-ramification in both sham and ischemic mice, suggesting that morphological changes in the microglia are closely related to the CSF1R cascade. Importantly, microglia proliferation and soma size are more obvious markers of activation; no changes in the microglial soma size and survival indicated that the microglia were not activated, although there were slight modifications in the microglial processes and microglia proliferation. In the sham group, ki20227, unlike other strong microglial inhibitors, did not cause the loss of a large number of microglia, but had a similar effect as GW2580, suggesting that the drug did not lead to microglial activation. Additionally, inflammatory cytokines, which are markers of activated microglia, were not significantly changed by ki20227 treatment. There results suggested that the drug did not lead to microglia activation in sham mice. Furthermore, ki20227 treatment resulted in a decline in the number of microglia and BrdU-labeled microglia in stroke mice. This result suggests that CSF1R inhibition reduced the number of newly proliferated microglia after global cerebral ischemia. Moreover, ki20227 treatment showed that a considerable number of microglial processes were retracted, suggesting that CSF1R inhibition induced excessive de-ramification of activated microglia after global cerebral ischemia. In addition to exerting surveillance functions, the microglia exhibit pro-inflammatory and neurotropic activities *via* increased expressions of cell-surface receptors and the release of cytokines and chemokines (Perego et al., 2011). During reperfusion, the increased release of microglial cytokines, chemokines, and other pro-inflammatory molecules in response to the ischemic stimuli suggested that these molecules play crucial roles in the activation, differentiation, regulation, and the functions of innate and adaptive immunity after stroke (Ramesh et al., 2013). These cytokine-related genes, such as TNF-α, iNOS, and TNF-β, which are pro- or anti-inflammatory, may contribute to the impairment of neuronal and brain damage after stroke (Lin et al., 2016). We observed a significant enhancement of the cytokine-related genes such as TNF-α and iNOS and the downregulated gene TNF-β in ischemic mice after ki20227 treatment, indicating that these cytokine-related genes may be a risk factor after stroke. Stroke caused an increased release of cytokines/chemokines such as CCL and its ligands MCP-1/CCL2, IP-10/CXCL10, and RANTES/CCL5. These cytokine/chemokine networks related to the activation of the microglia were reestablished after stroke,

suggesting that ki20227 treatment further caused excessive immune response after ischemia–reperfusion. Furthermore, we found that stroke induced a high expression of CSF1R, which is closely related to microglial proliferation. CSF1R expression was significantly decreased after ki20227 treatment, suggesting that stroke-related microglial proliferation may be dependent on the CSF1R signaling pathway. In addition, as a marker of monocytes, increased CCR2 mRNA expression is indicative of monocyte infiltration after stroke. However, it was previously shown that CCR2 mRNA expression is inhibited by ki20227 (Ohno et al., 2008). Whether the infiltration of monocytes has a robust effect on neuronal structure remains to be evaluated in future studies.

In sham-operated mice, the neurons of the somatosensory cortex were not affected by ki20227 treatment. However, ki20227 treatment exacerbated neurodegeneration after stroke, which suggested that CSF1R is necessary for the recovery of neurons damaged by stroke. In addition, the reversible recovery of dendritic structures was not affected by ki20227 treatment during reperfusion, suggesting that CSF1R inhibition has less influence on the integrity of neural networks than does local blood flow (Zhu et al., 2017b). Although ki20227 treatment did not change the reversible recovery of dendritic structures after ischemia, our study showed that ki20227 treatment exacerbated the loss of dendritic spines when combined with ischemia, indicating that CSF1R inhibition changed the plasticity of the dendritic spine during ischemia. Whether ki20227 has a long-term effect on the stability of the neuronal structure and the plasticity of cortical circuits remains to be evaluated in future studies. Damage to neurons is a major manifestation of stroke in the CNS. An unstable neuronal structural and functional state is considered crucial for neural development and circuit plasticity under normal physical conditions (Grutzendler et al., 2002; Davalos et al., 2005; Zuo et al., 2005; Bhatt et al., 2009); however, this state can be changed by ischemia and other pathological insults (Hasbani et al., 2001; Heiss et al., 2017; Suresh and Dunaevsky, 2017; Zhu et al., 2017b). The unstable neuronal structural and functional state after ischemia is thought to be related to the rewiring of neuronal circuits and to contribute to the recovery of cortical function (Dijkhuizen et al., 2001; Ward and Cohen, 2004; Murphy and Corbett, 2009). In our present study, the behavioral tests showed that ki20227 treatment alone did not affect the behavior of healthy mice but that ki20227 treatment further reduced the activity of the mice after stroke, suggesting that CSF1R inhibition may have accumulative and detrimental effects on the restoration of behavioral ability following ischemia.

In summary, this study suggests that pharmacological inhibition of CSF1R by ki20227 causes excessive microglial de-ramification and inflammatory responses, induces a decrease in microglial proliferation, and aggravates neuronal degeneration, the loss of dendritic spines, and behavioral deficits after transient global cerebral ischemia. Therefore, inhibition of CSF1R in the microglia may have a negative clinical effect following ischemic stroke.

DATA AVAILABILITY STATEMENT

All datasets generated for this study are included in the article.

ETHICS STATEMENT

This study was carried out in accordance with the regulations of Lanzhou University and the ARRIVE guidelines. All experimental procedures and protocols were approved by the Ethics Committee of Lanzhou University. Written informed consent was obtained from the owners for the participation of their animals in this study.

AUTHOR CONTRIBUTIONS

FJ, BH, and HR designed the study. FJ, BH, CJ, GW, ZW, DW, YK, JS, and PW performed the experiments. MZ and DW analyzed the data. FJ, BH, and CJ wrote the article.

FUNDING

This study was supported by Lanzhou Science and Technology Bureau Project, Lanzhou, Gansu, China (No. 2018-4-68), Cuiying Graduate Supervisor Applicant Training Program of Lanzhou University Second Hospital (No. CYDSPY201902), Cuiying Students Research Ability Training program of Lanzhou University Second Hospital (No. CYXZ2020-14), National Innovation and Entrepreneurship Training Program for College Students (No. 202010730223), Cuiying Scientific and Technological Innovation Program of Lanzhou University Second Hospital (No. CY2018-MS08), The Youth Innovation Promotion Association of the Chinese Academy of Sciences (2017413 PW), and Shenzhen Government Basic Research Grants (JCYJ20170411140807570 PW).

REFERENCES

Bell, R. D., Winkler, E. A., Sagare, A. P., Singh, I., Larue, B., Deane, R., et al. (2010). Pericytes control key neurovascular functions and neuronal phenotype in the adult brain and during brain aging. *Neuron* 68, 409–427. doi: 10.1016/j.neuron.2010.09.043

Bhatt, D. H., Zhang, S. X., and Gan, W. B. (2009). Dendritic spine dynamics. *Ann. Rev. Physiol.* 71, 261–282. doi: 10.1146/annurev.physiol.010908.163140

Davalos, D., Grutzendler, J., Yang, G., Kim, J. V., Zuo, Y., Jung, S., et al. (2005). ATP mediates rapid microglial response to local brain injury *in vivo*. *Nat. Neurosci.* 8, 752–758. doi: 10.1038/nn1472

Denes, A., Thornton, P., Rothwell, N. J., and Allan, S. M. (2010). Inflammation and brain injury: acute cerebral ischaemia, peripheral and central inflammation. *Brain Behav. Immun.* 24, 708–723. doi: 10.1016/j.bbi.2009.09.010

Denieffe, S., Kelly, R. J., Mcdonald, C., Lyons, A., and Lynch, M. A. (2013). Classical activation of microglia in CD200-deficient mice is a consequence of blood brain barrier permeability and infiltration of peripheral cells. *Brain Behav. Immun.* 34, 86–97. doi: 10.1016/j.bbi.2013.07.174

Dijkhuizen, R. M., Ren, J. M., Mandeville, J. B., Wu, O. N., Ozdag, F. M., Moskowitz, M. A., et al. (2001). Functional magnetic resonance imaging of reorganization in rat brain after stroke. *Proc. Natl. Acad. Sci. U S A* 98, 12766–12771. doi: 10.1073/pnas.231235598

Elmore, M. R. P., Najafi, A. R., Koike, M. A., Dagher, N. N., Spangenberg, E. E., Rice, R. A., et al. (2014). Colony-stimulating factor 1 receptor signaling is necessary for microglia viability, unmasking a microglia progenitor cell in the adult brain. *Neuron* 82, 380–397. doi: 10.1016/j.neuron.2014.02.040

Erblich, B., Zhu, L., Etgen, A. M., Dobrenis, K., and Pollard, J. W. (2011). Absence of colony stimulation factor-1 receptor results in loss of microglia, disrupted brain development and olfactory deficits. *PLoS One* 6:e26317.

Fontainhas, A. M., Wang, M., Liang, K. J., Chen, S., Mettu, P., Damani, M., et al. (2011). Microglial morphology and dynamic behavior is regulated by ionotropic glutamatergic and GABAergic neurotransmission. *PLoS One* 6:e15973. doi: 10.1371/journal.pone.0015973

Ginhoux, F., Greter, M., Leboeuf, M., Nandi, S., See, P., Gokhan, S. et al. (2014). Fate mapping analysis reveals that adult microglia derive from primitive macrophages. *Science* 330, 841–845.

Grutzendler, J., Kasthuri, N., and Gan, W. B. (2002). Long-term dendritic spine stability in the adult cortex. *Nature* 420, 812–816. doi: 10.1038/nature01276

Hasbani, M. J., Schlief, M. L., Fisher, D. A., and Goldberg, M. P. (2001). Dendritic spines lost during glutamate receptor activation reemerge at original sites of synaptic contact. *J. Neurosci.* 21, 2393–2403. doi: 10.1523/jneurosci.21-07-02393.2001

Heiss, J. K., Barrett, J., Yu, Z. Z., Haas, L. T., Kostylev, M. A., and Strittmatter, S. M. (2017). Early activation of experience-independent dendritic spine turnover in a mouse model of Alzheimer's disease. *Cereb. Cortex* 27, 3660–3674. doi: 10.1093/cercor/bhw188

Hou, B., Ju, F., Guo, X., Wang, D., Cheng, X., Khan, A., et al. (2016). Ki20227 influences the morphology of microglia and neurons through inhibition of CSF1R during global ischemia. *Int. J. Clin. Exp. Pathol.* 9, 12459–12469. Available online at: http://www.ijcep.com/files/ijcep0036593.pdf.

Iadecola, C., and Anrather, J. (2011). The immunology of stroke: from mechanisms to translation. *Nat. Med.* 17, 796–808. doi: 10.1038/nm.2399

Jolivel, V., Bicker, F., Biname, F., Ploen, R., Keller, S., Gollan, R., et al. (2015). Perivascular microglia promote blood vessel disintegration in the ischemic penumbra. *Acta Neuropathol.* 129, 279–295. doi: 10.1007/s00401-014-1372-1

Ju, F., Ran, Y., Zhu, L., Cheng, X., Gao, H., Xi, X., et al. (2018). Increased BBB permeability enhances activation of microglia and exacerbates loss of dendritic spines after transient global cerebral ischemia. *Front. Cell. Neurosci.* 12:236. doi: 10.3389/fncel.2018.00236

Kettenmann, H., Hanisch, U. K., Noda, M., and Verkhratsky, A. (2011). Physiology of microglia. *Physiol. Rev.* 91, 461–553. doi: 10.1152/physrev.00011.2010

Khan, A., Ju, F., Xie, W., Tariq Hafeez, M., Cheng, X., Yang, Z., et al. (2017). Transcriptomic analysis reveals differential activation of microglial genes after ischemic stroke in mice. *Neuroscience* 348, 212–227. doi: 10.1016/j.neuroscience.2017.02.019

Kreutzberg, G. W. (1996). Microglia: a sensor for pathological events in the CNS. *Trends Neurosci.* 19, 312–318. doi: 10.1016/0166-2236(96)10049-7

Lee, T. C., Kashyap, R. L., and Chu, C. N. (1994). Building skeleton models *via* 3-D medial surface axis thinning algorithms. *CVGIP: Graphical Models Image Process.* 56, 462–478. doi: 10.1006/cgip.1994.1042

Li, J., Chen, K., Zhu, L. and Pollard, J. W. (2006). Conditional deletion of the colony stimulating factor-1 receptor (c-fms proto-oncogene) in mice. *Genesis* 44, 328–335.

Lin, R., Cai, J., Kostuk, E. W., Rosenwasser, R., and Iacovitti, L. (2016). Fumarate modulates the immune/inflammatory response and rescues nerve cells and neurological function after stroke in rats. *J. Neuroinflammation* 13:269. doi: 10.1186/s12974-016-0733-1

Masuch, A., Shieh, C. H., Van Rooijen, N., Van Calker, D., and Biber, K. (2016). Mechanism of microglia neuroprotection: involvement of P2X7, TNFα and valproic acid. *Glia* 64, 76–89. doi: 10.1002/glia.22904

Masuda, T., Croom, D., Hida, H., and Kirov, S. A. (2011). Capillary blood flow around microglial somata determines dynamics of microglial processes in ischemic conditions. *Glia* 59, 1744–1753. doi: 10.1002/glia.21220

Michell-Robinson, M. A., Touil, H., Healy, L. M., Owen, D. R., Durafourt, B. A., Bar-Or, A., et al. (2015). Roles of microglia in brain development, tissue maintenance and repair. *Brain* 138, 1138–1159. doi: 10.1093/brain/awv066

Miyamoto, A., Wake, H., Ishikawa, A. W., Eto, K., Shibata, K., Murakoshi, H., et al. (2016). Microglia contact induces synapse formation in developing somatosensory cortex. *Nat. Commun.* 7:12540. doi: 10.1038/ncomms12540

Morrison, H. W., and Filosa, J. A. (2013). A quantitative spatiotemporal analysis of microglia morphology during ischemic stroke and reperfusion. *J. Neuroinflammation* 10:4. doi: 10.1186/1742-2094-10-4

Mosher, K. I., Andres, R. H., Fukuhara, T., Bieri, G., Hasegawa-Moriyama, M., He, Y., et al. (2012). Neural progenitor cells regulate microglia functions and activity. *Nat. Neurosci.* 15, 1485–1487. doi: 10.1038/nn.3233

Murphy, T. H., and Corbett, D. (2009). Plasticity during stroke recovery: from synapse to behavior. *Nat. Rev. Neurosci.* 10, 861–872. doi: 10.1038/nrn2735

Nimmerjahn, A., Kirchhoff, F., and Helmchen, F. (2005). Resting microglial cells are highly dynamic surveillants of brain parenchyma *in vivo*. *Science* 308, 1314–1318. doi: 10.1126/science.1110647

Ohno, H., Kubo, K., Murooka, H., Kobayashi, Y., Nishitoba, T., Shibuya, M., et al. (2006). A c-Fms tyrosine kinase inhibitor, Ki20227, suppresses osteoclast differentiation and osteolytic bone destruction in a bone metastasis model. *Mol. Cancer Ther.* 5, 2634–2643. doi: 10.1158/1535-7163.mct-05-0313

Ohno, H., Uemura, Y., Murooka, H., Takanashi, H., Tokieda, T., Ohzeki, Y., et al. (2008). The orally-active and selective c-Fms tyrosine kinase inhibitor Ki20227 inhibits disease progression in a collagen-induced arthritis mouse model. *Eur. J. Immunol.* 38, 283–291. doi: 10.1002/eji.200737199

Olmos-Alonso, A., Schetters, S. T., Sri, S., Askew, K., Mancuso, R., Vargas-Caballero, M., et al. (2016). Pharmacological targeting of CSF1R inhibits microglial proliferation and prevents the progression of Alzheimer's-like pathology. *Brain* 139, 891–907. doi: 10.1093/brain/awv379

Orr, A. G., Orr, A. L., Li, X. J., Gross, R. E., and Traynelis, S. F. (2009). Adenosine A(2A) receptor mediates microglial process retraction. *Nat. Neurosci.* 12, 872–878. doi: 10.1038/nn.2341

Otxoa-De-Amezaga, A., Miro-Mur, F., Pedragosa, J., Gallizioli, M., Justicia, C., Gaja-Capdevila, N., et al. (2019). Microglial cell loss after ischemic stroke favors brain neutrophil accumulation. *Acta Neuropathol.* 137, 321–341. doi: 10.1007/s00401-018-1954-4

Parkhurst, C. N., Yang, G., Ninan, I., Savas, J. N., Yates, J. R., Lafaille, J. J., et al. (2013). Microglia promote learning-dependent synapse formation through brain-derived neurotrophic factor. *Cell* 155, 1596–1609. doi: 10.1016/j.cell.2013.11.030

Perego, C., Fumagalli, S., and De Simoni, M. G. (2011). Temporal pattern of expression and colocalization of microglia/macrophage phenotype markers following brain ischemic injury in mice. *J. Neuroinflammation* 8:174. doi: 10.1186/1742-2094-8-174

Prinz, M., and Priller, J. (2014). Microglia and brain macrophages in the molecular age: from origin to neuropsychiatric disease. *Nat. Rev. Neurosci.* 15, 300–312. doi: 10.1038/nrn3722

Ramesh, G., Maclean, A. G., and Philipp, M. T. (2013). Cytokines and chemokines at the crossroads of neuroinflammation, neurodegeneration and neuropathic pain. *Mediators Inflamm.* 2013:480739. doi: 10.1155/2013/480739

Stence, N., Waite, M., and Dailey, M. E. (2001). Dynamics of microglial activation: a confocal time-lapse analysis in hippocampal slices. *Glia* 33, 256–266. doi: 10.1002/1098-1136(200103)33:3<256::aid-glia1024>3.0.co;2-j

Suresh, A., and Dunaevsky, A. (2017). Relationship between synaptic AMPAR and spine dynamics: impairments in the FXS mouse. *Cereb. Cortex* 27, 4244–4256. doi: 10.1093/cercor/bhx128

Szalay, G., Martinecz, B., Lenart, N., Kornyei, Z., Orsolits, B., Judak, L., et al. (2016). Microglia protect against brain injury and their selective elimination dysregulates neuronal network activity after stroke. *Nat. Commun.* 7:11499. doi: 10.1038/ncomms11499

Tremblay, M. E., Lowery, R. L., and Majewska, A. K. (2010). Microglial interactions with synapses are modulated by visual experience. *PLoS Biol.* 8:e1000527. doi: 10.1371/journal.pbio.1000527

Tremblay, M. E., Stevens, B., Sierra, A., Wake, H., Bessis, A., and Nimmerjahn, A. (2011). The role of microglia in the healthy brain. *J. Neurosci.* 31, 16064–16069. doi: 10.1523/JNEUROSCI.4158-11.2011

Turrin, N. P., and Rivest, S. (2006). Tumor necrosis factor α but not interleukin 1 β mediates neuroprotection in response to acute nitric oxide excitotoxicity. *J. Neurosci.* 26, 143–151. doi: 10.1523/jneurosci.4032-05.2006

Uemura, Y., Ohno, H., Ohzeki, Y., Takanashi, H., Murooka, H., Kubo, K., et al. (2008). The selective M-CSF receptor tyrosine kinase inhibitor

Ki20227 suppresses experimental autoimmune encephalomyelitis. *J. Neuroimmunol.* 195, 73–80. doi: 10.1016/j.jneuroim.2008.01.015

Vinet, J., Weering, H. R., Heinrich, A., Kalin, R. E., Wegner, A., Brouwer, N., et al. (2012). Neuroprotective function for ramified microglia in hippocampal excitotoxicity. *J. Neuroinflammation* 9:27. doi: 10.1186/1742-2094-9-27

Wake, H., Moorhouse, A. J., Jinno, S., Kohsaka, S., and Nabekura, J. (2009). Resting microglia directly monitor the functional state of synapses *in vivo* and determine the fate of ischemic terminals. *J. Neurosci.* 29, 3974–3980. doi: 10.1523/jneurosci.4363-08.2009

Wake, H., Moorhouse, A. J., Miyamoto, A., and Nabekura, J. (2013). Microglia: actively surveying and shaping neuronal circuit structure and function. *Trends Neurosci.* 36, 209–217. doi: 10.1016/j.tins.2012.11.007

Ward, N. S., and Cohen, L. G. (2004). Mechanisms underlying recovery of motor function after stroke. *Arch. Neurol.* 61, 1844–1848. doi: 10.1001/archneur.61.12.1844

Willis, E. F., Macdonald, K. P. A., Nguyen, Q. H., Garrido, A. L., Gillespie, E. R., Harley, S. B. R., et al. (2020). Repopulating microglia promote brain repair in an IL-6-dependent manner. *Cell* 180, 833.e16–846.e16. doi: 10.1016/j.cell.2020.02.013

Winship, I. R., and Murphy, T. H. (2008). *In vivo* calcium imaging reveals functional rewiring of single somatosensory neurons after stroke. *J. Neurosci.* 28, 6592–6606. doi: 10.1523/jneurosci.0622-08.2008

Zhan, Y., Paolicelli, R. C., Sforazzini, F., Weinhard, L., Bolasco, G., Pagani, F., et al. (2014). Deficient neuron-microglia signaling results in impaired functional brain connectivity and social behavior. *Nat. Neurosci.* 17, 400–406. doi: 10.1038/nn.3641

Zhang, S., Boyd, J., Delaney, K., and Murphy, T. H. (2005). Rapid reversible changes in dendritic spine structure *in vivo* gated by the degree of ischemia. *J. Neurosci.* 25, 5333–5338. doi: 10.1523/jneurosci.1085-05.2005

Zhu, L., Wang, L., Ju, F., Khan, A., Cheng, X., and Zhang, S. (2017a). Reversible recovery of neuronal structures depends on the degree of neuronal damage after global cerebral ischemia in mice. *Exp. Neurol.* 289, 1–8. doi: 10.1016/j.expneurol.2016.12.002

Zhu, L., Wang, L., Ju, F., Ran, Y., Wang, C., and Zhang, S. (2017b). Transient global cerebral ischemia induces rapid and sustained reorganization of synaptic structures. *J. Cereb. Blood Flow Metab.* 37, 2756–2767. doi: 10.1177/0271678x16674736

Zuo, Y., Lin, A., Chang, P., and Gan, W. B. (2005). Development of long-term dendritic spine stability in diverse regions of cerebral cortex. *Neuron* 46, 181–189. doi: 10.1016/j.neuron.2005.04.001

Conflict of Interest: The authors declare that the research was conducted in the absence of any commercial or financial relationships that could be construed as a potential conflict of interest.

frontiers in Cellular Neuroscience

BRIEF RESEARCH REPORT
published: 02 February 2021
doi: 10.3389/fncel.2021.633280

The Anti-apoptosis Effect of Single Electroacupuncture Treatment *via* Suppressing Neuronal Autophagy in the Acute Stage of Ischemic Stroke Without Infarct Alleviation

*Ying Xing[1], Min Zhang[2], Man-Man Wang[1], Ya-Shuo Feng[1], Fang Dong[3] and Feng Zhang[1,4]**

[1]Department of Rehabilitation Medicine, The Third Hospital of Hebei Medical University, Shijiazhuang, China, [2]Department of Pathophysiology, Hebei Medical University, Shijiazhuang, China, [3]Department of Clinical Laboratory Medicine, The Third Hospital of Hebei Medical University, Shijiazhuang, China, [4]Hebei Key Laboratory of Critical Disease Mechanism and Intervention, Shijiazhuang, China

OPEN ACCESS

Edited by:
Zhang Pengyue,
Yunnan University of Traditional Chinese Medicine, China

Reviewed by:
Long Yu Wei,
Beijing University of Chinese Medicine, China
Kewei Yu,
Fudan University, China

***Correspondence:**
Feng Zhang
zjk20019@126.com

Specialty section:
This article was submitted to Cellular Neuropathology, a section of the journal Frontiers in Cellular Neuroscience

Received: 25 November 2020
Accepted: 11 January 2021
Published: 02 February 2021

Citation:
Xing Y, Zhang M, Wang M-M, Feng Y-S, Dong F and Zhang F (2021) The Anti-apoptosis Effect of Single Electroacupuncture Treatment via Suppressing Neuronal Autophagy in the Acute Stage of Ischemic Stroke Without Infarct Alleviation. Front. Cell. Neurosci. 15:633280. doi: 10.3389/fncel.2021.633280

The main purpose of the study was to investigate the antiapoptotic effect of electroacupuncture (EA) in the acute stage of ischaemic stroke in rats. The cerebral ischemia model was established by middle cerebral artery occlusion (MCAO)/reperfusion in rats. A single EA treatment was performed at the acute stage of ischaemic stroke. The neurological function, brain water content, apoptotic cell number, and cerebral infarct volume were assessed in stroke rats. The expression of autophagy-related proteins (LC3II/I, Beclin1, P62, and LAMP1), Sirtuin 1 (SIRT1), p-JNK, p-ERK1/2, and cleaved caspase-3 (CCAS3) were measured by Western blot, immunofluorescence, and immunohistochemistry. Rapamycin (RAP, an activator of autophagy) was used to confirm the antiapoptotic effect of EA *via* regulating autophagy. The brain edema infarct size and apoptotic cell number were increasing within 3 days following stroke, and brain edema reached its peak at 24 h after stroke. EA treatment at 24 h after ischaemic stroke obviously suppressed the number of apoptotic cells and brain edema. However, there were no significant differences in infarct volumes among EA-12 h, EA-24 h, and MCAO/R group. Moreover, EA treatment at 24 h after ischaemic stroke obviously suppressed the expression of CCAS3, LC3II/I, Beclin1 while increasing the level of P62 and LAMP1 and hence mediating autophagy, which was reversed by RAP. Meanwhile, the expression of SIRT1, p-ERK1/2, p-JNK were promoted by EA at 24 h after ischaemic stroke. In conclusion, EA treatment may suppress apoptosis possibly *via* regulating autophagy in the acute period after ischaemic stroke, hence reducing brain injury.

Keywords: stroke, autophagy, apoptosis, electroacupuncture, SIRT1, JNK

INTRODUCTION

Stroke is a common disease that causes disability and death worldwide. The occurrence of acute first-ever ischaemic stroke is significantly higher than acute first-ever hemorrhagic and other types of stroke, according to the Global Burden of Disease (GBD) 2015 study (Roth et al., 2017). Ischaemic stroke is a fatal disease that is capable of resulting in neurological defects due to the occlusion of blood flow to certain brain areas (He et al., 2018). Recombinant tissue-type plasminogen activator (rt-PA) treatment has been well established for ischaemic stroke therapy, but only a few ischaemic stroke patients can obtain benefits from rt-PA treatment because of the restrained therapeutic time window (Shi et al., 2015). Therefore, effective and safe therapy is urgently required in a clinical setting.

Electroacupuncture (EA) is a modified technique based on traditional acupuncture therapy; EA stimulates selected acupoints *via* an electrical current, replacing manual manipulations and bringing more reproducible outcomes both in clinical settings and the laboratory (Liu et al., 2019). EA has been widely adopted as a rehabilitation method for stroke patients in clinical settings, which can alleviate neurological dysfunction without obvious adverse effects (Kim et al., 2018). According to the meridians theory of Traditional Chinese Medicine (TCM), spasticity and flaccid paralysis after stroke are two different performances involving in an imbalance of "liver qi," and the acupoints of the Stomach and Large Intestines, such as Zusanli and Quchi, could be used for rebalancing the "liver qi" (Chang et al., 2020; Zou et al., 2020). The EA at acupoints of Quchi and Zusanli is commonly applied in stroke (Zou et al., 2020). In our previous studies, we demonstrated that EA at Quchi and Zusanli acupoints might exert an anti-apoptosis effect by activating the MAPK pathway (Xing et al., 2018). However, whether EA can regulate neuronal autophagy levels to alleviate apoptosis remains unclear.

Autophagy is a catabolic process that occurs with the formation of autophagolysosome, which acts as removing impaired cellular and molecular components (Moreira et al., 2017). Autophagy may be activated in various conditions, including hypoxic stimulus, oxidative stress, starvation, and nonfunctional protein accumulation (Zhang and Chen, 2018). To the best of our knowledge, excessive activation of autophagy may facilitate neuronal death *via* precipitating neurocytes to self-digest their own constituents or by interacting with the apoptotic cascade around the ischaemic areas following ischaemic stroke (Liu et al., 2016). EA might improve cerebral ischemia/reperfusion (I/R) injury by suppressing excessive autophagy during the reperfusion period, which might be a vital cause of EA protecting neurocytes (Ting et al., 2017).

Sirtuin 1 (SIRT1) is a nicotine adenine dinucleotide (NAD^+)-dependent class III histone deacetylase and expresses in all cell types, and SIRT1 is associated with the alleviation of hippocampus ischemia/reperfusion injury, which is involved in neuronal autophagy and apoptosis (Zhou et al., 2018). The activation of SIRT1 plays a crucial role in maintaining redox balance and mitochondrial function and suppressing apoptosis *via* activating the MAPK signaling pathway (Becatti et al., 2018). Similar to ERKs, JNKs are a subfamily of MAPKs and are richly expressed in the central nervous system. Furthermore, the regulation of the JNK pathway has been proven to play a neuroprotective role after ischaemic stroke (Xing et al., 2018). Interestingly, the inhibition of the JNK pathway is also involved in mitigating autophagy and reducing neuronal apoptosis (Xue et al., 2017). Therefore, the JNK pathway might be a downstream pathway of SIRT1 when it comes to taking part in the regulation of autophagy.

In the current study, we explore the effect of EA treatment in the early stage of I/R and the detailed mechanism of EA in inhibiting apoptosis by regulating autophagy possibly through the SIRT1-JNK and ERK pathway.

MATERIALS AND METHODS

Experimental Animals

All experimental animal protocols were approved by the Animal Care and Use Committee of Hebei Medical University, and all the procedures were conducted according to the recommendations of the Laboratory Animal—Guide for Ethical Review of Animal Welfare (GB/T35892–2018). A total of male Sprague–Dawley rats (n = 284, 230–270 g) were purchased from the Laboratory Animal Centre of Hebei Medical University, Hebei, China.

Inclusion and Exclusion Criteria

A neurological behavior score assessment was used to determine the inclusion criteria of rats with I/R. Rats whose score was between 1 and 3 were included. All rats were randomly allocated to different groups by computer-generated randomization schedules. For drug experiments, the rats were randomly allocated to groups before drug administration, and rats with scores between 1 and 3 were included. The details are shown in **Supplementary Table 1**.

Animals' Groupings

The animal groupings are shown in **Figure 1A**. The details are shown in the **Supplementary Material**.

Drug Injection

Rapamycin (RAP, 3 mg/kg/day, Selleck Chemicals, United States) or control (2% DMSO, 30% PEG, 5% Tween 80) was injected intraperitoneally (i.p) for three consecutive days, and the last injection was conducted 30 min before the Middle cerebral artery occlusion (MCAO) surgery.

Middle Cerebral Artery Occlusion (MCAO)

Male Sprague–Dawley rats (250–280 g) were housed in the same condition during a 12 h light/dark cycle and used to establish the MCAO/reperfusion model, as previously described. In short, the rats were anesthetized *via* intraperitoneal injection of 3% sodium pentobarbital (50 mg/kg) and fixed on the operating table. The rectal temperature of the rats was kept at 37 ± 0.5°C during the whole procedure *via* a heating pad. Subsequently, the right common carotid artery (CCA), internal carotid artery (ICA), and external carotid artery (ECA) were isolated; then CCA and ECA were ligated with a thread. The origin of the middle cerebral artery was occluded for 2 h with a nylon suture,

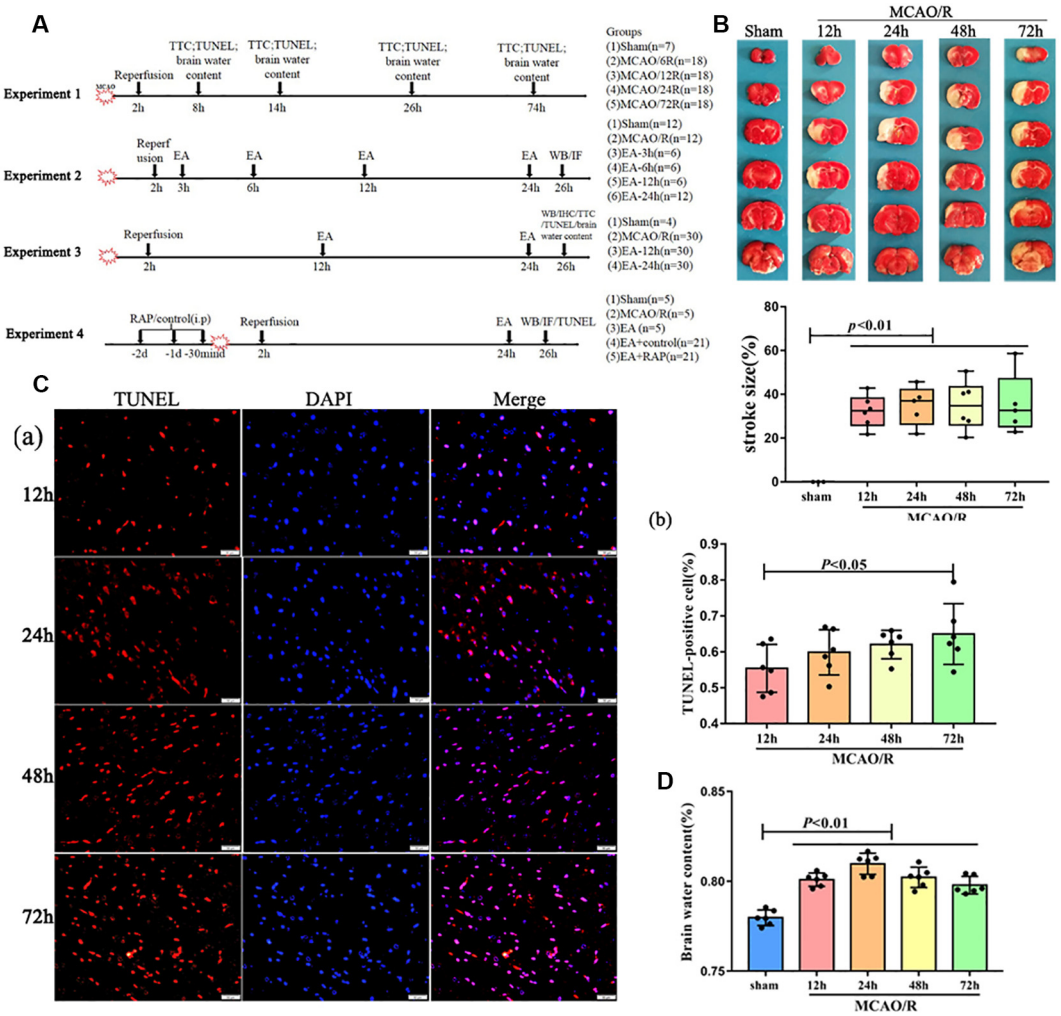

FIGURE 1 | The pathology damage after ischemia/reperfusion (I/R) within 3 days. **(A)** Experimental groups and the protocol. **(B)** 2,3,5-Triphenyltetrazolium Chloride (TTC) staining and the statistical analysis showing cerebral infarct volume of the rats. **(Ca)** Terminal deoxynucleotidyl transferase dUTP nick-end labeling (TUNEL) staining showing several apoptotic cells in the penumbra of the infarct area of rats. **(Cb)** Bar diagram showing the number of apoptotic cells. **(D)** Bar diagram showing the percentage of the water content of the brain.

which was inserted from the left ECA into the ICA. Afterward, the suture was withdrawn for blood reperfusion. The sham group underwent the same procedure without the insertion of the nylon suture. Finally, the rats returned to their cages and were permitted free access to water and food following recovery from anesthesia. Successful occlusions (<20% baseline) and reperfusion were confirmed by Laser-doppler flowmetry.

Neurological Behaviors Assessment

The neurological deficits score was used in all rats 2 h after reperfusion in the blind method, as described previously (Longa et al., 1989). The details are shown in the **Supplementary Material**.

Cerebral Edema Measurements

The brain tissues were immediately weighed to measure the wet weight (WW) and then were placed in a drying oven at 70°C. After drying for 72 h, brain tissues were measured again to obtain the dry weight (DW). A percentage of brain water content was calculated by the following formula: $(WW - DW)/WW \times 100\%$.

Electroacupuncture Stimulation

EA treatment was performed at the acupoints of Quchi (LI11) and Zusanli (ST36) in the right affected limb using an apparatus (Model G6805–2A; Shanghai Huayi Company, Shanghai, China). The specific methods were as per a previous method (Xing et al., 2018). The stimulation (disperse-dense waves of 4/20 Hz, 4 V) lasted for 30 min.

TTC (2,3,5-Triphenyltetrazolium Chloride) Staining

The infarct size was measured as described. Six rats in each group were sacrificed, and the fresh brains were quickly obtained and

then immediately frozen at −20°C for 20 min. Then, the brain tissues were sectioned coronally into six slices (2-mm/section) for TTC staining. The slices were stained in 2% TTC at 37°C for 30 min. Finally, the stained slices were photographed with a Canon camera, and the infarct size percentage (%) was calculated using ImageJ.

TUNEL Staining

Terminal deoxynucleotidyl transferase dUTP nick-end labeling (TUNEL) staining was used to assess neuronal apoptosis using the *in situ* Cell Death Detection Kit (Roche, Mannheim, Germany). The brains were treated with 4% formaldehyde at 4°C for 24 h, followed by embedding in paraffin. Subsequently, those brains were cut into 5-um-thick coronal slices. Afterward, brain slices were treated with proteinase K for 15 min and quenched with 3% H_2O_2 for 10 min at the door temperature. Following incubating in the TUNEL reaction mixture for 60 min, the cell nuclei were stained by DAPI, and red fluorescence of TUNEL-positive cells (apoptotic cells) was assessed with a light microscope (Olympus Corporation, Tokyo, Japan). The five high-power fields of the ischaemic penumbra were randomly selected. The number of apoptotic cells was counted by a blinded observer using the ImageJ software.

Western Blot

The expression levels of Beclin-1, LC3, P62, LAMP1, p-JNK, cleaved caspase-3 (CCAS3), SIRT1, and p-ERK1/2 in the peri-ischaemic hippocampus in each group were analyzed by Western blot. The rats in each group were sacrificed at different times following reperfusion. Subsequently, the peri-ischaemic hippocampus was quickly dissected and then lysised in the RIPA lysis buffer. BCA kits were used to measure protein concentration. Equal amounts of proteins (30 μg) from each sample were subjected to 12% or 15% SDS-PAGE and then transferred to PVDF membranes. Afterward, the PVDF membranes were blocked for 1 h at 37°C. We then prepare the primary antibodies: anti-Beclin1 (1:2,000; Abcam), anti-LC3 (1:1,000; Cell Signal Technology), anti-P62 (1:2,000; Proteintech), anti-LAMP1 (1:1,000; Abcam), anti-p-ERK1/2 (1:1,000; Cell Signal Technology), anti-SIRT1 (1:1,000; Abcam) and CCAS3 (1:300; Proteintech). After incubation with the diluted primary antibodies at 4°C overnight, the PVDF membranes were treated with horseradish peroxidase-conjugated secondary antibodies (1:5,000) for 2 h at room temperature and immunodetected by an enhanced chemiluminescent substrate. The protein expression level was normalized to the GAPDH (1:5,000; Proteintech) protein expression. The band density was analyzed with ImageJ software (1.46r).

Immunofluorescence (IF) and Immunohistochemistry (IHC) Staining

Twenty-four hours following reperfusion, the rats were sacrificed for IF staining. The brains were removed and immediately fixed with PBS containing 4% paraformaldehyde. After 24 h of fixation, the brains were dehydrated, tansparented, and then embedded into paraffin blocks. Paraffin blocks were sectioned into coronal slices of 5 μm thickness. The sections were treated with a blocking solution at 37°C for 30 min. The slices were incubated with an anti-LC3 antibody (1:200, Cell Signal Technology) at 4°C overnight. After washing in PBS for 5 min three times, a secondary antibody was then incubated at 37°C for 30 min. After washing in PBS (pH 7.4) for 15 min, the slices were incubated with DAPI at room temperature for 10 min. IHC was performed by anti-CCAS3 antibody (1:100, Cell Signal Technology) incubation and BDA, staining followed by dehydration. In all sections, the hippocampus fields were selected for photography and the expression levels of the LC3 and CCAS3 proteins were calculated in this area. The average fluorescence intensity and positive cell number were analyzed with the ImageJ software to evaluate the protein expression level in all groups.

Statistical Analysis

Statistical analyses were implemented using SPSS 25.0 software (IBM, Armonk, NY, USA). The data from multiple groups were analyzed using a one-way analysis of variance (ANOVA) followed by a least significant difference (LSD) test. All data are presented as mean ± $\overline{X}$. Statistical significance was set at $p < 0.05$.

RESULTS

The Pathological Changes After I/R Within 3 Days

As shown in **Figure 1**, to detect the injury of cerebral I/R, the rats at different reperfusion times were euthanized and tested with TTC staining, TUNEL staining, and assessment of brain water content. Our results showed that the brain infarct volume and the number of apoptotic cells were increasingly elevated by TTC and TUNEL staining with reperfusion time (**Figures 1B,C**). However, the brain water content of the rats was significantly increased within 3 days after surgery, especially at 24 h ($p < 0.01$; **Figure 1D**).

The Effect of EA Treatment on Autophagy in Ischaemic Stroke Outset

We assessed the levels of autophagy-related proteins (LC3, P62, LAMP1, and Beclin1) after a single EA treatment at 3, 6, 12, and 24 h following MCAO surgery, to clarify the speculation that EA may regulate the autophagy level. As shown in **Figures 2A,C**, the expression of LC3II/I and Beclin1 increased in the MCAO/R group than the sham group ($p < 0.01$). Compared with the MCAO/R group, LC3II/I was significantly increased in the EA-6 h ($p < 0.05$) and EA-12 h group ($p < 0.01$) and Beclin1 was significantly increased in the EA-6 h group ($p < 0.001$), but LC3II/I ($p < 0.05$) was significantly decreased in the EA-24 h group. Also, the expressions of P62 ($p < 0.01$) and LAMP1 ($p < 0.05$) were decreased in the MCAO/R group compared with the sham group. However, the expressions of P62 ($p < 0.05$) and LAMP1 ($p < 0.01$) in the EA-24 h group were increased compared with the MCAO/R group. LC3 levels found with immunofluorescence were significantly increased in the MCAO/R group ($p < 0.01$)

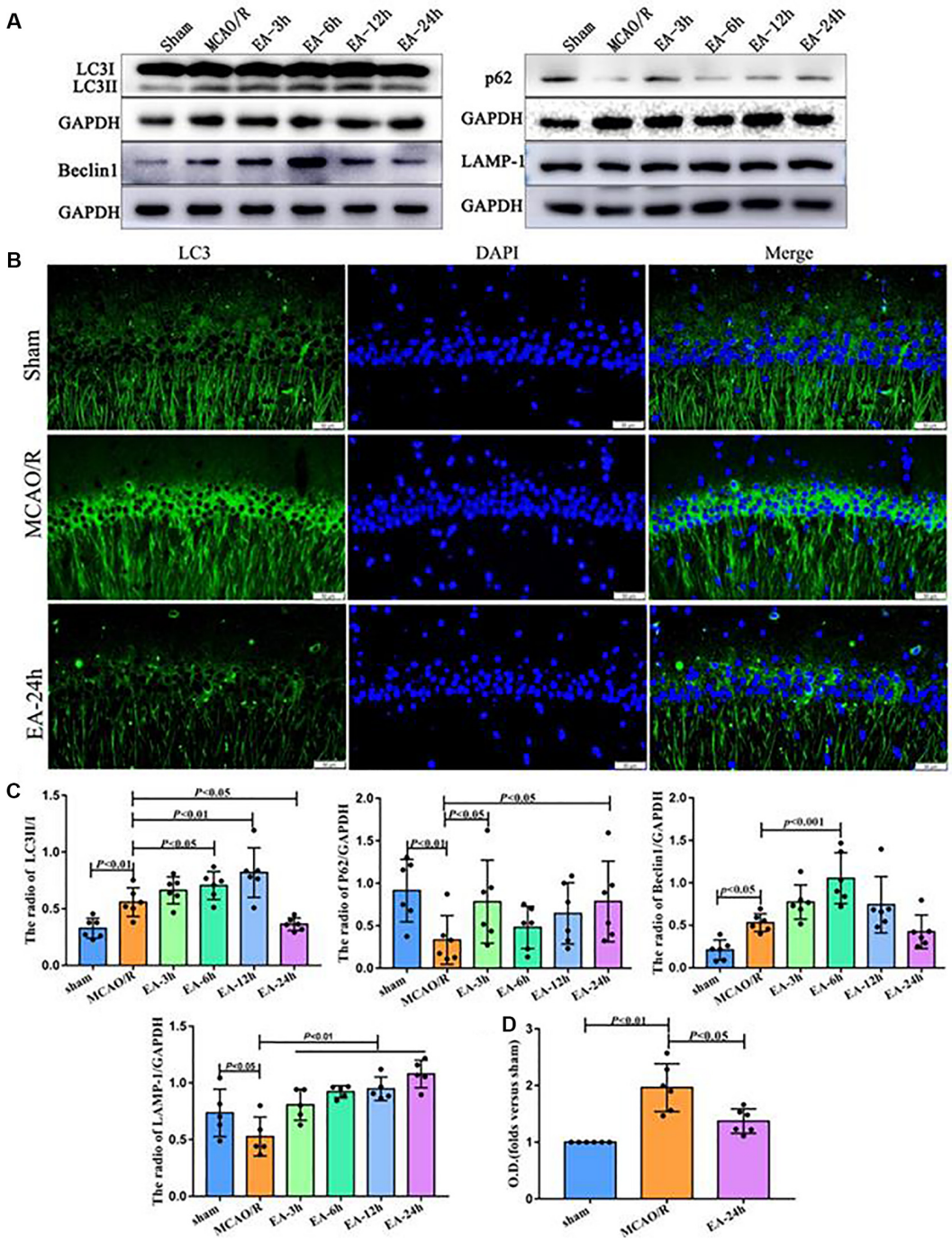

FIGURE 2 | The effect of electroacupuncture (EA) treatment on autophagy in ischaemic stroke outset. **(A)** Western blot analysis showing the difference of LC3II/I, P62, Beclin1, and LAMP-1 after EA treatment at 3, 6, 12, and 24 h *post*-middle cerebral artery occlusion (MCAO) surgery. **(B)** Immunofluorescence (IF) analysis showing the expression difference of LC3 after EA treatment among the sham, MCAO/R, and EA-24 h groups. **(C)** Statistical analysis of the expression of autophagy-related proteins assessed by Western blot. **(D)** Statistical analysis of the LC3 expression assessed by IF. The control images of GAPDH are re-used for illustrative purposes in **Figure 2**.

and decreased in the EA-24 h group ($p < 0.05$; **Figures 2B,D**). These results demonstrate that EA treatment at 24 h after surgery may inhibit autophagy, which might be related to the neuroprotection mechanism.

The Neuroprotective Effect of EA Treatment in Ischaemic Stroke Outset

Since the autophagy level had an obvious change after EA intervention at post-stroke 12 and 24 h, as shown in **Figure 3**,

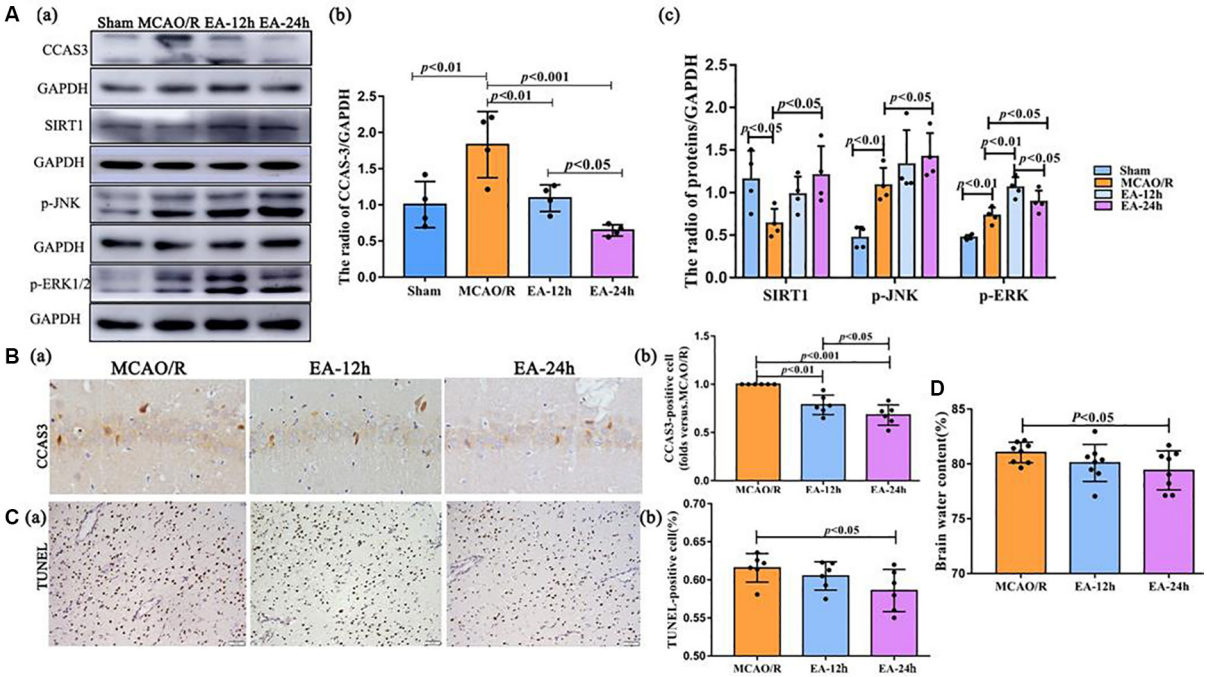

FIGURE 3 | The neuroprotective effect of EA treatment in ischaemic stroke outset. **(Aa–c)** The Western blot and bar diagram shows the expression of cleaved caspase-3 (CCAS3), Sirtuin 1 (SIRT1), p-JNK, and p-ERK1/2 after EA treatment. **(Ba,b)** Immunohistochemistry (IHC) and bar diagram show the number of CCAS3 positive cells in the ipsilateral hippocampus of the rats. **(Ca,b)** TUNEL staining and bar diagram shows the apoptotic cell number in the penumbra of the infarct area of the rats. **(D)** Bar diagram shows the percentage of brain water content. The control images of GAPDH are re-used for illustrative purposes in **Figure 3**.

we next explored the neuroprotective effect of EA at 12 and 24 h after surgery. The TUNEL staining, brain water content assessment, and TTC staining were performed to clarify the neuroprotection of EA against I/R injury. The number of apoptotic cells was obviously reduced in the EA-24 h group than the MCAO/R group ($p < 0.05$; **Figure 3C**). The brain edema was significantly alleviated in the EA-24 h group than the MCAO/R group ($p < 0.05$; **Figure 3D**). However, there was no obvious difference in infarct volume among MCAO/R, EA-12 h, and EA-24 h group ($p > 0.05$), as shown in **Supplementary Figure 1**.

Western blot and IHC were performed to assess the level of CCAS3. This was done because CCAS-3 plays a control role in the phase of apoptosis. As shown in **Figure 3A**, CCAS3 levels were significantly increased in the MCAO/R group than the sham (sham surgery) group ($p < 0.01$). As shown in **Figures 3A,B**, CCAS3 was significantly decreased in the EA-24 h and EA-12 h group compared with the MCAO/R group, and the expression of CCAS3 in the EA-24 h group had a more obvious decrease than the EA-12 h group ($p < 0.05$). These results demonstrate that EA treatment may effectively decrease the apoptosis level at 24 h after stroke.

Also, the levels of SIRT1 were significantly decreased in the MCAO/R group compared with the sham group ($p < 0.05$), but the EA treatment reversed this change at 24 h after MCAO surgery ($p < 0.05$). The p-JNK levels were significantly increased in the MCAO/R group than in the sham group ($p < 0.01$) and were further increased in the EA-24 h group than the MCAO/R group ($p < 0.05$). Furthermore, the p-ERK1/2 levels were significantly increased in the MCAO/R group than the sham group ($p < 0.01$) and were further increased in the EA-12 h ($p < 0.01$) and EA-24 h ($p < 0.05$) groups than the MCAO/R group; also, the expression of p-ERK1/2 in the EA-12 h group was higher than the EA-24 h group ($p < 0.05$; **Figure 3A**). Thereby, we speculate that the antiapoptotic effect of EA might be associated with the SIRT1/JNK pathway and the ERK1/2 pathway.

Rapamycin (Autophagy Activator) Aggravated Apoptosis After EA Treatment at 24 h After MCAO

Finally, we explored the role of autophagy in the process of EA regulating neuronal apoptosis through RAP administration. As shown in **Figures 4Aa,b**, the CCAS3 ($p < 0.001$), LC3-II/I ($p < 0.01$), and Beclin1 ($p < 0.01$) levels were significantly increased, and P62 ($p < 0.05$) and LAMP1 ($p < 0.05$) levels decreased in the MCAO/R group compared with the sham group ($p < 0.01$). EA treatment may reverse the expression of these proteins. After RAP (autophagy activator) treatment, CCAS3 ($p < 0.001$), LC3II/1 ($p < 0.01$), and Beclin1 ($p < 0.001$) levels in the EA + RAP group were significantly increased than the EA and EA+control groups. Moreover, the expressions of P62 and LAMP1 in the EA + RAP group were lower than the EA and

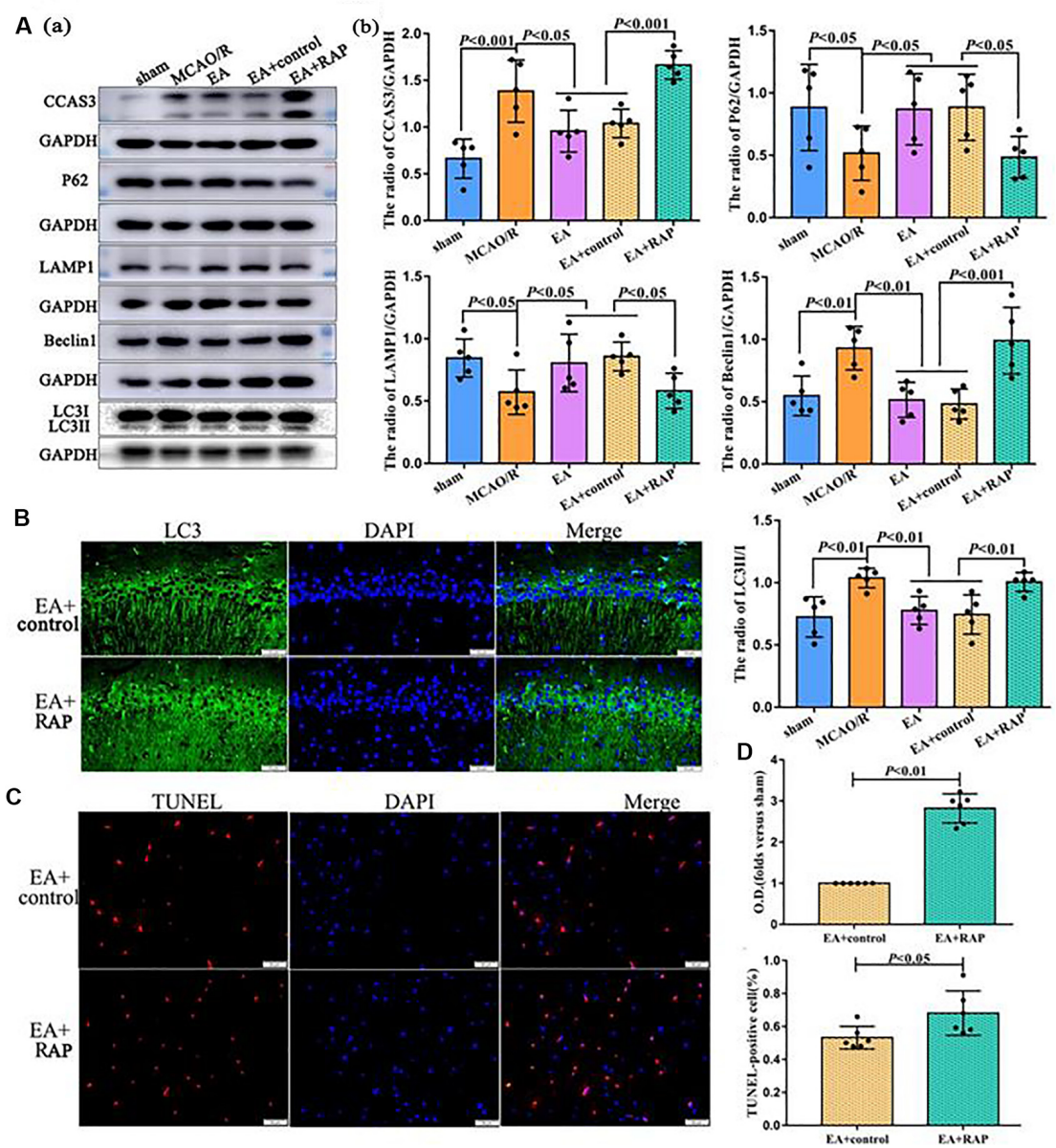

FIGURE 4 | Rapamycin (RAP, autophagy activator) aggravated apoptosis after EA treatment at 24 h after MCAO. **(Aa)** Western blot showing the level of CCAS3 and autophagy-related proteins in the ipsilateral hippocampus of the rats. **(Ab)** Statistical analysis of protein levels as assessed by Western blot. **(B)** IF showing the LC3 levels in the ipsilateral hippocampus of the rats. **(C)** TUNEL staining showing the apoptotic cell levels in the penumbra of the infarct area of rats. **(D)** Statistical analysis of the LC3 levels as assessed by IF staining and the number of apoptotic cells as assessed by TUNEL staining. The control images of GAPDH are re-used for illustrative purposes in **Figure 4**.

EA+control groups ($p < 0.05$). There was no difference in CCAS3, LC3-II/I, Beclin1, P62, and LAMP1 expression between the EA and EA+control groups ($p > 0.05$). The LC3 level as analyzed by immunofluorescence was also significantly increased in the EA + RAP group compared with the EA +control group ($p < 0.01$; **Figures 4B,D**). The number of apoptotic cells in the EA + RAP group was significantly increased compared with the EA+control group ($p < 0.05$; **Figures 4C,D**).

DISCUSSION

In this study, we provide new insights into the detailed mechanism for the antiapoptotic effect of EA and its ability to suppress neuronal autophagy in the early stage of ischaemic stroke, which might be associated with the SIRT1-JNK and ERK pathway. EA treatment is a potential strategy for promoting patient recovery in the acute stage of ischaemic stroke. Autophagy and its capacity to regulate apoptosis might be a

potential therapeutic target for exploring new therapies for ischaemic stroke in the future.

Previous studies have demonstrated that brain edema occurs immediately after cerebral infarction, and the most obvious promotion of cerebral edema has been observed at 24 h after reperfusion (Hu et al., 2014), which is as per our results. Also, as shown in our results, the cerebral infarct area and the number of apoptotic cells in the penumbra of the infarct area increased with time over a period of 3 days following I/R injury. Therefore, initiating early treatment through an effective and safe method is a rational therapeutic strategy to alleviate I/R injury.

EA is a technique that integrates electric stimulation and acupuncture to stimulate specific acupoints, creating more reproducible outcomes compared with acupuncture alone (Liu et al., 2019). EA is involved in regulating various pathological mechanisms pre and post-stroke, including apoptosis, autophagy, and inflammation, and so on (Wang et al., 2011; Shu et al., 2016). A single EA treatment in the acute stage of ischaemic stroke also may alleviate apoptosis, inflammation, and oxidative stress by activating the parasympathetic nervous system (Chi et al., 2018). As shown in our previous studies, EA treatment can significantly exert an antiapoptotic effect after cerebral I/R (Xing et al., 2018). However, the concrete mechanism for the antiapoptotic effect of EA in stroke remains unclear.

In a normal physiological state, the autophagy level in cells is always low; however, it may be significantly activated in response to nutritional deficiency (Sato et al., 2019), oxidative stress (Sun et al., 2019), and immune response (Padhi et al., 2019). Extensive and excessive autophagy may damage cellular components and ultimately cause cell death (Zhao et al., 2010). EA may regulate autophagy activity (Ting et al., 2017), which might be associated with various signaling pathways, including PI3K-AMPK and mTOR pathways (Codogno and Meijer, 2005). In the current study, we found that the expression level of P62 and LAMP1 were significantly increased in the hippocampus at 24 h compared to the MCAO/R group after stroke, and the LC3-II/I ratio was significantly increased at 12 h after MCAO surgery and was decreased at 24 h after MCAO surgery in the hippocampus after EA treatment; this result might be involved in the neuroprotective effect of EA and post-stroke 12 h and 24 h might be the key time points for stroke intervention methods application.

In the subsequent experiments, we found that even a single EA treatment could exert neuroprotective effects *via* reducing the percentage of brain edema and the numbers of apoptotic cells, especially at 24 h following ischemic stroke, which was associated with an antiapoptotic effect. We further confirmed the relationship between autophagy and apoptosis by RAP. The activation of autophagy by RAP reversed the antiapoptotic effect of EA, indicating that the antiapoptotic effect of EA is significantly regulated by the autophagy level.

SIRT1, one of the Sirtuin protein family members, is reported to play a crucial role in the neuroprotective effect against ischaemic injury, which is involved the regulation of autophagy and apoptosis (Zhou et al., 2018). The JNK pathway plays different roles in the early and late stages of cerebral ischaemic stroke (Murata et al., 2012). Also, ERK1/2 has been reported as being involved in EA pretreatment-inhibited apoptosis *via* cannabinoid receptor type 1 (Du et al., 2010). In our study, the expression level of SIRT1 was inhibited after I/R injury, and the expression level of p-ERK and p-JNK was activated following I/R injury. EA intervention markedly promoted the expression of SIRT1, p-ERK, and p-JNK and suppressed neuronal autophagy and apoptosis, thus alleviating brain damage following I/R. Thus, SIRT-1, ERK, and JNK might involve in regulating apoptosis and autophagy after EA treatment in the acute stage of ischaemic stroke.

CONCLUSION

Taken together, the present results demonstrate that EA exerts neuroprotection against cell apoptosis *via* regulating neuronal autophagy following ischaemic stroke. The current study provides novel insights that possibly SIRT1, JNK, and ERK1/2 might be potential therapeutic targets to alleviate neuronal apoptosis after ischaemic stroke. In summary, EA treatment might be a rational strategy for promoting patient recovery in the acute stage of ischaemic stroke, thus benefiting the increasing number of stroke patients worldwide.

DATA AVAILABILITY STATEMENT

The raw data supporting the conclusions of this article will be made available by the authors, without undue reservation.

ETHICS STATEMENT

The animal study was reviewed and approved by Animal Care and Use Committee of Hebei Medical University.

AUTHOR CONTRIBUTIONS

YX and FZ designed the study. YX, MZ, Y-SF, M-MW and FD performed the experiments. FD, M-MW and FZ analyzed the results together. YX and FZ wrote the article. All authors contributed to the article and approved the submitted version.

FUNDING

The present study was supported by the National Natural Science Foundation of China (Nos. 82072531 and 81971228).

SUPPLEMENTARY MATERIAL

The Supplementary Material for this article can be found online at: https://www.frontiersin.org/articles/10.3389/fncel.2021.633280/full#supplementary-material.

REFERENCES

Becatti, M., Barygina, V., Mannucci, A., Emmi, G., Prisco, D., Lotti, T., et al (2018). Sirt1 protects against oxidative stress-induced apoptosis in fibroblasts from psoriatic patients: a new insight into the pathogenetic mechanisms of psoriasis. *Int. J. Mol. Sci.* 19:1572. doi: 10.3390/ijms19061572

Chang, Y. Y., Chiu, C. W., Chen, C. Y., Chang, C. F., Lee, T. C., Lo, L. C., et al. (2020). Efficacy of electroacupuncture on acute abdomen emergency care: study protocol for a randomized controlled trial. *Trials* 224:224. doi: 10.1186/s13063-020-4071-3

Chi, L., Du, K., Liu, D., Bo, Y., and Li, W. (2018). Electroacupuncture brain protection during ischemic stroke: a role for the parasympathetic nervous system. *J. Cereb. Blood. Flow. Metab.* 38, 479–491. doi: 10.1177/0271678X17697988

Codogno, P., and Meijer, A. J. (2005). Autophagy and signaling: their role in cell survival and cell death. *Cell Death Differ.* 12, 1509–1518. doi: 10.1038/sj.cdd.4401751

Du, J., Wang, Q., Hu, B., Peng, Z., Zhao, Y., Ma, L., et al. (2010). Involvement of ERK 1/2 activation in electroacupuncture pretreatment *via* cannabinoid CB1 receptor in rats. *Brain. Res.* 1360, 1–7. doi: 10.1016/j.brainres.2010.07.034

He, Q., Liu, Q., Chen, Y., Meng, J., and Zou, L. (2018). Long-zhi decoction medicated serum promotes angiogenesis in human umbilical vein endothelial cells based on autophagy. *Evid. Based Complement. Alternat. Med.* 2018:6857398. doi: 10.1155/2018/6857398

Hu, J., Wen, Q., Wu, Y., Li, B., and Gao, P. (2014). The effect of butylphthalide on the brain edema, blood-brain barrier of rats after focal cerebral infarction and the expression of Rho A. *Cell Biochem. Biophys.* 69, 363–368. doi: 10.1007/s12013-013-9808-0

Kim, Y. R., Ahn, S. M., Pak, M. E., Lee, H. J., Jung, D. H., Shin, Y. I., et al. (2018). Potential benefits of mesenchymal stem cells and electroacupuncture on the trophic factors associated with neurogenesis in mice with ischemic stroke. *Sci. Rep.* 8:2044. doi: 10.1038/s41598-018-20481-3

Liu, W., Shang, G., Yang, S., Huang, J., Xue, X., Lin, Y., et al. (2016). Electroacupuncture protects against ischemic stroke by reducing autophagosome formation and inhibiting autophagy through the mTORC1-ULK1 complex-Beclin1 pathway. *Int. J. Mol. Med.* 37, 309–318. doi: 10.3892/ijmm.2015.2425

Liu, Y., Zhang, S., Ye, F., Yin, J., Li, S., and Chen, J. D. Z. (2019). Ameliorating effects and mechanisms of chronic electroacupuncture at ST36 in a rodent model of dyspepsia induced by cisplatin. *Neurogastroenterol. Motil.* 31:e13474. doi: 10.1111/nmo.13474

Longa, E. Z., Weinstein, P. R., Carlson, S., and Cummins, R. (1989). Reversible middle cerebral artery occlusion without craniectomy in rats. *Stroke* 20, 84–91. doi: 10.1161/01.str.20.1.84

Moreira, O., Estebanez, B., Martinez-Florez, S., de Paz, J. A., Cuevas, M. J., and Gonzalez-Gallego, J. (2017). Mitochondrial function and mitophagy in the elderly: effects of exercise. *Oxid. Med. Cell. Longev.* 2012798:2012798. doi: 10.1155/2017/2012798

Murata, Y., Fujiwara, N., Seo, J. H., Yan, F., Liu, X., Terasaki, Y., et al. (2012). Delayed inhibition of c-Jun N-terminal kinase worsens outcomes after focal cerebral ischemia. *J. Neurosci.* 32, 8112–8115. doi: 10.1523/JNEUROSCI.0219-12.2012

Padhi, A., Pattnaik, K., Biswas, M., Jagadeb, M., Behera, A., and Sonawane, A. (2019). Mycobacterium tuberculosis LprE suppresses TLR2-dependent cathelicidin and autophagy expression to enhance bacterial survival in macrophages. *J. Immunol.* 203, 2665–2678. doi: 10.4049/jimmunol.1801301

Roth, G. A., Johnson, C., Abajobir, A., Abd-Allah, F., Abera, S. F., Abyu, G., et al. (2017). Global, regional and national burden of cardiovascular diseases for 10 causes, 1990 to 2015. *J. Am. Coll. Cardiol.* 70, 1–25. doi: 10.1016/j.jacc.2017.04.052

Sato, S., Norikura, T., and Mukai, Y. (2019). Maternal quercetin intake during lactation attenuates renal inflammation and modulates autophagy flux in high-fructose-diet-fed female rat offspring exposed to maternal malnutrition. *Food Funct.* 10, 5018–5031. doi: 10.1039/c9fo01134j

Shi, H., Jing, X., Wei, X., Perez, R. G., Ren, M., Zhang, X., et al. (2015). S-allyl cysteine activates the Nrf2-dependent antioxidant response and protects neurons against ischemic injury *in vitro* and *in vivo*. *J. Neurochem.* 133, 298–308. doi: 10.1111/jnc.12986

Shu, S., Li, C. M., You, Y. L., Qian, X. L., Zhou, S., and Ling, C. Q. (2016). Electroacupuncture ameliorates cerebral ischemia-reperfusion injury by regulation of autophagy and apoptosis. *Evid. Based Complement. Alternat. Med.* 2016:7297425. doi: 10.1155/2016/7297425

Sun, J., Li, X., Liu, J., Pan, X., and Zhao, Q. (2019). Stigmasterol exerts neuroprotective effect against ischemic/reperfusion injury through reduction of oxidative stress and inactivation of autophagy. *Neuropsychiatr. Dis. Treat.* 15, 2991–3001. doi: 10.2147/NDT.S220224

Ting, Z., Jianbin, Z., and Luqi, H. (2017). Protective effect of electroacupuncture on neurons autophagy in perfusion period of cerebral ischemia. *Neurosci. Lett.* 661, 41–45. doi: 10.1016/j.neulet.2017.06.043

Wang, Q., Li, X., Chen, Y., Wang, F., Yang, Q., Chen, S., et al. (2011). Activation of epsilon protein kinase C-mediated anti-apoptosis is involved in rapid tolerance induced by electroacupuncture pretreatment through cannabinoid receptor type 1. *Stroke.* 42, 389–396. doi: 10.1161/STROKEAHA.110.597336

Xing, Y., Yang, S. D., Wang, M. M., Dong, F., Feng, Y. S., and Zhang, F. (2018). Electroacupuncture alleviated neuronal apoptosis following ischemic stroke in rats *via* midkine and ERK/JNK/p38 signaling pathway. *J. Mol. Neurosci.* 66, 26–36. doi: 10.1007/s12031-018-1142-y

Xue, T. F., Ding, X., Ji, J., Yan, H., Huang, J. Y., Guo, X. D., et al. (2017). PD149163 induces hypothermia to protect against brain injury in acute cerebral ischemic rats. *J. Pharmacol. Sci.* 135, 105–113. doi: 10.1016/j.jphs.2017.10.004

Zhang, Y., and Chen, N. (2018). Autophagy is a promoter for aerobic exercise performance during high altitude training. *Oxid. Med. Cell. Longev.* 2018:3617508. doi: 10.1155/2018/3617508

Zhao, L., Zhu, Y., Wang, D., Chen, M., Gao, P., Xiao, W., et al. (2010). Morphine induces Beclin 1- and ATG5-dependent autophagy in human neuroblastoma SH-SY5Y cells and in the rat hippocampus. *Autophagy.* 6, 386–394. doi: 10.4161/auto.6.3.11289

Zhou, S., Qiao, B., Chu, X., and Kong, Q. (2018). Oxymatrine attenuates cognitive deficits through SIRT1-mediated autophagy in ischemic stroke. *J. Neuroimmunol.* 323, 136–142. doi: 10.1016/j.jneuroim.2018.06.018

Zou, F., Lin, Y. F., Chen, S. G., Cao, L., Wang, H. R., Ye, B., et al. (2020). The impact of electroacupuncture at hegu, shousanli and quchi based on the theory "treating flaccid paralysis by yangming alone" on stroke patients' EEG: a pilot study. *Evid. Based. Complement. Alternat. Med.* 2020:8839491. doi: 10.1155/2020/8839491

Conflict of Interest: The authors declare that the research was conducted in the absence of any commercial or financial relationships that could be construed as a potential conflict of interest.

frontiers in Cellular Neuroscience

ORIGINAL RESEARCH
published: 12 March 2021
doi: 10.3389/fncel.2021.653487

Influence of iTBS on the Acute Neuroplastic Change After BCI Training

Qian Ding[1], Tuo Lin[1], Manfeng Wu[1], Wenqing Yang[1], Wanqi Li[1], Yinghua Jing[1], Xiaoqing Ren[1], Yulai Gong[2], Guangqing Xu[3] and Yue Lan[1]**

[1] Department of Rehabilitation Medicine, Guangzhou First People's Hospital, School of Medicine, South China University of Technology, Guangzhou, China, [2] Sichuan Provincial Rehabilitation Hospital, Chengdu University of Traditional Chinese Medicine, Chengdu, China, [3] Department of Rehabilitation Medicine, Guangdong Provincial People's Hospital, Guangdong Academy of Medical Sciences, Guangzhou, China

OPEN ACCESS

Edited by:
Zhang Pengyue,
Yunnan University of Traditional Chinese Medicine, China

Reviewed by:
Chunlei Shan,
Shanghai University of Traditional Chinese Medicine, China
Xiquan Hu,
Third Affiliated Hospital of Sun Yat-sen University, China

***Correspondence:**
Guangqing Xu
guangchingx@163.com
Yue Lan
bluemooning@163.com

Specialty section:
This article was submitted to Cellular Neurophysiology, a section of the journal Frontiers in Cellular Neuroscience

Received: 14 January 2021
Accepted: 22 February 2021
Published: 12 March 2021

Citation:
Ding Q, Lin T, Wu M, Yang W, Li W, Jing Y, Ren X, Gong Y, Xu G and Lan Y (2021) Influence of iTBS on the Acute Neuroplastic Change After BCI Training.
Front. Cell. Neurosci. 15:653487.
doi: 10.3389/fncel.2021.653487

Objective: Brain-computer interface (BCI) training is becoming increasingly popular in neurorehabilitation. However, around one third subjects have difficulties in controlling BCI devices effectively, which limits the application of BCI training. Furthermore, the effectiveness of BCI training is not satisfactory in stroke rehabilitation. Intermittent theta burst stimulation (iTBS) is a powerful neural modulatory approach with strong facilitatory effects. Here, we investigated whether iTBS would improve BCI accuracy and boost the neuroplastic changes induced by BCI training.

Methods: Eight right-handed healthy subjects (four males, age: 20–24) participated in this two-session study (BCI-only session and iTBS+BCI session in random order). Neuroplastic changes were measured by functional near-infrared spectroscopy (fNIRS) and single-pulse transcranial magnetic stimulation (TMS). In BCI-only session, fNIRS was measured at baseline and immediately after BCI training. In iTBS+BCI session, BCI training was followed by iTBS delivered on the right primary motor cortex (M1). Single-pulse TMS was measured at baseline and immediately after iTBS. fNIRS was measured at baseline, immediately after iTBS, and immediately after BCI training. Paired-sample *t*-tests were used to compare amplitudes of motor-evoked potentials, cortical silent period duration, oxygenated hemoglobin (HbO2) concentration and functional connectivity across time points, and BCI accuracy between sessions.

Results: No significant difference in BCI accuracy was detected between sessions ($p > 0.05$). In BCI-only session, functional connectivity matrices between motor cortex and prefrontal cortex were significantly increased after BCI training (p's < 0.05). In iTBS+BCI session, amplitudes of motor-evoked potentials were significantly increased after iTBS (p's < 0.05), but no change in HbO2 concentration or functional connectivity was observed throughout the whole session (p's > 0.05).

Conclusions: To our knowledge, this is the first study that investigated how iTBS targeted on M1 influences BCI accuracy and the acute neuroplastic changes after BCI training. Our results revealed that iTBS targeted on M1 did not influence BCI accuracy

or facilitate the neuroplastic changes after BCI training. Therefore, M1 might not be an effective stimulation target of iTBS for the purpose of improving BCI accuracy or facilitate its effectiveness; other brain regions (i.e., prefrontal cortex) are needed to be further investigated as potentially effective stimulation targets.

Keywords: transcranial magnetic stimulation, brain computer interface, functional near-infrared spectroscopy, intermittent theta burst stimulation, motor imagery

INTRODUCTION

Brain computer interface (BCI) can directly translate brain activities reflecting the subject's intention into motor commands for controlling an external device (Abiri et al., 2019). The external device can in turn provide BCI users with state-dependent sensory feedback, which is known as closed-loop BCI system (Johnson et al., 2018). Following stroke, the connection between the peripheral muscles and sensorimotor cortex is often disrupted due to cortical or subcortical lesions, which results in hemiparesis. With BCI, stroke survivors are able to control external devices bypassing the damaged physiological motor output system (Daly and Wolpaw, 2008), including those with severe hemiparesis who cannot actively participate in traditional motor training (Ramos-Murguialday et al., 2013). The closed-loop BCI system provides stroke survivors with a chance to actively participate in motor training and activate their motor-related cortices (Pichiorri et al., 2015). The effectiveness of BCI training on motor recovery following stroke has been reported in several clinical studies (Teo and Chew, 2014; Pichiorri et al., 2015; Sun et al., 2017; Wu et al., 2019).

However, a large portion of BCI users (∼30% of healthy adults and ∼40% stroke survivors) are unable to control BCI systems effectively (Blankertz et al., 2010). This phenomenon is called "BCI-illiteracy" problem (Vidaurre and Blankertz, 2010), which largely limits the effectiveness of BCI training. "BCI-illiteracy" has been suggested to result from insufficient event-related desynchronization (ERD) of the mu rhythm (Buch et al., 2008). Mu rhythm is typically observed over the sensorimotor area with a frequency of 8–13 Hz and is attenuated during motor imagery (i.e., mu ERD). As the amplitude of mu ERD plays a crucial role in BCI decoding accuracy (Buch et al., 2008), it is sometimes difficult for BCI systems to detect the subject's motion intention without a strong mu ERD (Kasashima et al., 2012). As the amplitude of mu ERD is related to motor-related cortical activation, it can be modulated by non-invasive brain stimulation (NIBS) techniques (Hummel and Cohen, 2006). Therefore, NIBS is a feasible approach for enhancing BCI performance and solving "BCI-illiteracy" problem. The influence of transcranial direct current stimulation (tDCS), a common form of NIBS, on BCI training has been extensively investigated (Ang et al., 2015; Kasashima-Shindo et al., 2015; Hong et al., 2017). It has been reported that anodal tDCS applied on motor cortex can increase mu ERD and improve BCI accuracy in both healthy adults (Wei et al., 2013) and stroke survivors (Ang et al., 2015; Kasashima-Shindo et al., 2015). Unfortunately, the increased BCI accuracy cannot be transferred to improved effectiveness of BCI training in motor recovery following stroke (Ang et al., 2015; Kasashima-Shindo et al., 2015; Hong et al., 2017); this is possibly because anodal tDCS could not facilitate neuroplastic changes induced by BCI training. Therefore, how other forms of NIBS influence the effects of BCI training needs to be investigated.

Repetitive transcranial magnetic stimulation (rTMS) is another popular NIBS technique, which is frequently applied to induce modulation of cortical activation. Among patterned rTMS protocols, a modified form of rTMS known as theta-burst stimulation (TBS) can induce longer-lasting neural effects with shorter application time and lower stimulation intensities compared with conventional rTMS paradigms. Intermittent TBS (iTBS) has been suggested to have facilitatory neural effects (Chung et al., 2016). When applied on the primary motor cortex (M1), robust increase in cortical excitability usually lasts for 20–30 min after iTBS (Huang et al., 2005, 2011; Chung et al., 2016). Based on its convenience of use and strong neural modulatory effect, iTBS has been widely applied as a powerful technique to upregulate cortical excitability in clinical studies (Chung et al., 2016; Chen et al., 2019). Therefore, iTBS might be an effective approach for increasing BCI accuracy and facilitating neuroplastic changes of BCI training.

Neuroplastic changes after BCI training can be investigated by many neuroimaging approaches, such as functional magnetic resonance imaging (fMRI), electroencephalography (EEG), and functional near-infrared spectroscopy (fNIRS), etc. (Yang et al., 2019). Although being able to provide accurate information about brain structure and neural activities, high cost and subject's head fixation have limited applications of fMRI in tasks that require constant movement or real-time monitor (Strangman et al., 2006; Mihara and Miyai, 2016). fNIRS is a non-invasive neuroimaging tool that monitors cerebral and myocardial oxygenation during tasks (Yang et al., 2019). Compared with fMRI, fNIRS has some advantages including real-time monitor, relatively low price, simplicity, and relatively high temporal resolution. Compared with EEG, fNIRS has higher spatial resolution and is less likely to be influenced by subject's head

Abbreviations: BCI, brain computer interface; ERD, event-related desynchronization; NIBS, non-invasive brain stimulation; tDCS, transcranial direct current stimulation; rTMS, repetitive transcranial magnetic stimulation; iTBS, intermittent theta-burst stimulation; MVC, maximal voluntary contraction; EMG, electromyography; FDI, first dorsal interosseus; M1, primary motor cortex; RMT, resting motor threshold; MEP, motor evoked potential; AMT, active motor threshold; fNIRS, functional near-infrared spectroscopy; CSP, cortical silent period; ROI, regions of interest; DLPFC, dorsal lateral prefrontal cortex; FP, frontal polar; HbO2, oxygenated hemoglobin; HRF, hemodynamic response function; PLV, phase locking value.

move during motor tasks (Yang et al., 2019). Therefore, fNIRS is a suitable approach for monitoring immediate neuroplastic changes after BCI training.

Here, we investigated how iTBS targeted on M1 influences the BCI accuracy and acute neuroplastic changes of BCI training. We used fNIRS to measure acute neuroplastic changes of BCI training. We anticipated that BCI training would increase brain activation and functional connectivity in the motor and prefrontal cortices. iTBS would improve BCI accuracy and boost the acute neuroplastic changes induced by BCI.

METHODS

Participants

Eight healthy adults volunteered for this two-session study [four males; mean age: 21.6 (SD = 1.2) years]. Participants were included only if they were right-handed assessed with the Edinburgh Handedness Inventory, and had no history of neurological disorders, including no head or hand injuries. Participants were excluded if: using medications that reduce seizure threshold; pregnant; or any implanted device or metal that might be affected by the magnetic field generated by TMS was present.

Participants gave their written informed consent for the experimental procedures that were approved by the Guangzhou First People's Hospital Human Research Ethics Committee. The study was performed in accordance with the Declaration of Helsinki.

Force Measurements

We tested maximal voluntary isometric pinch grip (MVC) in both hands of each participant. Grip force assessment system (BioFlex-H, Zhanghe Intelligent Co., Guangzhou, China) was used to measure isometric pinch grip force in the "standard" position (Ding and Patten, 2018) with real-time force feedback displayed on a 24-inch television screen. Three MVC trials were interspersed with rest intervals (2 min); the peak value was carried forward as MVC for each hand.

Physiological Measures

Transcranial Magnetic Stimulation

Surface electromyography (EMG) was recorded from the first dorsal interosseus (FDI) of both hands. Participants were seated in a comfortable chair with back supported. The EMG raw signal was amplified and band-pass filtered (3 Hz−3 kHz), digitized at a sampling rate of 2,048 Hz with a 50 Hz notch filter enabled. EMG data were written to disc for offline analysis.

TMS was performed using a NS5000 Magnetic Stimulator (YIRUIDE Medical Co., Wuhan, China). TMS was applied over M1 using a figure-of-eight-shaped coil (70 mm diameter) positioned tangentially 45° from midline to induce a posterior-anterior current in the hemisphere. Participants were asked to remain static while determining the optimal scalp position for eliciting maximal responses in the contralateral FDI. Resting motor threshold (RMT) was determined experimentally as the lowest stimulation intensity that produced motor evoked potentials (MEP) $\geq$ 50 uV in 50% of consecutive stimulations at rest (Chen et al., 1998). Active motor threshold (AMT) was determined experimentally as the lowest stimulation intensity that produced MEPs $\geq$ 200 uV in 50% of consecutive stimulations during grip at 10% MVC (Matsunaga et al., 2005; Takechi et al., 2014). A neuronavigation system (Visor2, ANT Neuro, Hengelo, Netherlands) was used to ensure reliable and consistent coil positioning over the hotspot throughout the experiment. Coil position error was controlled at $<$ 5 mm displacement and $<$ 3° relative to the target (Ding et al., 2018). Stimulations were delivered at every 5–8 s. Both hemispheres were tested in a random order.

Totally 40 single-pulse TMS pulses were delivered at 120% RMT, with 20 stimuli at rest and 20 during grip at 10% MVC. At rest condition, participants were instructed to completely relax. EMG signals displayed on a computer screen were used to provide feedback and assist participants in keeping the arm and hand muscles quiet. During grip, participants produced constant submaximal (10% MVC) isometric pinch grip with force feedback displayed visually as a target zone (10 $\pm$ 2% MVC) within which the participant was instructed to maintain force. Prior to the testing, participants practiced using visual feedback to maintain the force trace within the target zone. TMS was applied when the force trace was stable and maintained in the target zone.

MEPs were analyzed offline using custom written Matlab scripts (Matlab2019b, Mathworks, Inc., Natick, USA). EMG data were demeaned, filtered using a fourth order Butterworth filter (10–500 Hz), and signal averaged over 20 trials for each condition. Averaged peak-to-peak MEP amplitudes of both rest and grip condition were calculated (i.e., MEP_{rest} and MEP_{active}, respectively). Cortical silent period (CSP) was also calculated. CSP onset was defined as the point at which the average rectified EMG amplitude remained below threshold for 5 ms. CSP offset was defined as the point at which the amplitude returned to and remained above threshold for 5 ms. The CSP duration was quantified by the time interval between CSP onset and offset (Triggs et al., 1992; Classen et al., 1997; Urbin et al., 2015).

Functional Near-Infrared Spectroscopy

fNIRS data was acquired using a 46 multichannel fNIRS instrument (BS-3000, Wuhan Znion Technology Co., Wuhan, China). Channels between each transmitter and receiver were placed with reference to the 10–20 system. The two probe sets were inserted into a nylon cap and then placed on the participant's head. One of the probe sets was placed on the prefrontal area (24 optodes, 37 channels), and the other one was placed on the right motor cortex (8 optodes, 9 channels). The 46-channel montage placement is shown in **Figure 1**. A chin strap was used to secure the cap in place to reduce cap movement. Prior to recording, a NIR gain quality check was performed to ensure data acquisition was neither under-gained nor over-gained. Data were recorded at wavelengths of 695 and 830 nm.

For each fNIRS testing, participants were asked to rest for 60 s, followed by the force tracking task (60 s grip and 30 s rest for 3 times) (**Figure 2A**). At rest condition, participants were asked to sit in an armchair with eyes closed. During the force tracking task, subjects were asked to use a pinch grip to produce submaximal

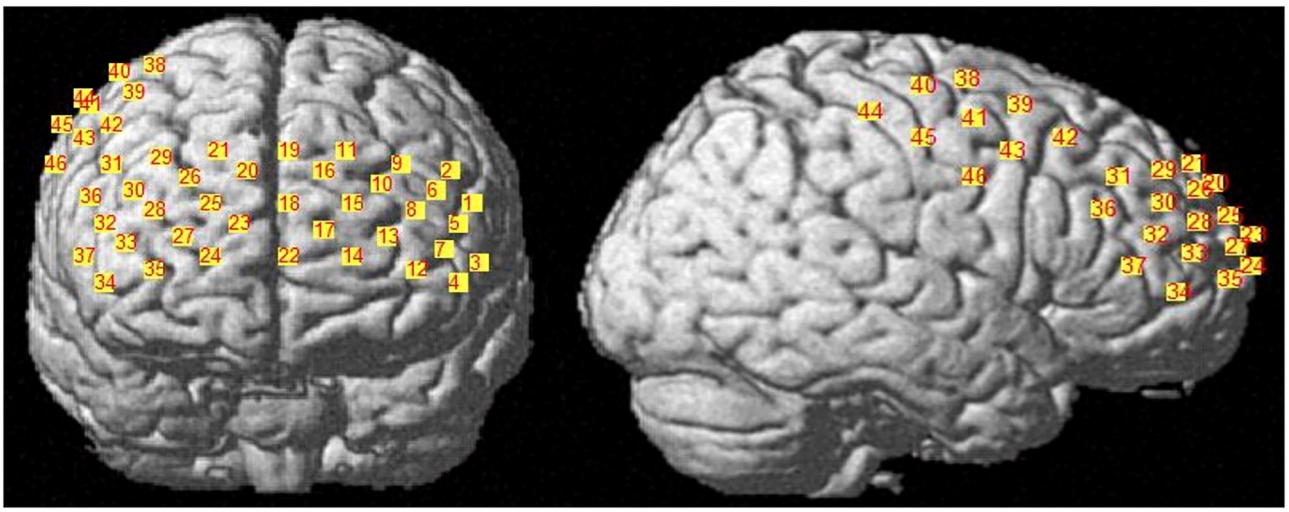

FIGURE 1 | fNIRS 46-channel montage placement. There were 37 channels placed on the prefrontal cortex, and eight channels placed on the right motor cortex.

isometric contraction to track the criterion trajectory (**Figure 2B**) as accurately as possible. The force tracking task included force production, force maintenance and force release phase.

Regions of interest (ROIs) were selected *via* Polhemus PATRIOT digitizer channel registration analyses. After tasks were completed, subjects were instructed to keep the fNIRS cap on while the experimenters carefully removed the optodes. A measuring tape was used to find the center point (i.e., Cz) on the head. Measurements were taken from the left auricular lobule to the right auricular lobule, and from the nasion to the inion. Once the Cz point was determined, a magnet was positioned on it and the subject was moved so that the inion was 10 cm away from the transmitter. Five head base reference points were measured using the stylus, which are nasion, left tragus, right tragus, inion, and Cz. All other optical fiber points were measured in numerical order afterwards. Selected ROIs were M1, left and right dorsal lateral prefrontal cortex (DLPFC), left and right frontal polar (FP). All channels with >50% overlap within a region were averaged together based on MRIcro registration (Rorden and Brett, 2000; Wan et al., 2018).

Fluctuations in concentration of delta oxygenated hemoglobin (HbO2) were calculated from changes in detected light intensity according to the modified Beer-Lambert Law, assuming constant scattering (Sakatani et al., 2006). Data preprocessing was performed after delta HbO2 signals were obtained. We used the moving average filter was 3 s (Huo et al., 2019). A processing method based on moving standard deviation and cubic spline interpolation was then applied to remove motion artifacts (Scholkmann et al., 2010). Artifacts were distinguished by identifying the sliding window standard deviation above a certain threshold and were removed by cubic spline interpolation. The physiologic signals are removed from the data using the low pass filer with a cut-off of 0.2 Hz. The low-frequency drift was removed by a high pass filter of 0.01 Hz cut-off frequency (Arun et al., 2020). 60s task period and 10s rest period before the trial were extracted from the data. Baseline correction was then performed on each trial to ensure that the beginning of each task period was approximately zero. The average time series for each ROI (i.e., hemodynamic response function, HRF) was calculated for the force tracking task. The averaged amplitude of each HRF was calculated for statistical analysis.

Functional connectivity was calculated in both time and frequency domain. In the time domain, correlation approach was used to estimate the strength of the pairwise Pearson's correlation between ROIs (Pannunzi et al., 2017). In frequency domain, coherence and phase locking value (PLV) were used to analyze the level of synchronization of the fNIRS signals. The Welch's averaged, modified periodogram method (Welch, 1967), was performed to calculate the squared coherence between ROIs. PLV was calculated to indicate the stability of the phase difference between two time series [for calculation details see Briels et al. (2020)]. All connectivity matrices were Fisher's z-transformed (Arun et al., 2020) to the set of Gaussian distributed values and the z scores were used for further statistical analysis.

Interventions

BCI Training

Motor imagery-based BCI training system was developed as shown in **Figure 3A**. EEG signals were recorded using 16 active electrodes (g.LADYbird, g.Tec Medical Engineering GmbH, Schiedlberg, Austria). The real-time EEG signals were amplified (g.USBamp, g.Tec Medical Engineering GmbH, Austria) and then computer processed. Video clips were played in a 24-inch computer screen to guide the participants to complete motor imagery tasks. An exoskeleton hand was used to provide sensory feedback in hand grasping/opening tasks. A mu ERD score (0–100) was displayed on the screen to provide real-time feedback. Subjects could adjust their motor imagery strategy according to

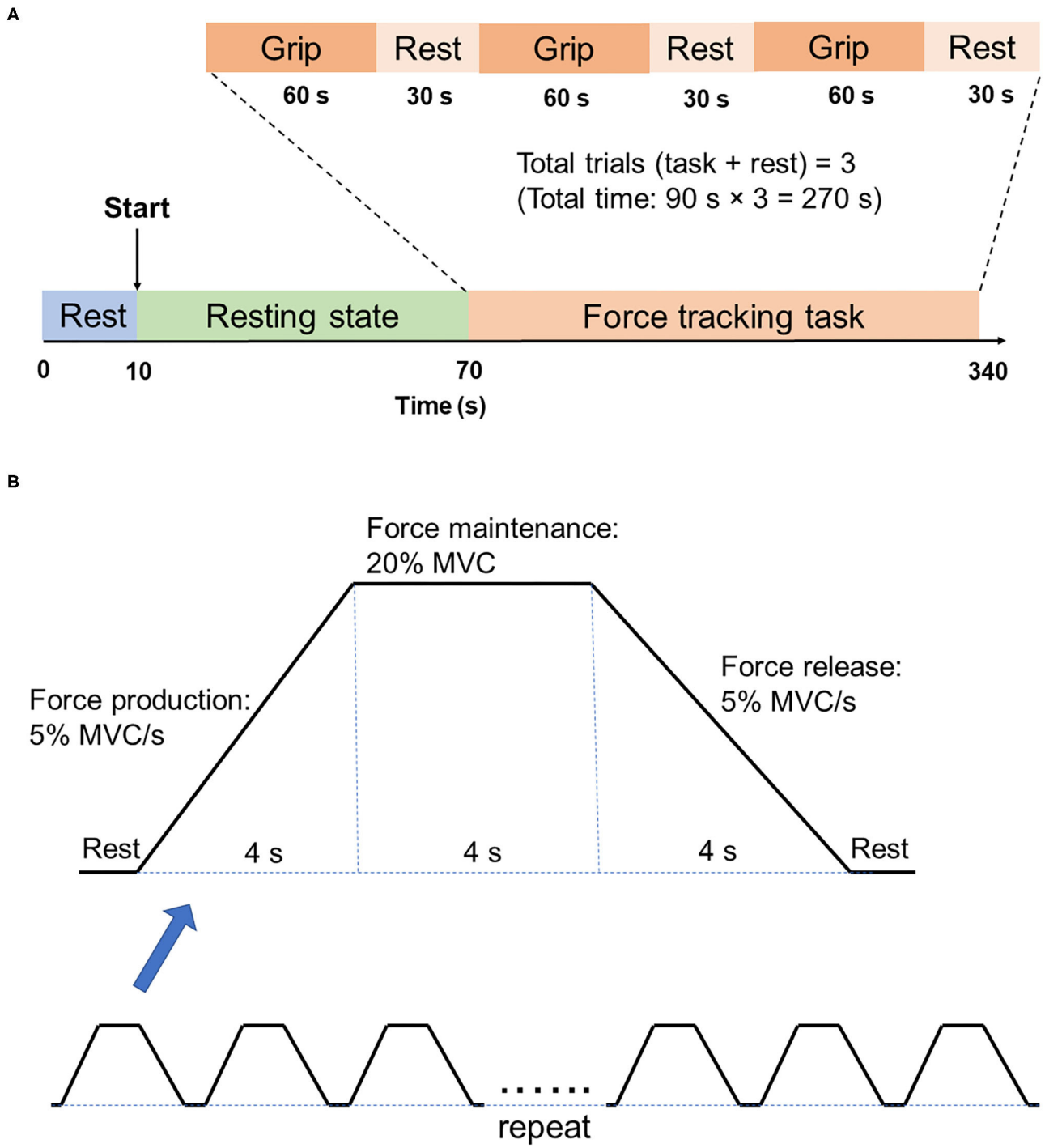

FIGURE 2 | Illustration of fNIRS testing. **(A)** fNIRS testing procedure. There are two states of fNIRS testing, which are the 60s resting state and 270s force tracking task. Force tracking task consists of three trials, with each trial followed by 30s rest. **(B)** Force tracking task paradigm. Each block of force tracking task includes force production phase, force maintenance phase and force release phase, with 4s rest break between two adjacent blocks.

this index to achieve higher scores and control the BCI robot more effectively (Sun et al., 2017).

EEG signals were referenced to a unilateral earlobe. The signal from 16 active electrodes was sampled at 256 Hz. The real-time EEG signals were processed by the amplifier using a band-pass filter (2–60 Hz) to remove artifacts and a notch filter (48–52 Hz) to remove power line interference. All electrodes were filled with salt water to ensure the transmission impedance remained below

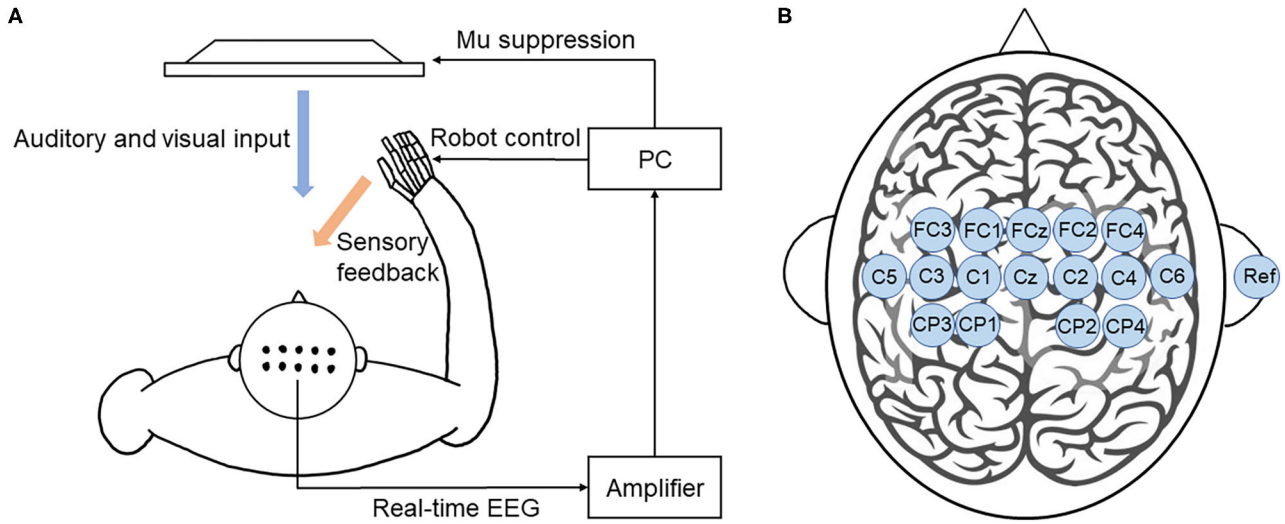

FIGURE 3 | BCI training system. **(A)** Illustration of the closed-loop system. This BCI system consists of an EEG amplifier collecting real-time EEG, a PC analyzing EEG signal and providing visual and auditory feedback, and a robot hand providing sensory feedback. **(B)** The location of EEG electrodes. There were 16 active electrodes placed on the motor and sensory area and a reference electrode placed on the right ear.

1 kOhm. The EEG electrodes were placed over the central area according to the 10–20 system (**Figure 3B**). EEG signals from the C3 and C4 electrodes were used for BCI control.

During the action observation, a dark screen was first displayed for 2 s, followed by a white cross for 2 s. Then, a text cue of "hand grasp" or "hand open" was displayed for 2 s. A video clip with a duration of 6 s was then displayed. Subjects were asked to observe the actions and imagine they were performing those actions without actually moving their hands. The mu ERD score was calculated based on the EEG signal during the video. If the mu ERD score was above 60, the robot hand would assist the subject in completing the hand grasp/open task during the following 3 s, which was considered as a successful trial. If the mu ERD score was below 60, the robot hand would not move, which was considered as an unsuccessful trial. The mu ERD score was then shown for 2 s. Each trial ended with the display of a dark screen for 3 s. During each BCI training, the trial repeated for 100 times and video clips of the grasping/opening hand was shown alternately at a random order. There was 30 s rest break after every 10 trials. Each BCI training took about 40–50 min in total. The BCI accuracy was then calculated by the number of successful trials divided by the number of total trials.

Intermittent Theta Burst Stimulation

iTBS was applied over the right M1 and was delivered using a NS5000 Magnetic Stimulator (YIRUIDE Medical Co., Wuhan, China). The TBS pattern consist of bursts containing three pulses at 50 Hz repeated at 5 Hz and an intensity of 80% AMT. A 2 s train of TBS was repeated every 10 s for a total of 190 s (600 pulses) (Huang et al., 2005). Participants were asked to stay relaxed during the application of iTBS.

Experimental Procedures

This study included a BCI-only session and iTBS+BCI session in a random order with approximately 7 days apart. The order of two sessions was determined by the random integers generated in Matlab2019b (Mathworks, Inc., Natick, USA). For the odd numbers, BCI-only session would be the first session and iTBS+BCI session would be the second session. For the even numbers, iTBS+BCI session would be the first session and BCI-only session would be the second session. In BCI-only session, fNIRS was tested at baseline and immediately after BCI tasks. In iTBS+BCI session, BCI training were followed by iTBS. Single-pulse TMS was tested at baseline and immediately after iTBS. fNIRS was tested at baseline, immediately after iTBS, and immediately after BCI training (**Figure 4**).

Statistical Analysis

All data analyses and statistics were performed in Matlab2019b (Mathworks, Inc., Natick, USA). Data were tested using the Kolmogorov-Smirnov test and found to be normally distributed. In the BCI-only session, paired-sample *t*-tests were used to compare averaged HbO2 amplitude and functional connectivity matrices (including correlation, coherence and PLV) in each ROI before and after BCI. In the iTBS+BCI session, repeated-measures ANOVA were used to compare averaged HbO2 amplitude and functional connectivity matrices at baseline, after TBS and after BCI. In the iTBS+BCI session, paired t-test was used to compare TMS measures (including MEP_{rest}, MEP_{active} and CSP) before and after iTBS. Paired-sample *t*-test was also used to compare the averaged mu ERD score during BCI training between two sessions. False discovery rate corrections were used for multiple comparisons. Statistical significance was established at $p < 0.05$.

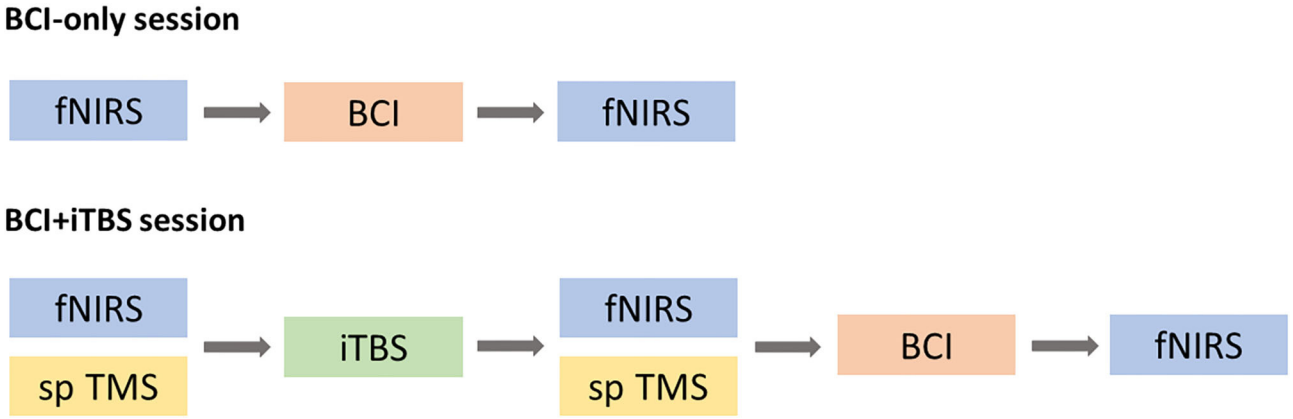

FIGURE 4 | Experimental procedure. In BCI-only session, fNIRS was tested at baseline and after BCI training (top panel). In iTBS + BCI session, fNIRS was tested at three times points: baseline, after TBS and after BCI. Single-pulse (sp) TMS was tested at baseline and after iTBS. The order of those two sessions was randomized.

RESULTS

All eight participants completed two sessions of experiment, with five participants completed BCI-only session first. No adverse effect was reported.

BCI Accuracy

The mean BCI accuracy was 82.63% (SD = 3.6) and 81.50% (SD = 3.0) in the BCI-only session and iTBS+BCI session, respectively. There was no difference in BCI accuracy between two sessions ($p > 0.05$).

TMS Measures

There was significant increase in amplitudes of MEP_{rest} and MEP_{active} in the contralateral hand (i.e., left hand) after iTBS (p's = 0.02 and 0.04, respectively) (**Figure 5**). No significant change in CSP duration was revealed in the contralateral hand after iTBS ($p > 0.05$). There was also no significant change in MEP amplitude or CSP duration in the ipsilateral hand (i.e., right hand) after iTBS (p's > 0.05).

HRF

There was no significant difference in averaged amplitude of HbO2 concentration change throughout the whole experiment in either session (**Figure 6**).

Functional Connectivity Analysis

For resting-state functional connectivity, increased correlation between motor cortex and right DLPFC was observed after BCI training in the BCI-only session ($p = 0.005$) (**Figure 7**). No significant difference in resting-state functional connectivity was observed throughout the iTBS+BCI session (p's > 0.05).

For functional connectivity measured during force tracking task, increased coherence between motor cortex and left DLPFC was observed after BCI training in the BCI-only session ($p = 0.032$) (**Figure 8**). In addition, increased PLV was observed between motor cortex and left FP after BCI training in the BCI-only session ($p = 0.037$). There was no significant difference in functional connectivity measured during force tracking task throughout the iTBS + BCI session.

DISCUSSION

This study for the first time investigated the acute neuroplastic changes after BCI training using fNIRS. We also investigated how iTBS targeted on M1 influenced BCI accuracy and neuroplastic changes induced by BCI training. Results revealed that functional connectivity between motor cortex and prefrontal cortex was acutely increased after BCI training. After iTBS, increased cortical excitability was observed, but brain activation or functional connectivity remained unchanged. iTBS targeted on M1 did not influence BCI accuracy or facilitate the neural effects induced by BCI training.

Acute Neuroplastic Change After BCI Training

Results revealed acute neuroplastic change in functional connectivity between motor cortex and prefrontal cortex after BCI training. To our knowledge, ours is the first study that investigated the acute neural plasticity induced by BCI training using fNIRS. The acute neural adaptation of BCI training has been investigated using TMS and MRI (Xu et al., 2014; Mrachacz-Kersting et al., 2016; Nierhaus et al., 2019). TMS studies reported that MEP amplitude was increased after BCI training for up to 30 min in both stroke survivors (Mrachacz-Kersting et al., 2016) and healthy adults (Xu et al., 2014), suggesting BCI training could induce a prolonged increase in cortical excitability in the trained hemisphere (Bai et al., 2020). Nierhaus et al. (Nierhaus et al., 2019) used functional and structural MRI after only 1 h of BCI training to investigate immediate brain plasticity. Results revealed increased BOLD activity in the left sensorimotor area of trained hemisphere during motor imagery after BCI training, suggesting BCI training facilitates recruitment of cortical motor neurons during motor imagery. Our findings extend the acute neural adaptations after BCI training from cortical excitability

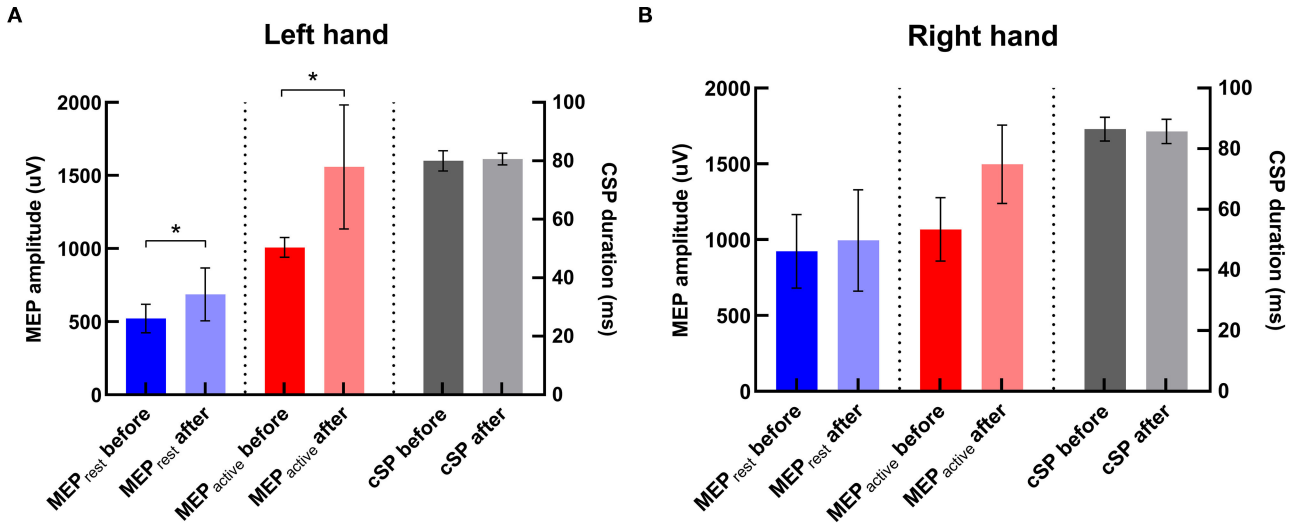

FIGURE 5 | Changes in TMS parameters after iTBS in two hemispheres. **(A)** In the left hand (i.e., the contralateral hand to iTBS), MEP_{rest} and MEP_{active} were significantly increased compared with baseline, and there was no significant change in CSP duration after iTBS. **(B)** In the right hand, there was no significant change in any TMS parameter after iTBS. *Indicates significant changes after iTBS.

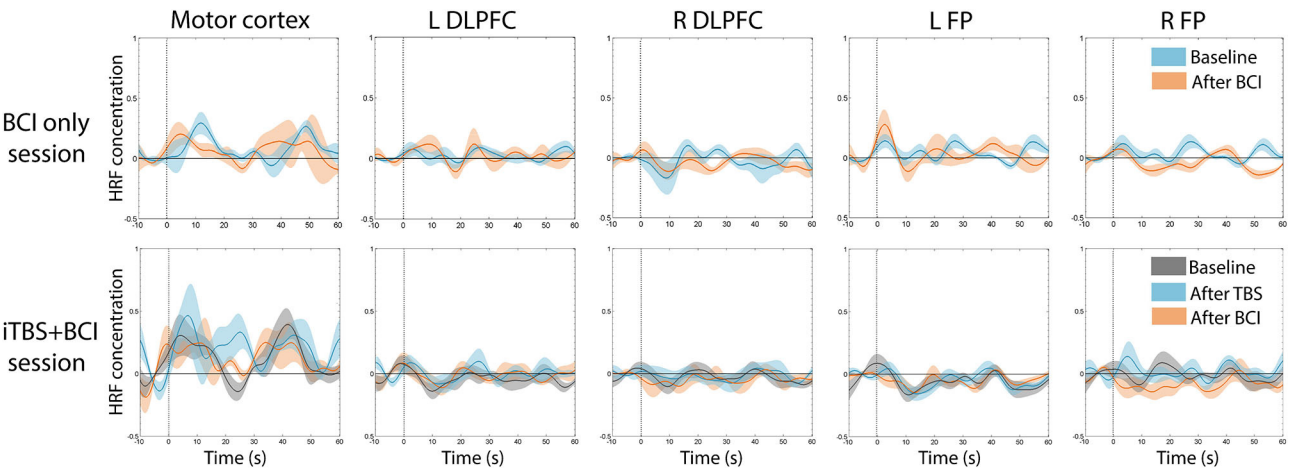

FIGURE 6 | Average time series of HRF across participants. There was no significant change in average HbO2 amplitude at any time point in either session. In BCI-only session (top panel), blue indicates HRF at baseline, and pink indicates HRF after BCI training. In iTBS+BCI session (bottom panel), gray indicates HRF at baseline; blue indicates HRF after TBS; and pink indicates HRF after BCI training. Error bars are standard error.

and brain activation to functional connectivity of the cortical networks which has not been previously investigated.

As reduced functional connectivity between brain regions has been observed in stroke survivors (Arun et al., 2020), our findings suggest a potential neural mechanism underlying the effectiveness of BCI training in neurorehabilitation. Based on results from our current study and previous studies (Xu et al., 2014; Mrachacz-Kersting et al., 2016; Nierhaus et al., 2019), the neuroplastic state of motor imagery-related cortical network (including sensorimotor cortex, prefrontal cortex, etc.) is elevated after BCI training. This provides a possibility for improving the effectiveness of traditional motor training in stroke survivors by priming with BCI training, which needs to be tested in future studies.

Acute Neuroplastic Change After iTBS

In line with previous literature (Huang et al., 2005, 2011; Cirillo et al., 2017), our results revealed increased MEP amplitudes after iTBS on M1. However, we did not observe any change in HbO2 concentration or functional connectivity in the motor cortex or prefrontal cortex after iTBS. To our knowledge, there was only one previous study using fNIRS to investigate acute neural adaptation after iTBS on M1 (Mochizuki et al., 2007). Similar to what we found in this current study, no change in HbO2

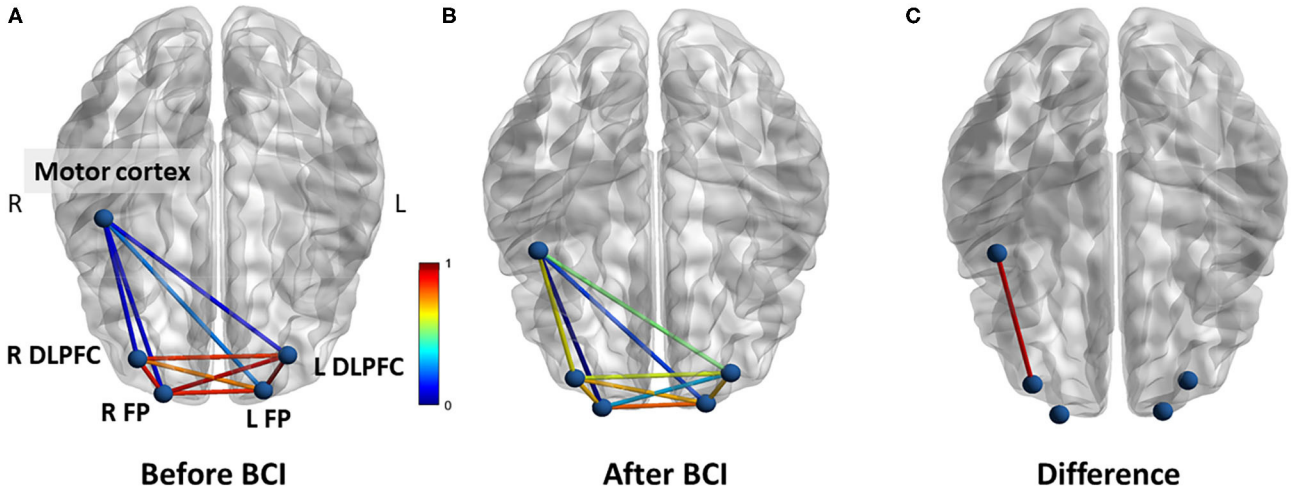

FIGURE 7 | Functional connectivity (correlation) change measured at rest in BCI-only session. **(A)** Correlations between each ROI at baseline. **(B)** Correlations between each ROI after BCI training. **(C)** The correlation between right motor cortex and right DLPFC was significantly increased after BCI training. L refers to left. R refers to right. DLPFC refers to dorsal lateral prefrontal cortex. FP refers to frontal polar area.

concentration in the ipsilateral motor cortex or prefrontal cortex was reported after iTBS in Mochizuki et al.'s study (Mochizuki et al., 2007).

Similar to iTBS, high-frequency rTMS is another type of non-invasive brain stimulation that has been used to upregulate cortical excitability. Some studies used fNIRS to investigate acute neural adaptation during and after high frequency rTMS on M1 (Li et al., 2017, 2019). Reduced HbO2 (Li et al., 2017) and functional connectivity (Li et al., 2019) in motor cortex and prefrontal cortex were observed in both hemispheres during rTMS, which returned to baseline after rTMS.

Collectively, there is lack of a direct relationship between hemodynamic response or functional connectivity and cortical excitability after iTBS or high-frequency rTMS. The neural mechanisms remain unclear. It has been suggested that the activation of sympathetic nervous system during rTMS application might be a possible mechanism (Li et al., 2019). The activation of sympathetic nervous system maintains a constant cerebral blood flow through vasoconstriction. This may prevent the potential dilatation of cerebral vessels induced by iTBS or high-frequency rTMS, thus no change in HbO2 concentration can be detected after stimulation (Li et al., 2019). Further studies are needed to investigate the mechanisms underlying the disassociated relationship between cortical excitability and hemodynamic response after NIBS.

The Influence of iTBS on BCI Training

Inconsistent with our hypothesis, iTBS targeted on M1 did not influence BCI accuracy or facilitate the neuroplastic changes induced by BCI training. The mechanism is still unclear. To our knowledge, no published study has investigated the acute effect of excitatory rTMS (including iTBS) on BCI training. There were some studies investigating the influence of excitatory tDCS on BCI training (Wei et al., 2013; Ang et al., 2015; Kasashima-Shindo et al., 2015; Hong et al., 2017). It has been reported that anodal tDCS effectively increased mu ERD during BCI training and improved BCI accuracy in both healthy adults (Wei et al., 2013) and stroke survivors (Ang et al., 2015; Kasashima-Shindo et al., 2015). The different results might be due to the different stimulation paradigms. Although similar neural mechanisms are shared by iTBS and tDCS, iTBS has much higher temporal resolution compared with regular tDCS. In those aforementioned studies (Wei et al., 2013; Ang et al., 2015; Kasashima-Shindo et al., 2015; Hong et al., 2017), tDCS electrodes were relatively large and placed on motor cortex that covers not only M1 but also premotor cortex and supplementary motor cortex, while in our current study iTBS was precisely targeted on M1 with the guidance of neuronavigation system. It has been suggested that motor imagery requires not only M1 but also a distributed brain network including premotor cortex, supplementary motor cortex and prefrontal cortex, etc. (Sharma et al., 2009; Bauer et al., 2015). Because of the low spatial resolution, tDCS applied on the motor cortex might activate a broader motor imagery-related cortical network compared with iTBS targeted on M1, and thus effectively influence BCI performance. Based on this speculation, dual or multiple sites of iTBS might be more likely to improve BCI performance, which needs to be tested in the future. Difference between stroke and healthy adults may also contribute to different results between ours and previous studies (Ang et al., 2015; Kasashima-Shindo et al., 2015). As stroke survivors often have reduced mu ERD and the poorer BCI performance, there is larger room for stroke survivors to increase mu ERD or improve BCI accuracy compared with healthy adults.

Apart from BCI accuracy, iTBS on M1 did not facilitate the acute neuroplastic change induced by BCI training either. Similarly, previous studies reported that anodal tDCS on motor cortex did not facilitate neuroplastic change or improve the effectiveness of BCI training in stroke survivors (Ang et al., 2015; Kasashima-Shindo et al., 2015; Hong et al., 2017). Possibly

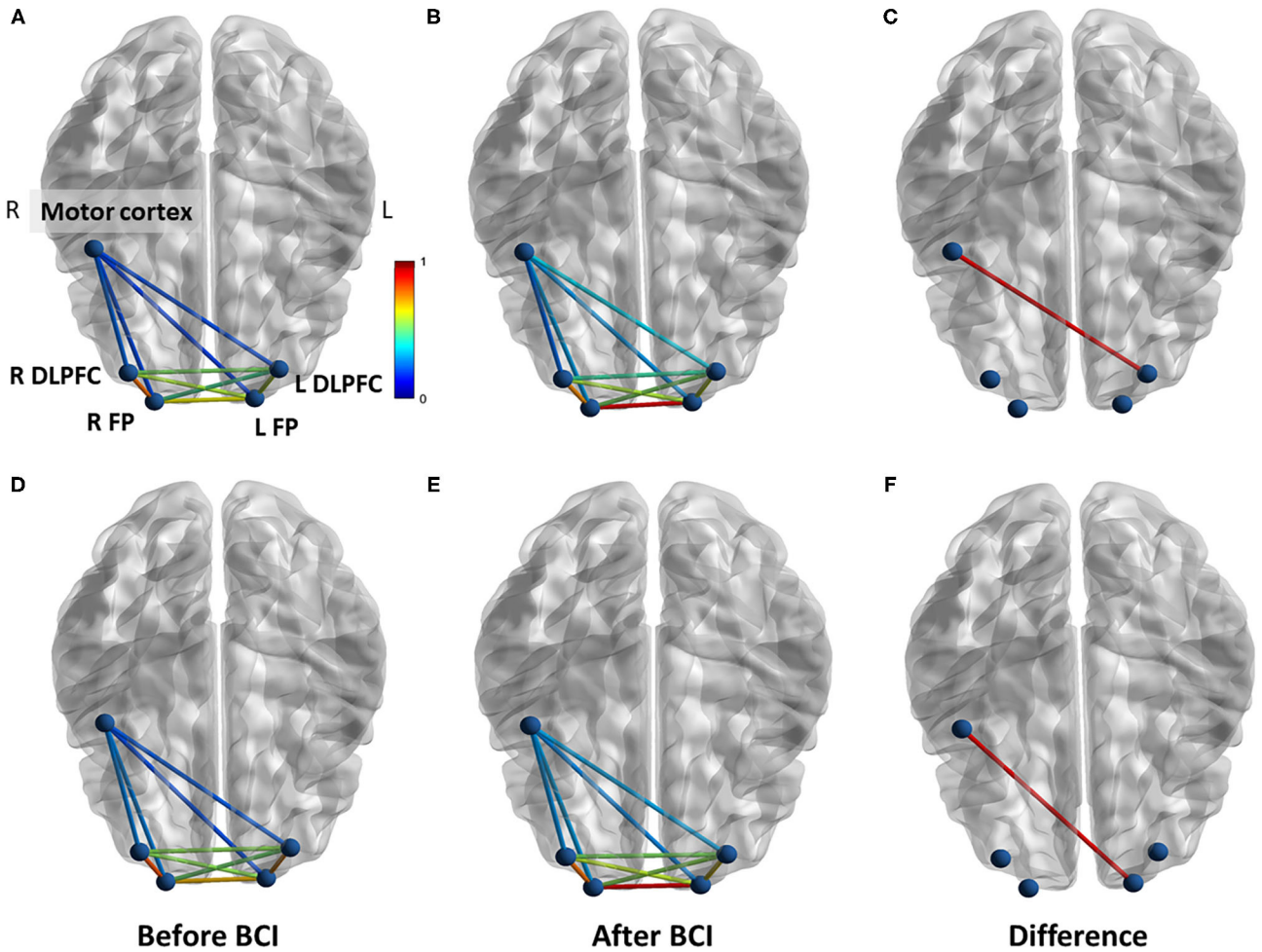

FIGURE 8 | Functional connectivity change measured during force tracking task in BCI-only session. **(A)** Coherence between each ROI at baseline. **(B)** Coherence between each ROI after BCI training. **(C)** Coherence between right motor cortex and left DLPFC was significantly increased after BCI training. **(D)** PLV between each ROI at baseline. **(E)** PLV between each ROI after BCI training. **(F)** The PLV between right motor cortex and left FP was significantly increased after BCI training. L refers to left. R refers to right. DLPFC refers to dorsal lateral prefrontal cortex. FP refers to frontal polar area.

because the use of BCI-only requires modulation of neural activities in M1 (Wander et al., 2013), M1 has been the most common target of NIBS in BCI literature (Wei et al., 2013; Ang et al., 2015; Kasashima-Shindo et al., 2015; Hong et al., 2017; Shu et al., 2017). However, acquisition of BCI proficiency requires a distributed brain network, including prefrontal cortex, premotor cortex, and posterior parietal cortex, etc. (Wander et al., 2013). In addition, the role that M1 plays in the process of motor imagery might not be as important as brain regions with higher cortical functions (e.g., prefrontal cortex) (Moghadas Tabrizi et al., 2019); this may explain why iTBS on M1 did not positively influence the effect of BCI training. Taken together, M1 may not be the best stimulation target for improving BCI accuracy or effectiveness. Further studies are needed to explore other brain regions as potentially effective stimulation targets for improving the effectiveness of BCI training.

Limitations

As a pilot study, the sample size of current study is small ($N = 8$). In addition, our sample only includes young adults, so cautions are needed when generalizing our findings to other populations, such as aging population or stroke survivors. Future studies are needed to test our results in other populations with larger sample sizes.

Another limitation is that current study did not include sham iTBS condition in our study design. We acknowledge that the lack of sham iTBS condition may weaken the convincingness of the conclusions. In addition, due to the limited number of fNIRS channels, we did not monitor the neuroplastic changes in the left M1 (the non-stimulated hemisphere) and may miss some neuroplastic changes. Further studies are still needed to include sham iTBS condition and measure neuroplastic changes in both motor cortices.

CONCLUSIONS

Our pilot study systematically investigated how iTBS targeted on M1 influences BCI accuracy and the acute neuroplastic changes induced by BCI training. Our results revealed that iTBS targeted on M1 did not influence BCI accuracy or facilitate the neuroplastic changes induced by BCI training, suggesting that M1 might not be an effective stimulation target of iTBS for the purpose of improving BCI accuracy or facilitate the effectiveness of BCI training. Other brain regions (i.e., prefrontal cortex) are needed to be further investigated as potentially effective stimulation targets.

DATA AVAILABILITY STATEMENT

The raw data supporting the conclusions of this article will be made available by the authors, without undue reservation.

ETHICS STATEMENT

The studies involving human participants were reviewed and approved by Guangzhou First People's Hospital Human Research Ethics Committee. The patients/participants provided their written informed consent to participate in this study.

AUTHOR CONTRIBUTIONS

QD, YL, and GX designed the experiment. QD, TL, MW, WY, WL, YJ, XR, and YG conducted the experiments. QD reduced and analyzed the data. QD, YL, and GX interpreted the data. QD and YL wrote the manuscript. All authors contributed to the article and approved the submitted version.

FUNDING

This work was supported by the National Science Foundation of China [Grant Numbers: 81772438 (YL), 81974357 (YL), 82072548 (GX), and 81802227 (TL)]; the Guangzhou Municipal Science and Technology Program [Grant Number: 201803010083 (YL)]; the Fundamental Research Funds for the Central University [Grant Number: 2018PY03 (YL)]; National Key R&D Program of China [Grant Number: 2017YFB1303200 (YL)]; Guangdong Basic and Applied Basic Research Foundation [Grant Number: 2020A1515110761 (QD)]; and Guangzhou Postdoctoral Science Foundation (QD).

ACKNOWLEDGMENTS

We would like to thank all our participants for their interest and time investment.

REFERENCES

Abiri, R., Borhani, S., Sellers, E. W., Jiang, Y., and Zhao, X. (2019). A comprehensive review of EEG-based brain-computer interface paradigms. *J. Neural. Eng.* 16:011001. doi: 10.1088/1741-2552/aaf12e

Ang, K. K., Guan, C., Phua, K. S., Wang, C., Zhao, L., Teo, W. P., et al. (2015). Facilitating effects of transcranial direct current stimulation on motor imagery brain-computer interface with robotic feedback for stroke rehabilitation. *Arch. Phys. Med. Rehabil.* 96, S79–87. doi: 10.1016/j.apmr.2014.08.008

Arun, K. M., Smitha, K. A., Sylaja, P. N., and Kesavadas, C. (2020). Identifying resting-state functional connectivity changes in the motor cortex using fNIRS during recovery from stroke. *Brain Topogr.* 33, 710–719. doi: 10.1007/s10548-020-00785-2

Bai, Z., Fong, K. N. K., Zhang, J. J., Chan, J., and Ting, K. H. (2020). Immediate and long-term effects of BCI-based rehabilitation of the upper extremity after stroke: a systematic review and meta-analysis. *J. Neuroeng. Rehabil.* 17:57. doi: 10.1186/s12984-020-00686-2

Bauer, R., Fels, M., Vukelic, M., Ziemann, U., and Gharabaghi, A. (2015). Bridging the gap between motor imagery and motor execution with a brain-robot interface. *Neuroimage* 108, 319–327. doi: 10.1016/j.neuroimage.2014.12.026

Blankertz, B., Sannelli, C., Halder, S., Hammer, E. M., Kubler, A., Muller, K. R., et al. (2010). Neurophysiological predictor of SMR-based BCI performance. *Neuroimage* 51, 1303–1309. doi: 10.1016/j.neuroimage.2010.03.022

Briels, C. T., Schoonhoven, D. N., Stam, C. J., De Waal, H., Scheltens, P., and Gouw, A. A. (2020). Reproducibility of EEG functional connectivity in Alzheimer's disease. *Alzheimers Res. Ther.* 12:68. doi: 10.1186/s13195-020-00632-3

Buch, E., Weber, C., Cohen, L. G., Braun, C., Dimyan, M. A., Ard, T., et al. (2008). Think to move: a neuromagnetic brain-computer interface (BCI) system for chronic stroke. *Stroke* 39, 910–917. doi: 10.1161/STROKEAHA.107.505313

Chen, R., Tam, A., Butefisch, C., Corwell, B., Ziemann, U., Rothwell, J. C., et al. (1998). Intracortical inhibition and facilitation in different representations of the human motor cortex. *J. Neurophysiol.* 80, 2870–2881. doi: 10.1152/jn.1998.80.6.2870

Chen, Y.-J., Huang, Y.-Z., Chen, C.-Y., Chen, C.-L., Chen, H.-C., Wu, C.-Y., et al. (2019). Intermittent theta burst stimulation enhances upper limb motor function in patients with chronic stroke: a pilot randomized controlled trial. *BMC Neurol.* 19:1302. doi: 10.1186/s12883-019-1302-x

Chung, S. W., Hill, A. T., Rogasch, N. C., Hoy, K. E., and Fitzgerald, P. B. (2016). Use of theta-burst stimulation in changing excitability of motor cortex: a systematic review and meta-analysis. *Neurosci. Biobehav. Rev.* 63, 43–64. doi: 10.1016/j.neubiorev.2016.01.008

Cirillo, G., Di Pino, G., Capone, F., Ranieri, F., Florio, L., Todisco, V., et al. (2017). Neurobiological after-effects of non-invasive brain stimulation. *Brain Stimul.* 10, 1–18. doi: 10.1016/j.brs.2016.11.009

Classen, J., Schnitzler, A., Binkofski, F., Werhahn, K. J., Kim, Y. S., Kessler, K. R., et al. (1997). The motor syndrome associated with exaggerated inhibition within the primary motor cortex of patients with hemiparetic stroke. *Brain* 120, 605–619. doi: 10.1093/brain/120.4.605

Daly, J. J., and Wolpaw, J. R. (2008). Brain-computer interfaces in neurological rehabilitation. *Lancet Neurol.* 7, 1032–1043. doi: 10.1016/S1474-4422(08)70223-0

Ding, Q., and Patten, C. (2018). External biomechanical constraints impair maximal voluntary grip force stability post-stroke. *Clin. Biomech. (Bristol, Avon)* 57, 26–34. doi: 10.1016/j.clinbiomech.2018.06.001

Ding, Q., Triggs, W. J., Kamath, S. M., and Patten, C. (2018). Short intracortical inhibition during voluntary movement reveals persistent impairment post-stroke. *Front. Neurol.* 9:1105. doi: 10.3389/fneur.2018.01105

Hong, X., Lu, Z. K., Teh, I., Nasrallah, F. A., Teo, W. P., Ang, K. K., et al. (2017). Brain plasticity following MI-BCI training combined with tDCS in a randomized trial in chronic subcortical stroke subjects: a preliminary study. *Sci. Rep.* 7:9222. doi: 10.1038/s41598-017-08928-5

Huang, Y. Z., Edwards, M. J., Rounis, E., Bhatia, K. P., and Rothwell, J. C. (2005). Theta burst stimulation of the human motor cortex. *Neuron* 45, 201–206. doi: 10.1016/j.neuron.2004.12.033

Huang, Y. Z., Rothwell, J. C., Chen, R. S., Lu, C. S., and Chuang, W. L. (2011). The theoretical model of theta burst form of repetitive transcranial magnetic stimulation. *Clin. Neurophysiol.* 122, 1011–1018. doi: 10.1016/j.clinph.2010.08.016

Hummel, F. C., and Cohen, L. G. (2006). Non-invasive brain stimulation: a new strategy to improve neurorehabilitation after stroke? *Lancet Neurol.* 5, 708–712. doi: 10.1016/S1474-4422(06)70525-7

Huo, C., Xu, G., Li, Z., Lv, Z., Liu, Q., Li, W., et al. (2019). Limb linkage rehabilitation training-related changes in cortical activation and effective connectivity after stroke: a functional near-infrared spectroscopy study. *Sci. Rep.* 9:6226. doi: 10.1038/s41598-019-42674-0

Johnson, N. N., Carey, J., Edelman, B. J., Doud, A., Grande, A., Lakshminarayan, K., et al. (2018). Combined rTMS and virtual reality brain-computer interface training for motor recovery after stroke. *J. Neural. Eng.* 15:016009. doi: 10.1088/1741-2552/aa8ce3

Kasashima, Y., Fujiwara, T., Matsushika, Y., Tsuji, T., Hase, K., Ushiyama, J., et al. (2012). Modulation of event-related desynchronization during motor imagery with transcranial direct current stimulation (tDCS) in patients with chronic hemiparetic stroke. *Exp. Brain Res.* 221, 263–268. doi: 10.1007/s00221-012-3166-9

Kasashima-Shindo, Y., Fujiwara, T., Ushiba, J., Matsushika, Y., Kamatani, D., Oto, M., et al. (2015). Brain-computer interface training combined with transcranial direct current stimulation in patients with chronic severe hemiparesis: proof of concept study. *J. Rehabil. Med.* 47, 318–324. doi: 10.2340/16501977-1925

Li, R., Potter, T., Wang, J., Shi, Z., Wang, C., Yang, L., et al. (2019). Cortical hemodynamic response and connectivity modulated by sub-threshold high-frequency repetitive transcranial magnetic stimulation. *Front. Hum. Neurosci.* 13:90. doi: 10.3389/fnhum.2019.00090

Li, R., Wang, C., Huang, K., Shi, Z., Wang, J., and Zhang, Y. (2017). Blood oxygenation changes resulting from subthreshold high frequency repetitive transcranial magnetic stimulation. *Annu. Int. Conf. IEEE Eng. Med. Biol. Soc.* 2017, 1513–1516. doi: 10.1109/EMBC.2017.8037123

Matsunaga, K., Maruyama, A., Fujiwara, T., Nakanishi, R., Tsuji, S., and Rothwell, J. C. (2005). Increased corticospinal excitability after 5 Hz rTMS over the human supplementary motor area. *J. Physiol.* 562, 295–306. doi: 10.1113/jphysiol.2004.070755

Mihara, M., and Miyai, I. (2016). Review of functional near-infrared spectroscopy in neurorehabilitation. *Neurophotonics* 3:031414. doi: 10.1117/1.NPh.3.3.031414

Mochizuki, H., Furubayashi, T., Hanajima, R., Terao, Y., Mizuno, Y., Okabe, S., et al. (2007). Hemoglobin concentration changes in the contralateral hemisphere during and after theta burst stimulation of the human sensorimotor cortices. *Exp. Brain Res.* 180, 667–675. doi: 10.1007/s00221-007-0884-5

Moghadas Tabrizi, Y., Yavari, M., Shahrbanian, S., and Gharayagh Zandi, H. (2019). Transcranial direct current stimulation on prefrontal and parietal areas enhances motor imagery. *Neuroreport* 30, 653–657. doi: 10.1097/WNR.0000000000001253

Mrachacz-Kersting, N., Jiang, N., Stevenson, A. J., Niazi, I. K., Kostic, V., Pavlovic, A., et al. (2016). Efficient neuroplasticity induction in chronic stroke patients by an associative brain-computer interface. *J. Neurophysiol.* 115, 1410–1421. doi: 10.1152/jn.00918.2015

Nierhaus, T., Vidaurre, C., Sannelli, C., Mueller, K. R., and Villringer, A. (2019). Immediate brain plasticity after one hour of brain-computer interface (BCI). *J. Physiol*. doi: 10.1113/JP278118

Pannunzi, M., Hindriks, R., Bettinardi, R. G., Wenger, E., Lisofsky, N., Martensson, J., et al. (2017). Resting-state fMRI correlations: from link-wise unreliability to whole brain stability. *Neuroimage* 157, 250–262. doi: 10.1016/j.neuroimage.2017.06.006

Pichiorri, F., Morone, G., Petti, M., Toppi, J., Pisotta, I., Molinari, M., et al. (2015). Brain-computer interface boosts motor imagery practice during stroke recovery. *Ann. Neurol.* 76, 891–898. doi: 10.1002/ana.24390

Ramos-Murguialday, A., Broetz, D., Rea, M., Laer, L., Yilmaz, O., Brasil, F. L., et al. (2013). Brain-machine interface in chronic stroke rehabilitation: a controlled study. *Ann. Neurol.* 74, 100–108. doi: 10.1002/ana.23879

Rorden, C., and Brett, M. (2000). Stereotaxic display of brain lesions. *Behav. Neurol.* 12, 191–200. doi: 10.1155/2000/421719

Sakatani, K., Yamashita, D., Yamanaka, T., Oda, M., Yamashita, Y., Hoshino, T., et al. (2006). Changes of cerebral blood oxygenation and optical pathlength during activation and deactivation in the prefrontal cortex measured by time-resolved near infrared spectroscopy. *Life Sci.* 78, 2734–2741. doi: 10.1016/j.lfs.2005.10.045

Scholkmann, F., Spichtig, S., Muehlemann, T., and Wolf, M. (2010). How to detect and reduce movement artifacts in near-infrared imaging using moving standard deviation and spline interpolation. *Physiol. Meas.* 31, 649–662. doi: 10.1088/0967-3334/31/5/004

Sharma, N., Baron, J. C., and Rowe, J. B. (2009). Motor imagery after stroke: relating outcome to motor network connectivity. *Ann. Neurol.* 66, 604–616. doi: 10.1002/ana.21810

Shu, X., Yao, L., Sheng, X., Zhang, D., and Zhu, X. (2017). Enhanced motor imagery-based BCI performance via tactile stimulation on unilateral hand. *Front. Hum. Neurosci.* 11:585. doi: 10.3389/fnhum.2017.00585

Strangman, G., Goldstein, R., Rauch, S. L., and Stein, J. (2006). Near-infrared spectroscopy and imaging for investigating stroke rehabilitation: test-retest reliability and review of the literature. *Arch. Phys. Med. Rehabil.* 87, S12–19. doi: 10.1016/j.apmr.2006.07.269

Sun, R., Wong, W. W., Wang, J., and Tong, R. K. (2017). Changes in electroencephalography complexity using a brain computer interface-motor observation training in chronic stroke patients: a fuzzy approximate entropy analysis. *Front. Hum. Neurosci.* 11:444. doi: 10.3389/fnhum.2017.00444

Takechi, U., Matsunaga, K., Nakanishi, R., Yamanaga, H., Murayama, N., Mafune, K., et al. (2014). Longitudinal changes of motor cortical excitability and transcallosal inhibition after subcortical stroke. *Clin. Neurophysiol.* 125, 2055–2069. doi: 10.1016/j.clinph.2014.01.034

Teo, W. P., and Chew, E. (2014). Is motor-imagery brain-computer interface feasible in stroke rehabilitation? *PM R* 6, 723–728. doi: 10.1016/j.pmrj.2014.01.006

Triggs, W. J., Macdonell, R. A. L., Cros, D., Chiappa, K. H., Shahani, B. T., et al. (1992). Motor inhibition and excitation are independent effects of magnetic cortical stimulation. *Ann. Neurol.* 32, 345–351. doi: 10.1002/ana.410320307

Urbin, M. A., Harris-Love, M. L., Carter, A. R., and Lang, C. E. (2015). High-Intensity, unilateral resistance training of a non-paretic muscle group increases active range of motion in a severely paretic upper extremity muscle group after stroke. *Front. Neurol.* 6:119. doi: 10.3389/fneur.2015.00119

Vidaurre, C., and Blankertz, B. (2010). Towards a cure for BCI illiteracy. *Brain Topogr.* 23, 194–198. doi: 10.1007/s10548-009-0121-6

Wan, N., Hancock, A. S., Moon, T. K., and Gillam, R. B. (2018). A functional near-infrared spectroscopic investigation of speech production during reading. *Hum. Brain Mapp.* 39, 1428–1437. doi: 10.1002/hbm.23932

Wander, J. D., Blakely, T., Miller, K. J., Weaver, K. E., Johnson, L. A., Olson, J. D., et al. (2013). Distributed cortical adaptation during learning of a brain-computer interface task. *Proc. Natl. Acad. Sci. U.S.A.* 110, 10818–10823. doi: 10.1073/pnas.1221127110

Wei, P., He, W., Zhou, Y., and Wang, L. (2013). Performance of motor imagery brain-computer interface based on anodal transcranial direct current stimulation modulation. *IEEE Trans. Neural. Syst. Rehabil. Eng.* 21, 404–415. doi: 10.1109/TNSRE.2013.2249111

Welch, P. D. (1967). Use of fast fourier transform for estimation of power spectra—a method based on time averaging over short modified periodograms. *IEEE Trans. Audio Electroacoust.* 15, 70–73. doi: 10.1109/TAU.1967.1161901

Wu, Q., Yue, Z., Ge, Y., Ma, D., Yin, H., Zhao, H., et al. (2019). Brain functional networks study of subacute stroke patients with upper limb dysfunction after comprehensive rehabilitation including BCI Training. *Front. Neurol.* 10:1419. doi: 10.3389/fneur.2019.01419

Xu, R., Jiang, N., Mrachacz-Kersting, N., Lin, C., Asin Prieto, G., Moreno, J. C., et al. (2014). A closed-loop brain-computer interface triggering an active ankle-foot orthosis for inducing cortical neural plasticity. *IEEE Trans. Biomed. Eng.* 61, 2092–2101. doi: 10.1109/TBME.2014.2313867

Yang, M., Yang, Z., Yuan, T., Feng, W., and Wang, P. (2019). A systemic review of functional near-infrared spectroscopy for stroke: current application and future directions. *Front. Neurol.* 10:58. doi: 10.3389/fneur.2019.00058

Conflict of Interest: The authors declare that the research was conducted in the absence of any commercial or financial relationships that could be construed as a potential conflict of interest.

frontiers in Cellular Neuroscience

ORIGINAL RESEARCH
published: 30 March 2021
doi: 10.3389/fncel.2021.654340

Cannabidiol Induces Autophagy to Protects Neural Cells From Mitochondrial Dysfunction by Upregulating SIRT1 to Inhibits NF-κB and NOTCH Pathways

Shaolei Kang[2†], Jinglin Li[2†], Zhihui Yao[1,3] and Jiaxin Liu[1]*

[1] Medical School, Kunming University of Science and Technology, Kunming, China, [2] Department of Radiology, The First Affiliated Hospital of Kunming Medical University, Kunming, China, [3] Department of Burn and Plastic Surgery, 926 Hospital of People's Liberation Army, Kaiyuan, China

OPEN ACCESS

Edited by:
Zhang Pengyue,
Yunnan University of Traditional Chinese Medicine, China

Reviewed by:
Jinhui Zhang,
Yan'an Hospital Affiliated to Kunming Medical University, China
Daoqun Li,
Shandong First Medical University, China

***Correspondence:**
Jiaxin Liu
jiaxin_iphone@163.com

[†] These authors have contributed equally to this work

Specialty section:
This article was submitted to Cellular Neurophysiology, a section of the journal Frontiers in Cellular Neuroscience

Received: 16 January 2021
Accepted: 09 March 2021
Published: 30 March 2021

Citation:
Kang S, Li J, Yao Z and Liu J (2021) Cannabidiol Induces Autophagy to Protects Neural Cells From Mitochondrial Dysfunction by Upregulating SIRT1 to Inhibits NF-κB and NOTCH Pathways. Front. Cell. Neurosci. 15:654340. doi: 10.3389/fncel.2021.654340

The protective effect of Cannabidiol on Parkinson's disease (PD) has been found in recent study. However, the specific mechanism of the protective effect of Cannabidiol on PD nerve damage require further exploration. This study aims to investigate effect of Cannabidiol on MMP-induced Neural Cells (SH-SY5Y) mitochondrial dysfunction. MMP^+ and Cannabidiol were used to treat SH-SY5Y cells, the cells viability was measured by MTT assay. The expression of Tyrosine hydroxylase (TH) in cells was measured by western blotting and Immunofluorescence staining. The relationship among Cannabidiol, Silent mating type information regulation 2 homolog-1 (SIRT1) and NOTCH signaling, NF-κB signaling was examined by western blotting. The effect of Cannabidiol on MMP^+-induced mitochondrial dysfunction of SH-SY5Y cells was measured by western blotting. Cannabidiol alleviated loss of TH expression and cytotoxicity in the MPP^+-induced SH-SY5Y cells. Further mechanistic investigation showed that Cannabidiol induced SH-SY5Y cells autophagy to protects cells from mitochondrial dysfunction by upregulating SIRT1 to Inhibits NF-κB and NOTCH Pathways. Taken together, Cannabidiol acts as a protector in PD.

Keywords: Cannabidiol, SIRT1, NF-κB, NOTCH, PD, SH-SY5Y cells

INTRODUCTION

Parkinson's disease (PD) is a common neurodegenerative disease (Jasmin et al., 2020). More than 6 million individuals suffering from PD globally, which seriously endangers human health in their lives (Nobre et al., 2020). Pathologically, the characteristics of PD include the gradual loss of dopaminergic neurons in substantial nigra pars compacta and the abnormal accumulation of α-synuclein, which further leads to motor dysfunction (Sveinbjornsdottir, 2016; Opara et al., 2017). Currently, the common treatment for PD is the administration of a dopamine precursor to relieve the clinical symptoms of PD patients (Santiago et al., 2017). However, there are still no effective

drugs or method to restore and prevent neuronal damage. Therefore, the development of new adjuvant therapies and therapeutic targets is crucial.

Cannabidiol is a component extracted of non-psychoactive natural from cannabis, It has antioxidant and anti-inflammatory properties (Atalay et al., 2019). A series of studies have confirmed that Cannabidiol are effective against Neurodegenerative disease, such as PD (Santos et al., 2015), AD (Watt and Karl, 2017). Although current studies have confirmed that Cannabidiol plays an active role in neurological diseases through G protein-coupled receptors, TRPV1 ion channels, and peroxisome proliferator-activated receptors (Santos et al., 2015), the specific protective mechanism of Cannabidiol on PD nerve damage has not been fully elucidated.

Insufficiency of mitochondria leads to mitochondrial dysfunction, contributing to the progression of PD characterized by dysfunctional energy metabolism (Wang et al., 2016). Previous studies have shown that mitochondrial dysfunction is related to the pathogenesis of PD progression. Moreover, the regulation of autophagy may be an important therapeutic strategy in PD, When mitochondrial damage causes mitochondrial dysfunction in nerve cells, it further leads to the development of PD. Therefore, promoting damaged mitochondrial autophagy can remove the aggregates of α-synuclein and other abnormal proteins, and protect nerve cells from mitochondrial dysfunction (Ho et al., 2020). In addition, Cannabidiol protects cell survival by improving mitochondrial dysfunction (Ammal Kaidery et al., 2019). However, the specific mechanism of Cannabidiol on improving mitochondrial dysfunction and autophagy is still unclear.

In this study, we exposed SH-SY5Y cells to MPP^+ to mimic a cellular model of PD. simultaneously, the protective effect of Cannabidiol and its possible molecular mechanism were investigated through this model. We found that SIRT1 is closely related to the protection of SH-SY5Y cells from mitochondrial dysfunction by Cannabidiol. Further analysis showed that Cannabidiol induces autophagy to protect SH-SY5Y cells from mitochondrial dysfunction by upregulating SIRT1 to inhibits NF-κB and NOTCH pathways.

MATERIALS AND METHODS

Materials

Cannabidiol (purity > 98%)were purchased from Biopurify (Chengdu, China). 3-(4,5-dimethyl-2-thiazolyl)-2, 5-diphenyltetrazolium bromide (MTT) and 1-Methyl-4-phenylpyridine (MPP^+) were purchased from Sigma-Aldrich (St. Louis, MO, United States); Dulbecco's modified Eagle medium and 10% fetal bovine serum (FBS) were purchased from Gibco (Grand Island, NY, United States). penicillin and streptomycin were purchased from Sigma-Aldrich (St. Louis, MO, United States). Primary antibodies against TH, SIRT1, α-synuclein, p62, LC3-I/II, Atg5/7, Parkin, PINK-1, Nrf2, SOD-1, DJ-1, GSH, NOTCH1, Hes1, p-p65, p65, p-Ikb, Ikb, and GAPDH were purchased from Cell Signaling Technology (Danvers, MA, United States).

Cell Culture and Treatments

The SH-SY5Y human neuroblastoma cell line was purchased from Cell Bank, Shanghai Institutes for Biological Sciences (Shanghai, China), Cells were cultured in the DMEM with 10% fetal bovine serum, 100 U/ml penicillin and 100 μg/ml streptomycin (Sigma, United States) at 37°C in a 5% CO_2 humidified incubator. The medium is replaced every 2 days. When the monolayer cell confluence reaches 75% or more, the cells are subculture. SH-SY5Y cells were pretreated with different concentrations of Cannabidiol for 24 h followed by incubation with MPP^+ for another 24 h to observe the effects of Cannabidiol on autophagy in MPP^+-induced cells.

Western Blotting

The whole-cell proteins were extracted from the SH-SY5Y cells lysed in RIPA lysis buffer (Invitrogen, United States), and the protein concentrations were determined assessed using Bradford protein assay (Invitrogen, United States). After boiling and denaturation, Protein samples were separated by a 10% SDS-PAGE and transferred onto PVDF membranes. Then, the membranes were blocked with 50 g/L skim milk for 4 h at room temperature and incubated with primary antibodies (TH, SIRT1, α-synuclein, p62, LC3-I/II, Atg5/7, Parkin, PINK-1, Nrf2, SOD-1, DJ-1, GSH, NOTCH1, Hes1, p-p65, p65, p-Ikb, Ikb, and GAPDH) at 4°C overnight. The next day, the membranes were washed three times with PBS and incubated with secondary antibodies at room temperature for 1 h. The membranes were rinsed with TBST buffer and visualized using an enhanced chemiluminescence kit (Bio-Rad Laboratories, Inc). Finally, the protein bands were quantified using ImageJ software (NIH, Bethesda, MD, United States).

MTT Assay

Cell viability was determined using the MTT assay. Briefly, the SH-SY5Y cells seeded into 96-well plates at a density of 2×10^5 cells/ml for 24 h. The cells were pretreated with different concentrations of Cannabidiol for 24 h followed by incubation with MPP^+ for another 24 h. The medium was removed and incubated with 20 μl of MTT (5 mg/ml in phosphate buffered saline) for 4 h. Next, added 150 μl DMSO to per well, and the absorbance at 570 nm was measured using a microplate (Thermo Fisher Scientific, United States).

Immunofluorescence Staining

SH-SY5Y cells were placed in a 12 well plate and treated with or without Cannabidiol, and MPP^+ for 24 h. The SH-SY5Y cells were fixed with 4% paraformaldehyde for 30 min at room temperature, next, the cells were permeabilization with 0.2% Triton X 100 for 20 min, Then, the cells were blocked with 1% BSA for 1 h and incubated with primary antibody overnight. The next day, After washing with PBS, the cells were incubated with specific secondary antibodies for 1 h, The cellular nuclei were stained with 4',6-diamidino-2-phenylindole (DAPI) and cells were evaluated using a fluorescence microscope (IX71; Olympus, Miami, FL, United States).

Statistical Analysis

All data were presented as mean values ± standard deviation (SD), and the results of the experiment are repeated three times. The difference between the two groups were calculated through the *t*-test, Other statistical variances among multigroups were calculated through the One-way analysis of variance (ANOVA). Statistical analyses were performed by GraphPad Prism 8.0 software (GraphPad Software, Inc). $P < 0.05$ was considered to indicate a statistically significant difference.

RESULTS

Cannabidiol Alleviated Cytotoxicity in the MPP^+-Induced SH-SY5Y Cells

The viability of SH-SY5Y cells were detected using the MTT assay. The treatment of Cannabidiol (0, 5, 10, 15, 25, and 50 μM) had no significant effect on SH-SY5Y cells viability (**Figure 1A**). Compared with untreated cell, the treatment of MPP^+ (0, 1, 2, 3, 4, and 5 mM) significantly reduced SH-SY5Y cells viability (**Figure 1B**). Based on the MTT results, we chooses 3 mM MPP^+ used to evaluate the protective effects of Cannabidiol on SH-SY5Y cells. The results showed that treatment with 25 and 50 μM Cannabidiol significantly attenuated MPP^+-induced loss of SH-SY5Y cells viability (**Figures 1C,D**). These results suggest that Cannabidiol ameliorated MPP^+-induced loss of Tyrosine Hydroxylase (TH) expression and cytotoxicity in SH-SY5Y cells.

Cannabidiol Alleviated Loss of Tyrosine Hydroxylase Expression in the MPP^+-Induced SH-SY5Y Cells

Tyrosine hydroxylase is the rate-limiting enzyme in DA biosynthesis, the decrease in TH expression leads to PD. The TH expression of SH-SY5Y cells were detected using the western blotting and Immunofluorescence staining, the results showed that treatment with 25 and 50 μM Cannabidiol significantly increased TH expression compared with MPP^+-induced cells (**Figures 2A,B**). These results suggest that Cannabidiol alleviated loss of TH expression in the MPP^+-induced SH-SY5Y cells.

Cannabidiol Alleviated Mitochondrial Dysfunction in MPP^+-Induced SH-SY5Y Cells

Having determined that Cannabidiol could alleviated loss of TH expression and cytotoxicity in the MPP^+-induced SH-SY5Y Cells, we next studied the effect of Cannabidiol on autophagy in cells treated with MPP^+. The results of western blotting showed that the Cannabidiol significantly enhanced the expression of autophagy-related proteins LC3-II, Atg5/7, decreased the expression p62, and α-synuclein. Simultaneously, pretreatment with Cannabidiol significantly restored the expression of antioxidant proteins Nrf2, SOD-1, and GSH (**Figures 3A,B**). Thus, Cannabidiol enhanced autophagy in MPP^+-induced SH-SY5Y cells.

Blockade of Autophagy and Knockdown of SIRT1 Attenuated the Alleviation Effect of Cannabidiol on the Dysfunction of Mitochondrial Induced by MPP^+

SIRT1 is a protein that is downregulated in PD mitochondrial dysfunction and induces autophagy. To find out whether Cannabidiol could induced autophagy in SH-SY5Y Cells by acting on SIRT1, we construct si-SITR1 transfected cells. western blotting showed that SITR1 expression decreased in MPP^+-induced cells; simultaneously, compared with MPP^+ induction, Cannabidiol treatment upregulated the expression level of SITR1 (**Figures 4A,B**). In addition, si-SITR1 transfected and 3-MA (autophagy inhibitor) treatmented decreased the expression of SIRT1 in SH-SY5Y cells compared with the pretreatment of cells with Cannabidiol alone, As shown in **Figure 4B**. The results of western blotting showed that si-SITR1 transfected and 3-MA treatmented decreased the expression of LC3-II, Atg5/7 and Nrf2, SOD-1, GSH, enhanced the expression p62, α-synuclein, compared with the pretreatment of cells with Cannabidiol alone (**Figures 4C,D**). This data indicates that blockade of autophagy and knockdown of SIRT1 attenuated the alleviation effect of Cannabidiol on the dysfunction of mitochondrial induced by MPP^+.

Cannabidiol Protected SH-SY5Y Cells Mitochondrial Proteins Through SIRT1

Mitochondrial proteins are destroyed during the development of PD, which may lead to the pathogenesis of PD. We examined the effect of Cannabidiol on the mitophagy regulators Parkin, PINK-1, DJ-1 in MPP^+-induced SH-SY5Y cells. The results of western blotting showed that MPP^+ significantly decreased the expression levels of Parkin and DJ-1, compared with untreated cell, as shown in **Figure 5**. Cannabidiol treatment significantly enhanced the expression levels of Parkin and DJ-1, compared with MPP^+ alone, as shown in **Figure 5**. Furthermore, si-SITR1 transfected attenuated the protective effect of Cannabidiol on mitochondrial proteins, as shown in **Figure 5**. This data indicates that Cannabidiol protected cells mitochondrial proteins through SIRT1.

Cannabidiol Induced Cell Autophagy by Upregulating SIRT1 to Inhibits NF-κB and NOTCH Pathways

To further clarify the mechanism of SIRT1 Cannabidiol in PD, we measured the expression levels of signaling molecules involved in the NF-κB and NOTCH pathways. The results of western blotting showed that MPP^+ significantly enhanced the expression levels of NOTCH1, Hes 1 and phosphorylated p65, iκBα, as shown in **Figure 6**. Cannabidiol treatment significantly decreased the expression levels of NOTCH1, Hes 1 and phosphorylated p65, iκBα, Furthermore, si-SITR1 transfected attenuated the inhibitory effect of Cannabidiol on inhibitors NF-κB and NOTCH pathways, as shown in **Figure 6**. Therefore, Cannabidiol inhibits NF-κB and NOTCH pathways by upregulating SIRT1.

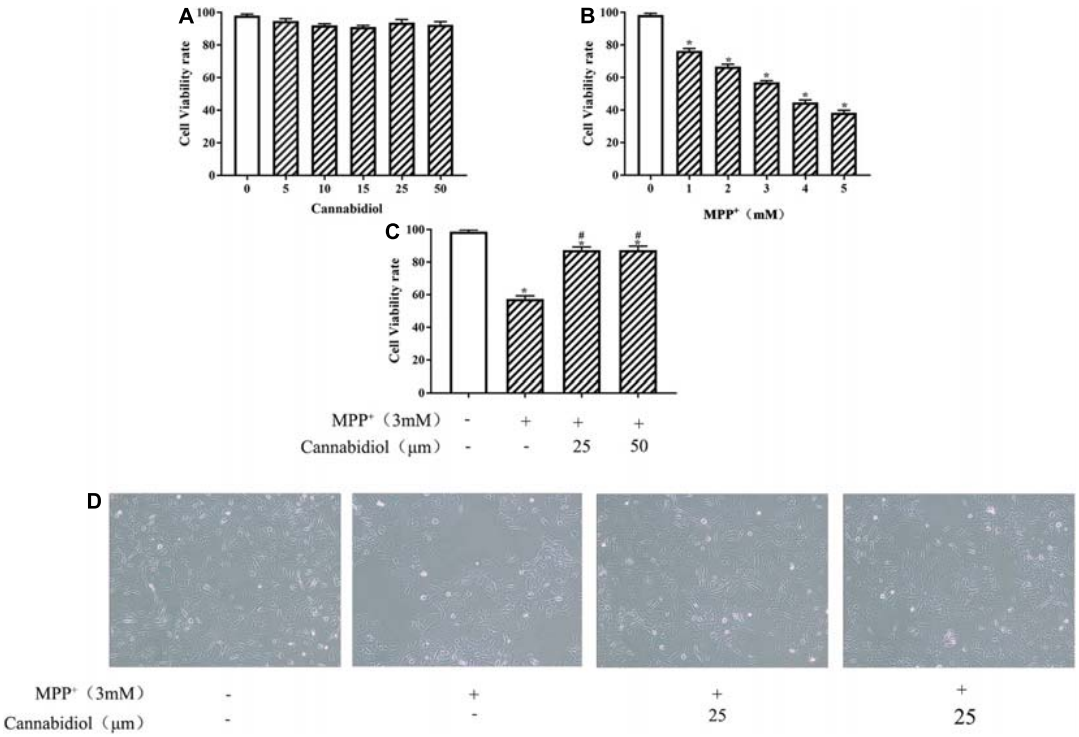

FIGURE 1 | Cannabidiol protected SH-SY5Y cells against MPP^+-induced cytotoxicity and Loss of Tyrosine Hydroxylase (TH) expression. **(A–C)** SH-SY5Y cells were treated with different concentrations of Cannabidiol or MPP^+ for 24 h and Cells viability was measured by the 3-(4,5-dimethylthiazol-2-yl)-2,5-diphenyltetrazolium bromide (MTT) assay. **(D)** Cells viability was Observed by Microscopic (100×); The expression of TH in SH-SY5Y cells were measured by western blotting; $^*p < 0.05$, compared with control group, $^\#p < 0.05$ compared with MPP+ alone.

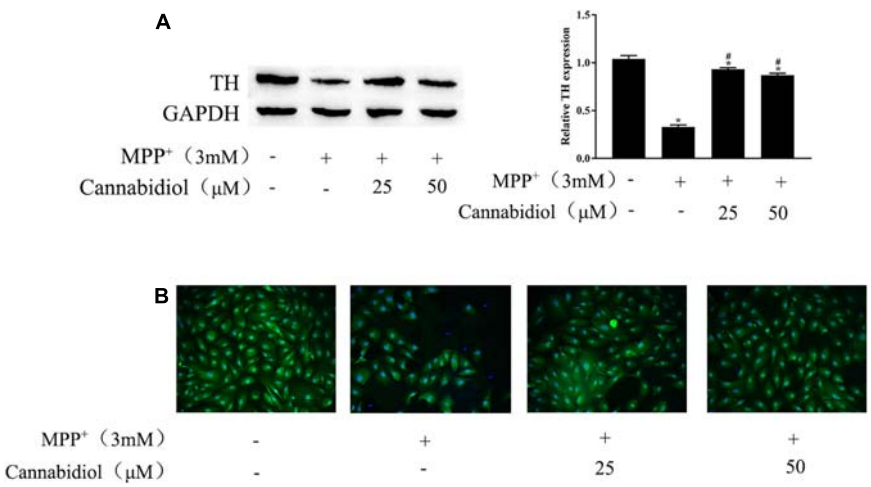

FIGURE 2 | Cannabidiol protected SH-SY5Y cells against MPP^+-induced Loss of Tyrosine Hydroxylase (TH) expression. **(A)** The expression of TH in SH-SY5Y cells were measured by western blotting; **(B)** The expression of TH in SH-SY5Y cells were measured by Immunofluorescence staining (200×); $^*p < 0.05$, compared with control group, $^\#p < 0.05$ compared with MPP^+ alone.

DISCUSSION

The identification of effective protective candidate agents for neurodegenerative diseases is one of the research hotspots in the treatment of PD, Cannabidiol has been reported to treated the psychosis in Parkinson's disease (Ding et al., 2015; Cassano et al., 2020; Silvestro et al., 2020), However, the neuroprotective potential of Cannabidiol against MPP^+-mediated PD in SH-SY5Y cells is unclear. In our present study we demonstrated that Cannabidiol induces autophagy to protects SH-SY5Y cells from

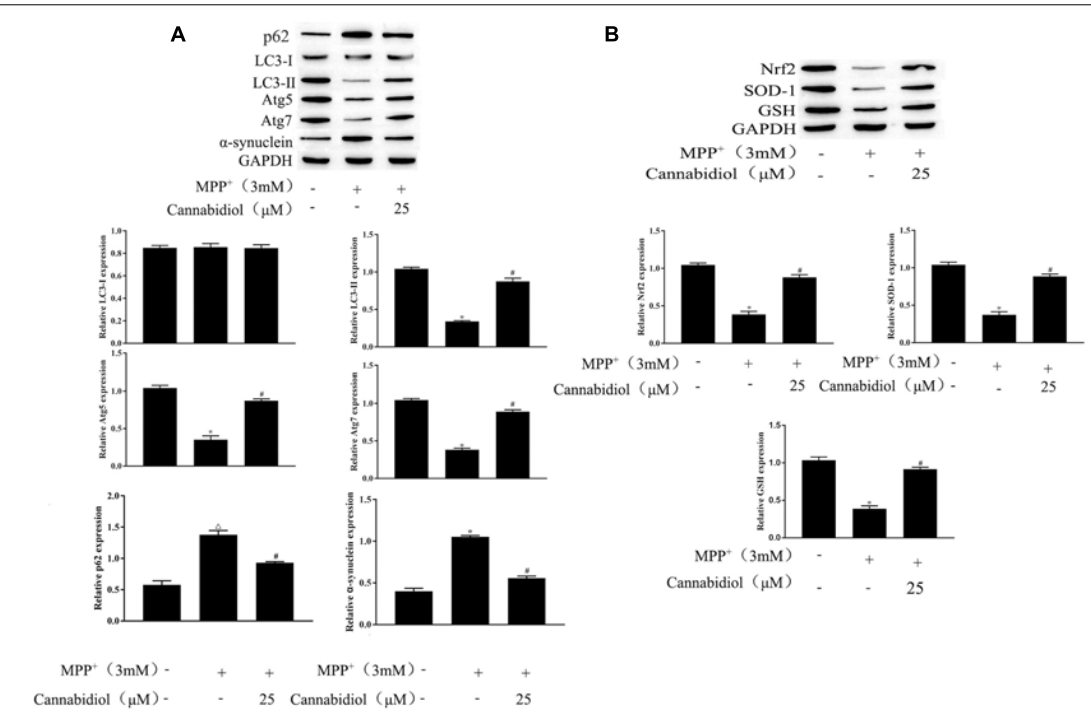

FIGURE 3 | Cannabidiol alleviated mitochondrial dysfunction in MPP^+-induced SH-SY5Y cells. **(A,B)** The expression of autophagy-related proteins and antioxidant proteins in SH-SY5Y cells were measured by western blotting; $^*p < 0.05$, compared with control group, $^{\#}p < 0.05$ compared with MPP^+ alone.

MPP^+-mediated mitochondrial dysfunction by upregulating SIRT1 to inhibits NF-κB and NOTCH pathways. We provide evidence that Cannabidiol attenuated the loss of TH and the accumulation of α-synuclein expression, simultaneously restored the levels of antioxidant protein and autophagy protein in SH-SY5Y cells induced by MPP^+. In addition, STRI1 is highly expressed under the action of Cannabidiol, blockade of autophagy and knockdown of SIRT1 attenuated the alleviation effect of Cannabidiol on the dysfunction of mitochondrial induced by MPP^+. The current findings reveal that Cannabidiol induces Autophagy to protects SH-SY5Y cells from MPP^+-mediated mitochondrial dysfunction by upregulating SIRT1 to inhibits NF-κB and NOTCH pathways.

Mitochondrial dysfunction has an integral role in the development of PD (Buneeva et al., 2020; Imam Aliagan et al., 2020), Many studies have reported that MPP^+-induction is the main source of neuronal cells mitochondrial dysfunction (Xu et al., 2020), MPP^+-induction causes defects in the activity of the mitochondrial electron transport complex, causes transitions of mitochondrial permeability and increases of oxidative stress, causes death of dopaminergic neurons (Bose and Beal, 2016). A previous study showed that Cannabidiol protects cell survival by improving mitochondrial dysfunction (Vidyadhara et al., 2019). However, the specific mechanism of Cannabidiol in mitochondrial dysfunction remains unclear. In the development of mitochondrial dysfunction, Nrf-2, as an important redox-sensitive transcription factor, reduces cell damage caused by reactive oxygen species by regulating antioxidant proteins (Choi et al., 2017). In the present study, we found that Cannabidiol treatment significantly restored the expression levels of Nrf-2, the most important antioxidant enzyme SOD in the antioxidant system, and the non-enzymatic antioxidant GSH. PINK-1/Parkin pathway is related to mitochondrial damage (Quinn et al., 2020), PINK1 promoted Parkin's mitochondrial translocation and modification, thus protecting mitochondrial DNA from damage by reactive oxygen species and stimulating the self-repair process of mitochondria (Xu et al., 2020). DJ-1 is a redox sensor of oxidative stress, upregulating DJ-1 antagonize the mitochondrial dysfunction caused by PINK1 mutation, thus, DJ-1 can be used as an important indicator of mitochondrial damage (Lei et al., 2020). In the present study, we found that Cannabidiol pretreatment reduced MPP^+-mediated mitochondrial damage via activation of PINK-1/parkin and DJ-1.

In the development of PD, the regulation of autophagy is essential (Zhu et al., 2019; Wan et al., 2020). The damage to the autophagy pathway and the resulting accumulation of misfolded α-synuclein and other proteins aggregates represent the common pathobiological characteristics of neurodegenerative diseases such as PD (Erb and Moore, 2020; Kwon et al., 2020). A previous study showed that neurons need autophagy for catabolism to mediate the replacement of damaged organelles and promote synaptic remodeling, thus, autophagy impairment can lead to PD (Moors et al., 2017). In order to deal with the neurological diseases caused by mitochondrial damage, it is necessary to increase the physiological process of mitochondrial autophagy. Previous studies have shown that PINK-1/Parkin pathway is related to mitochondrial damage, Parkin translocation to damaged mitochondria induces mitochondrial autophagy

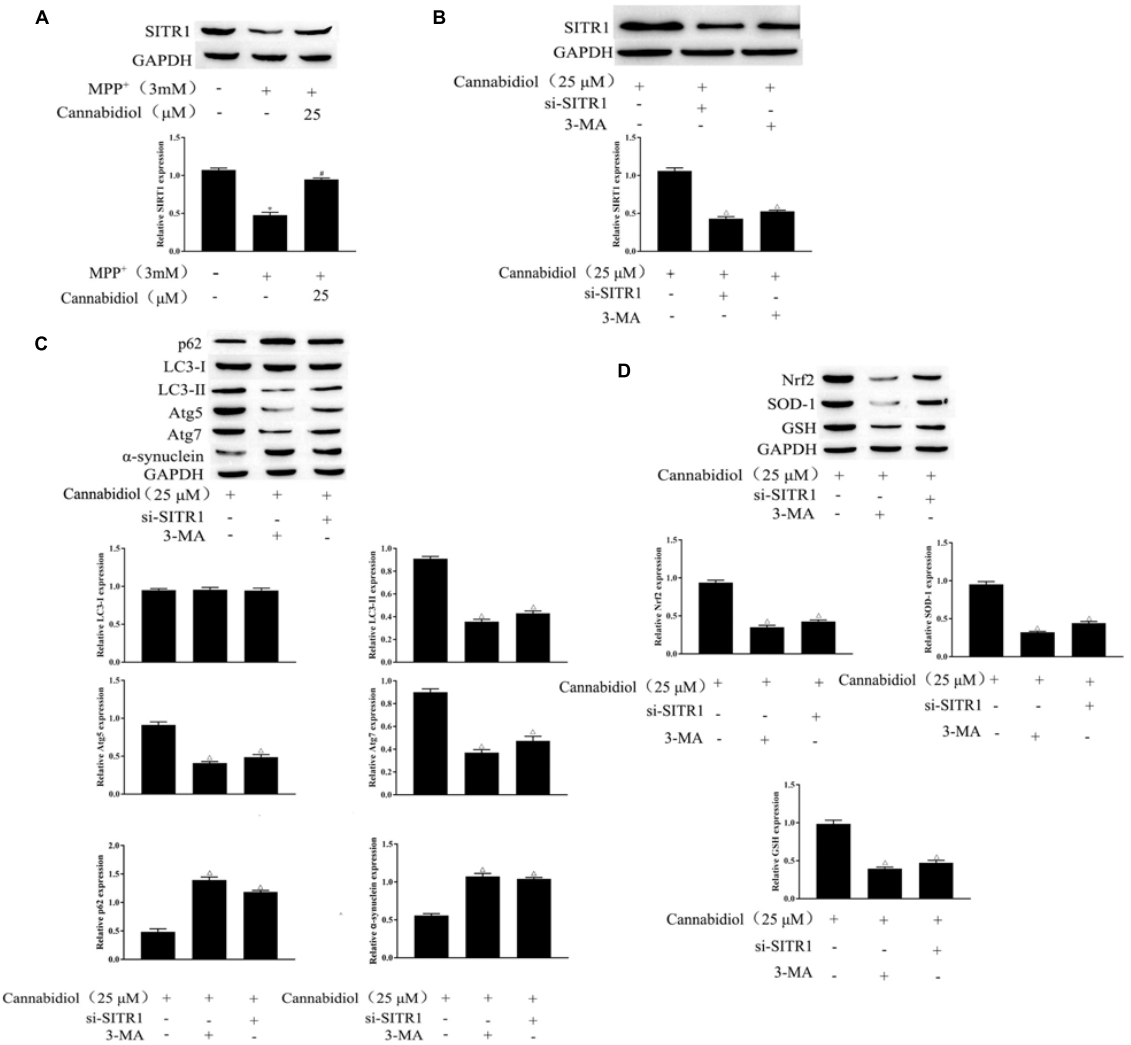

FIGURE 4 | Blockade of autophagy and knockdown of SIRT1 attenuated the alleviation effect of Cannabidiol on the dysfunction of mitochondrial induced by MPP^+. **(A,B)** The expression of SIRT1 in Cannabidiol treatment SH-SY5Y cells were measured by western blotting; **(C,D)** The expression of autophagy-related proteins and antioxidant proteins in SH-SY5Y cells were measured by western blotting; $^*p < 0.05$, compared with control group, $^\#p < 0.05$ compared with MPP^+ alone, $^\Delta p < 0.05$ compared with Cannabidiol alone.

(Quinn et al., 2020). Common antioxidants can reduce oxidative stress damage, but they cannot eliminate the increase of misfolded α-synuclein and other proteins (Yan et al., 2020). Here, we found that Cannabidiol could increase the LC3 levels and decrease the protein expression of p62 and α-synuclein. Combined with the results of Cannabidiol's effect on oxidative stress, we demonstrated that Cannabidiol can reduce oxidative stress damage, eliminate the increase in misfolded α-synuclein and other proteins, induce autophagy, and alleviate mitochondrial dysfunction.

Mitochondrial biogenesis is a key process in the maintenance of mitochondrial mass, SIRT1 is the main regulator of mitochondrial biogenesis (Mao et al., 2020). The increase of SIRT1 has been considered as a therapeutic strategy for PD, previous research showed that SIRT1 has neuroprotective effects in both *in vivo* and *in vitro* PD models (Li et al., 2020). Simultaneously, SIRT1 was significantly downregulated in neurons treatmented with rotenone or MPP^+ (Chen et al., 2019). In addition, HA et al. found that Cannabidiol increases the protein expression level of SIRT1 during the activation of white adipocytes (Parray and Yun, 2016). Thus, we speculate that Cannabidiol alleviating PD may be related to the level of SIRT1. In the present study, we found that Cannabidiol significantly increased the expression of SIRT1 in cells, and knockdown of SIRT1 attenuated the alleviation effect of Cannabidiol on the dysfunction of mitochondrial induced by MPP^+. NF-κB and NOTCH signaling pathway are confirmed to be downstream signaling pathways of SIRT1, SIRT1 could deacetylate the NICD, leading to NOTCH transcriptional inhibition (Bai et al., 2018). Simultaneously, SIRT1 could deacetylate the p65/RELA at lysine 310, leading to NF-κB transcriptional inhibition (Back et al., 2011). Moreover, We also observed that NF-κB and NOTCH

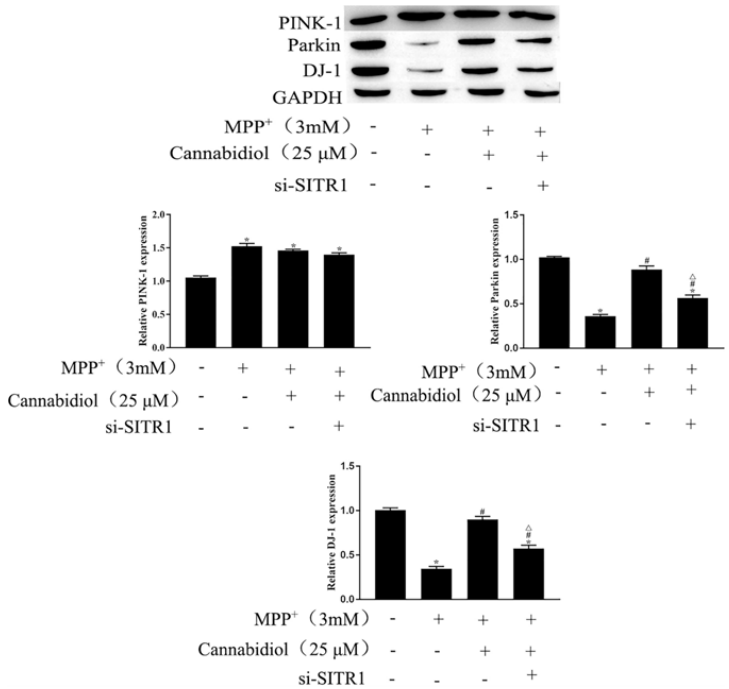

FIGURE 5 | Cannabidiol protected SH-SY5Y cells mitochondrial proteins through SIRT1. The expression of Parkin, PINK-1, DJ-1 in SH-SY5Y cells were measured by western blotting; $^{*}p < 0.05$, compared with the control group, $^{\#}p < 0.05$ compared with MPP^{+} alone, $^{\triangle}p < 0.05$ compared with MPP^{+} + Cannabidiol.

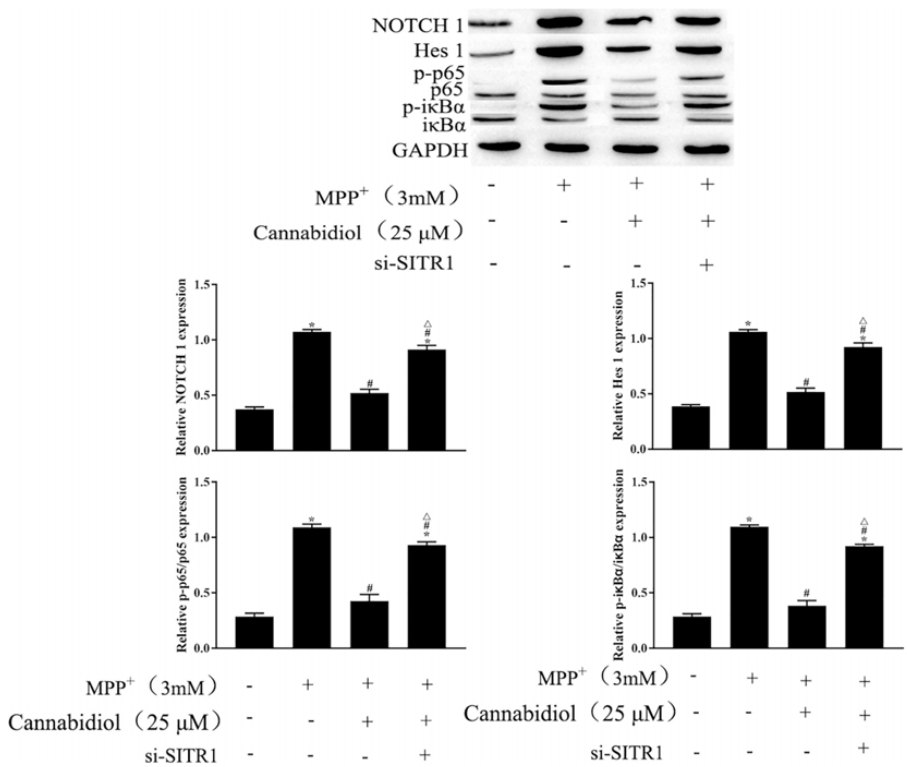

FIGURE 6 | Cannabidiol inhibits NF-κB and NOTCH pathways by upregulating SIRT1. The expression of p65, NOTCH in SH-SY5Y cells were measured by western blotting; $^{*}p < 0.05$, compared with the control group, $^{\#}p < 0.05$ compared with MPP^{+} alone, $^{\triangle}p < 0.05$ compared with MPP^{+} + Cannabidiol.

signaling pathway participates in the development process of PD (Gan et al., 2020). In this study, we found that Cannabidiol induced cell autophagy by upregulating SIRT1 to inhibits NOTCH1, Hes 1 expression and p65, iκBα phosphorylation.

In summary, the present study showed that Cannabidiol induces autophagy to ameliorate MPP^+ induced SH-SY5Y cell damage, rescued mitochondrial dysfunction, We further found that Cannabidiol induced cell autophagy by upregulating SIRT1 to inhibits NOTCH and NF-κB pathway. In conclusion, based on our findings, Cannabidiol is a potential candidate for the therapeutic treatment of PD.

DATA AVAILABILITY STATEMENT

The original contributions presented in the study are included in the article/supplementary material, further inquiries can be directed to the corresponding author/s.

ETHICS STATEMENT

This study was approved by the Ethics Committee of Kunming University of Science and Technology.

AUTHOR CONTRIBUTIONS

JXL designed the experiments. SLK and JLL wrote the article. SLK, JLL, and ZHY performed experiments and analyzed data. All the authors read and approved the final manuscript.

FUNDING

This study was supported by the National and Regional Science Foundation Projects 81860338 and Yunnan Province Foundation of Talent Cultivation (KKSY201960025).

REFERENCES

Ammal Kaidery, N., Ahuja, M., and Thomas, B. (2019). Crosstalk between Nrf2 signaling and mitochondrial function in Parkinson's disease. *Mol. Cell Neurosci.* 101:103413. doi: 10.1016/j.mcn.2019.103413

Atalay, S., Jarocka-Karpowicz, I., and Skrzydlewska, E. (2019). Antioxidative and anti-inflammatory properties of cannabidiol. *Antioxidants (Basel)* 9:21. doi: 10.3390/antiox9010021

Back, J. H., Rezvani, H. R., Zhu, Y., Guyonnet-Duperat, V., Athar, M., Ratner, D., et al. (2011). Cancer cell survival following DNA damage-mediated premature senescence is regulated by mammalian target of rapamycin (mTOR)-dependent Inhibition of sirtuin 1. *J. Biol. Chem.* 286, 19100–19108. doi: 10.1074/jbc.M111.240598

Bai, X., He, T., Liu, Y., Zhang, J., Li, X., Shi, J., et al. (2018). Acetylation-Dependent regulation of notch signaling in macrophages by SIRT1 affects sepsis development. *Front. Immunol.* 9:762. doi: 10.3389/fimmu.2018.00762

Bose, A., and Beal, M. F. (2016). Mitochondrial dysfunction in Parkinson's disease. *J. Neurochem.* 139(Suppl. 1), 216–231. doi: 10.1111/jnc.13731

Buneeva, O., Fedchenko, V., Kopylov, A., and Medvedev, A. (2020). Mitochondrial dysfunction in Parkinson's disease: focus on Mitochondrial DNA. *Biomedicines* 8:591. doi: 10.3390/biomedicines8120591

Cassano, T., Villani, R., Pace, L., Carbone, A., Bukke, V. N., Orkisz, S., et al. (2020). From *Cannabis sativa* to cannabidiol: promising therapeutic candidate for the treatment of neurodegenerative diseases. *Front. Pharmacol.* 11:124. doi: 10.3389/fphar.2020.00124

Chen, C., Xia, B., Tang, L., Wu, W., Tang, J., Liang, Y., et al. (2019). Echinacoside protects against MPTP/MPP(+)-induced neurotoxicity via regulating autophagy pathway mediated by Sirt1. *Metab. Brain Dis.* 34, 203–212. doi: 10.1007/s11011-018-0330-3

Choi, H. I., Kim, H. J., Park, J. S., Kim, I. J., Bae, E. H., Ma, S. K., et al. (2017). PGC-1α attenuates hydrogen peroxide-induced apoptotic cell death by upregulating Nrf-2 via GSK3β inactivation mediated by activated p38 in HK-2 Cells. *Sci. Rep.* 7:4319. doi: 10.1038/s41598-017-04593-w

Ding, W., Ding, L. J., Li, F. F., Han, Y., and Mu, L. (2015). Neurodegeneration and cognition in Parkinson's disease: a review. *Eur. Rev. Med. Pharmacol. Sci.* 19, 2275–2281.

Erb, M. L., and Moore, D. J. (2020). LRRK2 and the endolysosomal system in Parkinson's disease. *J. Parkinsons Dis.* 10, 1271–1291. doi: 10.3233/jpd-202138

Gan, P., Ding, L., Hang, G., Xia, Q., Huang, Z., Ye, X., et al. (2020). Oxymatrine attenuates dopaminergic neuronal damage and microglia-mediated neuroinflammation through Cathepsin D-Dependent HMGB1/TLR4/NF-κB pathway in Parkinson's disease. *Front. Pharmacol.* 11:776. doi: 10.3389/fphar.2020.00776

Ho, P. W., Leung, C. T., Liu, H., Pang, S. Y., Lam, C. S., Xian, J., et al. (2020). Age-dependent accumulation of oligomeric SNCA/α-synuclein from impaired degradation in mutant LRRK2 knockin mouse model of Parkinson disease: role for therapeutic activation of chaperone-mediated autophagy (CMA). *Autophagy* 16, 347–370. doi: 10.1080/15548627.2019.1603545

Imam Aliagan, A. D., Ahwazi, M. D., Tombo, N., Feng, Y., and Bopassa, J. C. (2020). Parkin interacts with Mitofilin to increase dopaminergic neuron death in response to Parkinson's disease-related stressors. *Am. J. Transl. Res.* 12, 7542–7564.

Jasmin, M., Ahn, E. H., Voutilainen, M. H., Fombonne, J., Guix, C., Viljakainen, T., et al. (2020). Netrin-1 and its receptor DCC modulate survival and death of dopamine neurons and Parkinson's disease features. *Embo J.* 40:e105537. doi: 10.15252/embj.2020105537

Kwon, Y., Bang, Y., Moon, S. H., Kim, A., and Choi, H. J. (2020). Amitriptyline interferes with autophagy-mediated clearance of protein aggregates via inhibiting autophagosome maturation in neuronal cells. *Cell Death Dis.* 11:874. doi: 10.1038/s41419-020-03085-6

Lei, H., Ren, R., Sun, Y., Zhang, K., Zhao, X., Ablat, N., et al. (2020). Neuroprotective effects of safflower flavonoid extract in 6-Hydroxydopamine-induced model of Parkinson's disease may be related to its anti-inflammatory action. *Molecules* 25:5206. doi: 10.3390/molecules25215206

Li, X., Feng, Y., Wang, X. X., Truong, D., and Wu, Y. C. (2020). The critical role of SIRT1 in Parkinson's Disease: mechanism and therapeutic considerations. *Aging Dis.* 11, 1608–1622. doi: 10.14336/ad.2020.0216

Mao, K., Chen, J., Yu, H., Li, H., Ren, Y., Wu, X., et al. (2020). Poly (ADP-ribose) polymerase 1 inhibition prevents neurodegeneration and promotes α-synuclein degradation via transcription factor EB-dependent autophagy in mutant α-synucleinA53T model of Parkinson's disease. *Aging Cell* 19:e13163. doi: 10.1111/acel.13163

Moors, T. E., Hoozemans, J. J., Ingrassia, A., Beccari, T., Parnetti, L., Chartier-Harlin, M. C., et al. (2017). Therapeutic potential of autophagy-enhancing agents in Parkinson's disease. *Mol. Neurodegener.* 12:11. doi: 10.1186/s13024-017-0154-3

Nobre, C. M. G., Pütz, N., König, B., Rupf, S., and Hannig, M. (2020). Modification of in situ biofilm formation on titanium by a hydroxyapatite nanoparticle-based solution. *Front. Bioeng. Biotechnol.* 8:598311. doi: 10.3389/fbioe.2020.598311

Opara, J., Małecki, A., Małecka, E., and Socha, T. (2017). Motor assessment in Parkinson's disease. *Ann. Agric. Environ. Med.* 24, 411–415. doi: 10.5604/12321966.1232774

Parray, H. A., and Yun, J. W. (2016). Cannabidiol promotes browning in 3T3-L1 adipocytes. *Mol. Cell Biochem.* 416, 131–139. doi: 10.1007/s11010-016-2702-5

Quinn, P. M. J., Moreira, P. I., Ambrósio, A. F., and Alves, C. H. (2020). PINK1/PARKIN signalling in neurodegeneration and neuroinflammation. *Acta Neuropathol. Commun.* 8:189. doi: 10.1186/s40478-020-01062-w

Santiago, J. A., Bottero, V., and Potashkin, J. A. (2017). Biological and clinical implications of comorbidities in Parkinson's disease. *Front. Aging Neurosci.* 9:394. doi: 10.3389/fnagi.2017.00394

Santos, N. A., Martins, N. M., Sisti, F. M., Fernandes, L. S., Ferreira, R. S., Queiroz, R. H., et al. (2015). The neuroprotection of cannabidiol against MPP^+-induced toxicity in PC12 cells involves trkA receptors, upregulation of axonal and synaptic proteins, neuritogenesis, and might be relevant to Parkinson's disease. *Toxicol. In Vitro* 30(1 Pt. B), 231–240. doi: 10.1016/j.tiv.2015.11.004

Silvestro, S., Schepici, G., Bramanti, P., and Mazzon, E. (2020). Molecular targets of cannabidiol in experimental models of neurological disease. *Molecules* 25:5186. doi: 10.3390/molecules25215186

Sveinbjornsdottir, S. (2016). The clinical symptoms of Parkinson's disease. *J. Neurochem.* 139(Suppl. 1), 318–324. doi: 10.1111/jnc.13691

Vidyadhara, D. J., Lee, J. E., and Chandra, S. S. (2019). Role of the endolysosomal system in Parkinson's disease. *J. Neurochem.* 150, 487–506. doi: 10.1111/jnc.14820

Wan, T., Weir, E. J., Johnson, M., Korolchuk, V. I., and Saretzki, G. C. (2020). Increased telomerase improves motor function and alpha-synuclein pathology in a transgenic mouse model of Parkinson's disease associated with enhanced autophagy. *Prog. Neurobiol.* 199:101953. doi: 10.1016/j.pneurobio.2020.101953

Wang, W., Wang, X., Fujioka, H., Hoppel, C., Whone, A. L., Caldwell, M. A., et al. (2016). Parkinson's disease-associated mutant VPS35 causes mitochondrial dysfunction by recycling DLP1 complexes. *Nat. Med.* 22, 54–63. doi: 10.1038/nm.3983

Watt, G., and Karl, T. (2017). In vivo evidence for therapeutic properties of Cannabidiol (CBD) for Alzheimer's disease. *Front. Pharmacol.* 8:20. doi: 10.3389/fphar.2017.00020

Xu, Y., Zhi, F., Mao, J., Peng, Y., Shao, N., Balboni, G., et al. (2020). δ-opioid receptor activation protects against Parkinson's disease-related mitochondrial dysfunction by enhancing PINK1/Parkin-dependent mitophagy. *Aging (Albany NY)* 12, 25035–25059. doi: 10.18632/aging.103970

Yan, J., Huang, J., Liu, A., Wu, J., Fan, H., Shen, M., et al. (2020). Atorvastatin improves motor function, anxiety and depression by NOX2-mediated autophagy and oxidative stress in MPTP-lesioned mice. *Aging (Albany NY)* 13, 831–845. doi: 10.18632/aging.202189

Zhu, Z., Yang, C., Iyaswamy, A., Krishnamoorthi, S., Sreenivasmurthy, S. G., Liu, J., et al. (2019). Balancing mTOR signaling and autophagy in the treatment of Parkinson's disease. *Int. J. Mol. Sci.* 20:728. doi: 10.3390/ijms20030728

Conflict of Interest: The authors declare that the research was conducted in the absence of any commercial or financial relationships that could be construed as a potential conflict of interest.

frontiers in Cellular Neuroscience

ORIGINAL RESEARCH
published: 16 April 2021
doi: 10.3389/fncel.2021.653881

NF-κB-Induced Upregulation of miR-146a-5p Promoted Hippocampal Neuronal Oxidative Stress and Pyroptosis *via* TIGAR in a Model of Alzheimer's Disease

Bo Lei[1,2], *Jiaxin Liu*[3], *Zhihui Yao*[3,4], *Yan Xiao*[3], *Xiaoling Zhang*[3], *Yueting Zhang*[5]* and *Jianguo Xu*[1]*

[1]Department of Neurosurgery, West-China Hospital, Sichuan University, Chengdu, China, [2]Department of Neurosurgery, People's Hospital of Leshan, Leshan, China, [3]Medical School, Kunming University of Science and Technology, Kunming, China, [4]Department of Burn and Plastic Surgery, 926 Hospital of People's Liberation Army, Kaiyuan, China, [5]Special Ward, The Second Affiliated Hospital of Kunming Medical University, Kunming, China

OPEN ACCESS

Edited by:
Zhang Pengyue,
Yunnan University of Traditional Chinese Medicine, China

Reviewed by:
Yongbo Kang,
Shanxi Medical University, China
Jian Wang,
Yunnan University of Traditional Chinese Medicine, China

***Correspondence:**
Yueting Zhang
Yueting_1985@163.com
Jianguo Xu
xujg@scu.edu.cn

Specialty section:
This article was submitted to Cellular Neuropathology, a section of the journal Frontiers in Cellular Neuroscience

Received: 15 January 2021
Accepted: 18 March 2021
Published: 16 April 2021

Citation:
Lei B, Liu J, Yao Z, Xiao Y, Zhang X, Zhang Y and Xu J (2021) NF-κB-Induced Upregulation of miR-146a-5p Promoted Hippocampal Neuronal Oxidative Stress and Pyroptosis via TIGAR in a Model of Alzheimer's Disease. Front. Cell. Neurosci. 15:653881. doi: 10.3389/fncel.2021.653881

Alzheimer's disease (AD) is a common neurodegenerative disorder that places a heavy burden on patients and society. Hippocampal neuronal loss is a hallmark of AD progression. Therefore, understanding the mechanism underlying hippocampal neuronal death would be of great importance for the diagnosis and treatment of AD. This study aimed to explore the molecular mechanism *via* which nuclear factor kappa β (NF-κB) promotes hippocampal neuronal oxidative stress and pyroptosis in AD. We collected serum samples from 101 healthy elderly people and 112 patients with AD at the Affiliated Hospital of Kunming University of Science and Technology between January 2017 and January 2020. Commercially available human hippocampal neurons (HHNs) were used to establish an AD model (AD-HHN) following Aβ25–35 treatment. The mRNA expression levels of NF-κB and pyroptosis markers [NLR family pyrin domain-containing 3, caspase-1, interleukin (IL)-1β, and interleukin-18] mRNA and the expression level of miR-146a-5p in the serum samples of patients with AD and AD-HHNs were determined by quantitative reverse transcription polymerase chain reaction. Oxidative stress indices (reactive oxygen species, malondialdehyde, nicotinamide adenine dinucleotide phosphate, superoxide dismutase, glutathione, and catalase) were measured by Enzyme-Linked Immunosorbent Assay (ELISA). The expression of proteins [NF-κB, TP53-induced glycolysis and apoptosis regulator (TIGAR), and pyroptosis markers] was tested by western blotting. The relationship between miR-146a-5p and TIGAR was investigated using a dual luciferase reporter gene assay. We found that NF-κB and miR-146a-5p were highly expressed, while TIGAR was low expressed in patients with AD and AD-HHNs. In addition, there was a significant positive correlation between the expression levels of NF-κB and miR-146a-5p, but a negative correlation between NF-κB mRNA and TIGAR mRNA in patients with AD, as well as miR-146a-5p and TIGAR mRNA in patients with AD. In AD-HNNs, miR-146a-5p targeted and downregulated

the expression of TIGAR. Knockdown of NF-κB or overexpression of TIGAR markedly attenuated oxidative stress and pyroptosis in AD-HHNs, while concurrent overexpression of miR-146a-5p inhibited these effects. In conclusion, NF-κB-induced upregulation of miR-146a-5p promoted oxidative stress and pyroptosis in AD-HNNs by targeting TIGAR.

Keywords: pyroptosis, oxidative stress, NF-κB, miRNA, hippocampus, Alzheimer's disease, TP53-induced glycolysis and apoptosis regulator

INTRODUCTION

Alzheimer's disease (AD) is a common age-related neurodegenerative disorder characterized by a functional decline (Høgh, 2017). AD has a high incidence its prevalence and mortality rates, and its treatment and care are costly, thus placing a tremendous burden on caregivers and society (Yilmaz, 2015; Alzheimer's Association, 2016; Hodson, 2018). The hippocampus is a brain area critical for learning and memory, and it has become increasingly clear that loss of hippocampal neurons occurs in AD (Mu and Gage, 2011). The fate of hippocampal neurons is essential for the occurrence and development of AD (Richetin et al., 2015; Hu et al., 2019). Therefore, understanding the mechanism underlying hippocampal neuronal death would be of great importance for the diagnosis and treatment of AD.

AD is highly correlated with neuroinflammation and oxidative stress in the brain causing neuronal loss. Nuclear factor kappa β (NF-κB) is a proinflammatory, redox-sensitive transcription factor that plays an important role in AD (Ju Hwang et al., 2019). It also regulated hippocampal neuron apoptosis and cognitive impairment (Fang et al., 2019). Besides, NF-κB plays a key role in cytokine-induced gene expression, there was a previous study has found a consistent upregulation of several brain-enriched miRNAs (miR-9, miR-34a, miR-125b, miR-146a, and miR-155) that are under the transcriptional control of NF-kB in AD brain tissues (Zhao et al., 2014). Among the several upregulated miRNAs, miR-146a-5p (miR-146 or miR-146a) drew our attention: miR-146a-5p is deregulated in the peripheral blood of patients with AD and might serve as a diagnostic or therapeutic biomarker for AD (Gupta et al., 2017; Fransquet and Ryan, 2018). It is also involved in the progression from mild cognitive impairment to AD (Ansari et al., 2019). However, the molecular mechanism *via* which miR-146a-5p promotes progression to AD is still unknown.

Network analysis has revealed that miRNAs, including miR-146a-5p, are associated with the immune system, cell cycle, gene expression, cellular response to stress, and neuron growth factor signaling (Swarbrick et al., 2019). When we predicted the target genes of miR-146a-5p using bioinformatics, TP53-induced glycolysis and apoptosis regulator (TIGAR) drew our attention due to its role in oxidative stress in AD (Katsel et al., 2013). Therefore, we studied the role of miR-146a-5p/TIGAR in AD.

Oxidative stress contributes to AD by promoting amyloid-beta peptide (Aβ) deposition, hyperphosphorylated tau protein accumulation, and synapse and neuronal cell loss (Chen and Zhong, 2014; Tönnies and Trushina, 2017). Oxidative stress products can activate cells, induce pyroptosis, and promote disease progression (Wang et al., 2019). Pyroptosis is a recently discovered type of programmed cell death that depends on the activation of caspase-1 and the release of a large number of proinflammatory factors (Shi et al., 2017). Increasing evidence has indicated that the pyroptosis of neuronal cells is closely related to the progression of AD (Fricker et al., 2018; Han et al., 2020).

This study aimed to explore the molecular mechanism *via* which NF-κB-induced regulation of miR-146a-5p/TIGAR promotes oxidative stress and pyroptosis in AD.

MATERIALS AND METHODS

Collection of Serum Samples

Serum samples were collected from 101 healthy elderly individuals (49 men, 52 women; mean age, 63.57 ± 5.89 years) and 112 patients with AD (59 men, 53 women; mean age, 65.13 ± 6.05 years) at the Affiliated Hospital of Kunming University of Science and Technology between January 2017 and January 2020. There was no significant difference in sex and age between the group of healthy elderly individuals and the group of patients with AD. All the participants were informed of the details of the study and gave written informed consent to participate. The study was approved by the Ethics Committee of Kunming University of Science and Technology (No. KMUST-MEC-041). All experiments were performed following the guidelines of the Helsinki Declaration.

Cell Culture and Construction of AD Model

Human hippocampal neurons (HHNs; #P10153; Innoprot, Spain) were purchased *via* Beijing Biolead Biological Science and Technology Co., Ltd. and cultured in Dulbecco's Modified Eagle Medium/Nutrient Mixture F-12 (DMEM-F12, #P008–2; Yaji, Shanghai, China) containing 10% fetal bovine serum (#C0257; Yaji), 2% B-27 (#PB180630; Yaji), and 0.3 mg/ml glutamine (#Q112655; Yaji) at 37°C and 5% CO_2. After 7 days, cultured HHNs were used to establish a model of AD. Briefly, HNNs were treated with 10 μmol/L Aβ25–35 (#A4559–1MG; Sigma, USA) for 72 h, and named AD-HHNs.

Cell Transfection

AD-HHNs were seeded at 1×10^5 cells/well in a 6-well plate and maintained in a humidified incubator at 37°C and 5% CO_2. When AD-HHNs reached 70% confluency after 24 h, cell transfection was performed. Guangzhou Ruibo Biotechnology

Company, Limited (China) designed and produced si-NF-κB, miR-146a-5p inhibitor, miR-146a-5p mimics, and pcDNA-TIGAR. AD-HHN cell transfection was performed by using Lipofectamine 2000 (#11668–019; Invitrogen, Carlsbad, CA, USA) according to the manufacturer's instructions.

Quantitative Reverse Transcription Polymerase Chain Reaction (qRT-PCR)

The total RNA of serum samples and HHNs was isolated using the TRIzol RNA Extraction Kit (#WE0192-EYI; BioMart, Beijing, China). Isolated total RNA was reverse transcribed into cDNA using a reverse transcription kit (#QN0931-OSF; BioMart). Subsequently, SYBR Premix Ex Taq II (#RR820A; Takara, Japan) was used to perform qRT-PCR using the following steps: denaturation at 90°C for 5 min, followed by 45 cycles of denaturation at 90°C for 1 min, annealing at 60°C for 40 s, and extension at 75°C for 30 s, and a final extension at 75°C for 5 min. The relative expression of mRNA and miRNA was analyzed using the 2-ΔΔCt method. The forward and reverse primers were as follows: NF-κB F: 5′-AGCACAGA TACCACCAAGACC-3′ and R 5′-GGGCACGATTGTCAAA GAT-3′; miR-146a-5p F: 5′-GGCGGTGAGAACTGAATTCC-3′ and R 5′-TTGCACTGGATACGACAACC-3′; NLR family pyrin domain containing 3 (NLRP3) F: 5′-CAGACCTCCAAGACCA GGACTG-3′ and R 5′-CATCCGCAGCCAATGAACACAC-3′; caspase-1 F: 5′-TGCCTGGTCTTGTGACTTGGAG-3′ and R 5′-ATGTCCTGGGAAGAGGTAGAAACG-3′; interleukin (IL)-1β F: 5′-ACAGATGAAGTGCTCCTTCCA-3′ and R 5′-GTCG GAGATTCGTAGCTGGAT-3′; IL-18 F: 5′-ATATCGACCGAA CAGCCAAC-3′ and R 5′-TTCCATCCTTCACAGATAGGG-3′; GAPDH F: 5′-TCGACAGTCAGCCGCATCTTCTTT-3′ and R 5′-GCCCAATACGACCAAATCCGTTGA-3′; and U6 F: 5′-CT CGCTTCGGCAGCACA-3′ and R 5′-AACGCTTCACGAATTT GCGT-3′.

Western Blotting

The total protein of HHNs was extracted using a total protein extraction kit (#BB-3101; BestBio, Shanghai, China) and the concentration of isolated total protein was measured using a BCA protein quantification kit (#BB-3401; BestBio). Next, equivalent amounts of protein were separated by 10% sodium dodecyl sulfate polyacrylamide gel electrophoresis (SDS PAGE, #YJ0014B; Yiji, Shanghai, China) and transferred onto a polyvinylidene difluoride (PVDF, #SD7966555; Yiji) membrane. Subsequently, the PVDF membrane was blocked with 5% skim milk at room temperature for 1 h, then treated with primary antibodies against NF-κB (1:1,000, #ER0815; HUABIO, Hangzhou, China), anti-NLRP3 (1:1,000, #ER1706-72; HUABIO), anti-caspase-1 (1:1,000, #ET1608-69; HUABIO), anti-IL-1β (1:1,000, #ET1701-39; HUABIO), anti-IL-18 (1:1,000, #EM170401; HUABIO), anti-TIGAR (1:1,000, #ER62495; HUABIO), and anti-GAPDH (1:1,000, #ER1901-65; HUABIO) overnight at 4°C. The next day, a secondary antibody (1:1,000, #HA1024; HUABIO) was used to treat the PVDF membrane at 37°C for 1 h. Protein bands were visualized using an ECL chemiluminescence detection kit (#BB-3501; BestBio). ImageJ was used to analyze the gray values of bands.

Enzyme-Linked Immunosorbent Assay (ELISA)

Oxidative stress indices [reactive oxygen species (ROS), malondialdehyde (MDA), nicotinamide adenine dinucleotide phosphate (NADPH), superoxide dismutase (SOD), glutathione (GSH), and catalase (CAT)] in HNNs were measured using ELISA kits according to the manufacturer's instructions. All ELISA kits were purchased from Wuhan Chundu Biological Science and Technology Company Limited, including human ROS ELISA kit (#CD-100411-ELISA; Chundu), human MDA ELISA kit (#CD-100334-ELISA; Chundu), human NADPH ELISA kit (#CD-101534-ELISA; Chundu), human SOD ELISA kit (#CD-100247-ELISA; Chundu), human GSH ELISA kit (#CD-101068-ELISA; Chundu), and human CAT ELISA kit (#CD-102196-ELISA; Chundu).

Dual Luciferase Reporter Genes Gene Assay

A dual luciferase reporter gene assay kit (#11402ES60; Yeasen, Shanghai, China) was used to investigate the relationship between miR-146a-5p and TIGAR. In detail, the 3′-UTR of TIGAR wild type (TIGAR-WT) or TIGAR mutant type (TIGAR-MUT) was cloned into the pGLO luciferase vector, and transfected into HHNs, with or without miR-146a-5p mimics, using Lipofectamine 2000. After 48 h, the luciferase activity of HHNs was detected using a dual luciferase reporter assay system (Promega Corporation, Madison, WI, USA).

Statistical Analysis

In this study, data from three independent experiments were presented as means ± standard deviation and analyzed using SPSS 19.0 software. The difference between the two groups was compared by using Student's *t*-test, and that among groups was assessed by one-way analysis of variance (ANOVA). The correlation between NF-κB mRNA and miR-146a-5p, NF-κB mRNA and TIGAR mRNA, miR-146a-5p, and TIGAR mRNA were calculated using linear regression analysis. $P < 0.05$ was considered statistically significant.

RESULTS

The Expression of NF-κB Is Correlated With miR-146a-5p in Patients With AD and AD-HNNs

NF-κB plays an important role in AD, and miR-146a-5p is one of the target miRNAs of NF-κB. To study the function of NF-κB or miR-146a-5p in the progression of AD, we first determined their expression levels in patients with AD. qRT-PCR results showed that the expression levels of NF-κB mRNA (**Figure 1A**) and miR-146a-5p (**Figure 1B**) in serum samples from patients with AD were higher than those in healthy individuals. A linear analysis revealed a positive correlation between NF-κB mRNA and miR-146a-5p in patients with AD (**Figure 1C**).

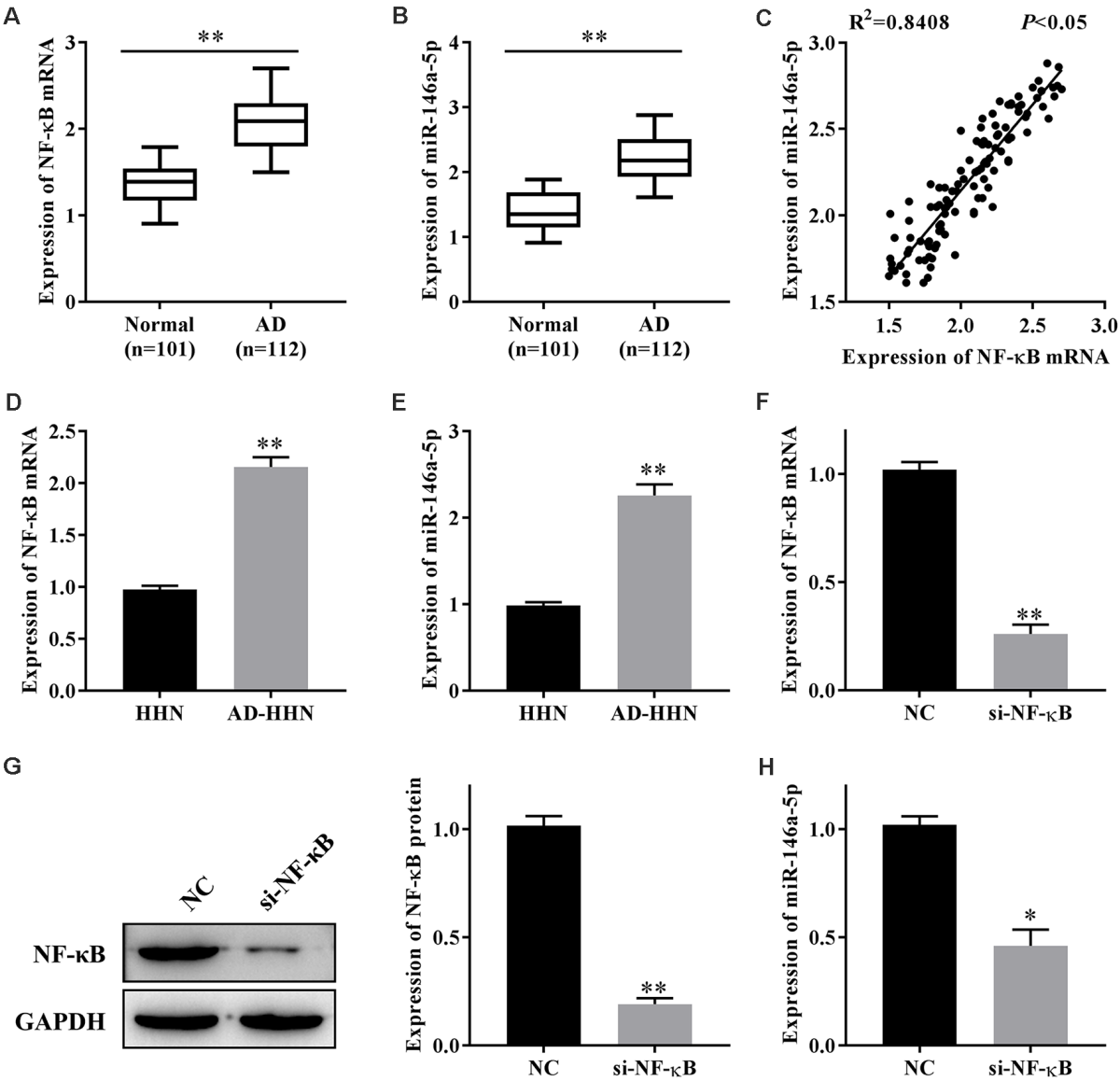

FIGURE 1 | The expression of nuclear factor kappa β (NF-κB) is correlated with that of miR-146a-5p in patients with Alzheimer's disease (AD) and a cell culture model of AD in human hippocampal neurons (AD-HNNs). **(A)** Relative expression level of NF-κB mRNA. $^{**}P < 0.01$ vs. normal group. **(B)** Relative expression level of miR-146a-5p. $^{**}P < 0.01$ vs. normal group. **(C)** Linear analysis between NF-κB mRNA and miR-146a-5p. **(D)** NF-κB mRNA in AD-HNNs. $^{**}P < 0.01$ vs. HHN group. **(E)** NF-κB protein in AD-HNNs. $^{**}P < 0.01$ vs. HHN group. **(F)** Transfection efficiency of si-NF-κB into AD-HNNs. $^{**}P < 0.01$ vs. NC group. **(G)** Expression of NF-κB protein after si-NF-κB transfection into AD-HNNs. $^{**}P < 0.01$ vs. NC group. **(H)** Expression of miR-146a-5p after si-NF-κB transfection into AD-HNNs. $^{*}P < 0.05$ vs. NC group.

Next, we established a cell culture model of AD by treating HNNs with Aβ25–35 (AD-HNNs). qRT-PCR results showed that the expression levels of NF-κB mRNA (**Figure 1D**) and miR-146a-5p (**Figure 1E**) in AD-HHNs were higher than those in HHNs. To knockdown NF-κB, we transfected si-NF-κB into AD-HHNs, and confirmed the transfection efficiency by qRT-PCR (**Figure 1F**) and western blotting (**Figure 1G**). When the transfection was successful, we determined the expression level of miR-146a-5p by qRT-PCR (**Figure 1H**). Knockdown of NF-κB in AD-HHNs significantly reduced the expression of miR-146a-5p. Therefore, we speculated that one way NF-κB might play a role in AD is through the upregulation of miR-146a-5p.

NF-κB Promotes Oxidative Stress and Pyroptosis in AD-HNNs *via* miR-146a-5p

Hippocampal neuronal loss is a hallmark of AD progression, and oxidative stress and pyroptosis can lead to hippocampal neuronal loss. The experiments described above showed that NF-κB might play a role in AD through miR-146a-5p. Next,

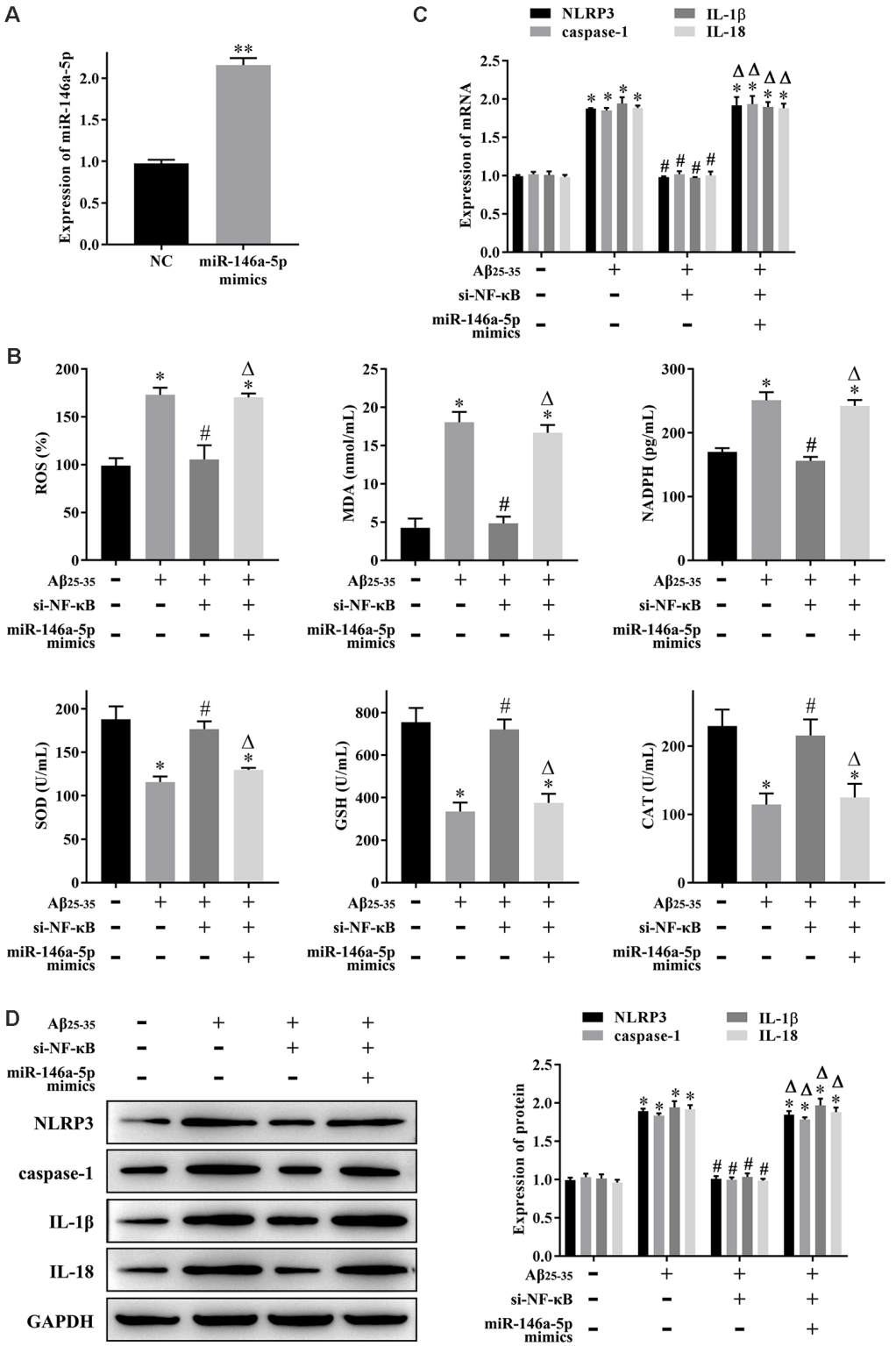

FIGURE 2 | NF-κB promotes oxidative stress and pyroptosis in a cell culture model of Alzheimer's disease in human hippocampal neurons (AD-HNNs) *via* miR-146a-5p. **(A)** Transfection efficiency of miR-146a-5p mimics into AD-HNNs. $^{**}P < 0.01$ vs. NC group. **(B)** Level of oxidative stress indices [reactive oxygen species (ROS), malondialdehyde (MDA), nicotinamide adenine dinucleotide phosphate (NADPH), superoxide dismutase (SOD), glutathione (GSH), and catalase (CAT)]. **(C)** mRNA expression of pyroptosis markers (NLRP3, caspase-1, Interleukin (IL)-1β, and IL-18). **(D)** Protein expression of pyroptosis markers (NLRP3, caspase-1, IL-1β, and IL-18). $^{*}P < 0.05$ vs. HHN group; $^{\#}P < 0.05$ vs. AD-HHN group; $^{\Delta}P < 0.05$ vs. AD-HHN+si-NF-κB group.

we studied the effect of NF-κB-induced upregulation of miR-146a-5p on oxidative stress and pyroptosis in AD-HHNs. After knockdown of NF-κB (**Figures 1F,G**) or overexpression of miR-146a-5p (**Figure 2A**) in AD-HHNs, we checked the transfection efficiency of miR-146a-5p by qRT-PCR. Next, we measured the levels of oxidative stress in each group of cells (**Figure 2B**). The levels of ROS, MDA, and NADPH were increased, while those of SOD, GSH, and CAT were decreased in AD-HHNs compared to HHNs. Knockdown of NF-κB attenuated oxidative stress in AD-HHNs. Moreover, knockdown of NF-κB combined with overexpression of miR-146a-5p restored all oxidative stress indices in AD-HHNs to levels similar to those in HHNs. We also measured pyroptosis markers (**Figures 2C,D**). The levels of NLRP3, caspase-1, IL-1β, and IL-18 mRNA and protein were increased in AD-HHNs compared to HHNs. Knockdown of NF-κB in AD-HHN reduced their expression in AD-HHNs. However, knockdown of NF-κB combined with overexpression of miR-146a-5p and elevated their expression compared to only knockdown of NF-κB in AD-HHNs. These results suggested that NF-κB might promote oxidative stress and pyroptosis in AD-HHNs through the upregulation of miR-146a-5p.

miR-146a-5p Reduces the Expression of TIGAR

We have previously predicted the target genes of miR-146a-5p by using bioinformatics. TIGAR aroused our great interest, and the binding sites are shown in **Figure 3A**. To confirm the relationship between miR-146a-5p and TIGAR, we transfected miR-146a-5p mimics into HHNs and checked the transfection efficiency by qRT-PCR. The results showed that the expression level of miR-146a-5p was substantially increased in the miR-146a-5p mimic group compared to the NC group (**Figure 3B**). Moreover, a dual luciferase reporter gene assay revealed that overexpression of miR-146a-5p markedly reduced the luciferase activity of TIGAR-WT but had no significant effect on TIGAR-MUT (**Figure 3C**). In addition, western blotting revealed that overexpression of miR-146a-5p significantly reduced the expression of TIGAR (**Figure 3D**). These results indicated that miR-146a-5p targeted and downregulated TIGAR in HHNs.

miR-146a-5p Regulates Oxidative Stress and Pyroptosis in AD-HHNs *via* TIGAR

To clarify whether NF-κB regulates oxidative stress and pyroptosis through the miR-146a-5p/TIGAR axis, we first measured the expression levels of TIGAR mRNA in patients with AD, and qRT-PCR results showed that it was lower in serum samples from patients with AD than that in healthy individuals (**Figure 4A**). The linear analysis revealed a negative correlation between NF-κB mRNA and TIGAR mRNA in patients with AD (**Figure 4B**), as well as miR-146a-5p and TIGAR mRNA (**Figure 4C**). Furthermore, we transfected pcDNA-TIGAR or miR-146a-5p mimics into AD-HHNs, then measured the expression of TIGAR protein by western blotting. The results showed that the expression of TIGAR protein in HHNs was higher than that in AD-HHNs. Transfection of pcDNA-TIGAR into AD-HHNs increased its expression.

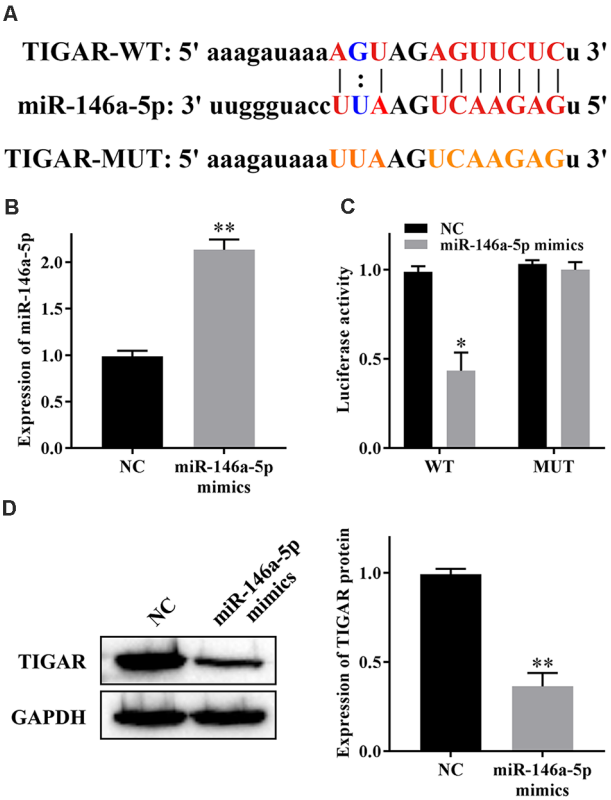

FIGURE 3 | miR-146a-5p reduces the expression of TIGAR. **(A)** Binding sites between miR-146a-5p and TIGAR. **(B)** Transfection efficiency of miR-146a-5p mimics. **(C)** Dual luciferase reporter gene assay. **(D)** Expression of TIGAR protein. $^{*}P < 0.05$ vs. NC group; $^{**}P < 0.01$ vs. NC group.

However, transfection of pcDNA-TIGAR combined with miR-146a-5p mimics into AD-HHNs resulted in an expression level of TIGAR protein similar to that of non-transfected AD-HHNs (**Figure 4D**). Overexpression of TIGAR relieved oxidative stress (**Figure 4E**) and pyroptosis (**Figures 4F,G**) in AD-HHNs. However, transfection of pcDNA-TIGAR combined with miR-146a-5p mimics reverted these improvements. These results indicated that miR-146a-5p exacerbated oxidative stress and pyroptosis in AD-HHNs through TIGAR.

DISCUSSION

AD is a neurodegenerative disorder and the most common and devastating form of dementia, which impacts the lifestyle of patients and their families, and society, due to the high costs of social and medical care (Di Resta and Ferrari, 2019). Therefore, understanding the pathogenic mechanisms of this disorder has great social, academic, and clinical implications. In this study, we explored the molecular mechanism *via* which NF-κB promotes oxidative stress and pyroptosis in AD. We found that NF-κB-induced upregulation of miR-146a-5p promoted oxidative stress and pyroptosis in a hippocampal neuronal cell model of AD through TIGAR.

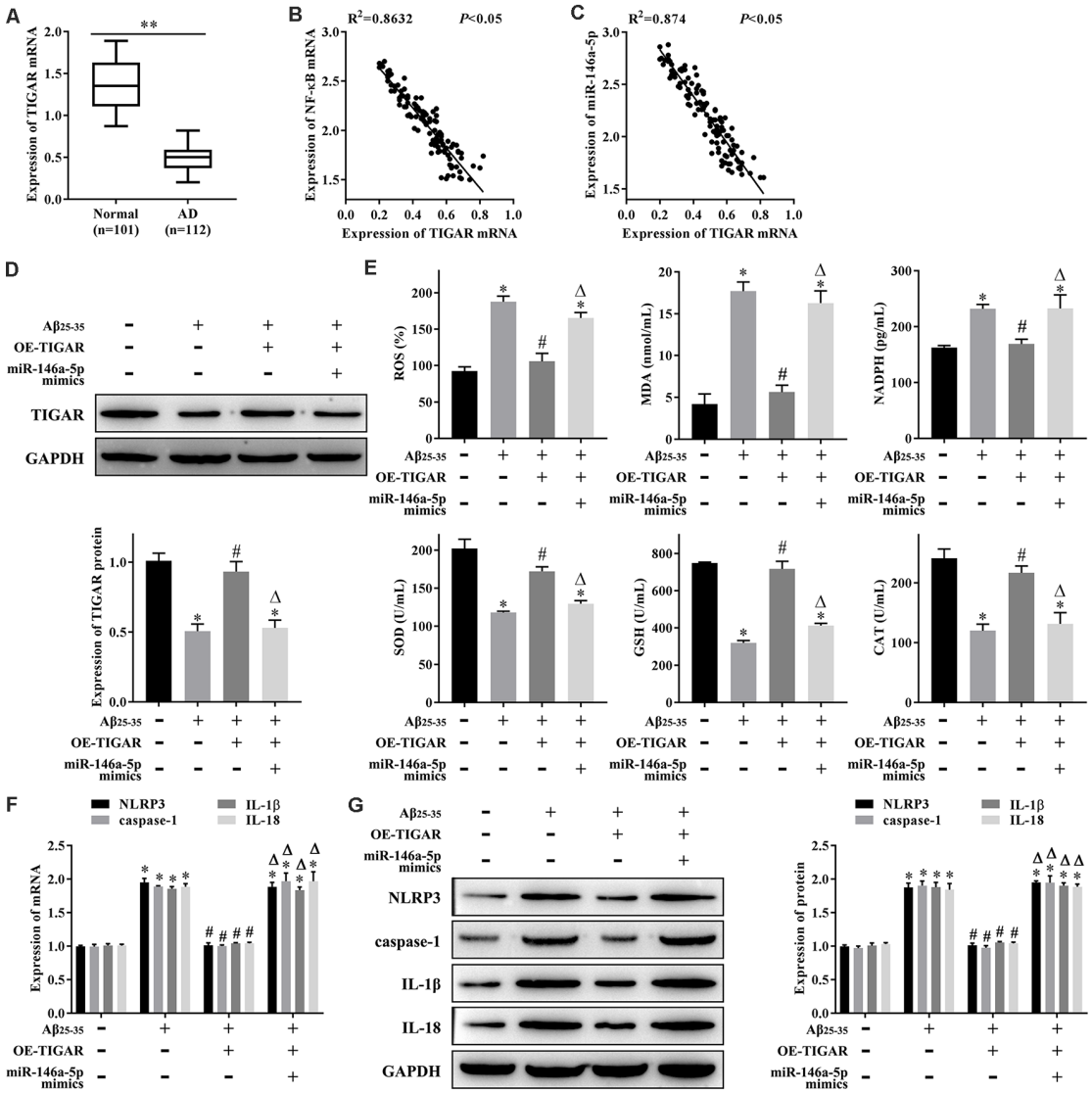

FIGURE 4 | miR-146a-5p regulates oxidative stress and pyroptosis in a cell culture model of Alzheimer's disease in human hippocampal neurons (AD-HNNs) *via* TIGAR. **(A)** Relative expression level of TIGAR mRNA. $^{**}P < 0.01$ vs. normal group. **(B)** Linear analysis between NF-κB mRNA and TIGAR mRNA. **(C)** Linear analysis between miR-146a-5p and TIGAR mRNA. **(D)** Protein expression of TIGAR. **(E)** Level of oxidative stress indices (ROS, MDA, NADPH, SOD, GSH, and CAT). **(F)** mRNA expression of pyroptosis markers (NLRP3, caspase-1, IL-1β, and IL-18). **(G)** Protein expression of pyroptosis markers (NLRP3, caspase-1, IL-1β, and IL-18). $^{*}P < 0.05$ vs. HHN group; $^{\#}P < 0.05$ vs. AD-HHN group; $^{\Delta}P < 0.05$ vs. AD-HHN+OE-TIGAR group.

NF-κB contributes to the pathogenesis of AD by participating in synaptic plasticity, learning and memory, insulin resistance, oxidative stress, neuroinflammation, and metabolism (Marwarha and Ghribi, 2017). Another study confirmed that inhibitors of NF-κB might be a novel therapeutic opportunity for AD (Seo et al., 2018). In our study, we found that NF-κB was highly expressed in patients with AD and AD-HHNs, and that knockdown of NF-κB effectively relieved oxidative stress and pyroptosis in AD-HHNs. The most well-known factor leading to AD is changes in amyloid precursor protein cleavage and production of Aβ (Soria Lopez et al., 2019). One study has proved that $A\beta_{25–35}$ induces neuronal inflammation by reducing the nuclear import of NF-κB (Liu et al., 2017). Our results add evidence to the links between the role of NF-κB in hippocampal neurons and the progression of AD.

At the molecular level, NF-κB plays a role in AD by regulating various downstream effectors, including the molecules involved in signaling pathways, such as the PI3K/AKT, MAPK, and AGE/RAGE/GSK-3, and newly discovered noncoding RNAs (ncRNAs), which mediate neuronal toxicity or protection (Shi et al., 2016). miRNA is a type of ncRNA. In our study, we found a significant positive relationship between the level of NF-κB and miR-146a-5p in patients with AD, and knockdown of NF-κB in AD-HHNs markedly reduced the expression of miR-146a-5p. A previous study indicated that NF-κB-sensitive miR-

146a-mediated modulation of complement factor H (CFH), an important repressor of the inflammatory response in the brain, regulates the inflammatory response in AD brains and human neuronal cell models of AD (Lukiw et al., 2008; Pogue et al., 2009). According to that study, NF-κB-induced upregulation of miR-146a-5p promotes the inflammatory response in AD and neuronal cells, and there exists a cause–effect relationship between inflammatory response and pyroptosis. That previous study supported our findings. It has been proven that the inflammasome platform leads to activation of caspase-1 through proximity-induced self-cleavage, which further induces the activation and secretion of IL-1β and IL-18. Activated caspase-1 also cleaves gasdermin D, which results in a particular form of lytic, programmed cell death named pyroptosis (Jorgensen and Miao, 2015; Malik and Kanneganti, 2017).

In our study, we found that overexpression of TIGAR, a target of miR-146a-5p, inhibited oxidative stress and pyroptosis in AD-HHNs. TIGAR is a p53-inducible gene that correlates with an ability to protect cells from ROS-associated apoptosis, in detail, TIGAR expression lowered fructose-2,6-bisphosphate levels in cells, resulting in an inhibition of glycolysis and an overall decrease in intracellular ROS levels, and consequently, knockdown of endogenous TIGAR expression sensitized cells to p53-induced death (Bensaad et al., 2006). A previous study has shown that TIGAR inhibits microglial pyroptosis and plays a protective role in neonatal hypoxic-ischemic brain damage; in that study, knockdown of TIGAR in rats markedly worsened pyroptosis and brain damage after hypoxia/ischemia *in vivo* and *in vitro* (Tan et al., 2021). Moreover, a study has suggested that overexpression of TIGAR increases the levels of NADPH, reduced GSH, and inducible nitric oxide synthase (iNOS), reduces intracellular ROS and increases the release of proinflammatory cytokines IL-1β and tumor necrosis factor-α in cultured primary astrocytes (Chen et al., 2018). Our work further strengthens the evidence that TIGAR affects pyroptosis through a regulated inflammatory response.

In summary, our results showed that NF-κB and miR-146a-5p were highly expressed in patients with AD and AD-HHNs and that there was a positive relationship between NF-κB and miR-146a-5p. Therefore, we speculated that one way NF-κB might play a role in AD through the upregulation of miR-146a-5p. Moreover, knockdown of NF-κB relieved oxidative stress and pyroptosis in AD-HHNs, while miR-146a-5p overexpression inhibited these effects. In addition, miR-146a-5p targeted and downregulated the expression of TIGAR in HHNs. Furthermore, the inhibition of oxidative stress and pyroptosis in AD-HHNs caused by overexpression of TIGAR was reversed by overexpression of miR-146a-5p. Therefore, our results indicated that NF-κB promoted oxidative stress and pyroptosis in AD-HHNs through the miR-146a-5p/TIGAR axis. This molecular mechanism of oxidative stress and pyroptosis in AD hippocampal neurons probably has some guiding significance for exploring new therapeutic targets, such as the knockdown of NF-κB or miR-146a-5p, overexpression of TIGAR, inhibition of oxidative stress, and pyroptosis in AD hippocampal neurons.

The major limitation of this study is that all the *in vitro* experiments were performed in normal HHNs and AD-HHNs. However, the hippocampus is more complex. It is possible that some special conditions in the hippocampus of AD patients could influence the results. Hence, we are performing further studies on this mechanism in mice with AD. In addition, it is worth noting that NF-κB plays a dualistic role in the pathogenesis of AD. In our study, we focused on the function and mechanism of NF-κB in oxidative stress and pyroptosis in a hippocampal neuronal cell model of AD. On the other hand, NF-κB might be beneficial in AD. Thus, to provide the potential pathogenesis and treatment targets of AD, more research on NF-κB in AD is warranted.

CONCLUSION

This study demonstrated that NF-κB-induced upregulation of miR-146a-5p promoted oxidative stress and pyroptosis *via* TIGAR in a hippocampal neuronal cell model of AD.

DATA AVAILABILITY STATEMENT

The raw data supporting the conclusions of this article will be made available by the authors, without undue reservation.

ETHICS STATEMENT

The studies involving human participants were reviewed and approved by Ethics Committee of Kunming University of Science and Technology. The patients/participants provided their written informed consent to participate in this study. Written informed consent was obtained from the individual(s) for the publication of any potentially identifiable images or data included in this article.

AUTHOR CONTRIBUTIONS

BL, JL, YZ, and JX designed the experiments. JL and ZY wrote the article. YX and XZ performed experiments and analyzed data. All authors contributed to the article and approved the submitted version.

FUNDING

This study was supported by National and Regional Science Foundation Projects 81860338, Yunnan Province Foundation of Talent Cultivation (KKSY201960025) and West China Hospital Sichuan University 1.3.5 project for disciplines of excellence (ZYJC18007).

REFERENCES

Alzheimer's Association. (2016). 2016 Alzheimer's disease facts and figures. *Alzheimers Dement.* 12, 459–509. doi: 10.1016/j.jalz.2016.03.001

Ansari, A., Maffioletti, E., Milanesi, E., Marizzoni, M., Frisoni, G. B., Blin, O., et al. (2019). miR-146a and miR-181a are involved in the progression of mild cognitive impairment to Alzheimer's disease. *Neurobiol. Aging* 82, 102–109. doi: 10.1016/j.neurobiolaging.2019.06.005

Bensaad, K., Tsuruta, A., Selak, M. A., Vidal, M. N., Nakano, K., Bartrons, R., et al. (2006). TIGAR, a p53-inducible regulator of glycolysis and apoptosis. *Cell* 126, 107–120. doi: 10.1016/j.cell.2006.05.036

Chen, J., Zhang, D.-M., Feng, X., Wang, J., Qin, Y.-Y., Zhang, T., et al. (2018). TIGAR inhibits ischemia/reperfusion-induced inflammatory response of astrocytes. *Neuropharmacology* 131, 377–388. doi: 10.1016/j.neuropharm.2018.01.012

Chen, Z., and Zhong, C. (2014). Oxidative stress in Alzheimer's disease. *Neurosci. Bull.* 30, 271–281. doi: 10.1007/s12264-013-1423-y

Di Resta, C., and Ferrari, M. (2019). New molecular approaches to Alzheimer's disease. *Clin. Biochem.* 72, 81–86. doi: 10.1016/j.clinbiochem.2019.04.010

Fang, H., Li, H.-F., Yang, M., Liao, R., Wang, R.-R., Wang, Q.-Y., et al. (2019). NF-κB signaling pathway inhibition suppresses hippocampal neuronal apoptosis and cognitive impairment *via* RCAN1 in neonatal rats with hypoxic-ischemic brain damage. *Cell Cycle* 18, 1001–1018. doi: 10.1080/15384101.2019.1608128

Fransquet, P. D., and Ryan, J. (2018). Micro RNA as a potential blood-based epigenetic biomarker for Alzheimer's disease. *Clin. Biochem.* 58, 5–14. doi: 10.1016/j.clinbiochem.2018.05.020

Fricker, M., Tolkovsky, A. M., Borutaite, V., Coleman, M., and Brown, G. C. (2018). Neuronal cell death. *Physiol. Rev.* 98, 813–880. doi: 10.1152/physrev.00011.2017

Gupta, P., Bhattacharjee, S., Sharma, A. R., Sharma, G., Lee, S. S., and Chakraborty, C. (2017). miRNAs in Alzheimer disease—a therapeutic perspective. *Curr. Alzheimer Res.* 14, 1198–1206. doi: 10.2174/1567205014666170829101016

Han, C., Yang, Y., Guan, Q., Zhang, X., Shen, H., Sheng, Y., et al. (2020). New mechanism of nerve injury in Alzheimer's disease: β-amyloid-induced neuronal pyroptosis. *J. Cell. Mol. Med.* 24, 8078–8090. doi: 10.1111/jcmm.15439

Hodson, R. (2018). Alzheimer's disease. *Nature* 559:S1. doi: 10.1038/d41586-018-05717-6

Høgh, P. (2017). Alzheimer's disease. *Ugeskr Laeger* 179:V09160686.

Hu, K., Li, Y., Yu, H., and Hu, Y. (2019). CTBP1 Confers protection for hippocampal and cortical neurons in rat models of Alzheimer's disease. *Neuroimmunomodulation* 26, 139–152. doi: 10.1159/000500942

Jorgensen, I., and Miao, E. A. (2015). Pyroptotic cell death defends against intracellular pathogens. *Immunol. Rev.* 265, 130–142. doi: 10.1111/imr.12287

Ju Hwang, C., Choi, D.-Y., Park, M. H., and Hong, J. T. (2019). NF-κB as a key mediator of brain inflammation in Alzheimer's disease. *CNS Neurol. Disord. Drug Targets* 18, 3–10. doi: 10.2174/1871527316666170807130011

Katsel, P., Tan, W., Fam, P., Purohit, D. P., and Haroutunian, V. (2013). Cell cycle checkpoint abnormalities during dementia: a plausible association with the loss of protection against oxidative stress in Alzheimer's disease [corrected]. *PLoS One* 8:e68361. doi: 10.1371/journal.pone.0068361

Liu, Y.-C., Gao, X.-X., Chen, L., and You, X.-Q. (2017). Rapamycin suppresses $A\beta_{25-35}$- or LPS-induced neuronal inflammation *via* modulation of NF-κB signaling. *Neuroscience* 355, 188–199. doi: 10.1016/j.neuroscience.2017.05.005

Lukiw, W. J., Zhao, Y., and Cui, J. G. (2008). An NF-κB-sensitive micro RNA-146a-mediated inflammatory circuit in Alzheimer disease and in stressed human brain cells. *J. Biol. Chem.* 283, 31315–31322. doi: 10.1074/jbc.M805371200

Malik, A., and Kanneganti, T.-D. (2017). Inflammasome activation and assembly at a glance. *J. Cell Sci.* 130, 3955–3963. doi: 10.1242/jcs.207365

Marwarha, G., and Ghribi, O. (2017). Nuclear factor κ-light-chain-enhancer of activated B cells (NF-κB)—a friend, a foe, or a bystander—in the neurodegenerative cascade and pathogenesis of Alzheimer's disease. *CNS Neurol. Disord. Drug Targets* 16, 1050–1065. doi: 10.2174/1871527316666170725114652

Mu, Y., and Gage, F. H. (2011). Adult hippocampal neurogenesis and its role in Alzheimer's disease. *Mol. Neurodegener.* 6:85. doi: 10.1186/1750-1326-6-85

Pogue, A. I., Li, Y. Y., Cui, J.-G., Zhao, Y., Kruck, T. P., Percy, M. E., et al. (2009). Characterization of an NF-κB-regulated, miRNA-146a-mediated down-regulation of complement factor H (CFH) in metal-sulfate-stressed human brain cells. *J. Inorg. Biochem.* 103, 1591–1595. doi: 10.1016/j.jinorgbio.2009.05.012

Richetin, K., Leclerc, C., Toni, N., Gallopin, T., Pech, S., Roybon, L., et al. (2015). Genetic manipulation of adult-born hippocampal neurons rescues memory in a mouse model of Alzheimer's disease. *Brain* 138, 440–455. doi: 10.1093/brain/awu354

Seo, E.-J., Fischer, N., and Efferth, T. (2018). Phytochemicals as inhibitors of NF-κB for treatment of Alzheimer's disease. *Pharmacol. Res.* 129, 262–273. doi: 10.1016/j.phrs.2017.11.030

Shi, J., Gao, W., and Shao, F. (2017). Pyroptosis: gasdermin-mediated programmed necrotic cell death. *Trends Biochem. Sci.* 42, 245–254. doi: 10.1016/j.tibs.2016.10.004

Shi, Z.-M., Han, Y.-W., Han, X.-H., Zhang, K., Chang, Y.-N., Hu, Z.-M., et al. (2016). Upstream regulators and downstream effectors of NF-κB in Alzheimer's disease. *J. Neurol. Sci.* 366, 127–134. doi: 10.1016/j.jns.2016.05.022

Soria Lopez, J. A., González, H. M., and Léger, G. C. (2019). Alzheimer's disease. *Handb. Clin. Neurol.* 167, 231–255. doi: 10.1016/B978-0-12-804766-8.00013-3

Swarbrick, S., Wragg, N., Ghosh, S., and Stolzing, A. (2019). Systematic review of miRNA as biomarkers in Alzheimer's disease. *Mol. Neurobiol.* 56, 6156–6167. doi: 10.1007/s12035-019-1500-y

Tan, L.-L., Jiang, X.-L., Xu, L.-X., Li, G., Feng, C.-X., Ding, X., et al. (2021). TP53-induced glycolysis and apoptosis regulator alleviates hypoxia/ischemia-induced microglial pyroptosis and ischemic brain damage. *Neural Regen. Res.* 16, 1037–1043. doi: 10.4103/1673-5374.300453

Tönnies, E., and Trushina, E. (2017). Oxidative stress, synaptic dysfunction, and Alzheimer's disease. *J. Alzheimers Dis.* 57, 1105–1121. doi: 10.3233/JAD-161088

Wang, S., Ji, L.-Y., Li, L., and Li, J.-M. (2019). Oxidative stress, autophagy and pyroptosis in the neovascularization of oxygen-induced retinopathy in mice. *Mol. Med. Rep.* 19, 927–934. doi: 10.3892/mmr.2018.9759

Yilmaz, U. (2015). Alzheimer's disease. *Radiologe* 55, 386–388. doi: 10.1007/s00117-014-2796-2

Zhao, Y., Bhattacharjee, S., Jones, B. M., Hill, J., Dua, P., and Lukiw, W. J. (2014). Regulation of neurotropic signaling by the inducible, NF-kB-sensitive miRNA-125b in Alzheimer's disease (AD) and in primary human neuronal-glial (HNG) cells. *Mol. Neurobiol.* 50, 97–106. doi: 10.1007/s12035-013-8595-3

Conflict of Interest: The authors declare that the research was conducted in the absence of any commercial or financial relationships that could be construed as a potential conflict of interest.

frontiers in Cellular Neuroscience

ORIGINAL RESEARCH
published: 19 May 2021
doi: 10.3389/fncel.2021.654521

Dynamic Changes of Arc Expression in Dorsal Striatum of Mice After Self-Administration of Sucrose

Xue Li[1†], Jing-Wang Zhao[2†], Qian Ding[3†], Cheng Wu[3], Wan-Qi Li[1], Yan-Chen Guo[4], Di Wang[4], Guang-Qing Xu[5], Ti-Fei Yuan[4,6,7*], Wan-Kun Gong[4*] and Yue Lan[1,3*]*

[1] Department of Rehabilitation Medicine, Guangzhou First People's Hospital, Guangzhou Medical University, Guangzhou, China, [2] School of Rehabilitation Science, Shanghai University of Traditional Chinese Medicine, Shanghai, China, [3] Department of Rehabilitation Medicine, Guangzhou First People's Hospital, School of Medicine, South China University of Technology, Guangzhou, China, [4] Shanghai Key Laboratory of Psychotic Disorders, Shanghai Mental Health Center, Shanghai Jiao Tong University School of Medicine, Shanghai, China, [5] Department of Rehabilitation Medicine, Guangdong Provincial People's Hospital, Guangdong Academy of Medical Sciences, Guangzhou, China, [6] Translational Research Institute of Brain and Brain-Like Intelligence, Shanghai Fourth People's Hospital Affiliated to Tongji University School of Medicine, Shanghai, China, [7] Co-innovation Center of Neuroregeneration, Natong University, Nantong, China

OPEN ACCESS

Edited by:
Zhang Pengyue,
Yunnan University of Traditional Chinese Medicine, China

Reviewed by:
Wen Wu,
Southern Medical University, China
Jean-Pascal Morin,
National Autonomous University of Mexico, Mexico

***Correspondence:**
Guang-Qing Xu
guangchingx@163.com
Ti-Fei Yuan
ytf0707@126.com
Wan-Kun Gong
15111010008@fudan.edu.cn
Yue Lan
bluemooning@163.com

[†] These authors have contributed equally to this work

Specialty section:
This article was submitted to Cellular Neurophysiology, a section of the journal Frontiers in Cellular Neuroscience

Received: 16 January 2021
Accepted: 13 April 2021
Published: 19 May 2021

Citation:
Li X, Zhao J-W, Ding Q, Wu C, Li W-Q, Guo Y-C, Wang D, Xu G-Q, Yuan T-F, Gong W-K and Lan Y (2021) Dynamic Changes of Arc Expression in Dorsal Striatum of Mice After Self-Administration of Sucrose. Front. Cell. Neurosci. 15:654521. doi: 10.3389/fncel.2021.654521

Region-specific plasticity in the striatal circuit plays an important role in the development and long-term maintenance of skills and sequential movement procedures. Studies investigating the molecular substrates that contribute to the plasticity changes during motor skill processes have documented a transition in expression from the dorsomedial striatum (DMS) to the dorsolateral striatum (DLS); however, few studies have explored the expression pattern of molecular substrates in the dorsal striatum during progression of instrumental learning. To address this issue, the activity-regulated cytoskeleton-associated protein (Arc) expressions in the subregional dorsal striatum were analyzed during the early and late learning phases of the 10-day sucrose self-administration process. We found that Arc protein is primarily detected in the DMS only in the initial learning stage; however, it is expressed in the DLS during both early and late learning stages. Moreover, Arc expression in the DMS correlated with the number of rewards received later in the training. These data indicated that the Arc expression in subregions of the dorsal striatum shows region-specific transfer and that Arc expression in the DMS contributes to obtaining reward in later learning stage during the process of instrumental learning.

Keywords: Arc, the dorsomedial striatum, the dorsolateral striatum, instrumental learning, self-administration

INTRODUCTION

Instrumental or operant conditioning can be considered as learning about specific behavior and its consequences. Such processes are believed to be flexible and convertible, to produce rewarding outcomes or to avoid undesirable outcomes (Corbit, 2018). One of the most commonly used tasks to investigate instrumental conditioning is the self-administration (SA) paradigm, wherein hungry or thirsty animals perform seemingly random movements, such as nose-poking, to obtain food or water. Previous studies have shown that chronic access to highly palatable foods or sucrose water can promote a shift from goal-directed performance to habit-based performance (Avena et al., 2008;

Kenny, 2011; Furlong et al., 2014). Several studies have investigated the neuronal activity during this shift process; however, the neural plasticity mechanism controlling instrumental learning is not well characterized.

The basal ganglia were earlier believed to control executive motor functions; however, several studies have demonstrated that the basal ganglia also affect cognition and motivational behavior (Graybiel, 2008; Witt, 2021). As a major part of the basal ganglia, the dorsal striatum plays an essential role in the acquisition of new skills. The striatum is composed of two parts, i.e., the dorsal medial striatum (DMS) and the dorsal lateral striatum (DLS). The DMS receives afferents from the prefrontal and associative cortex, and mainly participates in goal-oriented learning (Balleine and O'Doherty, 2010). The DLS receives afferents from the sensorimotor cortex (Voorn et al., 2004; Hawes et al., 2015) and is mainly involved in habitual learning. Numerous studies, including our previous study (Gong et al., 2020), have documented a transition in the engaged dorsal striatal subregions (from dorsomedial to dorsolateral) with the shift in skill performance from an initial attentive phase to a more automatic or habitual phase during motor skill tasks (Yin et al., 2008; Balleine and O'Doherty, 2010; Kupferschmidt et al., 2017; Bergstrom et al., 2018). In a long SA test, the DLS was found necessary for habitual performance. However, as a more complex behavioral paradigm than skill learning, the pattern of involvement of the two major sub-regions of the dorsal striatum in the SA learning process has rarely been explored.

Activity-regulated cytoskeleton-associated protein (Arc) is an immediate early gene that has been strongly suggested as a molecular marker for neuronal plastic changes underlying the formation and stabilization of long-term memory in striatum, hippocampus, and cortex (Noe et al., 2019; Guan et al., 2021). Several studies have documented an increase in the expression of Arc in the dorsal and ventral striatum after cocaine SA (Gao et al., 2017). However, the expression pattern in the dorsal striatum in different stages of instrumental learning has not been explored yet. In this study, we attempted to determine the regional Arc expression in the different regions of the dorsal striatum during formation and consolidation of instrumental learning. The sucrose SA task was used to assess the acquisition and consolidation of instrumental learning. The Arc-positive cells in the DMS and DLS were calculated during the early and later phases in the 10-day sucrose SA process. Furthermore, by assessing the correlation between density of Arc-positive cells in the dorsal striatum and behavior, we investigated the link between dorsal striatal Arc expression and instrumental learning in mice. Our results suggested that the Arc expression in subregions of dorsal striatum shows region-specific transfer and that Arc expression in the DMS contributes to obtaining a reward in the later learning stage, during the process of instrumental learning.

MATERIALS AND METHODS

Animals

Male C57BL/6J mice (weight: 25–30 g) were purchased from the Shanghai Reagan Biotechnology Co., Ltd. Mice were housed in standardized environmental conditions (12 h light, 50% humidity, temperature: 18–22°C) and provided *ad libitum* access to water and food. Male mice aged 6 to 8 weeks were used for behavioral experiments. All animal experiments were approved by the Commission on animal experiments and application of the Shanghai Jiao Tong University School of Medicine. All efforts were made to minimize the pain caused to animals. Only the minimum number of animals required to generate credible data were used in this study.

Sucrose Self-Administration

C57 mice were handled by the experimenter for 3 min each day, starting at least 4 days before the sucrose SA training, in an operant conditioning box (Anilab, China). The program was set as follows: An active nose-poke led to delivery of sucrose (10% solution; 0.083 mL/infusion; duration: 5 s) followed by a tone (20 dB) for 5 s + turning off of house lights at each sucrose delivery. There was a 20 s interval after each infusion. During this period, only the number of nose pokes was recorded, but there was no sucrose delivery.

Prior to the initiation of the experiment, the mice were deprived of water and food for 12 h. The training lasted 3 h (from 8:00 to 11:00) and was carried out in a soundproof and ventilated operating cage. Mice were trained to respond to a 10% sucrose solution at a fixed ratio of 1 (FR1). Each active poking of the nose delivered 0.083 mL of sucrose solution. After 10 days of training, the number of nose-poke responses was stable. The number of nose-pokes executed, and the rewards obtained were recorded using the LabStat Standard Edition software. In the final 3 days, mice with fewer than 10 active nose-poke responses were excluded from further experiments.

Immunohistochemistry

Arc is vital to the formation of memory and its expression changes dynamically during the learning process. A previous study has shown that the expression of Arc increases over a period of 30 min to 2 h upon the increase in network activity, exposure to new environments, or detailed study programs (Wall et al., 2018). To assess the expression of Arc during instrumental learning, the mice were sacrificed 90 min after the time they were placed in the box. Mice in the training group were required to undergo the FR1 program, while mice in the control group were just placed in the operation box, without the program being performed. Mice were anesthetized with pentobarbital (50 mg/kg, i.p.) and the left ventricle was perfused with 0.9% normal saline followed by fixation with 4% paraformaldehyde (PFA). Brains were harvested and placed in 4% PFA overnight. Sections of brain tissue (40-μm thick) were prepared with a concussion microtome, and then placed in 0.01 M PBS for immunohistochemistry. The floating slices containing striatum were rinsed in PBS three times. The sections were then incubated overnight at 4°C with polyclonal antibody of rabbit-anti-Arc (SYSY, 156002) diluted with 0.25% Triton X-100 (v/v) and 3% normal donkey serum (v/v) (1:1,000). After washing in PBS at least three times, the sections were transferred into biotinylated goat-anti-rabbit antibody (Vector laboratories, BA1000) that was diluted with 0.25% Triton X-100 (v/v) (1:1,000) at 37°C for

1 h. After repeated washing in PBS, the sections were incubated with Alexa Fluor 546 (1:1,000; Invitrogen) for 2 h at room temperature. Finally, the sections were rinsed in 0.01 M PBS.

Imaging Analysis

A train of brain sections containing striatum was imaged under a confocal microscope equipped with a 20× objective lens (Olympus, Japan). To facilitate a comparison between the groups, all fluorescence images in the experiment were assessed using the same laser and scan settings. The photoshop software counting tool was applied to manually count the Arc immunoreactive cells in the DMS and DLS. Arc-positive cells were marked and calculated by different investigators, and the average values were used for statistical analysis. Arc-positive cells in brain sections of striatum were calculated in an area about + 1.10 to −0.10 mm from the anterior to the posterior direction (Gong et al., 2020; **Figure 2B**).

Statistical Analysis

All data are expressed as mean ± standard error of the mean (SEM). The mean scores for the behavioral and immunohistochemical experiments were subjected to multivariate analysis of variance. Multiple comparisons were performed using Tukey *post hoc* analysis. Data management and analysis were performed using GraphPad Prism 8 software. P values < 0.05 were considered indicative of statistical significance.

RESULTS

Acquisition of FR1 Response for Sucrose

To evaluate the expression of Arc during different periods of instrumental learning, mice were self-administered sucrose using the conventional training protocol described in a previous report (Mahler and Aston-Jones, 2012). In our study, mice were trained in sucrose SA for 3 h a day, for 10 consecutive days in operant conditioning boxes. The design of the box is shown in **Figure 1A**. Sucrose flows out when the mouse nose touches the active port, at which point the house light was turned on and a sound was activated to indicate that a reward was available. On the contrary, there were no programmed consequences upon touching another (inactive) nose-poke port. **Figure 1B** shows the total number of active and inactive nose pokes during the training process of the FR1 response to the sucrose solution. Optional increase in nose poking on the active hole reached an asymptote in 10 sessions. The number of rewards also increased on consecutive days, reaching a plateau on the third day, which was maintained until the 10th day. It is worth noting that the rate of rewards and the ratio of active pokes declined. The number of pokes without rewards increased, which means that the correct rate of poke decreased during training (**Figures 1C,D**).

Regional Specificity of Arc Protein Expression in the Dorsomedial and Dorsolateral Striatum During Instrumental Learning

To detect the Arc expression in the different regions of the dorsal striatum, during various periods of instrumental learning, all brain tissues of mice were obtained on the first and 10th day of training (**Figures 2A,B**). The expression of Arc in the DMS changed dynamically during the 10-day sucrose SA process [one-way ANOVA, $F(2,21) = 4.724$, $P < 0.05$]. On the first day, there was no significant increase in the number of Arc-positive cells (**Figures 2C,D**), while there was an obvious difference of Arc-positive cells between day 10 and day 1 (**Figures 2C,D**).

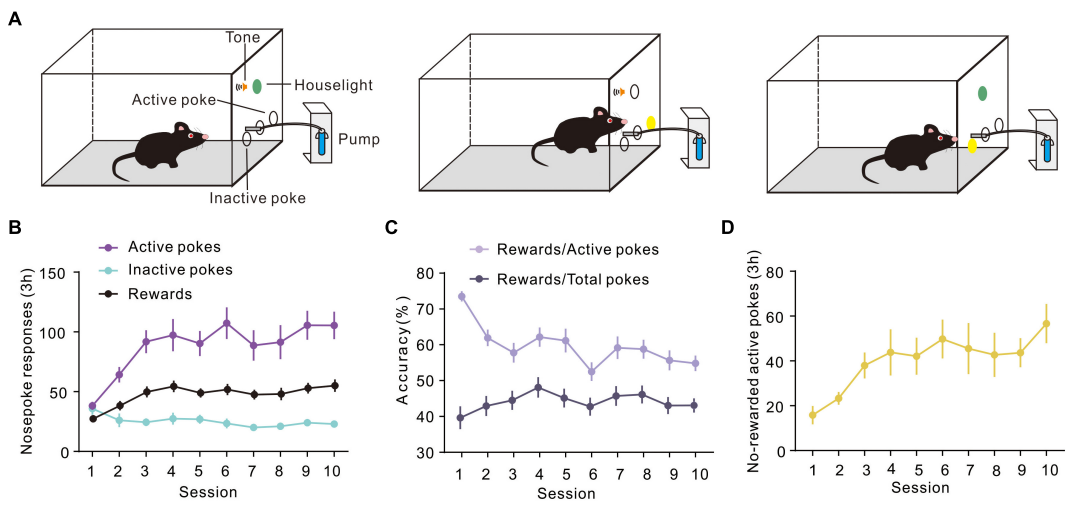

FIGURE 1 | Performance of sucrose self-administration behavior. **(A)** Schematic illustration of sucrose self-administration. **(B)** Under the fixed ratio 1 (FR1) program, active and inactive nose pokes in response to 10% sucrose were calculated during training ($n = 20$). **(C)** Curve showing the proportion of the number of rewards and the number of pokes. **(D)** The number of No-rewarded active pokes in 3 h.

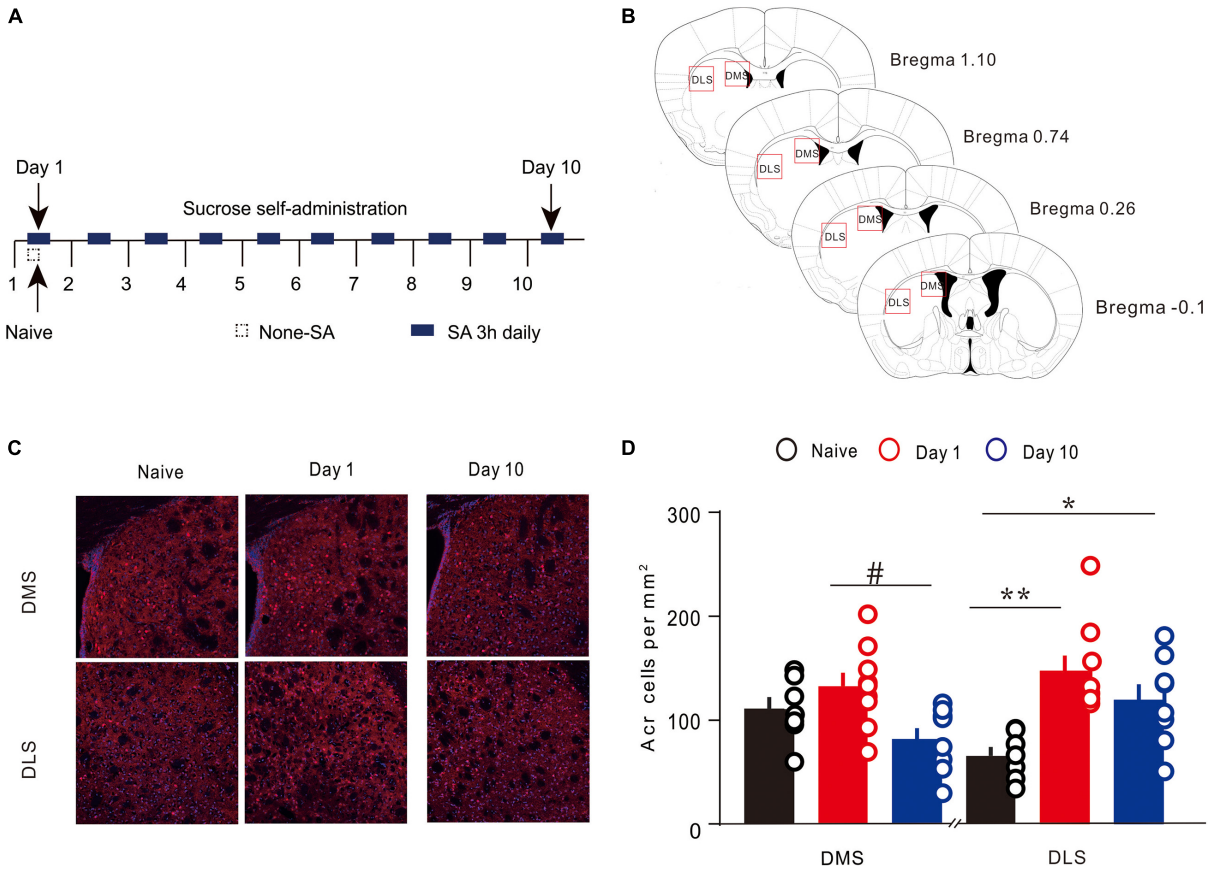

FIGURE 2 | Expression of Arc in the specific regions of the dorsal striatum during sucrose self-administration. **(A)** Self-administration of sucrose solution in mice (n = 20). Arrows represent the time of sampling. **(B)** George and Franklin's (2001) coronal section map with Bregma coordinates. Reference modified from Gong et al. (2020), quantitative explanation of Arc in the brain regions. **(C)** Representative images of the DMS and DLS showing Arc expression in different groups on day 1 and day 10. Scale bar = 300 μm. **(D)** The density of Arc$^+$ cells in the DMS and DLS on day 1 (n = 9), day 10 (n = 8), and in the naive group (n = 7) mice. *P < 0.05, **P < 0.01 versus naive group by one-way ANOVA. #P < 0.05 versus day 10 in the DMS by Tukey *post hoc* tests. Data are expressed as mean ± SEM. cc, corpus callosum DMS, dorsomedial striatum; LV, lateral ventricle; IHC, immunohistochemistry; DLS, dorsolateral striatum.

Results of the *post hoc* Tukey test showed that the density of Arc-positive cells on day 1 was significantly higher (132.67 ± 13.14 cells/mm^2, 8 n = 9; vs. 81.36 ± 11.07, n = 8 P < 0.05) than that on day 10. The expression of Arc in the DLS also showed a dynamic change during the 10-day sucrose SA process [one-way ANOVA, $F(2,21) = 8.884$, $P < 0.01$]. Results of the *post hoc* Tukey test showed that the density of Arc-positive cells in the DLS was significantly higher on day 1 (147.39 ± 14.71, n = 9 vs. 65.56 ± 8.49 cells/mm^2, n = 7; P < 0.01) and on day 10 (119.25 ± 15.19, n = 8 vs. 65.56 ± 8.49 cells/mm^2, n = 7; P < 0.05) as compared to that in the naive group. In addition, the expression of Arc in DLS did not differ between day 1 and day 10. These results indicate that Arc showed area-specific expression in the striatum during the instrumental learning process.

Correlation Between the Number of Rewards and the Density of Arc$^+$ Cells

Next, we sought to assess the correlation between density of Arc-positive cells in the dorsal striatum and behavior. We conducted a correlation analysis to determine the relationship of current behavioral data with Arc expression in the striatum during different stages of sucrose SA. On day 1, no pronounced correlation was observed in DMS (R^2 = 0.02298, $P > 0.05$) and DLS (R^2 = 0.03975, $P > 0.05$) (**Figure 3**). However, in the DMS, the number of rewards showed a significant positive correlation with the density of Arc$^+$ cells on day 10 (R^2 = 0.3115, $P > 0.05$). There was also no apparent association between the number of rewards and the density of Arc$^+$ cells in the DLS (R^2 = 0.1452, $P > 0.05$) on day 10.

DISCUSSION

In this study, we investigated instrumental learning using sucrose SA in which thirsty animals can obtain sucrose water by poking the active port. The results showed region-specific expression of Arc in the dorsal striatum during the formation and stabilization stage of SA instrumental learning. Arc expression in the DMS was increased during the early stage of instrumental learning and

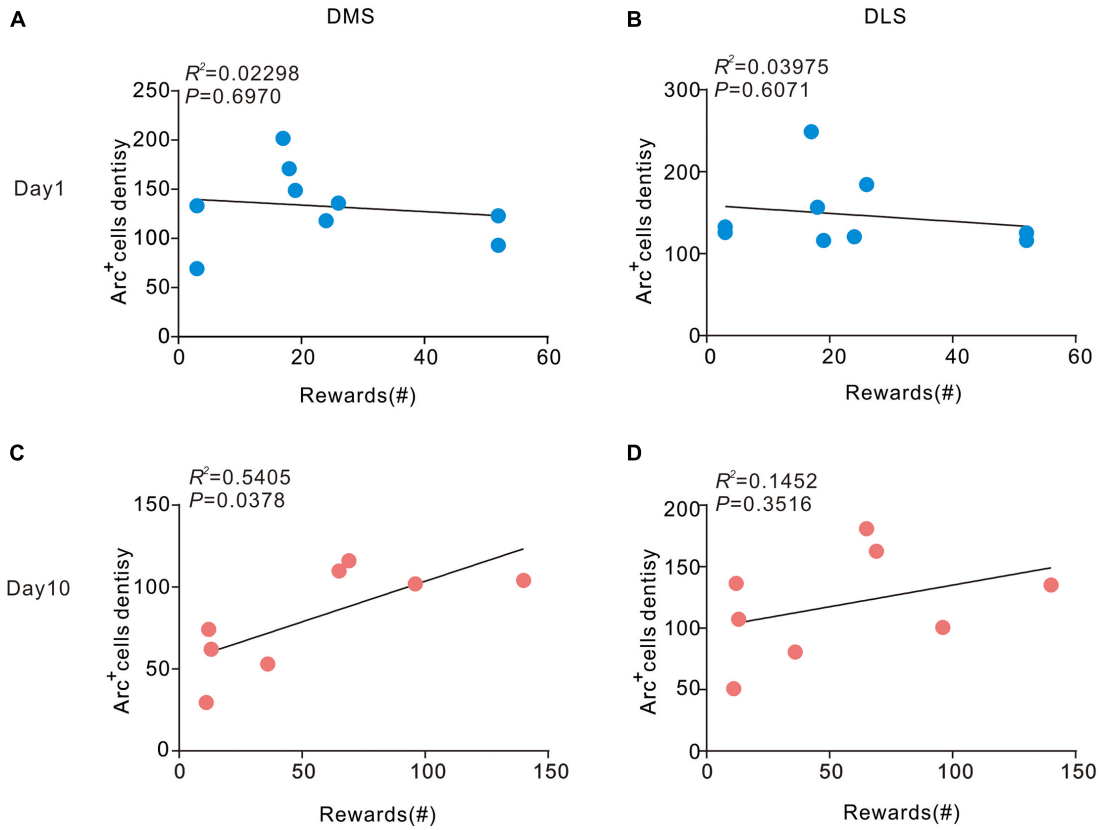

FIGURE 3 | Correlation between Arc expression and reward times in the DMS and DLS. **(A,B)** Arc expression during instrumental learning did not correlate with sucrose self-administration behavior on day 1 (n = 9). **(C)** Day 10, the density of Arc positive cells correlated with the magnitude of the number of rewards in the DMS ($P < 0.05$, $R^2 = 0.5405$) Pearson's product-moment correlation coefficients. **(D)** In the DLS, Arc expression did not correlate with the number of rewards on day 10. n = 8 mice for the day 10 group.

reduced to the basic levels when the procedural operation was automated; in contrast, Arc expression in the DLS was increased both in the early stage and the later stage.

A wide body of evidence supports the essential role of the basal ganglia circuit in instrumental learning and operation (Groenewegen, 2003). However, these two functions are generally considered to be distinct and independent. Instrumental learning mainly depends on glutamatergic projections from the frontal cortex and limbic lobe to the dorsal striatum, while the execution of instrumental learning tasks is primarily dependent on the dorsal striatal output pathways (Kreitzer and Malenka, 2008). Previous studies have shown the involvement of dorsal striatum in several kinds of learning (Graybiel and Grafton, 2015); however, the precise dynamic role of the DLS and DMS in SA instrumental learning is not well characterized (Devan et al., 2011; Kupferschmidt et al., 2017). From a neuroanatomical perspective, the DMS and DLS are two distinct regions which receive different projections from the cortex and the midbrain dopaminergic nucleus (Hintiryan et al., 2016). The DMS receives afferents from the cognition-related cortex, such as the prefrontal cortex and the associative cortex, while the DLS receives afferents from the motor execution cortex (Voorn et al., 2004; Hawes et al., 2015).

The sucrose SA can be roughly divided into two stages: (1) the early learning/training stage (first 3 days) during which the mouse learns how to operate the equipment motivated by the reward (sucrose); and (2) the later stage (4 to 10 days) when the mouse has already learnt and transferred it into a proficient skill and may perform it habitually. During the early stage of training, the mouse initially explores the environment aimlessly; it typically pokes the active side and inactive side randomly until it obtains the reward (sucrose) after an active nose poke, which is followed by a light and tone; subsequently, it tends to poke more purposively to obtain sucrose. As shown in **Figure 1**, nose pokes of the two sides are almost equal at first (session 1); however, the active pokes increased very soon after (especially the first three sessions), with a simultaneous gradual decrease in the inactive pokes. The prefrontal cortex and DMS are mainly involved in this process of cognition; consistently, DMS was preferentially activated in the early stage with an increase in Arc expression. Previous studies have shown that the DMS plays an important part in the early acquisition of dynamic foraging, motor skill learning (Sheng et al., 2019), habitual drug seeking (Corbit et al., 2012), and instrumental learning (Vicente et al., 2016; Peak et al., 2019). Our results are consistent with the results of previous studies.

With the progression of training in the later stage (4–10 days), mice had already learnt and transferred the learning into a proficient skill. The reduced involvement and dependence of DMS led to downregulation of Arc in this stage. The characteristics of Arc expression showed that the DLS is activated during both the early and later stages of instrumental learning. Earlier studies have shown the participation of DLS in the consolidation of skilled actions in operant tasks, habitual drug-seeking, and motor skill learning (Kimchi and Laubach, 2009; Thorn et al., 2010; O'Hare et al., 2016). The results of Arc expression in our study are consistent with those of previous studies, indicating that Arc expression is indispensable for the acquisition and consolidation of instrumental learning.

Immediate early genes, including Arc/Arg3.1 and c-Fos, are a group of genes that are expressed dynamically and rapidly in brain regions that are closely related to the formation of memory and learning procedures (Ramírez-Amaya et al., 2005). The protein products of immediate early genes have been regarded as biomarkers of neurons that activate or exhibit plasticity changes. In a previous study, expression of c-Fos was shown to increase in the dorsal part of the striatum during motor learning; however, no dynamic change was observed among the different phases of learning (Bureau et al., 2010). This suggests that c-Fos may not be an appropriate biomarker for representing dynamic changes of plasticity between the different motor learning stages (Yin et al., 2009). However, a previous study documented dynamic changes in the expression of Arc in the dorsal striatum during the learning phase of a touchscreen task (Bergstrom et al., 2018). At the molecular level, Arc is functionally involved in the maintenance of homeostatic synaptic plasticity by accelerating endocytosis of AMPA-type glutamate receptors (Tzingounis and Nicoll, 2006; Jakkamsetti et al., 2013). Our study indicates region-specific dynamic changes in Arc expression in the dorsal striatum during SA learning. Therefore, Arc is an eligible biomarker for neurons that undergo plasticity transformation during different phases of learning. With a decrease of Arc expression in the DMS while showing an obviously positive correlation with the number of rewards received in the later stages, our study shows a dissociation between Arc expression in the DMS and learning stages in the instrumental learning of sucrose SA.

In summary, our study demonstrates regional and temporal variations of neural plasticity in DMS during different phases of sucrose SA instrumental learning through Arc expression.

DATA AVAILABILITY STATEMENT

The original contributions presented in the study are included in the article/supplementary material, further inquiries can be directed to the corresponding authors.

ETHICS STATEMENT

The animal study was reviewed and approved by the Ethics Committee of Medical College of Shanghai Jiao Tong University.

AUTHOR CONTRIBUTIONS

YL, W-KG, G-QX, and T-FY designed the experiment. XL, J-WZ, QD, and CW collected the data. XL, J-WZ, QD, Y-CG, W-QL, and DW analyzed the data. XL, J-WZ, and QD wrote the manuscript. All authors contributed to the article and approved the submitted version.

FUNDING

This work was supported by the National Science Foundation of China [grant numbers 81772438 (YL), 81974357 (YL), and 82072548 (G-QX)], the Guangzhou Municipal Science and Technology Program [grant number 201803010083 (YL)], the Fundamental Research Funds for the Central University [grant number 2018PY03 (YL)], Guangdong Grant "Key Technologies for Treatment of Brain Disorders" [grant number 2018B030331001 (T-FY)], the Medicine and Engineering Interdisciplinary Research Fund of Shanghai Jiao Tong University [grant numbers ZH2018ZDA30 (T-FY) and YG2021QN132 (W-KG)], the Guangdong Basic and Applied Basic Research Foundation [grant number 2020A1515110761 (QD)], and the Guangzhou Postdoctoral Science Foundation (QD). The study is also supported by Shenzhen-Hong Kong Institute of Brain Science – Shenzhen Fundamental Research Institutions [NYKFKT20190020 (T-FY)].

REFERENCES

Avena, N. M., Rada, P., and Hoebel, B. G. (2008). Evidence for sugar addiction: behavioral and neurochemical effects of intermittent, excessive sugar intake. *Neurosci. Biobehav. Rev.* 32, 20–39. doi: 10.1016/j.neubiorev.2007.04.019

Balleine, B. W., and O'Doherty, J. P. (2010). Human and rodent homologies in action control: corticostriatal determinants of goal-directed and habitual action. *Neuropsychopharmacology* 35, 48–69. doi: 10.1038/npp.2009.131

Bergstrom, H. C., Lipkin, A. M., Lieberman, A. G., Pinard, C. R., Gunduz-Cinar, O., Brockway, E. T., et al. (2018). Dorsolateral Striatum Engagement Interferes with Early Discrimination Learning. *Cell. Rep.* 23, 2264–2272. doi: 10.1016/j.celrep.2018.04.081

Bureau, G., Carrier, M., Lebel, M., and Cyr, M. (2010). Intrastriatal inhibition of extracellular signal-regulated kinases impaired the consolidation phase of motor skill learning. *Neurobiol. Learn. Mem.* 94, 107–115. doi: 10.1016/j.nlm.2010.04.008

Corbit, L. H. (2018). Understanding the balance between goal-directed and habitual behavioral control. *Curr. Opinion Behav. Sci.* 20, 161–168. doi: 10.1016/j.cobeha.2018.01.010

Corbit, L. H., Nie, H., and Janak, P. H. (2012). Habitual alcohol seeking: time course and the contribution of subregions of the dorsal striatum. *Biol. Psychiat.* 72, 389–395. doi: 10.1016/j.biopsych.2012.02.024

Devan, B. D., Hong, N. S., and Mcdonald, R. J. (2011). Parallel associative processing in the dorsal striatum: segregation of stimulus-response and

cognitive control subregions. *Neurobiol. Learn. Mem.* 96, 95–120. doi: 10.1016/j.nlm.2011.06.002

Furlong, T. M., Jayaweera, H. K., Balleine, B. W., and Corbit, L. H. (2014). Binge-like consumption of a palatable food accelerates habitual control of behavior and is dependent on activation of the dorsolateral striatum. *J. Neurosci.* 34, 5012–5022. doi: 10.1523/jneurosci.3707-13.2014

Gao, P., Limpens, J. H., Spijker, S., Vanderschuren, L. J., and Voorn, P. (2017). Stable immediate early gene expression patterns in medial prefrontal cortex and striatum after long-term cocaine self-administration. *Addict. Biol.* 22, 354–368. doi: 10.1111/adb.12330

George, P., and Franklin, K. B. J. (2001). *The Mouse Brain in Stereotaxic Coordinates*, Vol. 200 (Cambridge, MI: Acadmic press), 65–69.

Gong, W. K., Ni, J., Yu, L. F., Wang, L., and Huang, Z. L. (2020). Temporal dynamics of Arc/Arg3.1 expression in the dorsal striatum during acquisition and consolidation of a motor skill in mice. *Neurobiol. Learn. Mem.* 168:107156. doi: 10.1016/j.nlm.2019.107156

Graybiel, A. M. (2008). Habits, rituals, and the evaluative brain. *Annu. Rev. Neurosci.* 31, 359–387. doi: 10.1146/annurev.neuro.29.051605.112851

Graybiel, A. M., and Grafton, S. T. (2015). The striatum: where skills and habits meet. *Cold Spring Harb. Perspect. Biol.* 7:a021691. doi: 10.1101/cshperspect.a021691

Groenewegen, H. J. (2003). The basal ganglia and motor control. *Neural. Plast.* 10, 107–120.

Guan, S. Z., Fu, Y. J., Zhao, F., Liu, H. Y., Chen, X. H., Qi, F. Q., et al. (2021). The mechanism of enriched environment repairing the learning and memory impairment in offspring of prenatal stress by regulating the expression of activity-regulated cytoskeletal-associated and insulin-like growth factor-2 in hippocampus. *Environ. Health. Prev. Med.* 26:8.

Hawes, S. L., Evans, R. C., Unruh, B. A., Benkert, E. E., Gillani, F., Dumas, T. C., et al. (2015). Multimodal Plasticity in Dorsal Striatum While Learning a Lateralized Navigation Task. *J. Neurosci.* 35, 10535–10549. doi: 10.1523/jneurosci.4415-14.2015

Hintiryan, H., Foster, N. N., Bowman, I., Bay, M., Song, M. Y., Gou, L., et al. (2016). The mouse cortico-striatal projectome. *Nat. Neurosci.* 19, 1100–1114. doi: 10.1038/nn.4332

Jakkamsetti, V., Tsai, N. P., Gross, C., Molinaro, G., Collins, K. A., Nicoletti, F., et al. (2013). Experience-induced Arc/Arg3.1 primes CA1 pyramidal neurons for metabotropic glutamate receptor-dependent long-term synaptic depression. *Neuron* 80, 72–79. doi: 10.1016/j.neuron.2013.07.020

Kenny, P. J. (2011). Common cellular and molecular mechanisms in obesity and drug addiction. *Nat. Rev. Neurosci.* 12, 638–651. doi: 10.1038/nrn3105

Kimchi, E. Y., and Laubach, M. (2009). The dorsomedial striatum reflects response bias during learning. *J. Neurosci.* 29, 14891–14902. doi: 10.1523/jneurosci.4060-09.2009

Kreitzer, A. C., and Malenka, R. C. (2008). Striatal plasticity and basal ganglia circuit function. *Neuron* 60, 543–554. doi: 10.1016/j.neuron.2008.11.005

Kupferschmidt, D. A., Juczewski, K., Cui, G., Johnson, K. A., and Lovinger, D. M. (2017). Parallel, but Dissociable, Processing in Discrete Corticostriatal Inputs Encodes Skill Learning. *Neuron* 96, 476-489.e5.

Mahler, S. V., and Aston-Jones, G. S. (2012). Fos activation of selective afferents to ventral tegmental area during cue-induced reinstatement of cocaine seeking in rats. *J. Neurosci.* 32, 13309–13326. doi: 10.1523/jneurosci.2277-12.2012

Noe, E., Bonneau, N., Fournier, M. L., Caillé, S., Cador, M., and Le Moine, C. (2019). Arc reactivity in accumbens nucleus, amygdala and hippocampus differentiates cue over context responses during reactivation of opiate withdrawal memory. *Neurobiol. Learn. Mem.* 159, 24–35. doi: 10.1016/j.nlm.2019.02.007

O'Hare, J. K., Ade, K. K., Sukharnikova, T., Van Hooser, S. D., Palmeri, M. L., Yin, H. H., et al. (2016). Pathway-Specific Striatal Substrates for Habitual Behavior. *Neuron* 89, 472–479. doi: 10.1016/j.neuron.2015.12.032

Peak, J., Hart, G., and Balleine, B. W. (2019). From learning to action: the integration of dorsal striatal input and output pathways in instrumental conditioning. *Eur. J. Neurosci.* 49, 658–671. doi: 10.1111/ejn.13964

Ramírez-Amaya, V., Vazdarjanova, A., Mikhael, D., Rosi, S., Worley, P. F., and Barnes, C. A. (2005). Spatial exploration-induced Arc mRNA and protein expression: evidence for selective, network-specific reactivation. *J. Neurosci.* 25, 1761–1768. doi: 10.1523/jneurosci.4342-04.2005

Sheng, M. J., Lu, D., Shen, Z. M., and Poo, M. M. (2019). Emergence of stable striatal D1R and D2R neuronal ensembles with distinct firing sequence during motor learning. *Proc. Natl. Acad. Sci. U. S. A.* 116, 11038–11047. doi: 10.1073/pnas.1901712116

Thorn, C. A., Atallah, H., Howe, M., and Graybiel, A. M. (2010). Differential dynamics of activity changes in dorsolateral and dorsomedial striatal loops during learning. *Neuron* 66, 781–795. doi: 10.1016/j.neuron.2010.04.036

Tzingounis, A. V., and Nicoll, R. A. (2006). Arc/Arg3.1: linking gene expression to synaptic plasticity and memory. *Neuron* 52, 403–407. doi: 10.1016/j.neuron.2006.10.016

Vicente, A. M., Galvão-Ferreira, P., Tecuapetla, F., and Costa, R. M. (2016). Direct and indirect dorsolateral striatum pathways reinforce different action strategies. *Curr. Biol.* 26, R267–R269.

Voorn, P., Vanderschuren, L. J., Groenewegen, H. J., Robbins, T. W., and Pennartz, C. M. (2004). Putting a spin on the dorsal-ventral divide of the striatum. *Trends Neurosci.* 27, 468–474. doi: 10.1016/j.tins.2004.06.006

Wall, M. J., Collins, D. R., Chery, S. L., Allen, Z. D., Pastuzyn, E. D., George, A. J., et al. (2018). The Temporal Dynamics of Arc Expression Regulate Cognitive Flexibility. *Neuron* 98, 1124–1132.e7.

Witt, K. (2021). The Impact of the Basal Ganglia on Working Memory: Evidence from Parkinson's Disease. *Mov. Disord.* 36, 13–15. doi: 10.1002/mds.28358

Yin, H. H., Mulcare, S. P., Hilario, M. R., Clouse, E., Holloway, T., Davis, M. I., et al. (2009). Dynamic reorganization of striatal circuits during the acquisition and consolidation of a skill. *Nat. Neurosci.* 12, 333–341. doi: 10.1038/nn.2261

Yin, H. H., Ostlund, S. B., and Balleine, B. W. (2008). Reward-guided learning beyond dopamine in the nucleus accumbens: the integrative functions of cortico-basal ganglia networks. *Eur. J. Neurosci.* 28, 1437–1448. doi: 10.1111/j.1460-9568.2008.06422.x

Conflict of Interest: The authors declare that the research was conducted in the absence of any commercial or financial relationships that could be construed as a potential conflict of interest.

Advantages of publishing in Frontiers

OPEN ACCESS
Articles are free to read for greatest visibility and readership

FAST PUBLICATION
Around 90 days from submission to decision

HIGH QUALITY PEER-REVIEW
Rigorous, collaborative, and constructive peer-review

TRANSPARENT PEER-REVIEW
Editors and reviewers acknowledged by name on published articles

Frontiers
Avenue du Tribunal-Fédéral 34
1005 Lausanne | Switzerland

Visit us: www.frontiersin.org
Contact us: frontiersin.org/about/contact

REPRODUCIBILITY OF RESEARCH
Support open data and methods to enhance research reproducibility

DIGITAL PUBLISHING
Articles designed for optimal readership across devices

FOLLOW US
@frontiersin

IMPACT METRICS
Advanced article metrics track visibility across digital media

EXTENSIVE PROMOTION
Marketing and promotion of impactful research

LOOP RESEARCH NETWORK
Our network increases your article's readership